CONCEPTUAL DESIGN AND ANALYSIS OF THE TRACKED MAGNETICALLY LEVITATED VEHICLE TECHNOLOGY PROGRAM (TMLV) - REPULSION SCHEME

VOLUME I - TECHNICAL STUDIES
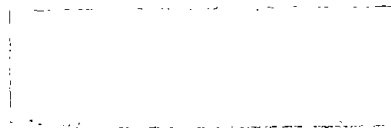
February 1975

FINAL REPORT
DOT-FR-40024 (Task I)

Prepared for:

Department of Transportation

Federal Railroad Administration
Office of Research, Development and Demonstrations
Washington, D.C. 20590

NOTICES

The United States Government does not endorse products of
manufacturers. Trade or manufacturers' names appear herein
solely because they are considered essential to the object
of this report.

This document is disseminated under the sponsorship of the
Department of Transportation in the interest of information
exchange. The United States Government assumes no liability
for its contents or use thereof.

PREFACE

The study documented in this Final Report was conducted by Ford Motor
Co. under contract to the U.S. Department of Transportation (DOT), Federal
Railroad Administration, Office of Research, Development and Demonstrations.
The DOT Program Manager was Dr. John T. Harding. Additional support was
provided by Mr. Arnold Gross of DOT and Dr. Roger Katz of MITRE Corp.

Overall program management and levitation magnet design were the respon-
sibility of the Ford Scientific Research Staff. Vehicle and guideway con-
ceptual designs, vehicle dynamic analysis, and overall systems analysis were
the responsibility of the Aeronutronic Division of Philco-Ford Corp.

Levitation magnet design and cost analysis were provided by Magnetic
Corp. of America, Waltham, Mass., under subcontract to Ford. Subcontractors
to the Aeronutronic Division of Philco-Ford and their areas of responsibility
were: The Cardan Co., Inc., Beverly Hills, Ca., for the design and cost esti-
mates of the supporting structure for the at-grade and elevated guideways;
the Raytheon Company, Equipment Division for linear synchronous motor studies;
and the Hamilton Standard Division of United Aircraft Corp. for the analysis
and cost estimates of air propulsion systems. The latter contract was sup-
ported by Philco-Ford in-house funds at no cost to the contract.

Additional no-cost information was provided by the AiResearch Division
of Garrett Corp. (linear induction motor design and performance data, and
information on superconducting rotary electric motors), Jet Propulsion Labo-
ratory (conceptual single-sided linear induction motor performance), and the
United Aircraft Research Laboratory (cost analysis of high-speed ground trans-
portation systems).

The key technical personnel on the project are listed below:

- Ford Motor Co. Scientific Research Laboratory

  J. R. Reitz . . . . . Program Manager

  R. H. Borcherts . . . Deputy Program Manager for Magnetics

  L. C. Davis . . . . . Consultant for Magnetics

- Aeronutronic Division, Philco-Ford Corporation

  R. L. Pons . . . . . Deputy Program Manager for Systems

  T. B. Clark . . . . . System Design and Analysis

  D. A. Rodriguez . . . Vehicle Dynamics and Control

  R. R. Auelmann . . . Vehicle Dynamics and Control

  C. C. Wan . . . . . . Vehicle Dynamics and Control

  L. C. Sutherland . . Vehicle Dynamics and Control

  R. M. Taylor . . . . Vehicle and Guideway Structures

  J. R. Dowty . . . . . Vehicle Design

  R. E. England . . . . Electrical Systems

- Magnetic Corp. of America

  Z. J. J. Stekly . . . Principal Investigator, Levitation Magnets

- Cardan Co.

  B. H. Cardan . . . . At-Grade and Elevated Guideway Structures

  Bernard Cardan . . . Consulting Engineer, Structures

- Raytheon Co., Equipment Division

  M. Kolker . . . . . . Task Manager

  C. H. Tang . . . . . Principal Investigator, LSM

- Hamilton Standard and United Aircraft Corp. Research Labs.

  B. S. Gatzen . . . . Principal Investigator, Air Propulsion
  Systems

  F. B. Metzger . . . . Acoustics

  F. W. Gobetz . . . . Economic Analysis

Messrs. T. B. Clark and R. L. Pons were the editors of this report.

CONTENTS

VOLUME I

CONTENTS (Continued)

CONTENTS (Continued)

CONTENTS (Continued)

ILLUSTRATIONS

ILLUSTRATIONS (Continued)

ILLUSTRATIONS (Continued)

ILLUSTRATIONS (Continued)

ACOUSTICALLY
TREATED DUCTED FAN

REGENERATIVE
GAS TURBINES

AUXILIARY POWER
UNIT AND CABIN CONDITIONING
EQUIPMENT

HELIUM LIQUIFIER AND COMPRESSOR

DEWAR AND
MAGNETS

LAVATORIES

AFT STORAGE
& WARDROBES

PASSENGER
COMPARTMENT
(80 SEATS)

FUEL
TANKS

ADDITIONAL
CARGO CAPACITY

LANDING/SWITCHING
GEAR

GALLEY

CREW
COMPARTMENT

FORWARD
STORAGE
& WARDROBES

MAGLEV REVENUE VEHICLE SYSTEM/BASELINE CONFIGURATION

xviii

SECTION 1

INTRODUCTION

1.1 BACKGROUND

This report summarizes the studies conducted by the Ford Motor Co. and its subcontractors under Task I of the Tracked Magnetically Levitated Vehicle (TMLV) Technology Program - Repulsion scheme. The purpose of the program is to establish the technology of magnetic suspension for ultimate use in a passenger-carrying high-speed ground transportation (HSGT) system - at speeds on the order of 134 m/s (300 mph).

Magnetic Levitation (MAGLEV) is one of several advanced vehicle suspension concepts being studied under U.S. Department of Transportation (DOT) sponsorship as alternatives to conventional transportation modes in the short-haul regime. The search for transportation alternatives is motivated by predictions of heavy traffic congestion - in the 1985-1990 time frame - in highly populated regions of the United States with attendant environmental damage, and substantial hazard to public safety. Also, the national energy shortage has intensified the search for more energy-efficient as well as cost-effective transportation modes.

In 1971-72, DOT sponsored initial MAGLEV research studies at Ford Motor Co. and at Stanford Research Institute (SRI). The results of these studies indicated that magnetic levitation is feasible, and that it offers several unique advantages and should be considered competitive, for example, with tracked air cushion vehicles for the ultimate HSGT role.

The TMLV Technology Program contract was awarded to Ford Motor Co. on 31 May 1974 (Contract DOT-FR-40024) for the purpose of developing MAGLEV technology relating to the Repulsion, or superconducting concept. The program consisted of two tasks:

- Task I - A conceptual design of the total suspension and associated guideway for an 80-passenger repulsion MAGLEV vehicle

1-1

meeting the specified ride quality requirements at all speeds
below 134 m/s.

* Task II - The detailed design, construction and test of a high-
  speed test platform incorporating a scaled version of the sus-
  pension system designed in Task I. Also included was the asso-
  ciated guideway (to be constructed at the U.S. Naval Weapons
  Center (NWC), China Lake, California).

This report contains only the results of Task I; Task II was cancelled shortly
after initiation due to cuts in the Federal budget.

The original scope of Task I has been expanded to include larger capacity
vehicles, preliminary propulsion studies, conceptual vehicle design (other
than suspension-related elements), system engineering studies of the overall
system (vehicle, guideway, etc.), and cost studies of the major elements of
the system. A simplified cost model has been derived to establish cost/
effectiveness trends and help make preliminary judgements as to such factors
as optimum cruise speed, magnet and guideway configuration, system energy
efficiency, etc.

1.2 ORGANIZATION OF REPORT

A summary of the important results obtained from this study are contained
in Section 2. The system requirements specified by DOT and those derived
during the program are given in Section 3. Section 4 contains the design and
analysis of the vehicle, suspension, propulsion, and guideway (both at-grade
and elevated). The system analysis and tradeoffs are given in Section 5,
followed by the cost estimates for the suspension subsystem and guideway.
Volume I is concluded by the Conclusions and Recommendations, Section 7.

Volume II is an Appendix which contains the mathematical details of
various portions of the vehicle dynamics and control work (Appendices A-D),
followed by a Hamilton Standard Summary of the Q-fan propulsion system acoustic
characteristics and the Raytheon work on the linear synchronous motor.

Volume III (Appendix G) is a description of the five degree-of-freedom
(5 DOF) computer program that was developed to analyze the dynamics and ride
quality of the Repulsion MAGLEV vehicle.

SECTION 2

SUMMARY

A baseline Revenue TMLV system is identified as a reference point for comparative performance and cost analysis. The salient features of this system, supporting tradeoffs, and alternate design approaches are summarized in the following paragraphs.

2.1 BASELINE SYSTEM DESCRIPTION

The reference system consists of an 80-seat vehicle (with a 2 + 2 seating arrangement, i.e., 2 seats on each side of an aisle) powered by two noise-suppressed ducted fans driven by regenerative gas turbines. The vehicle is designed to operate at 134 m/s (300 mph) over a hat-shaped (wide inverted tee) guideway. The route profile is nominally 750 km long with five intermediate, equidistant stops.

A sketch of the vehicle is shown in Figure 2-1 and the frontispiece; it has a cabin cross section 3.45 m (11.3 ft) high x 2.94 m (9.6 ft) wide and is 33.7 m (111 ft) long, with a gross weight (including JP fuel at 15% reserve) of 366.5 kN (82,400 lb).

Levitation and guidance is provided by eight cryogenically cooled superconducting magnets encased in insulated dewars and arranged in four modules at the corners of the vehicle. The magnetic fields interact with L-shaped aluminum guideway elements to provide levitation and guidance at a nominal 30 cm (12 in.) clearance (measured from coil centerline to guideway surface). For operation at speeds below ~ 30 m/s (67 mph), an auxiliary suspension system is provided consisting of retractable, pneumatic-tired bogies at the front and rear of the vehicle.

Active control of vehicle dynamic motion is accomplished with conventional electromagnets mounted below the levitation/guidance magnets and external to the dewars. The control magnets interact with the levitation/guidance magnets and the aluminum guideway elements to damp the vehicle

2-1

HAT-SHAPE GUIDEWAY

INLETS FOR
GAS TURBINES

7.01
(276)

33.67
(1326)

DIMENSIONS: METERS (INCHES)

TWIN "Q-FANS"
(Q JET FANS)

MAGNET MODULE

LANDING/SWITCHING
WHEELS

80 PASSENGERS

15.15
(596)

24
(946)

2
(78.8)

0.9
(35.5)

3.2
(126)

2.15
(84.8)

4.92
(194)

3.45
(136)

0.19
(7.5)

3.51
(138)

2.94
(116)
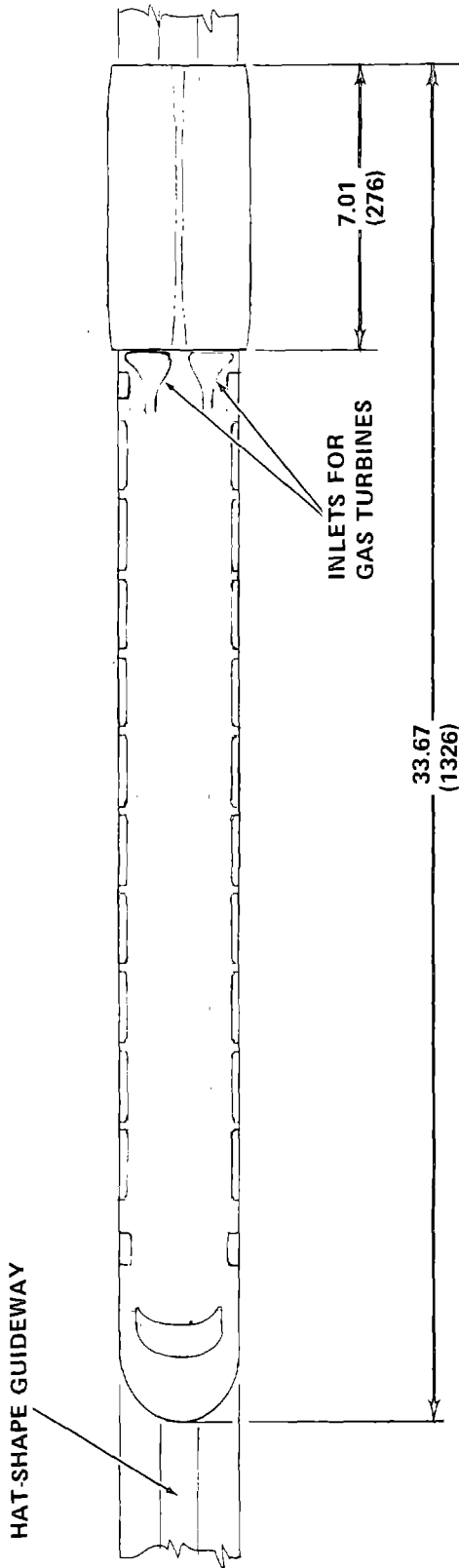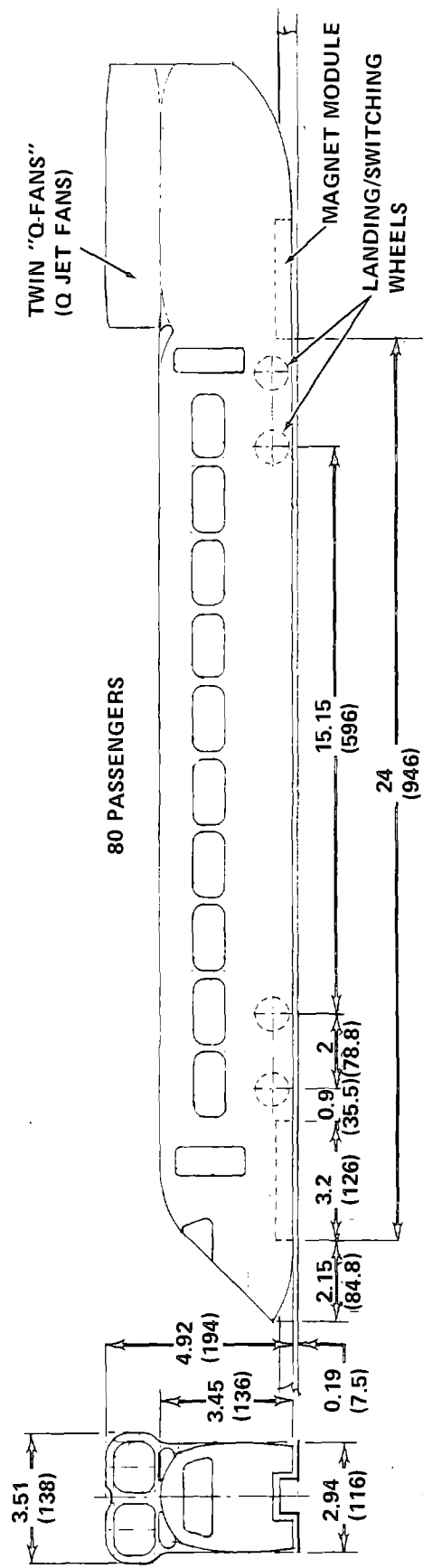
FIGURE 2-1. BASELINE TMLV (MAGLEV) VEHICLE

oscillatory motion. This is accomplished by varying the current and polarity of the control magnets in response to onboard motion and position sensor data, processed according to a specified control strategy.

2.2 OVERALL SYSTEM PERFORMANCE

Each superconducting magnet module* has an effective coil size of 0.5 x 3 m, and a magnetic lift/drag ratio at 134 m/s of 45.5 for 2.54 cm thick, high-conductivity aluminum (1100-H14 series) guideway elements. For the baseline 80-seat 366.5 kN vehicle, the total drag power in level, no-wind operation at 134 m/s is 3,739 kW (5,014 hp); for operation on a 2% grade with a 13.4 m/s (30 mph) headwind, the total drag power is 5,279 kW (7,079 hp).

With a two minute allowance for passenger loading/unloading and a maximum deceleration rate of 0.15 g, the vehicle will traverse the nominal 750 km (466 mile) route in 120 minutes with five intermediate stops and in 98 minutes without intermediate stops (the express case).

For a two minute headway, the 80-seat vehicle can handle $\sim 17 \times 10^6$ passengers per year, assuming 60% load factor and 16 hr/day operation; $\sim 1.3 \times 10^{10}$ passenger-km/yr are accommodated for the 750 km route. A 140-seat configuration can handle $\sim 5,000$ passengers/hr, 30×10^6 passengers per year or $\sim 2.2 \times 10^{10}$ passenger-km/yr, which is close to the predictions for the Northeast Corridor (NEC) in the year 1990. The larger capacity vehicle has the added advantage of reducing the energy intensity at 134 m/s from 2.18 MJ/seat-km (3,324 BTU/seat-mile) to 1.65 MJ/seat-km (2,516 BTU/seat-mile).

For headways greater than two minutes, or peak capacity greater than 5,000 passengers/hr, two or more 140-seat vehicles should be coupled together. A train set of three 140-seat vehicles shows an energy intensity of 1.33 MJ/seat-km (2028 BTU/seat-mile) at 134 m/s. At a cruise speed of 110 m/s (246 mph), the energy intensity of the three 140-seat coach arrangement is only 1 MJ/seat-km (1525 BTU/seat-mile).

---

*Two 0.5 x 1.5 m magnets, in separate dewars, are mounted end-to-end within each suspension module.

2.3 SUBSYSTEM CHARACTERISTICS

2.3.1 Vehicle Design

A. Suspension

(1) Dynamics and Control. The baseline Revenue TMLV control system incorporates moderate damping of vehicle motion (damping ratio, $\zeta \sim 0.6$-1.0) based on feedback of vehicle absolute (inertial) velocity data and vehicle position relative to the guideway. The effective natural frequency of the system is 0.6 Hz; non-linear position feedback reduction is provided to avoid possible vehicle instability in negotiating a transition to a 2% downgrade. Gap sensors and accelerometers provide the necessary input signals. In addition to the sensors, the ride control system is comprised of: (1) a set of control electronics to process the sensor data and compute low-power ride control signals, (2) a power control unit to provide power switching, (3) a set of power amplifiers to drive the control magnets, and (4) an emergency back-up power supply.

For guideway surface roughness approximately equal to that for airport runways, the DOT ride quality requirements are achieved in all dynamic modes (heave, pitch, roll, sway, and yaw) for straight and level operation as well as for turns and transitions to a 2% grade. The associated vehicle displacements from the steady-state position are small (maximum stroke ~ 5 cm) and power consumption is low (25 to 50 kW)*. Maximum vehicle sway (the lateral displacement of c.g.) in response to a 20 m/s (45 mph) crosswind is 8 cm.

Alternate active control strategies were briefly studied; e.g., acceleration feedback (in conjunction with absolute velocity feedback) and heavy absolute damping, and offer potential advantages since they do not require the use of gap sensors (which could be a problem in an all-weather environment). These alternate strategies achieve acceptable ride quality/stroke performance but require increased grade transition lengths (Table 2-1). Since evaluation of this tradeoff is clearly route-specific, no optimum ride control system or strategy can be identified at this time.

---

*This corresponds to the long-time power consumption for straight and level operation. The short-time multimode power demand for negotiating a 1 km transition to a 2% upgrade is ~ 150 kW; comparable power for a downgrade is ~ 60 kW.

TABLE 2-1. OVERALL CONTROL SYSTEM COMPARISON

CONTROL STRATEGY	VEHICLE OPERATION				
	LEVEL GUIDEWAY		TRANSITION TO 2% GRADE		HORIZONTAL TURN
	MEETS RIDE SPECIFICATIONS?	INPUT POWER (KW)	LENGTH FOR 5 CM MAX STROKE	MEETS RIDE SPECIFICATIONS?	
(1) POSITION FEEDBACK • MODERATE ABSOLUTE DAMPING ($\zeta = 0.6 - 1.0$) • WITH OR WITHOUT RELATIVE DAMPING • GAP SENSOR • $f_N^{(2)} = 0.6$ HZ	YES	$\sim 17^{(1)}$ FOR HEAVE MODE ~ 25 FOR ALL MODES (BETTER WITHOUT RELATIVE DAMPING)	< 1 KM	YES	GAIN MODIFICATION OR ELIMINATION OF INERTIAL RATE SIGNAL REQUIRED (REDUCED ABSOLUTE DAMPING)
(2) ACCELERATION FEEDBACK • MODERATE ABSOLUTE DAMPING ($\zeta = 0.6 - 1.0$) • NO RELATIVE DAMPING • NO GAP SENSOR • $f_N = 0.6$ HZ	YES	$\sim 17^{(1)}$ FOR HEAVE MODE ~ 30 FOR ALL MODES	6.5 KM	YES	GAIN MODIFICATION OR ELIMINATION OF INERTIAL RATE SIGNAL REQUIRED (REDUCED ABSOLUTE DAMPING)
(3) HEAVY DAMPING • ABSOLUTE DAMPING ONLY ($\zeta = 3\text{-}4$) • $f_N = 1.41$ HZ • NO GAP SENSOR	YES	~ 32.5 FOR HEAVE MODE ~ 50 FOR ALL MODES	8-10 KM AT $f_A^{(3)} = 0.6$ HZ 4 KM AT $f_A^{(3)} = 0.25$ HZ	YES	NOT EVALUATED

(1) I^2R LOSS = 16.0 kW, MECHANICAL POWER = 0.6 kW

(2) f_N IS THE NATURAL FREQUENCY

(3) f_A IS THE ABSOLUTE DAMPER FILTER FREQUENCY

(2) Magnets. The liquid helium-cooled, superconducting, levitation/guidance magnets are fabricated of niobium-titanium multi-filament twisted wire, wrapped on a stainless-steel racetrack-shaped coil form approximately 0.5 m (19.7 in.) wide by 1.5 m (59.1 in.) long. Levitation and guidance forces are transmitted from the coil to the top of the evacuated dewar structure via epoxy-fiberglass struts specially designed for low heat conduction. Each magnet supports 1/8 of the weight of the vehicle at the design clearance and speed, and operates at ~ 350,000 ampere-turns in the persistent mode; the coil winding is intrinsically stabilized, with a current density of 300 A/mm^2. Active shielding is accomplished with a 0.5 x 1.5 m bucking coil mounted within each dewar and 30 cm above the levitation/guidance magnet; the maximum magnetic field at the seat level in the vehicle passenger compartment is held to acceptable levels (~ 70 gauss) without severe weight penalty.* Overall magnet lift/weight ratio is ~ 16.8 with the shielding coil; heat leak per vehicle is 20.8 W.

A closed-cycle refrigeration system is provided, consisting of two electrically-driven Claude cycle expansion engines served by a single compressor, with an additional back-up compressor for added reliability. The associated cryogenic system includes 16-liter liquid helium storage containers inside each magnet dewar, transfer lines, etc.

B. Structure and Configuration. The basic vehicle structure employs aircraft-type aluminum sheet-stringer construction, modified in fore and aft sections to support the levitation and guidance magnets, landing wheels, and the propulsion system. In these areas, an I-beam structure replaces the sheet-stringer construction below the floor level. "Z" section transverse frames 5.1 cm (2 in.) deep are provided on 45.7 cm (18 in.) centers to support the outer structure and prevent buckling during compressive loading. The outer structure consists of 0.102 cm (0.040 in.) thick 2024-T3 alloy sheet flush-riveted to stringers 15.2 cm (6 in.) on centers. A 1.27 cm (0.5 in.) thick aluminum honeycomb-core floor panel is provided, supported by 20.3 cm (8 in.) deep transverse U-channel members tied to the side frames.

The vehicle structure is essentially a lightly loaded, very stiff hollow beam configuration. It is designed for a fundamental bending frequency of

____

*Maximum magnetic field occurs directly over the magnets, the average magnetic field in the passenger compartment is approximately 5 to 10 gauss.

4 to 5 Hz, which is substantially larger than the suspension heave-motion frequency and avoids the necessity for considering structural elastic effects on ride control system design. The baseline structural design approach has been extended to encompass larger vehicles (up to 140 seats) and different seating arrangements. A small decrease in bending frequency is allowed, however, since excessive structure weight would result with the longer configurations if the bending frequency is held constant. Preliminary vehicle synthesis analyses show that the 140-seat configuration exhibits 24% less energy consumption per passenger than the baseline 80-seat vehicle; the optimum seating arrangement for the larger vehicle is 2 + 3.

The particular vehicle cross section required to straddle the hat-shaped guideway is a favorable shape. It results in a high section modulus and a relatively short vehicle since the part of the structure below floor level provides for convenient packaging of the suspension elements, wheels, fuel and additional cargo. Both factors contribute to a lightweight, low power vehicle design.

C. Propulsion. The baseline propulsion system is comprised of twin rear-mounted ducted Q-fans, remotely driven by twin regenerative gas turbine engines. The regenerative engines provide high operating efficiency; cruise specific fuel consumption is estimated at 5.63×10^{-4} kN/MJ (0.34 lb/hp-hr). The Q-fan is a product of Hamilton Standard Division of the United Aircraft Corp. and is specifically designed for low-noise operation. Noise suppression materials and techniques are also applied to the engines as well as inlet/exit ducting for both the fans and the engines. Estimated total propulsion system noise for level, no-wind cruise at 134 m/s is 86 dbA* (at 15 m sideline distance); for maximum power operation during acceleration or at 134 m/s on a 2% grade with 13.4 m/s (30 mph) headwind, the noise level is 92 dbA (at 15 m). A further reduction in propulsion system noise (~ 5 to 6 db) is achievable by slightly increasing the separation distance between the fan inlet and the top surface of the vehicle or moving the propulsion system to the front of the vehicle. The Ducted Fan/GT system is a reliable lightweight concept (80.6 kN (18,000 lb) including fuel with 15% reserve) with good

---

*At 134 m/s, the vehicle self-generated (aerodynamic) noise is estimated at 92 dbA, also at 15 m (50 ft).

acceleration (0-134 m/s in ~ 180 sec), relatively low energy consumption, and the lowest total cost (including guideway) of all the propulsion systems studied. It is entirely self-contained, thereby permitting complete freedom in guideway selection. Also, it supplies all propulsion necessary for off-line (including switching) as well as on-line operations. Thrust control is provided by varying fan blade pitch; emergency braking can also be provided with full pitch reversal. If necessary, the gas turbines can be operated on a variety of chemical fuels (fossil or synthetic). With current design techniques, exhaust emissions are controllable to very low levels, particularly on a passenger-km basis.

2.3.2 Guideway

The hat-shaped guideway configuration is preferred for its favorable stability characteristics, its compatibility with the proposed passive failsafe switch concept, its low cost, and the fact that it can be fabricated quite easily with standard slip-form highway construction techniques.

A. At-Grade Construction. The at-grade guideway is essentially a continuously-reinforced concrete slab 20.3 cm (8 in.) thick and 3.05 m (120 in.) wide, laid on a treated, compacted combination of fill materials; the roadbed preparation is similar to that for airports and interstate highways. The steel reinforcement is employed with appropriate size and stand-off distance so as to minimize its influence (drag) on the vehicle. The central "spine" is a reinforced concrete beam, 79 cm (31 in.) wide and 53 cm (20.7 in.) high, anchored to the primary slab.

The guideway levitation elements are 2.54 cm (1 in.) thick, high conductivity aluminum (1100-H14 series) plates fabricated in L-shaped sections approximately 30 m (100 ft) in length. The aluminum sections are laid end-to-end with transverse gaps on the order of 2 to 3 cm wide, and attached to the concrete surfaces in a manner which permits longitudinal expansion, thus avoiding buckling due to thermal expansion. The use of nearly pure aluminum is essential for achieving a high vehicle magnetic lift/drag ratio.

Since the aluminum plates are non-structural elements, the roughness of the guideway is essentially the roughness of the supporting concrete surfaces.

The roughness for the long wavelengths of interest is dictated by the foundation under the concrete, i.e., the roadbed characteristics. On the basis of airport runway evaluation — which generally shows minimal time-dependent roughness degradation — no design allowance for post-installation adjustment is deemed necessary for good soil conditions. Preliminary analysis of conventional roadbed grading and concrete-laying techniques indicates that the achievable guideway vertical roughness level (at the appropriate wavelengths) is actually less than the roughness level used for the vehicle dynamics analysis. The lateral roughness level of the central guideway spine is expected to be even lower, so there is potential for further improvement in ride quality without resort to non-standard (i.e., expensive) construction techniques.

B. Elevated Construction. The baseline elevated guideway design approach is predicated on cost and the guideway influence on vehicle dynamic response. The conceptual TMLV revenue vehicle has a low natural frequency (0.6 Hz) with minimal relative damping; this results in a girder design which is relatively light and flexible compared with those designed for a more highly damped tracked air cushion vehicle. The baseline design (Frontispiece) employs simply supported pre-stressed concrete box-beam girders with a depth of 1.07 m (3.5 ft) and a span of approximately 23 m (75 ft). The beam has an integral top cap 15.2 cm (6 in.) thick by 3.05 m (10 ft) wide; this cap and an attached central reinforced concrete spine serve as the riding surfaces of the guideway. The box-beam girders are supported on columns with sliding joints at one end to accommodate differential thermal expansion, and pinned joints at the other end to transmit longitudinal loads. A uniform pre-stress is employed to eliminate post-fabrication camber effects.

C. Switching. To avoid long radii of curvature and excessive switch size, all switching operations are designed to take place at low speed; i.e., at or below the lift-off speed of 30 m/s (67 mph). Upon slowdown to this speed, the wheeled suspension bogies are extended down and out from the vehicle envelope to engage non-movable L-shaped reinforced concrete ramps located outboard of the main guideway. These ramps subsequently rise above the guideway and lead to an apron where the vehicle can "taxi" to the appropriate loading platform. The maneuver is similar to current aircraft procedure; the forward bogies are fully steerable to facilitate the taxi operation.

The passive method of switch operation permits the "express" vehicles to pass through the switch area at top speed with complete safety. Failure to extend the wheels also permits a vehicle to pass through the switch area without danger. Premature wheel extension is precluded by means of a dynamic pressure activated linkage, similar to that used on aircraft to prevent inadvertent landing gear extension at high speeds.

2.4 ALTERNATE PROPULSION SYSTEMS

If necessary, the Revenue TMLV can be propelled electrically — by any one of a number of systems currently in various stages of research and development. These include the single-sided linear induction motor (SLIM), the linear synchronous motor (LSM) and a superconducting rotary electric motor (REM) used in conjunction with ducted Q-fans. The guideway cost for all of the electric systems studied is substantially larger than the basic (non-electrified) guideway required with the Ducted Fan/Gas Turbine system. The effect of this increased cost, however, can be reduced if very high passenger capacity is achievable and/or the cost of chemical fuels becomes large in comparison with the cost of electricity.

The SLIM has the most development effort behind it; it is reasonably efficient but is excessively heavy — about 105 kN (23,600 lb) with onboard power conditioning. This results in high energy consumption, but the problem can be partially alleviated by employing wayside power conditioning with an associated 50% reduction in onboard propulsion system weight. Although not yet demonstrated, wayside power conditioning is probably feasible. High-speed power pickup is still necessary, however, and the motor appears difficult to switch — at least under the switch criteria established for all propulsion concepts studied herein. Preliminary analysis indicates that the (narrow-gap) motor cannot be suspended from the (large-gap) vehicle without the suspension forces adversely affecting vehicle ride quality and/or stroke. However, this problem is resolvable in principle by operating the motor as a tug, i.e., with its own separate suspension system — which could be an air cushion or a stiff, short-stroke repulsion magnet system. However, this approach seems overly complex and the dynamical incompatibility between the motor and the vehicle is not likely to be easily resolved. For this reason, the linear induction motor does not appear attractive for a Repulsion MAGLEV system.

The LSM is at a very early stage of development, but appears to have substantial potential for Repulsion MAGLEV applications. Thrust forces are developed by interaction of onboard superconducting magnets with a moving electrical field generated in "meander" coils embedded in the guideway and carrying large currents, appropriately phased and switched. The principal advantages of an LSM are that it is a large-gap (~ 30 cm) device, no power pick-up is required, and, depending on the design, good power transfer efficiency ($\sim 70\%$) can be achieved. Principal disadvantages are that more and higher-current superconducting magnets are required on the vehicle leading to additional shielding problems and the problem of combining levitation and propulsion functions in the same set of magnets since efficient designs for these functions are at cross purposes. That is, long narrow levitation magnets give high magnetic lift/drag, while many short, wide magnets result in efficient LSM propulsion. In principle, the LSM can also provide for vehicle ride control as well as for propulsion. Preliminary analysis, however, shows that this would require additional active guideway surfaces with substantial increase in guideway cost and complexity. Also, there is no clear system advantage connected with LSM control of vehicle dynamic motion. While the optimum LSM configuration is unknown at this time (in terms of number and size of vehicle magnets, guideway voltage, current and frequency), the LSM shows good potential for improvement and merits further study, particularly when "trained" vehicles are considered.

The REM-driven ducted fan concept is a lightweight propulsion option for MAGLEV if the superconducting motors can be developed at the target values of weight and volume used herein. Current U.S. Navy development efforts on superconducting motors and generators should provide early verifi-

2-11

cation of these estimates. However, energy consumption is the highest of all systems studied, due to the combination of low fan/duct efficienty and low efficiency for the electric generation, distribution, and collection process. Nevertheless, no reaction rail is required and the total guideway cost is the lowest of all the electric systems. Also, switching is made easier by the system's ability to provide propulsion for off-line as well as on-line operations. From a systems viewpoint, an additional advantage could result from using this concept as a back-up to the baseline Ducted Fan/GT system. For example, if the Revenue system is initially implemented with gas turbine drive, the superconducting REM drive could be substituted with minimal design change at such time that electric power is deemed necessary.

An advanced concept propulsion system — the superconducting paddle wheel — was also considered and shows long-term potential. With this concept, an onboard circular array of superconducting magnets is rotated about an axis perpendicular to the longitudinal axis of the vehicle. Both thrust and lift forces (or even drag for deceleration) can be developed by interaction of the moving magnetic field with the aluminum guideway elements, depending upon the peripheral speed of the magnets. An integrated propulsion/levitation system is thus possible; propulsive efficiency is high (~ 65%) and, when driven by regenerative gas turbines, the concept has the lowest energy consumption of all the systems studied. Basic feasibility has not been demonstrated, however, and this concept cannot be considered a realistic candidate for near-term application.

2.5 COST ANALYSIS

2.5.1 Baseline System

The Ducted Fan/GT-propelled, 80-seat vehicle estimated production cost is ~ \$2.3 x 10^6 which includes \$272,000 for the ride control subsystem. Basic at-grade, double-track guideway cost is ~ \$2 x 10^6/km with land at \$30,000/

acre; elevated guideway cost is $3.7 to 4.0 x 10^6/km depending on the type of footings used. The total guideway cost, assuming the NEC mix of at-grade, elevated, tunnel and bridge elements* and certain ancillary equipment is ~ $3.3 x 10^6/km.

The estimated guideway and vehicle costs have been converted to an annualized basis (with debt service) and combined with other investment costs (facilities), direct operating costs (fuel, crew, maintenance, and terminal operations), and estimated indirect operating costs to ascertain total system cost. For 134 m/s operation over the nominal 750 km route, total system cost using 80-seat vehicles at two minute headway is 4.4 to 5¢/passenger-km for JP fuel at 5.3 to 10.6¢/liter (20 to 40¢/gal); 16 hr/day operation is assumed, with a load factor of 60%. Operation with 140-seat vehicles drops the cost to 2.9 to 3.3¢/passenger-km. For train sets composed of three 140-seat coaches (also at 2 minute headway) the cost drops further, to about 1.7 to 2.1¢/passenger-km.

With JP fuel costs between 5¢/liter (20¢/gal) and 30¢/liter ($1.13/gal), the optimum thickness of the aluminum guideway elements is between 2 and 3 cm. The cruise speed for minimum energy cost is between 80 m/s (179 mph) and 95 m/s (212 mph); cruise speed for minimum total system cost is between 90 m/s (201 mph) and 110 m/s (246 mph) although total cost is not very sensitive to cruise speed for fuel cost up to 15¢/liter (57¢/gal).

2.5.2 Alternate Systems

The estimated vehicle production costs for the five propulsion systems studied range from ~ $2 x 10^6 (SLIM) to $2.6 x 10^6 (paddle wheel). The total guideway cost variation is from ~ $3.3 x 10^6/km (Fan/GT) to ~ $4.7 x 10^6/km (LSM). For electricity at 3¢/kw-hr, total system cost for the 80-seat electrically-propelled systems varies from 5.4 to 5.6¢/passenger-km compared with 5¢/passenger-km for the Fan/GT system at the same headway and speed. With 140-seat vehicles, the range is 3.5 to 3.6¢/passenger-km compared to 3.3¢/passenger-km for the Fan/GT, indicating some reduction in the overall influence of guideway cost with increasing capacity, as expected.

---

*1% bridges, 4% tunnels, 16% elevated, 79% at grade.
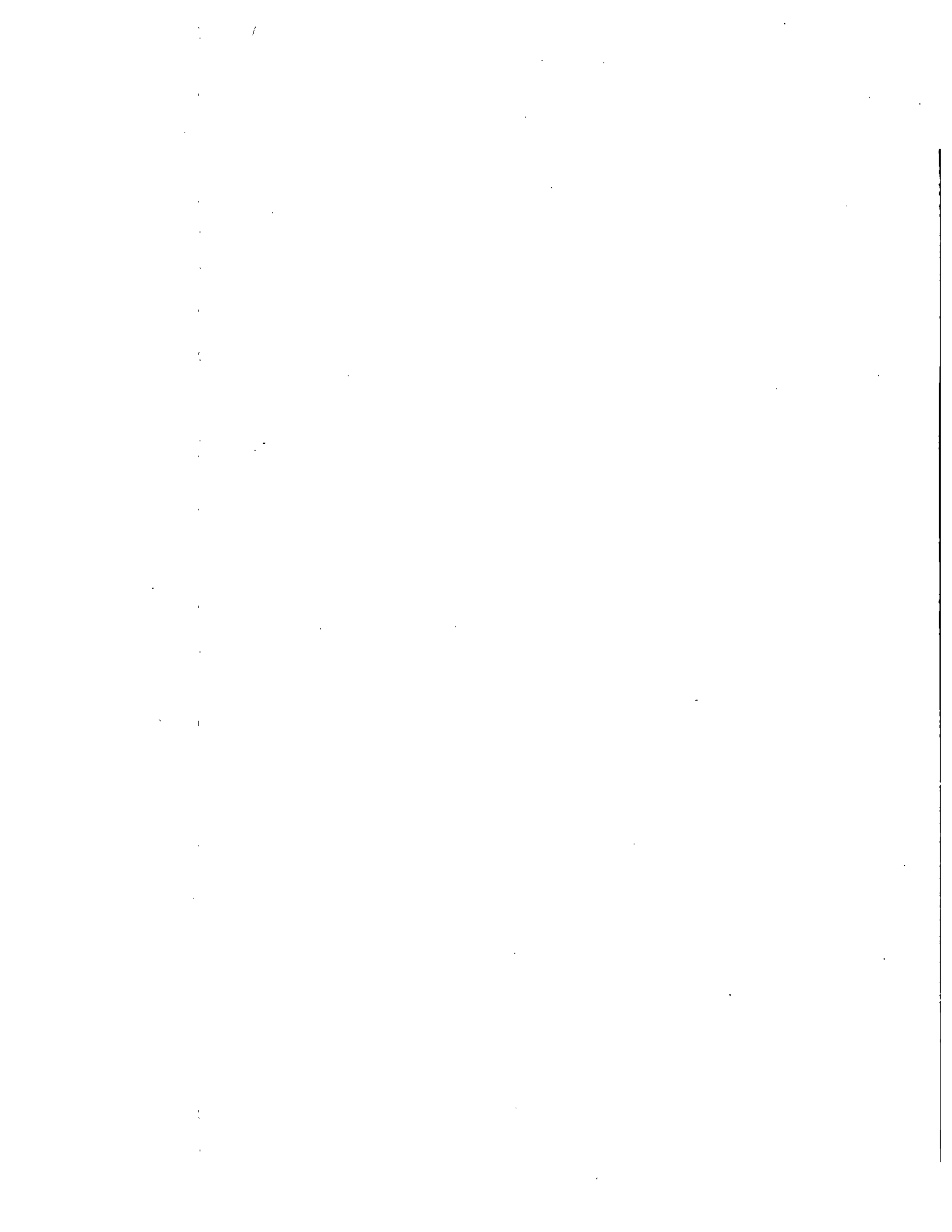
SECTION 3

SYSTEM REQUIREMENTS

3.1 OBJECTIVES

The objective of Task I of the TMLV Technology Program is to achieve a conceptual design of a passenger-carrying MAGLEV "Revenue" vehicle and its associated guideway. The major portion of the Task I study is directed at the levitation and guidance aspects of the problem. The purpose of the conceptual design effort is to provide the basis for the subsequent Task II experimental program as well as to obtain a preliminary systems evaluation of the Repulsion MAGLEV concept in the HSGT role. The potential HSGT application is in the heavily-travelled Northeast and California corridors for the 1985 - 1995 time frame.

3.2 SYSTEM REQUIREMENTS

The primary system requirement is to satisfy the DOT-supplied ride quality specification given below (Section 3.2.1E) for an 80-passenger vehicle at all speeds up to 134 m/s (300 mph). The secondary requirement is to meet various other criteria related to a high-speed passenger-carrying system 10 to 20 years in the future. The secondary criteria specified herein should be regarded as goals, since further system studies are necessary before firm requirements can be established.

3.2.1 Operational Goals

A. System Capacity. The passenger demand for a high-speed TMLV System for the Northeast Corridor in the 1985-1995 time period is projected as approximately 40 to 50 x 10^6 per year. Sufficient capacity must be provided to serve this level of demand, with provisions for future traffic growth. A nominal peak capacity of 10,000 passengers per hour per guideway is an objective. Freight has not been considered, although it offers an attractive means of increasing the utilization of the system (i.e., at night).

B. Operating in Trains. The conceptual studies considered only single coaches. However, analysis shows that the operation of multi-car trains is

necessary to provide safe headway for the peak passenger capacities; thus the system should eventually be capable of operating vehicles either separately or in trains.

C. <u>Passenger Capacity Per Vehicle</u>. The nominal baseline coach contains 80 passenger seats although the effect of larger numbers of passenger seats has been investigated in the System Studies (Section 5).

D. <u>System Control</u>. Much of the system for maintaining speed, headway, switching, etc., is expected to be fully automatic, with over-riding manual systems and onboard operators for abnormal operating conditions and as a safety backup.

E. <u>Switching</u>. High-speed switching (>45 m/s or 100 mph) is impractical, and a nominal switching speed of 30 m/s (67 mph) is used. Passive "fail-safe" switches will be required, and through-traffic should be able to pass switches without reducing speed.

F. <u>Headway</u>. All vehicles will operate under a safe stopping headway policy based on the normal or service braking rate of 0.15 g.

3.2.2 <u>System Performance Requirements</u>

The following cruise and acceleration performance requirements apply to single coaches only, not operation in trains.

A. <u>Thrust - Speed</u>. The nominal cruise speed is 134 m/s (300 mph), and the propulsion system should have sufficient short-duration performance to provide this speed on a positive 2% grade with a 13.4 m/s (30 mph) headwind. The maximum duration of the 134 m/s speed for a 2% grade, 13.4 m/s headwind is 20 minutes. The propulsion system shall be capable of one hour operation on a level grade with a 13.4 m/s headwind. Continuous operation is required for a level grade, no headwind cruise at 134 m/s.

B. <u>Acceleration</u>. The propulsion system should have the capability of providing sufficient short-duration thrust to accelerate a 445 kN (100,000 lb) vehicle on a positive 2% grade with a 13.4 m/s headwind through the lift-off drag peak (which occurs at ~ 30 m/s). The average acceleration between lift-off and 134 m/s for the level grade, no headwind condition should be approximately 0.08 g. The peak vehicle acceleration for any condition shall not exceed 0.15 g.

C. Normal Braking. The normal or service brake system shall be capable of decelerating a 445 kN vehicle at the normal limit of 0.15 g on a 1% downgrade with a 13.4 m/s tailwind. Normal stops should not exceed the jerk limit of 0.03 g/sec.

D. Emergency Braking. The emergency braking system shall be independent of the normal braking system or wayside power pick-up (if any), and shall be capable of decelerating a 445 kN vehicle at the 0.4 g emergency limit on a 1% downgrade with a 13.4 m/s tailwind.

E. Ride Quality.* Under any normal operating condition and all speeds below 134 m/s (300 mph), the following DOT-specified values of sustained or steady-state acceleration and rate of change of acceleration (jerk) shall not be exceeded at any time:

Direction	Sustained Acceleration (±g)	Jerk (±g/sec)
Longitudinal	0.15	0.03
Lateral	0.08	0.03
Vertical	0.10	0.04

These are human-comfort criteria, thus the response of the vehicle should be accounted for in determining the conditions sensed by passengers. According to Ref. 3-1, these limiting values do not apply to cabin vibrations but are based on vehicle maneuvers which result in durations exceeding 1 to 2 seconds. An additional passenger ride comfort constraint given in Ref. 3-1 is a maximum roll rate of 15°/sec., and this value has been used as a nominal value for this system.

The spectral composition of acceleration/time histories over any sample collected over a 1-km length of guideway or greater, over the frequency range of 0.1 to 50 Hz, shall not exceed the limits shown in Figure 3-1. Comparison with Figure 3-1 shall be made on the basis of a power spectral density analysis with a frequency resolution of 1 Hz intervals in the passband.

---

*Requirements for the aluminum levitation/guidance elements are given in Section 4.5.1A. The roughness index, A, used in this analysis is 1.5×10^{-6} m (5×10^{-6} ft).
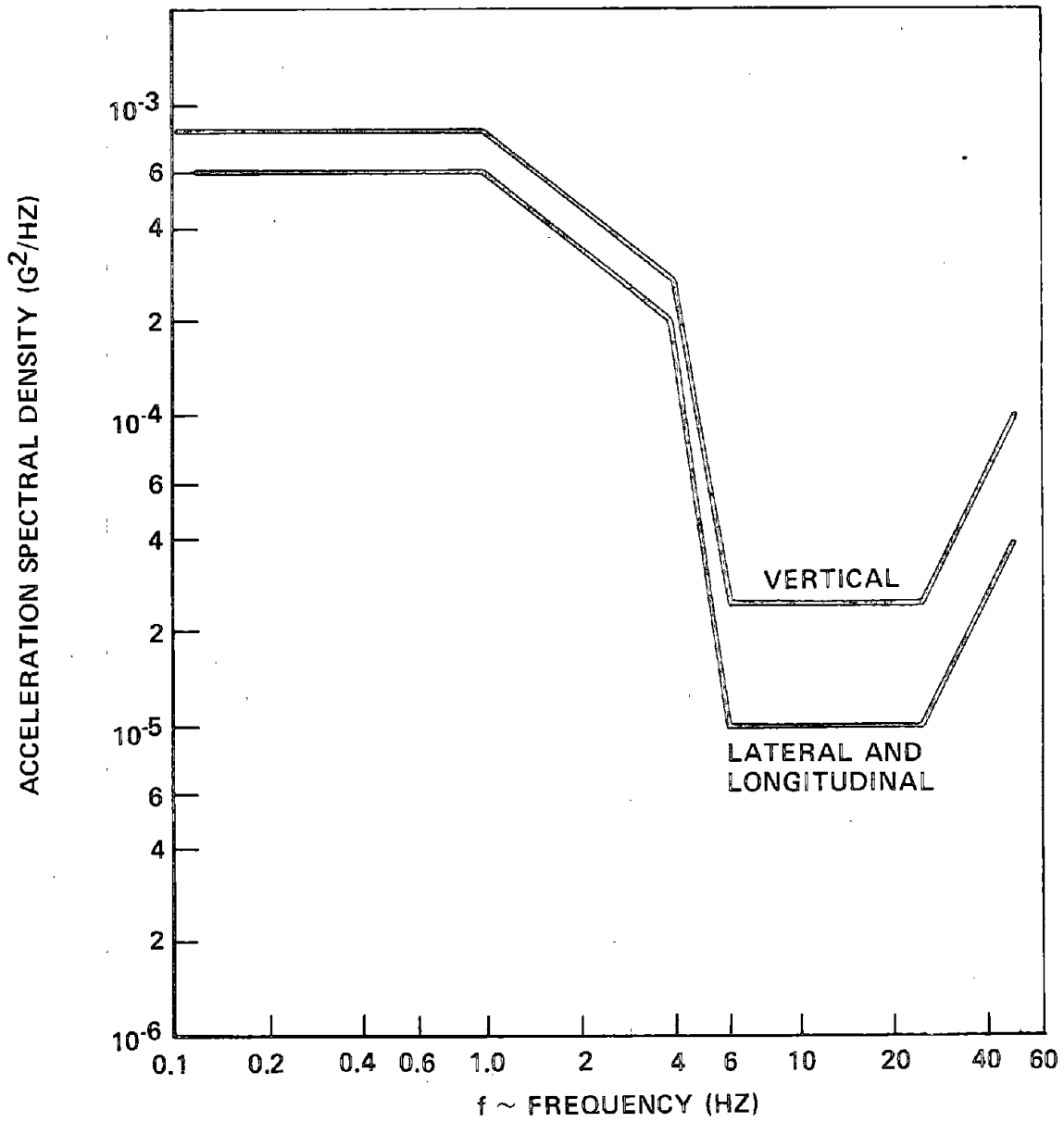
FIGURE 3-1. DOT SPECIFICATION FOR SPECTRAL COMPOSITION
OF ACCELERATION

F. __Guideway Superelevation and Vehicle Bank Limits__. The radii or guide-
way curvature required to satisfy the ride quality specification given above
can obviously be reduced by the use of guideway banking (superelevation) and/
or vehicle cabin bank. The guideway superelevation for a vehicle which does
not have the capability of rolling the cabin with respect to the undercarriage
is normally limited to approximately 10°, since greater angles are uncomfort-
able for passengers should the vehicle stop or negotiate curves considerably
below the design speed of the curve (Ref. 3-1). The maximum vehicle bank
angle is 24.6° which includes any guideway superelevation.* For any speed,
a 24.6° bank angle and the specified 0.08 g lateral acceleration limit define
the minimum radius turn. Typical results are shown in Figure 3-2 for speeds
of 134, 89.3 and 45 m/s (300, 200, and 100 mph). The curves labeled "coordi-
nated turn" denote a turn with no lateral acceleration.

The minimum vertical radius of curvature for a transition to a grade at a
nominal cruise velocity of 134 m/s (300 mph) is 18.3 km (60,000 ft). At
89.3 m/s (200 mph), this value is reduced to 8.1 km (26,670 ft.). Combined
horizontal and vertical curves, in general, require larger radii of curvature
than either the horizontal or vertical case, and must be calculated for the
parameters of interest. The acceleration limits at the beginning or end of the
transition sections are dictated by the ride comfort values given above.

G. __Operation in Crosswinds and Gusts__. The vehicle shall be designed to
operate normally (i.e., without exceeding the ride quality limits) for con-
tinuous winds and sharp-edged gusts up to 20.1 m/s (45 mph). The encounter
with a "sharp-edged" crosswind (a spatial step function in wind velocity) is
likely to be the worst aerodynamic loading condition, and can occur as the
vehicle emerges from a sheltered portion of the guideway into an open area
where a 20 m/s crosswind is blowing (Ref. 3-2). The design value of 20 m/s
is based upon the British Tracked Hovercraft study (Ref. 3-3), which demon-
strates that wind gusts of this magnitude are not likely to be exceeded 99.5%
of the time for a three-second gust for a Mildenhall, England location. Since
the Mildenhall data are similar to that for the Northeast Corridor or the
California Corridor of the United States, the 20 m/s value is used for these

_____

*Dictated by the vertical (heave) acceleration constraint of 1.1 g.
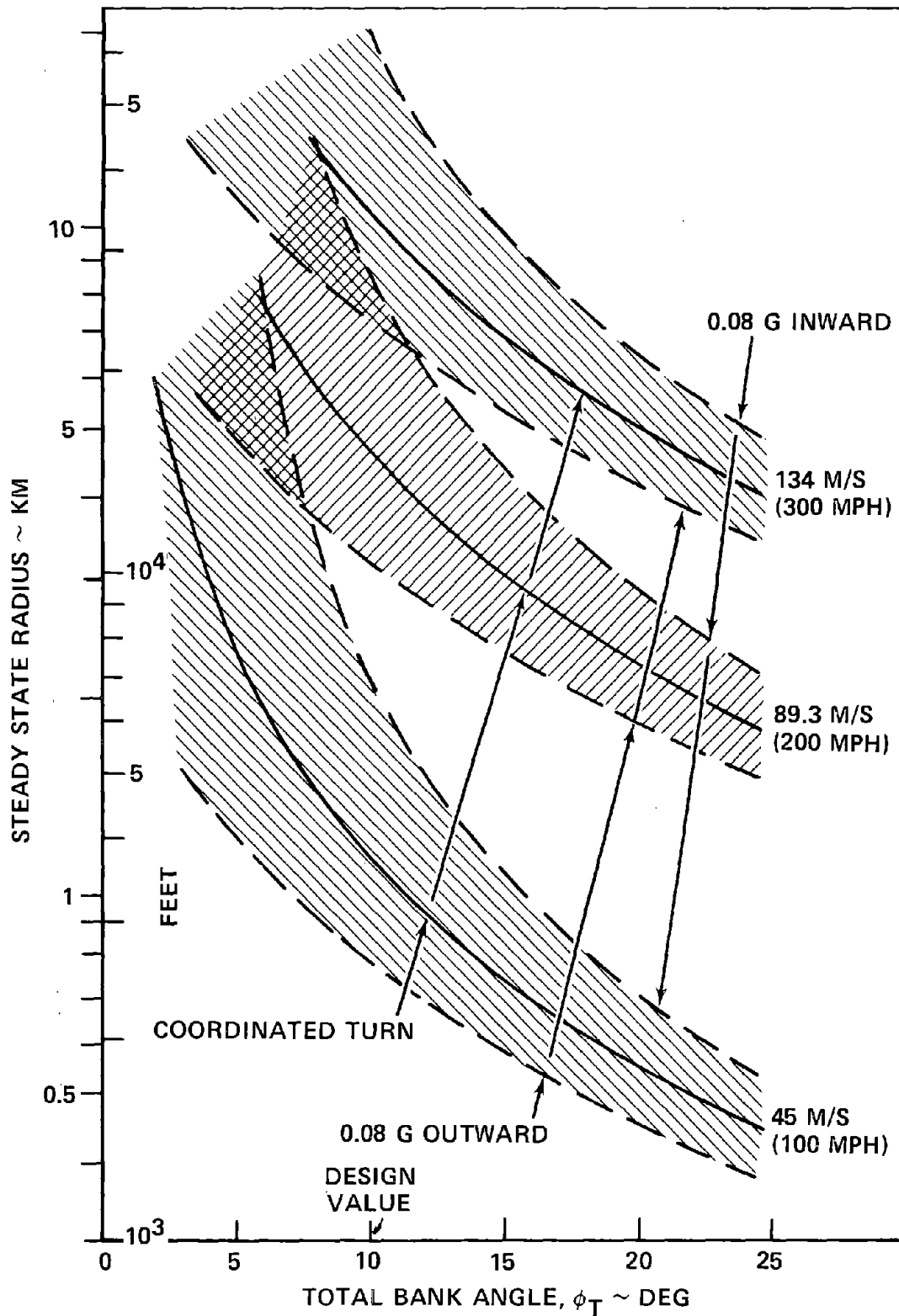
FIGURE 3-2. TURN RADII REQUIREMENTS VERSUS
TOTAL BANK ANGLE

studies. The vehicle can operate safely at crosswind speeds greater than 20 m/s, however at reduced vehicle speeds, based on early warning from guideway anemometers. If a warning is not received, then this is classified as an abnormal operating condition and the ride quality could be exceeded until the vehicle speed is reduced or the crosswind velocity abates.

3.2.3 Environmental Requirements

A. Vehicle Noise. The primary noise sources at cruise speed are the noise radiated from the vehicle boundary layer and wake, and the noise from the onboard propulsion system. The latter source may emit negligible noise if an electrical motor is used and power is supplied from the way-side. However, the noise of the electrical pick-up must still be included. The noise "limits" specified in Ref. 3-4 for High-Speed Ground Transportation Systems are listed below.

FRA/DOT Specified HSGT Noise "Limits"

Exterior Noise "Limit" at Cruise Speed....... 73 dbA

Exterior Noise "Limit" Braking, Idling,
in Terminals................................. 63 dbA

- 50 feet from vehicle centerline,
  measured at 90° to guideway for
  cruise speed, measured 50 feet
  in front of and behind the nearest
  noise source on the vehicle for
  braking, idling, or in terminals

- Includes specified tone corrections

Interior Noise Limits:

- Passenger compartment.................... 65 dbA

- Crew compartment........................ 75 dbA

However, the noise of the vehicle passing at 134 m/s without onboard propulsion has been estimated to be substantially higher than the 73 dbA "limits" (Section 4.2.5). Therefore, a more realistic requirement has been set for a propulsion system, i.e., the noise level of the propulsion unit shall not exceed either 73 dbA or the noise level of the vehicle without propulsion

when moving at 134 m/s, whichever is higher. Firm requirements for lower speeds have not been established, but tentatively a goal of maintaining the propulsion system sound level at or below the vehicle aerodynamic noise level down to the speed where 73 dbA is reached has been set. The final noise regulations that are used for HSGT systems should be based on the effect of the noise on people along the guidway and inside the vehicle.

B. Emissions for Onboard Gas Turbines. The use of an onboard gas turbine for driving a ducted fan or a superconducting paddle wheel has several advantages, however the noise and emissions must be within acceptable limits. Noise goals are summarized in the previous paragraph. The initial emission requirements used in the study were based on the information given in the DOT "High Speed Ground Transportation Alternatives Study" (Ref. 3-5). The values for emissions for a nonregenerative gas turbine were 1.4, 5.2, and 4.4 lb/10^3 hp-hr for unburned hydrocarbons (UHC), carbon monoxide (CO) and oxides of nitrogen (NO_x), respectively[*]. Values for regenerative gas turbines were approximately a factor of two lower.

A study of the Alternatives Study emissions revealed they were based upon automotive gas turbines having a pressure ratio of about 1/4 that of the aircraft-type gas turbine required for MAGLEV applications. Also the factor of two reduction between nonregenerative and regenerative turbines is apparently due to an assumed 50% reduction in specific fuel consumption (SFC). Such an improvement in SFC may be possible for automotive turbines, but is unrealistic for the high pressure ratio turbines for MAGLEV. Finally, the emissions given above were based on operation at constant power, whereas a more realistic approach is the use of a complete operating cycle where idle time is considered (where UHC and CO are highest), as well as acceleration and cruise. (NO_x is highest at maximum power, and appears to be the biggest problem.)

---

[*]Ref. 3-6 was given as the source of the information on gas turbine emissions. However these original values were considerably lower than that quoted in the Alternatives Study, i.e., 0.48, 5.4, and 3.4 lb/10^3 hp-hr for UHC, CO, and NO_x, respectively. For a regenerative system the values were exactly a factor of two lower.

3-8

To alleviate the problem of defining a pollution level based on automotive applications, the Environmental Protection Agency (EPA) standards for aircraft engines are used for the emission calculations (Ref. 3-7). This standard is listed below.

1979/81 EPA STANDARD FOR P2 CLASS (TURBOPROP) AIRCRAFT ENGINES

(Grams of pollutant per kilogram of fuel burned or pounds of pollutant per 1000 pounds of fuel)

TOTAL UNBURNED HYDROCARBONS (UHC) -IDLE-	CARBON MONOXIDE (CO) -IDLE-	OXIDES OF NITROGEN (NO_x) -MAX. POWER-
4	20	10

(To apply these standards to a turbine-powered vehicle, it is first necessary to define a route profile and the corresponding turbine cycle (i.e., horsepower/time requirements), then determine the percent of maximum UHC, CO and NO_x emissions and SFC as a function of horsepower for the particular gas turbine of interest. These factors can then be combined to yield the total pollutants emitted for the cycle or pollutants per horsepower-hour-cycle. Note that the proposed emission standards for aircraft published in Ref. 3-8 are considerably higher than those given above when converted to a typical cycle.)

Articles published in the past have referred to electric propulsion from wayside power pick-up as "pollution-free," however this is misleading. Most of the electrical power generated between the present time and at least the year 1990 will be from the combustion of fossil fuels (Ref. 3-5). This type of power plant emits pollutants which must be accounted for in comparing the overall emissions of gas turbines with electric motors. As nuclear power and electrical power from other non-fossil-fuel sources becomes more important, the power plant-generated pollution should then be proportionately reduced.

C. Magnetic Field/Shielding. The superconducting levitation magnets generate an intense magnetic field close to the magnet coil, e.g., ~0.15 to 0.2 tesla (T) (1500 to 2000 gauss) at 0.3 m above the coil for the worst case of no magnetic shielding and the vehicle is at rest. The field is roughly 0.04 T (400 gauss) at the floor of the passenger cabin for an unshielded

magnet if the vehicle is not moving, and 0.02 T (200 gauss) when moving at
high speed (Section 4.3.1B). Since no environmental requirements now exist
for magnetic fields, what are believed to be realistic limits are specified
in order to determine the amount of magnetic shielding required for passengers.

Reference 3-9 summarizes the pre-1970 literature on the biological effects
of magnetic fields with emphasis on human exposure to static fields. Since
that time there have been no decisive biomagnetic experiments which show harm-
ful effects to man in fields of 0.1 T (1000 gauss) or less. However, much
lower fields can cause some problems, for example a field of 0.02 T (200 gauss)
will affect the operation of some watches and may influence electronic pace-
makers. A field of 0.005 T (50 gauss) or less will affect some sensitive
electronic equipment.

In a recent paper, Beisher and Reno (Ref. 3-10) reviewed the literature
on biomagnetic effects and included some recommended limits for human exposure
to magnetic fields. These recommendations come from two sources: the Stanford
Linear Acceleration Center (SLAC) and the Soviets. The SLAC limits were based
on biomagnetic research on animals and also experience gained through main-
taining careful records on exposure of members of the Center. The Soviet
recommendations were based on studies of long-term health records of workers
engaged in the fabrication of permanent magnets. The recommendations are
summarized below.

RECOMMENDED LIMITS OF HUMAN
EXPOSURE TO MAGNETIC FIELDS FOR EXTENDED PERIODS (HOURS)
(REF. 3-10)

Type of Exposure	SLAC	USSR
Whole Body or Head	200 Gauss	300 Gauss
Arms and Hands	2000 Gauss	700 Gauss

Taking into account factors such as recommended limits to human exposure,
inconvenience to passengers, problems in shielding the magnetic field to low
levels, etc., the following recommendation is made: The maximum whole body or
head exposure for passengers and crew will be 0.008 T (80 Gauss), and the
maximum magnetic field at any point in the passenger compartment which is

accessible to people will be 0.02 T (200 Gauss). Potential problems with onboard electronic equipment will be alleviated by the proper selection of components, locating the equipment away from the magnets, and additional local shielding of equipment, if required.

D. Other Environmental Effects. Abrupt cabin pressure changes upon entry and exit from tunnels and the less severe case of pressure changes on grades must be avoided, and the obvious solution is the use of a sealed, pressurized cabin. The discomfort experienced by a person by a reduction in pressure depends on the rate of change of pressure and if the middle ear can adjust to it (Ref. 3-11). Any pressure changes due to cabin conditioning system should be limited to a rate of less than approximately 0.005 psi/sec, and the pressure change from the initial ambient must be limited to a few tenths of a psi.

The environmental impact of the elevated or at-grade guideway, passenger terminals, parking lots, and other facilities should be minimal. This effect is highly route-specific, and requires careful planning and design.

The visual effects of nearby objects passing the vehicle at high speed has an unsettling effect on people. Optokinetic (train) nystagmus and intermittent photic (flicker) stimuli must be maintained within acceptable levels by not having large vertical objects close to the track and/or restricting the visual field of the passengers. The latter may be accomplished by limiting the location, size, and number of side windows or having a technique of making the windows partially opaque when high speeds are reached. Envelopes of critical optical effects are given in Ref. 3-11.

3.2.4 Route Characteristics

A 750 km (466 mi.) linear, double-track route with five intermediate stops is selected to permit meaningful evaluation of energy consumption (acceleration, deceleration, and station idle operation), switch location and associated off-line loading arrangements, passenger handling capacity, etc.

Deceleration from cruise speed into each city area takes place at 0.15 g with subsequent station dwell for two minutes to allow for passenger loading and unloading. Acceleration time and distance out of the station and up to

3-11

cruise speed varies depending upon the particular vehicle and propulsion combination under analysis. Between the cities, 10% of the route (75 km) is assumed to have a 2% grade with a simultaneous headwind of 13.4 m/s (30 mph); the remainder of the intercity distance corresponds to level, no-wind operation at cruise speed.

3.2.5 Safety and Reliability

Detailed safety requirements have not been determined, however guidelines for various aspects of system safety have been formulated. The safety of any passenger-carrying system is of the highest importance. This is best accomplished during the design phase by conservative design approaches, redundant systems, and other standard safety techniques. The design objectives are that no accidents occur during normal operating conditions, and any malfunction that could result in an unsafe condition occur in a fail-safe manner (Ref. 3-11). It is anticipated that many of the aircraft-type safety procedures will be specified, particularly if gas turbines are used.

A. Vehicle Safety. Provisions will be made for automatic fire detection and extinguishing. Fire retardant and nontoxic materials will be used for the interior. The loading/unloading doors will be designed so that the passengers and crew can evacuate quickly. The vehicles will be designed to act as energy absorbers in event of a collision to minimize injuries. Braking the vehicle will be accomplished by two or three systems, with fail-safe provisions. Switching will be accomplished by onboard mechanisms which do not rely on moving any guideway element. This allows the vehicle to pass safely through the switch in event the switching mechanism fails.

The levitation system will have redundancy in the key components such as the lift magnets. Thus, failure of a single magnet will not result in contact with the guideway. The magnets will be protected from contact with the guideway by wheels and skids, and protected against the impact of small iron pieces attracted by the magnetic field by an external shroud. The baseline propulsion system has two separate and independent engines so that in the event of an engine failure the vehicle can reach the next terminal (at reduced speed) for repairs.

B. Guideway Safety. The guideway structure will be designed to withstand all normal loads. The design wind loads will be 45 m/s (100 mph) for the Northeast corridor with no vehicles operating, and 27 m/s (60 mph) with the vehicles operating. The normal height of the vehicle above the guideway (~ 19 cm) allows it to pass over relatively large objects, as well as a considerable amount of ice, snow, sand, etc. Low-speed areas will probably require clearance and the removal of most of the ice and snow due to the reduced clearance and the use of wheels. Selection of the final guideway shape will depend, in part, on the tendency to collect snow and other debris and the ease of removal. A system for the detection of objects on the guideway may be required onboard the vehicle or on the guideway.

Sufficient side clearance must be allowed between vehicles to reduce the passing loads to reasonable levels (~ 10 ft. at 300 mph). The right-of-way must be completely dedicated, i.e., no grade crossings are allowed. Fencing must be provided at the edges of the right-of-way to prevent people or animals from approaching the track or throwing objects directly at the vehicles. The number of overpasses above the MAGLEV guideway should be minimized, and they must be fenced to reduce the possibility of objects being dropped on the vehicles or onto the track. Elevated guideways will be required in some urban areas to ensure the safety of the vehicles. This will also help to reduce the amount of right-of-way required in these areas.

If electrical power is picked up from the guideway, the usual provisions of protecting people or other objects from contacting the power rails must be provided. The electrical system must be properly grounded and protected from overloads caused by lightning, etc. Communication links and the system for detecting vehicles or other objects on the track must be redundant.

3.3 REFERENCES

3-1. Walston, T.C., Graham, H.R. and Dietrich, W.H., "Operational Potential of Suspended Vehicle Systems (SVS)," Final Report, TRW, Report FRA-ORD&D-74-7B, July 1973.

3-2. Meisenholder, S.G., McGinnis, N.F. and Graham, H.R., "Suspended Vehicle Systems (SVS); Volume I, System Engineering Studies," Final Report, TRW, FRA-ORD&D-74-7, March 1974.

3-13

3-3. "A Cost Comparison of Three Tracked Air Cushion Configurations," Tracked Hovercraft Limited Report, PB 197501, July 1970.

3-4. Ward, E.J., "Noise in Ground Transportation Systems," High-Speed Ground Transportation Journal, Vol. 7, No. 3, pp 297-306, Fall 1973.

3-5. "High-Speed Ground Transportation Alternatives Study," Office of the Assistant Secretary for Policy and International Affairs (DOT/TPI), U.S. Department of Transportation (NTIS PB 220079), June 1973.

3-6. Fraize, W.E., and Lay, R.K., "A Survey of Propulsion Systems for Low-Emission Urban Vehicles, ASME paper 70-Tran-49, 1970.

3-7. Yaffee, M.L., "NASA Seeks Clean Combustors by 1976," Aviation Week, Vol. 101, No. 8, pp, 56-59, August 26, 1974.

3-8. Federal Register, Vol. 38, No. 136, July 17, 1973.

3-9. Reitz, J.R., et al., "Preliminary Design Studies of Magnetic Suspensions for High-Speed Ground Transporation, " U.S. Dept. of Transportation Report PB 223237, 1973.

3-10. Beischer, D.E., and Reno, V.R., "Magnetic Fields and Man: Where Do We Stand Today?" Aerospace Medical Panel Specialist Meeting, Luchon, France, 1971. AGARD Conference Proceedings No. 95, Part III.

3-11. "High Speed Rail Systems," FRA Report No. FRA-RT-70-36, PB 192506, February 1970.

SECTION 4

SYSTEM DESIGN ANALYSIS

4.1 INTRODUCTION

This section contains the discussion of the design and analysis of the major components of the system: the vehicle (Section 4.2), the suspension subsystem (Section 4.3), the propulsion subsystem (Section 4.4), and the guideway (Section 4.5). The basic purpose of this effort is to obtain a cost-effective conceptual design of the levitation and guidance elements of a passenger-carrying MAGLEV revenue vehicle and its guideway which meets or exceeds the ride quality standard.

A baseline conceptual design has been selected after considering the many options available; options related to the types of control strategies, the magnet design, the propulsion system and its effects on the vehicle and levitation/guidance elements, the type of guideway and its effects, etc. Preliminary tradeoffs were conducted among these options to obtain the baseline system — a system that is feasible for the near term (10 to 15 years). With development, some of the more exotic systems such as superconducting paddle wheel propulsion, could well become the optimum system in the future.

4.2 VEHICLE DESIGN

A conceptual design has been performed to obtain a baseline vehicle considering such parameters as vehicle size and shape, structural design, mass properties, and subsystems. The philosophy used in this study has been based on the ultimate purpose of a system of this type — that of providing high-speed intercity transportation typical of the high-density Northeast and California corridors in the United States. "Express" service from one end of a corridor to the other can involve travel times up to 100 minutes duration, and a high level of passenger comfort should be provided during the transit time, commensurate with other aspects such as vehicle cross-sectional area and cost.

4-1

The vehicle configuration is dependent upon the type of propulsion sub-system and guideway that is chosen. System tradeoffs indicate that a Ducted Fan/Gas Turbine is the leading propulsion candidate for the near term and that the hat-shape (wide inverted Tee) configuration is the first choice for the guideway. The baseline system shown in the following sections is based upon these selections.

Since the levitation magnets do not generate lift at zero speed, wheels must be provided. These support and guide the vehicle up to the lift-off (or landing) speed of $\sim$ 30 m/s (67 mph). An arrangement has been devised wherein the landing wheels are used to engage a passive switch and enable the vehicle to switch to an alternate guideway such as into a passenger loading/unloading station. The Ducted Fan/Gas Turbine propulsion system is relatively simple and compatible with various switch designs, whereas other systems require switching a power pick-up and/or complicated guideways such as an active track (i.e., the LSM). An evaluation of the various propulsion candidates is given in Section 4.4.6.

4.2.1 General Configuration

Initial weight and size estimates were established for the 80-passenger vehicle in order to have a common reference point for the structural, aero-dynamic, and dynamics analyses. The maximum weight was set at 445 kN (100,000 lb), and the external envelope at 3 x 3 x 30 m (10 x 10 x 100 ft). Calculations of the propulsion power demonstrated the value of minimizing the weight, and the detailed weight estimates* for the baseline vehicle resulted in a gross weight of 366.5 kN (82,400 lb). The external envelope of the base-line vehicle with the Ducted Fan/Gas Turbine is 3.45 x 2.94 x 33.67 m (11.3 x 9.7 x 110.5 ft). These dimensions are close to the original envelope; the additional 3 m length is required for the extensive sound treatment required in the fan duct. Details of the overall vehicle configuration are shown in figures 4-1, 2-1 and the frontispiece.

---

*Section 4.2.4
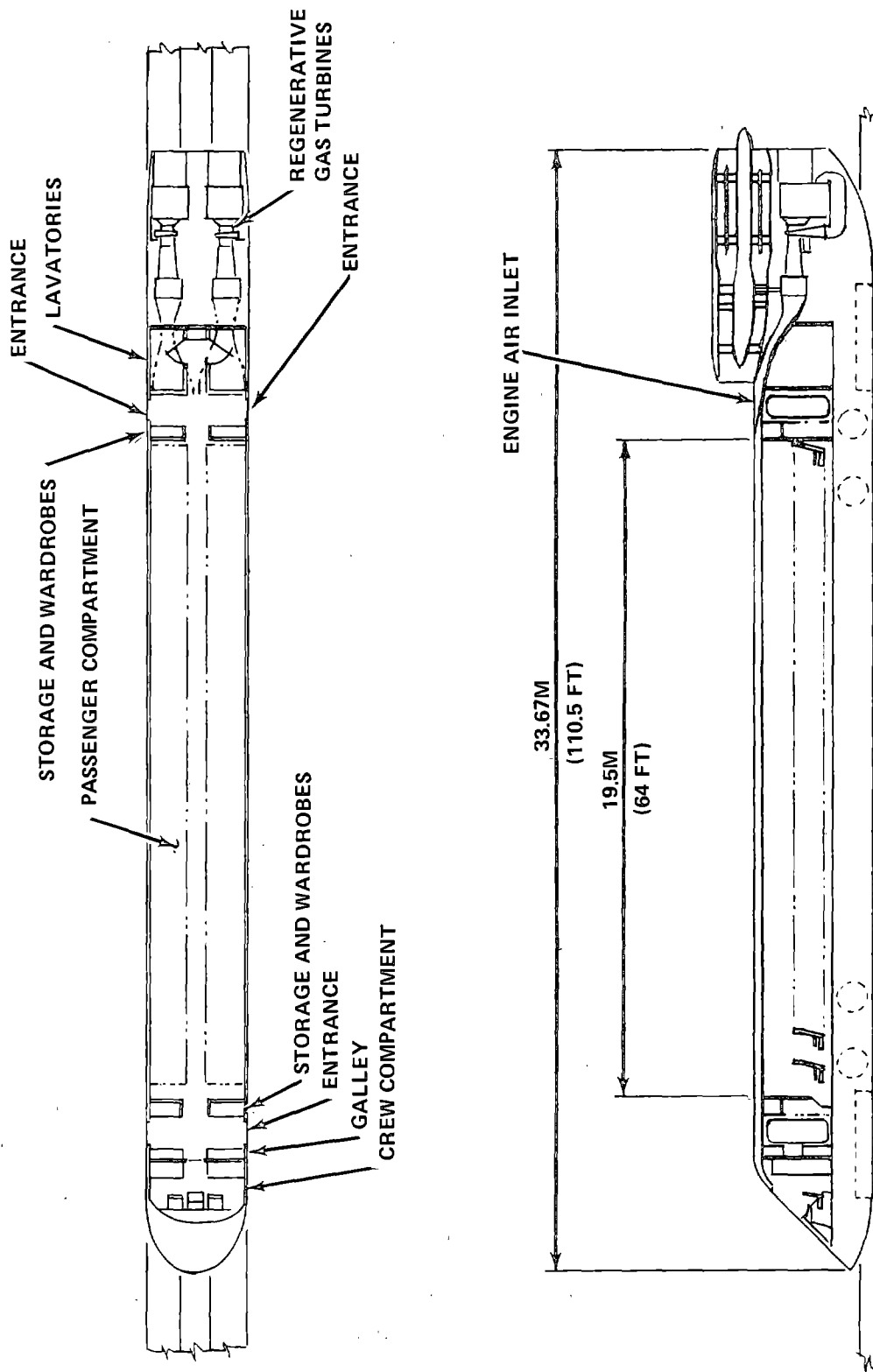
FIGURE 4-1. BASELINE CONFIGURATION – AIR PROPULSION WITH FAN/TURBINE DRIVE

Preliminary tradeoffs between passenger seating options and the need for minimum cross-section area (minimum aerodynamic drag), resulted in a vehicle with a cross section of 8.45 m^2 (91 ft^2). The baseline design shows the magnet modules near the front and rear ends of the vehicle to minimize the magnetic field in the passenger cabin. However, if the shielding coils are as effective as predicted, the magnets can be located directly under the passenger cabin if this is desirable from the standpoint of vehicle ride, packaging, etc.

Discussion of the various propulsion systems available for the vehicle — including the baseline Ducted Fan/Gas Turbine — is given in Section 4.4. The general vehicle configurations for these different propulsion systems are also shown in Section 4.4.

4.2.2 Passenger Cabin

Details of the 80-passenger cabin for the baseline configuration is given in Figures 4-2 and 4-3. A minimum cabin area has been defined consistent with large seats; seats equivalent to those of a DC-10 aircraft. The internal dimensions are a height (headroom) of 2.05 m (81 in.), a width of 2.79 m (110 in.), and a cabin length of 19.5 m (64 ft). A four-seat row with center aisle (2 x 2) has been used, with an aisle width of 0.533 m (21 in.). Both the aisle width and headroom dimensions are the same as a DC-9 aircraft. A seat pitch of 0.96 m (38 in.) is used to ensure adequate leg room.

The magnets, fuel, and landing/switching gear are located in channels or "sponsons" on either side of the vehicle. The distance between the floor of the cabin and the bottom of the vehicle is primarily dictated by the diameter of the landing/switching wheels. The cross section of the vehicle can be reduced by placing the magnets and wheels in front of and behind the passenger cabin and replacing the baseline hat-shape guideway with a U-channel shape, but this results in a considerably longer vehicle. System tradeoffs demonstrate that this arrangement is not as optimum as the one shown in Figure 4-2.

Figure 4-3 shows the baseline passenger compartment and service area arrangement. The seats for the 80 passengers will face forward to take advantage of the higher allowable longitudinal accelerations. Two door openings of

2.94
(116)

2.79
(110)

0.53
(21)

0.53
(21)

3.45
(136)

2.05
(81)

0.38
(15)

1.2
(47)

DIMENSIONS: $\dfrac{M}{(IN.)}$

0.4
(16)

SEAT
PITCH

0.76
(30)

0.51
(20)

0.96
(38)

0.23
(9)
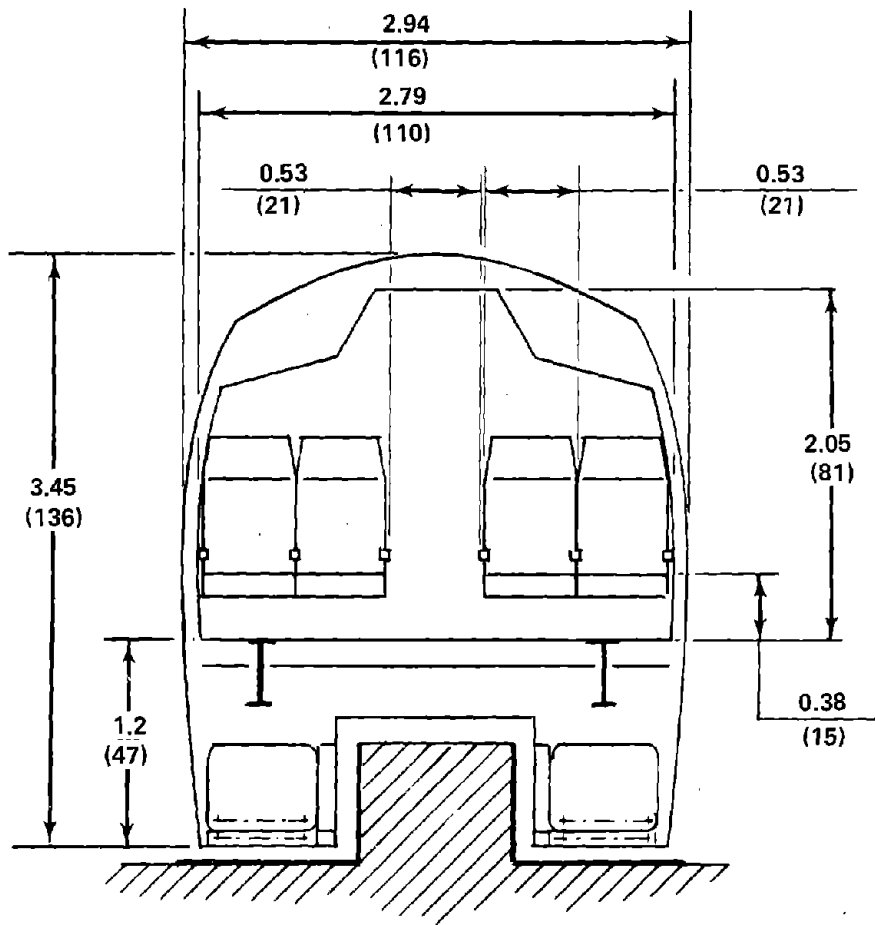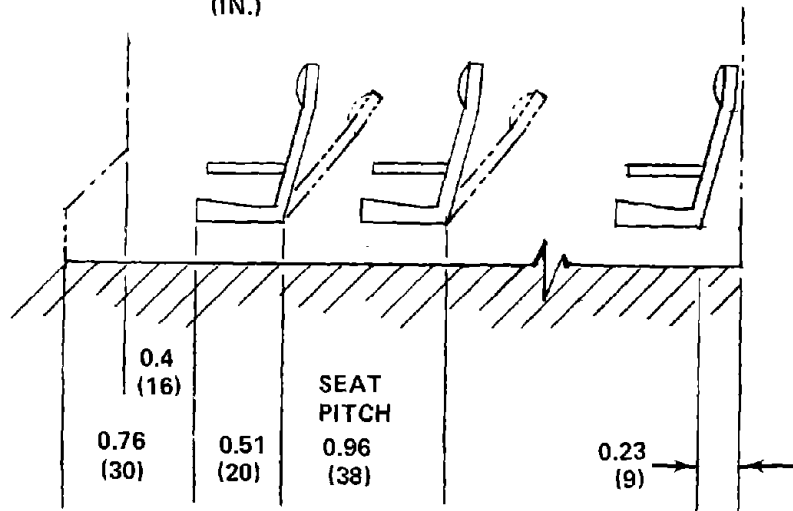
FIGURE 4-2.   BASELINE CABIN CROSS SECTION
AND SEATING CONFIGURATION

4-5

80 PASSENGERS

STORAGE AND WARDROBES

LAVATORIES

STORAGE AND WARDROBES

GALLEY

24.75M
(81.26 FT)

19.5M
(64 FT)

3.37M
(11 FT)

1.88M
(6.2 FT)
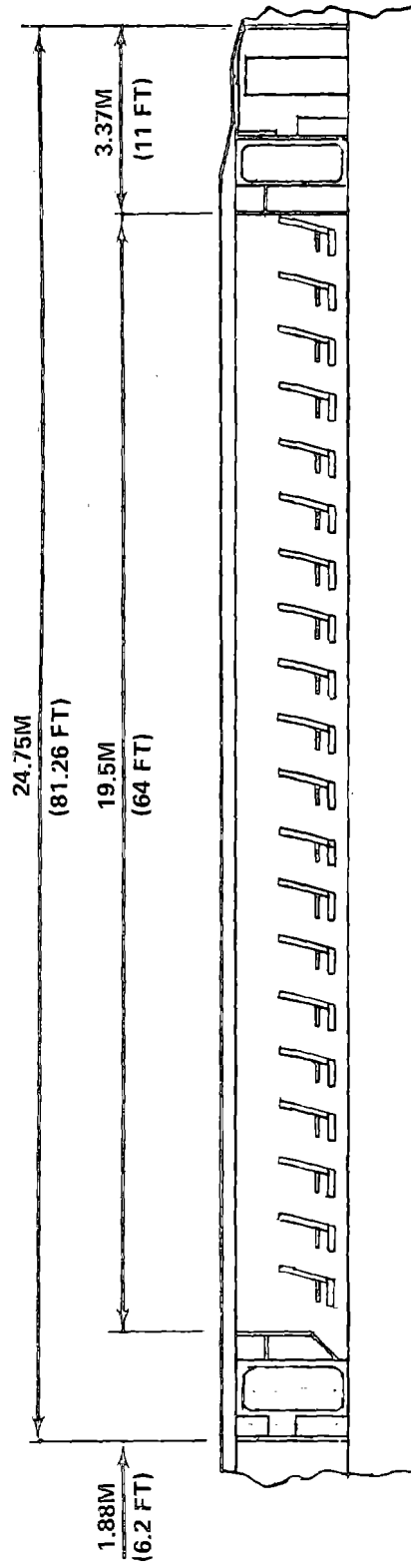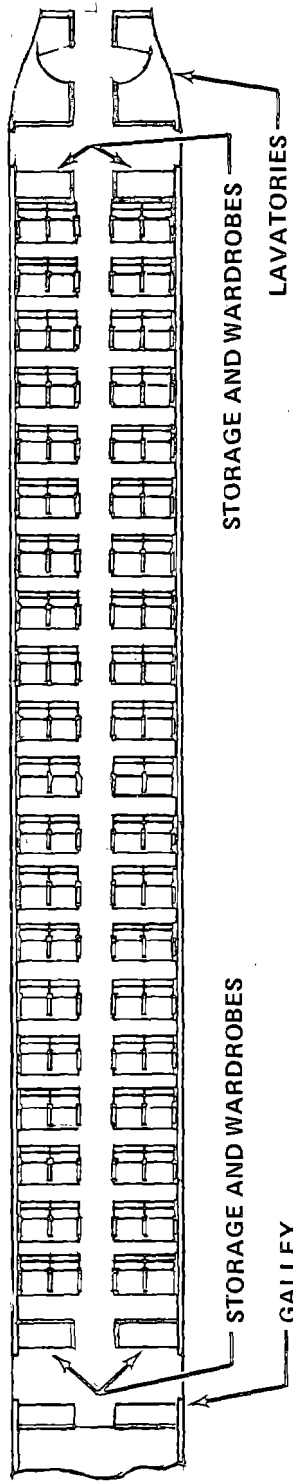
FIGURE 4-3. BASELINE PASSENGER COMPARTMENT AND SERVICE AREA ARRANGEMENT

single passage each are planned for each side of the vehicle for passenger ingress/egress. At any given time it is likely that only the two doors on one side will be utilized. The door opening will be approximately 0.76 m (30 in.) wide with a loading/unloading capacity of one passenger per second (Ref. 4-1). For 80 passengers, the loading/unloading time is 40 seconds (or 20 seconds for an emergency exit from all four doors). Eventually it may prove economical to add another door near the center of the vehicle to improve the load/unload time, and thus the average speed, particularly if the passenger capacity per vehicle is increased.

4.2.3 Structural Design

A. **Introduction.** A preliminary structural analysis of the conceptual vehicle design is presented which defines the primary structural elements and estimates the structural weight. The calculations are based upon the initial estimates of a vehicle with a weight of 445 kN and a length of 30 m. Scaling relationships are developed so the structural weight can be estimated for the baseline vehicle. Since vehicle ride quality requirements limit the allowable vehicle accelerations, dynamic loading of the vehicle during cruise conditions will be low. The most severe bending loads occur at low speeds when the vehicle drops down on the landing wheels. Normally, the transition from magnetic levitation to wheeled support will be smooth; however, a 2 g vertical acceleration of the vehicle is conservatively assumed for any adverse landing conditions.

Since the vehicle structure is lightly loaded, stiffness considerations become the primary structural design constraint. To simplify the vehicle dynamic control problem, the fundamental natural frequencies of the vehicle structure should be high relative to the vehicle/suspension system rigid-body heave-motion natural frequency of 0.6 Hz. Calculations based on the assumption that the vehicle could be represented by a uniform free-free beam were used to predict the value of the bending stiffness required to give a fundamental vehicle bending frequency of 5 Hz ($\sim$ 8 times the heave-motion frequency). Based on this goal of 5 Hz, a bending stiffness requirement of $EI = 2530$ MN-m^2 (8.83×10^{11} lb-in^2) was established. Various structural configurations have been studied in an attempt to meet this stiffness requirement, and the selected design is defined below.

B. Structural Configuration. Aluminum aircraft-type sheet-stringer
construction is used for the basic structure. This structure is modified in
the forward and aft vehicle sections to support the levitation and guidance
magnets, landing wheels, and propulsion system. In the center section of the
vehicle (the passenger section), the efficient sheet-stringer construction
provides the entire external perimeter of the vehicle. In the forward and
aft sections — where large, massive vehicle subsystems must be supported — an
I-beam frame structure replaces the sheet-stringer construction below the
floor level. Nonstructural fairings will be provided to enclose the lower
portion of the vehicle in the forward and aft sections.

The proposed vehicle cross sections are illustrated in Figure 4-4. The
vehicle cross sections employ two stringer designs; the stringers along the
top and bottom of the vehicle are considerably larger than the side stringers
in order to support the higher vertical loads through the vehicle and to com-
pensate for the reduced vertical height in the forward and aft sections. The
lateral stiffness provided by the side stringers is reinforced by the floor
panels and the component support beams.

To prevent buckling during compressive loading, 5.1-cm-deep (2 in.)
aluminum "Z"-section frames have been specified to support the outer structure
every 45.7 cm (18 in.). Aluminum honeycomb-core floor panels supported by
transverse beams tied to the frames on each side of the vehicle were designed
to support a 4787 N/m^2 (100 lb/ft^2) maximum load. All components of the
primary structure are illustrated in Table 4-1 along with tabulated weight
data.

C. Structural Analysis. A lumped-mass-beam analytical model was used to
calculate the fundamental bending frequencies for the vehicle structure. The
weight and stiffness distributions for the model are shown in Figure 4-5.
Fundamental bending natural frequencies of 6.9 Hz and 5.8 Hz were calculated,
assuming the beam model to be simply supported at the lift and guidance mag-
nets (joints 4 and 10 in Figure 4-5). These two frequencies were calculated
for the motion in the vertical and transverse planes, respectively. The
fundamental torsional mode was calculated to occur at approximately 6 Hz.

CENTER SECTION

3.18 (1.25)

5.08 (2.0)

TOP AND BOTTOM STRINGERS

15.2 (6.0)

0.102 (0.040)

FRAME (45.7 SPACING)

50.8 (2.0)

15.2 (6.0)

1.91 (0.75)

SLIDE STRINGERS

FORWARD AND AFT SECTIONS

SANDWICH FLOOR PANEL (DELETE IN AFT SECTION)

38.1 (15)

1.27 (0.5)

20.3 (8.0)

45.7 (18)

A

A

COMPONENT SUPPORT BEAMS
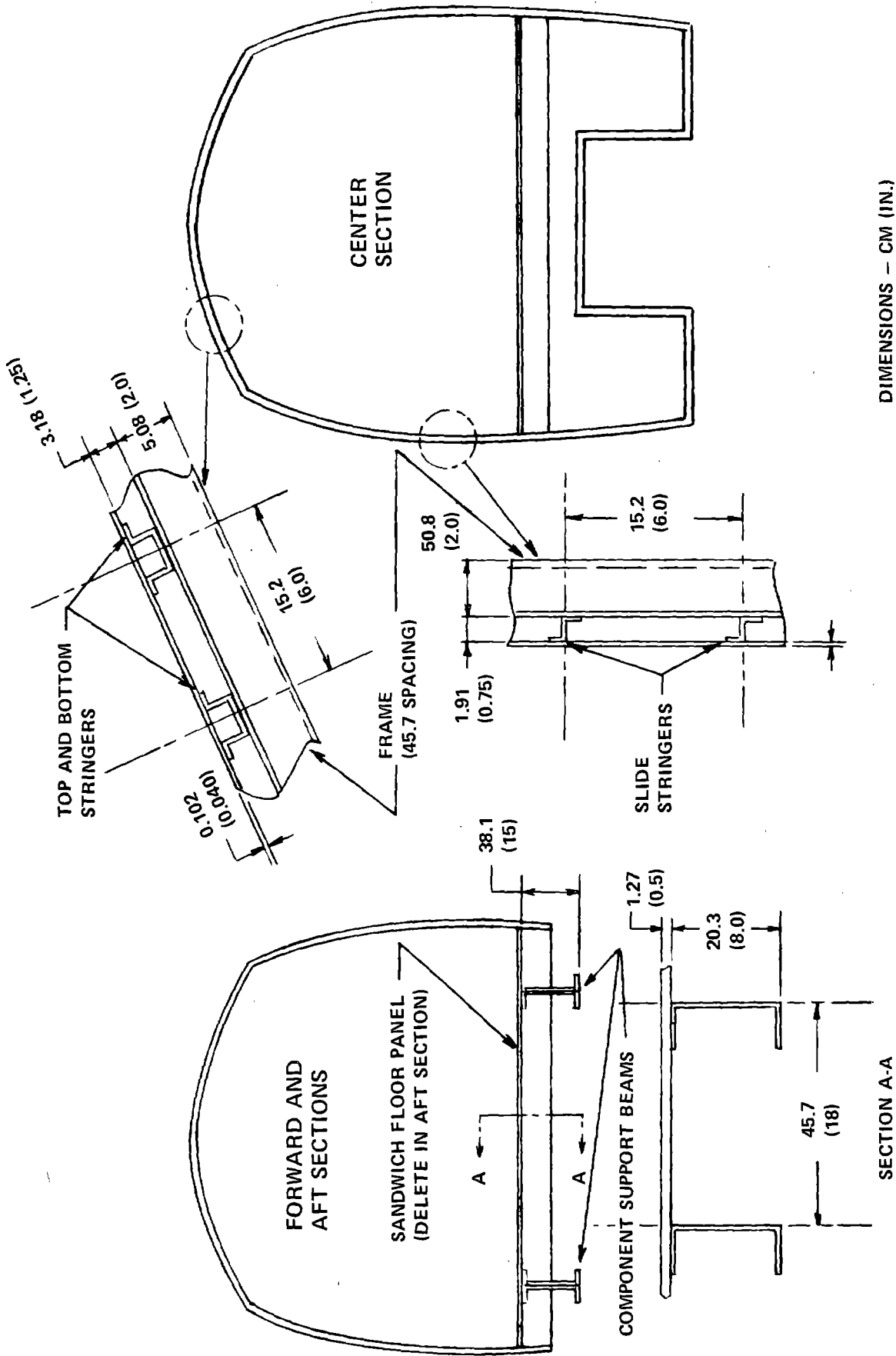
SECTION A-A

DIMENSIONS — CM (IN.)

FIGURE 4-4. VEHICLE PRIMARY STRUCTURE

4-9

TABLE 4-1. PRIMARY STRUCTURE AND ESTIMATED WEIGHT (FOR 445 kN GROSS WEIGHT VEHICLE)

STRUCTURAL ELEMENT (ALUMINUM)	DIMENSIONS cm	FORWARD SECTION			CENTER SECTION			AFT SECTION			WEIGHT TOTALS N (lb)
		QUANTITY	PERIMETER OR WIDTH cm	WEIGHT N (lb)	QUANTITY	PERIMETER OR WIDTH cm	WEIGHT N (lb)	QUANTITY	PERIMETER OR WIDTH cm	WEIGHT N (lb)	
Outer Sheet	0.102	–	742	1810 (406 lb)	–	1430	5250 (1180 lb)	–	742	1700 (382 lb)	8760 (1968)
Top and Bottom Stringers		21 (Top Only)	–	1730 (389)	42	–	5220 (1173)	21 (Top Only)	–	1620 (365)	8560 (1927)
Side Stringers		26	–	516 (116)	42	–	1254 (282)	26	–	485 (109)	2255 (507)
Frames		19	742	516 (116)	30	1430	1570 (352)	18	742	489 (110)	2575 (579)
Transverse Beams		19	300	738 (166)	30	300	1170 (262)	18	300	698 (157)	2610 (585)
Floor		–	300	2510 (565)	–	300	3800 (854)	No Floor in This Section	–	–	6310 (1419)
Component Support Beams		4	–	6160 (1386)	0	–	–	4	–	5790 (1302)	12,000 (2688)
Weight Totals N (lb)				13,980 (3144)			18,300 (4103)			10,800 (2425)	43,100 (9670)

Total Estimated Structural Weight = 1.24 X 43,100 = 53,400 N (~12,000 lb)

Allowance for Secondary Structure and Fairings

30.5m (1200 IN.)

8.83m (348 IN.) — FORWARD SECTION

13.3m (525 IN.) — CENTER SECTION

8.30m (327 IN.) — AFT SECTION

4-10
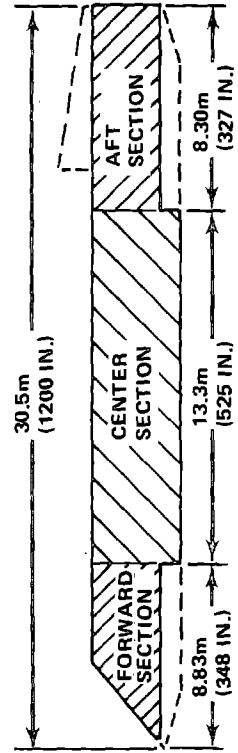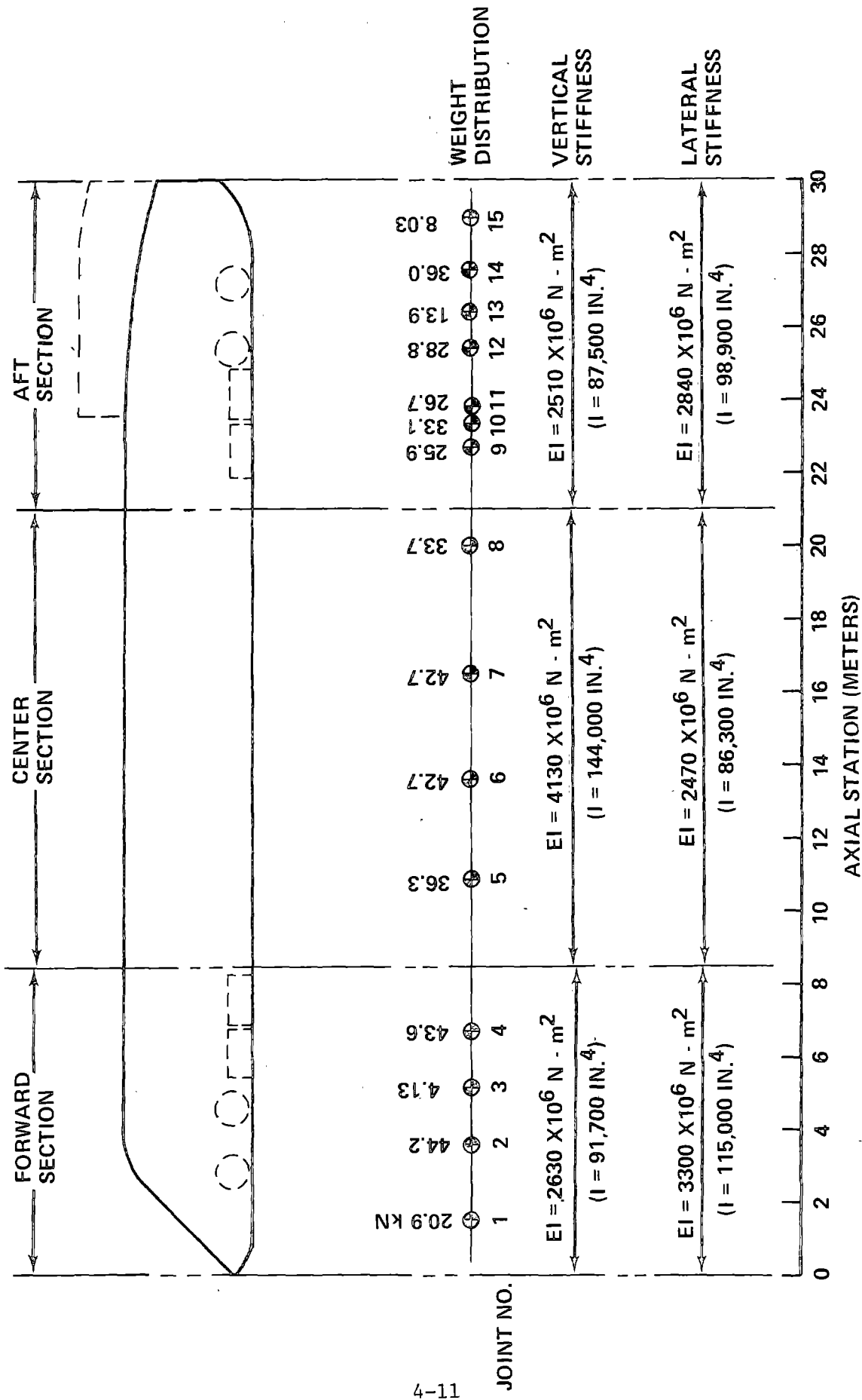
FIGURE 4-5.   ANALYTICAL MODEL FOR STRUCTURAL ANALYSIS

The 2 g landing condition induces the maximum compressive stresses in the top of the vehicle and maximum tensile stresses along the bottom. The axial position of the maximum stresses is approximately midway between the forward and aft landing wheels. The calculations of the structural margins of safety during landing are based on the assumption the outer sheet is fully effective in tension and partially effective in compression. (This is a common practice in aircraft fuselage stress analysis, e.g., Ref. 4-2.) Margins of 480 percent to local buckling of the sheet-stringer structure between frames on the top of the vehicle, and 390 percent to tensile yield along the bottom of the vehicle are calculated. These results are based on the properties of 2024-T3 aluminum alloy construction given in Ref. 4-3.

The possibility of general instability of the vehicle structure (buckling of the sheet-stringer structure through the frames) is prevented by designing the frames to be effectively rigid relative to the stringer bending stiffness, thus forcing the sheet-stringer panels to buckle between frames. Two approaches are taken to estimate the frame stiffness required. First, the frame stiffness requirement (EI) is estimated to be 4680 N-m^2 (1.63 x 10^6 lb-in^2) from data for ring-stiffened circular cylinders presented in Ref. 4-4. As an alternate approach, the sheet-stringer structure forming the top of the vehicle structure is assumed to be an orthotropic simply-supported flat plate, and an analysis predicts a required frame stiffness (EI) of 4220 N-m^2 (1.47 x 10^6 lb-in^2). The frame structure proposed in Table 4-1 gives a bending stiffnes (EI) of 40,800 N-m^2 (14.2 x 10^6 lb-in^2) which is considerably larger than either of the requirements derived above; therefore, a large margin exists before general instability takes place.

The margin to yielding for the transverse beams supporting the floor panels is calculated to be 150 percent for a maximum floor loading of 4790 N/m^2 (100 lb/ft^2). For a nominal floor loading of 1436 N/m^2 (30 lb/ft^2), the maximum floor deflection should be no greater than about 0.38 cm (0.15 in).

D. <u>Scaling Relationships for Structural Weight</u>. Relationships have been derived to allow an estimation of the structural weight required for alternate vehicle geometries and gross weights. The estimated structural weight can be scaled from the values given in Table 4-1 by assuming certain

conditions are valid. The primary assumption is that the vehicle structure is idealized by a rectangular tube with height, h, width, b, length, L, and gross weight, W. Supporting assumptions are:

- Vertical vehicle stiffness is provided only by the top and bottom sheet-stringer structures.

- Lateral vehicle stiffness is provided only by the side sheet-stringer structures.

- Frame bending stiffness and spacing for the baseline design is adequate for all configurations to be considered, therefore frame weight scales linearly with the vehicle surface area.

- The weight of the honeycomb-core floor panels scales linearly with floor area.

- The transverse beams supporting the floor should maintain a constant floor deflection for all vehicle designs.

With the above assumptions, structural weight can be estimated from the following relations:

$$W_{structure} = 1.25 \ (w_{s/s} + w_{fr} + w_{fp} + w_{tb})$$

where

$$w_{s/s} = \left(\frac{\omega_y}{\omega_y^*}\right)^2 \left(\frac{W}{W^*}\right) \left(\frac{\ell}{\ell^*}\right)^4 \left(\frac{h^*}{h}\right)^2 w_1^* + \left(\frac{\omega_z}{\omega_z^*}\right)^2 \left(\frac{W}{W^*}\right) \left(\frac{\ell}{\ell^*}\right)^4 \left(\frac{b^*}{b}\right)^2 w_2^*, \text{ weight of sheet-stringer panels and component support beams}$$

$$w_{fr} = \frac{(b+h)\ell}{(b^* h^*)\ell^*} w_{fr}^*, \text{ weight of frames}$$

$$w_{fp} = \frac{b\ell}{b^* \ell^*} w_{fp}^*, \text{ weight of floor panels}$$

$$w_{tb} = \left(\frac{b^*}{b}\right)^2 \left(\frac{\ell}{\ell^*}\right), \text{ weight of transverse beams}$$

ω_y and ω_z are the desired minimum fundamental bending frequencies of the vehicle structure.

The values for the initial vehicle design are:

$W^* = 445,000$ N (100,000 lb)

$L^* = 30.5$ m (100 ft)

$h^* = 3.4$ m (134 in.)

$b^* = 3.0$ m (118 in.)

$w_1^* = 18,200$ N (4086 lb)

$w_2^* = 13,300$ N (3000 lb)

$w_{fr}^* = 2570$ N (578 lb)

$w_{fp}^* = 6310$ N (1419 lb)

$w_{tb}^* = 2600$ N (9585 lb)

E. **Conclusions.** The vehicle structure described in Table 4-1 and Figure 4-4 provides adequate stiffness and strength for the expected TMLV environment. A structural weight of 53.4 kN ($\sim$ 12,000 lb) was calculated for the primary and secondary structure based on a vehicle 30.5 m long with a gross weight of 445 kN. As a conservative approach, the structural weight estimate of 53.4 kN was retained for the lighter, longer baseline vehicle. This results in a slight drop in the fundamental bending frequency, but the weight-length ratio compares favorably with prior TRW correlations, as discussed in Section 4.2.6.

4.2.4 Mass Properties

The detailed weight estimates for the baseline 80-passenger vehicle powered by a Ducted Fan/Gas Turbine are given in Table 4-2. The results reflect what are considered to be reasonable estimates of each significant component of the vehicle. The major portion of the total vehicle weight of 366.5 kN (82,400 lb) is contained in the suspension system (66.8 kN or 18%), the structure (53.4 kN or 15%), the propulsion system (80.6 kN or 22%), and the passenger payload (71 kN or 19%). The remaining 26% of the weight is contained in furnishings, auxiliaries, brakes, and approximately 5% of the total weight for contingencies.

4-14

TABLE 4-2. DETAILED WEIGHT BREAKDOWN SUMMARY FOR BASELINE MAGLEV VEHICLE

ITEM		WEIGHT	
		KN	(lb)
o SUSPENSION		66.8	(15,000)
LIFT/GUIDANCE MAGNET MODULES[1] (4 SETS)	21.8 KN		
CRYOGENIC REFRIGERATION[2]	7.1		
LANDING/SWITCHING WHEELS, BOGIES & BRAKES (4 SETS)	19.6		
CRYOGENIC PIPING, INSULATION, ATTACHMENTS, ETC.	4.4		
ELECTRONIC CONTROL FOR LIFT/GUIDANCE MAGNETS	13.9		
o STRUCTURE		53.4	(12,000)
PRIMARY STRUCTURE	42.7		
SECONDARY STRUCTURE	10.7		
o FURNISHINGS		24.5	(5,500)
SEATS (80)	11.0		
CARPETING AND LINING	8.1		
WINDOWS AND EXTERIOR DOORS	5.4		
o AUXILIARIES		21.0	(4,700)
AIR CONDITIONING (AIR CYCLE MACHINES PLUS DUCTING)	6.2		
AUXILIARY POWER UNIT AND LIGHTING	3.6		
PARTITIONS AND BAGGAGE RACKS	7.6		
LAVATORIES (TWO), POTABLE WATER AND TANK	3.6		
o BRAKES (AERODYNAMIC PANELS & EMERGENCY PARACHUTE)		20.2	(4,500)
o CREW COMPARTMENT		15.6	(3,500)
COMMUNICATIONS	2.2		
ELECTRICAL DISTRIBUTION	9.1		
GALLEY	2.7		
CONSOLE, INSTRUMENTS, & FURNISHINGS	1.6		
o PROPULSION		80.6	(18,200)
FANS (TWO 4.5 FT DIAMETER)	4.4		
ENGINES (TWO ~ 7000 HP REGENERATIVE TURBOSHAFTS PLUS DUCTS AND NOISE TREATMENT)	17.1		
FUEL[3] (INCLUDING 15% RESERVE AND FUEL TANKS)	34.1		
FAN DUCTS AND NOISE TREATMENT	21.6		
GEAR BOXES	3.4		
o CONTINGENCY		13.4	(3,000)
o EMPTY VEHICLE WEIGHT		295.5	(66,400)
o PAYLOAD (100% LOAD FACTOR)		71.0	(16,000)
PASSENGERS – 80 PLUS 4 CREW MEMBERS (AVERAGE PASSENGER & CREW WEIGHT PLUS LUGGAGE = 0.845 KN)			
• GROSS VEHICLE WEIGHT		366.5	(82,400)

[1] INCLUDES LEVITATION/GUIDANCE COILS, SHIELDING COILS, DEWARS AND CONTROL COILS.

[2] INCLUDES BASIC SYSTEM CONSISTING OF ONE COMPRESSOR AND TWO REFRIGERATORS PLUS ONE BACK-UP COMPRESSOR.

[3] EVALUATED FOR BASELINE TRIP PROFILE OF 750 KM LENGTH WITH FIVE EQUIDISTANT INTERMEDIATE STOPS.

Additional details on the weight breakdown for some of the items such as the lift and guidance modules, control electronics, and structure is given in Sections 4.3.1, 4.3.5, and 4.2.3, respectively. An average passenger weight of 716 N (161 lb) is used, plus 129 N (29 lb) for luggage, clothing, etc. This is the same as the value used by domestic airlines. Weights of the furnishings and auxiliaries are primarily based upon similar equipment for airlines. As in the case of aircraft, it is important to keep vehicle weight as low as possible in order to minimize the propulsion system power requirements.

Further discussion of weight breakdowns for alternate propulsion systems and for vehicles with greater passenger capacity are given in Section 5.4.

The location of the baseline vehicle center of gravity is indicated in Figure 4-6, i.e., 16.22 m aft of the nose and 1.32 m above the bottom of the vehicle. The estimated moments of inertia are:

- Roll Moment of Inertia = 6.24×10^{4} kg-m^{2} (1.48×10^{6} lb$_{m}$-ft^{2})

- Pitch and Yaw Moment of Inertia = 3.52×10^{6} kg-m^{2} (8.35×10^{7} lb$_{m}$-ft^{2})

Z = 0 AT GUIDEWAY
SURFACE, LEVITATION
MAGNET COIL
HEIGHT = 0.3 M

COORDINATE SYSTEM   -Y   +Y
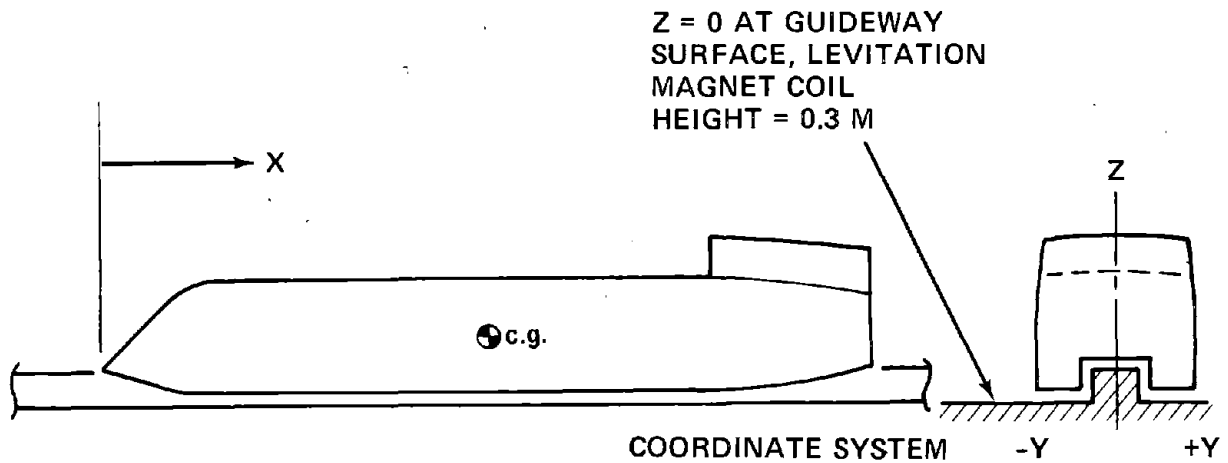
X_{CG} = 16.22 M (53.2 FT)
Y_{CG} = 0
Z_{CG} = 1.51 M (4.95 FT)

FIGURE 4-6. BASELINE VEHICLE CENTER OF GRAVITY LOCATION

4.2.5 Aerodynamics

A. <u>Introduction</u>. The aerodynamics analysis primarily consists of estimating the aerodynamic loads and moments on the vehicle for the design crosswind condition. These estimates are made in order to determine the effect of aerodynamics on the ride quality and stroke, and if the guidance and control system can accommodate the baseline crosswind forces and moments without special provisions. The vehicle shape is not aerodynamically optimized. Ultimately this must be done as well as evaluating the effect of transient airloads and the investigation of other problems such as passage through tunnels, etc.

The baseline system utilizes a hat-shape (wide inverted Tee) guideway. The fully exposed sides of the vehicle make it vulnerable to large side forces and moments induced by crosswinds. Therefore, a brief study was concerned with the design changes that may ultimately be required to alleviate the crosswind problem. A summary of the results and recommendations are given below. Additional details of the aerodynamic analyses are given in Ref. 4-5.

B. <u>Aerodynamic Data</u>. The data of Grunwald (Ref. 4-6) have been selected as the basis for the aerodynamic coefficients after a review was made of the limited information applicable to vehicles exposed to a crosswind in ground proximity. Grunwald's report represents the most comprehensive and representative compilation of data at this time. However, even these data have shortcomings when applied to the conceptual vehicle, particularly for the lift and pitching moment coefficients.

The first category of problems involves the test setup of Grunwald, and at least three differences exist between the test technique and actual MAGLEV operation. First, the moving ground plane fails to simulate properly the resultant wind-to-ground angle and velocity, as observed by Bowman (Ref. 4-7) and Ruetenik (Ref. 4-8). For the best simulation, the moving ground plane or belt should move in the direction of the model axis rather than in the direction of the tunnel airflow. For this reason, the stationary ground plane data are used. A second difference between Grunwald's models and the revenue vehicle concerns the guideway configuration. The baseline hat-shaped guideway has a raised section down the center whereas Grunwald used a flat belt.

4-17

These first two differences will affect the vehicle lift and pitching moment. The third difference exists in the base region. A ducted fan is the baseline propulsion system, with some or all of the flow deflected into the wake, while Grunwald used the model base for sting attachment. Also the vehicle has a partial boat-tail whereas the models did not. The third difference reduces base drag for the revenue vehicle as compared to the models.

The other category of problems relates to the model shape vs. the conceptual shape of the MAGLEV vehicle. Grunwald obtained aerodynamic data for six body geometries, three of which are more representative of the MAGLEV configuration. Grunwald refers to these shapes as square, triangular, and half-circle with long extended sides. The square cross section best matches the current baseline vehicle shape, but considerable differences still exist. Also the nose shape, base shape and especially the bottom configuration are considerably different. The overall effect of these differences is unclear. The triangular and half-circle shapes are aerodynamically superior to the square configuration in crosswind conditions due to their lower yawing forces and moments. Therefore these two shapes provide guidelines for improved aerodynamic designs. The aerodynamic coefficients for the square configuration of Grunwald are used to compute the forces and moments for this study.

The aerodynamic analysis was completed before the final vehicle configuration was derived. Figure 4-7 presents the shape used in the analysis*; the length and width of the vehicle is slightly less than the baseline configuration shown in Figure 4-1. The computed loads are based on a cross-sectional area of 8.5 m^2 (91.5 ft^2), and height above ground (ground clearance) of 0.15 m (6 in.). The large lateral area of the fan ducts is not included in the analysis. This area will increase the yaw force but reduce the yawing moment due to its location well aft of the vehicle center of gravity. The vehicle/guideway gap of 0.15 m corresponds to a height-to-effective-circular-diameter (H/d_e) of 0.045, which is within the range of values tested by Grunwald. The aerodynamic moments were transferred from the location used by Grunwald to the center of gravity location shown in Figure 4-7 by a simple mathematical transformation.

---

*This preliminary vehicle was also used for the structural and dynamic analyses.

30.5
(1200)

16.22
(638.4)

1.35
(53)

SUSPENSION MAGNETS

RETRACTABLE WHEELS

2.8
(110.6)

3.4
(134)

0.15
(6)

1.93
(76)

0.5
(19.7)

FRONTAL AREA = 8.5 M^2
(91.5 FT^2)
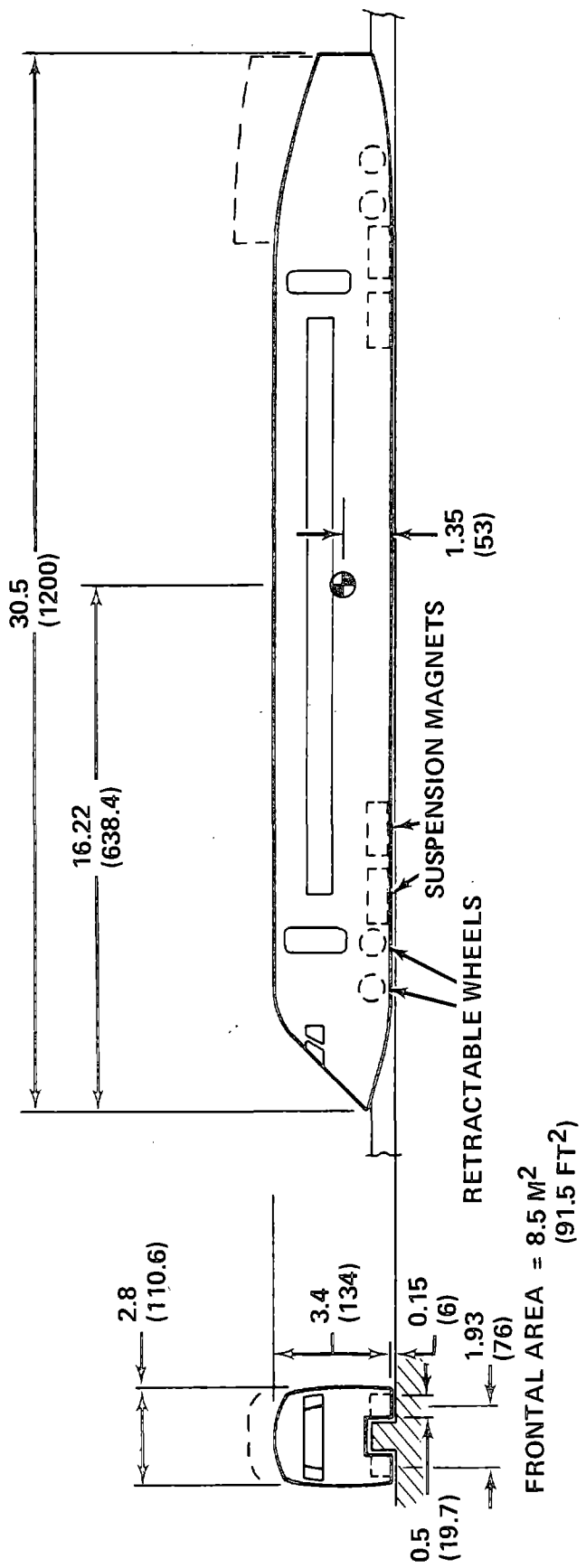
DIMENSIONS: METERS
(INCHES)

FIGURE 4-7. PRELIMINARY CONFIGURATION USED FOR AERODYNAMIC ANALYSIS

At the design yaw angle of 8.5° — which corresponds to a 20.1 m/s (45 mph) crosswind on a vehicle traveling at 134 m/s (300 mph) — the steady-state loads and coefficients are the values presented in Table 4-3.

TABLE 4-3. DESIGN AERODYNAMIC COEFFICIENTS AND LOADS FOR STEADY CROSSWIND

PARAMETER	COEFFICIENT	FORCE, KN (LB)	MOMENT, KN-m (FT-LB)
DRAG	$C_D = 0.255$	24.4 (5480)	—
LIFT	$C_L = -0.085$	-8.5 (-1910)	—
YAW	$C_Y = 0.525$	49.0 (11,010)	—
PITCH MOMENT	$C_m = -0.48$	—	-150 (-110,000)
YAW MOMENT	$C_n = 1.0$	—	320 (237,000)
ROLL MOMENT	$C_\ell = -0.10$	—	-3 (2210)

NOTE: FAN DUCTS NOT INCLUDED, MOMENTS ABOUT VEHICLE cg

In addition to the design case given above, aerodynamic coefficients and derivatives are computed from Grunwald's results for three configurations (square, triangular, and half-circle with extended sides) for yaw angles of 0, 4, 8, and 12 degrees (Ref. 4-5). The yawing and pitching moment coefficients exhibited the greatest variation with yaw. For high crosswinds, these moments tend to force the nose away laterally and lift the aft end of the vehicle.

C. <u>Conclusions and Recommendations</u>. Based on the magnitude of the forces and moments at the 8.5° yaw angle, only the yaw force and yawing moment appear to pose any potential problems. These loads, of course, depend on the body geometry, and the differences between the test models and the conceptual vehicle may mean that the Grunwald data are not accurate for the baseline configuration. Further test data are required to determine this. Approximately a 30% reduction of the yaw force and moment can be achieved by using the half-circular or triangular shapes rather than the square configuration. As observed by Ruetenik (Ref. 4-8), rounded corners on the bottom of the vehicle

are to be avoided since they tend to increase the side force and make it more sensitive to H/d_e. Although aft control surfaces (e.g., the fan ducts or a tail) will reduce the yawing moment, these will also increase the yaw force. No real advantage is realized by the use of a tail for yaw loads. The present baseline configuration has a relatively large height-to-width ratio, and this tends to result in high side forces. If these forces and moments (for applicable test models) prove to be too great a problem for the control system to overcome, consideration should be given to using a U-channel guideway and a longer, lower vehicle. A U-channel also provides a better shield for crosswinds, especially if additional wind barriers are erected along the sides.

The pitching moment is controlled by the lift. The Grunwald data show the lift for the square configuration to be slightly negative and acts far forward on the vehicle. Bowman (Ref. 4-9) has found that lift is particularly sensitive to the nose and tail shape. A minimum lift force requires that the nose stagnation region be kept low to the ground and rounded to the sides. The base should be square with the vehicle, avoiding the fastback slope. The vertical portion of the hat-shape guideway will cause a reduction in the Grunwald-derived lift and moments by reducing the airflow under the vehicle. Since the Grunwald configurations are not similar to the revenue vehicle nose, tail, or guideway; the lift and pitching moment data are probably only representative in magnitude. The conceptual revenue vehicle will likely have a slightly negative lift and moment.

The rolling moment is very small since the center-of-mass is near the geometric center of the vehicle. Vehicle drag was not investigated in detail since it does not significantly affect stability; additional information on the aerodynamic drag coefficients is given in Section 4.2.6B.

The problems associated with the theoretical predictions of subsonic aerodynamics in the presence of a ground plane and the configurational and test set-up problems with the existing test data make it necessary to have extensive subscale tests of the shapes of interest prior to the fabrication of any full-scale vehicle. One important problem that must be addressed further before testing is how to obtain the best simulation of the ground effects and crosswinds. Wind-tunnel testing should provide accurate

measurements of the side force and yawing moments. The data obtained by NASA (Ref. 4-6) and Hovercraft (Ref. 4-10) show that lift and pitching moment vary substantially with body and guideway geometry, but side force and yawing moments remain nearly the same. As observed by Beauvais (Ref. 4-11), the ground plane simulation technique may give as much as 25% variation in pitching moment. The fixed plane technique appears to provide the best results in the pitch and yaw plane when compared to full-scale model test data (Ref. 4-7).

A second approach to acquiring the test data is through the use of a moving model facility (fixed track) as suggested by Ruetenik and Zartarian (Ref. 4-8). This setup provides the correct body and track wind angle and can also be used for gust load and passing load measurements. This technique has a number of attractive features and existing test facilities have the potential of reaching the test conditions needed for MAGLEV.

D. Other Aerodynamic Phenemoma

(1) Passing Loads. Transient loads such as wind gusts and vehicles passing in opposite directions will give higher side loads and yawing moments than produced from steady-state side winds. Some work has been done on finding the force of one train exerted on a second train passing in opposite directions (Refs. 4-12 and 4-13). Typical results based on experiments and potential flow theory are given in Ref. 4-13. It was found that: (1) the force on the vehicle remains nearly constant over the length of the train, and (2) the force is proportional to $(a/a+S)^4$, where "a" is the half-width of the body and "S" is the physical separation distance between the two trains. A high side force builds up as they approach, followed by a negative force of approximately the same strength. At a separation distance of one-half the train width, the force exerted by a passing train is equal to the force of a steady crosswind of 30.9 m/s (69 mph) on a vehicle with a speed of 134 m/s (300 mph) (for this case $\beta = 13°$). To maintain an acceptably low force between passing trains, a good rule of thumb is to keep a minimum separation distance of at least one train width (S = 2a). A nominal separation distance of 3 m (10 ft) is specified for locations in which 134 m/s cruise speeds are reached.

(2) <u>Vehicle Flow Field Effects</u>. The aerodynamic flow field produced by a high-speed vehicle will be felt by objects close to the guideway. This effect will be in the form of a wind gust of short duration ($\lesssim$ 1 second), and the magnitude of the gust will be influenced by the distance from the passing vehicle, the vehicle characteristics (shape, speed, method of propulsion), and the magnitude of any crosswind.

The principal aerodynamic phenomena due to the vehicle body results from the pressure field created by the vehicle nose, and the wake aft of the vehicle base. Hammitt (Ref. 4-14) presents graphical estimates of these phenomena in parametric form for a representative vehicle configuration. The results of Hammitt have been used to determine the approximate magnitude of the wind gusts that would be experienced from passage of a single vehicle traveling at 134 m/s (300 mph) with no crosswind. Figure 4-8 shows the estimated maximum induced gust velocity as a function of side distance from the vehicle centerline. The results indicate the wake is more important than the nose effect. Figure 4-8 demonstrates that the induced velocity for an aerodynamically smooth body representative of MAGLEV is hardly noticeable at distances greater than about 9 m (30 ft) from the vehicle centerline. Therefore, a distance of 15 m (50 ft) to the edge of the wide right-of-way should provide sufficient distance to eliminate gust effects at the edge even with crosswinds, however additional test data are needed to confirm this conclusion.

A Ducted Fan/Gas Turbine exhausting into the base region will completely change the wake effect by changing the direction of the wake velocity. Hamilton Standard Division of United Aircraft conducted a brief study to evaluate the exhaust plume characteristics of the fan and the gas turbine for the MAGLEV application. Velocity and temperature profiles were obtained for three turboshaft gas turbines at static conditions and maximum power. The results showed that the significant increase in the velocity and temperature for the engine alone is confined to a relatively small volume extending about 1 m (3.3 ft) on either side of the centerline of the turbine exhaust and approximately 23 m (75 ft) downstream.

The Q-fan exhaust is larger than that of the gas turbine, the exit velocity is higher, but there is no temperature increase. Some recent exhaust

4-23
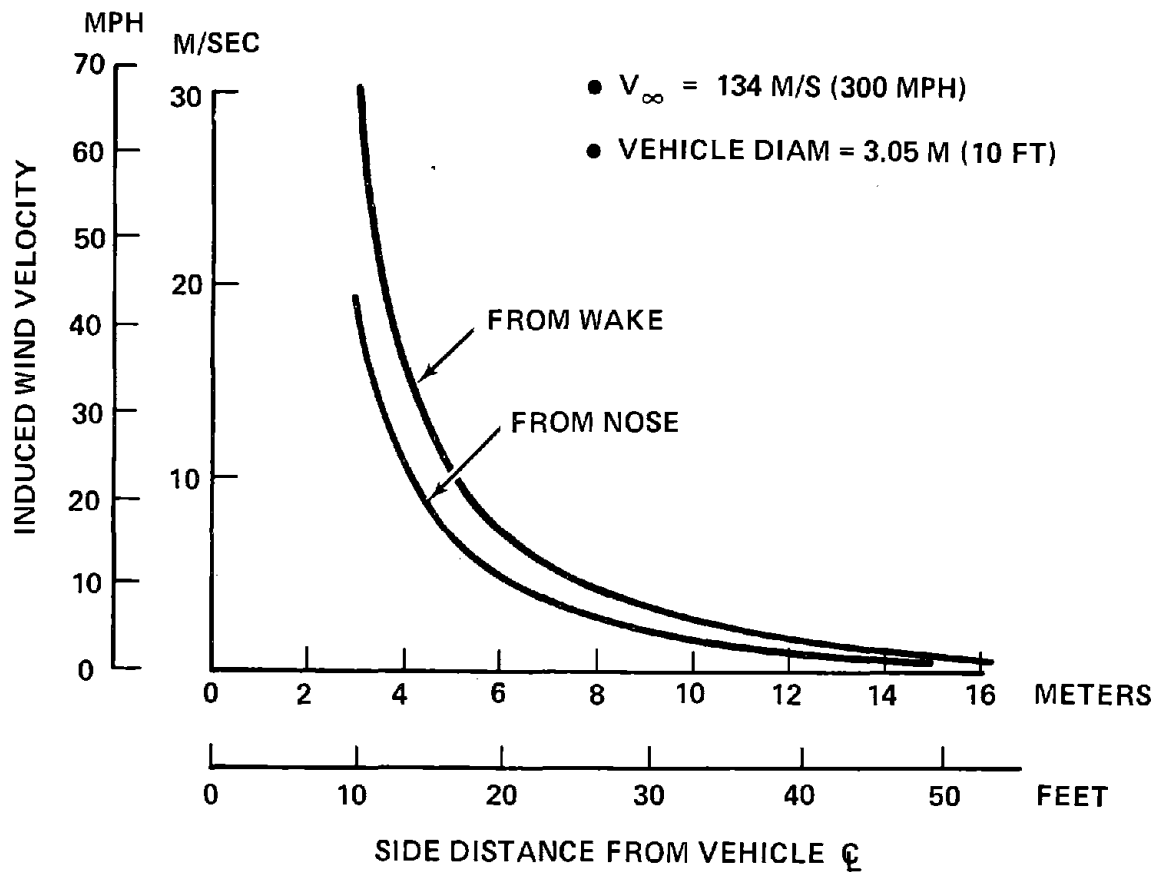
FIGURE 4-8. INDUCED WIND VELOCITY RESULTING FROM PASSAGE OF HIGH SPEED VEHICLE

measurements on the Hamilton Standard Q-fan demonstrator have been used to prepare velocity profiles for the static, maximum thrust condition. The results show that the area of significant velocity increase is roughly 6 m (20 ft) maximum on either side of the Q-fan exhaust centerline and approximately 60 m (200 ft) downstream. The region of high velocity is considerably smaller than this. No problems for the static exhaust of either the gas turbine or Q-fan exist at the edge of reasonably sized ($\geq$ 50 ft from centerline) rights-of-way. The problem of the exhaust in the passenger loading/unloading areas is minimized by using low thrust and/or by having protective loading and unloading ramps similar to present-day airports.

4-24

When the vehicle is in motion the plume velocity perceived by a station-
ary observer is the difference between the static plume velocity and the
vehicle velocity. Thus, the static conditions are the worst case, and the
flow field effect at the edge of the right-of-way for the Q-fan and turbine
at cruise speed are expected to be even less than that due to the flow field
from the body alone.

(3) <u>Passage Through Tunnels</u>. Although a study of the problems of
high-speed travel through tunnels was beyond the scope of the conceptual
design, the presence of tunnels has substantial implications on the ultimate
system design. For example, Kurtz and Dayman (Ref. 4-15) show that aerodyna-
mics should be a major factor in the design and operation of high-speed sys-
tems in tunnels. Either large tunnels are required or special techniques must
be used to vent the tunnel, otherwise the power required and/or the vehicle
velocity loss become prohibitive. A pressurized vehicle will be required to
eliminate the problem of rapid pressure changes in the cabin upon entry into a
tunnel. A large increase in the temperature of the air in the tunnel is also
a potential problem. Detailed systems studies must address these areas and
determine the most cost-effective solutions. As in the case of guideway con-
struction, tunnel construction and the necessity of having significant numbers
of tunnels is a highly route-specific problem.

(4) <u>Vehicle Aerodynamic Noise</u>. Substantial noise or sound is gener-
ated by the passage of a high-speed vehicle through the air. This sound is
due to the boundary layer on the body, vortex shedding, and the presence of
mixing and shear regions. The sound level increases rapidly as a function of
the vehicle speed. This phenomenon was apparently not fully appreciated when
the preliminary HSGT noise limits were set by FRA/DOT (see Section 3.2.3).
Although FRA/DOT has specified the total vehicle noise limit as 73 dbA at
50 feet from the vehicle centerline, this value should be considered as an
optimistic goal rather than a requirement. This is because the aerodynamic
noise level of the vehicle without propulsion traveling at 134 m/s (300 mph)
or even considerably lower speeds, is predicted to be substantially greater
than this value. In order to obtain a realistic basis for specifying the
sound level requirements for the propulsion system, it was decided that the

propulsion system should not have a sound level greater than that of the vehicle itself at 134 m/s, and, as a goal, should not exceed the sound level of the vehicle at any speed above which the aerodynamic noise is greater than 73 dbA. The task of predicting what the noise level of the vehicle would be without a propulsion system was undertaken by the Hamilton Standard Division of United Aircraft.

A literature review of prediction procedures for vehicle noise radiation shows that most of the methods had been established for, and correlated with, gliding aircraft (e.g., Ref. 4-16). The primary mechanism of noise generation for gliding aircraft is vortex shedding off the wings — an unrealistic condition for the MAGLEV vehicle. Thus, wing vortex noise equations provide, at best, only a rough conservative guide as to the noise levels.

Figure 4-9A presents noise data for various types of transportation vehicles with and without propulsion systems (from Refs. 4-17 and 4-18), and a summary of predictions for the unpowered MAGLEV vehicle. The recommended Hamilton Standard correlation was based on work by LTV (Ref. 4-19). Figure 4-9B is an updated summary of the information presented in the previous figure. The most applicable data are enclosed by the shaded border. Note that the Hamilton Standard correlation for the unpowered MAGLEV vehicle lies considerably outside the shaded area.

The recommended Hamilton Standard correlation results in a prediction of the unpowered MAGLEV sound level of 92 dbA (50 ft) at 134 m/s (300 mph), dropping to the DOT noise "limit" of 73 dbA at 77 m/s (174 mph). The importance of vehicle aerodynamic noise is obvious at high speeds. An upward revision of the DOT noise limit is required, otherwise future high-speed ground transportation vehicles typical of MAGLEV will be restricted to speeds roughly below 77 m/s (174 mph), even if the propulsion system, wayside pickup (if any) etc., contribute no increase in the bare-body aerodynamic noise level. Further test measurements are needed to determine aerodynamic sound levels of HSGT systems, since supporting data for magnetically levitated vehicles are non-existent for the speeds and vehicle configurations of interest.

SOURCE: HAMILTON STANDARD

LATEST NASA PROCEDURE
BASED ON GLIDING AIRCRAFT
(TMLV EST)

ESTIMATE OF VEHICLE
SOUND LEVEL WITHOUT
PROPULSION = 92 DBA

TAC V PROJECTED
FOR 1985

H.S. CORRELATION FOR
MAGLEV VEHICLE W/O PROPULSION
(BASED ON LTV WORK)

LATEST NASA CORRELATION
FOR BOUNDARY LAYER
SOUND ONLY

CONVAIR 240
GLIDING

MITRE
PROCEDURE
FOR B.L.
NOISE

AEROTRAIN
WITH
PROP

JAPAN
NEW
TOKAIDO

METROLINER

TURBO-
TRAIN

METROLINER

BART

AEROTRAIN
WITH
LIM

DUCTED
PROP TACV
W/O PROP

FRENCH
TACV
WITH
PROP
(GOMETZ)

FREEWAY TRAFFIC

DIESEL
LOCOMOTIVE

DIESEL TRUCK

VERY LONG
RAPID TRANSIT
TRAIN

PHILA
PATCO

FRENCH
TACV
WITH LIM
(GOMETZ)

FREIGHT TRAIN CARS

FRA/DOT SPECIFIED NOISE GOAL
(INCLUDES TONE CORRECTION)

AUTO

PASSENGER
TRAIN

150~M/S

125

VEHICLE SPEED (MPH)

SOUND LEVEL AT 50 FT (DB(A))

100 95 90 85 80 75 70

FIGURE 4-9A. NOISE DATA SUMMARY AND NOISE CORRELATION FOR
UNPOWERED MAGLEV VEHICLE

4-27
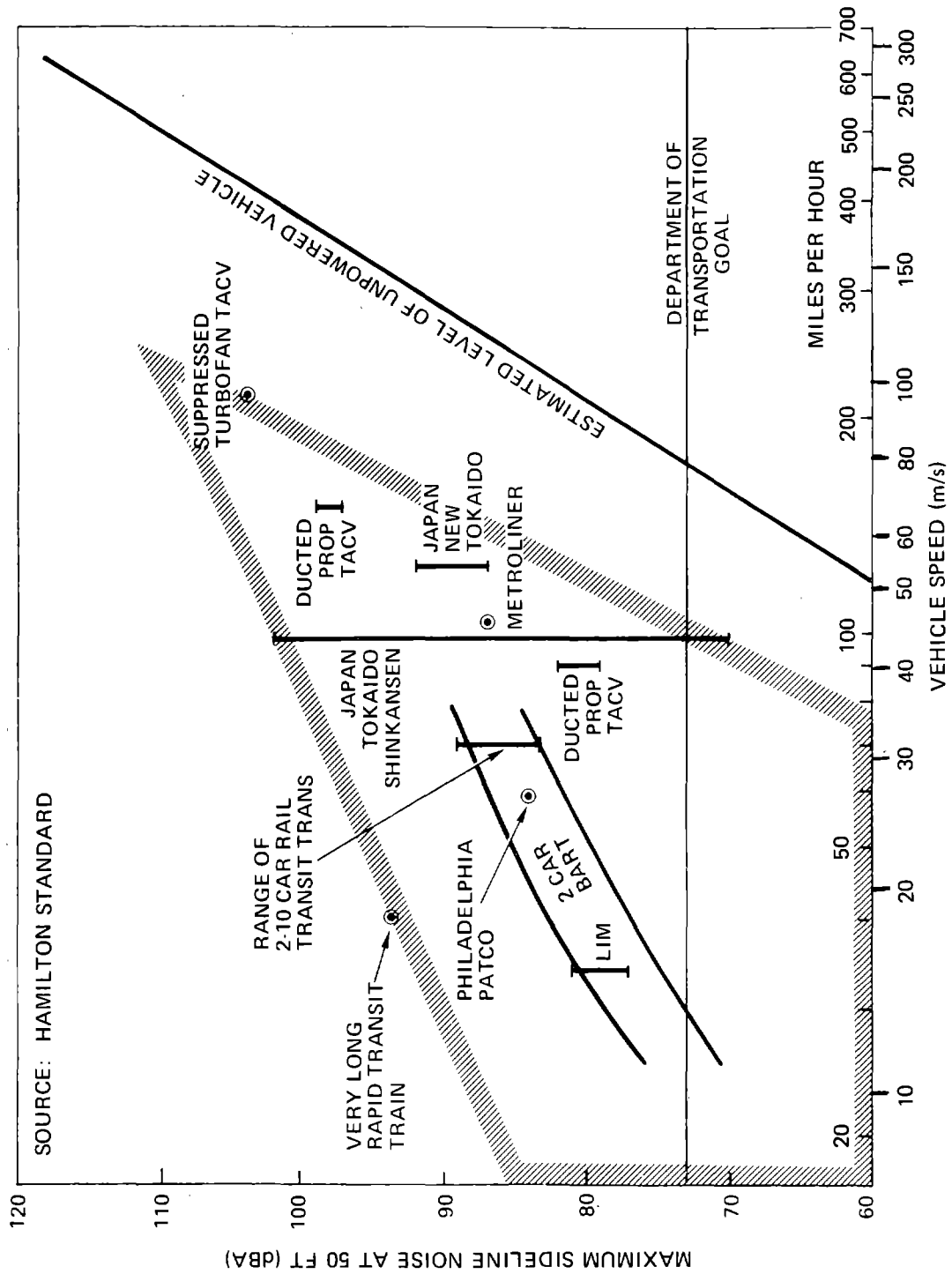
FIGURE 4-9B. VEHICLE NOISE TRENDS

4-28

4.2.6 Vehicle Synthesis

A matrix of 80- to 140-seat vehicles is synthesized to ascertain the relative merits of different seating arrangements*, e.g., 2 + 1, 2 + 2, 2 + 3, 3 + 3. The basic objective of this effort is to determine the "minimum energy" configurations for subsequent input to the systems analysis reported in Section 5. In particular, reasonably detailed syntheses are necessary to properly account for growth factor effects due to changes in the weight of individual vehicle components.

All vehicles are designed for a cruise speed, V_C, of 134 m/s (300 mph) and employ the baseline Ducted Fan/Gas Turbine propulsion system. Four 0.5 x 3 m (or eight 0.5 x 1.5 m) superconducting magnets are used for levitation and guidance, separated 0.3 m (horizontal and vertical) from L-shaped aluminum guideway elements of 2.54 cm thickness arranged in a hat-shape configuration. The magnetic lift-drag ratio is 45.5 at 134 m/s (300 mph).

The major tradeoff parameters are as follows:

- Seating Arrangement — The seating arrangement, together with the number of seats (N_{SV}) sets the basic vehicle dimensions.

- Aerodynamic Drag — Aerodynamic drag power increases with vehicle cross-sectional area and length. Long slender shapes are preferred for fixed payload volume.

- Magnetic Drag — Magnetic drag power increases with vehicle gross weight (as does the energy expended during acceleration); gross weight is in turn influenced by the structure and other component weights. Structure weight is adversely affected by vehicle length; for fixed payload volume, short squat shapes are preferred.

A. <u>Seating Arrangements</u>. Table 4-4 shows vehicle length for each seating arrangement and capacity under consideration. The seating accommodations are the same as DC-10 values, as shown previously.

---

*A 2 + 1 seating arrangement is two seats on one side of an aisle and one on the other, 2 + 2 is two seats on each side of an aisle, etc.

TABLE 4-4. VEHICLE LENGTH, ℓ (m)

PASSENGER CAPACITY, N_{SV}	SEATING ARRANGEMENT 2 + 1	2 + 2	2 + 3	3 + 3
80	40.42	33.67	29.81	27.88
100	47.2	38.5	33.6	30.8
120	54.5	44.9	39.1	35.2
140	61.3	49.7	42.9	39.1

Two lavatories are provided for $N_{SV} \leq 100$ whereas four lavatories are provided for $N_{SV} \geq 120$. Also, the length includes ~ 8.6 m over the basic passenger compartment length to accommodate the crew compartment (forward) and the propulsion system compartment (aft).

Cross-sectional data are shown in Table 4-5, based on an effective rectangular shape, i.e., the rectangular cross section has the same height and frontal area of the actual cross section. This approach was taken to simplify certain of the aerodynamic and structural calculations used in the tradeoff analysis.

TABLE 4-5. CROSS SECTION DATA

	SEATING ARRANGEMENT 2 + 1	2 + 2	2 + 3	3 + 3
HEIGHT, h (m)	3.454	3.454	3.454	3.454
EFFECTIVE WIDTH, b (m)	2.044	2.45	2.80	3.12
FRONTAL AREA, A_C (m^2)	7.06	8.45	9.66	10.77

B. Aerodynamics. A simplified aerodynamic drag analysis is employed based on the data of Ref. 4-20*. The aerodynamic drag coefficient for this general class of configurations may be written as:

$$C_D = C_D \text{ (Nose, Prot)} + C_D \text{ (Friction)} + C_D \text{ (Base)} + C_D \text{ (Gap)}$$

where

$$C_D \text{ (Nose, Prot)} \approx 0.098 \qquad\qquad 4-1$$

$$C_D \text{ (Friction)} = C_F \left(\frac{A_w}{A_c}\right) \qquad\qquad 4-2$$

$$C_D \text{ (Base)} \approx \frac{3.625 \times 10^{-3}}{\sqrt{C_F \left(\frac{A_w}{A_c}\right)}} @ \frac{D_b}{D} = 0.5 \qquad\qquad 4-3$$

$$C_D \text{ (Gap)} \approx 3.62 \times 10^{-4} \left(\frac{A_w}{A_c}\right) \qquad\qquad 4-4$$

and

$$C_F = 0.455 \, (\log Re_\ell)^{-2.58} \qquad\qquad 4-5$$

$$Re_\ell = 9.1745 \times 10^6 \, \ell @ \text{ sea level}, \ell \text{ in meters}$$

$$A_w/A_c = 2 \, (b+h) \, \ell/bh$$

All vehicle surfaces are assumed smooth, corresponding to aircraft design practice; all doors, windows, etc., are likewise flush-fitting. The protuberance and nose drag (Equation 4-1) are estimates for carefully streamlined vehicles. The base drag (Equation 4-3) is computed on the assumption of partial boat-tailing, i.e., $D_b/D = 0.5$. For a large ducted fan or gas turbine exhausting into the base region, the base drag should be lower than the value obtained from Equation 4-3. The skin friction coefficient, C_F (Equation 4-5)

---

*The referenced work was conducted by Avco Corporation for Ford Motor Company on prior DOT-sponsored MAGLEV research.

is based on the Prandtl-Schlichting formula, for $\text{Re}_\ell > 2 \times 10^8$. Equation 4-4 estimates the non-two-dimensional influence of secondary flow venting from the gap under the bottom of the vehicle in the circumferential direction. Fully developed flow in the gap is not expected to occur except toward the rear of the vehicle, i.e., where the boundary layer thickness approximates the gap dimension.

The resultant C_D values are tabulated in Table 4-6.

TABLE 4-6. AERO DRAG COEFFICIENTS

PASSENGER CAPACITY, N_{SV}	SEATING ARRANGEMENT			
	2 + 1	2 + 2	2 + 3	3 + 2
80	0.244	0.213	0.197	0.188
100	0.263	0.255	0.206	0.195
120	0.284	0.242	0.219	0.204
140	0.303	0.254	0.228	0.213

The aerodynamic drag power, P_A (in kW), is determined by

$$P_A = C_D A_c \rho V_C^3 / 2000 \qquad\qquad 4\text{-}6$$

where

A_c = Cross-section area = bh $\quad(\text{m}^2)$

ρ = Ambient air density = 1.225 kg/m^3 at sea level

The aerodynamic drag power for the various vehicle design points is shown in Figure 4-10.

C. Structure. Detailed structural weight calculations are reported in previous paragraphs. These calculations are made for a baseline (2 + 2, N_{SV} = 80) configuration at an arbitrary gross weight of 445 kN (10^5 lb) and at ℓ = 30.5 m, with the criterion that the structural modal frequencies be larger ($\sim$ 8 times) than the natural frequency of the suspension system. This
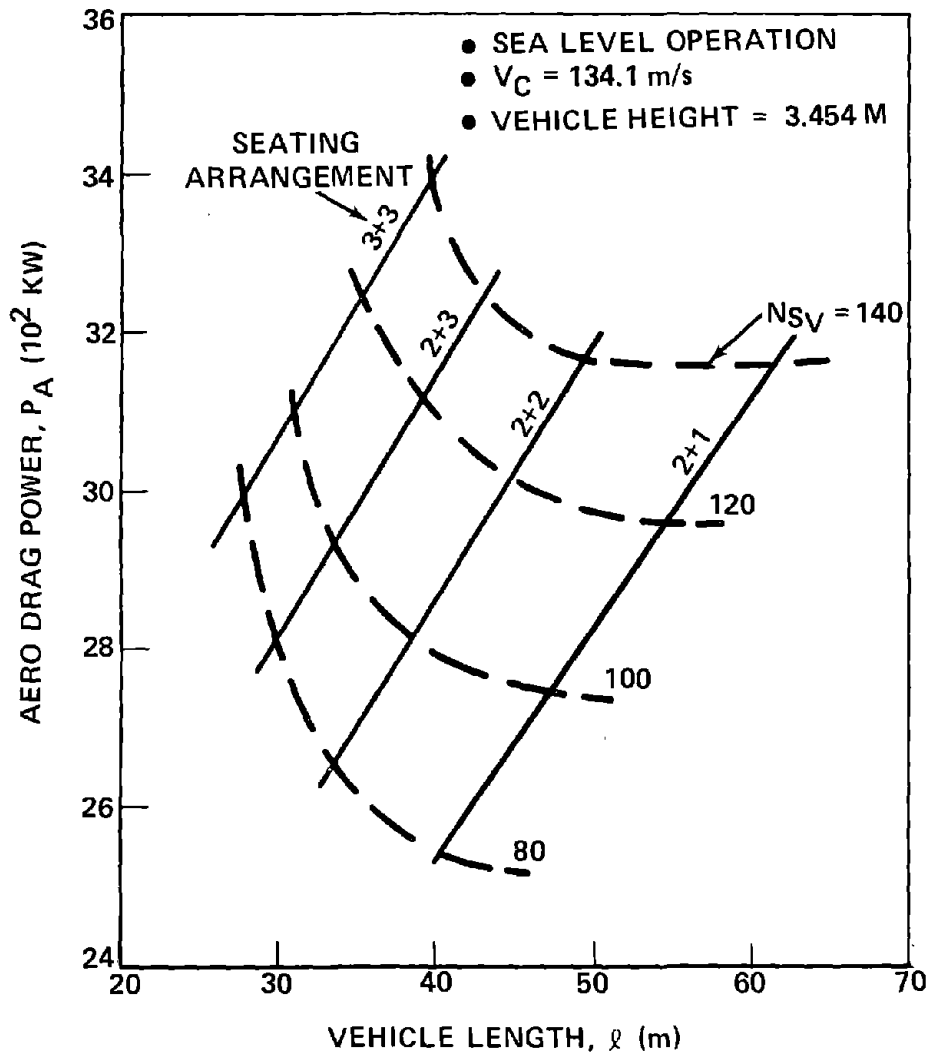
FIGURE 4-10. AERO DRAG POWER

permits the suspension system to be designed without consideration of struc-
tural elasticity. Using aircraft-type construction, this gives a weight/
length ratio ($\sim$ 1.78 kN/m) which compares favorably with a trend line devel-
oped by TRW in Ref. 4-21.

Subsequent iterative calculations show that the baseline configuration
would approximate 366.5 kN (82,400 lb) gross weight at ℓ = 33.67 m. The
baseline structural weight has been adjusted to these new values, and a new
trend-line developed which fits the following equation.

$$W \text{ (Structure)} = \frac{\ell}{b^2} (6.393 + 0.0283 \ \ell^{1.338})$$

Equation 4-7 is the basis for the structure weight data shown in Figure 4-11.
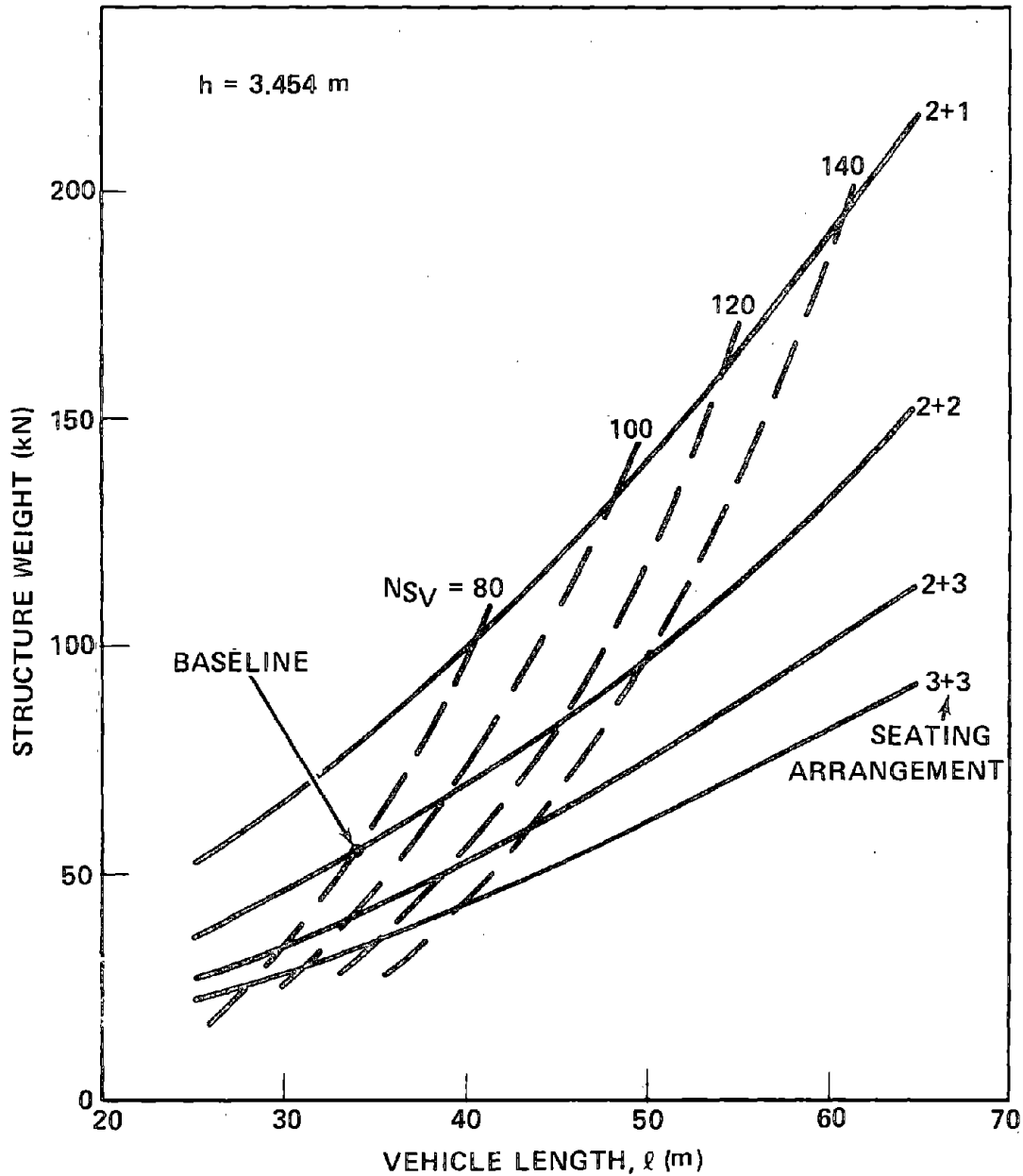
FIGURE 4-11. GENERALIZED STRUCTURE WEIGHT

Note that the structural frequencies are not held fixed for all the data points on Figure 4-11. Constant frequency designs would result in intolerably high (and unrealistic) structure weights for vehicle lengths in excess of approximately 40 m (131 ft), particularly for narrow configurations.

D. Propulsion. On the basis of data supplied by the Hamilton Standard Division of UAC, the propulsion system was scaled for vehicles of arbitrary gross weight operating over the baseline 750 km route with N_i intermediate, equidistant stops. A generalized propulsion system weight equation was derived:

$$W \text{ (Propulsion)} = 21.2 + \left[\frac{0.0124 \; W_g^{\;0.0265(N_i+1)}}{(N_i + 1)^{0.385}}\right] P_C, \text{ (kN)} \qquad 4\text{-}8$$

where

W_g = Vehicle gross weight (kN)

P_C = Cruise Power (kW)

Equation 4-8 includes fuel weight, with 15% reserve, for a one-way 750 km run* including level-cruise, grade-cruise, acceleration, deceleration, and station idle operation. The weight of fuel consumed (in kN) is correlated by:

$$W(\text{Fuel}) = 1.204 \times 10^{-6} \; (P_C - 378.7) \left[5800 + 1.167 \; (N_i + 1)^{0.728}\right.$$
$$\left.\cdot (W_g - 9.6)\right] \qquad 4\text{-}9$$

E. Weight Summary. Scaling law estimates were made for the weight of the remaining components. Table 4-7 summarizes the component weight equations.

For V_C = 134 m/s (300 mph) and magnetic L/D = 45.5, cruise power, P_C, can be expressed (in kW) as

$$P_C = P_A + 2.95 \; W_g \qquad 4\text{-}10$$

---

*Refueling at the route terminus is assumed.

TABLE 4-7. VEHICLE WEIGHT BREAKOUT (kN)

- SUSPENSION

  $48.5 + 0.05\ W_g$

- STRUCTURE

  $\dfrac{\ell}{b^2}\left(6.393 + 0.0283\ \ell^{1.338}\right)$

- FURNISHINGS

  $0.225\ N_{SV} + 0.0361\ (b + 3.545)\ \ell$

- AUXILIARIES

  $0.2625\ N_{SV}$

- BRAKES

  $4.5 + 0.043\ W_g$

- CREW COMPARTMENT

  15.6

- PAYLOAD

  $0.8877\ N_{SV}$

- PROPULSION $(N_i = 5)$

  $21.2 + 0.006221\ W_g^{0.159}\ P_C$

- CONTINGENCY

  13.4

Equation 4-10 can be combined with the summarized component weights from
Table 4-7 to determine vehicle gross weight and associated power data for
each configuration in the vehicle matrix. The Energy Intensity, ψ is then
computed* (in MJ/Seat-km) from

$$\psi = \frac{5.884\ W_F}{N_{SV}} \tag{4-11}$$

Figure 4-12 shows the Energy Intensity for the matrix of study vehicles. The
140-seat vehicle, as expected, is substantially better than the 80-seat con-
figuration; optimum seating arrangement for N_{SV} = 140 is 2 + 3, resulting in
a vehicle 42.9 m (141 ft) in length with a cross-sectional envelope of 3.454 x
3.454 m (11.3 x 11.3 ft).

Additional analyses have been carried out for the class of vehicles
designed to fit a U-channel, rather than the hat-shaped guideway. These vehi-
cles have less height and consequently lower cross-sectional area (lower aero-
dynamic drag). The magnetic and wheel suspension elements and fuel, however,

---

*Lower heating value for JP fuel is approximately 4412.1 MJ/kN.
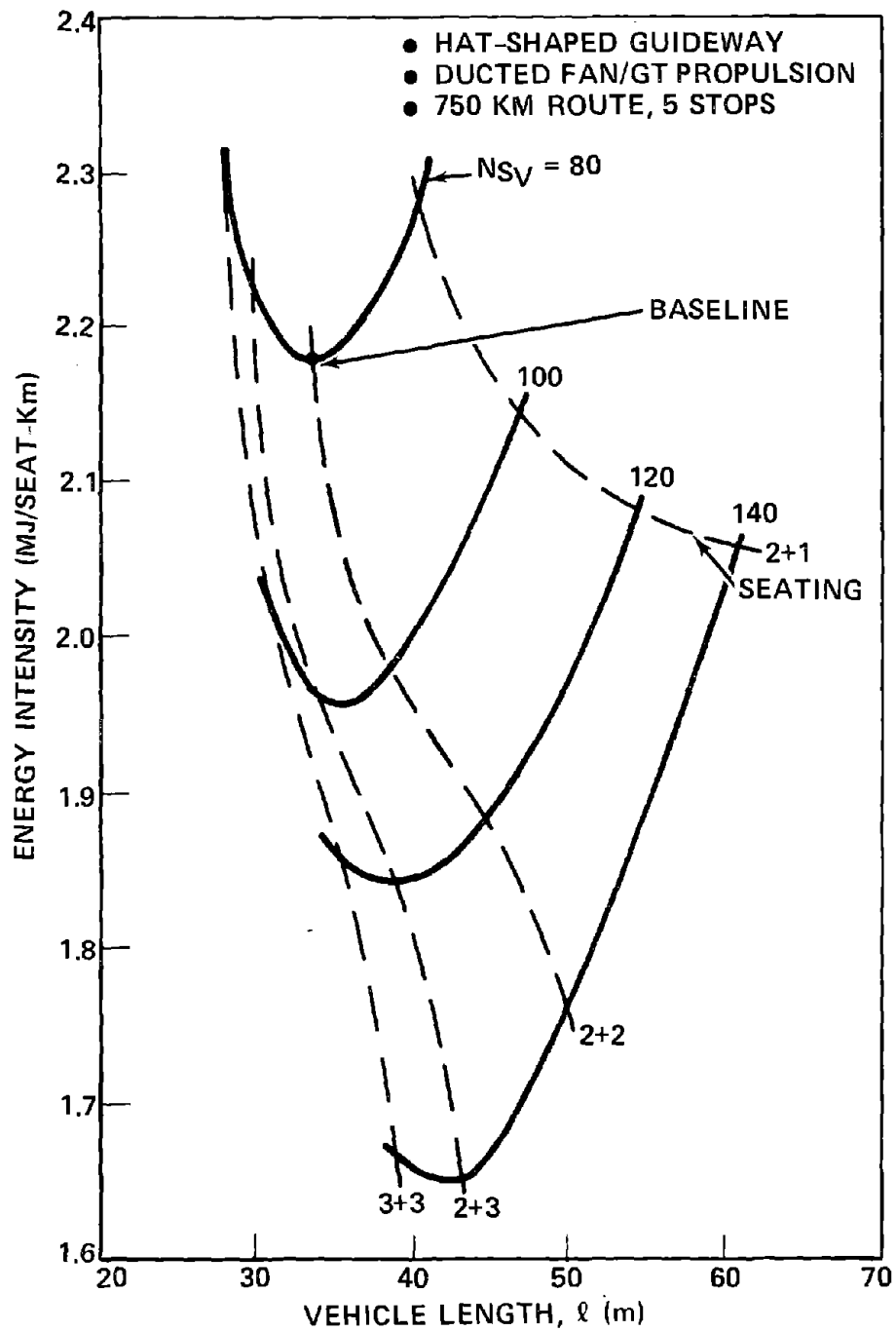
FIGURE 4-12. CONFIGURATION/ENERGY TRADEOFF

must be moved forward and aft of the primary passenger compartment, thus increasing length. The combination of lower section depth and increased length serves to increase structural weight and magnetic drag. These factors combine to produce a vehicle with higher total drag (and energy consumption) than the baseline design. It appears that the "sponsons" (the deep sections required to straddle the hat-shape guideway) on the baseline design are beneficial in that they provide a high section modulus and a relatively short vehicle — by encapsulating magnets, wheels, and fuel — thus permitting a lower weight, lower power system. Of course, this type of configuration could be used with the U-channel guideway just as well as with the hat guideway. The essential point of this analysis, however, is that it does not pay to reduce frontal area at the expense of length.

4.2.7 Common Subsystems

A summary of the general type of subsystems acceptable for the conceptual vehicle is contained in this section. These include air conditioning, landing/switching gear, brakes, auxiliary power unit, and onboard control/communication equipment. The term "common" subsystem refers to the fact that the subsystem will largely be the same for any type of propulsion system.

A. Air Conditioning. The air conditioning system must perform the functions of heating, cooling, humidity control and maintain a near-constant cabin pressure for the sealed cabin. The system must also be lightweight; all of these requirements imply the design must be more like that used on an airplane than a conventional train. An air cycle environmental control system has been chosen, since it fills the requirements stated above plus has the advantages of:

o Using air as the refrigerant

o Rapid cabin cooldown capability (high airflow)

o High reliability, low maintenance

o Compact, low weight design

An air-cycle machine is driven by compressed air, which is ideal if a gas turbine is used since the required air can be bled from the engine compressors.

4-38

The use of electrical propulsion systems will require a separate electric motor-driven air compressor to supply the required air. An air-cycle system has the disadvantages of requiring more power per ton of refrigeration and being more expensive than for a Freon-type system. Air-cycle machines are used on practically all modern aircraft and have proven to have all the advantages stated above.

Approximately 15 "tons" (53 kW) of air conditioning will be required, and the weight based on actual aircraft installations is estimated to be 1780 N (400 lb) for the air-cycle machine, (including heat exchangers, ducts, valves, sensors, etc.) plus approximately 4450 N (1000 lb) for the ducting required throughout the vehicle.

B. Landing/Switching Gear. The landing/switching gear has been designed to perform the following functions:

o   Support the vehicle on wheels up to the lift-off speed and be capable of rapid downward extension in the event of an emergency condition, such as power or magnet failure.

o   Extend down and out to engage the switching ramps used for the baseline switching concept. (Small lateral guidance wheels will be used to guide the vehicle in the ramp.)

o   Be steerable so that the vehicle can be maneuvered in the terminal areas.

o   Have wheel brakes for slowing and stopping in the switching and terminal areas.

o   Be fully retractable during cruise to minimize aerodynamic drag. An optional function during retraction would be to act as bumpers in event of extreme vehicle excursions, although this function may be better served by fixed skids.

The wheel design must allow for two positions when the wheels are lowered: first, directly down so that the wheels can engage the guideway during emergency conditions, and second, down and out to the sides to engage the switching ramps. These two cases are illustrated on the left side of Figure 4-13. A typical design is also schematically illustrated in Figure 4-13. A total of eight 36 x 11 inch aircraft-type tires are required to support the vehicle during emergency landing conditions. A hydraulic system will be used to actuate the gear, for steering, and to operate the wheel brakes, although a

VEHICLE BOTTOM

VEHICLE FLOOR

GUIDEWAY/RAMP

VERTICAL EXTENSION

VEHICLE C_L

VEHICLE SIDE

LATERAL EXTENSION

0.78
(30.7)

0.54
(21.3)

36 " X 11 "
TIRE

WHEELS FOR
LATERAL GUIDANCE

SWITCHING RAMP

WHEELS EXTENDED TO ENGAGE
LANDING/SWITCHING RAMP

0.28
(11)

WHEELS EXTENDED TO ENGAGE
GUIDEWAY FOR EMERGENCY CONDITION
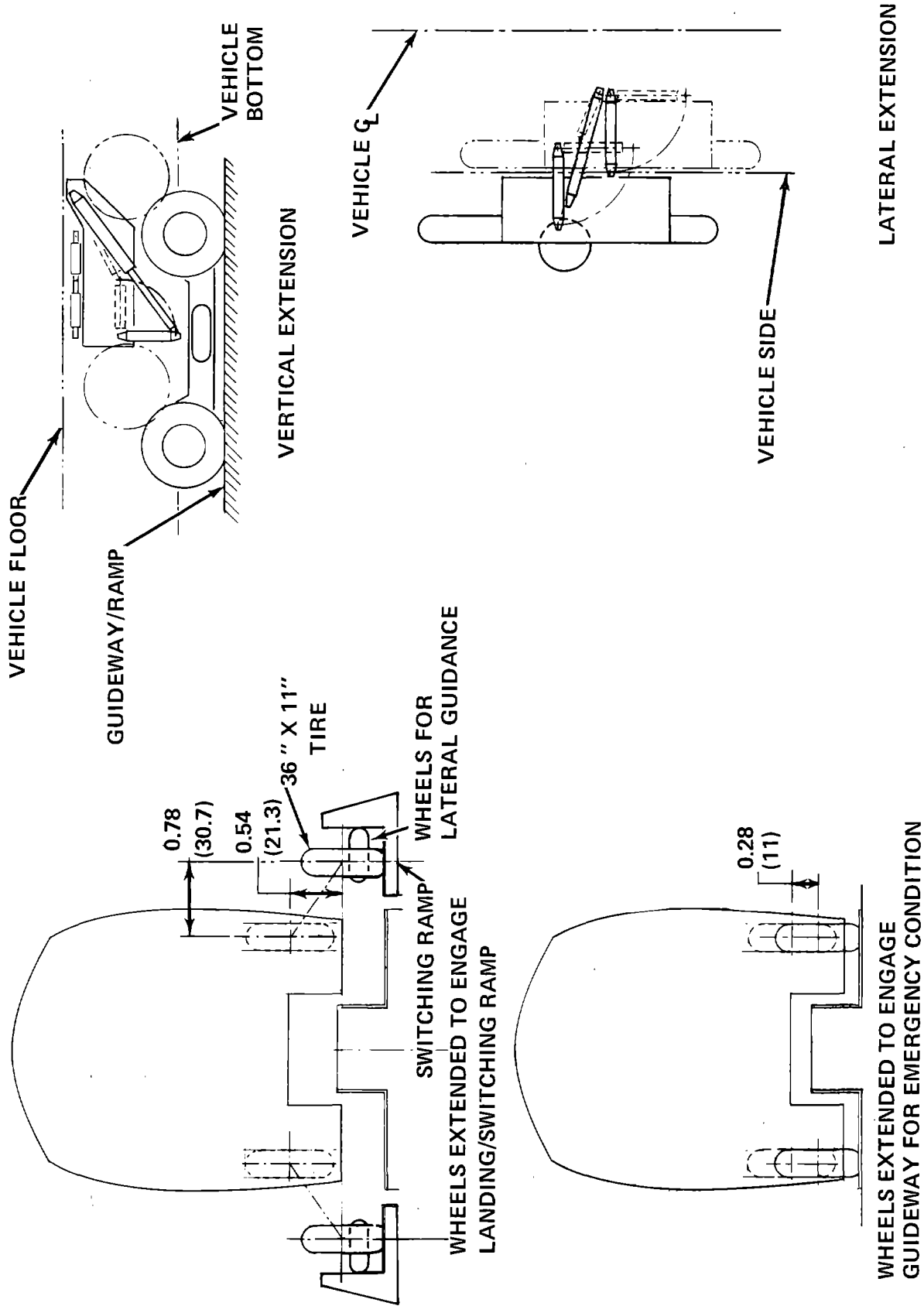
FIGURE 4-13. LANDING / SWITCHING GEAR ARRANGEMENT

back-up pneumatic system may be used for the rapid extension during emergency conditions. The entire system is estimated to weigh 19.6 kN (4,400 lb), based on aircraft landing gear design.

C. Brakes. Normal braking can be accomplished by reversing the pitch of the fan blades of the air propulsion system or by reversing the field of an electric motor. However, due to fuel consumption reasons, the air propulsion system will not be used for braking except in emergencies. Aerodynamic panels which extend into the airstream are the normal brakes for the baseline system. Typical deceleration calculations have been made to determine what size of aerodynamic panels are appropriate, based on the 0.15 g normal deceleration limit. The results were computed as a function of drag area of the brake (C_DA). Values of C_DA between 3 and 6 m^2 (30 to 60 ft^2) appear reasonable. A brake with $C_DA = 3$ m^2 reduces the stopping distance of the vehicle by 30% compared to a vehicle without an aerodynamic brake. For $C_DA = 6$ m^2 the distance is decreased by 44%. More rapid stops can be accomplished by varying the C_DA (modulating the panel position) so that a 0.15 g deceleration can be maintained at all speeds. Actuation of the panels will be accomplished with a hydraulic system. If all other systems fail to work properly, a back-up drag parachute may be used.

D. Auxiliary Power Unit (APU). Onboard power must be provided for lights, communication, control system, cryogenic refrigeration system, etc. The total power requirements are approximately 200 kW. This power could be provided by an alternator, gear-driven from the compressor shaft of one of the drive engines. If an electric propulsion system is used, the power can be provided from the wayside power rails via an electrical pick-up. For the baseline propulsion system, it was decided to use a separate APU incorporating its own small gas turbine drive. This system was chosen for maximum reliability in event of engine or power failure. It also has the advantage of more efficient operation during protracted idle conditions, e.g., long station dwell, turnaround, general maintenance operations, etc. The unit also contains the central hydraulic pump in addition to the alternator. High reliability, aircraft-quality gas-turbine APU packages are commercially available and directly suited to this application.

E. <u>Control and Communication</u>. The onboard control and communications equipment comprises the hardware defined in Figure 4-14. The basic control element is a stored program micro processor with up to 8K of memory operating at a cycle rate of approximately 1 MHz. This unit provides all of the requisite automatic flight control signals for vehicle operation. It receives inputs from the vehicle state transducers, the vehicle operator and the communications network. The state transducers provide information on the vehicle dynamic parameters required for active ride control. They also provide status monitoring of the onboard equipment for automatic housekeeping operations and for fault detection.

The communications network inputs in-station and en-route control information to the onboard computer from the wayside complex. It also transmits vehicle status information to the wayside.

The operator interface provides information to the operator display from the control computer and the vehicle state monitors. It also provides a means for the operator to input control instructions to the computer for in-station and en-route operations such as switching and main line ingress and egress.

The output of the computer comprises all of the static and dynamic control signals needed for vehicle operation. These signals are buffered in a Power Control Unit (PCU) and fed to the appropriate terminal devices. The PCU provides primary power to the various onboard elements in addition to the computer-generated control signals. Primary power switching, levitation magnet "charging," cryogenic refrigeration power, passenger-door operation, vehicle lighting, air conditioning, and passenger service communications are under manual operator control. Manual override of some of computer-generated control signals under some operational conditions is also provided. The manual override capability is constrained to those situations where the operator can be effective in real time control. These comprise terminal ingress, egress, switching, and emergency stop conditions. The latter case will involve operator actuation of special subroutines stored in the computer with direct manual control of the propulsion, wheels, and aerodynamic braking equipment.
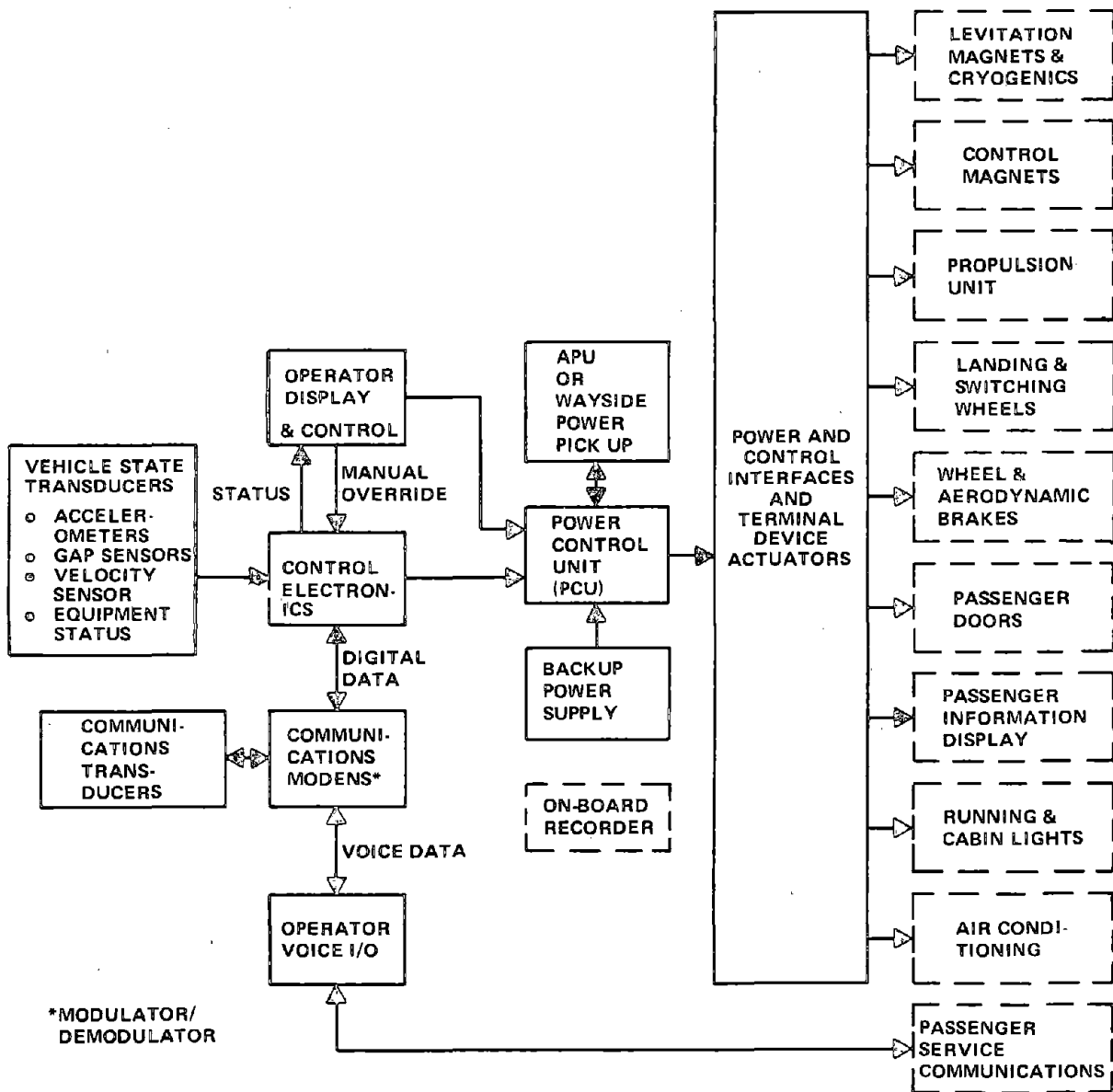
FIGURE 4-14. ON-BOARD CONTROL AND COMMUNICATIONS SUBSYSTEM BLOCK DIAGRAM

The vehicle control equipment will interface with the wayside complex via the communications transducers. The communications facilities will comprise a digital data link, a voice communications link, and any special links used for vehicle schedule control and vehicle safety. The digital data link provides a means to transmit route-control information to the onboard computer and to monitor vehicle status as noted previously. The voice link provides a direct channel for operator interface with the wayside complex to handle routine operational messages, passenger service communications, and emergency backup communications. The digital data link will be augmented with special links to control vehicle speed in real time from the wayside complex for schedule control and vehicle safety purposes. The latter function includes protection against foreign objects and inter-vehicle safety. These links will employ RF coupling to a combination of wayside antenna and cable networks.

4.3 SUSPENSION SUBSYSTEM

The suspension subsystem of the revenue vehicle consists of the superconducting levitation/guidance magnets, dewars and associated cryogenic system, helium liquifiers, control coils and control electronics. Also included are the details of the vehicle dynamics and control analysis (Section 4.3.2).

4.3.1 Superconducting Magnets and Associated Cryogenics

The levitation magnets selected for the suspension subsystem are flat, "racetrack"-shaped coils. More complicated shapes may ultimately be required if very stringent requirements for magnetic shielding of the passenger compartment are set. However, for the present requirements (Section 3.2.3C), a flat racetrack magnet with a shielding coil provides an acceptably low field in the passenger cabin. Parametric studies relating to coil geometry were carried out under an earlier contract (Ref. 4-22); these have been used in the present system studies to define a design which meets the overall system requirements. It was found that separate guidance coils are not required for the baseline concept; the levitation coil alone can supply an adequate guidance force provided it operates in the vicinity of the vertical leg of an L-shaped guideway element. In addition, calculations and experiments were carried out in an earlier study to determine the magnitude of the cryogenic loads due to projected thermal losses (Ref. 4-22 and 4-23).

A. Basic Magnet Design. Two important design parameters are the magnetic lift/magnetic drag ratio (F_L/F_D) and the lift/weight ratio (F_L/weight) of the suspension subsystem. Both of these parameters must be large to obtain a viable design. Large F_L/F_D leads to a magnet design with large aspect ratio (length/width). These narrow magnets can be used on a narrower "track" or guideway, and thus require less aluminum in the guideway. Although there is not a well-defined optimum size for the racetrack coils, consideration of the overall system parameters and requirements resulted in the selection of a coil geometry of 0.5 x 3 m at a nominal suspension height, h, of 30 cm. Approximately 3.5 x 10^5 ampere-turns are required to support one fourth of the weight of a 445 kN (100,000 lb) vehicle. Since the track width should exceed the magnet width by about twice the suspension height (2 h), narrowing the 0.5 x 3 m magnet will save some aluminum, but this small advantage is outweighed by the requirement for more magnet current to get the same lift (thus increasing magnet weight). An aluminum guideway composed of high electrical conductivity alloy (1100-type), 2.5 cm thick has been selected so as not to limit F_L/F_D at cruise speed by inadequate conductor thickness and resistivity. Tradeoffs of magnet performance, magnet size, conductor properties, etc., are discussed in Section 5.3.2.

A total of at least four magnets is required, one near each corner of the vehicle. However, to minimize the possibility of magnet failure and to increase system reliability, it is proposed that each 0.5 x 3 m superconducting coil be replaced by two 0.5 x 1.5 m coils, in tandem, with each coil in a separate dewar with separate refrigeration. It was shown in earlier studies that the long magnet can be replaced by two separate shorter coils with only a 5% reduction in F_L/F_D and a 3% loss in lift for high speed conditions when the coils are separated by 20 cm (Ref. 4-22). This is a small penalty to pay for the greatly increased reliability of a critical component.

Table 4-8 summarizes key magnet system characteristics and specifications. The nominal suspension height has been selected as 30 cm*, but a larger

---

*Defined as the distance from the center of the superconducting coil to the aluminum guideway. A nominal lateral guidance distance of 30 cm has also been selected. (See Figure 4-16.)

TABLE 4-8. MAGNET MODULE CHARACTERISTICS AND SPECIFICATIONS FOR BASELINE CONCEPTUAL VEHICLE

o NUMBER REQUIRED	4 MODULES
o COIL SIZE	0.5 X 3 M; TWO 0.5 X 1.5 M MAGNETS END-TO-END
o SUSPENSION HEIGHT	~ 30 CM
o LATERAL GUIDANCE DISTANCE	~ 30 CM
o AMPERE TURNS	~ 3.5 X 10^5 A-TURNS (NORMAL OPERATION)
LIFT TO DRAG RATIO FOR 1100 H14 ALUMINUM AT 134 M/S:	
INFINITE FLAT PLATE	61.7
CORNER (GUIDANCE FORCE = 0.36 F_L)	45.5
o LIFT TO WEIGHT RATIO	
WITHOUT SHIELDING COIL	20.5
WITH SHIELDING COIL	16.8
o CURRENT DENSITY	300 A/MM^2
o OPERATING CURRENT	1310A
o TYPE OF SUPERCONDUCTOR	NbTi MULTI-FILAMENT, TWISTED, LARGE – CORE BRAID
o PERSISTENT SWITCH RESISTANCE	$< 10^{-7} \Omega$
o HELIUM COOLING SYSTEM	GRAVITY FEED WITH 16 LITER CONTAINER
o MAGNET COIL SUPPORTS	LOW HEAT LOSS FOLDED EPOXY-FIBERGLASS COLUMNS
o CONTROL COIL	ALUMINUM WITH ~2 A/MM^2; FORCED AIR COOLING CAN BE PROVIDED, IF REQUIRED

suspension height will improve the ability to pass over objects on the track, reduce the aerodynamic drag of the underside and simplify some aspects of the dynamics/control problem. An increased suspension height, however, requires more magnet current to get the same lift. For example, F_L varies as $h^{-2.4}$ for constant current between h = 30 and 40 cm; thus it takes 1.41 times as much current at h = 40 cm to develop the same lift as at h = 30 cm. Since the amount of superconductor needed should be adjusted to an optimum current density, the h = 40 cm case will require more superconducting material, more structural material to accommodate the higher internal forces, and more cryogenic capacity. The 10 cm added height will roughly incur a 35% cost

increase for the magnets and refrigeration system relative to the baseline design. Furthermore, the magnetic fields will be 1.41 times higher and additional magnetic shielding will be required to obtain the same field level in the passenger cabin. On the other hand, a suspension height of 30 cm is near the minimum acceptable value since it is difficult to maintain adequate clearance between suspension system and guideway under various dynamic conditions for small distances.

B. Magnet Field/Shielding. Section 3.2.3C defined the recommended magnetic field limits as: 0.008 T (80 gauss) for the maximum whole body or head exposure for passengers and crew, and a maximum 0.02 T (200 gauss) at any point in the passenger cabin which is accessible to people.

The magnetic field at the guideway surface beneath the levitation coil must be in the vicinity of 0.1-0.5 T (1000-5000 gauss) in order to provide adequate magnetic "pressure" to support the vehicle. As a consequence, the magnetic field above and around the magnet is several orders of magnitude above ambient. For the worst case location, i.e., directly above the magnets, the results show that only a simple bucking-coil shield is needed to limit the average flux levels to the requirements given above. If substantially lower whole body exposure levels are required (e.g., 20 gauss), then passengers will not be able to sit directly over or within 1-2 m of the magnets*.

When the vehicle is in motion, circulating currents are generated in the guideway near each magnet which help shield the magnet. Thus, the magnetic field of the moving magnet is less than that of the stationary magnet. A very effective way (on a weight basis) to reduce the magnetic field above a coil is to use a bucking coil; if the main coil is located 30 cm above the conducting guideway, then an "optimum" bucking coil has the same dimensions as the main coil, has one-fourth the ampere-turns, and is located 30 cm above the main coil. This bucking weakens the lift force from the main coil slightly; it requires a 8.5% increase in the coil current to maintain the lift of an unshielded levitation coil.

_____

*Note that the baseline vehicle shown in Figures 2-1 and 4-1 have the magnets located at the ends of the vehicle so that the passenger seats are not above the magnets.

Figure 4-15 shows the magnetic field contours of the 0.5 x 3 m levitation coil in a longitudinal plane through the magnet (NI = 4 x 10^5 ampere-turns). The effects of the shielding coil and magnet motion are shown in the figure. The field contours were obtained from three-dimensional calculations of fields produced by currents in the main coil, bucking coil, and all developed "image coils". For the at-rest shielded case, the floor is at a maximum magnetic field level of 0.012 T (120 gauss), and the seat level at 0.007 T (70 gauss). However, a large majority of the time the vehicle will be moving, and the corresponding maximum shielded values are only about 0.0085 T (85 gauss) at floor level and 0.004 T (40 gauss) at seat level. Note that the field drops off rapidly in the longitudinal direction (and also in the lateral direction), therefore there is only a relatively small region above the magnets which are subjected even to these levels.

C. <u>Details of the Cryogenic Magnet Design</u>. The basic requirements for the levitation/guidance subsystem do not appear to offer unsolvable problems for superconductor/cryogenic technology. However, there are some areas of uncertainty, and what is vitally needed is a program to develop a practical, state-of-the-art levitation magnet — a new application with its own unique set of requirements. For example, magnet current densities of 300 A/mm^2 have been achieved in laboratory superconducting coils, and is felt to be a realistic value for the levitation magnets. Whether or not such high current density will create quench problems* because of the vibratory environment must be determined experimentally. If 300 A/mm^2 is not practical because the quench probability would be too large, more superconducting wire must be used. This will increase the magnet costs and magnet weight and reduce the magnet suspension height. For example, if 200 A/mm^2 is used for the operating current density of the magnet, the weight of the magnet module will increase by 8%, the costs by 16%, but the clearance will be reduced by only 0.35 cm. The cryogenic heat load will remain the same, but cooldown time will be increased by approximately 20%.

---

*Quenching is loss of the magnetic field when the superconductor is driven to the normal state.
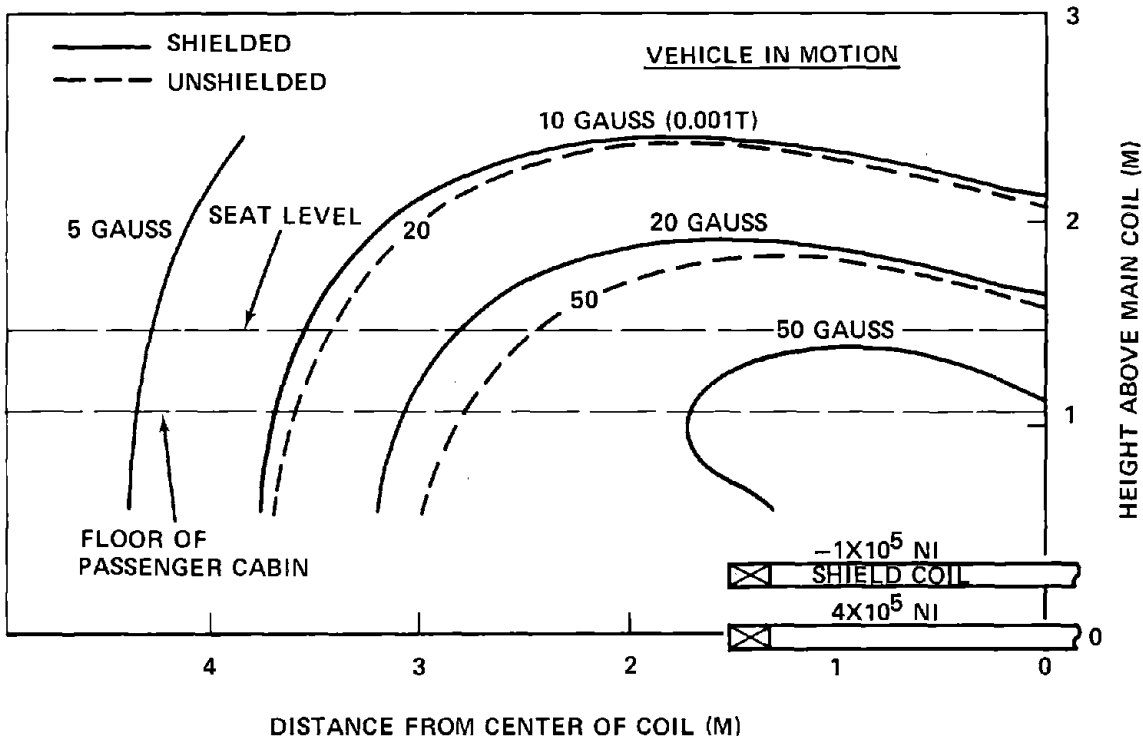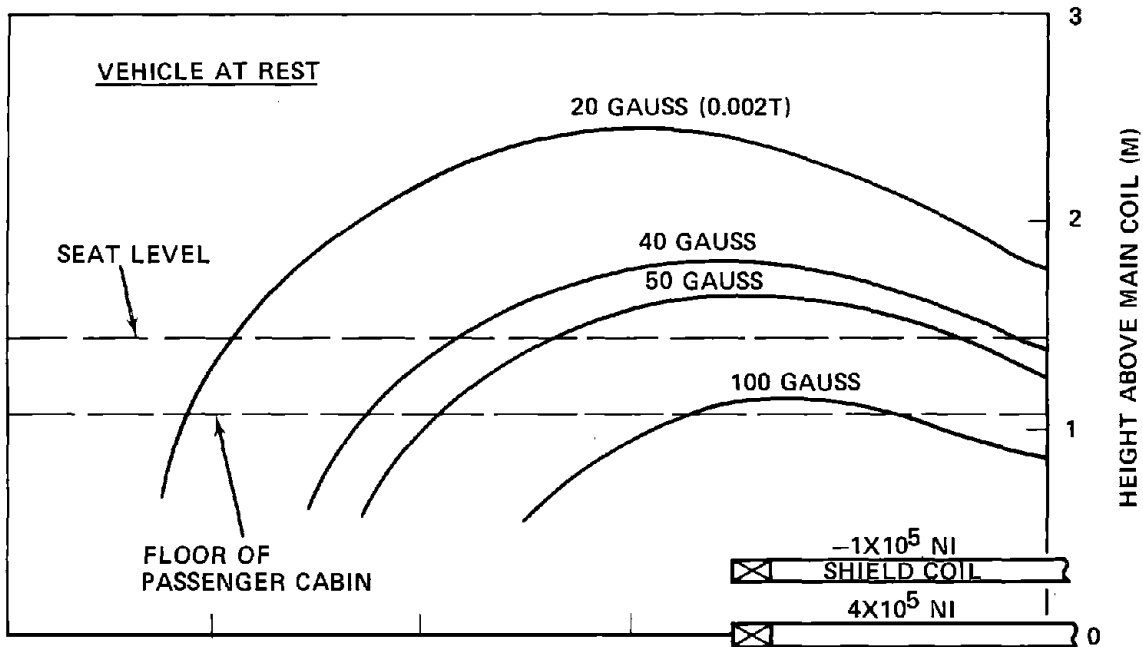
FIGURE 4-15. MAGNETIC FIELD CONTOURS

Another area of uncertainty is the important a.c. loss problem and its implication on superconductor design which is discussed below. Based on the potential problems, it is expected that several generations of experimental magnets will be required before acceptable low-weight, low-heat-leak, high-current-density magnets are available for a revenue vehicle. Note that the size of the magnets is of no concern. In fact, a number of large size super-conducting magnets are currently in operation and they work reliably (Ref. 4-24). Others in the advanced R&D stage are:

o Large bubble chambers in operation at high-energy physics installations all over the world. One of the largest (3.65 m dia.) has been on line at Argonne National Laboratory since 1967.

o Low speed homopolar motor. One such 3000 hp unit pumps water at the Fawley Generating Plant, England.

o Superconducting motors and generators being developed for the U.S. Navy and the electric utility industry.

o Immense plasma confinement magnets for fusion reactors.

The basic magnet/dewar designs and the cryogenic system specifications have been developed by Magnetic Corporation of America (MCA) with some inputs from Ford Motor Company (Scientific Research Staff). Discussions have also been held with Japanese scientists in the JNR MAGLEV program* concerning improvements in magnet design and construction. Based on these inputs, a conceptual design has been developed with and without a shielding coil.

Figures 4-16 and 4-17 show the cross section and the layout of the modular pair of unshielded magnets used for levitation and guidance. As discussed in Paragraph A, each module consists of two magnets, cryogenically isolated from each other, but which basically act like a single magnet. Each magnet is supported by six epoxy-fiberglass support columns which are canted as shown in the figures. Additional technical features of the magnet system are given in Table 4-9.

---

*Particularly, Professors T. Ohtsuka and Y. Ishizaki of Tohoku University and Tokyo University, respectively.

"FOLDED" SUPPORT COLUMN (G-10 IN COMPRESSION, STAINLESS STEEL IN TENSION)

3 CM SUPERINSULATION IN VACUUM REGION

SUPERCONDUCTING COIL (2.5 X 10 CM)

STAINLESS STEEL HELIUM AND COIL CONTAINER

COOLING PASSAGES

CONTROL COIL, AVAILABLE AREA ≅ 5 X 18 CM

LEVITATION COIL

VEHICLE SKIN

~22 CM

~19 CM

50 CM

2.54 CM

1100 AL

1.0 M

GUIDEWAY

~30 CM

~30 CM

50 CM
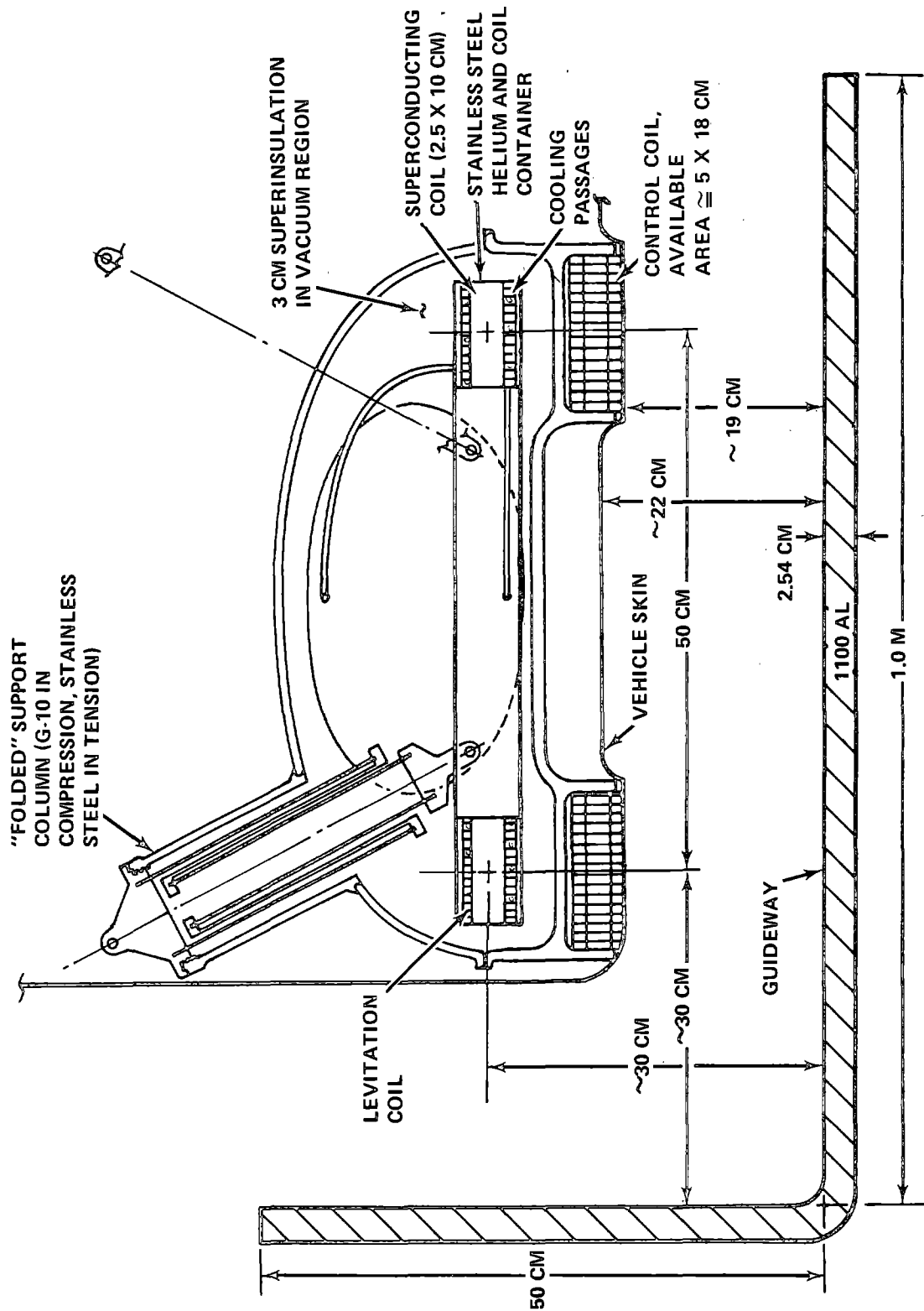
FIGURE 4-16. CROSS SECTION OF MAGNET ASSEMBLY WITHOUT SHIELDING COIL

WARM HE GAS
TO AND FROM SECOND
COMPRESSOR OR
REFRIGERATOR

MOTOR

310 CM

COMPRESSOR

REFRIGERATOR

~330 CM

VEHICLE

COAXIAL VAPOR-COOLED
HELIUM TRANSFER LINES
WITH SUPERINSULATION

LIQUID HELIUM TANK
FOR REFRIGERATOR
FAILURE

CRYOGENIC FILL
AND RETURN LINES

MAGNET CURRENT LEADS
(DISCONNECTIBLE WITH
PERSISTENT SWITCH)

SIX "G-10" FOLDED
SUPPORT COLUMNS
PER MAGNET

50

70 CM

FIGURE 4-17. LAYOUT OF LEVITATION MODULE (WITHOUT SHIELDING COILS)

TABLE 4-9. ADDITIONAL TECHNICAL FEATURES OF MAGNET MODULES

- REDUNDANT MAGNETS FOR SAFETY AND RELIABILITY

- HIGH-CURRENT-DENSITY, INTRINSICALLY-STABILIZED, SUPERCONDUCTING WINDING (300 A/mm^2)

- TWISTED, MULTI-FILAMENT, LARGE-CORE BRAID FOR LOW A.C. LOSSES

- SEPARABLE CURRENT LEADS FOR LOW-HEAT LOSS

- 3 cm SUPERINSULATION FOR RADIATION SHIELDING

- 16-LITER LIQUID HELIUM EMERGENCY STORAGE CONTAINER IN EACH DEWAR, GRAVITY FEED

- ALUMINUM OUTER CRYOSTAT

- MAGNETIC FIELD AND LIQUID HELIUM LEVEL INSTRUMENTATION

- MAGNET COOL-DOWN TIME ~ 16 HOURS

TABLE 4-10. MAGNET MODULE WEIGHTS AND HEAT LOSS

	WITHOUT SHIELDING COIL	WITH SHIELDING COIL
WEIGHT*		
Superconductor	757 N	947 N
Helium Container	300	410
Tension Plates	206	404
Outer Cryostat	1900	2250
Struts	181	272
Misc (Tubes, Leads, Persistent Switch)	200	250
Control Coil	928	928
Total (Module)	4472 N	5461 N
Total (Vehicle)	17.9 kN	21.8 kN
CRYOGENIC HEAT LOAD		
Radiation	0.5 W	0.8 W
Conduction	2.0	2.0
Current Leads	1.0	1.0
Cryogenic Lines	0.7	0.7
A.C. Losses	0.7	0.7
Total (Module)	4.9 W	5.2 W
Total (Vehicle)	19.6 W	20.8 W

*Values Adjusted for 366.5 kN Vehicle

Figure 4-18 shows a cross section of the baseline magnet design, i.e., the one containing a shielding coil. This design shows a different arrangement for the G-10, epoxy-fiberglass support columns. The main levitation/guidance coil is held in place by at least four vertical columns and four diagonal columns (two canted in the transverse direction and two canted longitudinally). Actually, the six-canted-column support structure shown in Figure 4-16 can also be used for the baseline design, but the cant angle and column positions must be modified in order that the columns clear the shield coil. The elevated shield coil is not attached to the outer cryostat, but is connected to the coil form of the main coil by lightweight tension members. The reserve liquid helium tank is not shown in Figure 4-18, although it will be used in an actual design.

Table 4-10 summarizes the weights of the various magnet components and lists the expected heat loads discussed in Paragraph D. The weights have been calculated for the baseline 366.5 kN vehicle rather than the preliminary weight estimate of 445 kN.

The G-10 (epoxy fiberglass) columns shown in the figures are folded to lengthen the thermal path and reduce the heat leak. Structurally, the G-10 is placed in compressive loading at 83 N/mm^2 (12,000 psi). This compares to the 140 N/mm^2 value for infinite fatigue life (Ref. 4-25). Dr. Y. Ishizaki of the University of Tokyo has noticed a "significant" increase in the thermal conduction of G-10 in a "loaded" condition (private communication). This subject needs further investigation to determine the heat losses through the folded columns under typical loads. Canting the column at approximately 30° minimizes the bending moments and maximizes the compressive loads on the column under stationary (non-dynamic) conditions. The use of superinsulation reduces the complexity of the module by eliminating the need for an intermediate temperature radiation shield. (The use of this type of shield is particularly troublesome since it must be strong enough to carry part of the transient dynamic loading of the magnet.)

The amount of superconductor required in the levitation magnet depends directly on the maximum current density which can be attained. As stated
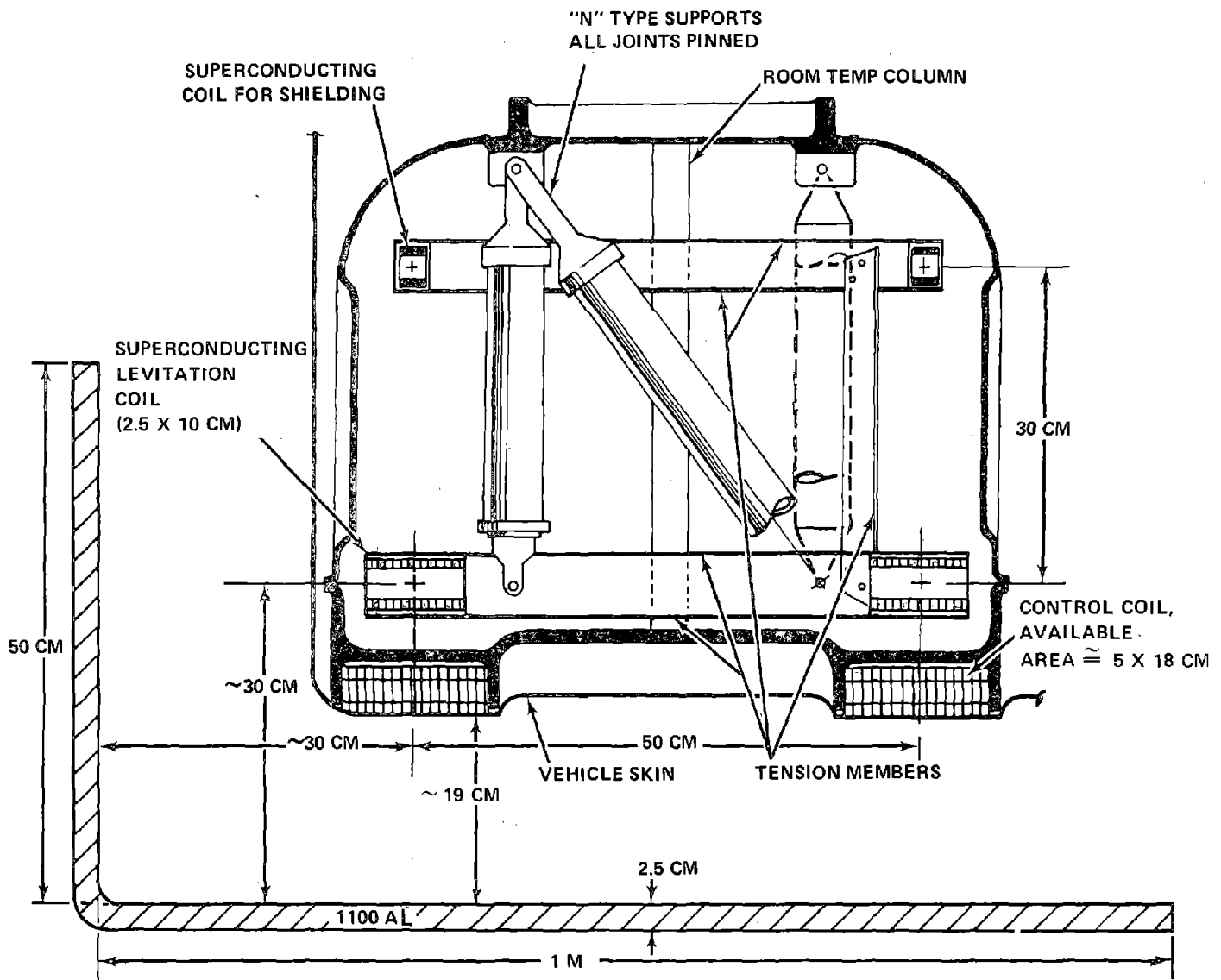
FIGURE 4-18. CROSS SECTION OF BASELINE MAGNET ASSEMBLY WITH SHIELDING COIL

above, superconducting magnets have been built and operated in a laboratory environment at design current density of 300 A/mm^2, but they have not been operated in the vibratory environment typical of a magnetically suspended vehicle. This is a subject for further development and test since the current density has substantial impact on magnet weight and cost; at 300 A/mm^2 the superconducting material is expected to account for 50 to 60% of the magnet cost.

Once the maximum practical current density has been established the current in the coil can be calculated for various operating conditions; typical values are shown in Table 4-11. Since the magnet is operating in persistent mode*, the flux linking the superconducting coil remains constant. Flux is proportional to inductance times current, and since the mutual inductance between the coil and guideway changes for different operating conditions, the current must also change. The maximum current of 420,000 ampere-turns shown for the worst-case condition determines the amount of superconductor required.

D. Cryogenic Heat Loads. The cryogenic heat loads can be broadly classified into three separate areas — radiation and conduction from external sources, and internal heat generation (a.c. losses).

(1) Radiation. Because of the large size of the magnets, radiation from the outer or room temperature container to the magnet container and the liquid storage vessel is the dominant effect for this type of heat load. Heat transfer through the superinsulation can be approximated empirically by a conduction-type equation (rather than radiation-type) of the form:

$$k \; A \; (T_1 - T_2)/\Delta \; t$$

where the k value for superinsulation is approximately 10^{-4}mW/cm-°K. The terms A, T, and Δt are area, temperature, and thickness, respectively. The

---

*Persistent mode operation of the levitation magnet refers to the energizing of the magnet from an external power supply and then providing a low resistance short (R < 10^{-7} Ω), usually at low temperature, across the magnet winding so that the external current supply can be disconnected. This low resistance, together with the inductance of the coil (0.2 H), results in a decay of the magnetic field with a time constant greater than 2 x 10^6 seconds.

TABLE 4-11. EFFECT OF OPERATING CONDITIONS ON THE CURRENT IN THE LEVITATION MODULE

(Persistent mode operation; F_L = 111 kN. Self inductance, L_O, = 182 mH)[1]

MODE	CURRENT (10^3 A-t)	HEIGHT (cm)	SIDE GAP (cm)	GUIDANCE FORCE, F_G (kN)
Normal Operation:				
● Initial Condition (Zero Speed)	358	–	–	–
● Nominal Guidance	393	30	30	40
One Coil Out:[2]				
● New Equilibrium	408	24.5	24.2	26
● At Largest Dynamic Excursion (Worst Case)	420	20.9	20.2	–

[1]L_O calculated for a coil with 270 turns and coil cross-section consistent with 300 A/mm^2 current density.

[2]See Section 4.3.6 for conditions.

baseline magnet module has an exposed surface at liquid helium temperature of 5 m^2 area, and a 3 cm thickness of superinsulation will result in a heat load of 0.5 watt per module. This value will be increased somewhat due to penetration of the superinsulation by current leads, struts and refrigeration tubing, and precautions must be taken to minimize the radiation load at these points.

(2) Conduction. Conduction of heat from high-temperature external regions into the cryostat can take place along the struts, current leads, and to a negligible degree along the instrumentation leads.

The heat losses down well-designed current-carrying leads is approximately 3xI watts, where I is in kiloamperes. This low value assumes the latent heat of the helium gas is used to cool the leads. Since the braided superconductor requires current levels of approximately 1300 amperes, persistent mode operation is necessary to minimize the heat loss associated with this current level. To reduce the heat load below that for persistent mode operation (∿ 1 watt), a mechanical disconnect should be incorporated inside the cryostat (probably

in the vacuum container). Then, the only heat input will be radiation between the disconnected leads.

The epoxy-fiberglass material used for the folded columns is very strong in compression and also has a very low thermal conductivity of 1.04 mW/cm-°K between 4°K and 80°K, rising to 5.2 mW/cm-°K at 300°K. These values are for no-load conditions and it remains to be determined what degradation, if any, is caused by loading. Thus even with a conservative stress design of 83 N/mm^2 (dictated by loading at the worst situation — one coil out, maximum dynamic excursion), the heat leak down the struts is predicted to be a relatively low 2 watts per module. Future designs may have part of the strut cooled to an intermediate temperature by, say, the warmed helium gas, and heat conduction loads of less than 0.2 watt could be expected for this type of design. Such an approach will only be recommended if the conduction heat leak is significantly larger than 2 watts, since this results in a more complex cooling system.

Compressed superinsulation has been used in some applications to transfer the levitation loads on the superconducting winding to room temperature structure (Ref. 4-27). However, the heat load using such a technique is predicted to be significantly larger than for the folded epoxy-fiberglass columns shown in Figures 4-16 and 4-18. Newer techniques using plastic honeycomb insulation (PHI) developed by Mitsubishi Electric Company show promise that cryostats of simple design with lift-to-weight ratios approaching 50 can be made, but at the expense of somewhat higher conduction heat loads.

(3) A.C. Losses. The third major loss — internal heat generation by a.c. losses — is more difficult to estimate because of the dependence on conductor design, the influence by the control coil and screening of the external fields by the outer cryostat. These losses can arise from flux flow through the superconductor (during current changes) as well as eddy current generation in the normal copper matrix, but the latter usually arises only during current oscillations with frequencies larger than that expected to be encountered in vehicle operation (i.e., greater than 10 Hz). It was shown experimentally in Ref. 4-22 that, because of the small oscillation of the

superconducting current about an equilibrium value, the choice of a large single-core superconductor could reduce the a.c. heat losses to 0.6 watt/ vehicle — several orders of magnitude lower than that expected for fine multi-filament wire. However, monofilament wire suffers from being less stable than twisted multi-filament wire, so that the selection of a particular supercon-ducting wire becomes a tradeoff. The choice of a braided cable where each strand is composed of one or several twisted filaments in a copper matrix appears to offer the best solution, but this approach must be tested experimentally.

E. Refrigeration Requirements. Figure 4-17 shows one refrigerator and compressor servicing the two modules at one end of the vehicle. This is a closed cycle refrigeration system in which the warm helium gas leaving the module is recompressed, liquified, and recirculated. Although the refrigera-tor should operate reliably with only routine servicing*, the baseline cryo-genic system is designed with liquid helium storage containers inside each magnet dewar. These 16-liter containers are large enough to allow a maximum 4-hour vehicle operation should refrigerator failure occur. These containers also enable transient heat loads, such as magnet energizing, to be more easily dissipated, and provide a measure of the cryogenic performance of each magnet by means of a liquid level detector. Each storage container forms part of the cryogenic circulation system, with liquid helium from the refrigerator first entering the shield coil, then the storage container. The main coil is served by gravity feed from the 16-liter storage container with vapor return lines from the main coil to the storage container.

An evaluation of the tradeoffs involved in providing onboard refrigera-tion has been undertaken by MCA. Examination of the type of cooling cycle (Claude vs. Gifford-McMahon), the number of refrigerators (one per module or one per vehicle), and number of compressors led to the following conclusions for system optimization. A single compressor serving two Claude cycle expan-sion engines located at the two ends of the vehicle (between the magnet

_____

*For example, the Cryogenic Technology model 1400 liquifier/refrigerator requires routine servicing only every 3000 hours.

modules) offers the best compromise in terms of heat load, efficiency, size, weight and cost; however, the second compressor is added for reliability. The system utilizes compressors already under development and refrigerators that are currently available and can readily be adapted to the required conditions.

A closed-cycle refrigeration system is our choice for large-scale MAGLEV applications in order to avoid handling cryogenic fluids. However, it is possible to operate the magnets in sealed cryostats (with no onboard refrigerator) for several hours with the internal liquid helium reservoir, or even for a whole day with a sufficiently large reservoir (Ref. 4-26). A reassessment of the need for an onboard refrigerator should be made after more experience has been obtained with the cryogenic problems of MAGLEV vehicles.

4.3.2 Vehicle Dynamics and Control

A. Introduction

(1) Definition of Problem. The suspension system of a MAGLEV vehicle must provide acceptable ride quality without excessive vehicle excursions (stroke) in response to transient excitations and low-frequency periodic disturbances. In principle, acceptable ride quality can be achieved with a sufficiently soft (low stiffness) suspension and/or with sufficiently high damping. The Repulsion MAGLEV concept is essentially a large gap, low stiffness system; the natural frequency of the baseline Revenue TMLV (without active control) is 1.41 Hz at the nominal 30 cm levitation height selected. However, for realistic guideway roughness levels,* the suspension is not sufficiently soft to meet the ride quality standards without damping, and since there is very little inherent damping in the system, some form of external damping must be provided.

Damping can be provided by passive means, e.g., with copper or aluminum plates inserted between the levitation magnets and the guideway. Prior Ford analysis, however, shows that there is a large weight penalty with this approach, and it cannot meet the DOT-specified ride quality standards unless the guideway is substantially smoother than the guideway used here, or unless

---

*The guideway design presented in Section 4.5.2 is characterized by a statistical roughness coefficient, A, on the order of 1.5×10^{-6} m (slightly better at long wavelengths).

the vehicle is limited to low-speed operation. Recourse must be made, therefore, to an active damping system. In addition, as shown later, an active control system can reduce the effective suspension system stiffness thereby improving ride quality as well as the ability to negotiate turns and grade transitions.

Prior Ford studies also show that the vehicle dynamic motion can be damped with a force proportional to vehicle velocity (rate damping), generated by means of a conventional electromagnet mounted external to the dewars, i.e., between the levitation magnet and the guideway. The control magnet interacts with the aluminum guideway elements and the levitation magnet field to alter the force-velocity relationship; the force-displacement relationship is altered to change stiffness. The control magnet current and polarity are varied subject to signals derived from onboard sensors and processed according to the particular control strategy selected. The major problem addressed in this study is the integration of a particular control strategy with the development of multi-degree-of-freedom analyses to ascertain vehicle dynamic response to random, periodic, and transient disturbances. The effort is scoped to determine a feasible conceptual control system design, rather than an optimum design based on broad parametric analysis.

(2) General Approach. A baseline control concept — derived from prior Ford and Philco-Ford studies — was selected for detailed evaluation. Absolute rate damping, i.e., relative to an inertial reference frame, is provided, employing feedback of vehicle (absolute) velocity derived from onboard accelerometer data. This inhibits the vehicle response to small amplitude, high frequency guideway irregularities and produces a good ride. The level of rate damping is optimized by adjusting the control system gain parameters to achieve damping ratios as near to critical damping as possible, while maintaining stability in all vehicle response modes and avoiding excessively high or low natural frequencies in any of these modes.

Positive position feedback is also provided, based on data relating vehicle position to the aluminum guideway surface and derived from body-mounted gap sensors. This reduces the effective suspension system stiffness thereby improving the ride.

Because inertial damping is used with this concept, there was initial concern that the vehicle might not negotiate turns and grade transitions

efficiently, i.e., with short transition lengths. (This presumes, of course, that short transition lengths are desirable, i.e., they result in a cheaper guideway — a presumption which may not be correct for many route specific situations.) Since grades and turns essentially produce large amplitude, low frequency vehicle excursions, the vehicle's ability to follow grades and turns should be improved by damping the vehicle motion relative to the guideway at low frequencies. This is accomplished by generating a damping force proportional to vehicle velocity relative to the guideway. The appropriate feedback signals are derived from the aforementioned gap sensor data. The resulting baseline system would then combine absolute rate damping (with a high-pass filter), relative rate damping (with a low-pass filter), and positive position feedback to produce good ride quality with improved ability to follow grades and curves. However, subsequent analyses showed that for the baseline concept and parameter values chosen herein, relative rate damping is beneficial only at very short transition lengths, well below the length required to hold maximum vehicle stroke below the design goal. The preferred baseline control concept, therefore, is defined as positive position feedback with filtered absolute damping only. The recommended damping ratios are in the range of 0.6 to 1.0, and the effective natural frequency is selected at 0.6 Hz. Also nonlinear feedback reduction is employed to assure stable operation in a transition to a downgrade. Further details of the baseline control concept are given in subsequent paragraphs of this section. Where possible, performance results are given both with and without relative damping.

Two alternate control strategies were briefly examined, primarily out of concern that reliable, accurate gap sensors might not be available for operation over a wide range of environments. These are: (1) a simple velocity feedback system with very high absolute (inertial) damping only, e.g., with damping ratios $\sim$ 3 to 4, but without position feedback or gap sensors (the system natural frequency is 1.41 Hz), and (2) acceleration feedback in combination with absolute velocity feedback using moderate damping ratios ($\sim$ 0.6 to 1.0). This second strategy eliminates the need for gap sensors, and has the added advantage of improved response to crosswind gusts by virtue of the increased apparent mass of the vehicle. The effective natural frequency of the suspension system for the second alternate system is 0.6 Hz.

(3) Study Results. Detailed results of the vehicle dynamics analysis are presented in subsequent sections of this report. A brief overview of the study results is given here to summarize important points.

Overall performance characteristics of the three control concepts are summarized in Table 2-1. The previously defined baseline position feedback system meets the DOT ride quality specifications in all dynamic modes for straight and level operations as well as for turns and grade transitions. Note that the power spectral density criteria are essentially inapplicable for turns and grade transitions, so only the DOT criteria on maximum sustained acceleration and rate of change of sustained acceleration (jerk) are employed. In negotiating a transition to a 2% grade, the vehicle maximum stroke* is less than the design goal of 5 cm for transition lengths of 1 km. With the amount of positive position feedback necessary to produce a vehicle heave frequency of 0.6 Hz, the force-displacement relationship indicates an unstable situation for upward excursions (transition to a "down" grade) greater than several centimeters. This instability is remedied by employing nonlinear feedback reduction for upward excursions. The baseline control concept can also negotiate horizontal turns, but modification of gain constants is found necessary to improve vehicle dynamic behavior. Further improvement (primarily in stroke) is possible, if necessary, by decreasing the amount of absolute damping** during transit through the turn. The necessary signals can be obtained by wayside communication or by increasing the capacity of the onboard computer and employing it (in conjunction with the existing accelerometers) as a simplified inertial navigator. For straight and level operation, the heave mode power consumption for the baseline concept is ~ 17 kW;

_____

*Stroke is defined as the vehicle displacement from its nominal steady-state position relative to the guideway surface. The physical clearance between the bottom of the control coil and the guideway is nominally 19 cm so the design goal of 5 cm maximum stroke is very conservative. Lateral clearance is nominally 23 cm, but the same design goal on maximum stroke is employed.

**The absolute damper (in combination with centrifugal force) is essentially trying to pull the vehicle toward the guideway during passage through a turn thus decreasing the clearance between the vehicle and the guideway.

total power consumption for all modes is estimated at ~ 25 kW. The short-time multi-mode power demand for negotiating a 1 km transition to a 2% upgrade is estimated at ~ 150 kW; comparable power for a down-grade is ~ 60 kW.

The alternative acceleration feedback concept dispenses with the gap sensor, but still meets DOT ride quality specifications for all dynamic modes and on turn and grade transitions as well as on straight and level portions of the guideway. A grade transition length of 6.5 km, however, is required to prevent vehicle maximum stroke from exceeding the design goal of 5 cm during approach to a 2% grade. Horizontal turn negotiation was not examined in detail, but it appears that vehicle dynamic response is somewhat better than with the baseline concept. Further improvement in stroke performance is achievable by reducing the level of absolute damping (during passage through the turn) in the aforementioned manner. Heave mode power consumption for straight and level operation is ~ 17 kW; total power consumption for all modes is estimated at ~ 30 kW.

The alternative heavy damping concept also dispenses with the gap sensor and meets the appropriate DOT ride quality criteria. For an absolute damper filter frequency of 0.6 Hz, a (2% grade) transition length of 4 km is required to prevent vehicle maximum stroke from exceeding the 5 cm design goal. Heave mode power consumption for straight and level operation is ~ 32 kW, total power consumption for all modes is estimated at ~ 50 kW. No evaluation has been made for horizontal turn negotiation, but no insurmountable problems are expected.

The foregoing brief review of the vehicle dynamic analysis indicates that all of the above systems are feasible and meet the appropriate ride quality specifications. The baseline concept permits much shorter grade transitions but requires gap sensors. Further analysis involving route specific considerations is obviously required prior to final system selection.

B. <u>Control Concept</u>. This section presents a general discussion of the baseline TMLV control concept and its alternatives. Details are given in Section 4.3.2C and Appendices B and C. The present discussion considers the following subjects:

- Feedback Logic

- Signal Filtering

- Signal Mixing

- Modal Gains and Control Current Commands

(1) <u>Feedback Logic</u>. In general, a control concept can provide for feedback of any combination of the following signals:

- Position relative to the guideway (gap)

- Inertial acceleration

- Velocity relative to the guideway (relative rate)

- Inertial velocity (absolute rate)

Positive position feedback is employed with the baseline concept to reduce the effective suspension system stiffness in order to improve ride quality. Another technique — inertial acceleration feedback — also improves ride quality, since it increases the vehicle apparent mass thereby reducing the suspension system natural frequency. This has the same effect as reducing the suspension system natural frequency with positive position feedback, except that the effect of magnet force nonlinearities is less significant with acceleration feedback than it is with positive position feedback. As stated earlier, acceleration feedback was subsequently considered as an alternative to the baseline position feedback concept.

Rate feedback is used to provide increased damping (above the level provided by passive damping forces). Absolute rate feedback is used to provide damping relative to an inertial reference frame in order to improve ride quality and is common to all control concepts studied. Relative rate feedback provides damping relative to the guideway and may improve the vehicle's ability to follow grades and turns. The final, preferred baseline control concept, however, does not employ relative rate damping, as discussed earlier.

(2) <u>Signal Filtering</u>. Tradeoff analyses were conducted both with and without relative damping which incorporate signal filtering. Signal filtering is employed to allow satisfactory ride quality to be achieved simultaneously with the ability to follow grades and turns. In essence, weighting of relative rate signals is increased at low frequencies to improve track-following ability, while weighting of absolute rate signals is increased at high frequencies to enhance ride quality. This is accomplished by providing a combination of absolute rate damping with a high pass filter and relative rate damping with a low pass filter.

(3) <u>Signal Mixing</u>. Accelerometers and gap sensors located on the vehicle near each of the magnet coil assemblies provide inertial acceleration and relative position measurements, respectively. Absolute and relative rate signals are derived from the acceleration and position signals. These signals are then modified by gain constants selected to achieve the desired combination of acceleration, rate, and position feedback. (Detailed discussion of gain selection is given in Section 4.3.2C. and in Appendix C.) The rate signals are then filtered as described above, and the acceleration, position, and filtered rate signals from each of the sensor locations are combined to generate "pseudo state variables." These pseudo state variables constitute a set of five signals, each of which relates exclusively to one of the five fundamental degrees of freedom (pitch, heave, roll, sway, yaw) of the vehicle. Thus, the pseudo state variables are basically modal signals, and the signal mixing process is essentially a Fourier decomposition of the filtered sensor signals into their fundamental modal content. (Details are given in Appendix B and Section 4.3.2C.). These modal signals are then further modified and operated on, as indicated below, in order to generate the ultimate control signals wh... establish the appropriate currents in the control coils.

(4) <u>Modal Gains and Control Current Commands</u>. The modal signals derived from the sensor signals are modified by individual "modal gain constants" to produce "modal control signals." The gain constants are selected so that these modal control signals ensure stability with adequate damping in all modes. The modal control signals are then recombined to generate individual control signals to each of the control coils. These control signals

establish current levels in the control coils which produce the appropriate combination of forces and moments to damp the vehicle motion in all modes. Details are given in Appendices B and C and the following discussion.

C. Dynamic Model. Modeling of vehicle dynamics and studies of stability characteristics are summarized in this section. Detailed derivation of the relevant equations is described in three appendices. Formulation of the magnetic force model is treated in Appendix A, derivation of the equations of motion including the control function is presented in Appendix B, and techniques employed for stability studies and selection of gain values are detailed in Appendix C.

(1) Vehicle Schematic and Dynamic Model. The vehicle is treated as a rigid body supported at four coil modules by forces and moments resulting from interaction of the levitation coils with a pair of L-shaped guideways. A control coil is placed at the bottom of each levitation module assembly to provide the requisite control forces for maintenance of vehicle stability and ride quality. Control current commands are generated through appropriate filtering and mixing of both acceleration information and relative displacement data at each of the coil assemblies. The eight sets of information are reduced to four separate current commands. A schematic for signal mixing and current command generation is shown in Figure 4-19.

The state of motion of the vehicle is defined in terms of five state variables which represent the following five rigid body degrees of freedom:

Z downward displacement of vehicle c.g.

θ pitching rotation about the body pitch-axis

Y lateral displacement of vehicle c.g.

Φ rolling rotation about the body roll-axis

ψ yawing rotation about the body yaw-axis

For vehicle operation at constant speed the equation for forward displacement of the c.g. along the direction of motion is a trivial identity defining the amount of thrust necessary to maintain the speed. A block diagram showing the interaction of control forces and passive magnetic forces with the vehicle is shown in Figure 4-20.

4-67

FIGURE 4-19. SIGNAL MIXING AND CONTROL
CURRENT COMMANDS SCHEMATIC

Due to the symmetrical placement of the four coil assemblies, there is no dynamic coupling between the (Z, θ) group of equations and the (Y, Φ, Ψ) group. This allows separate studies of vertical and lateral dynamics.
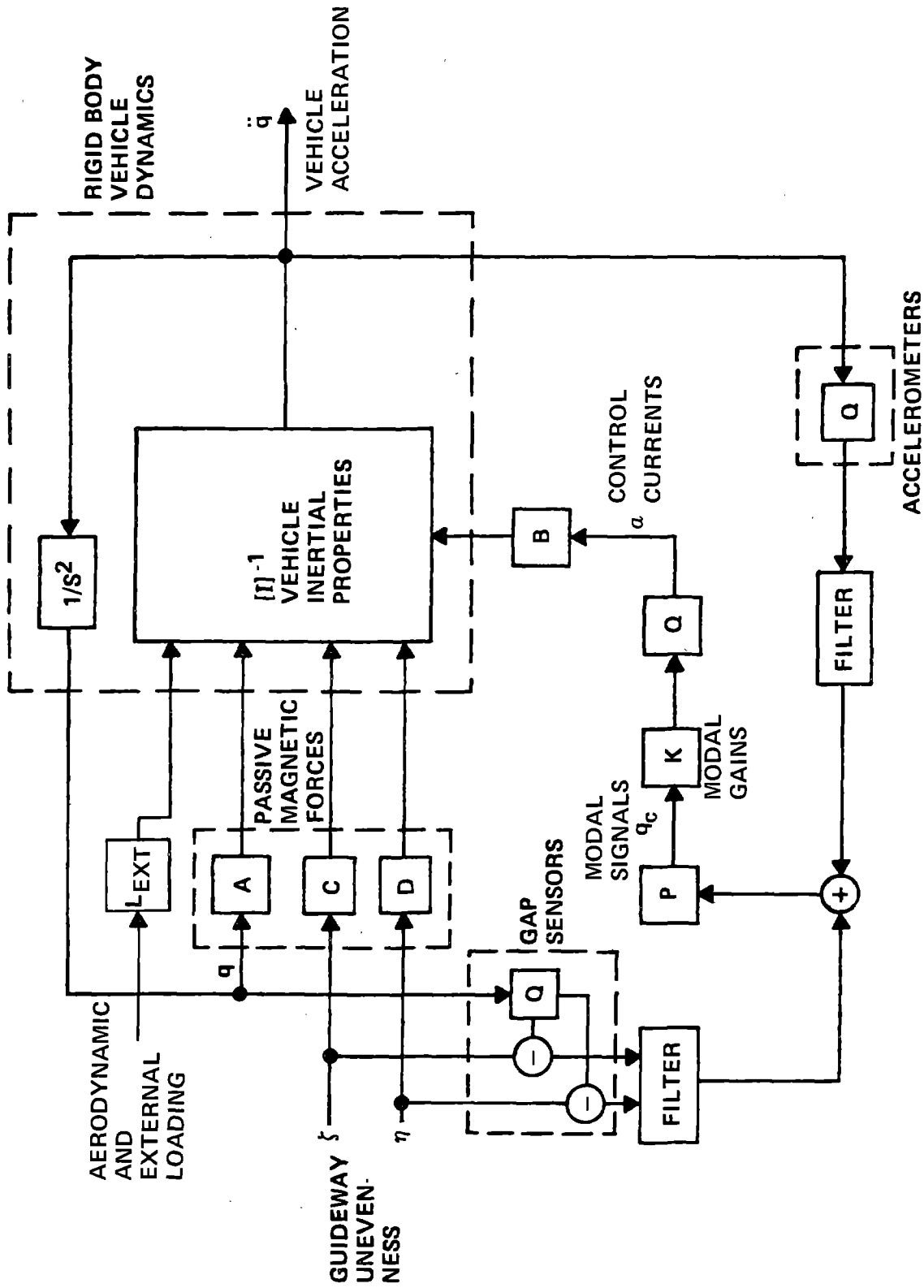
FIGURE 4-20. BLOCK DIAGRAM FOR TMLV CONTROL DYNAMICS AND RIDE QUALITY CHARACTERISTICS

The matrix equations defining the vehicle motion have the following form:

$$[s^2\ I_S - A_S + B_S\ Q_{SS}\ K_S\ K_{OS}]\begin{bmatrix} Z \\ \theta \end{bmatrix} = [B_S\ Q_{SS}\ K_S\ P_{SS}\ H_h + C_S]\ \zeta$$

$$+ [D_S]\ \eta + [L_S]$$

$$[s^2\ I_A - A_A + B_A\ Q_{AA}\ K_A\ K_{OA}]\begin{bmatrix} Y \\ \Phi \\ \Psi \end{bmatrix} = [B_A\ Q_{AA}\ K_A\ P_{AS}\ H_h + C_A]\ \zeta$$

$$+ [B_A\ Q_{AA}\ K_A\ P_{AA}\ H_{h'} + D_A]\ \eta + [L_A]$$

All matrices cited above are defined explicitly in Appendix B.

Note that in both groups of equations, dynamic coupling between the state variables of vehicle motion will vanish if the vehicle center of gravity lies in the plane of the coils (c=0) and if the vehicle center of gravity is at the midpoint between the front and rear coils ($a_F = a_R$). This suggests the possibility of simplified, approximate models in which the number of degrees of freedom is reduced by eliminating certain state variables. These simplified, approximate models are discussed in subsequent parts of this section.

Selection of control gain values is also discussed below.

(2) <u>Definition of Vehicle Parameters</u>. Mass properties and geometrical description of the preliminary conceptual vehicle configuration used in the vehicle dynamics calculations are summarized below:

m	vehicle mass	= 45400 kg (wt = 444.8 kN or 10^5 lb)
A	rolling moment of inertia	= 7.5×10^4 kg-m^2
B	pitching moment of inertia	= 3.4×10^6 kg-m^2
C	yawing moment of inertia	= 3.4×10^6 kg-m^2

These values were subsequently modified for the (lighter) baseline vehicle (baseline values are given in Section 4.2.4).

The vehicle is provided with four identical levitation coil assemblies. Each consists of two levitation coils end-to-end with overall centerline dimensions of 0.5 by 3.0 m and a control coil with identical centerline

dimensions, located 0.1 m below the levitation coil. The levitation coil is nominally located 0.3 m above the guideway surface with the center line of the nearside winding 0.3 m from the vertical surface of the guideway.

Positions relative to the vehicle c.g. are listed in Table 4-12 for individual coil modules and two other sets of related points. The thrust line is located at 2.72 m above the vehicle c.g. and it is assumed to be parallel to the direction of motion.

TABLE 4-12. COORDINATES OF MAIN COILS, VEHICLE EXTREMITIES, AND PASSENGER LOCATIONS*

	POSITION	INDEX	X	Y	Z	REMARK
MAIN COIL CENTER LINE	RIGHT FRONT	1	a_F	b	c	$a_F = 9.00$
	LEFT FRONT	2	a_F	$-b$	c	$a_R = 7.65$
	RIGHT REAR	3	$-a_R$	b	c	$b = 0.965$
	LEFT REAR	4	$-a_R$	$-b$	c	$c = 1.21$
VEHICLE EXTREMITIES	RIGHT FRONT	1	a_{VF}	b_v	c_v	$a_{VF} = 16.2$
	LEFT FRONT	2	a_{VF}	$-b_v$	c_v	$a_{VR} = 13.8$
	RIGHT REAR	3	$-a_{VR}$	b_v	c_v	$b_v = 0.55$
	LEFT REAR	4	$-a_{VR}$	$-b_v$	c_v	$c_v = 1.21$
CORNERS OF PASSENGER COMPARTMENT	RIGHT FRONT	1	a_{PF}	b_p	c_p	$a_{PF} = 8.2$
	LEFT FRONT	2	a_{PF}	$-b_p$	c_p	$a_{PR} = 11.2$
	RIGHT REAR	3	$-a_{PR}$	b_p	c_p	$b_p = 1.06$
	LEFT REAR	4	$-a_{PR}$	$-b_p$	c_p	$c = -0.39$

```
NOTE   X – AXIS     POSITIVE FORWARD
       Y – AXIS     POSITIVE TO THE RIGHT
       Z – AXIS     POSITIVE DOWNWARD
```

*VALUES FOR THE PRELIMINARY CONCEPTUAL VEHICLE USED FOR DYNAMICS AND CONTROL, STRUCTURES, AND AERODYNAMICS ANALYSES

(3) <u>Magnetic Force Model</u>. Forces and moments acting on a coil moving above a non-magnetic conducting medium are generated from interaction of current in the coil and an eddy current field created in the medium during the passage of the coil. Theoretical analyses and experimental measurements performed by the Scientific Research Staff of Ford Motor Company (Ref. 4-22) have established an adequate approach for the prediction of force and moment characteristics for rectangular coils moving at finite speeds over realistic guideway configurations. A detailed description of this approximate method may be found in Appendix A, including consideration of a control coil at a fixed distance from the levitation coil.

Pitching moment and yawing moments referred to the center of the main coil have been neglected in the derivation of the analytical force model for this study. This simplification is a good analytical approximation because amplitudes in pitch and yaw will be much smaller than amplitudes in roll due to the large longitudinal separation of the forward and rear coil assemblies compared to the lateral separation between the left side and right side coils. The magnet force components normal to the guideway surfaces and the rolling moment about the longitudinal axis through the center line of the main coil are given below in terms of coil orientation reckoned from its nominal position:

	Δh	$\Delta h'$	ϕ	α	X
$F_L = 1.1120(05)$	-8.9372(05)	+8.2437(04)	-1.2899(04)	+3.3981(05)	1
	-3.0328(06)	+2.4477(05)	+6.6260(03)	+2.7177(05)	α
	-2.6868(06)	+1.6119(05)	+2.9376(04)		α^2
$F_G = 3.9640(04)$	+8.2437(04)	-3.2430(05)	-4.7202(04)	+6.3715(04)	1
	+2.4477(05)	-5.4840(05)	-1.4250(05)	+2.7417(04)	α
	+1.6119(05)	-2.6359(05)	+9.2180(04)		α^2
$L = 1.1768(04)$	-1.2899(04)	-4.7202(04)	-2.3642(04)	+2.7473(04)	1
	+6.2601(03)	-1.4250(05)	-1.0240(05)	+1.4795(04)	α
	+2.9376(04)	+9.2180(04)	-1.0968(05)		α^2

The above values are for the preliminary conceptual vehicle of 444.8 kN (100,000 lb) gross weight and a speed of 134 m/s. The nominal position of

the coil assembly relative to the guideway is shown in Figure 4-21. The number of ampere turns in the main coil is $\sim 4.3 \times 10^5$ and the control current parameter α is the ratio of ampere turns in the control coil to that in the main coil.

The magnetically-induced drag force on each levitation coil module in a corner is given by the sum of F_L and F_G divided by 61.505, the value for lift/drag ratio for an infinite plate at a speed of 134 m/s. For speeds other than 134 m/s, the above result is multiplied by the ratio $F_{L,V}/F_{L,134}$. The variation of this ratio and the lift/drag ratio with speed is shown in Figure 4-23. The lift force capability of the levitation coil at 134 m/s and coil elevations other than 0.3 m is shown in Figure 4-22.

(4) <u>Nonlinear Magnetic Force Considerations</u>. Important considerations relative to magnet force nonlinearity are discussed in this paragraph.

The magnet force-displacement curve is quite nonlinear; hence, a linear approximation provides an accurate representation of force changes only over a very limited range of excursions from the nominal vehicle position. Figure 4-24 shows magnetic force characteristics with (0.6 Hz) and without (1.41 Hz) positive position feedback. It can be seen that without position feedback, a linear approximation results in errors exceeding 20% for excursions greater than about 3 cm from the nominal position. The errors are even larger with positive position feedback. This occurs because the slope of the force displacement curve is reduced by the position feedback. If linear feedback is employed, the nonlinear content of the force-displacement curve is unaltered, therefore, the nonlinear effect is larger relative to the linear term than without position feedback.

Furthermore, with the amount of linear positive position feedback required to produce a vehicle heave frequency of 0.6 Hz, the force-displacement relation indicates an unstable situation for upward excursions greater than several centimeters. This is shown by the dashed portion of the 0.6 Hz curve in Figure 4-24. This instability can be remedied by employing nonlinear feedback reduction for upward excursions, as indicated by the solid portion of the 0.6 Hz curve in Figure 4-24 to the right of the nominal 0.3 m elevation.
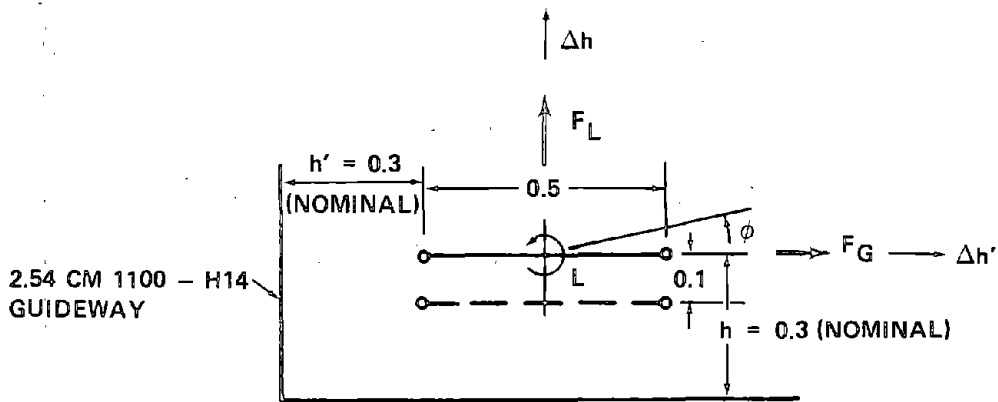
FIGURE 4-21. NORMAL POSITION OF COIL ASSEMBLY RELATIVE TO
GUIDEWAY
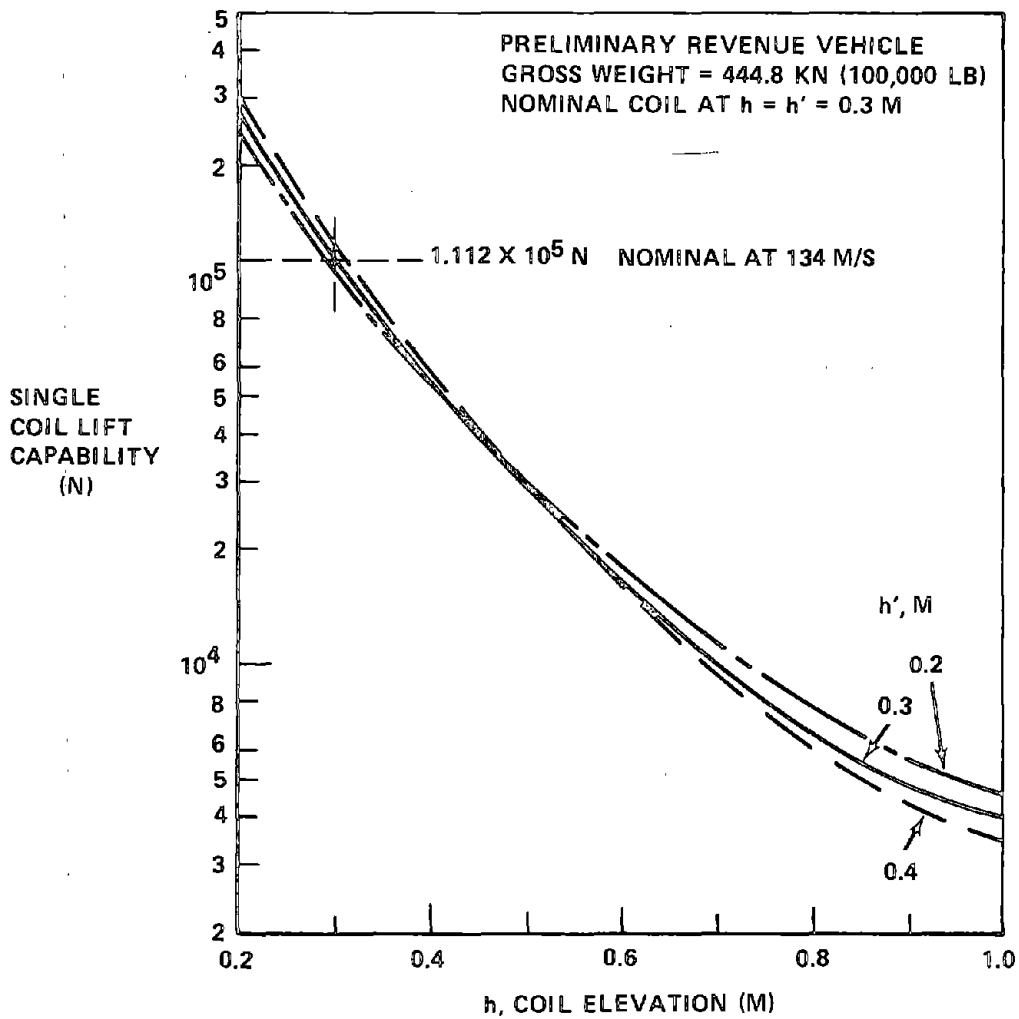
FIGURE 4-22. VARIATION OF COIL LIFT FORCE WITH
LEVITATION HEIGHT

VARIATION OF LIFT WITH SPEED

$\dfrac{F_{L,V}}{F_{L,134}}$

0.5 X 3.0 M COIL AT
0.3M ABOVE 2.54 CM
1100—H14 GUIDEWAY

134 M/S CRUISE SPEED

SPEED (M/S)

LIFT/DRAG RATIO

$\left.\dfrac{F_L}{F_D}\right|_\infty$ = 61.505 AT 134 M/S

$\left.\dfrac{F_L}{F_D}\right|_\infty$

V, SPEED (M/S)
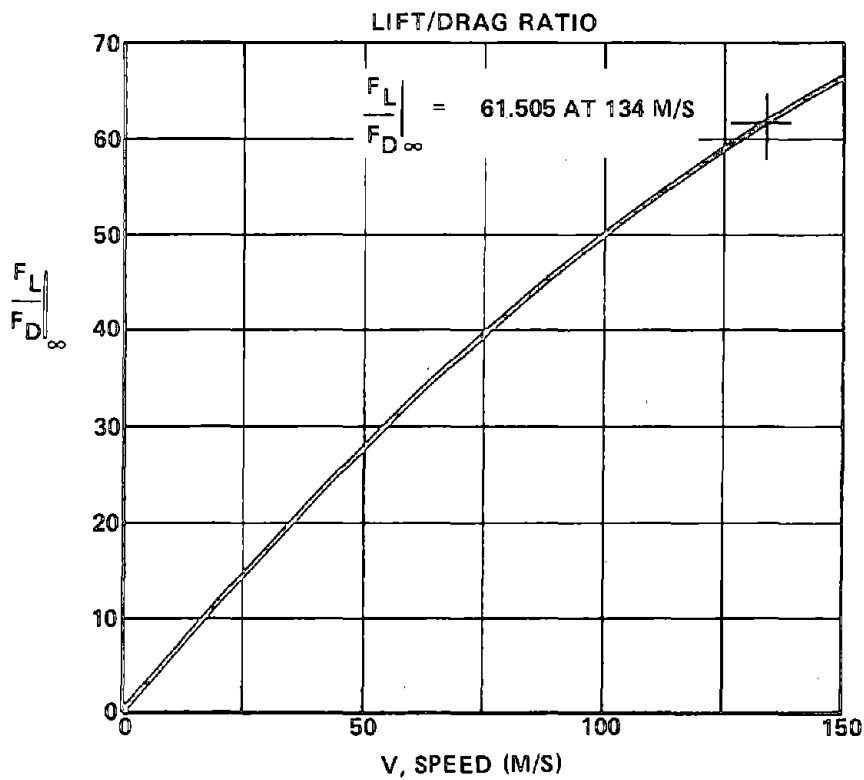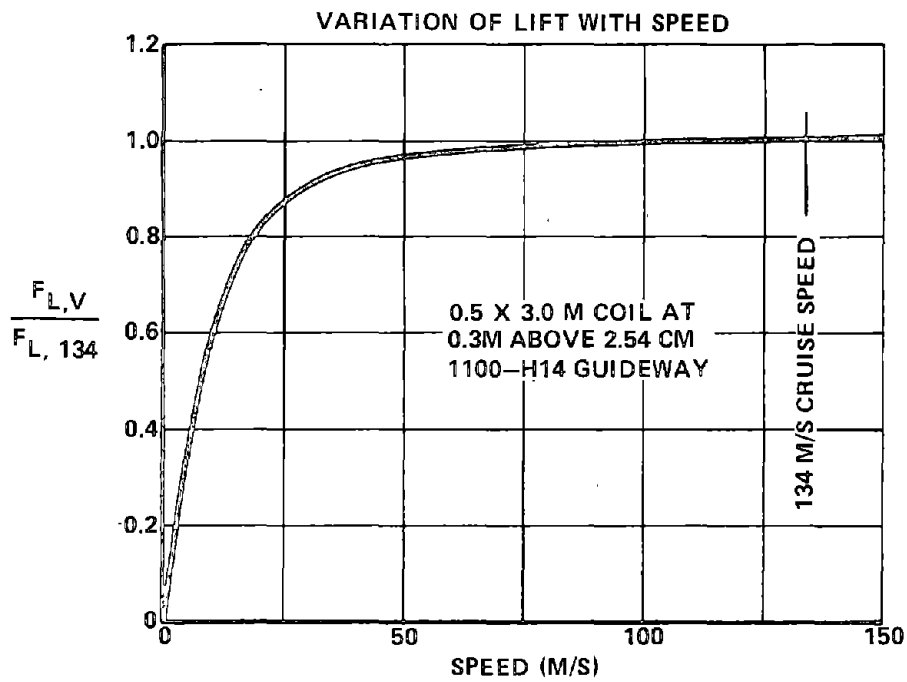
FIGURE 4-23.   VARIATION OF COIL LIFT FORCE AND
LIFT/DRAG RATIO WITH SPEED

4-75
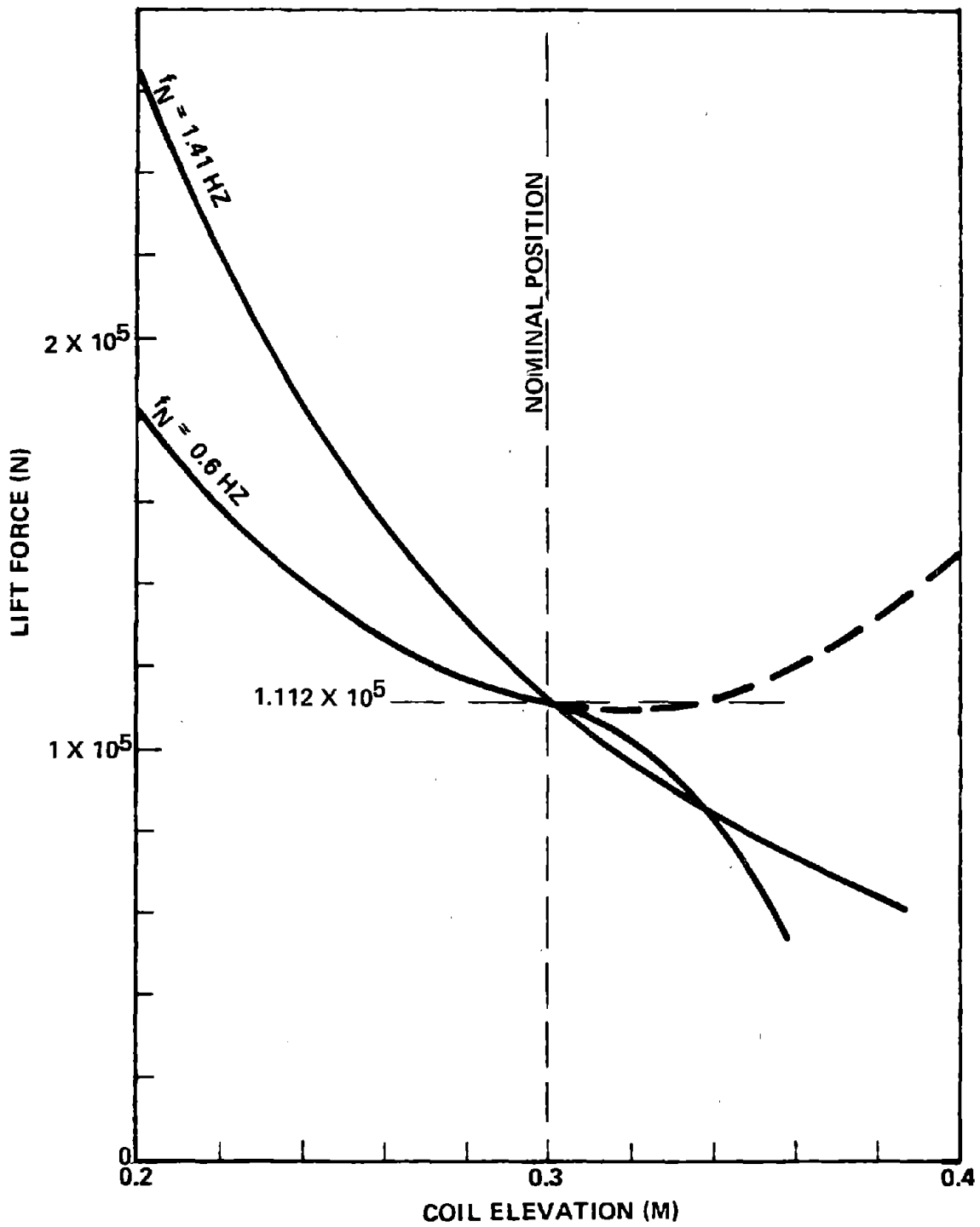
FIGURE 4-24. LIFT FORCE VERSUS COIL ELEVATION

The effect of nonlinear feedback reduction is shown parametrically in Figure 4-25. The value of the nonlinear feedback reduction parameter K_{h2} is selected on the basis of stroke limitation during negotiation of a grade transition; that is, the value of K_{h2} is selected so that the vehicle excursions from its nominal position while negotiating a grade transition is limited to acceptable values for grade transitions of reasonable length. In Paragraph 4.3.2D(2) it will be shown that a value of $K_{h2} = -2.5$ results in a stroke of about 4 cm for a 1 km grade transition, i.e., below the 5 cm design goal.

(5) <u>Simplified Heave Model</u>. A point mass heave model is obtained by retaining only the leading diagonal elements of the vertical equations developed in Appendix B. By virtue of the single mass point stipulation, guideway irregularities at all four coil locations must be identical, i.e.,

$$\zeta_1 = \zeta_2 = \zeta_3 = \zeta_4 = Z_g$$

The reduced equation and a formal solution for Z in terms of Z_g is given in Table 4-13. The functional relationships of various terms are also shown.

It is demonstrated in Appendix C that when the relative rate gain K_h and the absolute rate gain K_z take the same numerical value, the effect of the filter time constant can be ignored. An initial selection of gain values can thus be obtained from examination of the simplified heave model.

The following force coefficients apply for the preliminary conceptual vehicle:

$$F_{Lh} = -893720$$

$$F_{L\alpha} = 339800$$

The modal gain K_Z will be taken to be unity. For a vehicle weight of 444.8 kN, with both time constants set to zero it follows that

$$\frac{Z_1}{Z_g} = -\frac{K_h s + (K_h + 2.63)}{(0.0334 + K_z) s^2 + K_h s + (K_h + 2.63)}$$
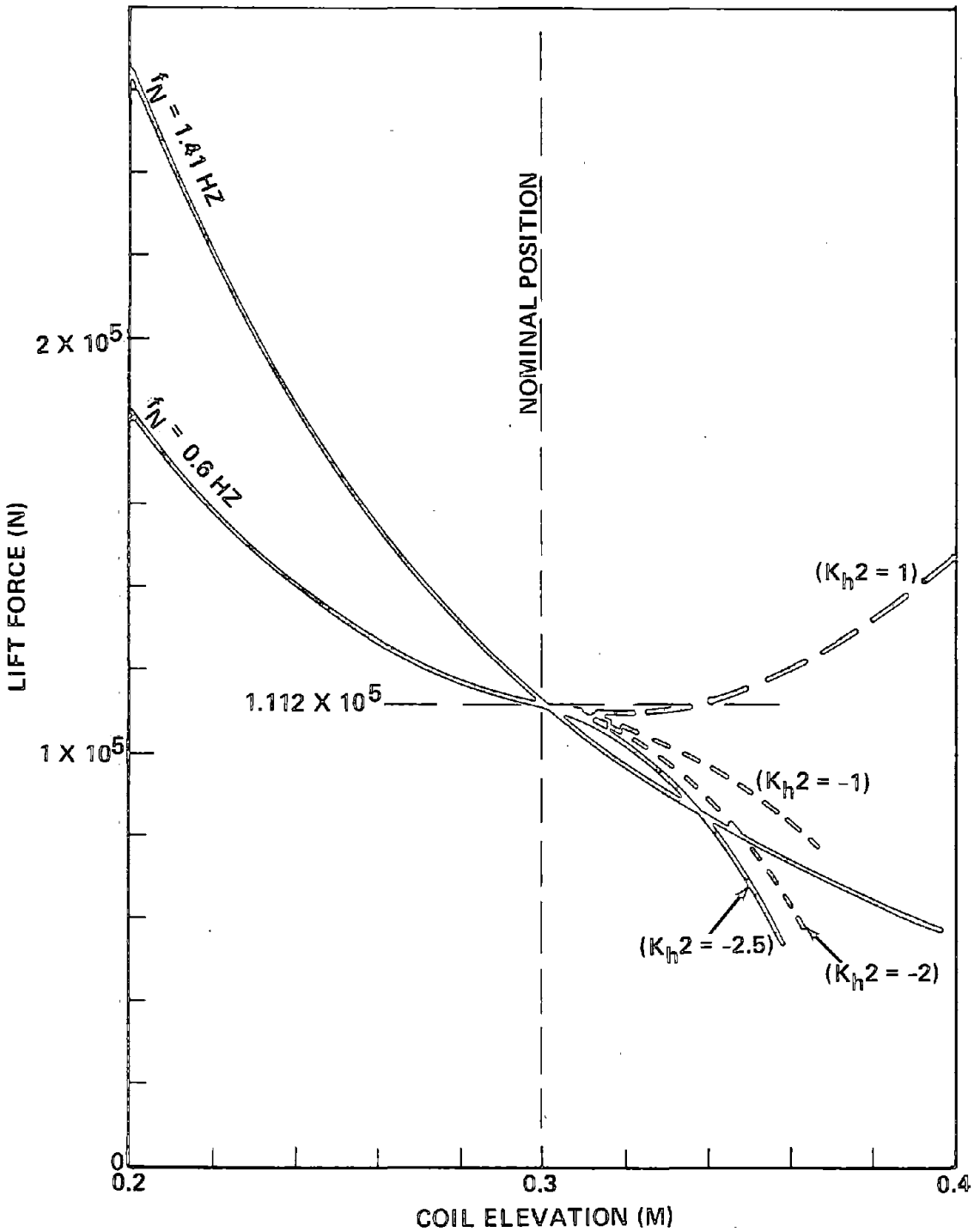
FIGURE 4-25. LIFT FORCE VERSUS COIL ELEVATION
(EFFECT OF NONLINEAR FEEDBACK REDUCTION)

TABLE 4-13. ONE DEGREE-OF-FREEDOM POINT MASS MODEL IN HEAVE

$$\left[ms^2 - 4F_{Lh} + 4F_{La}K_Z(s^2H_S + H_h)\right]Z = \left[4F_{Lh} - 4F_{La}K_Z H_h\right]Zg$$

$$H_S = K_{\ddot{z}} + \frac{K_{\dot{z}}\tau_Z}{1 + \tau_Z s} \; ; \; H_h = K_h + \frac{K_{\dot{h}}s}{1 + \tau_h s}$$

$$\frac{Z}{Zg} = -\frac{b_0 s^2 + b_1 s + b_2}{a_0 s^4 + a_1 s^3 + a_2 s^2 + a_3 s + a_4}$$

$$a_0 = \left(\frac{m}{4F_{La}K_Z} + K_{\ddot{z}}\right)\tau_h \tau_Z$$

$$a_1 = \left(\frac{m}{4F_{La}K_Z} + K_{\ddot{z}}\right)(\tau_h + \tau_Z) + K_{\dot{z}}\tau_h\tau_Z$$

$$a_2 = \left(\frac{m}{4F_{La}K_Z} + K_{\ddot{z}}\right) + \left(K_h - \frac{F_{Lh}}{F_{La}K_Z}\right)\tau_h\tau_Z + (K_{\dot{h}} + K_{\dot{z}})\tau_Z$$

$$a_3 = \left(K_h - \frac{F_{Lh}}{F_{La}K_Z}\right)(\tau_h + \tau_Z) + K_{\dot{h}}$$

$$a_4 = \left(K_h - \frac{F_{Lh}}{F_{La}K_Z}\right)$$

$$b_0 = \left(K_h - \frac{F_{Lh}}{F_{La}K_Z}\right)\tau_h\tau_Z + K_{\dot{h}}\tau_Z$$

$$b_1 = \left(K_h - \frac{F_{Lh}}{F_{La}K_Z}\right)(\tau_h + \tau_Z) + K_{\dot{h}}$$

$$b_2 = \left(K_h - \frac{F_{Lh}}{F_{La}K_Z}\right)$$

Previous studies have established that an undamped frequency of 0.6 Hz with 0.6 critical damping is desirable. Hence,

$$(K_h + 2.63)/0.0334 = (0.6 \times 2\pi)^2$$

$$K_{\dot{h}} = 2 \times 0.6 \sqrt{0.0334(K_h + 2.63)}$$

which results in

$$K_h = -2.1553 \qquad K_{\dot{h}} = 0.1511$$

The actual values used for subsequent analyses of ride quality are

$$K_{\dot{h}} = -2.155 \qquad K_{\ddot{h}} = 0.15$$

$$K_{\ddot{z}} = 0 \qquad K_{\dot{z}} = 0.15 \qquad K_{z} = 1$$

This completes the selection of gain values for vertical dynamics. Effects of varying the pitch mode gain K_θ have been presented in Appendix C, where it is shown that a value of $K_\theta = 1$ will produce acceptable stability characteristics.

(6) Simplified Sideway/Roll Model. A similar simplification of the lateral dynamics group leads to a sideway/roll model by ignoring the yaw variable. The resulting equations are displayed in Table 4-14.

(7) Gain Selection for Lateral Stability. In general, there will be three distinct natural frequencies in lateral dynamics (roll/sway/yaw). Gain values must be selected to ensure stability as well as to satisfy certain ride quality bounds for anticipated guideway irregularities. Attainment of the first objective of lateral stability calls for a systematic search for all relevant gain values for the lateral group, while accepting gain values already defined for the vertical group.

Due to the presence of time constants for signal filtering, the degree of the resulting polynominal is 12. This may be reduced to 9 by using the same time constant for all channels. Of these nine roots, three conjugate pairs pertain to lateral stability and the other three roots relate to the denominators of the filtering function. To ensure stability, all roots must have negative real parts.

The most direct search technique is to chart the movement of all roots as individual gain values are varied. In order to reduce the number of natural frequencies involved in the response analyses, it is also desirable to have at least one set of double roots among the selected conjugate pairs.

TABLE 4-14. TWO DEGREE-OF-FREEDOM MODEL FOR SIDESWAY / ROLL MODES

$$\left\{ \begin{bmatrix} m & o \\ o & A \end{bmatrix} s^2 - \begin{bmatrix} a_{yy} & a_{y\phi} \\ a_{\phi y} & a_{\phi\phi} \end{bmatrix} + \begin{bmatrix} 4\,K_y\,b_y\,\bar{K}_{oA} & 4cb_y\left[(K_y - K_\phi)K_{oS} - K_y\bar{K}_{oA}\right] + 4\,b_y\,K_y\,H_y\,g \\ 4\,K_y\,b_\phi\,\bar{K}_{oA} & 4cb_\phi\left[(K_y - K_\phi)K_{oS} - K_y\bar{K}_{oA}\right] + 4\,b_\phi\,K_y\,H_y\,g \end{bmatrix} \right\} \begin{bmatrix} Y \\ \Phi \end{bmatrix} = $$

$$\begin{bmatrix} 4\,K_y\,b_y\,H_{h'} + 4\,d_y & 4c\,(K_y - K_\phi)\,b_y\,H_h - 4\,bc_y + 4\,e_y \\ 4\,K_y\,b_\phi\,H_{h'} + 4\,d_\phi & 4c\,(K_y - K_\phi)\,b_\phi\,H_h - 4\,bc_\phi + 4\,e_\phi \end{bmatrix} \begin{bmatrix} y_g \\ \phi_g \end{bmatrix}$$

FOR

$$\begin{bmatrix} \zeta_1 \\ \zeta_2 \\ \zeta_3 \\ \zeta_4 \end{bmatrix} = \begin{bmatrix} o & -b \\ o & b \\ o & -b \\ o & b \end{bmatrix} \begin{bmatrix} y_g \\ \phi_g \end{bmatrix} \qquad \begin{bmatrix} \eta_1 \\ \eta_2 \\ \eta_3 \\ \eta_4 \end{bmatrix} = \begin{bmatrix} 1 & -c \\ -1 & c \\ 1 & -c \\ -1 & c \end{bmatrix} \begin{bmatrix} y_g \\ \phi_g \end{bmatrix} \qquad \begin{bmatrix} \phi_1 \\ \phi_2 \\ \phi_3 \\ \phi_4 \end{bmatrix} = \begin{bmatrix} \phi_g \\ -\phi_g \\ \phi_g \\ -\phi_g \end{bmatrix}$$

$$K_{oS} = s^2 H_S + H_h \qquad\qquad \bar{K}_{oA} = s^2 H_A + H_{h'}$$

$$H_S = K_{\ddot{z}} + \frac{K_{\dot{z}}\tau_z}{1 + \tau_z s} \qquad\qquad H_A = K_{\ddot{y}} + \frac{K_{\dot{y}}\tau_y}{1 + \tau_y s}$$

$$H_h = K_h + \frac{K_{\dot{h}}s}{1 + \tau_h s} \qquad\qquad H_{h'} = K_{h'} + \frac{K_{\dot{h}'}s}{1 + \tau_{h'}s}$$

$$a_{yy} = 4\,F_{Gh'} \qquad\qquad a_{y\phi} = a_{\phi y} = -4\,(b\,F_{Gh} + c\,F_{Gh'} + F_{G\phi})$$

$$a_{\phi\phi} = 4\left[\,b\,(b\,F_{Lh} + c\,F_{Lh'} + F_{L\phi} + L_h - F_{Go}) + c\,(b\,F_{Gh} + c\,F_{Gh'} + F_{G\phi} + L_{h'} + F_{Lo}) + L_\phi\right]$$

$$b_y = F_{Ga} \qquad\qquad b_\phi = -(b\,F_{La} + c\,F_{Ga} + L_a)$$

$$c_y = -F_{Gh} \qquad\qquad c_\phi = b\,F_{Lh} + c\,F_{Gh} + L_h$$

$$d_y = -F_{Gh'} \qquad\qquad d_\phi = b\,F_{Lh'} + c\,F_{Gh'} + L_{h'}$$

$$e_y = F_{G\phi} \qquad\qquad e_\phi = -b(F_{L\phi} - F_{Go}) - c\,(F_{G\phi} + F_{Lo}) - L_\phi$$

4-81

The above process has been carried out and a set of gain values has been found which will satisfy all stability requirements. These gain values are listed below:

	Vertical Channels	Lateral Channels
Modal Gains:	$K_z = 1$	$K_Y = 0.52$
	$K_\theta = 1$	$K_\phi = 1.25$
		$K_\psi = 3.5$
Abs. Rate Gain:	$K_{\dot{z}} = 0.15$	$K_{\dot{y}} = 0.29$
Acc. Feedback Gain:	$K_{\ddot{z}} = 0$	$K_{\ddot{y}} = -0.02$
Rel. Rate Gain:	$K_{\dot{h}} = 0.15$	$K_{\dot{h}'} = 0.29$
Pos. Feedback Gain:	$K_h = -2.155$	$K_{h'} = 0$

Undamped frequencies and system damping associated with the above set of gain values are:

0.515 Hz with 0.768 critical damping

0.734 Hz with 0.798 critical damping

1.016 Hz with 0.673 critical damping

A map of relevant roots in the vicinity of this region is shown in Figure 4-26. The points corresponding to the previously given set of gain values are shown circled in this figure. These values have been used for evaluation of ride quality discussed in Section 4.3.2D.

Further refined search revealed that a double root is located at $K_y = 0.5182$ and $K_{\dot{y}} = K_{\dot{h}'} = 0.2935$, corresponding to undamped frequencies and system damping of

0.60 Hz with 0.80 critical damping

1.02 Hz with 0.68 critical damping

These are shown as double circles in Figure 4-26.

A systematic process is presented above for the selection of gain values to ensure vehicle stability. However, additional iterations and search may

$K_h' = 0$ $K_{\dot{y}} = -0.02$ $K_\phi = 1.25$

$\tau_h' = 0.637$ $\tau_y = 0.637$ $K_\psi = 3.5$
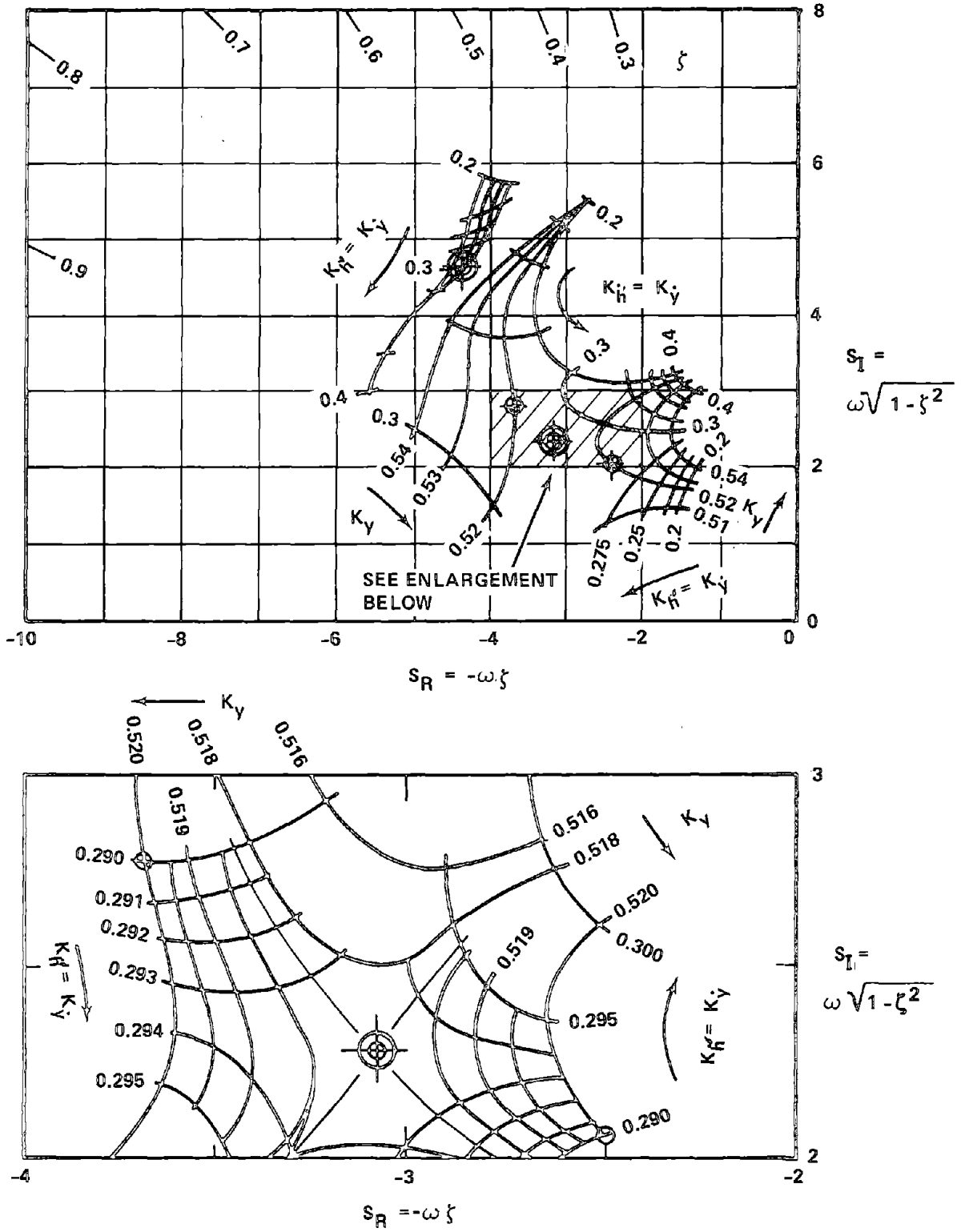
FIGURE 4-26. EXAMPLE OF LATERAL MODE PARAMETRIC STUDY

be needed to fulfill all other ride quality specifications and dynamic response limitations (e.g., stroke restrictions) imposed on the vehicle design.

D. Vehicle Response to Random and Periodic Guideway Disturbances. This section presents the results of an analysis of vehicle dynamic response to guideway random irregularities and periodic disturbances. The analysis provides an assessment of ride quality, stroke (vehicle excursion from its nominal position relative to the guideway), and control power requirements. A 1 DOF (heave) model is utilized for broad parametric studies, and a multimode (5 DOF) model is employed for detailed analyses of the dynamic response of the preliminary vehicle configuration.

(1) Single-Degree-of-Freedom Dynamic Studies. A 1 DOF (heave) model has been utilized for parametric investigation of vehicle dynamic response to guideway random irregularities and also for analysis of vehicle response to certain guideway periodic disturbances. The following analytical investigations were performed:

- Effects of position feedback and damping

- Effects of filter parameters

- Response to guideway roughness during negotiation of a grade transition

- Response to periodic gaps in the guideway

- Response to flexible guideway deformations

The results of these dynamic analyses are presented in the following sections. All analytical results are based on a guideway random roughness power spectral density (PSD) relation of the form $A\lambda^2$, where λ is the spatial wavelength and the roughness coefficient A is taken to be 1.5×10^{-6} m (5 $\times 10^{-6}$ ft).* This expression is believed to be inaccurate, however, for characterizing real guideways at long wavelengths of interest (or frequencies ≤ 2 Hz). Accordingly, investigations were conducted to assess the influence of roughness roll-off in this frequency domain.

---

*Although only a single value has been used for A, the PSD and rms values for acceleration, gap, current, power, etc., scale as a function of A, thus it is easy to extrapolate the results to other values.

a. <u>Effects of Position Feedback and Damping</u>. This paragraph discusses the effect of position feedback and damping on ride quality, stroke, and power requirements.

The natural frequency of the baseline MAGLEV suspension without position feedback is 1.41 Hz. Positive position feedback is employed to lower the suspension natural frequency and thereby improve ride quality. Figure 4-27 shows the effect of suspension natural frequency (f_N) on ride quality. The acceleration PSDs shown in this figure were calculated using a 1 DOF (heave) dynamic model with absolute (ζ_A) and relative (ζ_R) damping ratios equal to 1.0, and with filter corner frequencies* equal to 0.25 Hz.

It is seen from Figure 4-27 that the heave mode acceleration PSD exceeds the DOT ride quality specification in the vertical direction if the suspension frequency is greater than about 0.95 Hz. The ride quality specification can be met with higher values of the suspension natural frequency only if the absolute damping ratio is increased, as shown in Figure 4-28. This will be discussed in more detail below.

A suspension natural frequency of 0.6 Hz was selected for the baseline control concept. As seen in Figure 4-27 this provides some margin to allow for multimode (pitch-roll-heave) dynamic response effects without exceeding the ride quality specification.

Figure 4-28 shows the effect of damping on a system without position feedback (suspension frequency = 1.41 Hz). Acceleration PSDs are shown for several values of the absolute damping ratio, with the relative damping ratio equal to zero. (A gap sensor, which provides the relative rate signal required for relative damping, probably would not be used in a system without position feedback.) It is seen from Figure 4-28 that a damping ratio of 3 or 4 is required to meet the ride quality specification with some margin to allow for multimode dynamic response effects.

Figure 4-29 shows the effect of damping on the ride quality of the baseline control system with position feedback (suspension frequency = 0.6 Hz). It is seen that acceptable ride quality in the heave mode is obtainable over a wide range of damping ratios.

----

*The corner frequency is where the filter is rolled off.
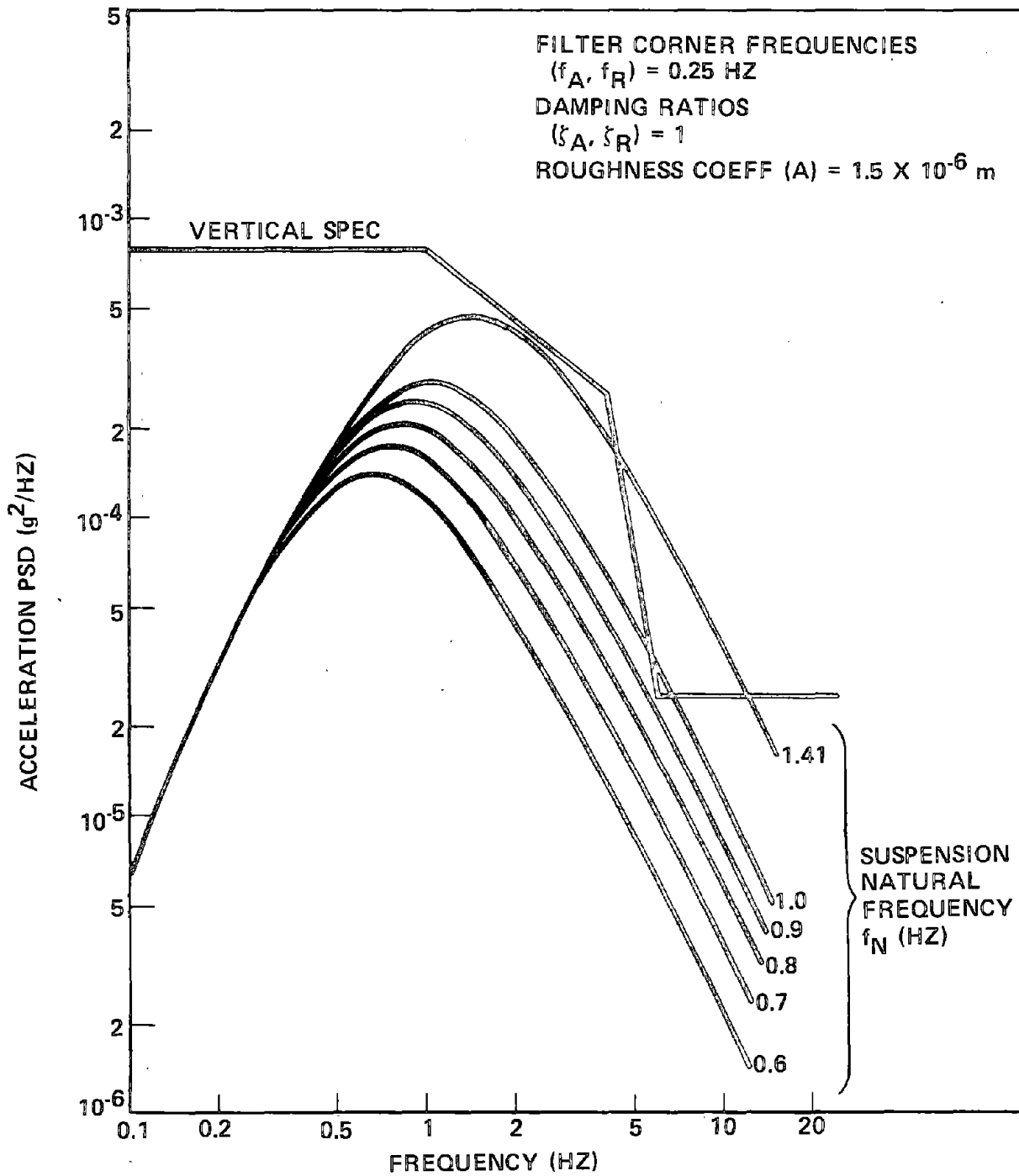
FIGURE 4-27. ACCELERATION POWER SPECTRAL DENSITY (PSD)
VERSUS NATURAL FREQUENCY

4-86
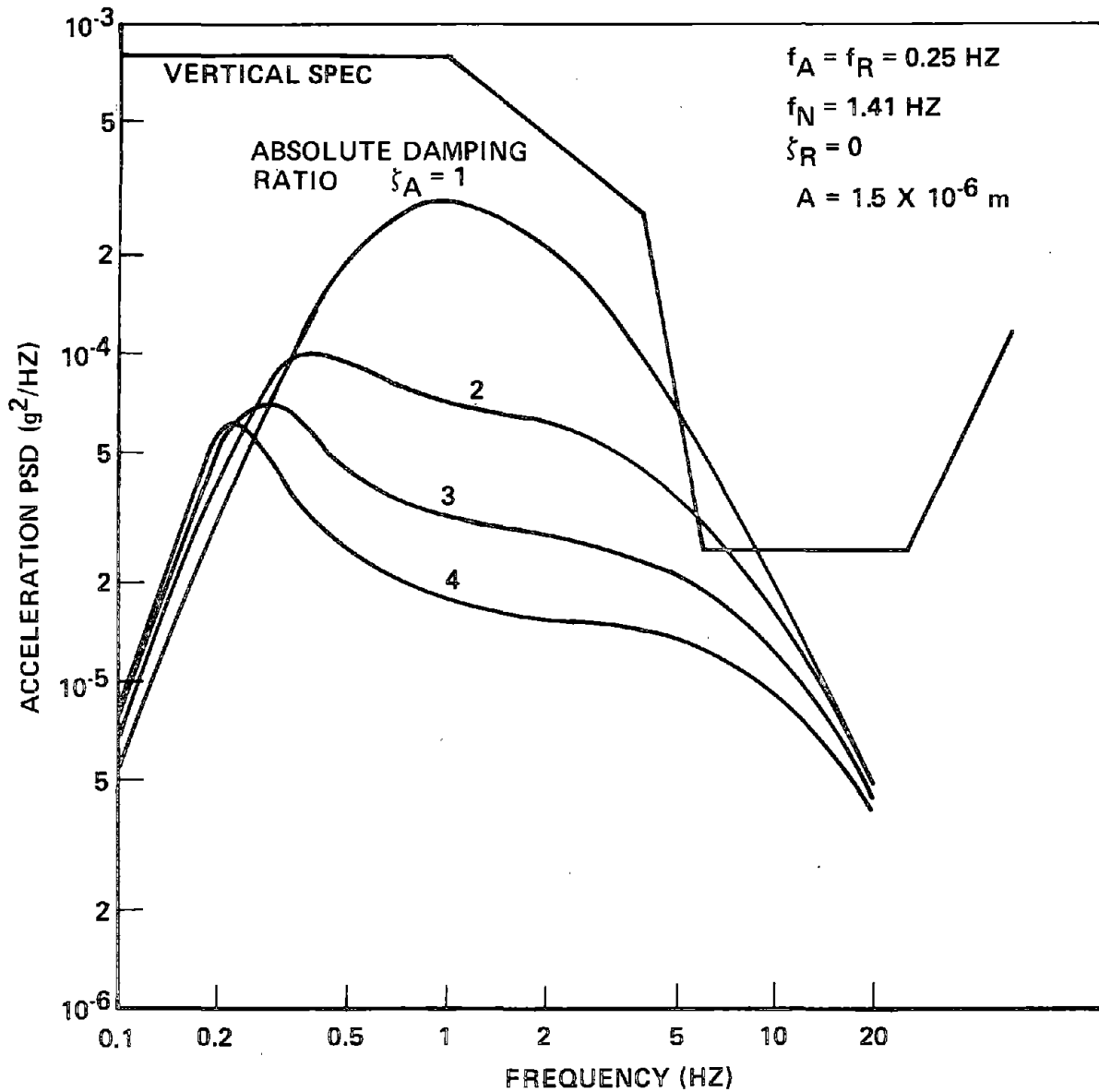
FIGURE 4-28. ACCELERATION PSD VERSUS ABSOLUTE DAMPING RATIO WITHOUT POSITION FEEDBACK
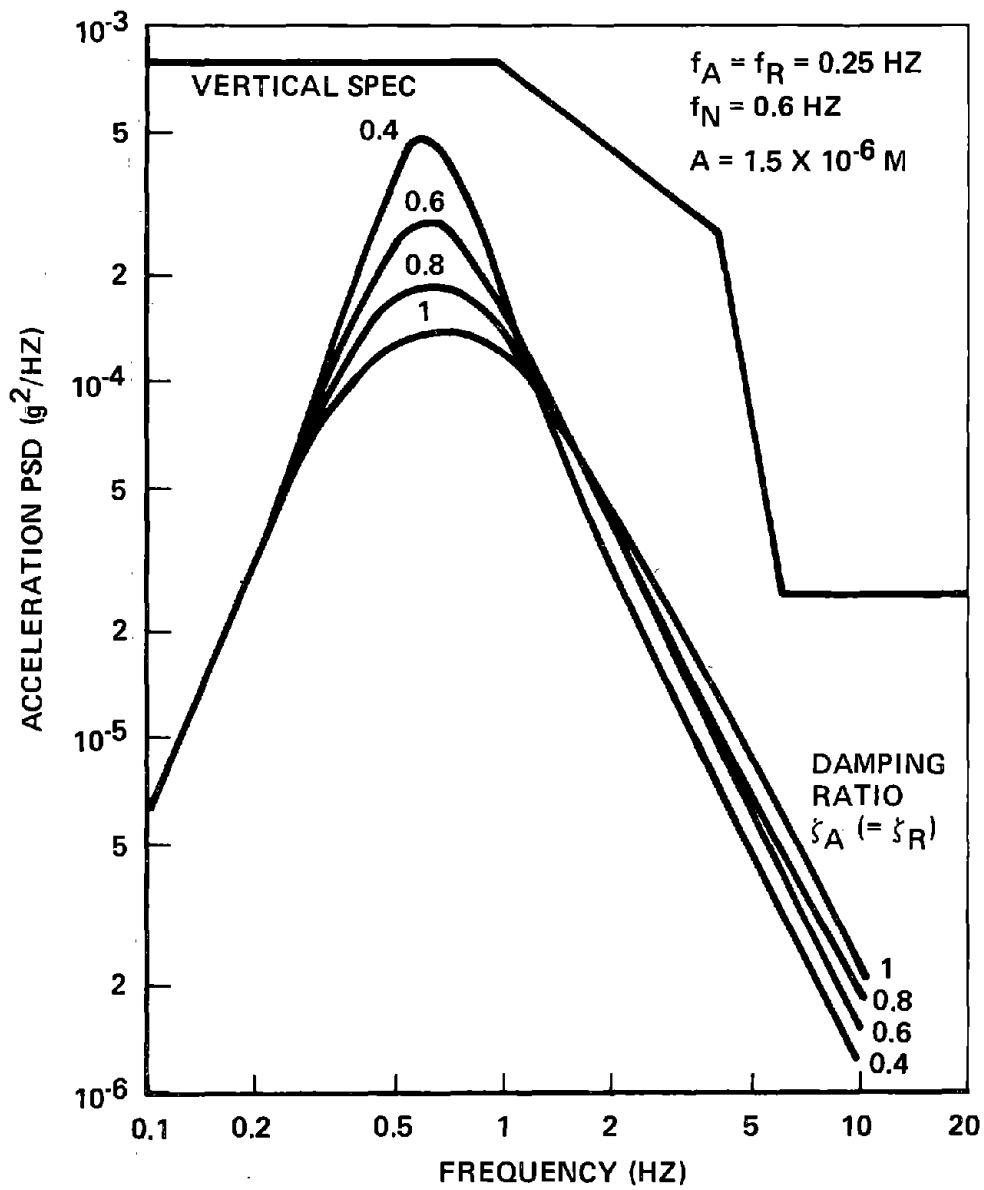
FIGURE 4-29. ACCELERATION PSD VERSUS DAMPING RATIO WITH POSITION FEEDBACK

4-88

Figure 4-30 shows the effect of damping on the rms stroke characterizing the vehicle response to guideway roughness. Curves of rms stroke vs. damping ratio are shown both for a system with (0.6 Hz) and a system without (1.41 Hz) position feedback (i.e., gap sensor). For a system without position feedback the rms stroke is somewhat higher at the higher values of damping required for acceptable ride quality. However, even without position feedback the rms stroke is only 1.7 cm or less.

Figure 4-31 shows that the ride quality of the baseline system is improved by eliminating relative damping. Relative damping can improve the
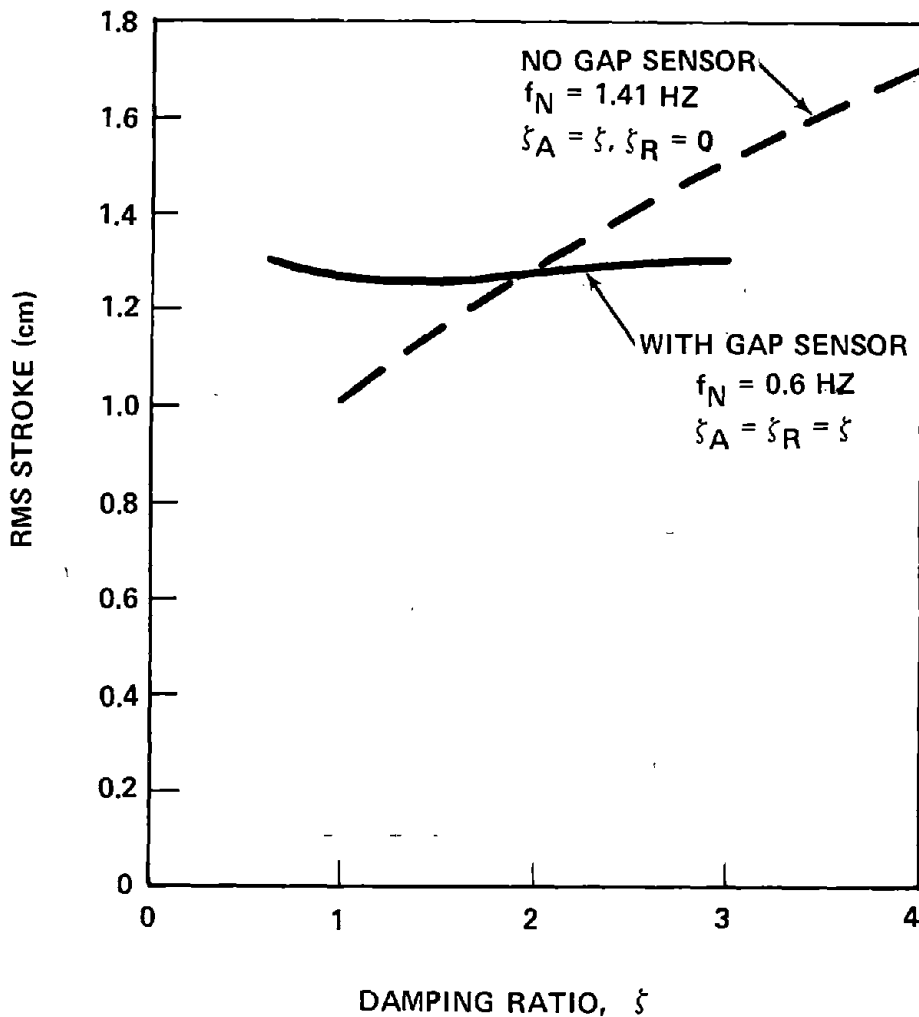
FIGURE 4-30. RMS STROKE VERSUS DAMPING RATIO

4-89

ability of the vehicle to follow grade transitions and turns. However, as is discussed in Paragraph 4.3.2.E(1) this effect is negligible in the case of the baseline system with position feedback for grade transitions of practical length. As indicated on Figure 4-31, the rms stroke characterizing the vehicle response to guideway roughness is smaller with relative damping than without. However, for the guideway roughness under consideration, the rms stroke without relative damping is only 1.71 cm. These considerations indicate that relative damping can be reduced or even eliminated without significant adverse effects on vehicle excursions relative to the guideway.
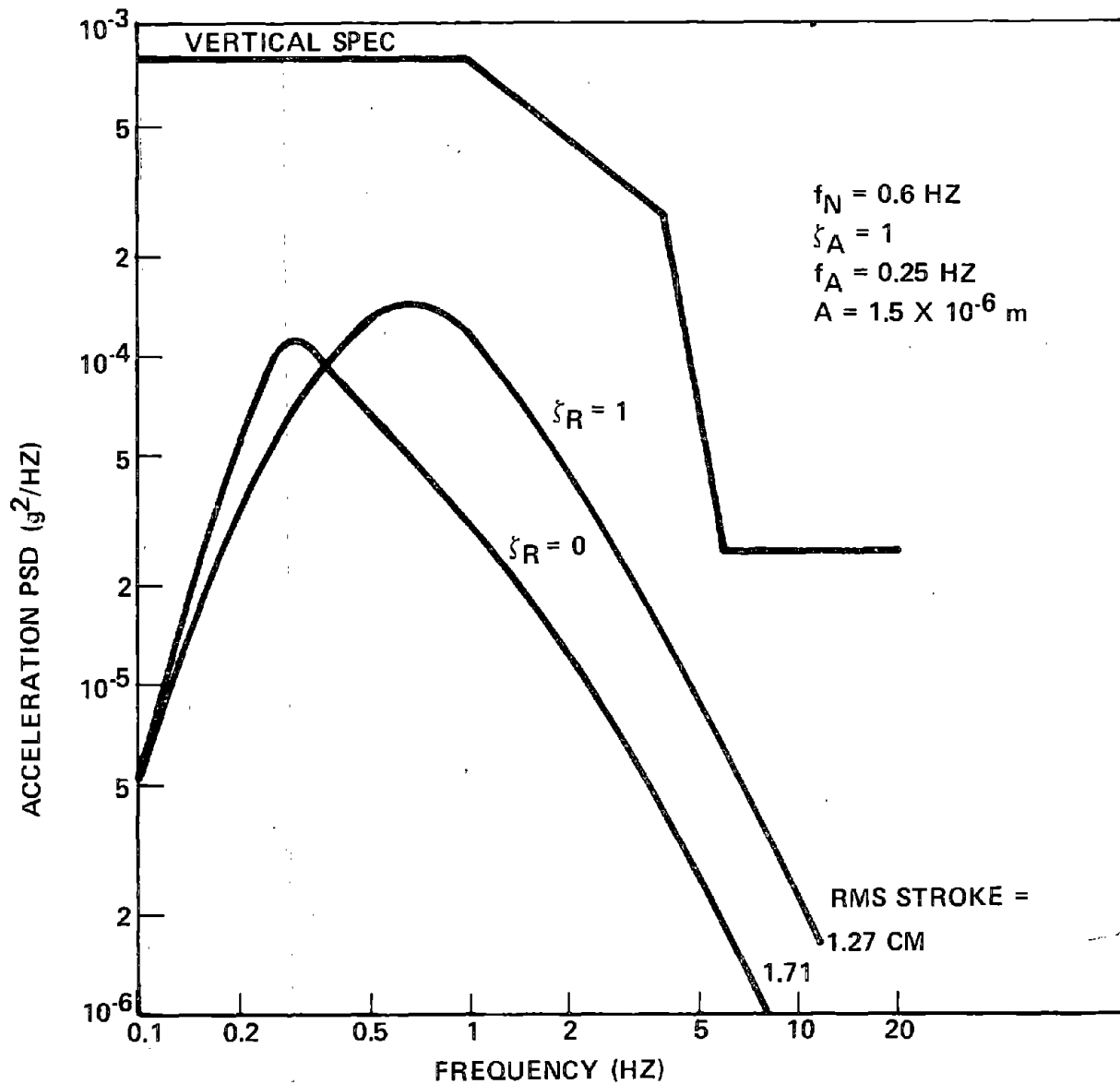
FIGURE 4-31. ACCELERATION PSD VERSUS RELATIVE DAMPING RATIO

4-90

Figure 4-32 shows power spectral density plots of the control current ratio α (ratio of control coil current to levitation coil current). These curves indicate the spectral composition of the I^2R power loss in the control coils. The control current PSDs are shown both with (0.6 Hz) and without (1.41 Hz) position feedback, and for two values of damping ratio in each case. The relative damping ratio is taken equal to the absolute damping ratio for the system with position feedback. For the system without position feedback, the relative damping is taken equal to zero, reflecting the absence of a gap sensor, as explained previously.

Figure 4-33 shows the influence of the damping ratio on the mean square control current ratio $\overline{\alpha^2}$. The mean square control current ratio is proportional to the average I^2R power loss in the control coils. The approximate value of the actual I^2R loss is indicated on the vertical scale at the right of the figure. Curves are presented both with and without position feedback, and, in each case, with and without relative damping. Relative damping is shown in the case of a system without position feedback for comparative purposes only, and as in the case of a system with position feedback, the relative damping is taken equal to the absolute damping. It is seen that the control power is significantly lower for a system with position feedback and relative damping than it is for the system without relative damping. For a system without position feedback and relative damping, the control power is significantly higher at the higher values of absolute damping required for acceptable ride quality. However, the heave mode control power is less than about 35 kW in all cases, except that the multimode dynamic response effects will result in somewhat higher control power requirements than the values indicated for the heave mode only. This will be discussed in more detail in a subsequent section.

      b. __Effects of Filter Parameters__. This paragraph presents the results of a parametric study of the effects of filter parameters on the ride quality of the vehicle.

      1. __First Order Filter Corner Frequencies__. The filter for the absolute damper is a high pass filter with a corner frequency f_A, and the one for the relative damper is a low pass filter with a corner frequency f_R. The corner frequencies f_A and f_R are the first order filter parameters

4-91
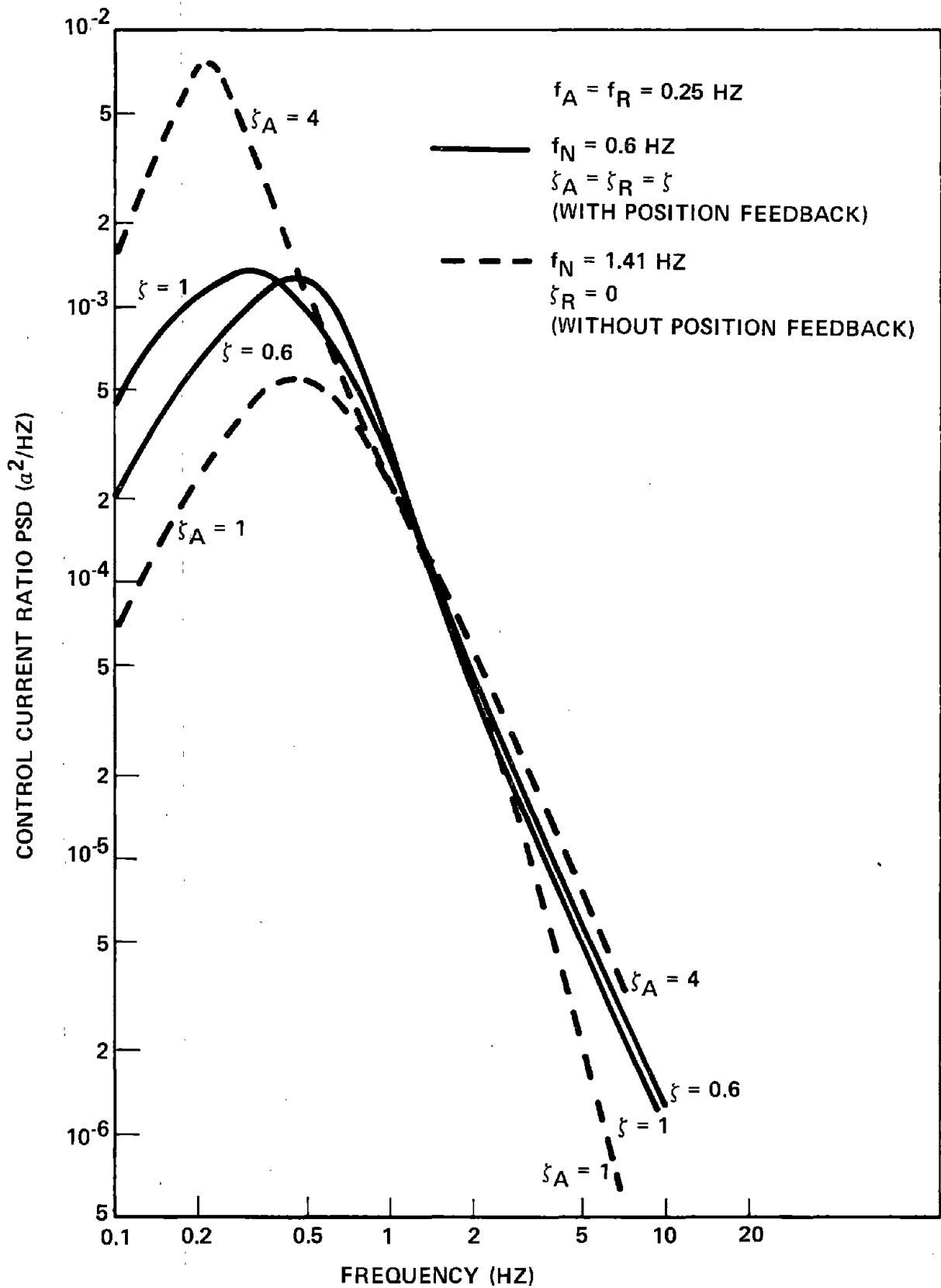
FIGURE 4-32. CONTROL CURRENT RATIO PSD VERSUS FREQUENCY AND DAMPING RATIO

4-92
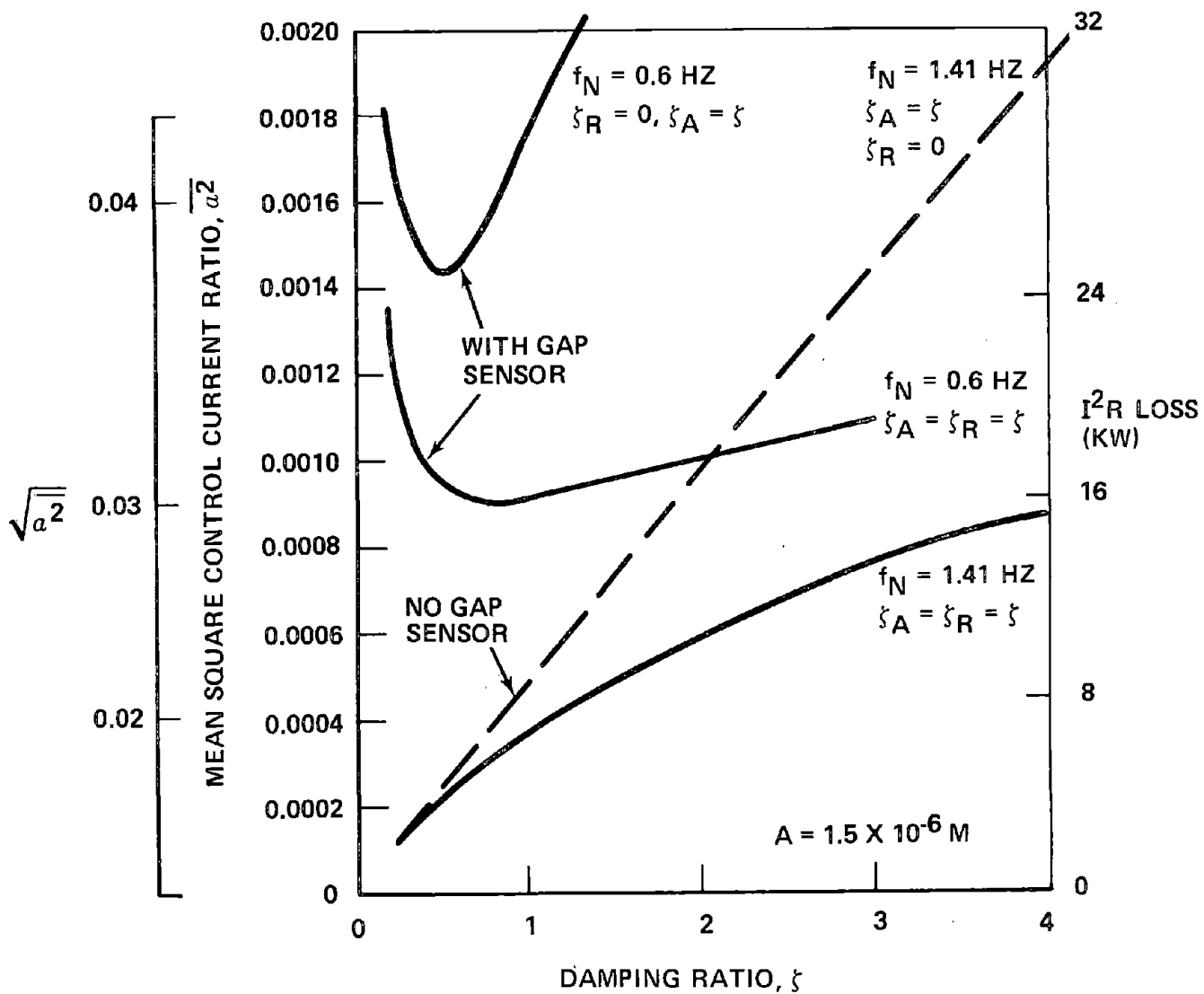
FIGURE 4-33. MEAN CONTROL CURRENT RATIO VERSUS DAMPING RATIO

which have been investigated in the present study. Absolute and relative damping ratios were taken equal to 1.0 for this investigation.

Figure 4-34 shows the effect of the corner frequencies on the ride quality for the case where $f_A = f_R$. It is seen that lower values of the corner frequencies result in improved ride quality. For the conceptual configuration a value of

$$f_A = f_R = 0.25 \text{ Hz}$$

was selected for the corner frequencies. Although heave mode acceleration PSDs corresponding to somewhat higher corner frequencies will not violate the ride quality specification, the value selected for the corner frequencies (0.25 Hz) provides margin to allow for multimode (pitch-roll-heave) dynamic response effects.
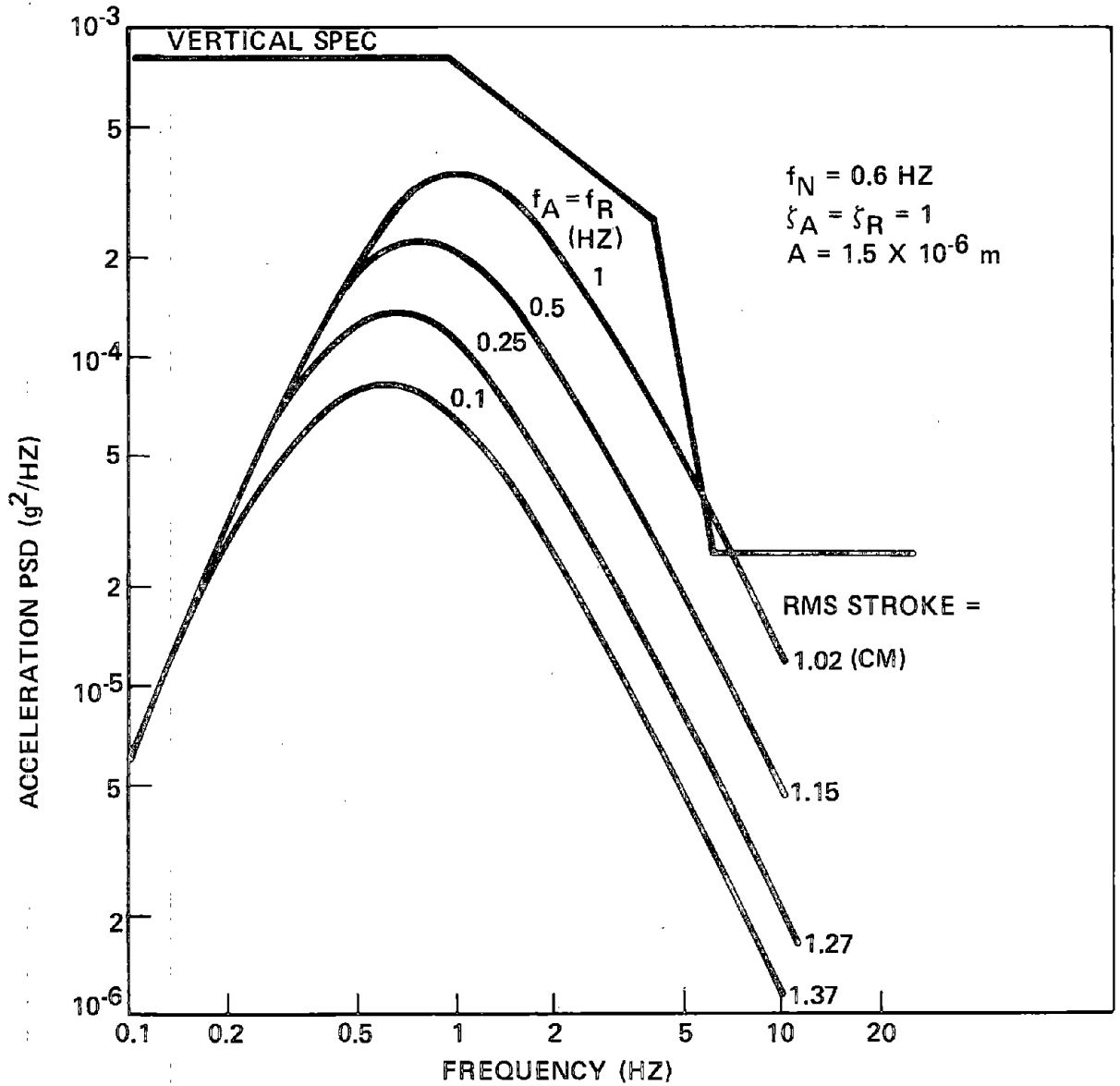
FIGURE 4-34. ACCELERATION PSD FOR DIFFERENT BREAK FREQUENCIES

Additional parametric investigations were conducted to assess the effects of using different corner frequencies for the absolute and relative dampers. Figure 4-35 shows the effect of varying f_R with $f_A = 0.25$ Hz, and Figure 4-36 is a similar plot with $f_A = 1.0$ Hz. Figure 4-37 shows the effect of varying f_A with $f_R = 0.25$ Hz. Separating the absolute and relative damper corner frequencies does not appear to improve ride quality, in fact in most cases it results in poorer ride quality. It is concluded there is no advantage to using different corner frequencies for the absolute and relative dampers.

2. <u>Second Order Filter</u>. The possibility of using a second order filter to achieve improved low frequency stroke response was also investigated. It was found that although improved low frequency (<0.2 Hz) stroke response can be achieved, the peak stroke response (which occurs near 0.5 Hz) is actually worse. Similarly, ride quality is better at high frequencies, but the peak acceleration response near 0.5 Hz is worse. It is concluded that a second order filter offers no clear advantage over a first order filter.

c. <u>Ride Quality in a Grade Transition</u>.* This paragraph discusses vehicle response to guideway roughness during a grade transition.

During negotiation of a grade transition, centrifugal forces and the action of the inertial (absolute) damper cause the vehicle to move to a new equilibrium position relative to the guideway. Because of the nonlinearities in the magnet force law, any vehicle excursion from the nominal position relative to the guideway results in an increase in the effective suspension stiffness.** The effective stiffness becomes greater as the vehicle excursions increase. As the transition length to a given grade becomes shorter, the vehicle accelerations increase, which in turn cause larger excursions of the vehicle from its nominal position (and an increasingly stiff suspension).

---

*DOT and MITRE Corp. personnel have suggested that the acceleration PSD criterion on ride quality is not appropriate for the short-time operation associated with turns and grade transitions. Pending establishment of a realistic criterion for these operations however, the acceleration PSD technique is used for the analysis reported in these paragraphs.

**This increase in stiffness occurs for both up and down excursions for the baseline control system, i.e., one with a gap sensor and feedback reduction.
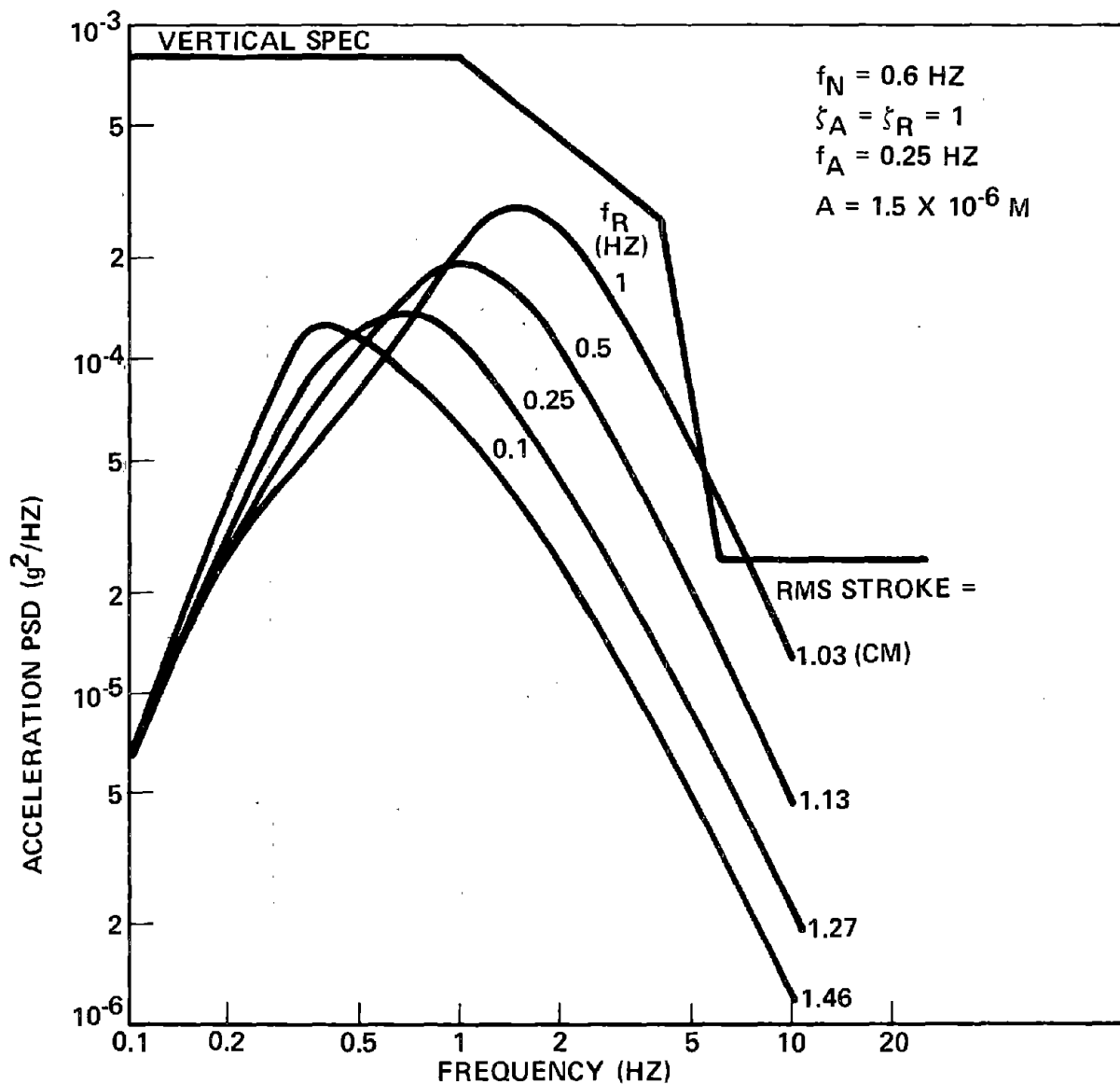
FIGURE 4-35. ACCELERATION PSD VERSUS CORNER FREQUENCY, F_R (f_A = 0.25 HZ)

The increased effective suspension stiffness in the grade transition results in poorer ride quality in response to guideway roughness. Figure 4-38 shows heave mode acceleration PSDs for various transition lengths to a 2% grade. Because the nonlinearities in the magnet force law are not symmetrical about the nominal vehicle position, the acceleration PSD for an "up transition" (increasing slope) differs from that for a "down transition" (decreasing slope). The acceleration PSDs shown in Figure 4-38 were computed for the

baseline configuration (with position feedback) and with the relative damping
ratio equal to the absolute damping ratio. It is seen that ride quality in
a grade transition is degraded relative to that on a level guideway. For the
conditions used in Figure 4-38, the ride quality specification is exceeded
for grade transitions less than ten kilometers in length. It should be noted
that consideration of multimode dynamic response effects will cause the ride
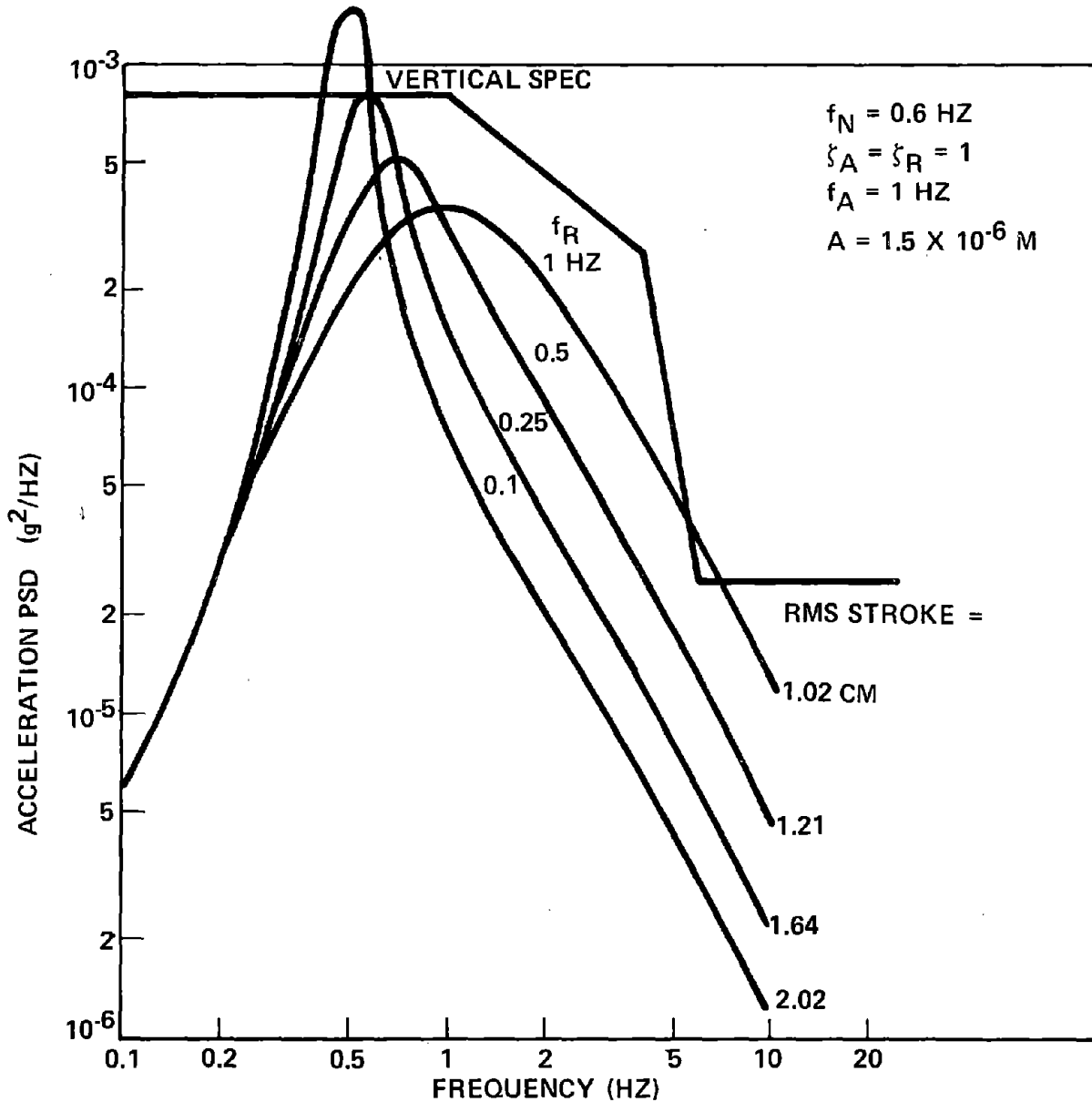
FIGURE 4-36. ACCELERATION PSD VERSUS CORNER FREQUENCY,
F_R (f_A = 1 HZ)

quality specification to be exceeded for even longer transition lengths. However, since a grade transition is a transient effect, it may be possible to exceed the ride quality for this short period without much passenger discomfort. For example at 134 m/s, the ride quality in a 5 km grade transition would be exceeded less than 37 seconds, and only seven seconds in a 1 km transition.
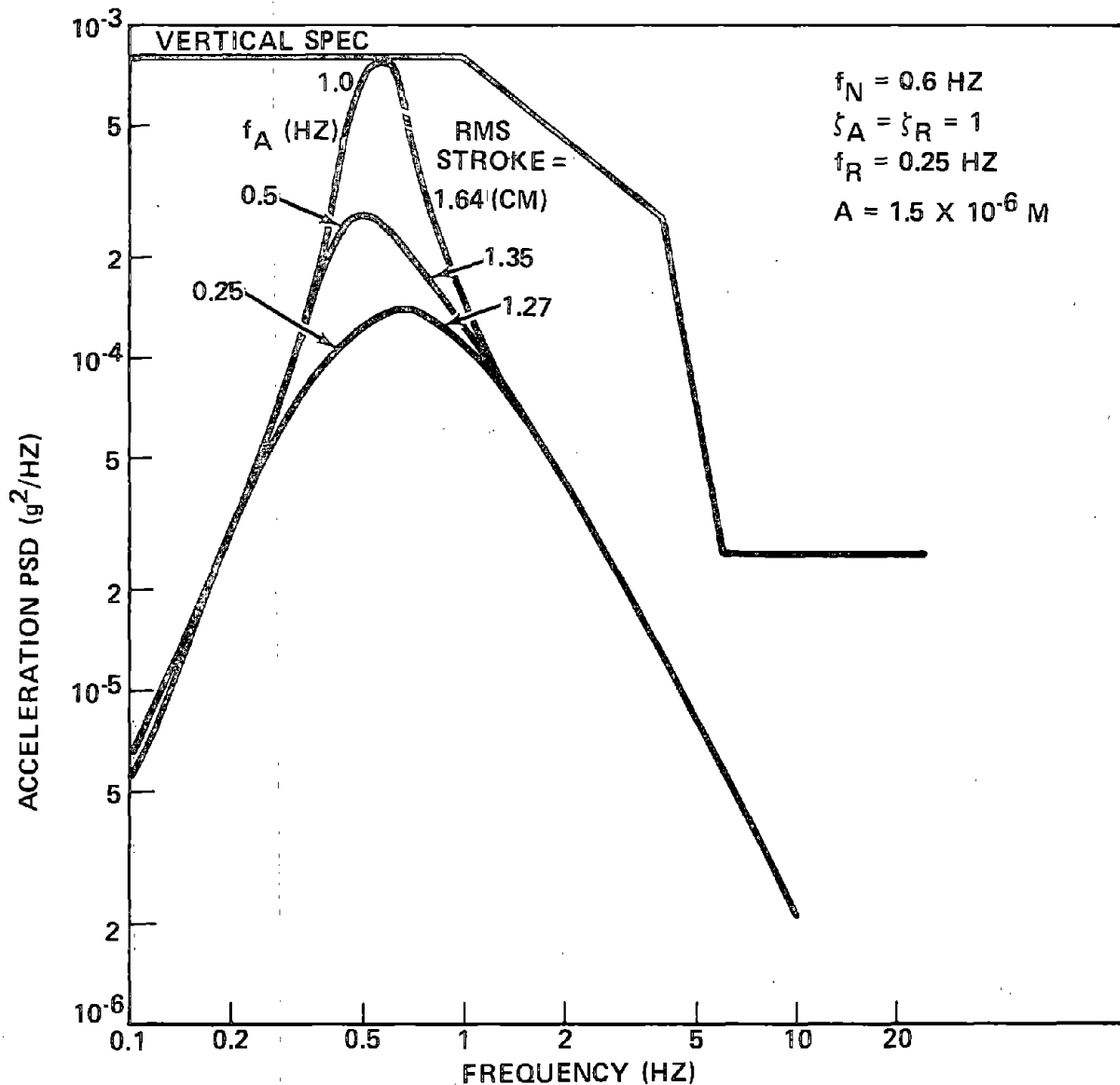
FIGURE 4-37. ACCELERATION PSD VERSUS CORNER FREQUENCY f_A (f_R = 0.25 HZ)
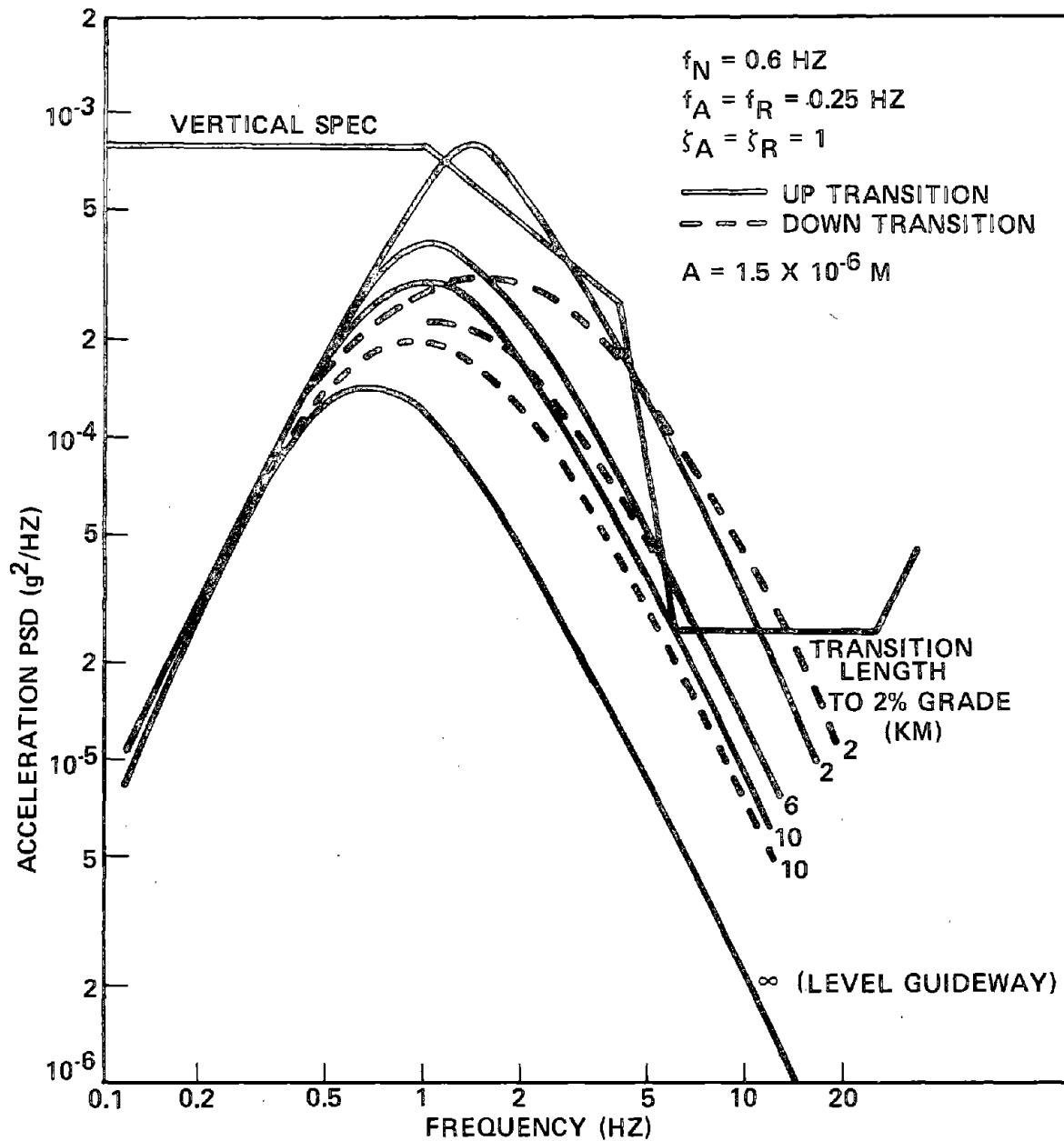
FIGURE 4-38. ACCELERATION PSD ON A TRANSITION TO A 2 PERCENT
GRADE - WITH POSITION FEEDBACK AND RELATIVE
DAMPING

Figure 4-39 presents similar heave mode acceleration PSDs for the base-
line conceptual configuration (with position feedback), but without relative
damping. Again, it is seen that ride quality is degraded relative to that on
a level guideway. However, comparison with Figure 4-38 indicates that ride
quality is improved by eliminating relative damping. Without relative damping,
heave mode acceleration PSDs exceed the ride quality criterion for grade

4-99

transitions less than 4 km (as compared with 10 km for a system with relative damping).
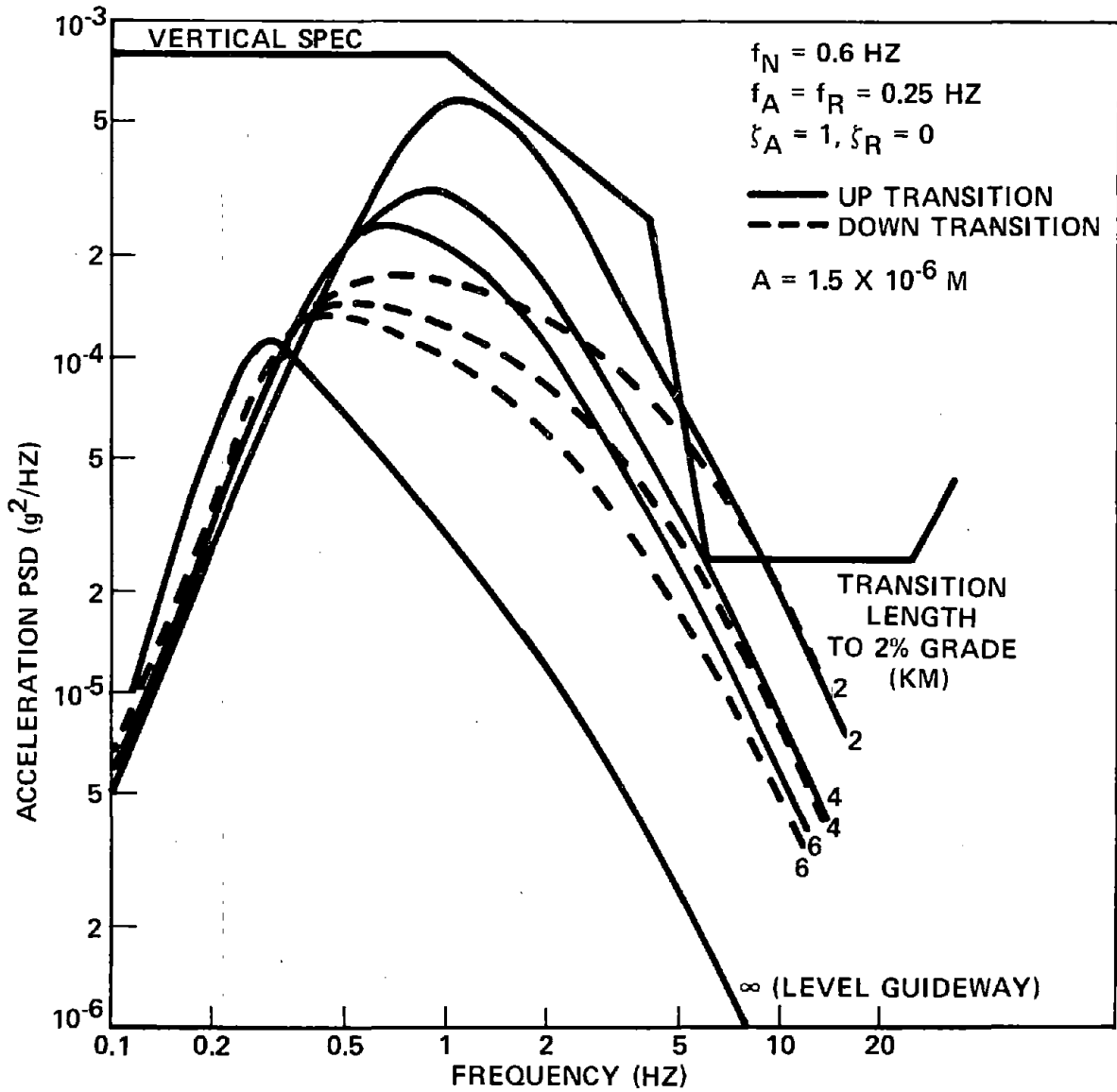
FIGURE 4-39. ACCELERATION PSD ON A TRANSITION TO A 2 PERCENT GRADE - WITH POSITION FEEDBACK BUT NO RELATIVE DAMPING

Figure 4-40 shows the dependence of ride quality on transition length
(to a 2% grade) for a system without position feedback and without relative
damping. For such a system, magnet force nonlinearities cause ride quality
degradation only on an "up transition", and the curves in Figure 4-40 are
for this case. It is seen that the heave mode acceleration PSDs exceed the
ride quality specification for transition lengths less than about 5 km.
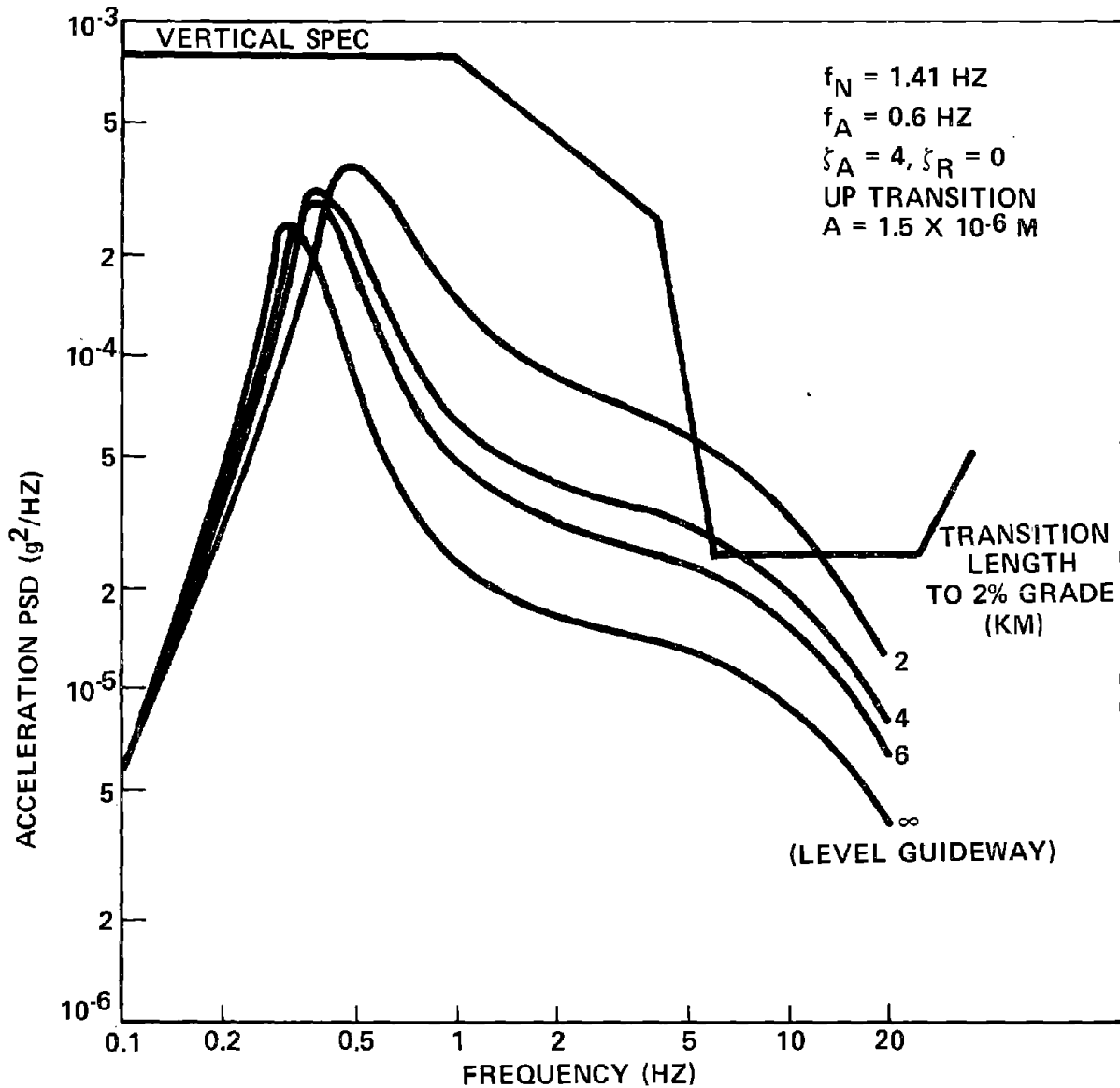
FIGURE 4-40. ACCELERATION PSD ON A TRANSITION TO A 2 PERCENT
GRADE - WITHOUT POSITION FEEDBACK

Figure 4-41 indicates how the rms stroke (in response to guideway rough-ness) varies as a function of transition length to a 2% grade. These results are presented for the baseline configuration with relative damping. It is seen that the rms stroke on a grade transition is less than that on a level guideway. Figure 4-42 shows how the increase in control current ratio (in response to guideway roughness) depends on transition length to a 2% grade for the baseline control scheme. The control current requirement (in response to guideway roughness) is less on a grade transition than on a level guideway.

d. Response to Periodic Gaps in the Guideway. The one DOF nonlinear dynamic model has been employed to evaluate vehicle response to periodic gaps in the guideway. The lift reduction due to the presence of a gap is given in Section 4.5.2D. Absolute and relative damping ratios were taken equal to 1.0. Figure 4-43 shows the time histories of vehicle motion after encountering gaps every 7.6, 15.2, and 30.5 m (25, 50, and 100 ft). A time history is also shown for a single, isolated gap. Physically, the plots represent the case of a vehicle traveling over a gap-free guideway then suddenly encountering, at time = 0, a section of guideway with evenly spaced gaps (or only a single gap). A momentary loss of lift occurs over each gap, and the closer the gaps are spaced, the more the reduction in integrated lift · and the closer the vehicle will approach the guideway. There is a transient period before the vehicle reaches the equilibrium position. Each small wave on the three lower curves shows the response to a single gap for the one DOF model. It is seen that the steady state excursion of the vehicle from its nominal equilibrium position is less than 1.5 cm for a gap spacing of 50 feet (15.2 m) or more.

Figure 4-44 shows passenger compartment acceleration as a function of gap spacing. It is seen that the peak acceleration is less than the minimum objective for gap spacings of 15.2 m (50 ft) or more.

e. Response to Elevated Guideway Deformations. Estimates are given in Section 4.5.2B of elevated guideway deformations under dynamic vehicle loading for the preliminary elevated span designs. These guideway deformations have been utilized as input excitation to the vehicle dynamic
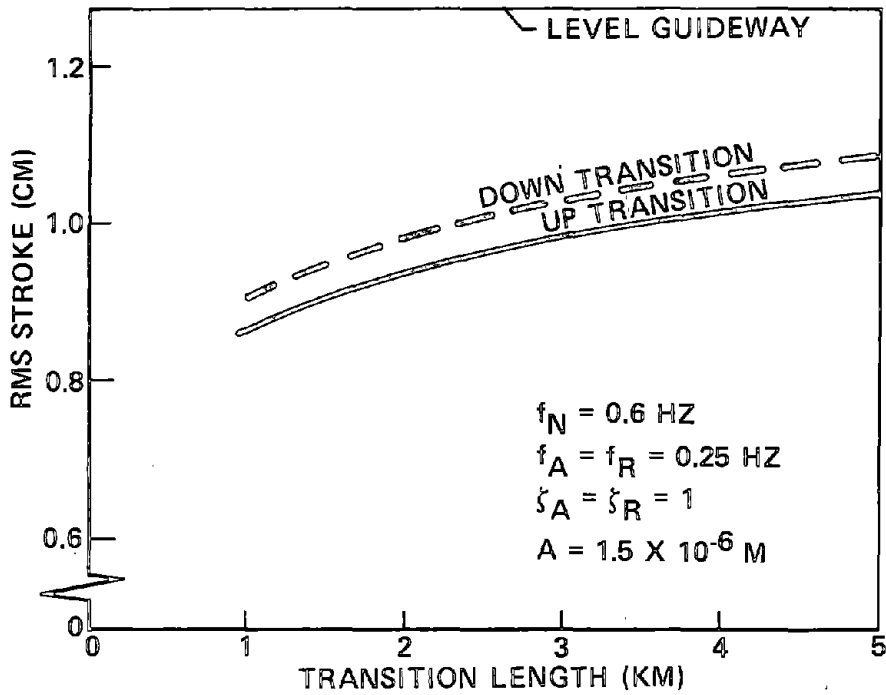
FIGURE 4-41. RMS STROKE ON A TRANSITION TO A 2 PERCENT GRADE - WITH POSITION FEEDBACK
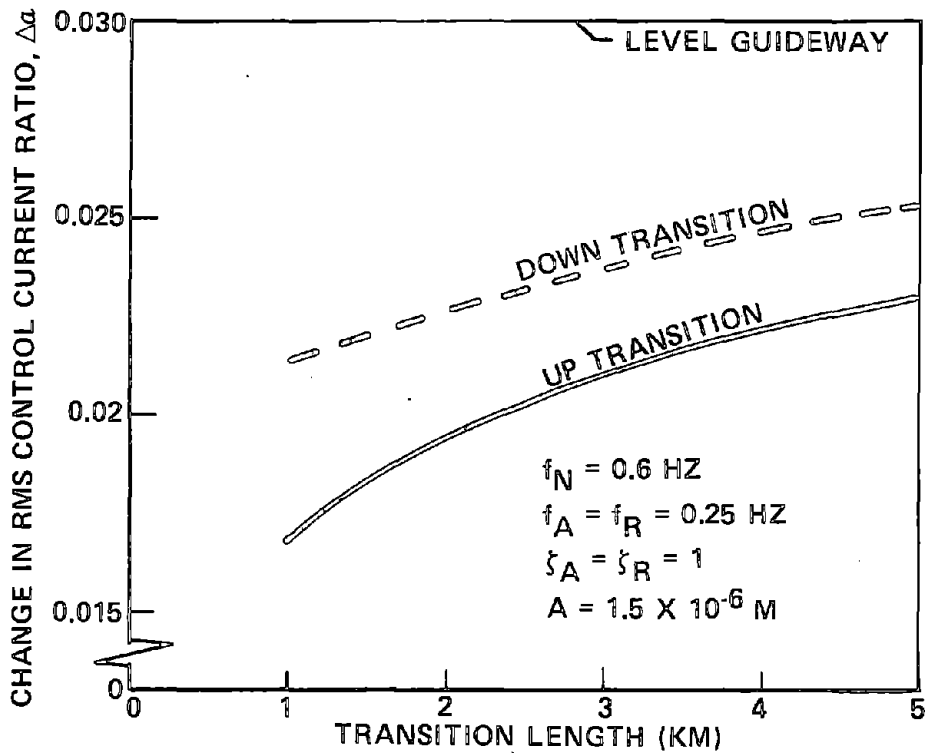
FIGURE 4-42. CHANGE IN RMS CONTROL CURRENT RATIO ON A TRANSITION TO A 2 PERCENT GRADE - WITH POSITION FEEDBACK
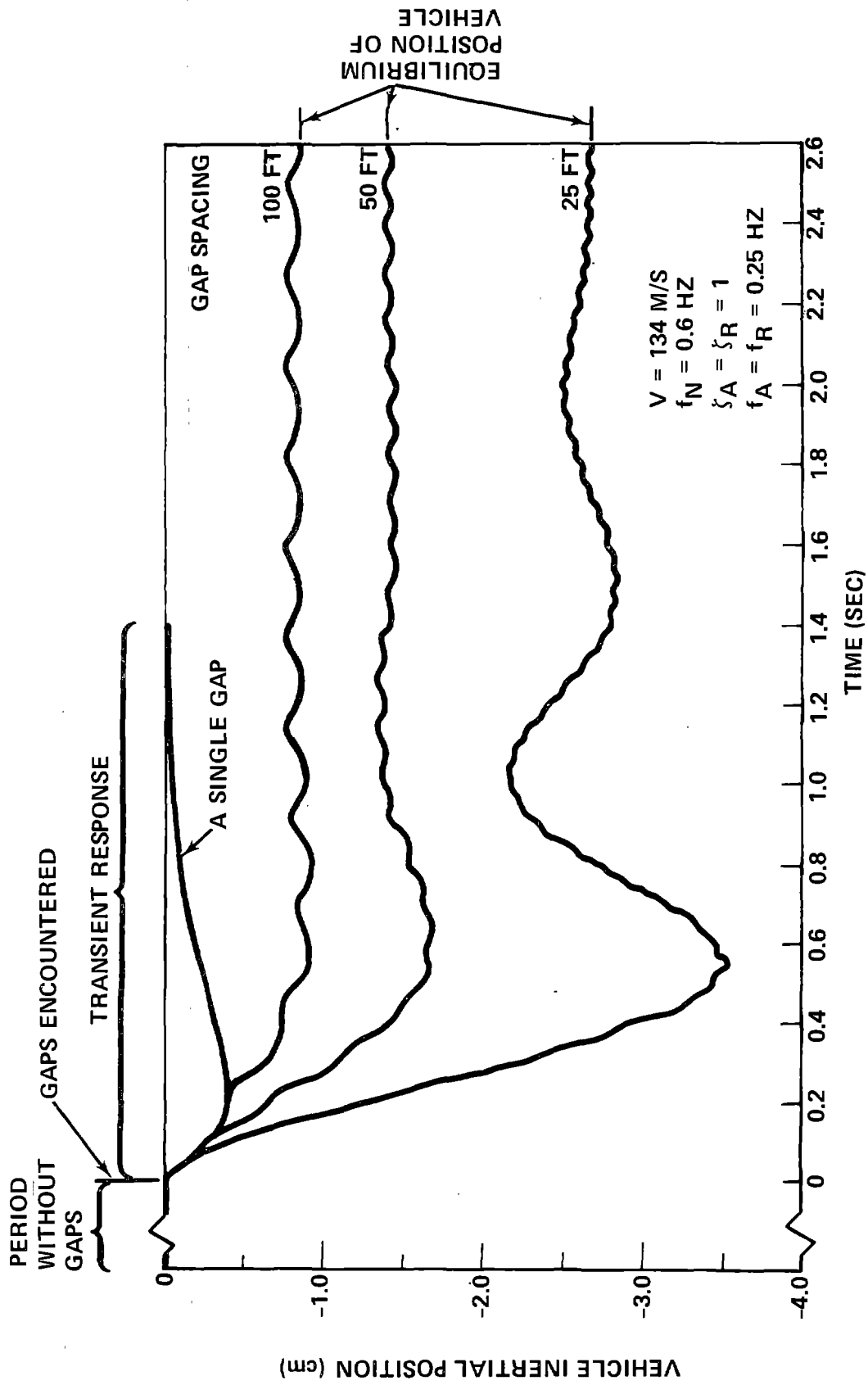
FIGURE 4-43. TRANSIENT VEHICLE RESPONSE TO REGULARLY SPACED GAPS IN GUIDEWAY
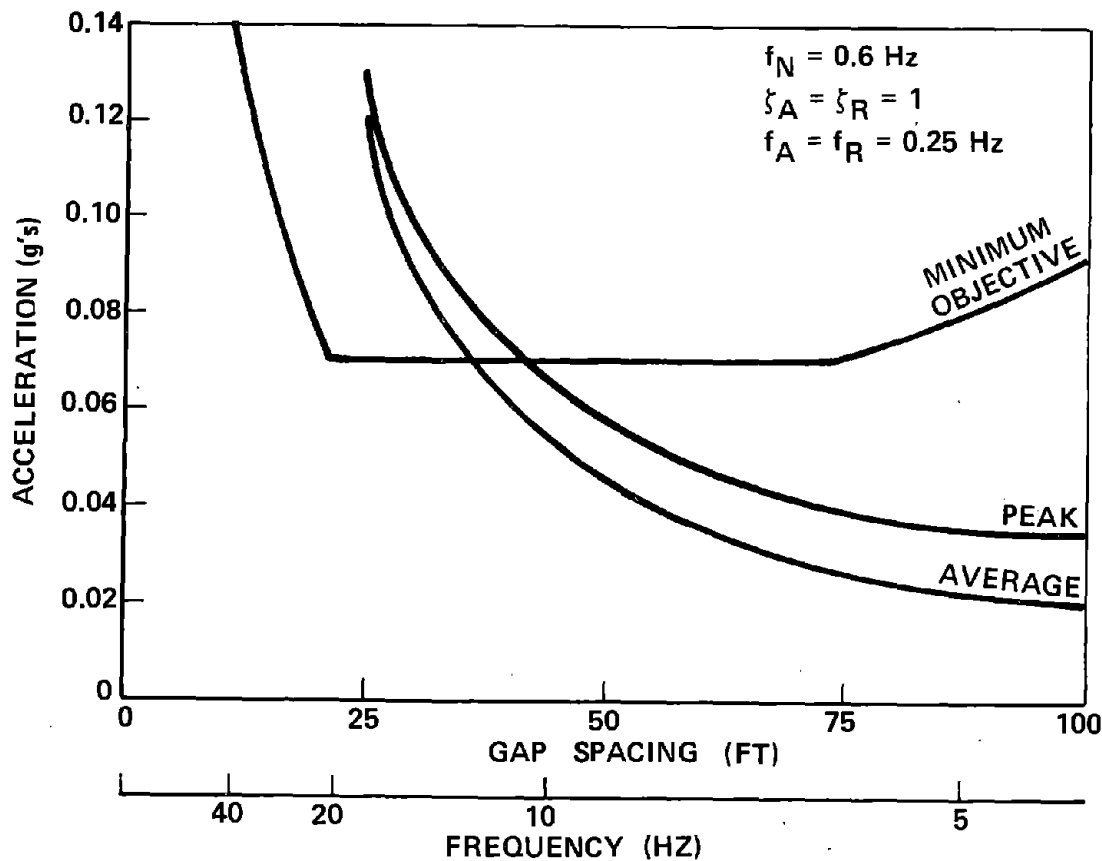
FIGURE 4-44. PASSENGER COMPARTMENT ACCELERATION AS A
FUNCTION OF GAP SPACING

model in order to provide a predynamic response. Maximum vertical accelera-
tion levels were found to be 0.055 g, indicating that the dynamic behavior
of a vehicle in response to a properly designed elevated guideway will not
result in unsatisfactory ride quality.

(2) Multi-Degree-of-Freedom Dynamic Studies. The results of an
analysis of the multimode dynamic response of the baseline control concept
to guideway random irregularities are given below. A five-degree-of-freedom
mathematical model is used for this analysis. Since the pitch/heave degrees
of freedom are decoupled from roll/sway/yaw, pitch coupling effects are
examined separately from roll/sway/yaw effects.

a. <u>Effects of Pitch Coupling</u>. Figure 4-45 shows vertical acceleration PSDs at the corners of the passenger compartment in response to guideway vertical random irregularities. The acceleration response is seen to be well below the ride quality specification, and the ride quality at the front and rear of the passenger compartment does not differ significantly.

The gain constants selected for the baseline configuration (see Section 4.3.2B) result in a damping ratio of about 0.6 in the pitch/heave mode. As was shown in Paragraph 4.3.2D(1)a., heave mode ride quality is
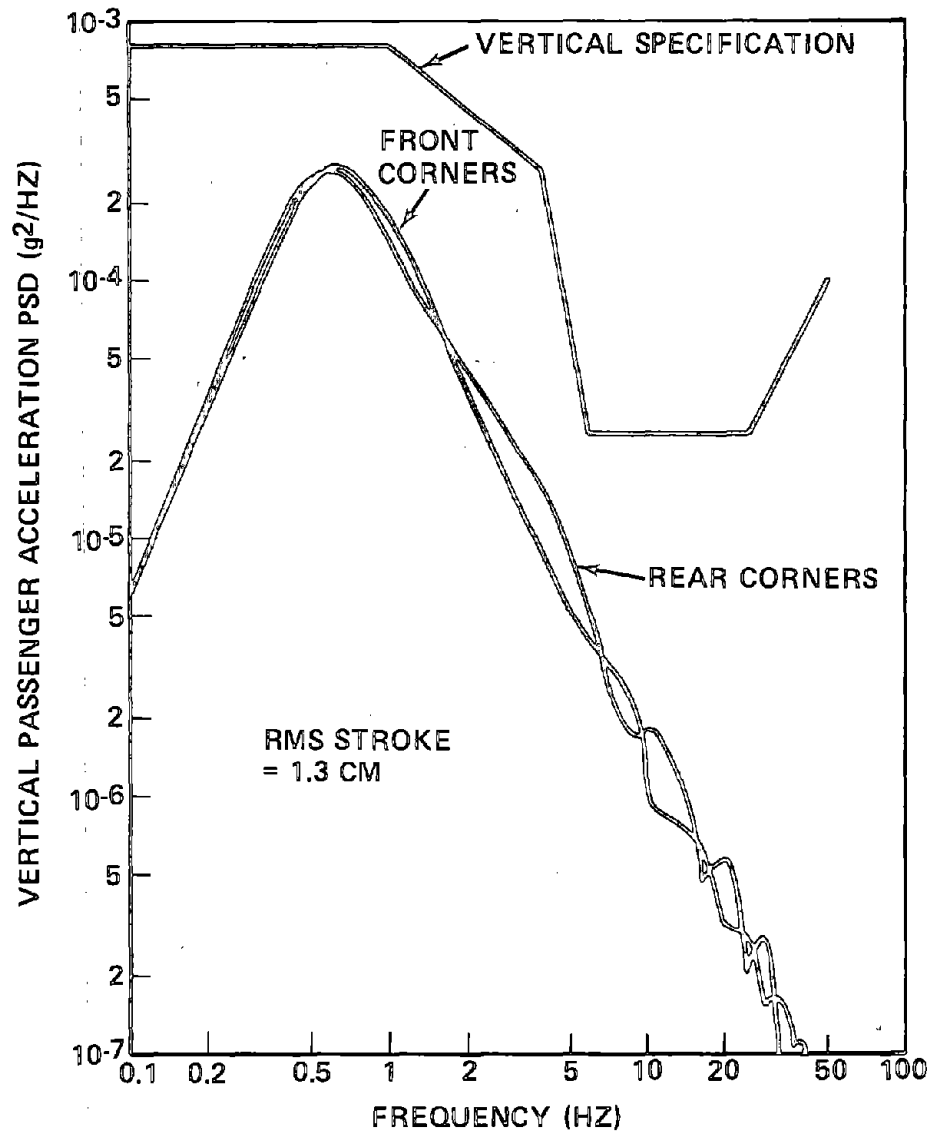
FIGURE 4-45. VERTICAL ACCELERATION RESPONSE TO GUIDEWAY VERTICAL RANDOM IRREGULARITIES

relatively insensitive to damping over a range of damping ratios from about 0.6 to 1.0 (see Figure 4-29). Also, Figures 4-30 and 4-33 show that for the baseline concept (with relative damping), the RMS stroke and control current ratio are not sensitive to damping over the same range of damping ratios. Comparison of Figure 4-45 with the heave mode acceleration PSD for a damping ratio of 0.6 in Figure 4-29 indicates that pitch coupling effects are not significant for the baseline concept. This is probably attributable to the fact that, for this concept, pitch and heave are only weakly coupled, and the selection of gain constants results in a pitch frequency which is very nearly equal to the heave frequency.

Figure 4-46 shows the control current ratio PSD for response to guideway vertical random irregularities. Curves are shown for the front and rear control coils and for the total control current. These curves indicate the spectral composition of the I^2R power loss in the control coils. Mean square control current ratios, indicated on Figure 4-46, are proportional to the average I^2R power loss in the control coils. The average I^2R loss is approximately 16 kW for the pitch/heave mode.

b. Roll/Sway/Yaw Effects. Guideway lateral random irregularities excite vehicle dynamic response in the coupled roll/sway/yaw modes, which involve both lateral and vertical vehicle motions. The power spectral density of guideway lateral roughness has been assumed to be the same as that for vertical roughness, as given in Paragraph 4.3.2D(1). This spectral density relation is probably conservative for lateral roughness and somewhat lower values could probably be used, at least for longer wavelength roughness components. This will be discussed further below.

Figure 4-47 presents the vertical acceleration PSD at the corners of the passenger compartment for vehicle response to guideway lateral random irregularities. This acceleration response is seen to be well below the ride quality specification, and is essentially the same at all four corners of the passenger compartment. The response to guideway lateral roughness combines statistically with the response to vertical roughness. The resultant statistically-combined acceleration response is estimated as the sum of the acceleration PSDs shown in Figures 4-45 and 4-47 and should be a conservative

value. It is seen that this sum does not exceed the ride quality specification.

Figure 4-48 shows the lateral acceleration PSDs at the corners of the passenger compartment for vehicle response to guideway lateral random irregularities. The curves designated by the solid lines show the vehicle response
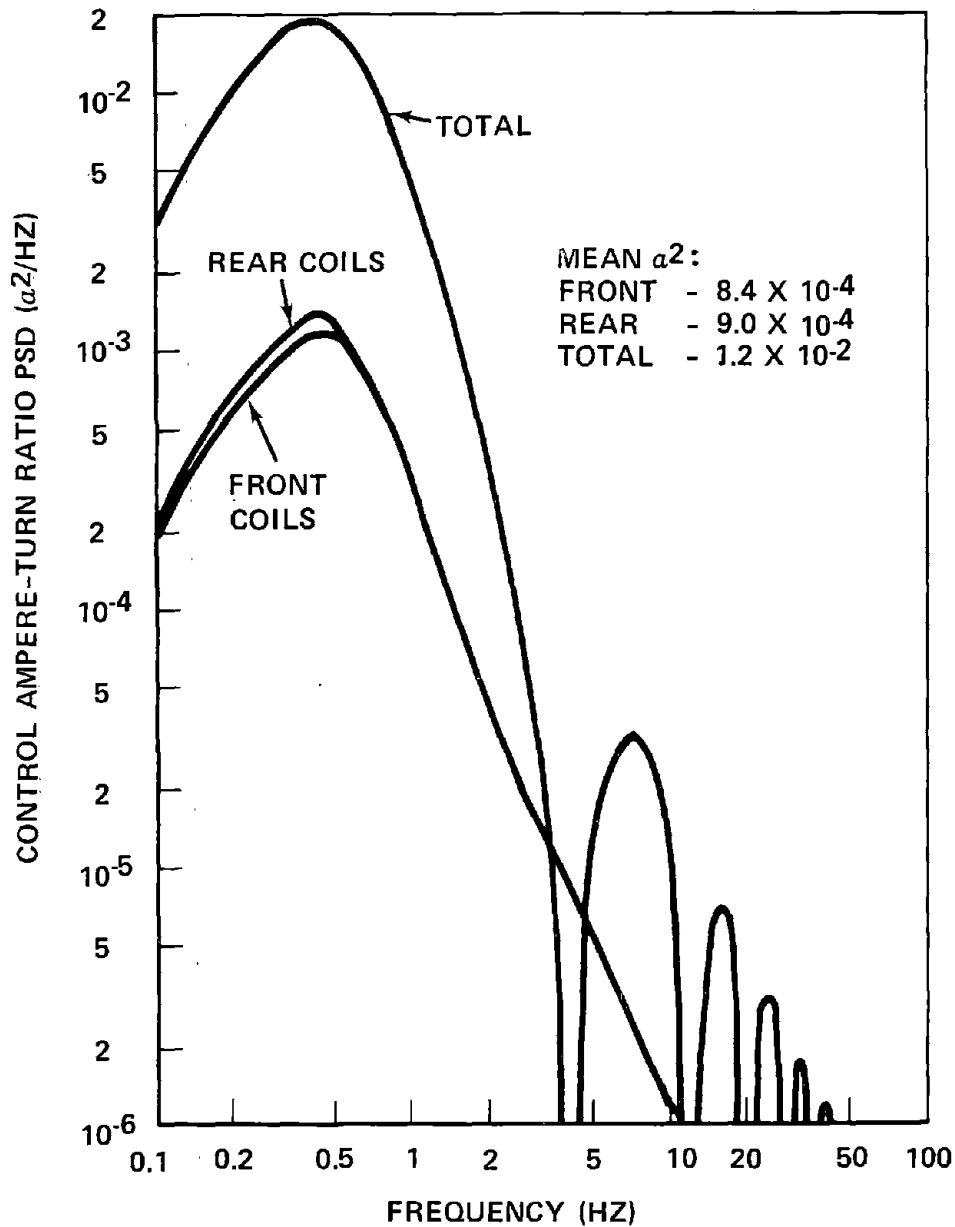
FIGURE 4-46. CONTROL CURRENT RATIO PSD'S FOR RESPONSE TO GUIDEWAY VERTICAL RANDOM IRREGULARITIES

to the guideway lateral roughness PSD given above. It is seen that the
vehicle lateral acceleration response corresponding to this guideway rough-
ness exceeds the lateral ride quality specification. However, as indicated
previously, the power spectral density relation which was utilized to repre-
sent guideway lateral roughness is the same as the vertical roughness PSD
and should be conservative, at least for longer wavelength roughness
components.
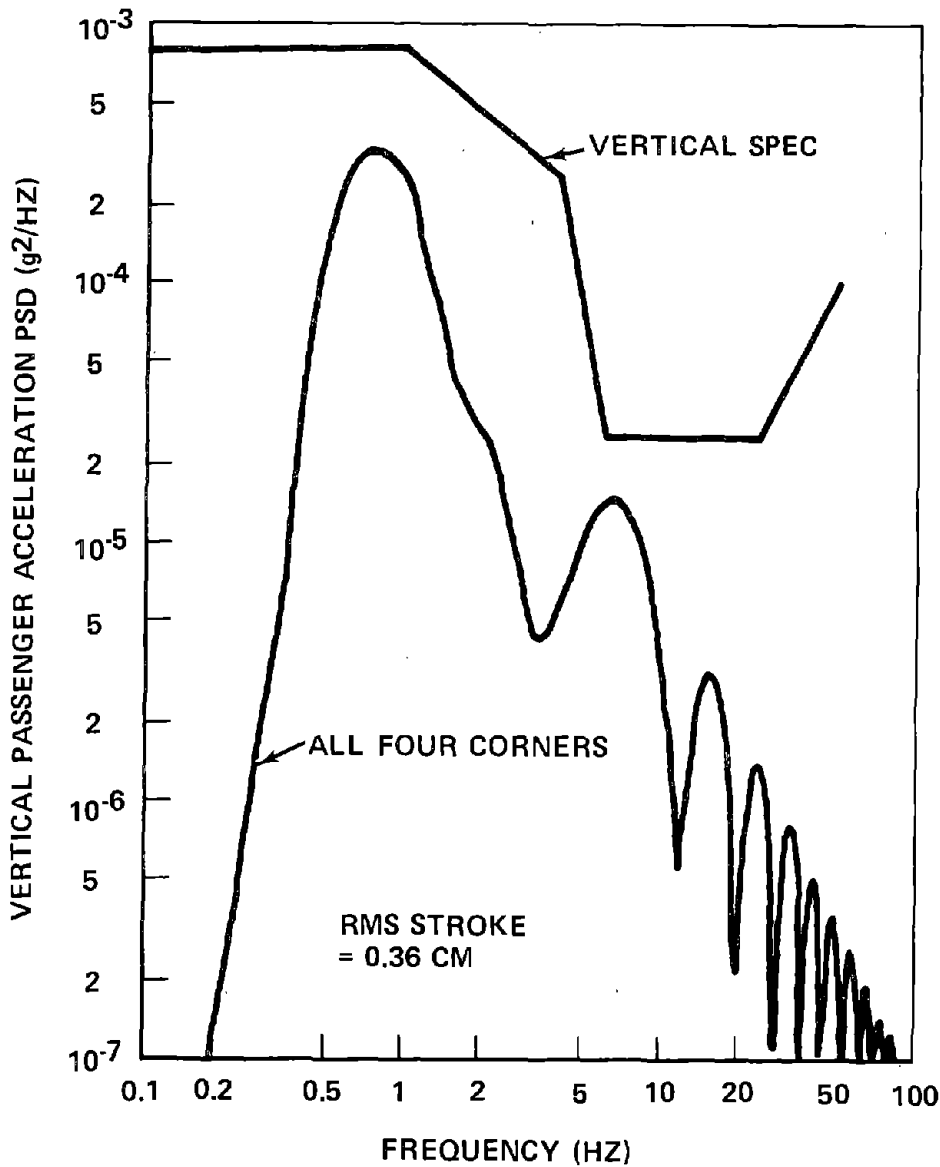
FIGURE 4-47. VERTICAL ACCELERATION RESPONSE TO GUIDEWAY LATERAL
RANDOM IRREGULARITIES
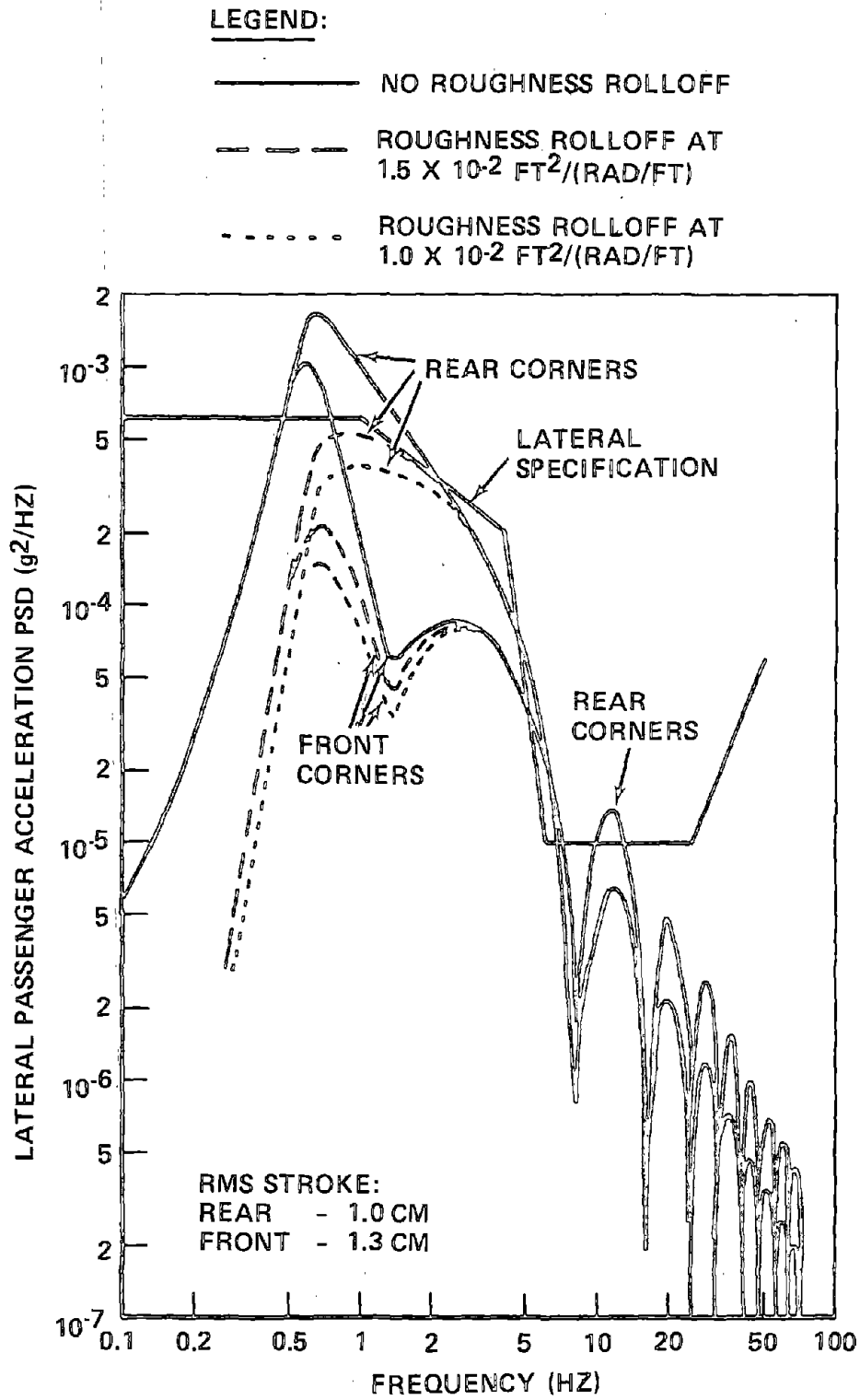
FIGURE 4-48. LATERAL ACCELERATION RESPONSE TO GUIDEWAY LATERAL
RANDOM IRREGULARITIES

It seems reasonable to assume that a long wavelength rolloff exists in the vertical roughness PSD. Figure 4-49 shows the assumed roughness power spectral density relation together with two different suggested* long wavelength (low frequency) rolloff characteristics. The lateral acceleration response corresponding to these two modified guideway roughness characteristics is indicated by the dashed and dotted curves in Figure 4-48. The dashed curve in Figure 4-48 corresponds to a roughness PSD rolloff at 1.5×10^{-2} ft^2/ (rad/ft) and the dotted curve corresponds to a rolloff at 1.0×10^{-2} ft^2/ (rad/ft). It is seen that the lateral acceleration PSDs corresponding to the modified guideway roughness characteristics do not exceed the ride quality specification near the response peak in the vicinity of 0.6 Hz. However, the roughness rolloff does not reduce the acceleration response at frequencies above 5 Hz, and so the ride quality specification is still exceeded slightly in the frequency range between 5 and 15 Hz.

A modification of the control system gain constants can be used to alter the acceleration response so that the ride quality specification is not exceeded. Figure 4-50 shows the acceleration response for the modified set of gain constants. The values of these gain constants are given in Table 4-15, along with the values for the original set of constants corresponding to Figure 4-48. The essential difference between the two sets is that the values corresponding to original results (Figure 4-48) incorporate lateral acceleration feedback (K_y) and no lateral position feedback ($K_h{}'$). Reversing the use of these two gain constants improves the ability to meet the lateral ride quality specification. (The definition of the symbols designating the gain constants is given in Section 4.3.2B, where the selection of gain constants is discussed.)

The curves designated by the solid lines in Figure 4-50 give the vehicle response to the lateral roughness PSD with no rolloff. For this case the lateral acceleration PSD does not exceed the ride quality specification at frequencies above about 1.1 Hz, but the peak acceleration response below 1 Hz is somewhat higher than the corresponding peak in Figure 4-48. However,

---

*Nathan Sussman, Mitre Corp., Personal Communication
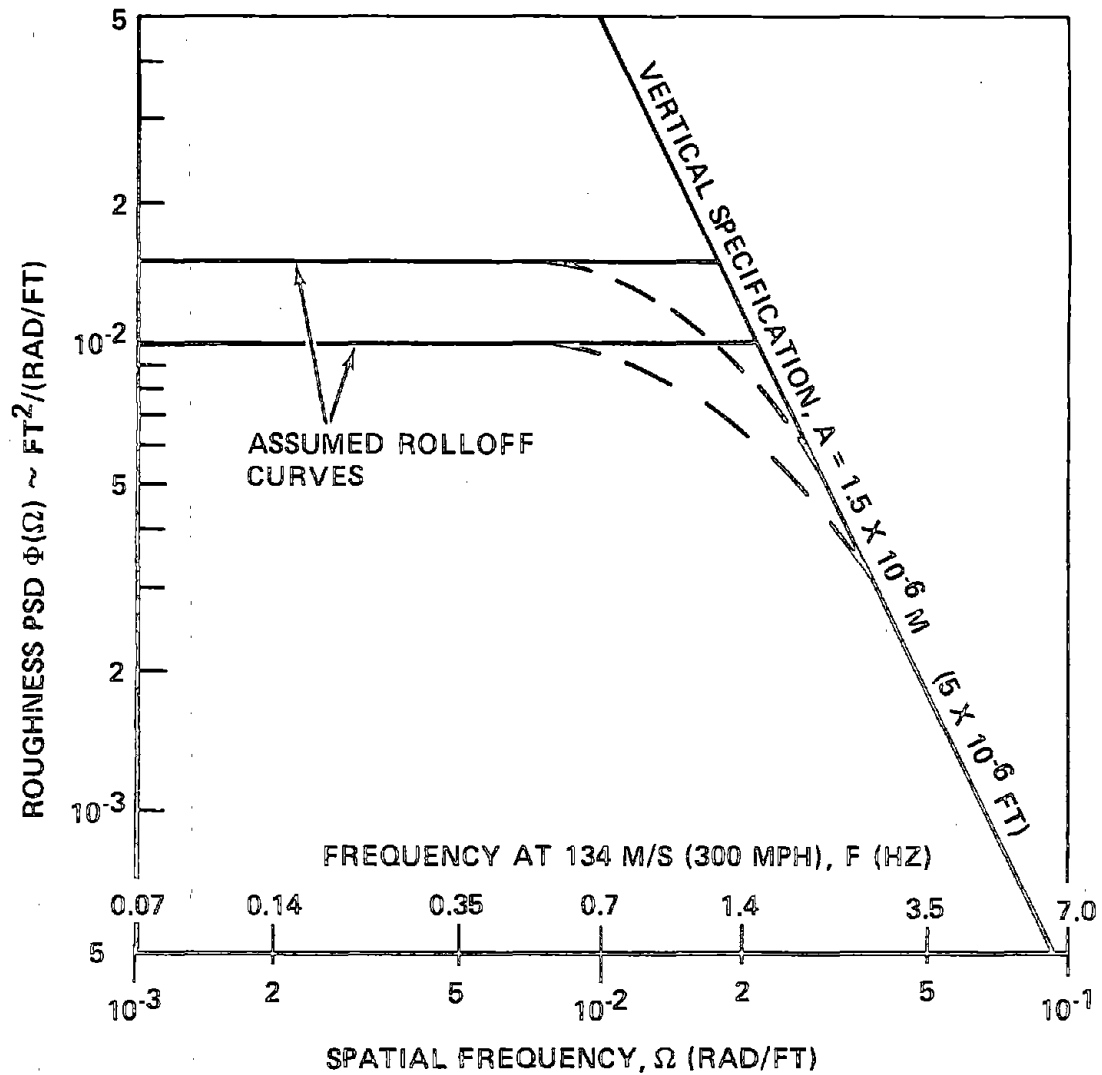
FIGURE 4-49. GUIDEWAY ROUGHNESS POWER SPECTRAL
DENSITY RELATIONS

the lateral acceleration PSD corresponding to a roughness rolloff at 1.0 x
10^{-2} ft^2/(rad/ft) is below the ride quality specification over the entire
frequency range.

Figure 4-51 shows the control current ratio PSDs for response to guide-
way lateral random irregularities. These control currents correspond to the
vehicle response shown in Figure 4-48. The mean square control current
ratios, indicated on Figure 4-51, are proportional to the average I^2R power

4-112
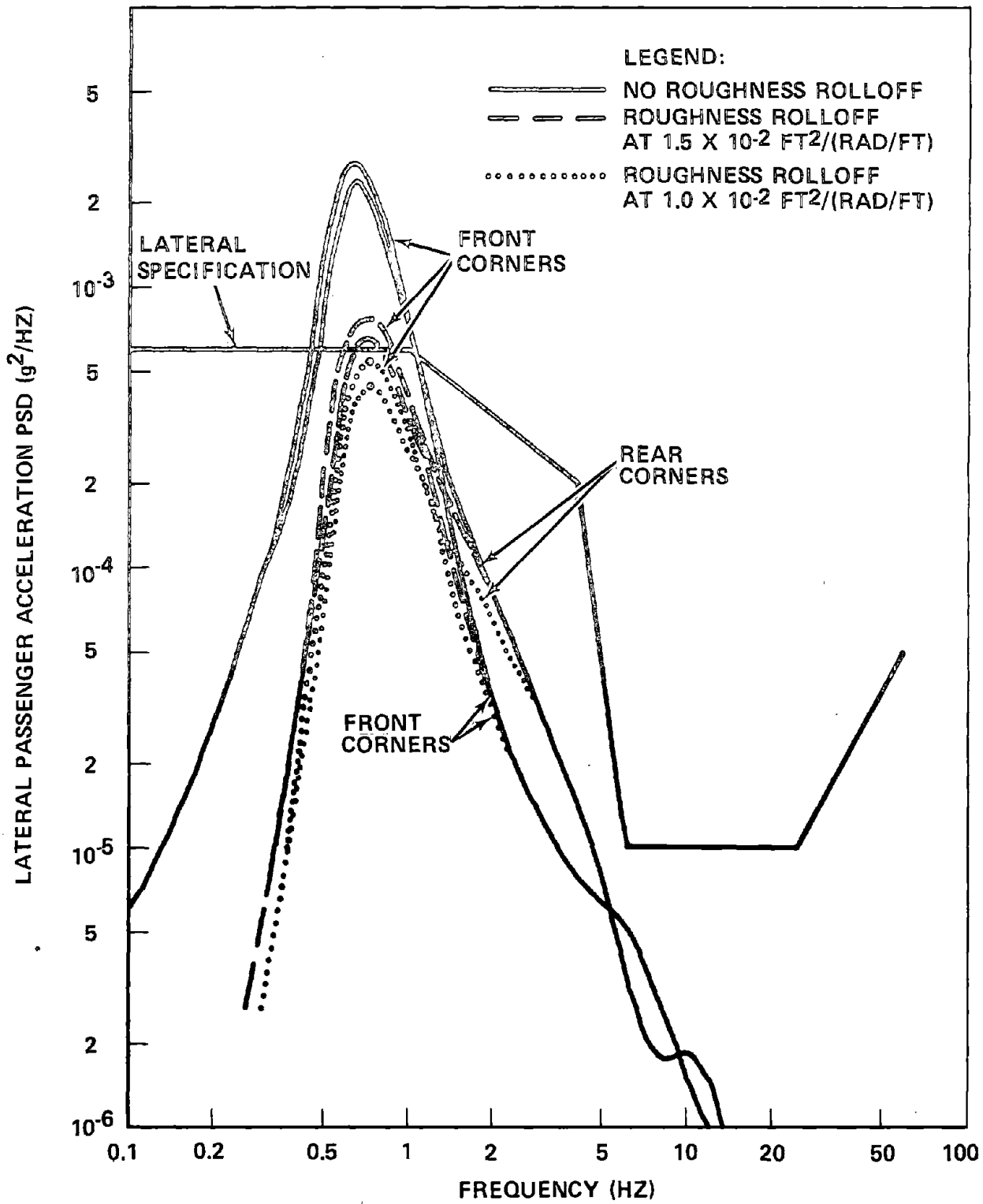
FIGURE 4-50. LATERAL ACCELERATION RESPONSE WITH MODIFIED CONTROL GAIN CONSTANTS

TABLE 4-15. GAIN CONSTANTS

GAIN PARAMETER	VALUES FOR FIG. 4-48	VALUES FOR FIG. 4-50
$K_{\ddot{y}}$	-0.02	0
$K_{\dot{y}}$	0.32	0.275
$K_{h'}$	0	-1
$K_{\ddot{z}}$	0	0
$K_{\dot{z}}$	0.15	0.15
K_h	-2.155	-2.155
K_z	1	1
K_θ	1	1
K_y	0.52	0.05
K_ϕ	1.25	1
K	3.5	3.25
$K_{\dot{h}'}$	0.32	0.275
$K_{\dot{h}}$	0.15	0.15

NOTE: ALL TIME CONSTANTS (τ's) = 0.637

loss in the coils. The average total I^2R loss in the front control coils is about 10 kW, and that for the rear coils is about 5 kW.

E. <u>Response to Non-periodic and Non-random Excitation</u>. This section presents the results of an analysis of the dynamic response of the vehicle to the following types of non-periodic and non-random excitation:

o Grade Transitions

o Steps and Gaps

o Horizontal Curves

o Crosswinds

(1) <u>Grade Transitions</u>. Results of an analysis of vehicle dynamic response during negotiation of a grade transition are presented here. The

nonlinear, single degree of freedom (1 DOF) dynamic model has been utilized for this analysis. Nonlinear effects have been found to be quite significant, and predictions based on a linearized model differ considerably from the results given by the nonlinear model.

As indicated in Paragraph 4.3.2.B(5), nonlinear feedback reduction is necessary in order to maintain acceptable values of stroke during upward
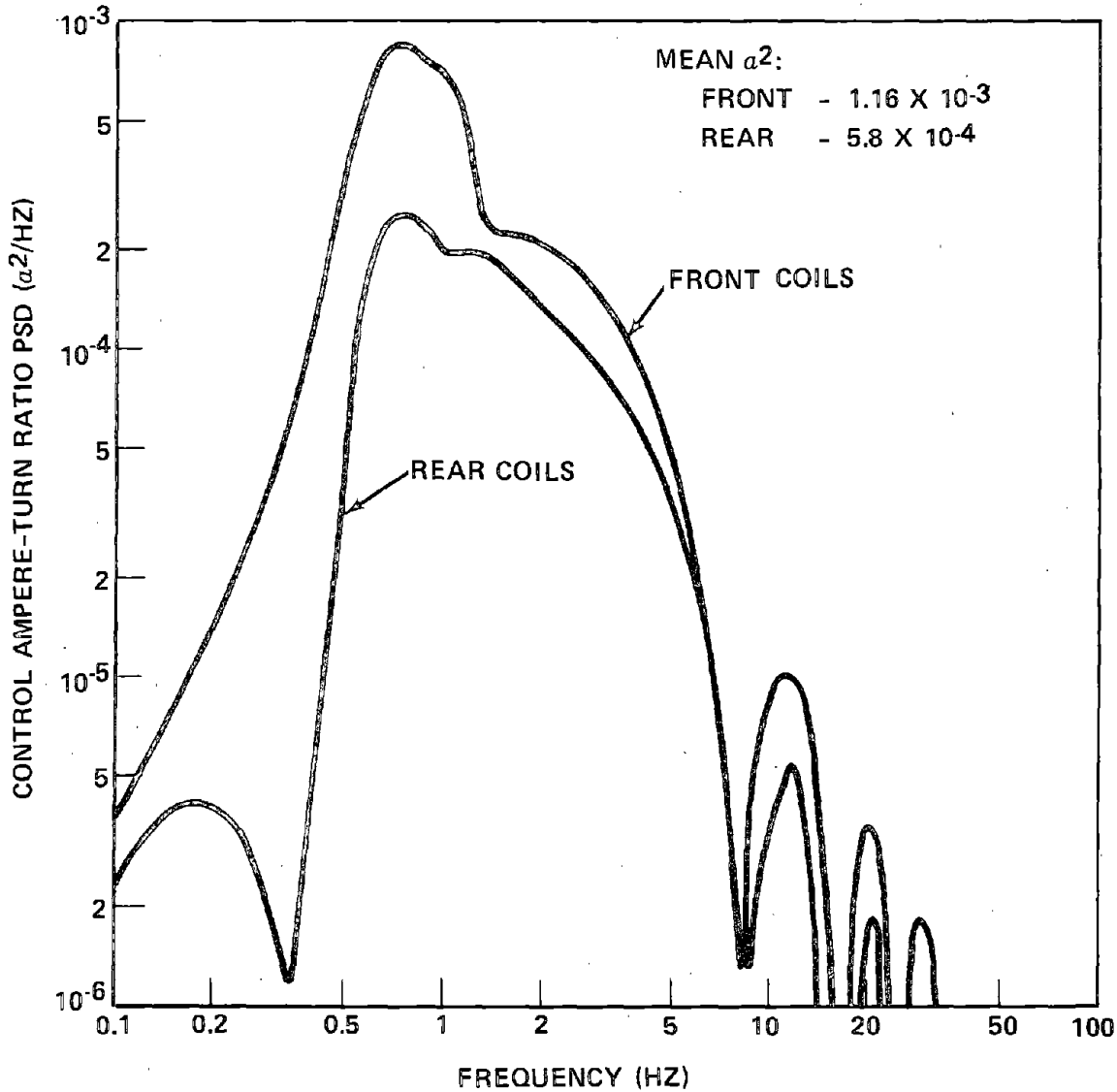
FIGURE 4-51. CONTROL CURRENT RATIO PSD'S FOR RESPONSE TO GUIDEWAY LATERAL RANDOM IRREGULARITIES

vehicle excursions from the nominal position. It has been found that a value of the feedback reduction parameter $K_{h2} = -2.5$ results in a stroke of about 4 cm for a 1 km grade transition, and this value is the basis for the analytical results presented herein.

Figure 4-52 shows the maximum stroke (vehicle excursion from its nominal position relative to the guideway) as a function of transition length to a 2% grade. Results are shown both for transition to an upgrade (increasing slope) and transition to a downgrade (decreasing slope). It is seen that higher strokes are experienced during negotiation of a transition to a downgrade (which corresponds to an upward vehicle excursion). This results from nonlinearities in the magnetic force law, which is not symmetrical about the nominal (or equilibrium) position of the vehicle relative to the guideway.

The maximum stroke is shown in Figure 4-52 as a function of transition length for the case of a vehicle with and without a gap sensor. It is seen that without a gap sensor, much longer transition lengths are required to maintain a specified value of allowable stroke. This results from the necessity of utilizing high damping ratios in a system without a gap sensor in order to meet ride quality requirements, as is demonstrated in Section 4.3.2D. For a system with a gap sensor, the maximum stroke is less than 4 cm for transition lengths greater than 1 km.

Figure 4-53 is a similar plot, showing the maximum value of α (ratio of control coil current to levitation coil current) as a function of transition length to a 2% grade. Again eliminating the gap sensor results in the need for much longer transition lengths to maintain the control coil current below a specified value; or, for a given transition length, a system with a gap sensor will require less control current (and power).

Figure 4-54 shows the effect of relative damping on maximum stroke in a downgrade transition. With a gap sensor, relative damping has a negligible effect on maximum stroke (for the range of transition lengths where the maximum stroke is not excessive). Without a gap sensor, large increases in relative damping produce only modest reductions in the transition lengths required to maintain a specified value of maximum stroke. This is clarified by Figures 4-55A and 4-55B which indicate that relative damping reduces stroke

4-116
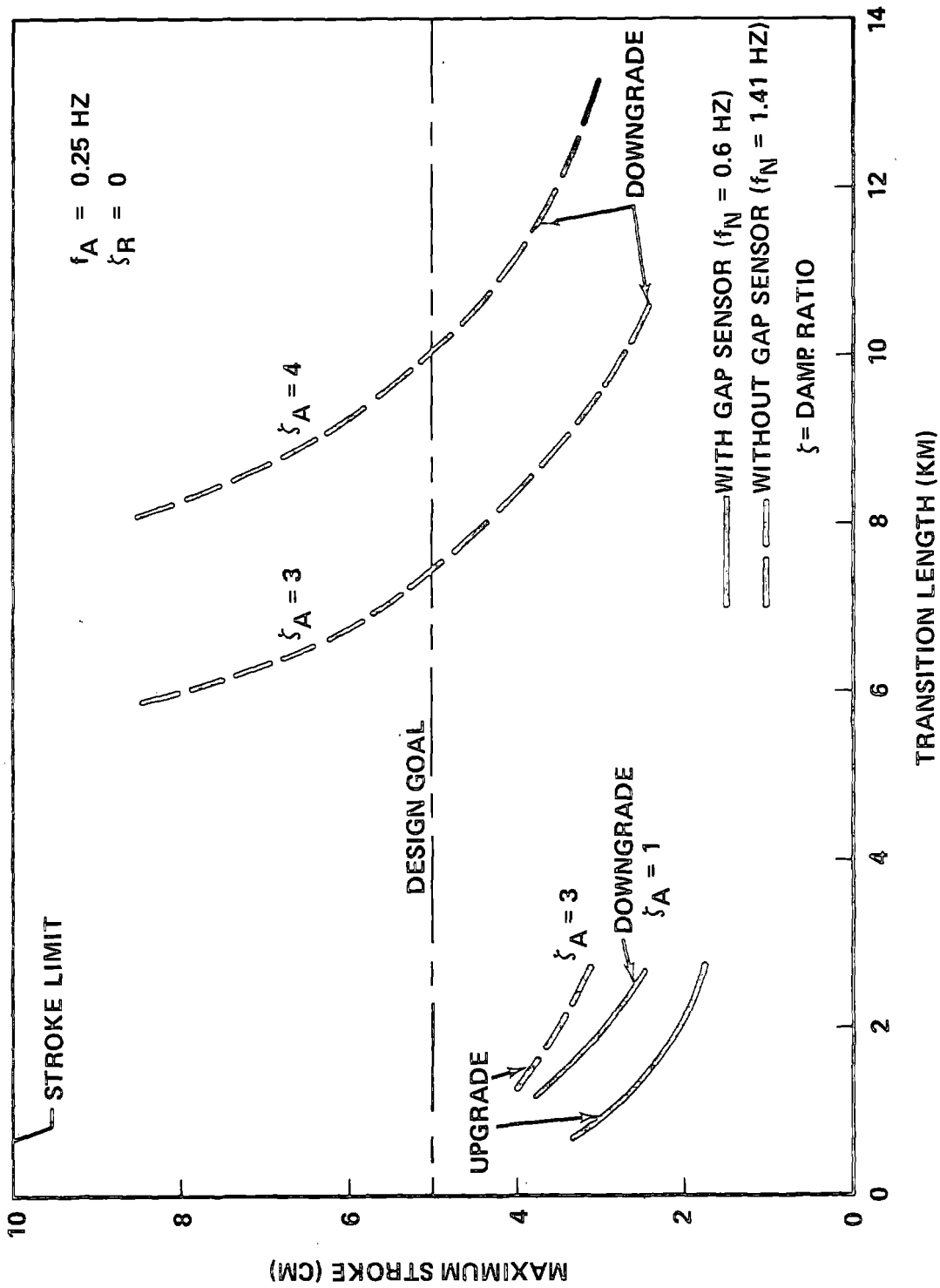
FIGURE 4-52. MAXIMUM STROKE VERSUS TRANSITION LENGTH TO A 2% GRADE
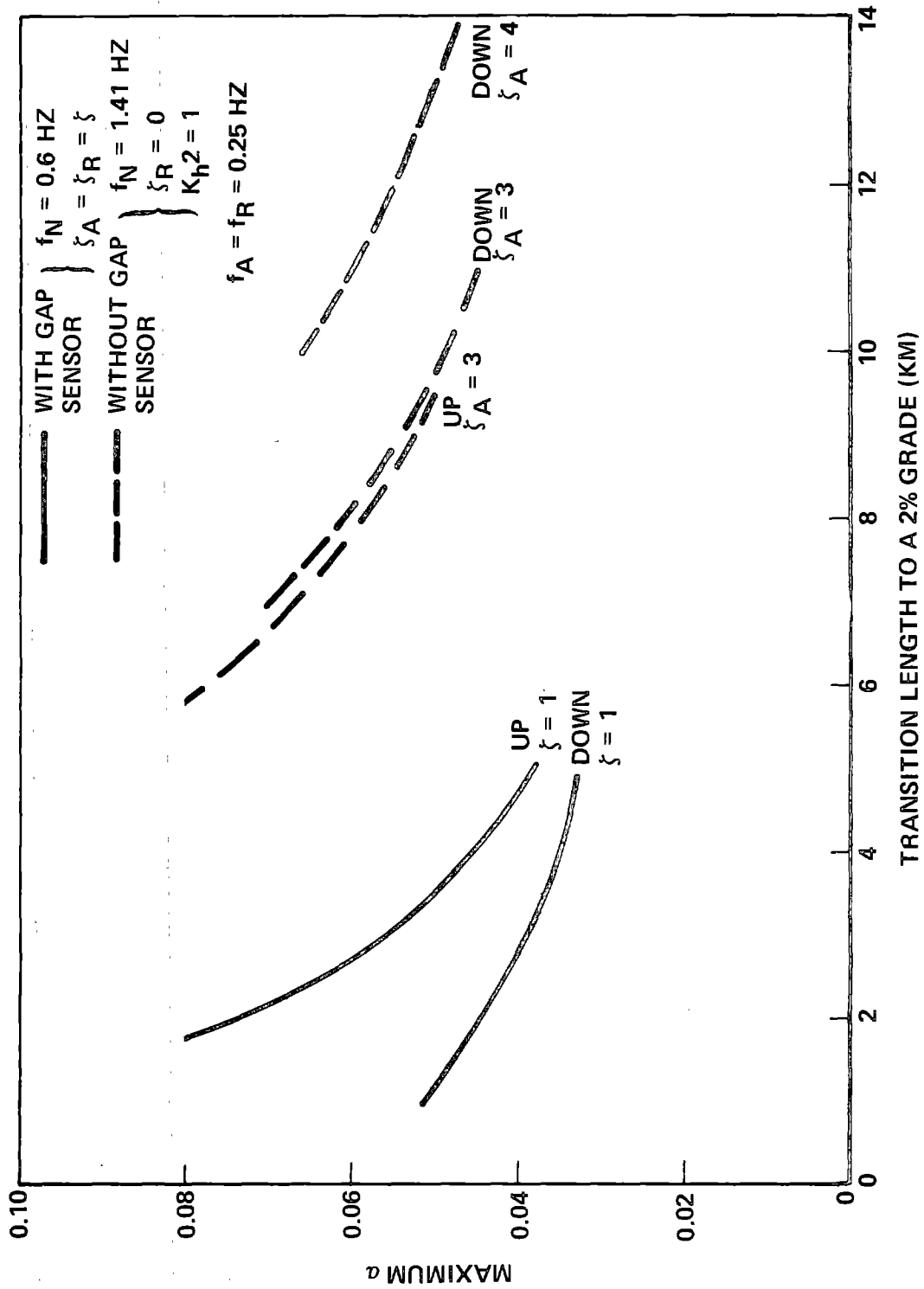
FIGURE 4-53. MAXIMUM CONTROL CURRENT RATIO ON A TRANSITION
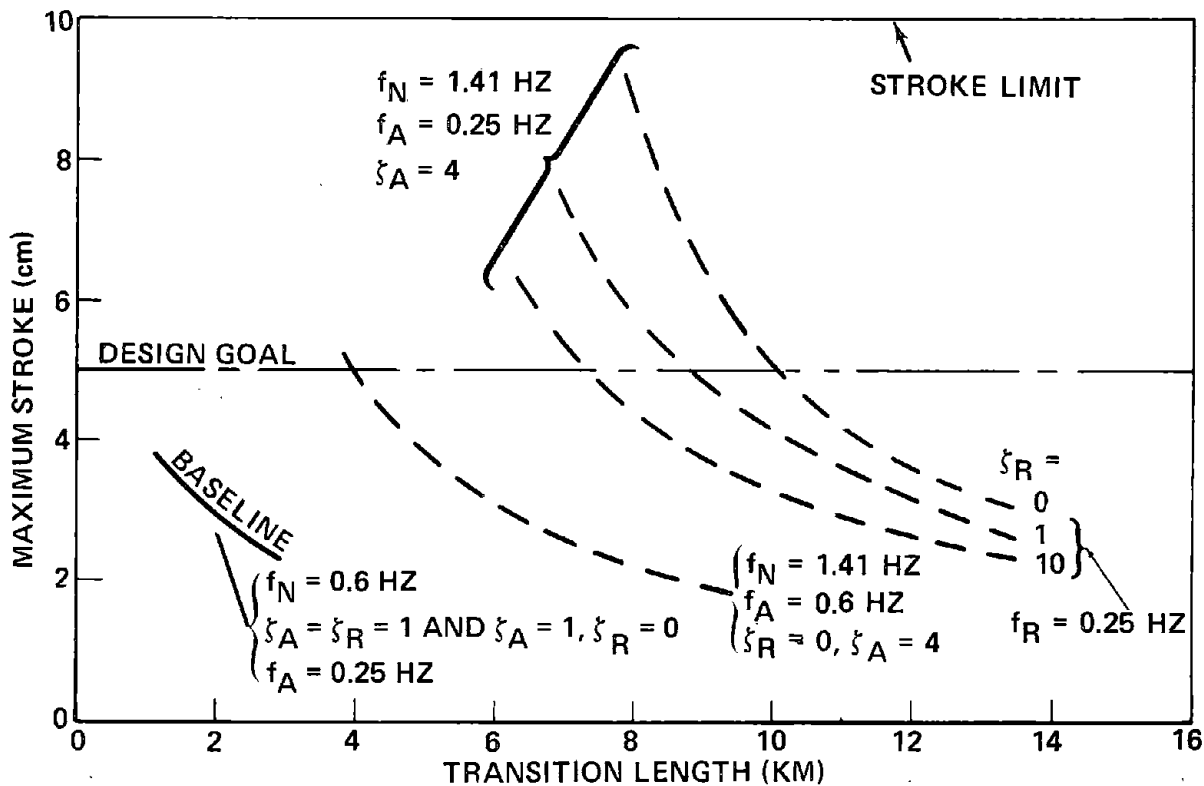
FIGURE 4-54. MAXIMUM STROKE VERSUS TRANSITION LENGTH TO 2% DOWNGRADE

overshoot above the steady state value, but does not affect the steady state value. For a system with a gap sensor (absolute damping ratio ≈ 1), the stroke overshoot is negligible, while without a gap sensor (absolute damping ratio ≈ 4), there is only a modest stroke overshoot.

Figure 4-54 also shows that without a gap sensor, significant reductions in required transition length can be achieved by increasing the absolute damper corner frequency (f_A) from 0.25 to 0.6 Hz. Nevertheless, a transition length of about 4 km is required to limit the maximum stroke to the design goal of 5 cm. (Increasing the corner frequency beyond 0.6 Hz results in undesirable degradation of ride quality characteristics.)

Figure 4-56 shows the maximum vehicle acceleration as a function of transition length. It is seen that the vehicle acceleration is somewhat greater than the grade acceleration, but for transition lengths greater than

FIGURE 4-55B. STROKE-TIME HISTORY ON A TRANSITION WITHOUT A GAP SENSOR

f_N = 1.41 HZ
ζ_A = 4
f_A = f_R = 0.25 HZ
$K_h{}^2$ = 1
L_T = 13.4 KM TO 2% DOWNGRADE

FIGURE 4-55A. STROKE – TIME HISTORY ON A TRANSITION WITH A GAP SENSOR

f_N = 0.6 HZ
ζ_A = 1
f_A = f_R = 0.25 HZ
L_T = 2 KM TO 2% DOWNGRADE

4-120
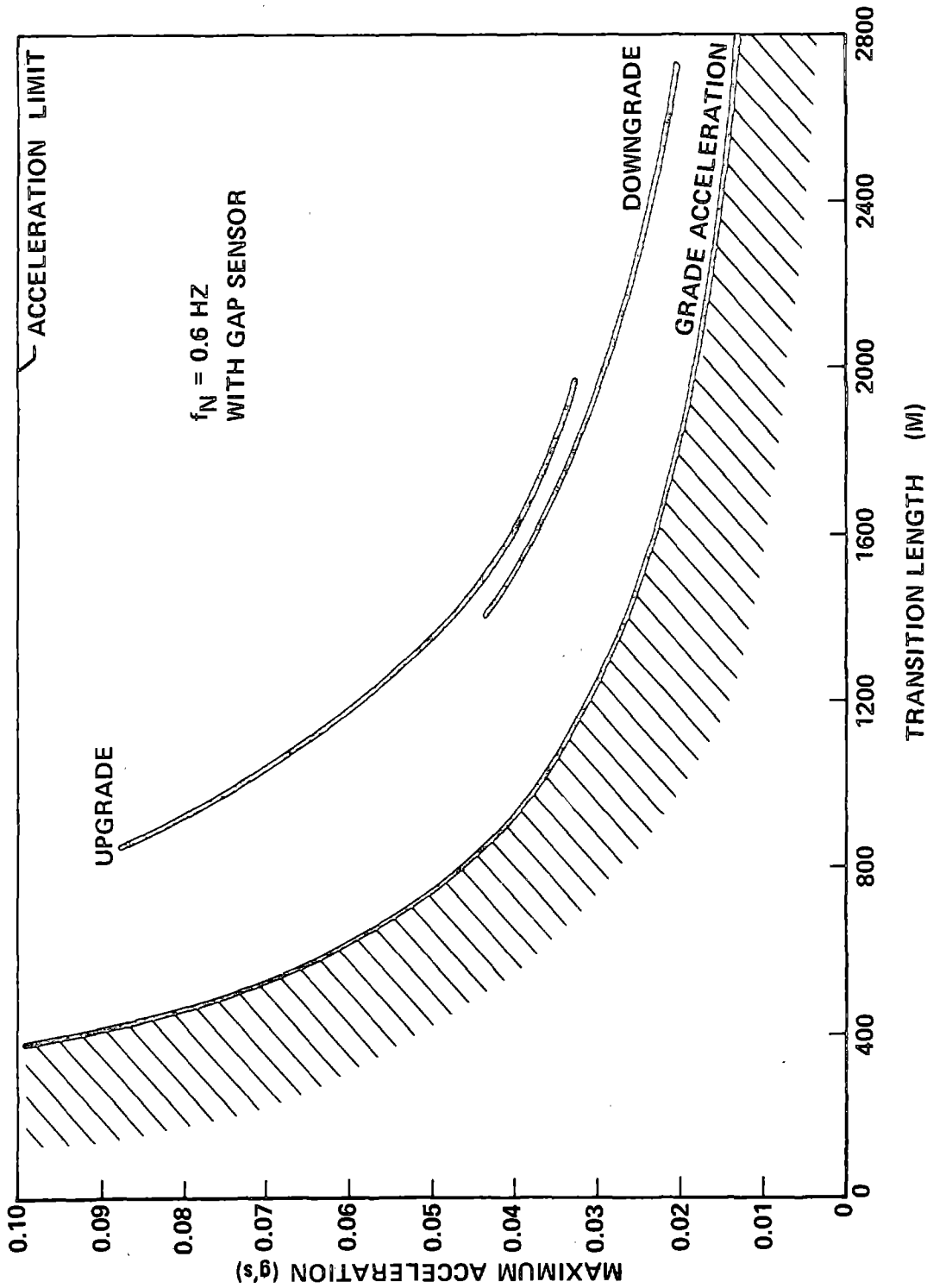
FIGURE 4-56. MAXIMUM ACCELERATION VERSUS TRANSITION LENGTH
TO A 2% GRADE

about 1 km, the maximum acceleration is significantly less than the allowable acceleration limit of 0.1 g.

Figures 4-57 and 4-58 demonstrate the effect of utilizing acceleration feedback instead of positive position feedback. Figure 4-57 shows that the maximum stroke in a grade transition is significantly higher with acceleration feedback than with position feedback. For example, with acceleration feedback a transition length in excess of 6.5 km is required to limit the maximum stroke to 5 cm for a transition to a 2% grade. Figure 4-58 shows that with acceleration feedback the maximum value of the control current ratio α is significantly greater than with position feedback.

(2) <u>Steps and Gaps</u>. The transient response of the vehicle to a step discontinuity in the guideway has been analyzed using both linear and non-linear one DOF dynamic models. The vehicle response has been analyzed both with and without the nonlinear feedback reduction described previously. Figure 4-59 shows the vehicle response to a step with an amplitude of 1 cm. The results of both linear and nonlinear analyses are presented for a system without feedback reduction. The nonlinear analysis shows that the vehicle response to an upward step is different from the response to a downward step. (The sign of the response curve for a down step is reversed to facilitate comparison.) The transient overshoot is greater in the case of an up step. This results from the fact that the nonlinearity in the magnet force law is not symmetrical about the nominal (equilibrium) position of the vehicle rela-tive to the guideway. It is seen that the maximum overshoot is about 0.3 cm and the motion relative to the guideway and is damped out in about 3 or 4 seconds.

Figure 4-60 shows the vehicle response to a 2 cm step. Results are pre-sented for both linear and nonlinear analyses. Results of the nonlinear analysis are shown both with nonlinear feedback reduction ($K_h2 = -2.5$), and without ($K_h2 = 1$). The nonlinear analysis shows that without feedback reduc-tion the vehicle does not follow a downward step. This results from the unstable magnetic force-displacement relation created by linear positive posi-tion feedback, as described in Paragraph 4.3.2.B(5). This situation is reme-died by employing nonlinear feedback reduction. The results in the figure
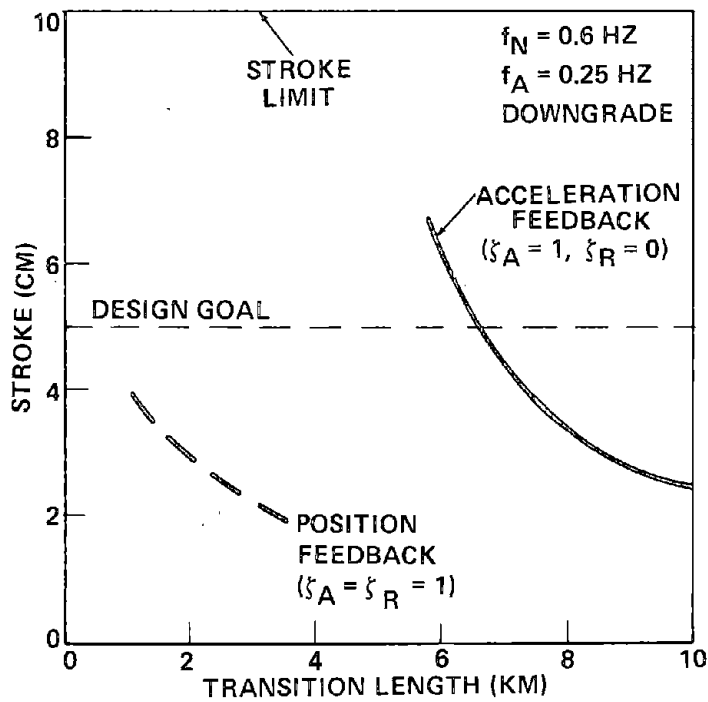
FIGURE 4-57. EFFECT OF ACCELERATION FEEDBACK ON MAXIMUM STROKE VERSUS TRANSITION LENGTH TO A 2% DOWNGRADE
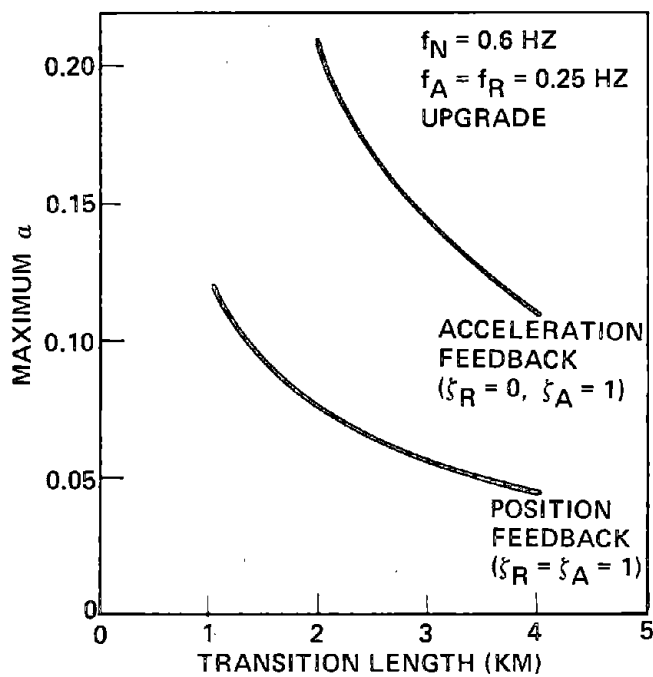
FIGURE 4-58. EFFECT OF ACCELERATION FEEDBACK ON MAXIMUM CONTROL CURRENT RATIO VERSUS TRANSITION LENGTH TO A 2% UPGRADE
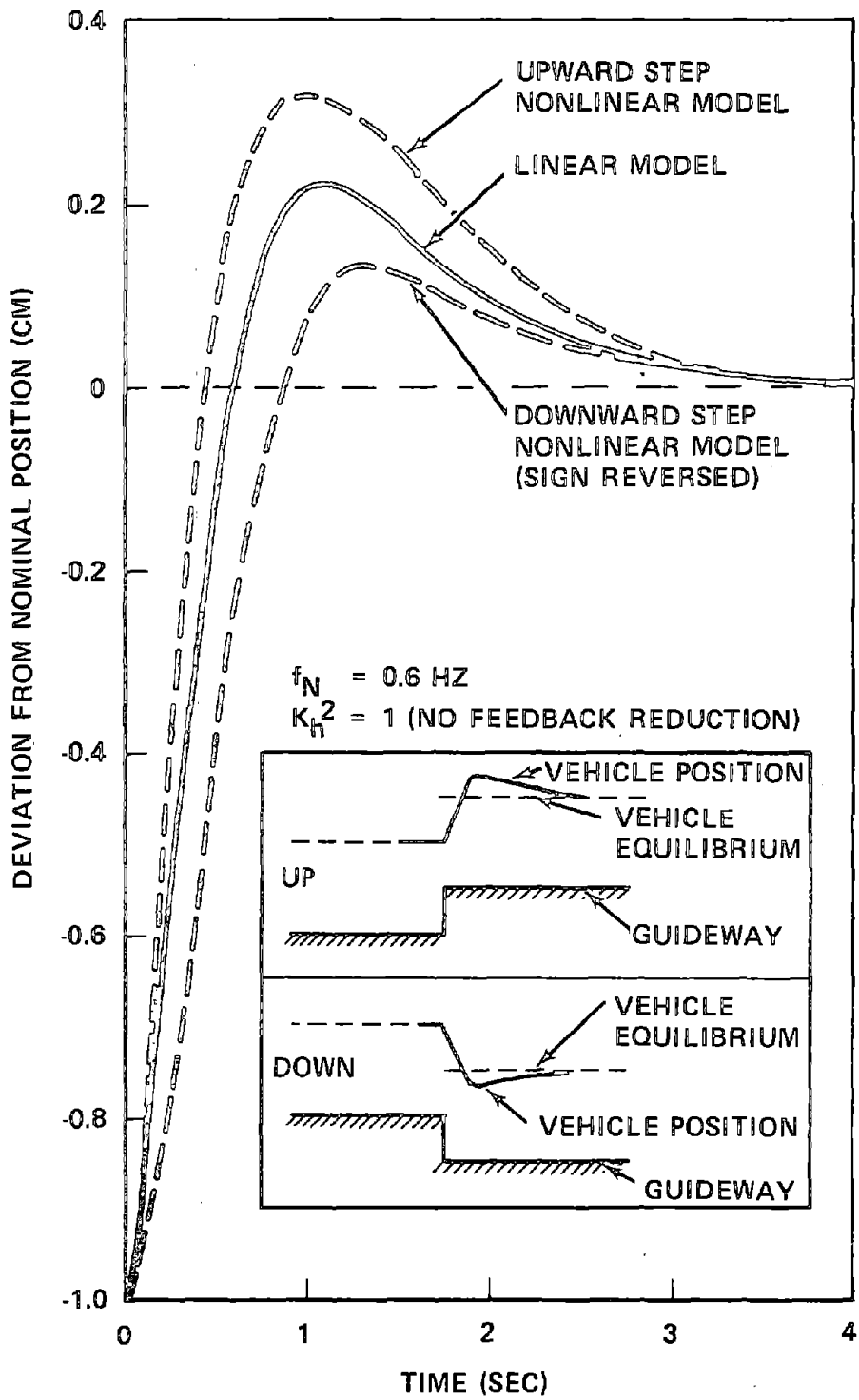
FIGURE 4-59. STROKE — TIME HISTORY IN RESPONSE TO A 1 CM STEP

4-124
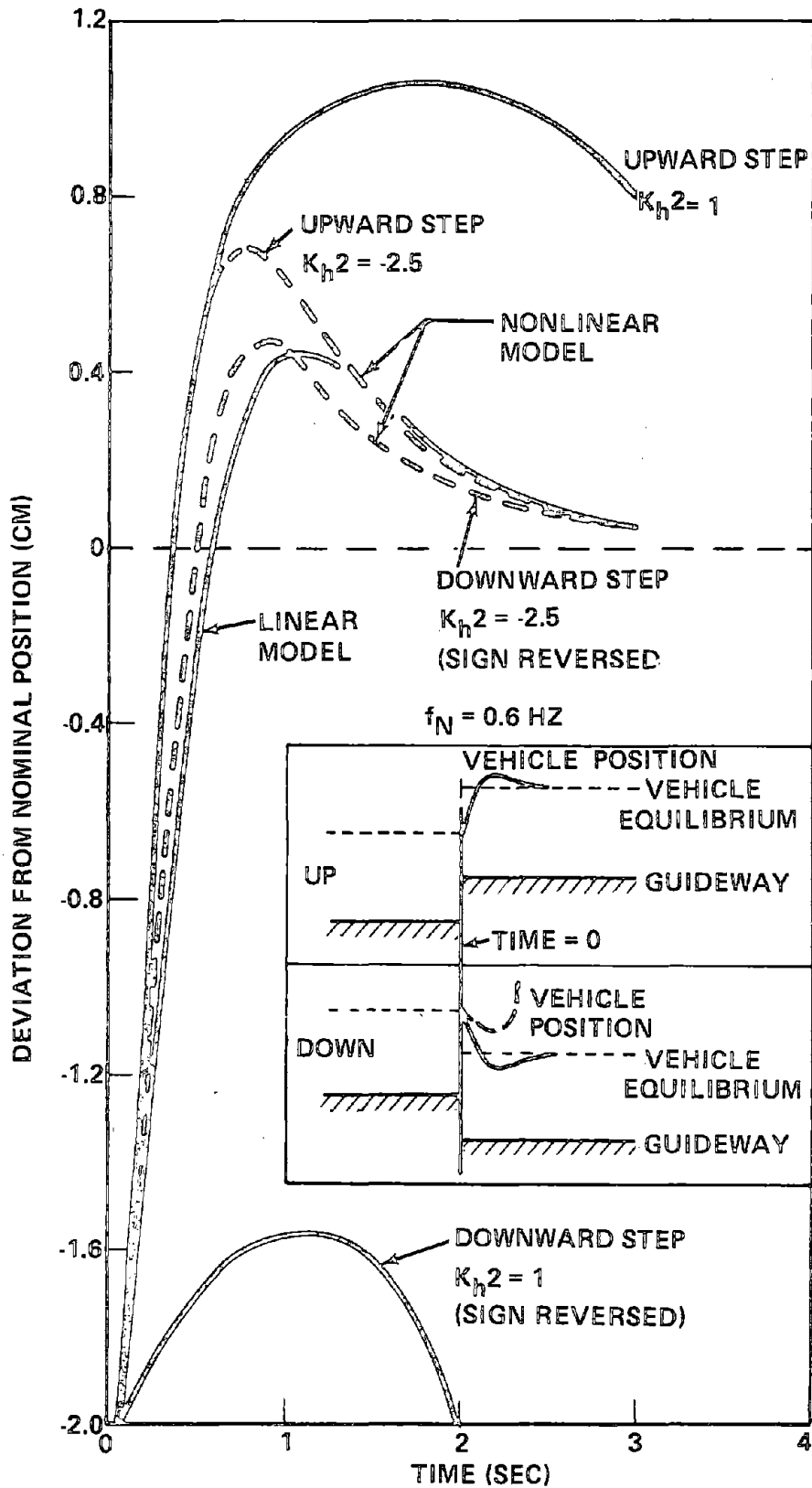
FIGURE 4-60. STROKE – TIME HISTORY IN RESPONSE TO A 2 CM STEP

show that the vehicle follows a 2 cm step discontinuity in the guideway if nonlinear feedback reduction is used. The maximum overshoot is about 0.7 cm and the motion is damped out in about 3 seconds.

The results of an analysis of dynamic response to periodic gaps in the guideway are presented in Section 4.3.2D. Figure 4-43 in that section also shows the vehicle response to a single, isolated gap in the guideway. It is seen that the maximum vehicle excursion in response to a single gap is about 0.4 cm and the motion damps out in about 1 second.

a. Horizontal Curves - Self Banking Capability. A study has been performed to investigate the feasibility of achieving a self banking capability by appropriately designing the guideway and/or vehicle magnet coils. The basic idea is as follows: the hat-shape guideway produces a small self-banking moment in a horizontal curve as a result of cross-coupling effects between lift forces and vehicle lateral motion. Although this moment is not large enough to achieve the equilibrium bank angle for a coordinated turn, the purpose was to determine whether modifications to the guideway configuration and/or vehicle coil geometry could result in increased cross-coupling effects sufficient to achieve the required bank angle. Specifically, canting (rotation) of the L-shaped guideway elements and/or canting of the vehicle magnetic coils has been analyzed to determine whether cross-coupling effects can be increased sufficiently to provide a self-banking capability.

The study indicated that the vehicle magnetic coils must be canted $30°$ or more relative to the horizontal in order to achieve non-negative bank angles. Furthermore, it is found that the maximum bank angle is achieved when the guideway element cant angle is also about $30°$. However, the maximum self banking angle attainable is only about 1/3 of the required equilibrium bank angle for a coordinated turn. This limited self-banking capability is not adequate and does not justify the complexity and cost of canted guideway elements and canted magnetic coils.

b. Coordinated Horizontal Turns. The horizontal turn transition problem and the associated lateral dynamics are somewhat analogous to the grade transition and heave dynamics. However, the horizontal turn problem is more complicated because of the sway/roll coupling, which requires the use

of 2 DOF dynamic modeling. A linearly increasing bank angle provides a coordinated turn transition with a constant rate of change of acceleration ("jerk"). This results in a cubic turn transition of the form: $\phi_g = \dfrac{\dot{a}}{g} t$ and $y_g = \dfrac{\dot{a}}{6} t^3$ where $\dot{a}$ is the guideway lateral jerk and t is time. The guideway cross section geometry used in the 2 DOF sway/roll model is illustrated in the following sketch.
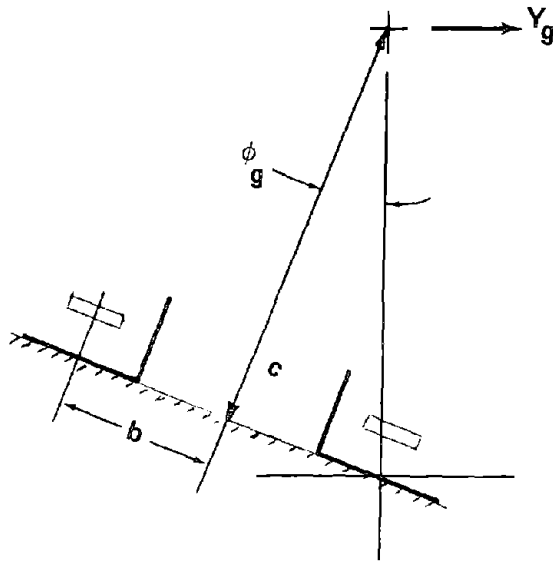
GUIDEWAY TURN GEOMETRY

After exiting from the transition, the vehicle enters the constant bank angle coordinated turn which has a constant lateral guideway acceleration.

In order to analyze the curve transition problem, a pseudo 3 DOF digital simulation has been written. The 2 DOF sway/roll model was augmented with a pseudo-steady state acceleration heave model in order to simulate the effect of heave depression (that is, the vehicle settling closer to the guideway in the turn). The steady state heave equation is:

$$Z - Z_g = \frac{-m + 4b_z K_z (K_{\dot{z}} \tau_z + K_{\ddot{z}})}{a_{zz} + 4b_z K_z K_h} \ddot{Y}_g \phi_g$$

The symbols are defined in Appendix B.

Adding roll to the guideway motion via the e_y and e_ϕ terms (see Section 4.3.2C) modified the equations of motion sufficiently to require a revised set of control gains in order to obtain satisfactory dynamic behavior.

Satisfactory performance was obtained by reducing K_y and K_h, from 0.35 to 0.01 s/m and reducing K_z from 0.15 to 0.075 s/m. Figure 4-61 shows the vertical and lateral strokes for this set of gains for the case of a 10° bank angle turn at the maximum jerk of 0.03 g/s. The transition length is 0.7876 km and the transition time is 5.88 seconds. The vehicle is making a right-hand turn and the strokes are computed at the right-hand (inside) corner. The vertical and lateral strokes are positive if the gaps are being reduced.

As the vehicle does into the transition, it rides down in the guideway (negative lateral stroke) and the right side or "inside" of the vehicle tends to stabilize out with about a 1.0 cm lateral gap increase (i.e., the vehicle moves to the right or inside with respect to the guideway). The left-hand side of the vehicle has a corresponding decrease in lateral gap. Also, there is about a 4.0 cm vertical gap increase on the right side because the vehicle roll angle lags the guideway roll. After the end of the transition (and the vehicle is in the constant bank angle turn), the lateral gap stabilizes out rapidly (Figure 4-61), but the vertical gap on the right side has been decreased by a maximum of about 6 cm. The steady state vertical gap on the right side in the turn is about 5 cm less due to the heave depression.

It has been found that somewhat better response can be obtained by replacing the position feedback in the heave mode with acceleration feedback ($K_{\ddot{z}} = 0.1517$ s^2/m) to lower the heave frequency to 0.6 Hz, and reduce the heave damping ratio to 0.25 with a $K_{\dot{z}} = 0.35$ s/m. All of the other gains are unchanged. Figure 4-62 shows the vertical and lateral strokes for this set of gains and the same 10° bank angle turn at the maximum jerk of 0.03 g/s. As the vehicle goes into the transition, it rides up into the guideway (positive lateral stroke) and the right-hand side tends to reach a steady state lateral stroke of about 0.6 cm and a maximum lateral stroke (reduced lateral gap) of about 1.0 cm. In addition, the vertical stroke shows an initial gap increase as the roll of the vehicle lags the roll of the guideway, but within about 2 seconds the vehicle motion is dominated by heave depression. The maximum vertical stroke (reduced vertical gap) is about 5.1 cm following the end of the transition, and the steady state stroke is about 4.5 cm in the turn. The lateral stroke is zero in the steady state turn.

4-128
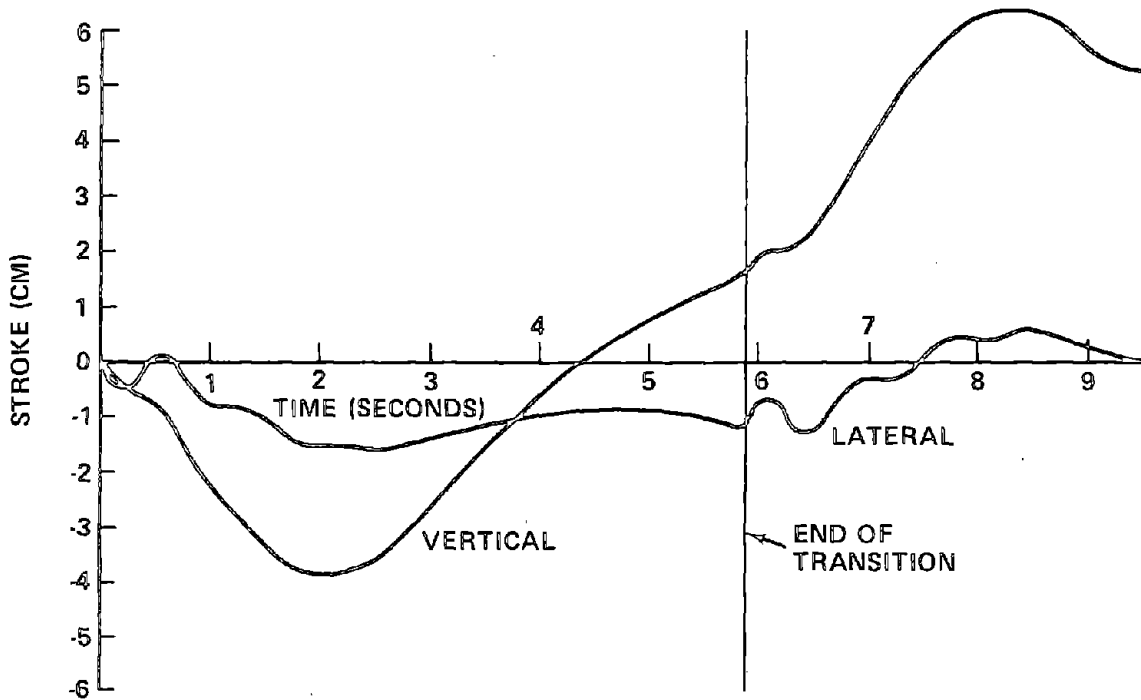
FIGURE 4-61. STROKES FOR A HORIZONTAL TRANSITION SECTION (WITH POSITION FEEDBACK IN HEAVE)

o FINAL BANK ANGLE = 10 DEGREES
o TRANSITION LATERAL JERK = 0.03 g/SEC
o TRANSITION LENGTH = 0.7876 KM
o RIGHT HAND TURN
o STROKES FOR RIGHT HAND CORNER OF VEHICLE
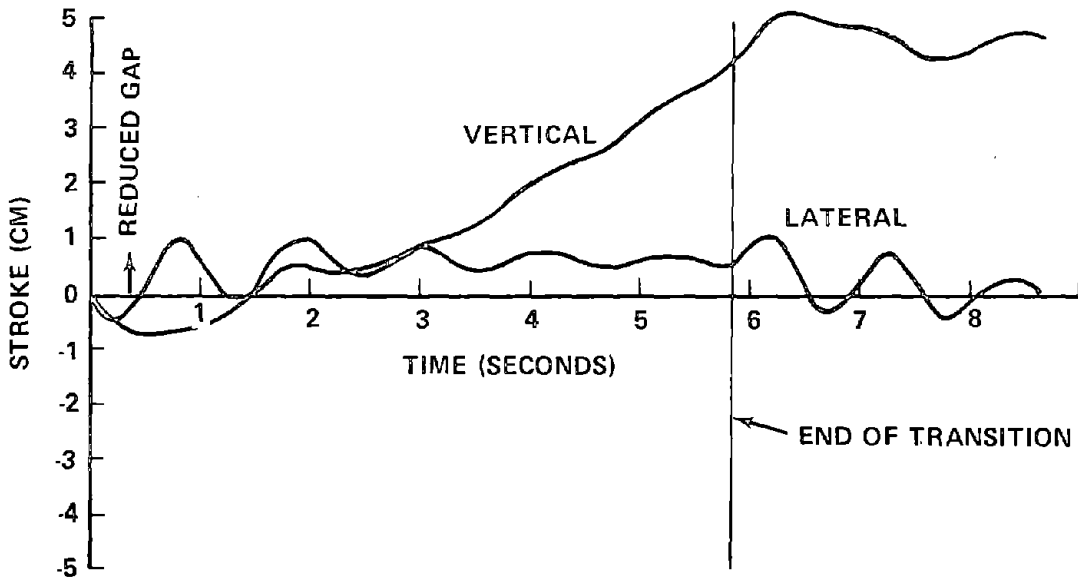
FIGURE 4-62. STROKES FOR A HORIZONTAL TRANSITION SECTION (WITH ACCELERATION FEEDBACK IN HEAVE)

The above results are preliminary in that magnetic force nonlinearities have not been treated and extensive gain parameter studies have not been performed to optimize the selection of gain constants, including consideration of the effects of gain constant modification on ride quality and dynamic behavior in a transition. Although these complete, detailed analyses remain to be performed, the results presented above indicate that horizontal turn transitions can be negotiated with appropriate selection of control system gain constants.

        c. <u>Crosswinds</u>. The response of the vehicle to crosswinds has been investigated using the 2 DOF sway/roll model. Of prime concern is the transient overshoot which may occur in the coupled sway/roll modes, since the mode coupling limits the amount of damping which can be achieved. Figure 4-63 shows the transient sway/roll response to a suddenly-applied 20.1 m/sec (45 mph) crosswind. The peak vertical displacement is 4.7 cm (1.85 in.) for an overshoot of 12% relative to the steady state value of 4.2 cm (1.71 in.). The peak lateral displacement is 2.6 cm (1.02 in.) for an overshoot of 18% relative to the steady state value of 2.2 cm (0.87 in.).

Since the yaw response can be damped independently of the sway/roll modes, sufficient damping can be put into the system to prevent significant yaw overshoot for crosswinds, and a steady state analysis can be used to determine the yaw response. The steady state yaw response, with no position feedback is

$$\psi = M_\psi / a_{\psi\psi}$$

where M_ψ is the aerodynamic yawing moment, 320 kN-m (237,000 ft-lb), and $a_{\psi\psi}$ the yaw spring constant, 9.04979×10^4 kN-m (6.7025×10^7 ft-lb). The resulting steady state yaw angle is 0.2 degree, corresponding to a lateral stroke at the forward corner of 5.7 cm. The total combined (roll/sway and yaw) steady state lateral stroke is 7.9 cm.

        F. <u>Dynamical Aspects of LSM and LIM Propulsion</u>. In accordance with the original program requirements for the scope of propulsion-related studies, consideration was given to the influence of certain types of propulsion
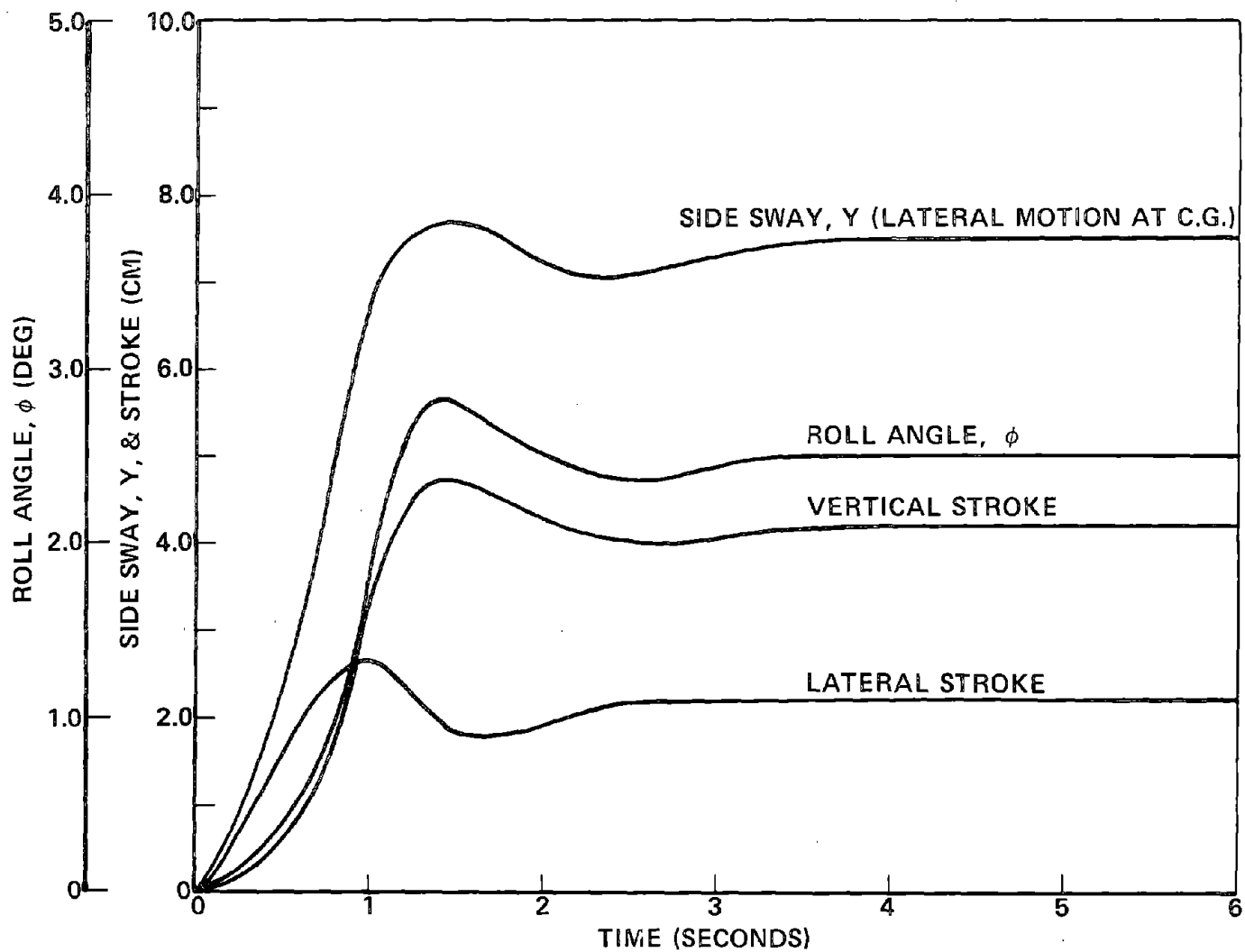
FIGURE 4-63. SWAY/ROLL RESPONSE TO A 45 MPH CROSSWIND

systems on vehicle dynamic behavior. The linear synchronous motor (LSM), for example, is claimed to be capable of providing damping, i.e., ride control, of all vehicle dynamic modes thereby obviating the need for an onboard control system power supply. Further advantages with regard to headway control are also claimed if all ride control functions - in addition to propulsion - are provided from the (active) guideway of the LSM. The Raytheon Company was contracted by Philco-Ford to study the problem of LSM ride control; the results of their study are presented in Appendix F. Essentially Raytheon performed an analysis of the forces and moments on an elemental LSM unit, presenting the results as a function of various vehicle displacements. In addition, the force and moment characteristics of the elemental LSM unit have been evaluated for vehicle control capability by identifying and analyzing a hybrid vehicle/guideway configuration which could provide dynamic forces and moments of sufficient magnitude and phase to accomplish damping of the vehicle sway/yaw degree-of-freedom, with the levitation magnets providing damping in all other dynamic modes. This hybrid configuration constitutes a compromise relative to the degree of vehicle/guideway complexity required to provide damping in all dynamic modes. The timing of this work and the limitations on Task I were such that no in-depth analysis could be undertaken to determine if the DOT ride quality specification can actually be achieved. Cursory examination, however, indicates that the LSM approach is feasible, but substantially more analysis is required to prove acceptable performance in all modes and for turns and grade transitions as well as straight and level operation. One disturbing aspect, however, is the increase in complexity of the guideway, e.g., due to the requirement for additional active surfaces (other than propulsion) to provide the necessary forces. As indicated in Sections 4.4.4 and 5, this increases guideway cost and could be counter-productive. Also, since onboard power supplies on the order of 100-200 kW are needed for lighting, air conditioning, communications, brake/wheel activation, etc. (compared with 25-50 kW* for ride control), there seems to be very little energy benefit in putting the control system power supply on the wayside. At this point, therefore, it is recommended that future research on LSM be directed to it purely as a propulsive device.

---

*Straight and level conditions, up to 150 kW for short-time (~ 7 sec) 1 km upgrades.

The linear induction motor (LIM) was also originally viewed solely for its relationship to vehicle dynamics. A LIM is a large, heavy, narrow gap device (~ 10 to 20 mm) with substantial performance penalties for significant gap variations during operation. The motor gap must be tightly controlled, and if the motor is suspended from the vehicle, the reactive forces from this (secondary) suspension system must not degrade vehicle ride quality and stroke. The double-sided LIM has some freedom in the vertical direction and Garrett recommends that it be rigidly attached to the vehicle in this direction. However, an active control system will be required for centering the motor relative to the aluminum reaction rail. The single-sided motor (SLIM) used in the propulsion studies of Section 4.4.3 has some freedom with regard to lateral stroke, but the vertical gap must be tightly controlled; with the added complexity of a downward attraction force (due to the iron in the reaction rail) varying with gap dimensions and vehicle speed. In either case, detailed analyses are required to firmly establish the feasibility of suspending the motor from the vehicle without adversely affecting vehicle ride quality and stroke. A brief examination of the problem, however, suggests operating it in a "tug" mode with its own suspension system, as is the case with the Grumman Air Cushion TLRV. In this way, the motor is effectively uncoupled from the vehicle, resulting in a somewhat lighter system.

G. Conclusions

(1) Straight and Level Operation. The following conclusions pertain to straight and level operation of a 445 kN (100,000 lb) Repulsion MAGLEV vehicle* at 134 m/s (300 mph) over the baseline guideway with a nominal statistical roughness coefficient, A, of 1.5×10^{-6} m (5×10^{-6} ft).

a. Ride Quality. The DOT vertical and lateral ride quality specifications are achievable for the baseline active control system employing position feedback in conjunction with absolute (inertial) velocity feedback. Alternate systems using acceleration feedback in place of position feedback or only heavy absolute damping also meet the ride quality specifications and do not require gap sensors. For the baseline control system, the following detailed conclusions are drawn:

---

*With appropriate scaling criteria, the results are applicable to the finalized, 366.5 kN (82,400 lb) baseline, 80-seat Revenue TMLV.

● Vertical acceleration response to guideway random irregularities is well below the specified limits.

● Lateral acceleration response to guideway random irregularities is below the specified limits, provided the guideway lateral roughness PSD has a long wavelength (low frequency) rolloff at 1.0×10^{-2} $ft^2/(rad/ft)$.

● Elimination of relative damping improves ride quality but requires increased control power.

b. <u>Gap Response</u>. Vehicle dynamic response to gaps in the aluminum guideway elements is acceptable. The vehicle maximum excursion is less than 0.5 cm for a single gap. For periodic gaps spaced 15 m (50 ft) apart, the cruise height above the guideway is reduced by less than 1.5 cm.

c. <u>Elevated Guideway</u>. The dynamic behavior of a properly designed elevated guideway will not result in unsatisfactory ride quality.

d. <u>Power Consumption</u>. The heavy damping control scheme consumes more power than either the baseline scheme or the acceleration feedback scheme, but the difference is small compared with the overall power requirements of the vehicle.

(2) <u>Grade Transitions</u>. The following conclusions pertain to operation of a 445 kN Repulsion MAGLEV vehicle at 134 m/s over a transition section connecting the straight and level guideway to a guideway at a 2% grade. The baseline hat-shaped guideway is employed, with a nominal statistical roughness coefficient, A, of 1.5×10^{-6} m (5×10^{-6} ft).

a. <u>Stroke</u>. All of the control system concepts studied permit negotiation of both up- and down-grade transitions for a design goal maximum stroke of 5 cm. The baseline position feedback system consumes the least control power, but the difference in power consumption compared with the alternate control schemes is probably not significant when compared with the overall vehicle power consumption. However, the required transition lengths differ substantially, as follows:

o The baseline position feedback system requires a transition length of $\sim$ 1 km. Nonlinear position feedback reduction is provided to avoid possible unstable dynamic behavior on transition to a down-grade. Relative damping has negligible effect on maximum stroke except for very short transitions, i.e., $\ll$ 1 km.

- The alternate highly damped system (without gap sensors) requires a transition length of ∼ 4 km with an absolute damper filter frequency of 0.6 Hz.

- The alternate acceleration feedback system (also without gap sensors) requires a transition length of ∼ 6.5 km.

- Improved vehicle dynamic behavior in a grade transition is possible for a system either with or without a gap sensor, if the amount of absolute damping is reduced during passage through the transition. The necessary signals can be obtained by wayside communication or by increasing the capacity of the onboard computer and employing it (in conjunction with the existing accelerometers) as a simplified inertial navigator. This permits subtraction of the component of the absolute rate signal due to the vertical curvature of the guideway, thus eliminating the damping forces which increase vehicle stroke relative to the guideway. Substantial reduction in transition length should be possible, particularly for the alternate concepts without gap sensors.

b. Ride Quality. Ride quality during passage over a grade transition is not as good as that on a level guideway. To meet the DOT ride quality specifications based on power spectral density criteria*, the following conclusions are drawn:

- The baseline position feedback system, without relative damping, requires a transition length ∼ 4 km. (For operation over the stroke-limited transition length of ∼ 1 km, the ride quality specification limit would be exceeded for approximately 7.5 seconds.)

- The alternate highly damped system (without gap sensors) requires a transition length ∼ 5 km.

- The alternate acceleration feedback system was not analyzed for ride quality during grade transition. However, it is our judgement that it would be slightly better (shorter transition length) than the baseline position feedback system.

(3) Horizontal Curves (Turns). Detailed analyses have not been performed to ascertain vehicle dynamic motion in horizontal turns. Preliminary, linear multi-DOF analyses, however, indicate that turns can be negotiated, with the following observations.

---

*It appears that the PSD criteria on ride quality are inappropriate for short-time, infrequent events such as grade and turn transitions. If the DOT criteria on maximum sustained acceleration and rate of change of acceleration (jerk) are used, then all control schemes considered will show acceptable ride quality for transition lengths ≪ 1 km.

- The baseline position feedback system can achieve acceptable dynamic behavior, subject to appropriate gain constant modification and damping reduction. However, more detailed studies are necessary to establish the concomitant effect of gain constant modification on ride quality and stroke in a grade transition.

- The alternate acceleration feedback system shows somewhat better performance in a turn than the baseline system. The alternate highly damped system was not analyzed for horizontal turn negotiation.

- Vehicle dynamic behavior (primarily stroke) in a horizontal turn can be improved, if desired, by reducing the amount of absolute damping provided during transit through the turn — as previously described for negotiating a grade transition.

(4) Crosswinds. Preliminary multi-DOF dynamic analysis of vehicle response to a 20 m/s (45 mph) crosswind shows a maximum side sway (lateral motion of the c.g.) of about 8 cm. Rolling motion also takes place and effectively reduces maximum lateral stroke to 2.6 cm. Maximum vertical stroke (due solely to roll) is ~ 5 cm. No serious problems are foreseen in withstanding crosswinds of 20 m/s.

H. Recommendations. A significant accomplishment of the Task I TMLV program effort in the area of vehicle dynamics is the development of multi-DOF computational techniques and associated computer programs for precise evaluation of MAGLEV vehicle dynamic response to a variety of input parameters and for various control system concepts/strategies*. This now permits rapid analysis of problems not studied in depth here (or not studied at all) because of scope/time limitations. Recommended analyses are as follows:

- Conduct multi-DOF analyses of vehicle transient and steady-state dynamic response to guideway gaps, grade transitions, horizontal curves, wind gusts and elevated guideway deformations. Nonlinear magnet force effects should be incorporated.

- Perform extensive, in-depth parametric investigations of control gain constant selection to optimize vehicle ride quality and dynamic response characteristics in horizontal curves.

---

*This program is documented in Appendix G, Volume III of this report.

o Perform in-depth analyses of alternate control concepts, e.g., acceleration feedback and/or revised signal mixing and filtering schemes, to improve ride quality and dynamic response in curves and grade transitions.

o Conduct multi-DOF analyses of vehicle dynamic behavior at speeds above and below 134.1 m/s and include response to wind gusts, guideway gaps, grade transitions and horizontal turns.

4.3.3 Control Magnets

Active control with control magnets is chosen over a secondary suspension for a number of reasons; it allows more freedom in meeting the ride quality requirements, it can be used on a rougher guideway, it is simpler and likely to be less costly, and it only requires a modest amount of control power under normal conditions. Previous work has shown that separate control coils are a necessity to allow persistent-mode operation of the levitation coils, and to keep the power requirements within reason. The control coils can be cryogenically cooled, or be at ambient temperature; ambient coils have been chosen for the conceptual design to simplify the driver interface and other aspects of the coil design. These magnets are most effective when mounted as close to the track as practical and coaxial with the levitation magnets. On the other hand, it is even more important to maximize the vehicle clearance above the track. Accordingly, the control magnets are located on the bottom of the dewar, coaxial with the levitation magnets. A control coil envelope of approximately 5 cm high by 18 cm wide is provided, as shown in Figures 4-16 and 4-18.

Eight control coils are specified to provide redundancy, each coil providing one-half of the total control force needed at the four levitation module locations. The windings of these coils will utilize aluminum tape interleaved with mylar or some other suitable tape insulation to minimize weight and maximize heat transfer from the core of the coil. Heat generated in the coils will be dissipated by conduction through the insulating overwrap to the outside container of the magnet module, and by radiation and convection to the vehicle skin on the bottom of the module and hence to the ambient air. Provisions are also included in the conceptual design to circulate cooling air over the underside of the control coils for direct convective cooling, if required.

4-137

Electrically, each magnet must supply 3% of the levitation magnet ampere turns to meet ride quality requirements when gap sensors are utilized in the control loops, and 4.5% when they are not. The operating levels required are then 10,500 ampere turns and 15,800 ampere turns RMS, respectively. The parameters of the baseline magnets for these two cases are listed in Table 4-16.

TABLE 4-16. CONTROL COIL PARAMETERS (PER COIL)[1]

| | AMPERE TURN RATIO | |
	$a = 0.03$	$a = 0.045$
o MATERIAL	ALUMINUM	ALUMINUM
o TURN SIZE (CM)	5 X 0.0233	5 X 0.0233
o OVERALL CROSS SECTION (CM)	5 X 18.4	5 X 18.4
o LENGTH (BETWEEN CENTERLINES)(CM)	150	150
o WIDTH (BETWEEN CENTERLINES)(CM)	50	50
o TURNS	750	750
o RESISTANCE (AT 120°C) (Ω)	10	10
o INDUCTANCE (H)	1.6	1.6
o CURRENT DENSITY, RMS (A/mm^2)	1.2	1.8
o CURRENT PEAK (A)	20	30
RMS	14	21
o REAL POWER, PEAK[2] (kW)	4	9
RMS	2	4.5

[1]VALUES FOR STRAIGHT AND LEVEL OPERATION.

[2]THE MECHANICAL POWER DELIVERED BY EACH COIL IS < 100 WATTS AND IS MUCH LESS THAN THE POWER REQUIRED TO SUPPLY THE COIL I^2R LOSSES.

Negotiation of grade transitions requires more net control force than for level conditions. A value of 7% of the levitation magnet ampere turns or 24,600 ampere turns is specified for the baseline condition with gap sensors. This value is predicated upon a transition distance of 4 km* while still maintaining ride quality (i.e , higher values would provide shorter trade transitions, but ride quality requirements cannot be met). When gap sensors are not used, a control current ratio of about 10% to 11% is required to maintain

---

*4 km is based on the minimum transition length for the conditions shown in Figure 4-39.

ride quality over transition distances of ∼ 10 km. The grade transition control force requirement is a transient peak-loading effect with a low duty cycle. The extra thermal load imposed on the control coil due to grade transitions is a short-term condition and can be "heat-sinked" into the control coil and dissipated normally after the grade is negotiated. The impact of the added power for grade transitions will fall on the control coil drivers which must be sized to provide the higher peak values.

4.3.4 Control Electronics

The suspension subsystem control electronics is diagrammed in Figure 4-64. The following paragraphs discuss the major elements of this subsystem.

A. Ride Control Sensors. The basic ride control sensors consist of eight accelerometers, a sensor for longitudinal velocity, one for longitudinal acceleration, and a set of eight gap sensors. Gap sensors are used on the baseline system, but a system has been examined which does not use gap measurements. Some of these sensors are duplicated for reliability purposes.

The accelerometers are used to measure the vertical and horizontal accelerations at each of the four levitation module locations. These data provide the necessary inputs to compute ride control signals for active damping. The accelerometer performance requirements are:

- Range ± 0.5 g
- Resolution $\pm 2 \times 10^{-4}$ g
- Accuracy (All Effects RSS'd) $\geq \pm 2\%$ of Full-scale
- Bandwidth (3 db) ≥ 25 Hz

These requirements can be met using existing commercial devices if provisions are made to limit the temperature range to about 100°F (30° to 130°F, typically). Also care must be taken to select units which are not susceptible to magnetic fields, or else appropriate magnetic shielding must be used.

The gap sensors measure the vertical and horizontal gap between the vehicle and the track at the eight accelerometer stations. This information is used with the accelerometer data to compute dynamic ride control commands. The requirements for this device preclude the use of any known instrument that currently exists. None of the available devices have all the necessary capabilities (i.e., measure gaps of 0 to 25 cm with 1% accuracy under all-weather

4-139

conditions). Optical, RF, acoustic, magnetic field, inductive, capacitive and mechanical methods of implementing the requirement have been investigated. All of these techniques have problems which either eliminate them or make it doubtful that the performance requirements can be met under all-weather conditions.
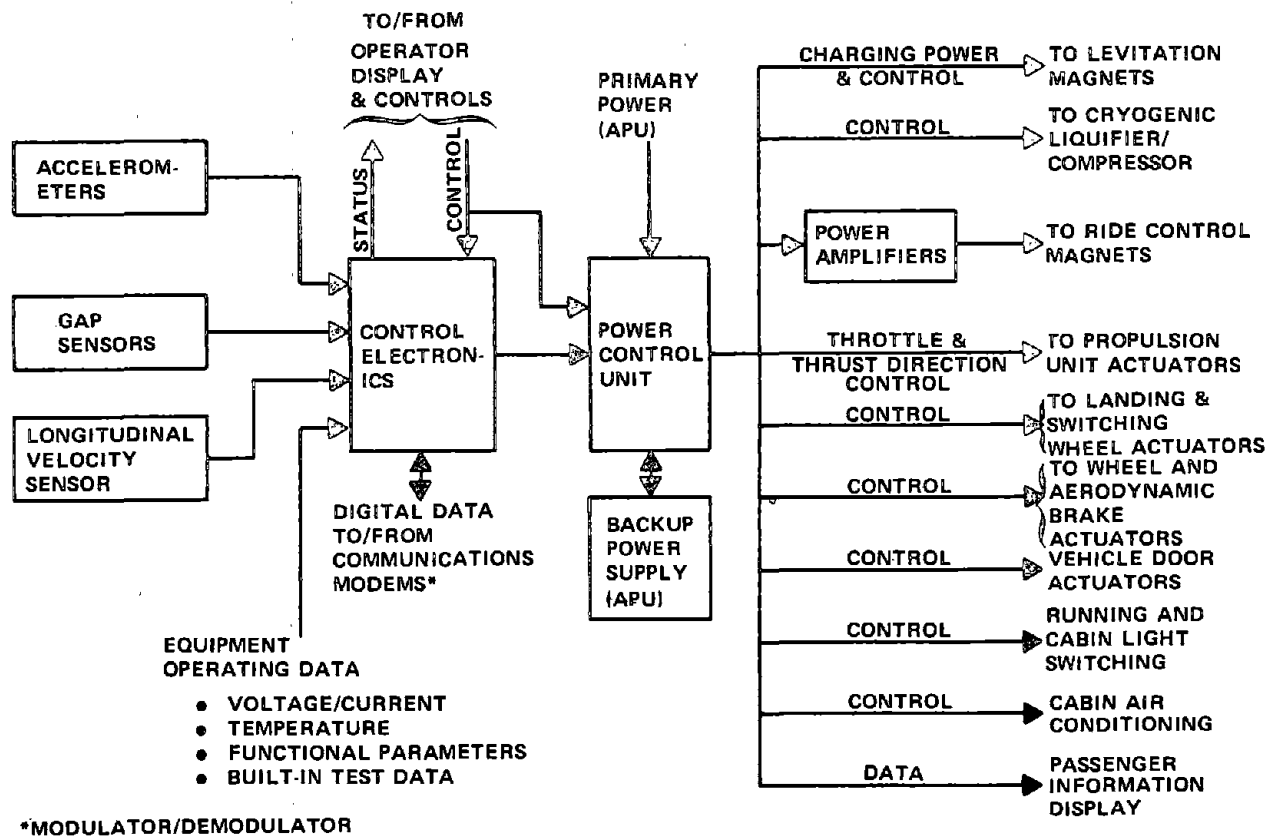
FIGURE 4-64. RIDE CONTROL SUBSYSTEM

Of the possible techniques, the inductive measurement approach currently appears to be the best candidate. This approach bases gap measurement on the variation in inductance of an a.c. excited coil with distance to the guideway. The approach is an extension of existing technology, currently capable of a maximum gap measurement of about 5 cm. The major problem anticipated is the maintenance of accuracy over a sufficiently wide temperature range. The design problems of this approach can probably be solved but will require considerable engineering development.

The RF approach utilizes either an interferometer to measure the phase shift of a fixed carrier or the frequency shift of a swept carrier as a function of gap. Both methods suffer from the problem of large errors due to

4-140

dielectrics, particularly ice, in the gap. It may be possible to devise ways to compensate for these errors, however. The feasibility of error compensation will have to be established, followed by engineering development. The total development costs of this approach are likely to exceed those of the inductive measurement alternative.

The other alternatives considered are judged less likely to yield working hardware in all-weather conditions. Overall, the gap sensor is the only suspension subsystem electronic element which has major unsolved development problems.

The longitudinal velocity and acceleration sensors provide the requisite information to control the vehicle forward motion to the desired profile. The velocity measurement can be made by the simple expedient of measuring the elapsed time between the guideway joints (provided constant guideway lengths are used). This method takes advantage of the large transient change in inductance of a coil during passage over the joints (Section 4.5.1D). An alternate approach could be the elapsed time between wayside distance markers. Obtaining hardware for this measurement is straightforward, using existing commercial devices.

B. Control Electronics. A digital computer is selected as the basic control element because of the variety and number of control functions to be performed. This element is augmented by extensive input/output (I/O) circuitry to mate it to the other subsystem hardware. The functions performed by the control electronics are:

(1) Multiplexing, analog to digital conversion, and processing of accelerometers, gap sensors, and longitudinal velocity sensor outputs.

(2) Computation of damping control signals for the control magnets based upon the sensor inputs.

(3) Computation of longitudinal velocity control signals for the propulsion unit throttle, and thrust direction controls during normal operations and emergency conditions.

(4) Automatic sequencing of aerodynamic drag brakes and wheel deployment, including the computation of braking control signals during switching, landing, and in-station operations.

(5) Buffering of en-route vehicle control information from the ground complex via the communications subsystem into the vehicle controls in both the pre-stored program and real-time control modes of operation.

(6) Automatic monitoring of vehicle subsystem status information, including key voltage, current and temperature readings, and subsystem functional parameters. Automatic initiation and monitoring of equipment built-in test routines.

(7) Automatic fault isolation based upon data from Item 6. Automatic notification of the operator and the ground complex of fault conditions and switching of redundant back-up systems.

(8) Computation of vehicle position as a function of time with respect to terminals in the ground complex. Computation of other operator and passenger display information such as time to next terminal, time to ultimate destination, etc.

(9) Output of appropriate vehicle status information to the onboard recorder, to the operator and passenger data displays, and to the wayside complex via the data communications link.

The computer characteristics required to meet only the ride-control requirements are: (1) a 2000-word 12-bits/word memory; (2) a basic instruction-cycle time of 1 microsecond or less; (3) a hardware signed multiplication capability with an execution time of 40 microseconds or less on two 12-bit words; (4) capability to handle double precision calculations; (5) an instruction set equivalent to those of current mini-computers; and (6) an option to add floating point computation facilities if needed. The basic I/O electronics needed consist of: (1) a 10 or 20 input analog multiplexer and an analog to digital converter to handle the inertial inputs, and (2) a set of eight digital to analog converters to provide magnet control signal outputs.

However, the control electronics must also handle the other functions and interfaces identified in Figure 4-64, in addition to the ride control. Thus, the overall capabilities must be increased from the values given above to the following: The memory capacity must be increased to 4000-8000 words, the hardware signed multiply execution time must be reduced to 20 microseconds, and the I/O capabilities must be greatly expanded.

It is obvious the control electronics mechanization will require a sophisticated, high-performance set of hardware. This hardware is, however,

well within the state-of-the-art and may be accomplished by straightforward adaptation of existing technology. This requirement will benefit from the current trend of development in digital microprocessor hardware. Future large-scale integration (LSI) can be expected to reduce the size and cost of the basic computer and a good deal of the I/O circuitry, but care must be exercised in estimating the cost impact of LSI. Section 6.1.2 contains a discussion of the estimated costs.

C. <u>Power Control Unit</u>. The Power Control Unit (PCU) mechanizes the following functions:

o Primary power switching to the onboard electronics including switchover to the back-up power source.

o All requisite power buffering between the low-power outputs of the Control Electronics/Operator Control Panel and the higher power inputs to the various control actuators except the control magnet power amplifiers.

o Secondary power conversion for the onboard electronics as required (i.e., for those subsystem elements without integral secondary power supplies).

o Voltage and current pick-offs for some of the vehicle status monitoring instrumentation.

The required power control circuitry can be implemented with application of existing relay and solid-state electronic technology.

D. <u>Control Magnet Power Amplifiers</u>. The control magnet PAs translate the low-power control signals from the control electronics to the power levels required by the control magnets. Eight independent amplifiers are required, driving the eight control magnets in parallel sets of two each. Each of these amplifiers must provide the drive capabilities specified in Section 4.3.3.

The power handling requirements for ride control on level roadways are relatively modest; 2 kW average and 4 kW peak with gap sensors, and 4.5 kW average and 9 kW peak without. These requirements go up by a factor of about 5.5 when grade transitions are considered; to 11 kW average and 22 kW peak with gap sensors, and 26 kW average and 52 kW peak without. The highest levels are of short-duration and low duty cycle, but they will still dictate the design voltage and current levels of the driver electronics. The only area that can take advantage of the short-term factor will be the thermal design of the units.

Power amplifier circuitry operating in the switching mode will be needed to gain efficiency. The selection of either transistor or silicon controlled rectifier (SCR) circuitry is subject to a detailed design and cost tradeoff between the requirements of the control magnet and the PA, considering the voltage and current levels required. The baseline system (with gap sensors) requires a PA capable of supplying a peak current of 47 amps at a peak voltage of 470 volts, which tends to favor the SCR approach. In either case, design of the hardware for the specific needs of this application is likely to be required but such design is well-supported by existing technology.

E. Back-Up Power Supply. The back-up power supply must supply the full suspension subsystem load for a minimum of 20 to 30 minutes to permit transit of any vehicle to the next stop with a main power source failure. The control coil amplifier load is large enough so that the use of batteries for this load is questionable from the standpoint of weight. A dedicated APU is selected for this purpose. A unit such as the Garrett GTP-36 series driving a suitable generator is well suited to the need. Automatic start (under control of the subsystem control electronics) will be employed with a switchover time requirement of $\leq$ 60 seconds. Batteries will be used to supply the low-power fault isolation and switching circuitry.

F. Suspension Subsystem State Instrumentation. A set of control system instrumentation is required to provide key operational parameter data to the control electronics and the operator. These data are needed for monitoring of the vehicle status and to mechanize fault detection, isolation and corrective actions. The hardware involved will include a central signal conditioner and pick-off devices distributed throughout the subsystem elements.

G. Reliability and Failsafe Operation. The feature of providing redundant control coils for each levitation module reduces the problems associated with the failure of a single control coil or its electronics. However, failure of several control coils or the complete control system must be avoided since the ride quality and stroke (position) of the vehicle will be adversely affected. To minimize the possibility of this happening, it is necessary to provide high reliability in the basic suspension subsystem equipment and to provide for failsafe operation. Equipment reliability is achieved by: (1) conservative design of the hardware; (2) a high level of quality control during manufacturing, test, and maintenance including use of high reliability,

screened parts; (3) adequate qualification and acceptance testing including exposure to expected environmental extremes; and (4) adequate in-service preventive maintenance. All of these elements should be included in the procurement and use of operational hardware.

Failsafe operation of the suspension control electronics is implemented by providing dual redundancy, fault isolation, and switching to augment those portions of the subsystem which do not have inherent redundancy. The equipment needing augmentation are the inertial sensors, the control electronics, the power control unit and part of the vehicle state instrumentation. The control coils, their power amplifiers, and the back-up power supply are inherently redundant. Incorporation of the additional hardware to implement failsafe operations is recommended.

4.3.5 Weight and Volume of Suspension/Guidance Elements

Table 4-17 summarizes the weight and volume of the three major components of the suspension and guidance subsystem. A more detailed weight summary of the magnet module is given in Table 4-10.

All of the major items in the control system electronics have been summarized, including a back-up APU to supply power to the control system in case of failure of the primary APU. Batteries are also supplied to provide low-level power in the transition period in case of primary APU failure. The "miscellaneous" category contains more contingency than required for the electronics alone, and it should be regarded as the contingency for the entire suspension subsystem.

4.3.6 Magnet Failure

One of the potential, and more serious, modes of failure is the loss of the magnetic field at one of the corners. The likelihood of failure is a function of the magnet and cryogenic design, i.e., the choice of superconducting current density, the stability of the coil in response to changes in the magnetic field, the loss of refrigerant, and/or loss of vacuum. While the magnets can be designed with excess copper and superconductor to minimize the probability of failure, the degree of "excess" is a judgment that must be determined by experiments during the magnet development program. In

TABLE 4-17. SUSPENSION SUBSYSTEM VOLUME AND WEIGHT

COMPONENT	VOLUME PER UNIT m³ (IN.³)		WEIGHT PER UNIT N (LB)		TOTAL WEIGHT KN (LB)	
o MAGNET MODULES[1] (4)					21.8	(4910)
LIFT/GUIDANCE MODULES	1.23	(75,200)	4,533	(1020)		
CONTROL COILS	0.06	(3600)	928	(210)		
o CRYOGENICS (1 SET)					11.5	(2585)
REFRIGERATION[2]	1.5	(91,500)	7,100	(1600)		
PIPING, INSULATION, ATTACHMENTS	—	—	4,400	(1000)		
o CONTROL SYSTEM ELECTRONICS (1 SET)					13.9	(3125)
ACCELEROMETERS (16)	120[3]	(7.5)	1.8	(0.4)		
GAP SENSORS (16)	1,400[3]	(800)	111.	(25)		
LONG. VELOCITY SENSOR (2)	400[3]	(25)	4.5	(1)		
CONTROL ELECTRONICS (1 SET)	0.08	(4800)	334.	(75)		
POWER CONTROL UNIT (1 SET)	0.17	(10,000)	1,112.	(250)		
POWER AMPLIFIERS (8)	0.047	(2800)	445.	(100)		
SIGNAL CONDITIONER (1)	0.019	(1100)	133.	(30)		
BATTERIES (2)	0.027	(1700)	356.	(80)		
CABLING (1 SET)	—	—	445.	(100)		
BACK-UP APU/FUEL (1)	1.6	(26,000)	1,334	(300)		
MISC[4](SUPPORT STRUCT, ATTACHMENTS, CONTINGENCY)	—	—	4,460.	(1000)		

[1]DETAILED WEIGHT BREAKDOWN IN TABLE 4-10, VALVES USED FOR SHIELDED COIL

[2]TWO COMPRESSORS AND TWO REFRIGERATORS

[3]UNITS ARE CM³ FOR THESE ITEMS

[4]CONTAINS CONTINGENCY FOR COMPLETE SUBSYSTEM

addition, the use of monofilament wire to minimize the heat generated by a.c. losses must be balanced against the stability obtained with multi-filament twisted superconducting composites. The possibility of using a braid to achieve both these goals appears very promising and deserves further consideration.

Magnet failure can be caused by loss of vacuum and/or loss of refrigeration. Loss of vacuum will cause rapid loss of superconductivity, due to the sudden large heat inputs. For this reason each of the redundant magnets has a separate cryostat. Loss of vacuum during normal operation is considered to

be a minimal risk as evidenced by the long and successful experience of industry with vacuum containers. For example, Western Airlines has flown liquid nitrogen in evacuated cryogenic containers for five years with no vacuum failures. A protective shroud encloses the magnet to minimize the possibility of dewar puncture by ferrous objects. Loss of refrigeration through compressor failure is considered a higher risk because the compressor seals cannot be lubricated due to the possible contamination of the helium. Experience has shown that normal replacement of these seals minimizes this failure; but to guard against this possibility two redundant features are added. First, a storage container of 16-liter capacity is placed in each cryostat, and finally a second compressor is placed on the vehicle.

Although magnet failure and loss of lift can still occur (whether by "chance" or deliberate action), the idea of redundant magnets in the corners of the vehicle tends to minimize the serious nature of this failure mode since the vehicle corner can be supported by the remaining magnet. The wheels required for low speed operation form a back-up system to prevent impact with the guideway; furthermore, the dedicated guideway provides confinement surfaces on which the vehicle will coast to low speeds on wheels in the event of complete loss of magnetic field at one of the corners.

The redundant magnet approach was suggested in a previous study in which an analysis of the failure mode of the vehicle was made, assuming an average force law over a flat guideway (Ref. 4-22). Table 4-18 updates this work by using the correct image calculations for a corner guideway for both the 0.5 x 3 m magnets (before failure) and the 0.5 x 1.5 m magnets (after failure).

The results show the new suspension height (h) and the lateral guidance distance (h') due to a failure of one of the two magnets at position 1 in Figure 4-65. The normal equilibrium values for these parameters h = h' = 30 cm, and $F_G = 0.36 \ F_{L_{Avg}}$. After failure the remaining operational magnet in the damaged module (position 1) drops 5.5 cm and moves 5.8 cm closer to the vertical surface in order to increase both the lift and guidance force that was lost. The adjacent support magnet module (position 2) also drops slightly (1.3 cm) and moves away from the vertical 5.8 cm so that the guidance

TABLE 4-18. MAGNET EQUILIBRIA POSITIONS AFTER FAILURE OF ONE OF THE EIGHT LEVITATION/GUIDANCE MAGNETS (See Figure Below)

MAGNET POSITION	LIFT FORCE, F_L (FRACTION OF NORMAL VALUE)	GUIDANCE FORCE, F_G (FRACTION OF NORMAL $F_{L_{AVG}}$)	SUSPENSION HEIGHT, h (cm)	LATERAL DISTANCE, h′ (cm)
1	0.83	0.23	24.5	24.2
2	1.17	0.23	28.7	35.8
3	0.83	0.36	32.6	30.5
4	1.17	0.36	28.0	29.5
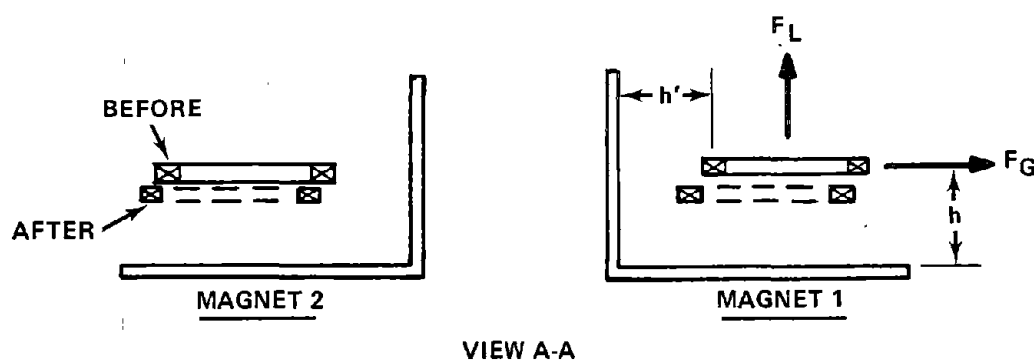
VIEW A-A
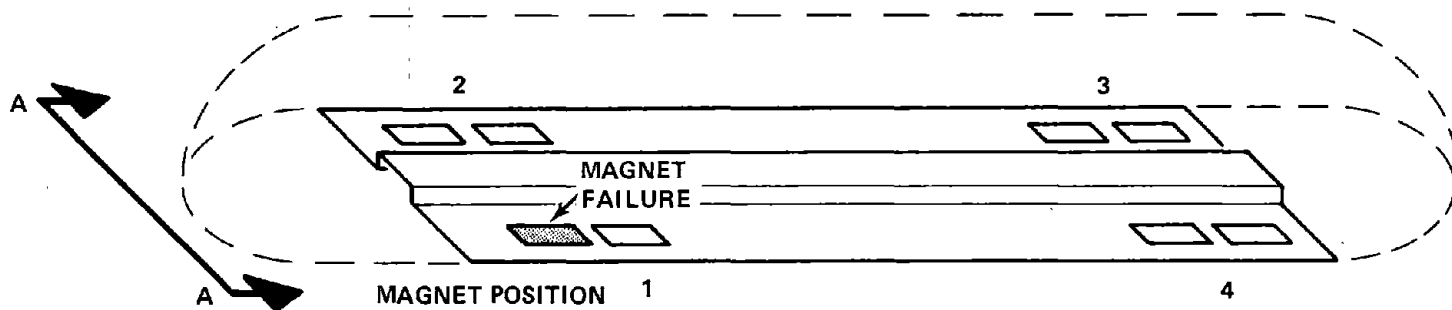
FIGURE 4-65. SCHEMATIC OF MAGNET FAILURE MODE

4-148

force at these positions are now 0.23 $F_{L_{Avg}}$ instead of the normal operating value of 0.36 $F_{L_{Avg}}$. Schematically this is shown in Figure 4-65.

The assumption of a rigid vehicle structure leads to the magnet forces and positions for magnets 3 and 4 listed in the table. However, an actual vehicle ~ 30 m long is expected to have some flexibility and the magnets at positions 3 and 4 will have force and position values between those listed in the table and the equilibrium values for normal operation.

The maximum dynamic excursion (minimum position) can also be obtained, assuming the failure of one magnet at position 1 to be catastrophic, i.e., instantaneous. These values for position 1 are h = 20.9 cm and h' = 20.2 cm. Should magnet failure occur over a finite time, i.e., several seconds, the equilibrium values listed in Table 4-18 will be reached with no overshoot. Other factors that will influence the new equilibrium position and the transient behavior are aerodynamics, propulsion, and the feedback control system for the control coils. A magnet field probe can be used to detect magnet failure, and the characteristics of the control system can be changed in order to minimize the effect of the loss.

4.4 PROPULSION SUBSYSTEM

This section presents the results of preliminary propulsion system analyses
conducted in support of the TMLV Revenue Vehicle (MAGLEV) conceptual design.
Specific attention is given to the Ducted Fan, the Linear Induction Motor (LIM),
the Linear Synchronous Motor (LSM) and the Superconducting Paddle Wheel concepts.

4.4.1 Introduction

The TMLV Technology Program is structured to consider propulsion primarily
in relation to its direct effect upon vehicle dynamic motion, e.g., as would
occur with an integrated propulsion/levitation concept. The LSM analyses
reported in Section 4.3 are in this category. Detailed analyses of the propul-
sion aspects of the aforementioned concepts thus are not within the original
scope of this program. Nevertheless, low-level preliminary analyses were
conducted to: (1) support vehicle synthesis/packaging studies, (2) make
preliminary compatibility assessments, and (3) assess energy implications and
the possible influence on cost effectivity of other MAGLEV system design
parameters.

4.4.2 Ducted Fan

Prior to initiation of the TMLV Technology Program, in-house MAGLEV system
studies at Philco-Ford indicated that a reaction propulsion system, using a
ducted fan, has merit provided noise and exhaust emissions can be reduced to
acceptable values. Subsequently, a contract* was issued to the Hamilton
Standard Division of UAC for preliminary design studies of a propulsion system
based on their Q-fan concept, with power supplied by gas turbine engines. The
results of this study are summarized in the following paragraphs.

A. Design Approach. The vehicle self-generated noise has been estimated
as a function of speed and compared with other vehicles as shown previously in
Section 3.2.3. The propulsion system noise goal was subsequently specified as
not to exceed the bare vehicle noise for maximum power operation at the cruise

---

*The work was carried out from 1 July 1974 to 1 November 1974 on Purchase
 Order P.O. A32835 under Philco-Ford Independent Research & Development (IR&D)
 Program, Work Order 7831.

velocity of 134 m/s (300 mph). Based on this constraint on noise (and additional constraints on vehicle envelope), Hamilton Standard optimization studies show that the most desirable* propulsion arrangement consists of twin ducted Q-fans of 1.37 m (4.5 ft) diameter, driven by two remotely-located gas turbine engines, as shown in Figure 4-66. In addition to the basic low-noise design of the fan, extensive noise treatment is provided along the duct walls, support struts, turning vanes and central pylons. Similar noise treatment is provided for the engines, primarily in the inlet and exhaust regions. The remote engine location is preferred because it is more favorable for sound suppression and permits inlet air filtering for longer engine life. Regenerative engines are highly desirable due to their ~ 15% lower fuel consumption, even though the weight and volume is substantially increased.

The propulsion system is sized to produce thrust at 134 m/s equal to vehicle total drag corresponding to 2% grade and 13.4 m/s (30 mph) headwind conditions. During acceleration the engines are operated at maximum power, i.e., at the power corresponding to the aforementioned design point, and fanblade pitch is varied to provide the desired thrust. For the level cruise and no-wind condition, the engines are throttled back to the lower power level when cruise velocity is reached. This method of operation results in the thrust/velocity relationship shown in Figure 4-67. Minimum specific fuel consumption (SFC) for the engines occurs at the level cruise, no-wind operating condition. The Q-fans are also fully reversible for braking, but this is employed only for emergency operation because the aerodynamic drag brakes combined with the inherent magnetic braking are easily capable of providing the maximum permissible 0.15 g deceleration rate under normal operating conditions down to the lift-off point.** Wheel brakes are provided for braking operations below the lift-off speed.

B. Noise. Propulsion system (engines and fans) noise level estimates are shown in Figure 4-68 together with the design goals and the bare vehicle noise estimate. For operation at 134 m/s on a 2% grade with 13.4 m/s headwind, the noise level is estimated at 92 dbA, 15 m (50 ft) from the centerline of a

---

*The selection criteria included size, noise, acquisition cost, maintenance cost, reliability, weight, and transmission (gear train) complexity.

**Note that the magnetic drag below lift-off ($\leq$ 30 m/s) is held constant by appropriate control of vehicle height above the guideway, while operating on its wheeled undercarriage.
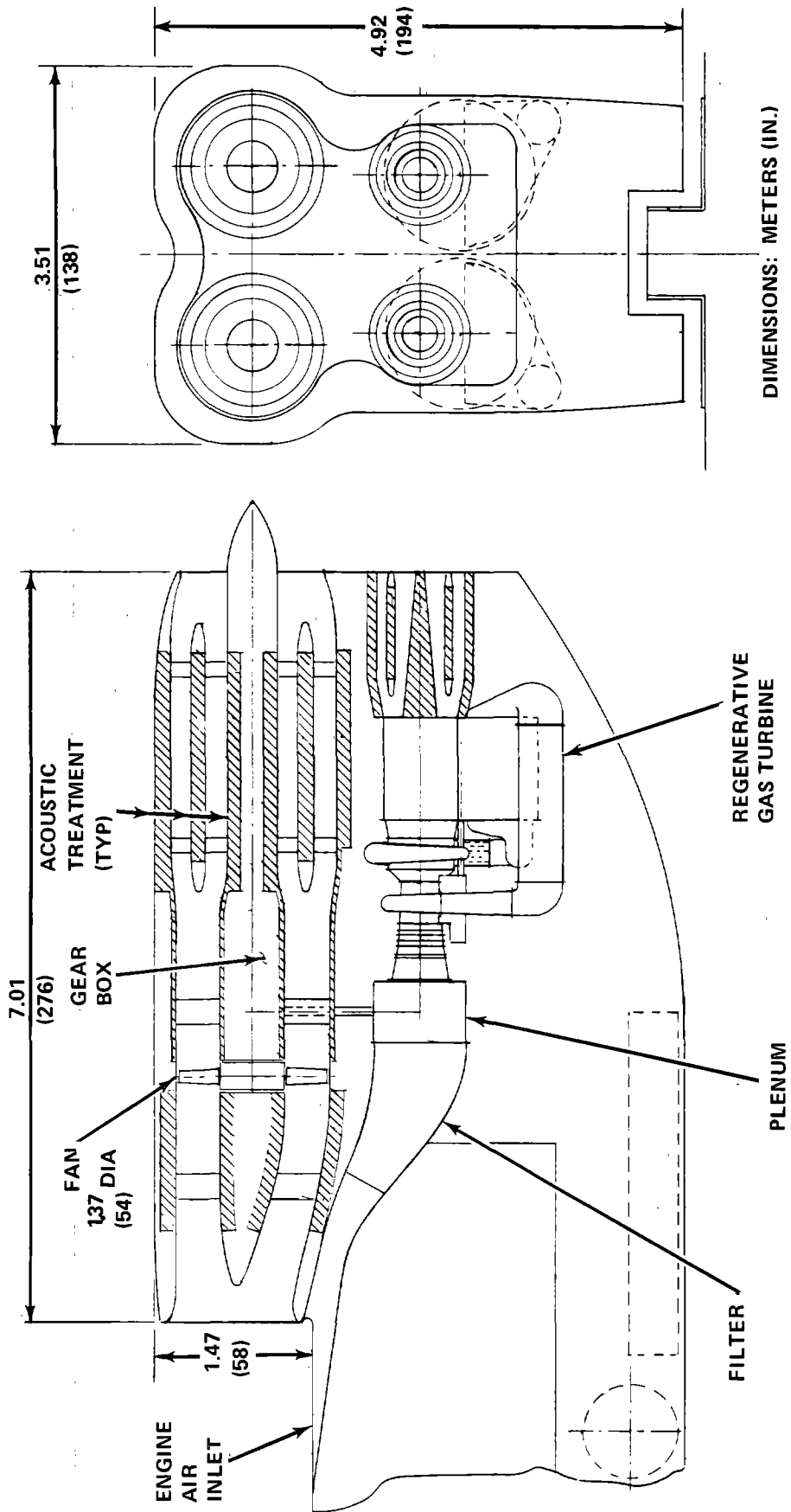
FIGURE 4-66. DUCTED FAN/GT GENERAL ARRANGEMENT

DIMENSIONS: METERS (IN.)

4.92 (194)

3.51 (138)

ACOUSTIC TREATMENT (TYP)

GEAR BOX

FAN 137 DIA (54)

7.01 (276)

1.47 (58)

ENGINE AIR INLET

REGENERATIVE GAS TURBINE

PLENUM

FILTER
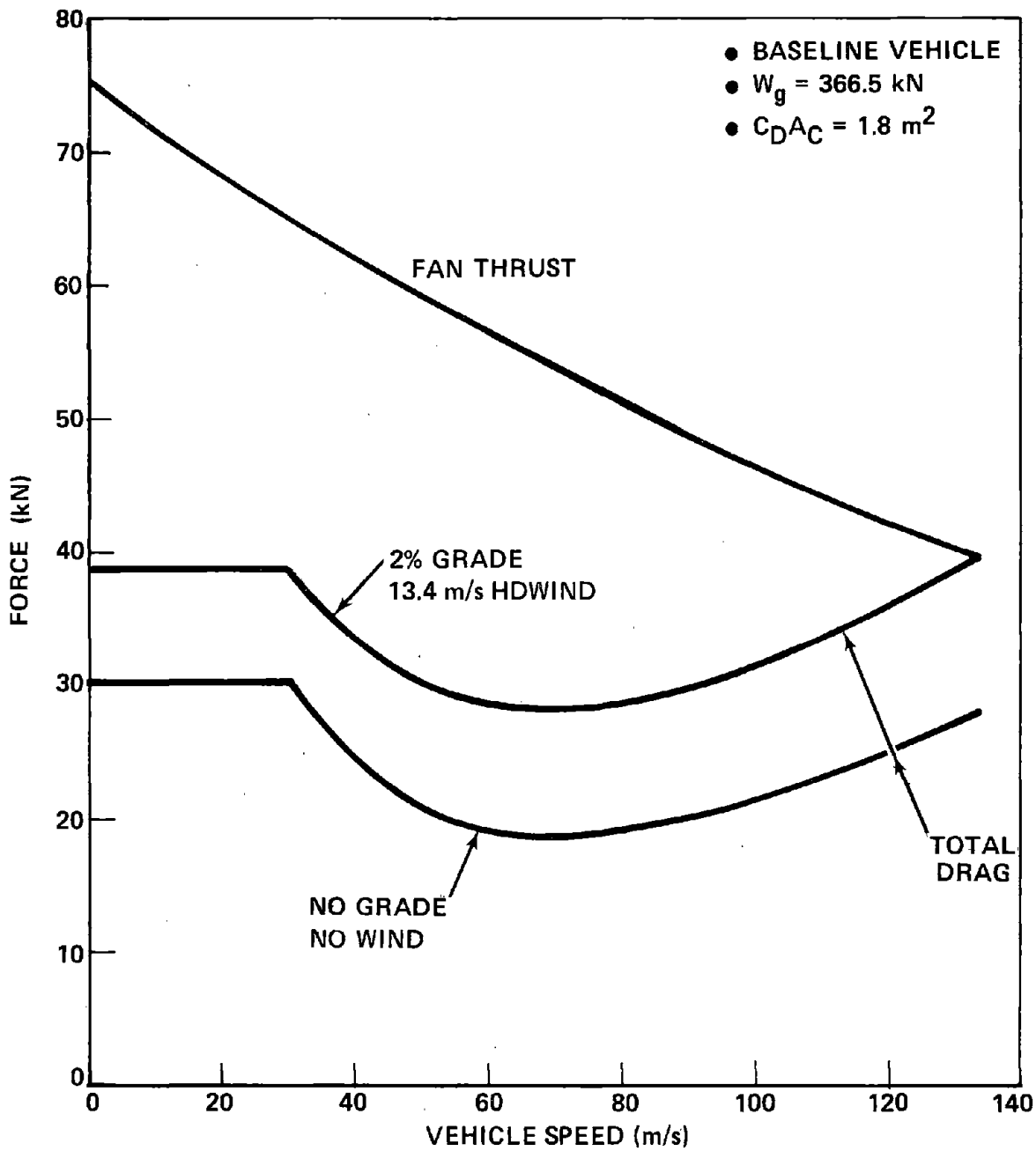
FIGURE 4-67. FAN/GT SYSTEM CHARACTERISTICS
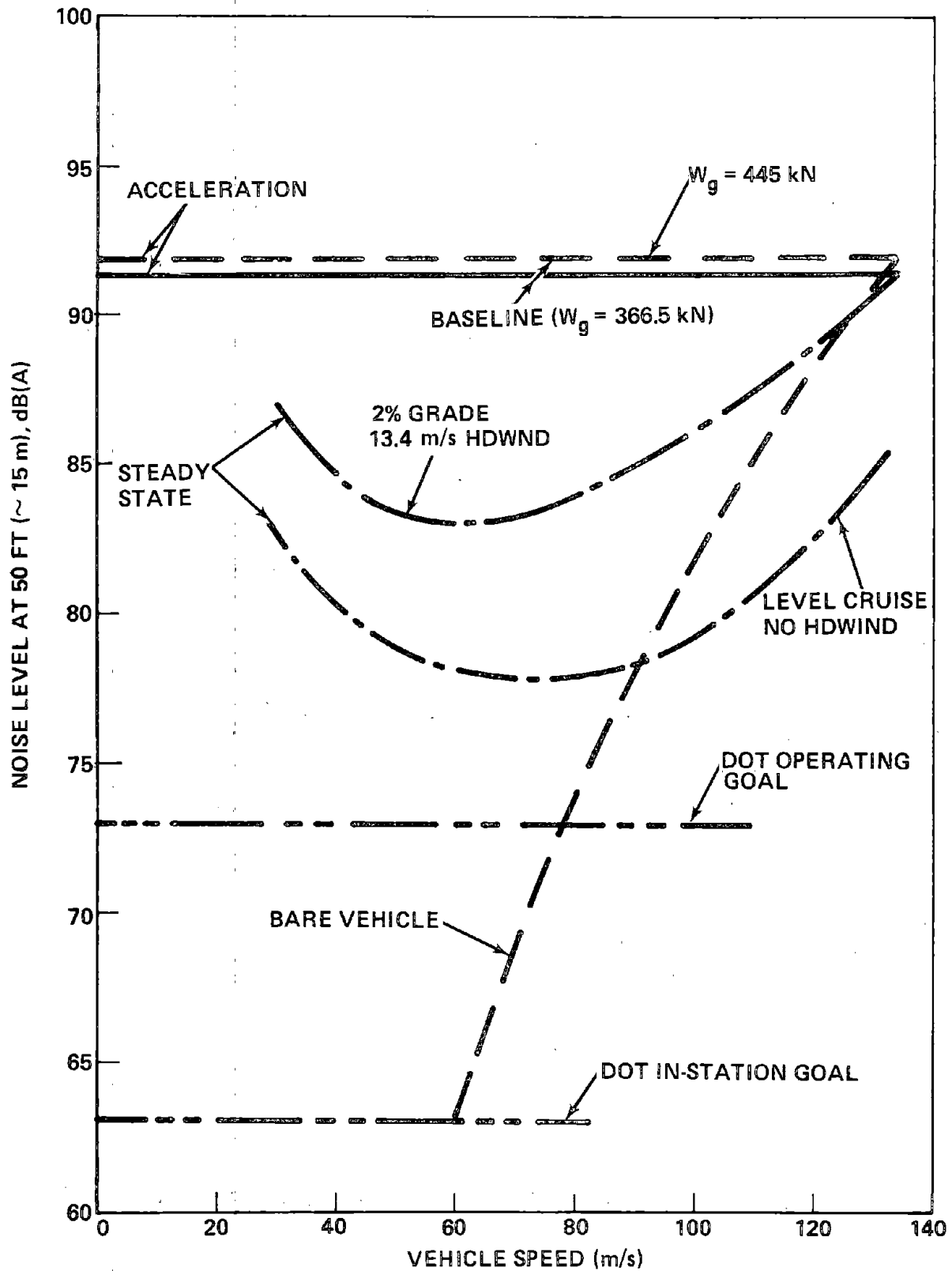
FIGURE 4-68. FAN/GT SYSTEM NOISE COMPARISON

445 kN (100,000 lb) vehicle. For the baseline vehicle at 366.5 kN (82,400 lb), the level reduces about 0.5 db, to 91.5 dbA. The noise level during acceleration is held constant by use of a variable area exhaust nozzle. For normal level-cruise operation, the propulsion noise level drops to 85.5 dbA at 134 m/s, 6.5 db less than that for the bare vehicle. Vehicle and propulsion system noise are equal (78.2 dbA) at approximately 90 m/s. Total vehicle noise is shown in Figure 4-69 for the Q-fan system with either gas turbine drive or the electric motor drive discussed in subsequent paragraphs.

FIGURE 4-69. TOTAL VEHICLE NOISE LEVEL

Overall untreated engine noise for the 445 kN vehicle is 99 dbA at 15 m, reduced to 86 dbA with treatment. Untreated fan noise is estimated at 106 dbA per fan, also reduced to 86 dbA with treatment. Hamilton Standard studies show that further noise reduction is possible by techniques such as increasing the fan diameter, moving the fans up so as to be out of the boundary layer (or forward on the vehicle) and the use of advanced technology noise suppression techniques. They estimate that the DOT "goal" of 73 dbA can be met, but the systems implications are such that further study would be required. Nevertheless, baseline noise performance must be regarded as quite good when compared with the performance goals of other transportation modes as shown in Table 4-19, prepared by Hamilton Standard. Appendix E presents a detailed discussion of Hamilton Standard's acoustic work relative to Q-fan propulsion for MAGLEV vehicles.

TABLE 4-19. COMPARISON OF NOISE OBJECTIVES

	dBA AT 60M
● DOT GOAL (73 dBA AT 15M)	61
● TMLV Q-FAN SYSTEM (~93 DBA AT 15M)	~81
● JAPAN (TRAINS)	75–80
● FRANCE (TRAINS)	75–80
● FUTURE STOL AIRCRAFT	92
● GENERAL AVIATION (USA AND EUROPE)	92
● FAR PART 36 (100,000 LB VEHICLE)	108
● 5-LANE INTERSTATE HIGHWAY	87

C. Performance. Figure 4-70 shows the acceleration of the baseline 80-seat vehicle for both cruise and grade/headwind conditions. The cruise condition occurs most frequently during corridor operations and represents the "design" condition. Thus, for sizing the propulsion system, maximum continuous power occurs during cruise at maximum velocity; acceleration and grade/headwind conditions represent time-limited overload operations. In general, Figure 4-70 shows that acceleration is very good, at least compared with railroad practice.*

---

*The advanced-technology Sikorsky 6-car Turbotrain 2, for example, is quoted at 0-80 mph in 156 sec, for an average acceleration of 0.023 g.

FIGURE 4-70. FAN/GT VEHICLE ACCELERATION

The speed-distance-time history for level, no-wind acceleration to cruise speed is shown in Figure 4-71. Note that the baseline vehicle takes 182.3 sec. and 14.17 km to reach 134 m/s. Figure 4-72 presents component efficiency during acceleration and at the cruise conditions. The component arrangements are shown below.
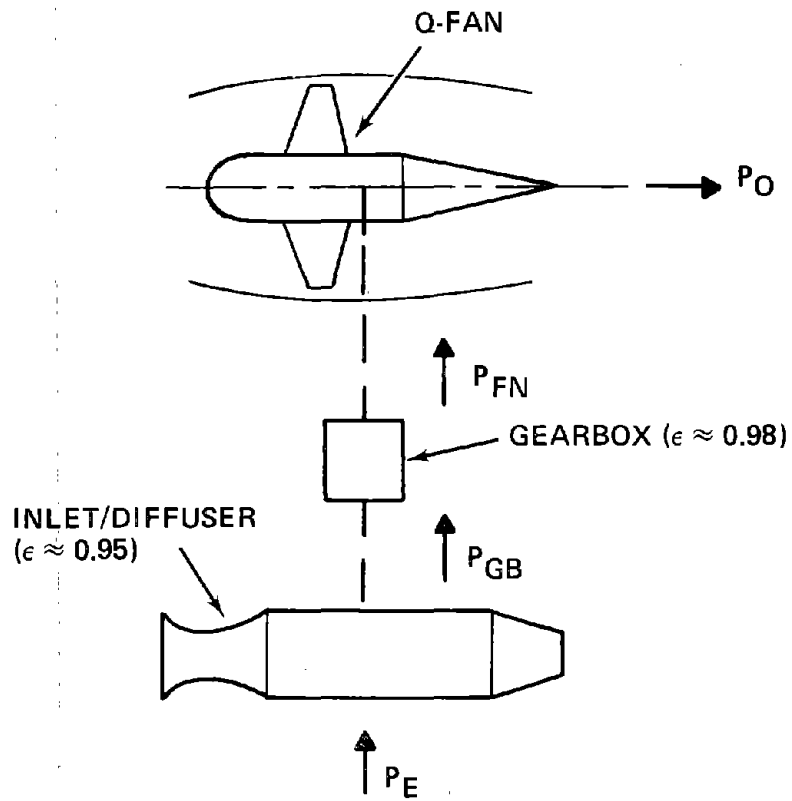
where

P_{FN} = Power delivered to fan

P_{GB} = Power delivered to gearbox

P_E = Power developed by (bare) engine

P_O = Output power = vehicle drag power
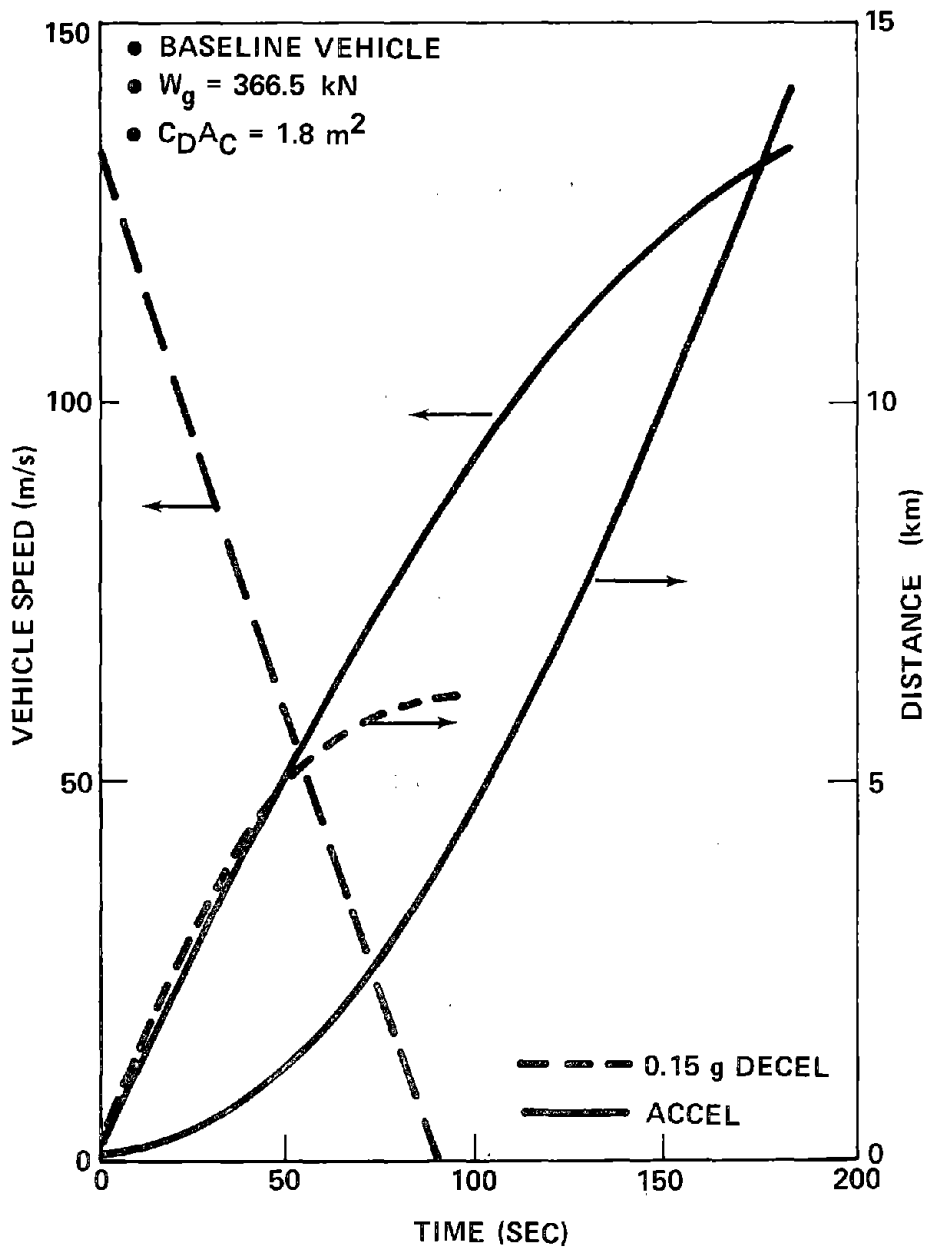
FIGURE 4-71. SPEED/DISTANCE/TIME
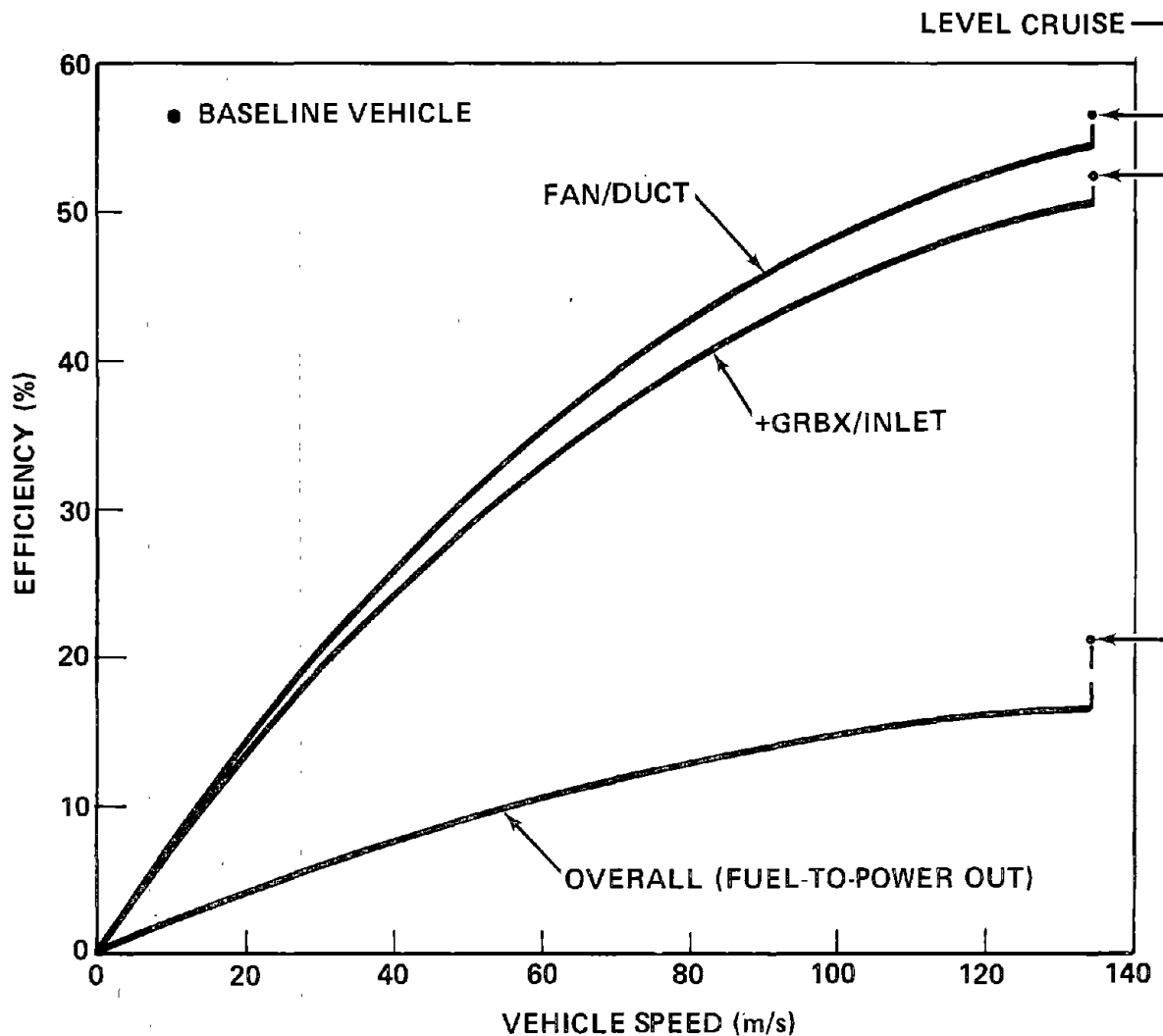
FIGURE 4-72. PROPULSION COMPONENT EFFICIENCY

Table 4-20 shows the power and efficiency values for the baseline vehicle $(366.5 \text{ kN}, C_D A_C = 1.8 \text{ m}^2)$.

The overall (fuel-to-power out) efficiency shown in Figure 4-72 and Table 4-20 is based on a fuel lower heating value (LHV) of 43.3 MJ/kg (18,600 Btu/lb). The quoted SFC values are estimates by Hamilton Standard based on current and advanced technology engines. The Detroit Diesel-Allison Division of General Motors is currently developing a number of derivatives of

4-160

TABLE 4-20. BASELINE POWER/EFFICIENCIES AT V = 134 m/s

	CRUISE	GRADE/HEADWIND
P_O (KW)	3739	5279
P_{FN} (KW)	6680	9742
P_E (KW)	7183	10,475
ϵ (FAN/DUCT)	0.560	0.542
ϵ (GEARBOX) X ϵ (INLET)	0.93	0.93
ϵ (OVERALL)	0.209	0.168
SFC (KN/MJ)	5.63×10^{-4}	6.63×10^{-4}
(LB/HP-HR)	(0.34)	(0.41)

their XT701-AD-700 turboshaft engine for the Boeing Vertol heavy-lift helicopter. One of these derivatives is a regenerative engine for a hydrofoil boat, developing 7640 hp (5700 kw) with an SFC $\approx$ 0.38 lb/hp-hr (0.23 kg/kw-hr).

D. Weight. Fuel weight is a function of the "trajectory" or mission profile employed. For design purposes, a 750 km route has been selected, with a maximum of five intermediate, equidistant stops as discussed in Section 3.2.4. The portion of the trajectory assumed for transit into and out of a hypothetical city is shown in Figure 4-73 for the baseline vehicle. Note that the total intra-city distance covered is 20.3 km and corresponding time is 423.5 sec., which includes 150 sec. for loading/unloading in the station. It is further assumed that 90% of the route (675 km minus the intra-city distance) represents the cruise condition and 10% (75 km) represents the grade/headwind condition. The fuel consumption rate for idle and deceleration is approximately 15% of the cruise value. SFC at grade/headwind conditions and under acceleration is approximately 21% above the cruise value.

Table 4-21 summarizes component and fuel weight for the baseline vehicle with five intermediate stops where the fuel weight includes a 15% reserve. For straight-through (express) operation, fuel consumption is 25.1 kN, and the
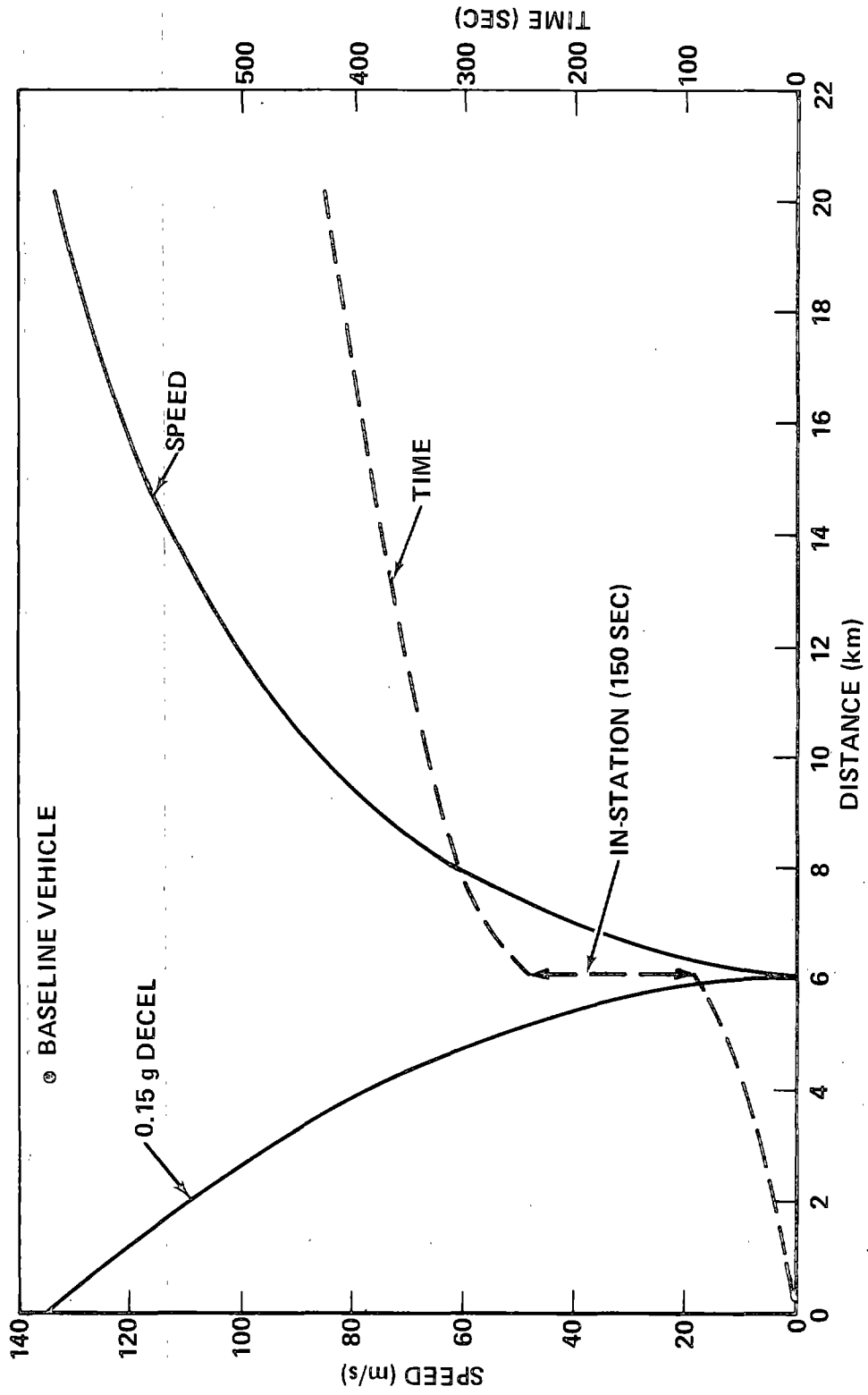
FIGURE 4-73. INTRA-CITY TRAJECTORY

4-162

comparative Energy Intensity, ψ, for the baseline 80-seat vehicle is

- ψ (N_i = 5) $\approx$ 2.18 MJ/seat-km (3326 Btu/seat-mile)

- ψ (N_i = 0) $\approx$ 1.84 MJ/seat-km (2807 Btu/seat-mile)

TABLE 4-21. PROPULSION SYSTEM WEIGHT BREAKOUT

COMPONENT	WEIGHT, KN	(lb)
● ROTOR GROUP	4.41	(991)
ROTOR ASSEMBLY		
PITCH ACTUATOR		
PITCH REGULATOR		
SYSTEM OIL		
● GEARTRAIN GROUP	3.42	(769)
GEARBOXES AND SHAFTING		
SYSTEM OIL		
● DUCT GROUP	21.62	(4,861)
NON-ROTATING SPINNER		
CENTERBODY		
VANES AND STRUTS		
FULL DUCT		
AFT SPLITTER		
● ENGINES (REGENERATIVE)	17.03	(3,829)
SUB-TOTAL, COMPONENTS	46.48	(10,450)
○ FUEL (29.7 X 1.15)	34.12	(7,670)
CRUISE 16.7		
GRADE/WIND 4.0 29.7 KN		
ACCELERATE 8.0 CONSUMED		
DECELERATE 0.4		
STATION 0.6		
TOTAL PROPULSION SYSTEM WEIGHT	80.6 KN	(18,120 lb)

Section 4.2.6 reports on a vehicle synthesis study carried out to ascertain the effect of vehicle seating arrangement and other parameters on energy consumption. The 140-seat vehicle with 2 + 3 seating (two seats on one side and three on the other side of an aisle) is found to have a substantially lower Energy Intensity, ψ, than the baseline 80-seat vehicle. Figure 4-74 shows ψ as
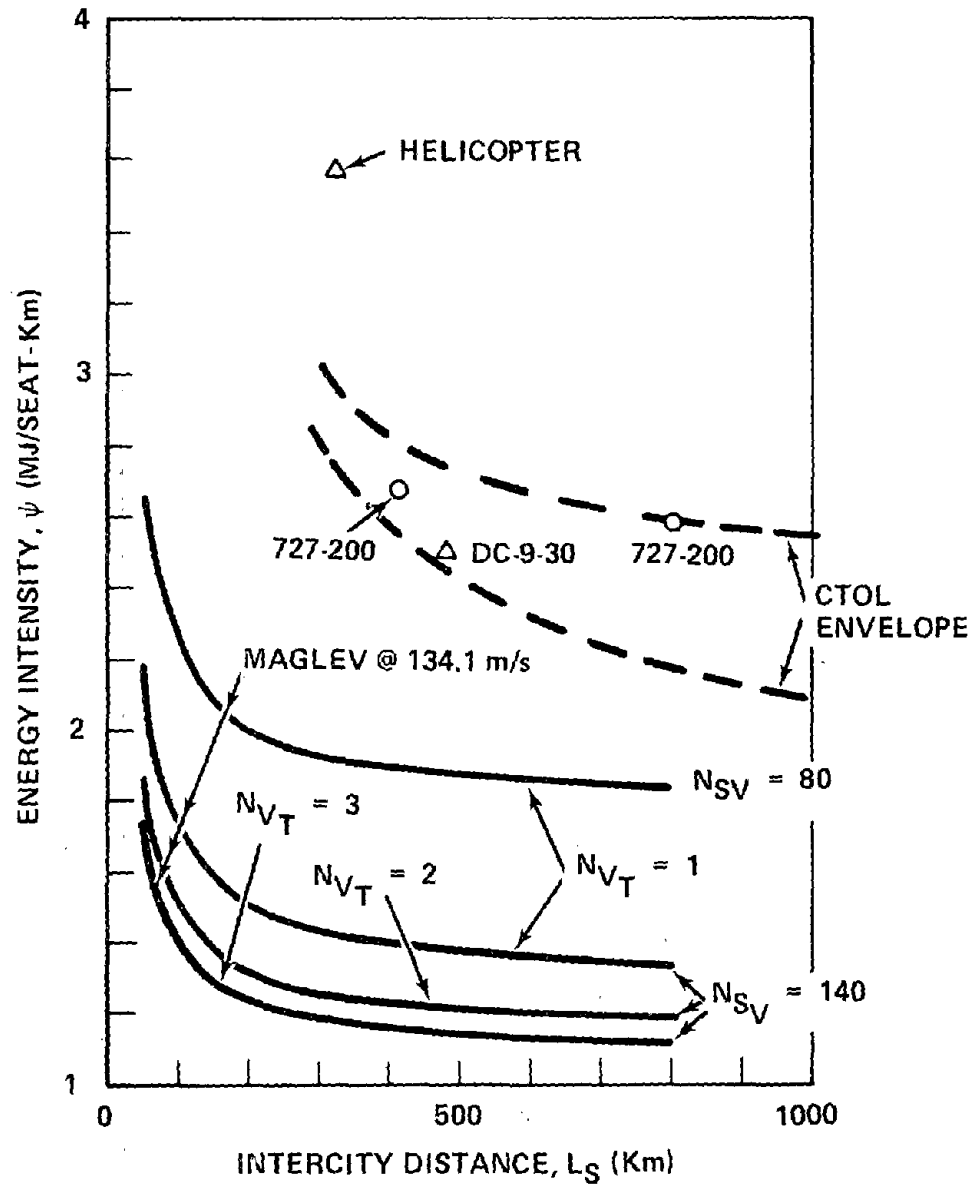
FIGURE 4-74. ENERGY VERSUS INTERCITY DISTANCE

a function of intercity distance for both the 80- and 140-seat vehicle as well as for trains of 140-seat vehicles, all at 134 m/s maximum speed. Note that the 3-coacn train shows a ψ of 1.33 MJ/seat-km (2029 Btu/seat-mile) for the 125 km intercity distance, corresponding to the baseline 750 km route with N_i = 5. For intercity distances less than 1000 km, the Ducted Fan/Gas Turbine-driven MAGLEV vehicle offers better than a 2 to 1 energy advantage (on a per seat basis) over current CTOL jet aircraft as well as a significant improvement over the personal automobile.

Figure 4-75 shows the effect of cruise speed on Energy Intensity. Note that the minimum energy point for the 3-coach train occurs at approximately 100 m/s (224 mph) with ψ = 0.9 MJ/seat-km (1373 Btu/seat-mile).

E. Emissions. Hamilton Standard believes that the gas turbines will easily meet the proposed 1979/81 EPA turbine regulations since some engines, e.g., the T-56, can currently meet or come very close to these values. Table 4-22 summarizes the emission performance for the 80-seat vehicle with five intermediate stops. The advanced system figures are based on the study data of Reference 4-28.

TABLE 4-22. ESTIMATED PROPULSION SYSTEM EMISSIONS

	NOX	UHC	CO
● 1979/81 EPA (G/KG FUEL)	10 (T.O.)	4 (IDLE)	20 (IDLE)
● BASELINE TMLV (KG/TRIP)	24.7	0.8	4
● BASELINE TMLV (KG/10³ SEAT-KM)	0.41	0.013	0.07
● ADVANCED SYSTEM (KG/10³ SEAT-KM)	0.057	0.005	0.09

A brief examination of alternate fuels was carried out, primarily to establish packaging requirements and performance capability associated with different fuel heating values. The major objectives for consideration of alternative fuels is reduced exhaust emissions and future fuel availability. The results are summarized in Table 4-23 for three fuels with lower emissions capability than the reference JP fuel. Note that the use of liquid hydrogen
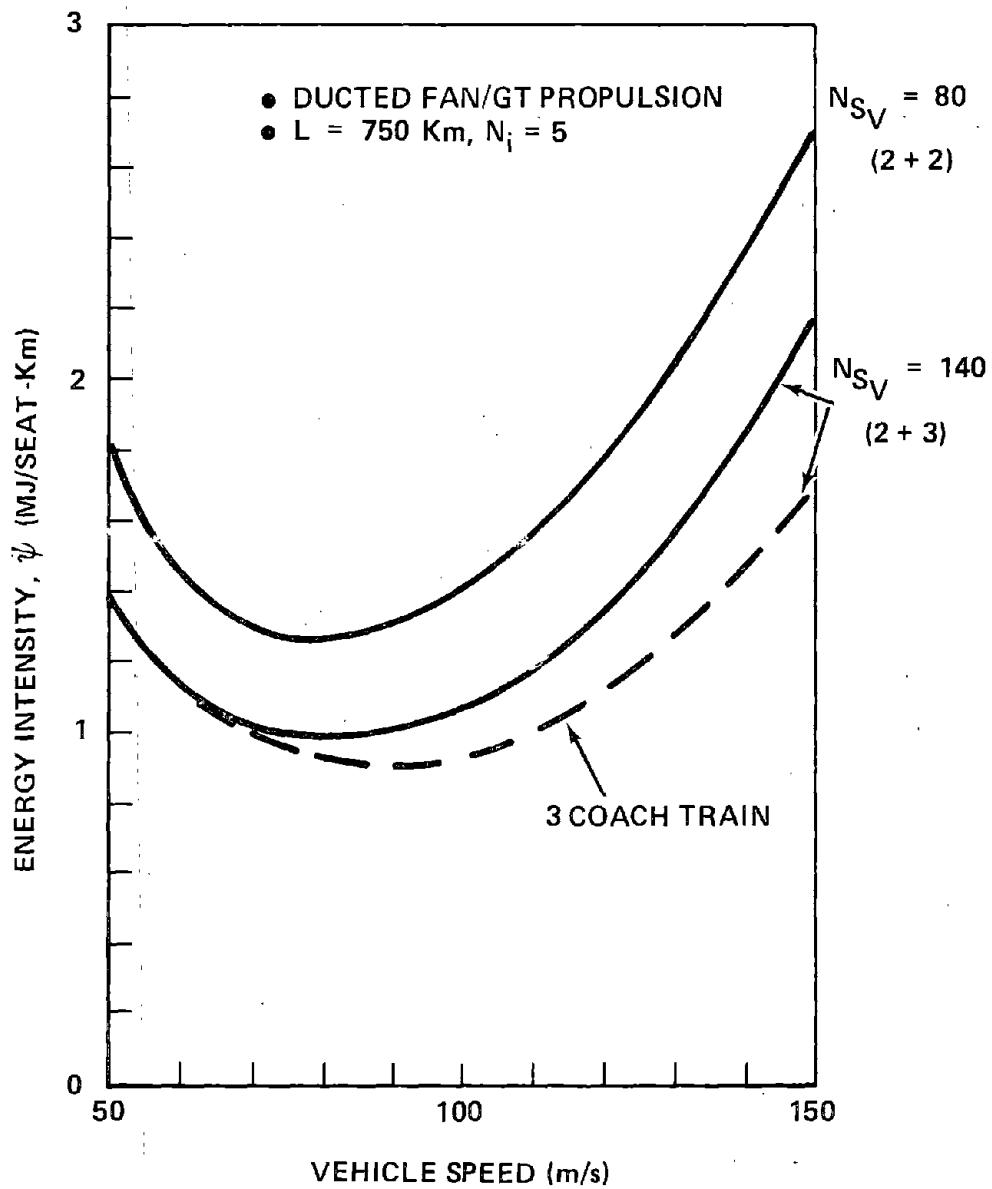
FIGURE 4-75. ENERGY VERSUS SPEED

reduces the fuel weight by 19.1 kN (4294 lb) — a 64.3% reduction compared with JP fuel. Although the storage volume is increased by a factor of four, it can be accommodated within the baseline vehicle.

TABLE 4-23. ALTERNATE FUELS COMPARISON (DUCTED FAN/GT BASELINE)

FUEL	LHV (MJ/KG)	FUEL WEIGHT CONSUMED W_F, KN (LB)	STORAGE VOLUME (M^3)
⊙ JP	43.2	29.7 (6677)	4.4
⊙ HYDROGEN	121.1	10.6 (2379)	17.6
⊙ ETHYL ALCOHOL	30	42.5 (9566)	6.8
⊙ METHYL ALCOHOL	20.2	63.3 (14,241)	14.5

F. Cost. For the baseline 80-seat vehicle, Hamilton Standard estimates the fan components (Q-fans, ducts, gearboxes, etc.) at $500,000 and the gas turbines at $700,000 for an onboard propulsion cost of $1,200,000 per vehicle, exclusive of development cost. Since the system is totally self-contained, there are no guideway-related costs as is the case with electric propulsion. Total vehicle cost is estimated at $2,316,000.

G. Preliminary Evaluation. The Ducted Fan/Gas Turbine combination is a feasible concept for MAGLEV vehicle propulsion, and has numerous advantages. Since it is totally self-contained, it is compatible with any vehicle/guideway configuration desired and any switch concept proposed. It provides propulsion for both primary operation as well as off-ramp and station operation. Overall efficiency is relatively high, total system energy consumption and cost is low, and a wide variety of chemical fuels can be employed, if desired, e.g., to reduce exhaust emissions to negligible levels. Performance is excellent and cruise noise levels by contemporary standards, are quite low. It has the unique advantage of essentially "off-the-shelf" development status and the obvious benefit of high reliability. At this point in time, the only dis-advantages are: (1) moderately high noise level (~ 90 dbA) during full-power acceleration, and (2) the requirement for chemical fuel, i.e., if the United States becomes an all-electric society.

H. Alternate Power Plant (Ducted Fan/REM). In the event that chemical
fuels (fossil or synthetic) prove undesirable because of cost, availability,
or unacceptable emissions characteristics, it will be necessary to propel the
MAGLEV vehicle with an electric system. Significant research efforts have
been devoted to a number of electric propulsion systems, such as the linear
induction motor (LIM) and the linear synchronous motor (LSM) discussed in
subsequent paragraphs. It is also possible to drive the ducted fans with
rotary electric motors (REMs), but the large volume and mass of conventional
electric motors in the power range of interest effectively make this approach
infeasible. However, recent research on superconducting electric motors and
generators (Ref. 4-29) indicates that substantial improvements are possible.
For the analyses reported herein, a power/weight ratio of 335 kW/kN (2 hp/lb)
is employed, together with a specific weight of 24.3 kN/m^3 (154.6 lb/ft^3),
based on the data of Ref. 4-29.

(1) Performance. An 80-seat (2 + 2 seating) vehicle has been synthesized
with this propulsion arrangement and the baseline hat-shaped guideway configu-
ration. With an onboard power control unit (PCU), the vehicle gross weight is
332.8 kN (74,800 lb) for operation at 134 m/s (300 mph) cruise speed. Indi-
vidual propulsion components are identified in Table 4-24. Table 4-25 shows
the weight of each major element comprising the vehicle. The general arrange-
ment of the Ducted Fan/REM drive system is shown in Figure 4-76.

TABLE 4-24. DUCTED FAN/REM SYSTEM COMPONENTS WEIGHTS

COMPONENT	WEIGHT, KN (LB)	
● FANS (2)	4.3	(967)
● GEARBOXES (2)	3.3	(742)
● DUCTING	21.6	(4,856)
● POWER CONDITIONING	4.5	(1,012)
● ELECTRIC MOTORS (2)	19.8	(4,451)
TOTAL	53.5 KN	(12,028 LB)

ACOUSTIC TREATMENT (TYP)

FAN

7.01 (276)

1.47 (58)

4.92 (194)

3.51 (138)

SUPERCONDUCTING REM

GEAR BOX

PCU

WAYSIDE POWER PICKUP

DIMENSIONS METERS (IN.)
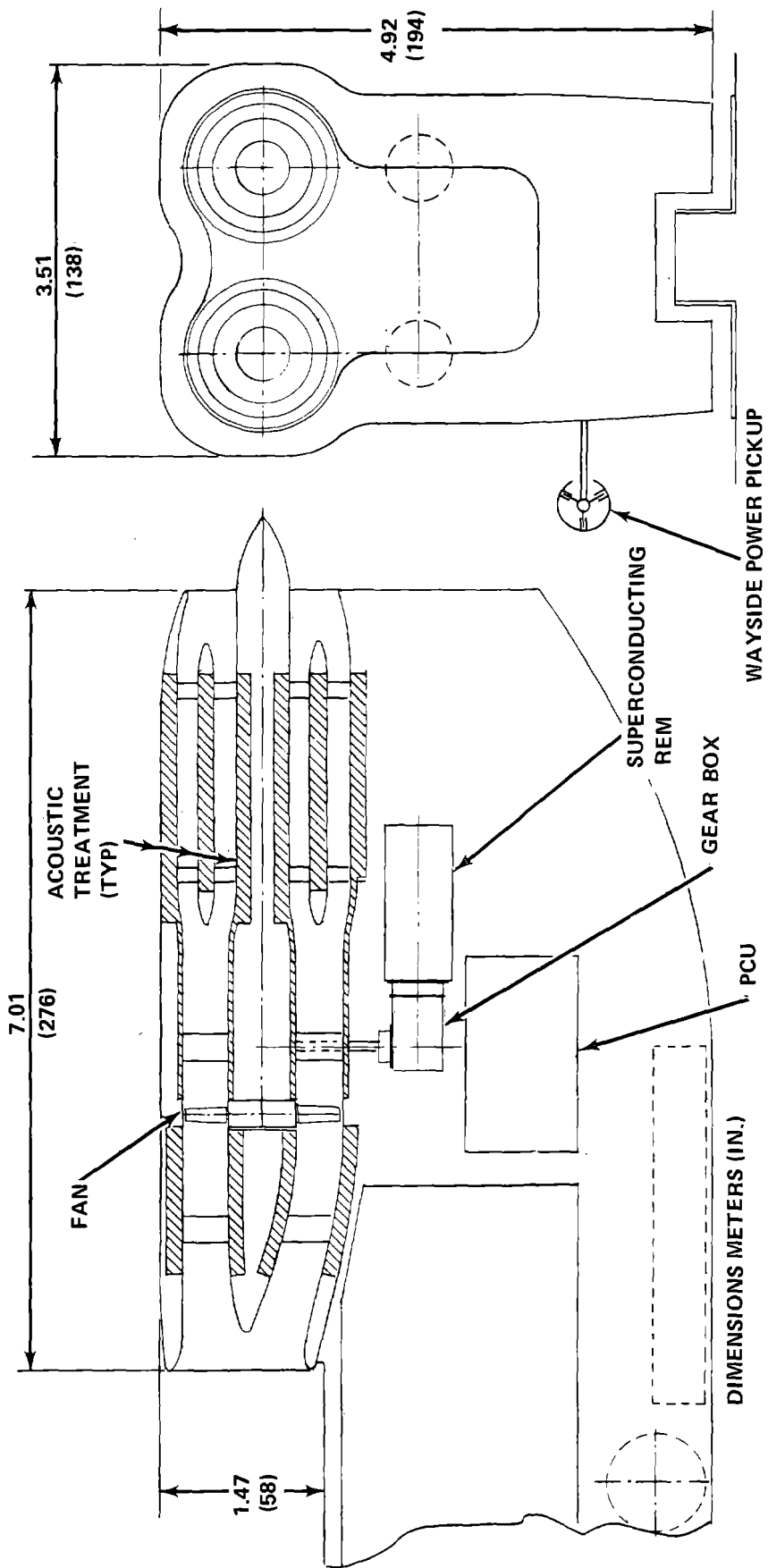
FIGURE 4-76. DUCTED FAN/REM SYSTEM GENERAL ARRANGEMENT

TABLE 4-25. DUCTED FAN/REM VEHICLE WEIGHT BREAKOUT

COMPONENT	WEIGHT, KN (LB)	
o SUSPENSION	65.2	(14,659)
o STRUCTURE	49.8	(11,196)
o FURNISHINGS	24.5	(5,508)
o AUXILIARIES	21.0	(4,721)
o BRAKES	18.8	(4,227)
o CREW COMPARTMENT	15.6	(3,507)
o PAYLOAD	71	(15,962)
o PROPULSION	53.5	(12,028)
o CONTINGENCY	13.4	(3,012)
VEHICLE GROSS WEIGHT	332.8 KN	(74,820 LB)

Figure 4-77 shows the thrust/drag characteristics of the system, and Figure 4-78 shows the resultant acceleration for operation on both level and grade conditions.

Overall system efficiency, i.e., from fuel to power out is approximately 14.9% at V_C = 134 m/s (300 mph) as shown in Table 4-26.

TABLE 4-26. OVERALL FAN/REM EFFICIENCY AT 134.1 M/S

o FAN/DUCT	0.56
o MOTOR	0.98
o POWER CONDITIONING	0.95
o GEARBOX	0.98
o TRANSMISSION LINES	0.9
o COLLECTION, DISTRIBUTION	0.9
o GENERATING PLANT	0.36
	ϵ_0 = 0.149
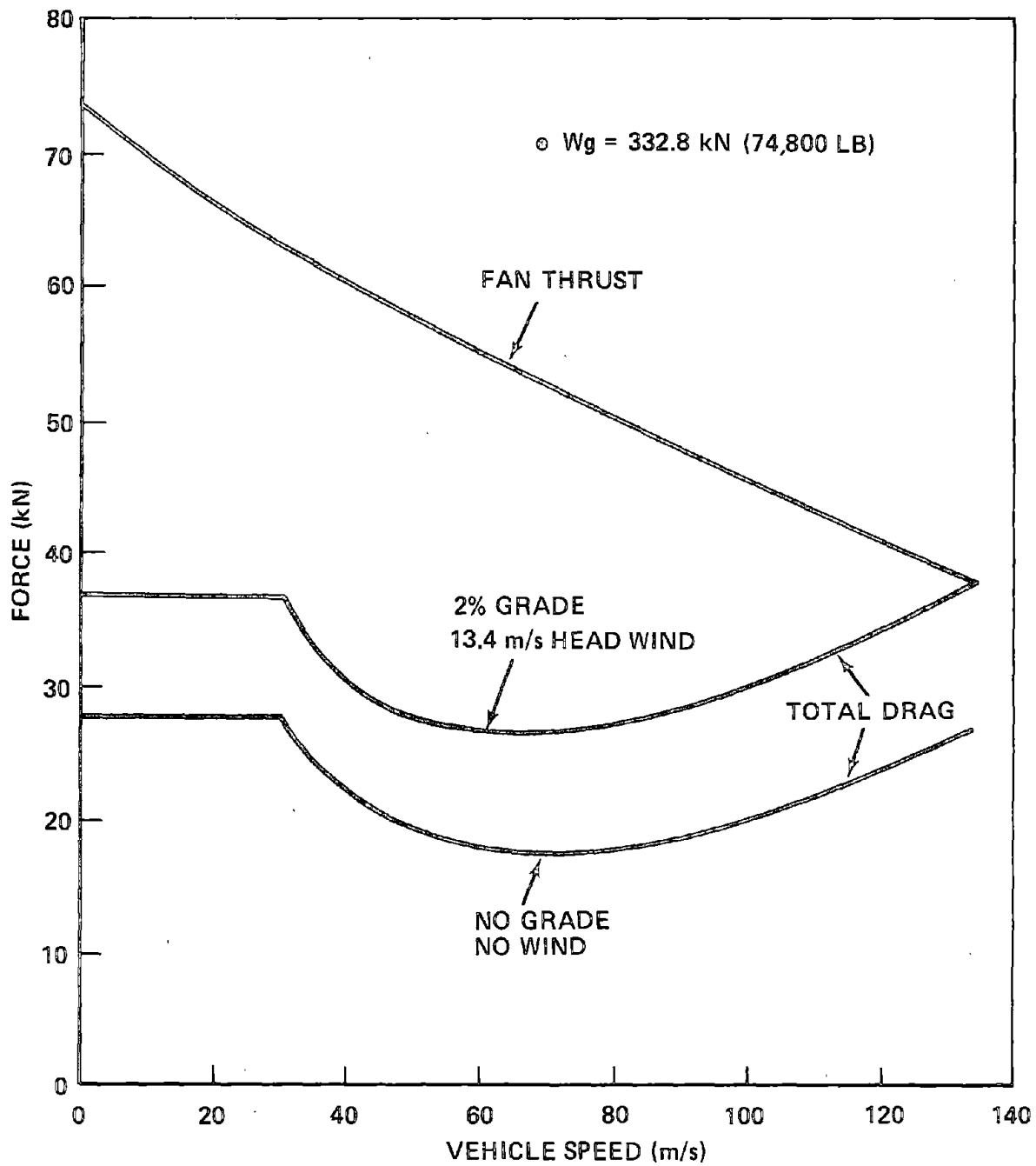
FIGURE 4-77. FAN/REM SYSTEM CHARACTERISTICS
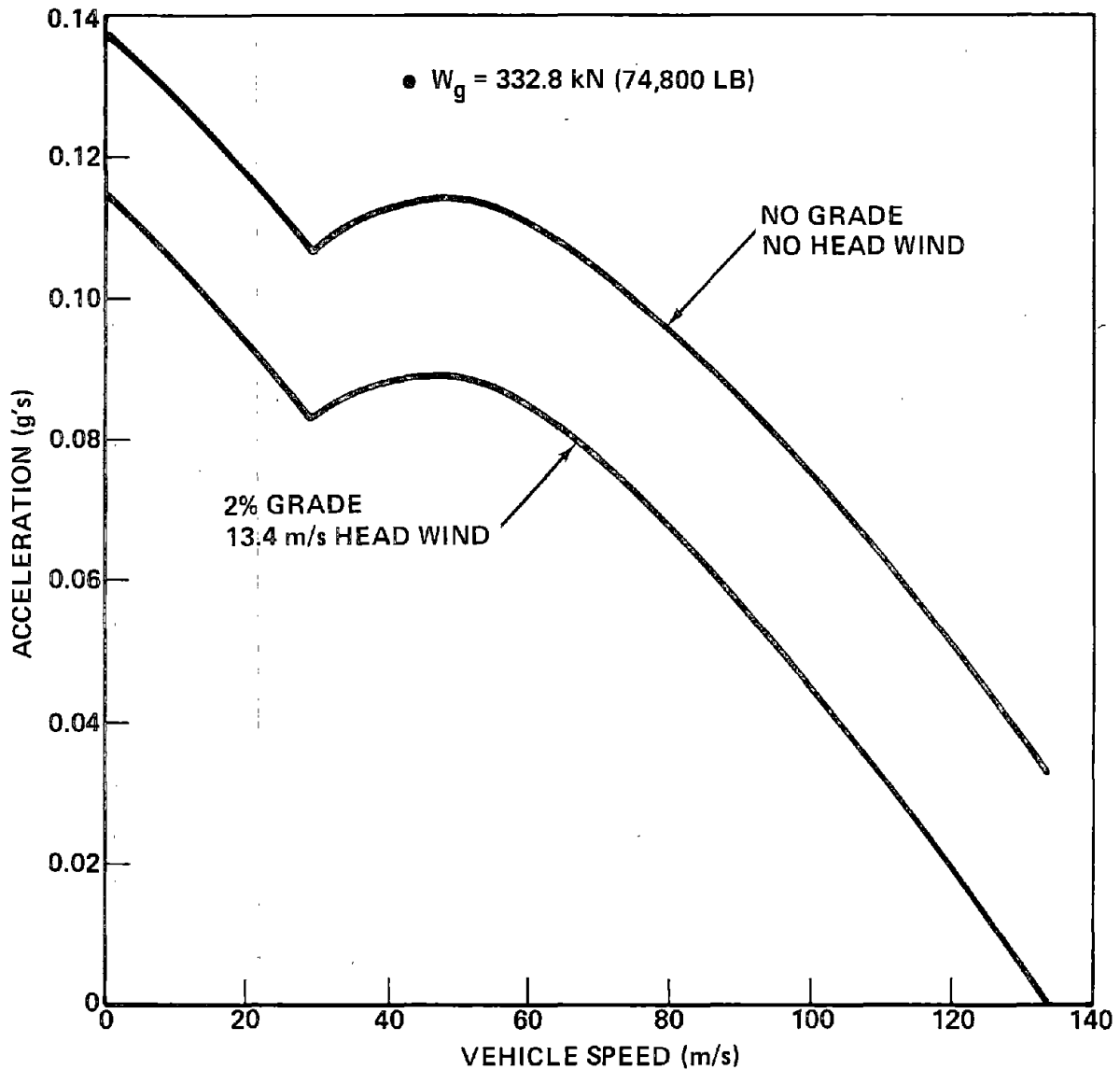
FIGURE 4-78. FAN/REM VEHICLE ACCELERATION

For the 80-seat Fan/REM-powered vehicle at 134 m/s, Energy Intensity, ψ, is approximately 2.59 MJ/seat-km (3951 Btu/seat-mile) for the 750 km route and $N_i = 5$, i.e., for an intercity distance of 125 km. The general variation of ψ with intercity distance is given in Table 4-27.

TABLE 4-27. FAN/REM VEHICLE ENERGY INTENSITY $V_C = 134.1$ M/S

INTERCITY DISTANCE, KM	ψ, MJ/SEAT-KM (BTU/SEAT-MI)	
50	2.96	(4,516)
100	2.66	(4,058)
125	2.59	(3,951)
200	2.52	(3,844)
300	2.47	(3,768)
500	2.43	(3,707)
800	2.41	(3,677)

(2) Switching. With the hat-shape guideway, the Ducted Fan/REM vehicle will switch in the same manner as the gas turbine-powered vehicle, but with the additional requirement that the power pick-up must be switched. This can be achieved by retracting the primary pick-up and engaging another one upon entering the off-ramp.

(3) Cost. Preliminary Fan/REM system cost estimates are given in Table 4-28.

TABLE 4-28. FAN/REM SYSTEM COST ESTIMATES

• MOTORS (INCL. PCU)	$950,000
• FANS (INCL. DUCT, GEARBOXES)	$500,000
• POWER RAILS	$497,000/km
• POWER STATIONS	$ 37,000/km

The 80-seat, 332.8 kN (74,800 lb) vehicle synthesized to accommodate a Fan/REM propulsion system is estimated to cost $2,546,000 exclusive of development cost. Section 5 summarizes the vehicle/guideway cost figures.

(4) <u>Preliminary Evaluation</u>. The Ducted Fan/REM propulsion concept appears feasible for a Repulsion MAGLEV system and is a viable alternative to a gas turbine drive if chemical fuels prove unacceptable. Fan noise is still present, but the previously presented acoustic data for Q-fans indicates that propulsion noise may not be a problem except during acceleration. System performance is good but overall efficiency is low, with consequent high energy consumption. The system is very compatible with the Repulsion MAGLEV concept, i.e., it is insensitive to the gap between vehicle and the guideway. Furthermore, the system provides propulsion for primary guideway operation, for switching, and at the passenger loading stations. Of all the electric propulsion systems studied, it appears easiest to switch. Motor cost is a rough estimate at this stage in its development, but the U. S. Navy programs on superconducting motor-generator systems should provide more accurate inputs in the near future.

4.4.3 Linear Induction Motor (LIM and SLIM)

A. <u>Background</u>. The linear induction motor has been the subject of substantial research effort both in the United States and abroad. Claimed advantages for this type of propulsion are low noise, no wayside emissions and the elimination of chemical fuels (fossil or synthetic) as the energy-producing source. Admitted disadvantages are the need for wayside power pick-up, reduced motor efficiency compared with conventional REMs due to end effects, power conversion losses and the reduced overall efficiency associated with Rankine-cycle power-station generation, and losses in the electrical transmission/distribution network. Furthermore, the motor and its associated power conversion equipment (PCUs) are quite heavy, e.g., about 105 kN (23,600 lb) with current technology. This problem can be alleviated, in principle, by locating all PCUs on the wayside, but there are substantial cost implications, as shown later in Section 5. Also, the plant-generated emissions problem is not eliminated until the nation's conversion to an all-nuclear (or solar) generation system. Even under such circumstances, the electrical transmission/distribution loss problem is such that there is strong advocacy of a synthetic fuel (e.g., hydrogen) system for those forms of energy utilization which are inefficient users of electricity.

B. Performance. More immediate difficulties with a LIM system for Repulsion MAGLEV systems relate to dynamic incompatibilities, i.e., related to the order-of-magnitude difference in clearance between the motor and its reaction surface and the vehicle and its reaction surface. Preliminary considerations on this subject (see Section 4.2) indicate that the motor cannot be attached to (or suspended from) the vehicle without, (1) adversely affecting vehicle ride quality, and/or (2) introducing unacceptable variations in the gap between the motor and its reaction surface. For design purposes, therefore, it is assumed that the motor has its own suspension system and functions strictly as a tug, thus transmitting only thrust forces by means of a low-friction thrust bearing/linkage arrangement. It is further assumed that the propulsion tug is suspended by means of superconducting magnets operating over the same aluminum surfaces which provide levitation to the passenger-carrying vehicle. Proper gap maintenance is achieved by operating the tug magnets (with damping control) at a small gap, with consequent higher natural frequency and much less stroke than for the main vehicle. Additional consideration has been given to supporting the propulsion tug by means of air cushions as employed on the Grumman TLRV. Although this approach could be more effective than the magnetic support approach, the necessary analyses were clearly out of scope for this program and no work has been done on air suspension.

LIM physical parameter and performance data have been provided by the Garrett Corp. (Ref. 4-30) based on scaling the existing TLRV double-sided motor to TMLV requirements. For analysis purposes, however, it was decided to consider the single-sided motor (SLIM) largely because it can be switched more easily and because the reaction rail configuration offers some technical advantages. At the direction of DOT, D. Elliott of JPL supplied some data for a SLIM (Ref. 4-31) based on a single-sided version of the Garrett LIMRV motor scaled to greater width and higher current density.* Since Elliott's estimate of the bare motor weight is essentially the same as Garrett's figure, the more detailed Garrett component weight data have been employed to support performance computations. Table 4-29 shows the weight and physical dimensions

---

*However, no data were provided on the associated power conditioning and control equipment.

TABLE 4-29. SLIM SYSTEM PHYSICAL DATA

COMPONENT	WEIGHT (KN)	DIMENSIONS (M)
● MOTOR (PRIMARY) (1)	53 (11,915 LB)	3.81 (L), 1.0 (W), 0.16 (H)
● SYNC.CONDENSERS (2)	37.3 (8,385 LB)	1.2 X 1.2 X 1.2 (EACH)
● CONVERTERS (2)	6.7 (1,506 LB)	1.65 (L), 0.55 (W), 1.2 (H) EACH
● SUPPORT EQUIPMENT (COOLING, AUX POWER, CONTROL)	7.8 (1,754 LB)	3.0 (L), 1.2 (W), 1.2 (H)
TOTAL*	104.8 KN (23,560 LB)	

*THESE FIGURES PROPERLY REPRESENT AN ON-BOARD SYSTEM; WITH WAYSIDE PCU, ONLY THE MOTOR AND SUPPORT EQUIPMENT ARE ON-BOARD AT A GROSS WEIGHT OF 60.8 KN (13,669 LB)

for a SLIM system exclusive of tug structure, thrust pad/linkage, and levitation/guidance (lev/guide) magnets. The tug structure and thrust pad/linkage equipment is estimated to weigh 9 kN (2,023 lb) with the levitation magnets and control equipment at 6 kN (1,349 lb) so the total SLIM propulsion system weight is 75.8 kN (17,042 lb) if wayside PCUs are employed. An 80-seat (2 + 2) vehicle was synthesized with this propulsion arrangement and the baseline guideway configuration; the resultant weight breakdown is shown in Table 4-30. With wayside PCUs, the vehicle gross weight is 347.2 kN (78,100 lb) whereas the gross weight with onboard PCUs is 402.2 kN (90,400 lb). The general arrangement of the vehicle and the propulsion tug is shown in Figure 4-79. The SLIM secondary (reaction surface) consists of a continuous laminated iron component 1 m wide by 0.125 m thick, overlayed with an aluminum conductor 2 mm thick. Note that this conductor is too thin (due to excessive drag force) to permit the propulsion tug to support itself magnetically above the motor reaction surface rather than above the vehicle reaction surfaces. A more serious problem associated with the thin aluminum conductor is the heat generated during motor start-up. Preliminary calculations indicate high temperatures in the aluminum with possible severe damage. Unfortunately, D. Elliott

TABLE 4-30. 80-SEAT SLIM VEHICLE WEIGHT BREAKOUT

COMPONENT	WEIGHT, KN (LB)	
● SUSPENSION	62.5	(14,051)
● STRUCTURE	44.0	(9,892)
● FURNISHINGS	24.5	(5,508)
● AUXILIARIES	21.0	(4,721)
● BRAKES	19.4	(4,361)
● CREW COMPARTMENT	15.6	(3,508)
● PAYLOAD	71	(15,962)
● PROPULSION	75.8	(17,042)
● CONTINGENCY	13.4	(3,012)
TOTAL	347.2 KN	(78,057 LB)

has indicated that an increase in aluminum thickness would substantially reduce SLIM performance. At this point, therefore, some aspects of the SLIM design data are questionable.

Thrust/drag characteristics are shown in Figure 4-80 for the Garrett LIM system as well as for the SLIM system. Note that the SLIM secondary exerts a very large down-force on the primary, particularly at low speed; this down-force introduces a drag force on the propulsion tug which serves to reduce the effective thrust of the system. Nevertheless, the gross thrust is so high that the vehicle acceleration will exceed the specified 0.15 g limit up to approximately 80 m/s (179 mph), as shown in Figure 4-81. Figures 4-80 and 4-81 also show Garrett LIM data for comparison. The substantial improvement in performance with the SLIM is probably due more to the "paper" aspect of the design, i.e., based on future expectations, rather than on actual performance.

Figure 4-82 shows the variation of SLIM efficiency with speed. Overall systems efficiency, i.e., from fuel to power out is approximately 18.8% at V_i = 134 m/s, as shown in Table 4-31.

PRIMARY

MOTOR
LEVITATION
MAGNETS

THRUST
MECHANISM

3.81
(150)

3.59
(141)

3.05
(120)

1.0
(39.4)

OUTRIGGERS

WAYSIDE POWER PICKUP

PRIMARY

MOTOR
LEVITATION
MAGNETS

SECONDARY
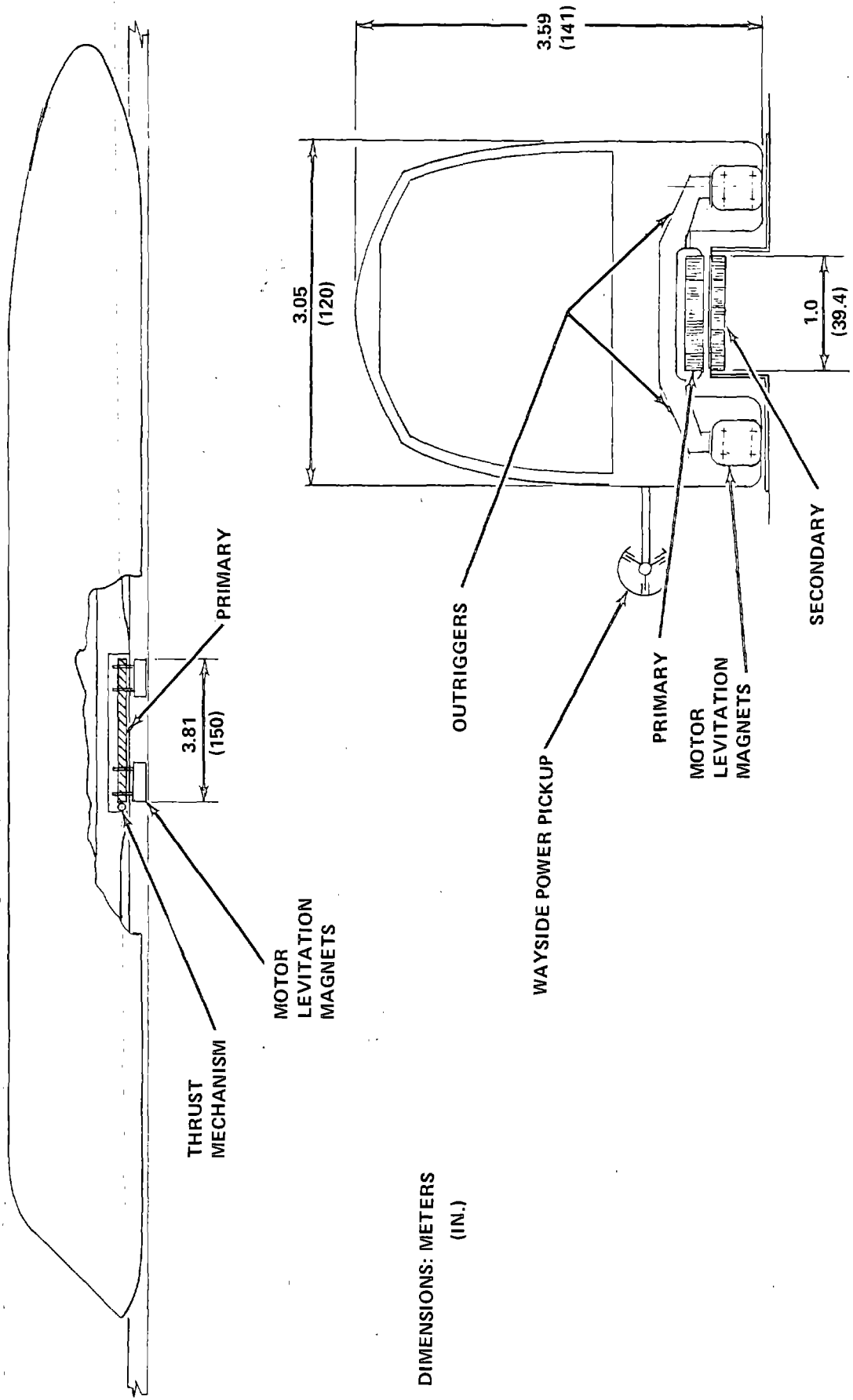
DIMENSIONS: METERS
(IN.)

FIGURE 4-79. SLIM SYSTEM GENERAL ARRANGEMENT
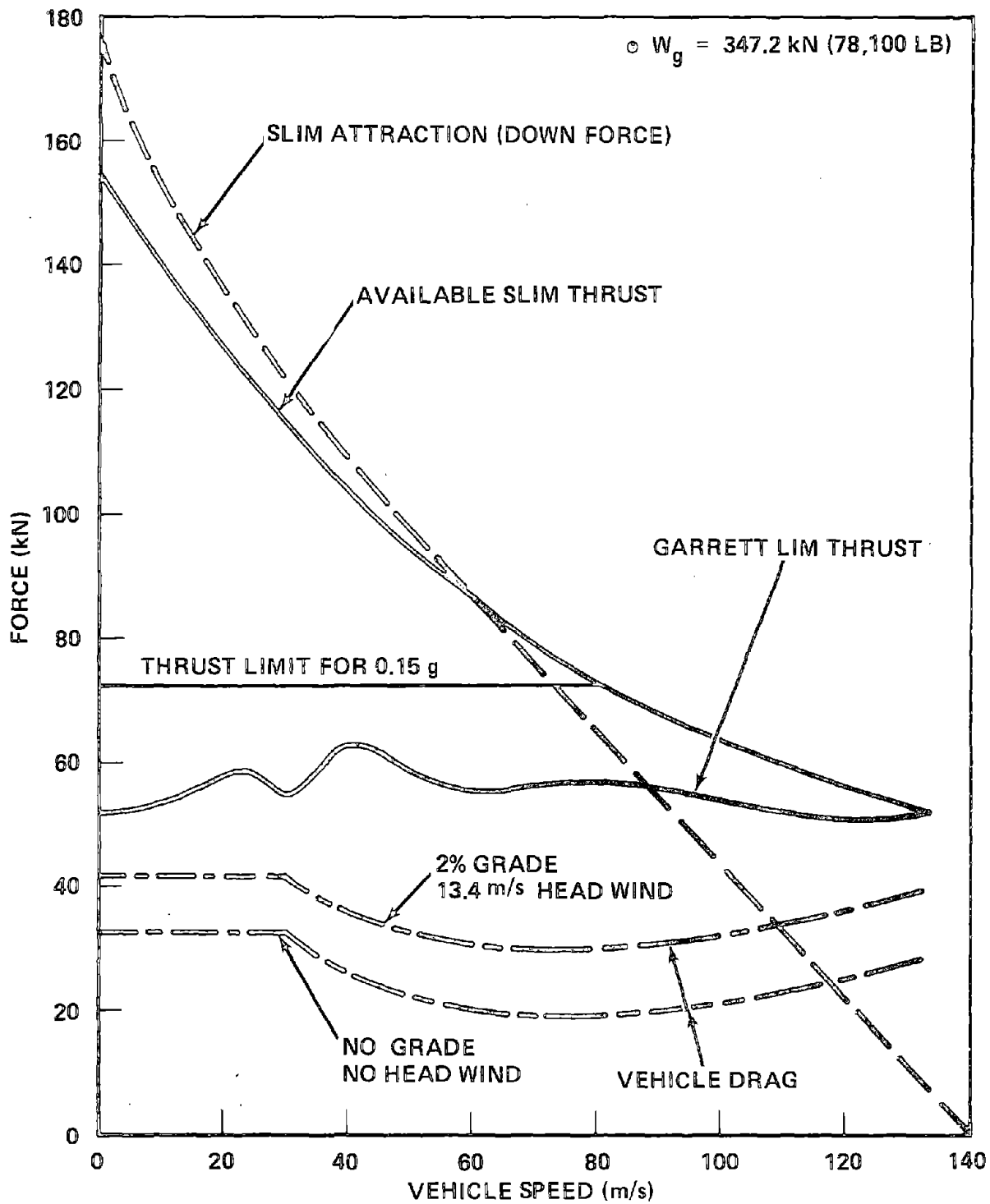
FIGURE 4-80. LIM SYSTEM CHARACTERISTICS
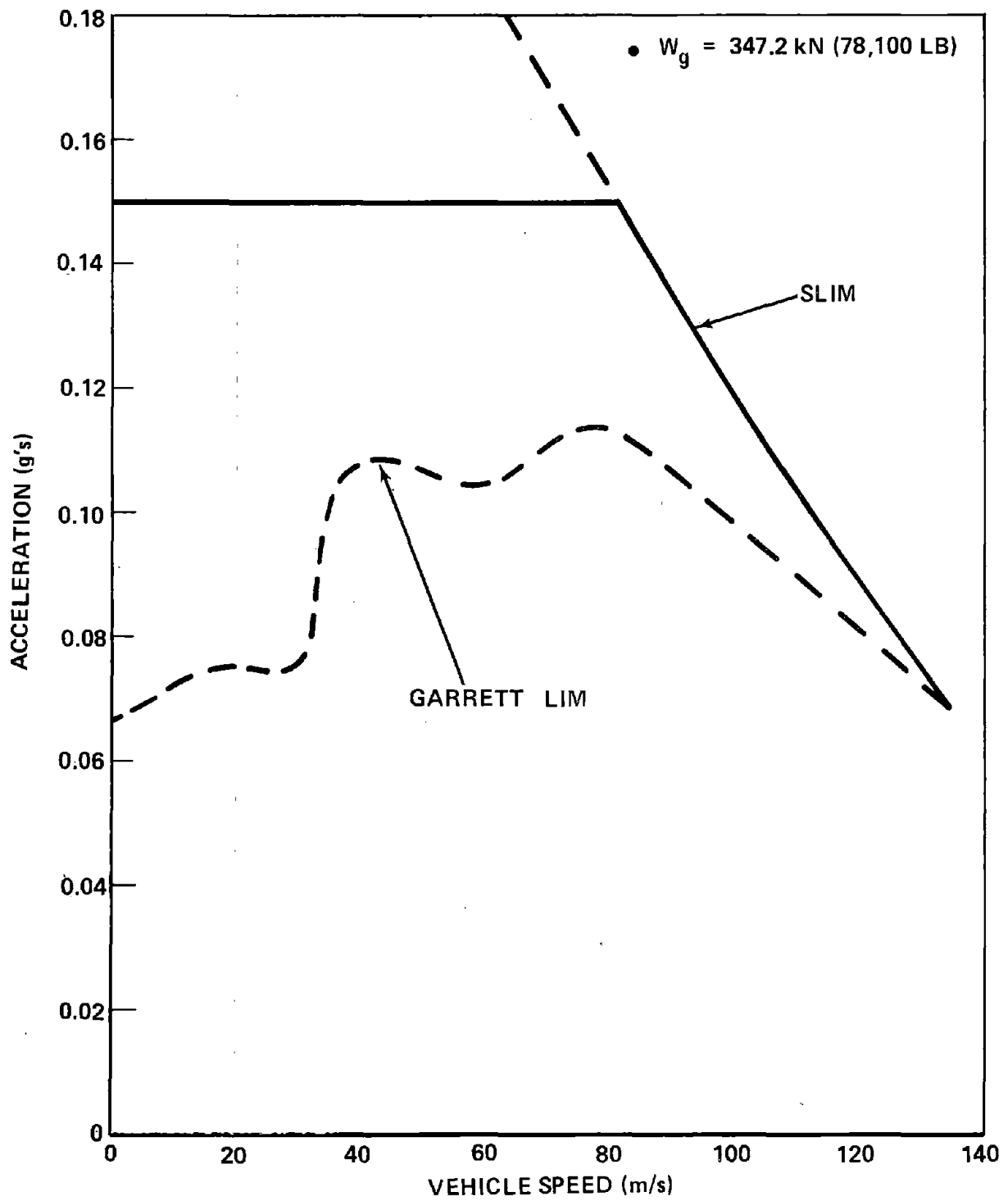
FIGURE 4-81. LIM VEHICLE ACCELERATION
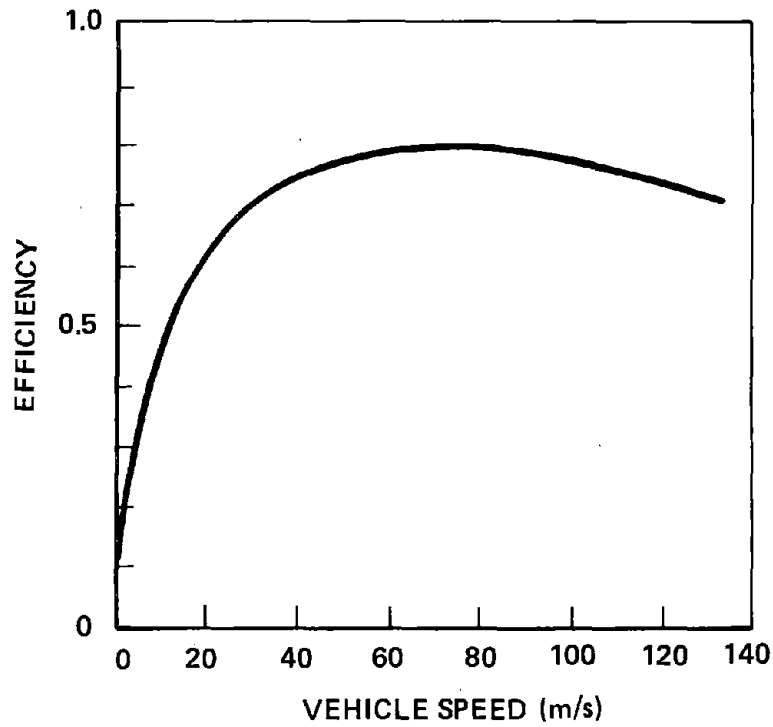
FIGURE 4-82. SLIM EFFICIENCY

TABLE 4-31. OVERALL SLIM EFFICIENCY AT 134.1 M/S

● MOTOR	0.7
● PCU	0.92
● TRANSMISSION LINES	0.9
● COLLECTION, DISTRIBUTION	0.9
● GENERATING PLANT	0.36
	ϵ_0 = 0.188

For the 80-seat SLIM-powered vehicle, Energy Intensity, ψ, is approximately 2.19 MJ/seat-km (3341 Btu/seat-mile) for the 750 km route with $N_i = 5$, which is equivalent to an intercity distance (stage length) of 125 km. The general variation of ψ with intercity distance is given in Table 4-32.

TABLE 4-32. SLIM VEHICLE ENERGY INTENSITY AT 134.1 M/S

INTERCITY DISTANCE, KM	ψ, MJ/SEAT-KM (BTU/SEAT-MI)	
50	2.31	(3,524)
100	2.21	(3,371)
125	2.19	(3,341)
200	2.16	(3,295)
300	2.14	(3,265)
500	2.13	(3,249)
800	2.12	(3,234)

C. <u>Switching</u>. If the hat-shaped guideway is employed with SLIM propulsion, switching is accomplished in a manner similar to the baseline Ducted Fan/GT system, with the exceptions that: (1) a separate propulsion system must be provided since the SLIM is nullified when the vehicle leaves the primary guideway, and (2) the power pick-up must also be switched. Since the vehicle engages the switch at speeds below lift-off, i.e., on wheels, the first exception above suggests separate electric motor drives for these wheels; a solution for the second exception is to retract the primary pick-up and extend a separate pick-up for engagement at the switch. Both of these approaches are complex but appear feasible, and retain the inherent safety of the basic switch concept. Of course, the U-channel guideway provides a simpler switching approach* and permits the SLIM to carry out the switch functions as well as the primary propulsion functions. This approach is not failsafe, however, and the U-channel suffers a number of other serious deficiencies when compared with the hat-shaped guideway.

---

*By extending an arm to engage either (left or right) outside reaction surface.

D. Cost. Preliminary SLIM system cost estimates supplied by DOT are summarized in Table 4-33.

TABLE 4-33. SLIM SYSTEM COST ESTIMATES

• MOTOR (PRIMARY)	$900,000
• REACTION RAIL (SECONDARY)	$311,000/KM
• POWER RAILS	$497,000/KM
• POWER STATIONS	$ 93,000/KM

The 80-seat, 347.2 kN (78,100 lb) vehicle synthesized to accommodate a SLIM propulsion system is estimated to cost $2,013,000 exclusive of development. See Section 5 for the derivation of the vehicle/guideway cost figures.

E. Preliminary Evaluation. In general, the brief analyses reported here show that a SLIM propulsion concept is feasible for a Repulsion MAGLEV system, and it has moderate efficiency and good performance provided wayside PCUs can be employed and high-speed power pick-up can be achieved. Substantially more research and development is required, however, to establish its desirability for Repulsion MAGLEV. The inherent difference between the operating gaps of the SLIM and the vehicle lev/guide magnets suggests a basic incompatibility which is not likely to be removed by clever linkage design, tugs, etc. Motor cost is reasonable, but the guideway cost is high, due primarily to the high electrification costs.

4.4.4 Linear Synchronous Motor (LSM)

A. Background. Consideration has been given to a linear synchronous motor of the type currently under study in Canada - namely 40-50 short magnets on the vehicle to be used only for propulsion. This large number of high-strength superconducting magnets are mounted on the vehicle and interact with a specially-designed part of the guideway. This guideway section is comprised of a matrix of aluminum conductors electrically powered,

phased and controlled so as to produce a moving field which interacts with the vehicle magnets and produces thrust. Since the LSM thrust is proportional to the product of the width of the magnets, the number of magnets, the magnet current and the guideway current (Ref. 4-22) it is obvious that for fixed magnet width and current, few vehicle magnets require high guideway currents while a large number of vehicle magnets require less guideway current, albeit of a higher frequency. Also, a larger number of vehicle magnets increases the vehicle weight requiring a corresponding increase in thrust.

Although the optimum configuration (magnet size, current and frequency) for lowest costs lies outside the scope of this study, work was initiated to obtain LSM magnet weights and costs from the Magnetic Corporation of America. This information together with appropriate modifications to the results of a report by United Engineers (Ref. 4-33) on the guideway electrification costs for the MIT Magneplane project formed the basis for the results in this section and the cost results in section 5.4. Also, the Raytheon Corporation, under contract to Philco-Ford, carried out a brief investigation (Ref. 4-32 and Appendix F) of the suitability of LSM for controlling the vehicle dynamic motions as well as for propulsion. Although is appears feasible to do this dual function, systems considerations suggest that a separate onboard system should be employed for ride control and use the LSM solely for the propulsion role. For example, additional "active" guideway surfaces will have to be provided in addition to the one for propulsion to assure the required damping forces in all degrees of freedom. Since these active surfaces are quite costly - compared with the basic guideway - there will have to be substantial benefit to justify the approach. The information

TRACK WINDINGS

LSM COIL

1.0 (39.4)

0.62 (24.4)

2.94 (116)

3.82 (150)

HYBRID (ALTERNATE)

DIMENSIONS: METERS (IN.)

SHIELDING COILS

LSM COILS

1.0 (39.4)

SHIELDING COILS

LEVITATION COILS

0.50 (19.7)

1.22 (48.1)

3.23 (127.3)

2.94 (116)

PROPULSION ONLY

LSM TRACK WINDINGS

3.45 (136)
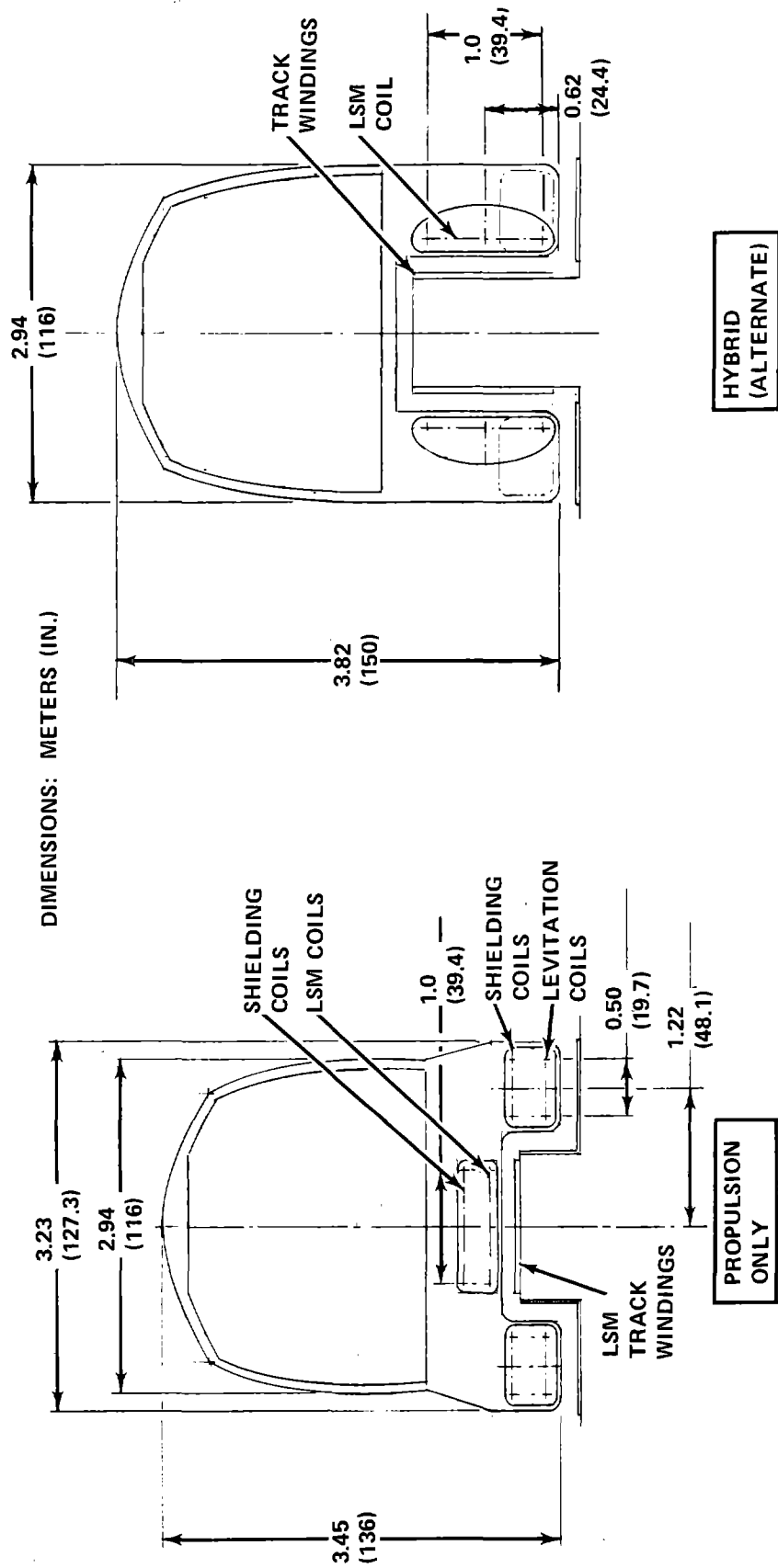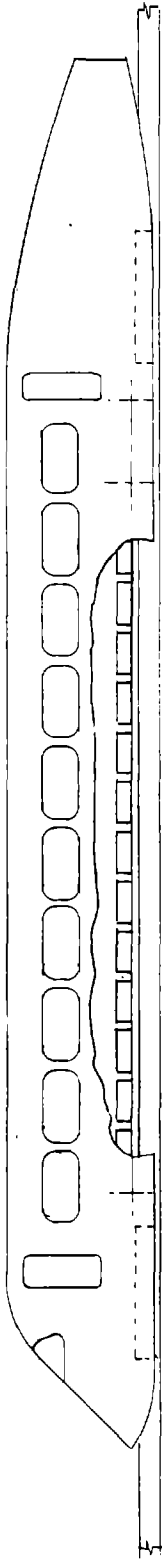
FIGURE 4-83. LSM-POWERED VEHICLE GENERAL ARRANGEMENT

4-185

exchange between vehicle and guideway is greater because of the need for handling multi-zxis dynamic motion data. Furthermore, an onboard power supply of about 100-200 kW is still necessary for lighting, air conditioning, communications, etc., whereas the average control power saved is only about 25-50 kW. Thus the benefits of having the LSM provide ride control appear outweighed by the disadvantages.

B. _Performance_. The propulsion-only LSM is reasonably compatible with the baseline guideway as shown in the general arrangement of Figure 4-83. (Note the layout of a hybrid system, where the LSM provides ride control of the sway/yaw motion in addition to propulsion.) There are a number of disadvantages with the LSM, however, that are pertinent to a MAGLEV system of the type considered here. For example, a large number of superconducting magnets and their associated cryogenic equipment requires a significant increase in vehicle weight and complexity. The guideway cost is high compared to the baseline ducted fan design because of the "active" nature of the propulsion-related components. Vehicle switching is also anticipated to be more complex although no in-depth analysis has apparently been made on this subject to date. If the LSM is coupled with the baseline guideway, auxiliary propulsion must be provided as the vehicle engages the off-ramps. One solution would be to provide electric motors for the wheeled suspension, to facilitate switching, off-ramp, and station operations. Power pick-up would thus be necessary, but at the low speeds involved this should be no problem.

Table 4-34 shows a weight estimate for the LSM magnets and associated cryogenic system, and Table 4-35 summarizes the component weights for a 134 m/s, 80-seat vehicle synthesized to accommodate an LSM propulsion system. The gross weight of the vehicle is 464 kN (104,300 lb).

The overall system efficiency at cruise conditions is approximately 19.6%. Table 4-36 identifies the individual component efficiencies. Note that the LSM efficiency corresponds to 2.5 km guideway-winding length, which results in lowest overall system cost, according to Ref. 4-33. It is claimed that LSM efficiency could be increased if shorter winding lengths were employed, but there would be a substantial cost increase. This is one area where more design and systems analysis is needed.

For the 80-seat vehicle operating at 134 m/s over the 750 km, 5-stop baseline route, the energy intensity, ψ, is estimated at 2.13 MJ/seat-km (3,249 Btu/seat-mile). The variation of ψ with intercity distance is shown in Table 4-37.

C. LSM Magnetic Field Strength. The magnetic field above an LSM is large in the immediate vicinity of the winding because of the $\sim 10^6$ ampere-turn coils, however the fall-off in field strength is quite rapid with distance since the LSM magnets alternate in polarity. This is verified by the calculations summarized in Table 4-38 for an unshielded LSM composed of 0.5x1.5 m magnets under the length of the vehicle.

Comparison of these results with those of the levitation magnets shows that the maximum unshielded LSM magnet field is not as large as the field of the shielded levitation coil, but the LSM field is spread over a much larger area. Also, the difference between the maximum and minimum LSM magnetic field strengths at a given height is only about 10%, whereas the field for the levitation coil drops off rapidly in both the longitudinal

4-186 a

TABLE 4-34. LSM PROPULSION SYSTEM WEIGHT

MAGNET SYSTEM	WEIGHT (KN)	
● SUPERCONDUCTOR	6	(349 LB)
● HELIUM CONTAINERS	6.7	(1,506)
● OUTER CRYOSTATS & SUPPORTS	9.5	(2,136)
SUB-TOTAL (PER MODULE)	22.2	(4,991)
SUB-TOTAL (5 MODULES/VEHICLE)	111	(24,955)
REFRIGERATION	43.5	(9,780)
TOTAL SYSTEM	154.5 KN	(34,735 LB)

TABLE 4-35. LSM VEHICLE WEIGHT BREAKOUT

COMPONENT	WEIGHT, KN (LB)	
● SUSPENSION	71.6	(16,097)
● STRUCTURE	63.9	(14,366)
● FURNISHINGS	24.5	(5,508)
● AUXILIARIES	25	(5,620)
● BRAKES	24.5	(5,508)
● CREW COMPARTMENT	15.6	(3,507)
● PAYLOAD	71	(15,962)
● PROPULSION	154.5	(34,735)
● CONTINGENCY	13.4	(3,013)
VEHICLE GROSS WEIGHT	464 KN	(104,316 LB)

TABLE 4-36. LSM COMPONENT EFFICIENCY

- LSM (INCL. PCU @ 0.85)   0.672
- TRANSMISSION LINE   0.9
- COLLECTION, DISTRIBUTION   0.9
- GENERATING PLANT   0.36

$$\epsilon_o \quad = \quad 0.196$$

TABLE 4-37. LSM ENERGY INTENSITY @ 134.1 M/S

INTERCITY DISTANCE, KM	ψ, MJ/SEAT-KM	(BTU/SEAT-MI)
50	2.24	(3,417)
100	2.15	(3,280)
125	2.13	(3,249)
200	2.10	(3,204)
300	2.08	(3,173)
500	2.07	(3,158)
800	2.06	(3,143)

TABLE 4-38. PREDICTED FIELD STRENGTH OF LSM MAGNETS

HEIGHT (m) (ABOVE MAGNET WINDING)	MAXIMUM FIELD STRENGTH (TESLA)	
0.3	0.310	(3100 gauss)
0.6	0.045	(450)
0.9	0.007	(70)
1.2	0.001	(10)

and lateral directions. The results presented above indicate that the unshielded magnetic field for LSM propulsion may not be a problem provided there is sufficient height ($\sim$ 1 m) above the windings — which is the case if the vehicle is configured to accommodate a U-channel guideway. For the baseline guideway however, there is less available height and shielding coils are provided.

D. <u>Cost</u>. The LSM costs are identified in detail in Section 6. With appropriate shielding coils, the total cost estimate is approximately $868,000 per vehicle, excluding refrigeration system cost and any development costs. Total cost of an LSM-powered, 80-seat vehicle is estimated at $2,086,000, exclusive of development. The guideway-related costs, based on Ref. 4-33 data, updated for 1974 dollars, are as follows:

- Conductors and Attach Hardware . . . . $ 320,000/km
- Fixed Equipment (115 kV and $180,000/km
  34.5 kV Transmission Systems)
- Variable Equipment (Power Stations, ... $234,000/km
  PCUs, Transformers, etc.)
                                                   _____
      LSM-Related Guideway Cost . . . . $ 734,000 /km

As stated in Section 5, the data presented in Ref. 4-33 actually indicates a cost of $1,280,000/km for the conductors after adjustment for 1974 dollars. However, because our vehicle has more LSM magnets (four times as many as assumed by Rahtheon) the guideway conductor costs have been reduced. The cost of transmission equipment estimated by Raytheon has not been changed here since the difference is not considered significant.

E. <u>Preliminary Evaluation</u>. The LSM appears to be a feasible propulsion system for a MAGLEV vehicle; its major advantages are compatibility with the Repulsion scheme and elimination of power pick-up equipment. Much R&D work remains, however, before a realistic assessment of the LSM can be made. The LSM-powered vehicle is very heavy and, although overall propulsive efficiency is good, energy consumption is adversely affected by the high weight. Much further work remains in the areas of vehicle switching, speed control and acceleration, and the LSM-part of the guideway design.

4.4.5 Superconducting Paddle Wheel

The superconducting paddle wheel is a novel propulsion scheme proposed by Davis and Borcherts (Ref. 4-34) to overcome the inherent small gap limitation of a conventional linear induction motor by using a superconducting winding.

Thrust is developed similar to the conventional induction motor, i.e., a moving magnetic field near a conducting surface generates eddy currents in the medium, and these eddy currents produce a force opposing the motion of this field. In the conventional induction motor, the moving magnetic field is created with multiphase power. However, only dc currents can be used in order to take advantage of the large fields produced by superconductors and to avoid severe ac loss problems. Hence, the moving magnetic field must be generated by mechanically moving the static magnetic field. One method of doing this is to mount the superconducting winding on the face of a drum and rotate the drum in proximity to a reaction rail. If the drum rotates fast enough, the part of the winding nearest the reaction rail is moving backward relative to the rail. In this manner, the "drag" force created is in the forward direction, providing thrust in analogy to the conventional paddle wheel used for ship propulsion. (By changing the relative speed of rotation, braking action can be obtained.) Since this superconducting motor does not generate its own power, a prime mover such as a gas turbine or a rotary electric motor (REM) would have to be provided.

For this application, the superconducting paddle wheel uses the levitation surface of the guideway as its reaction rail for producing thrust. The generalized thrust of the paddle wheel (per unit width) at constant current is shown in Figure 4-84 as a function of both vehicle speed and relative speed*. Note that the high "stall" thrust is a favorable feature for a Repulsion MAGLEV vehicle with its characteristic low-speed drag peak. The winding current must be in the vicinity of 10^6 ampere turns to provide the desired thrust. Figure 4-85 shows the generalized efficiency, also as a function of

---

*Relative speed is the difference between the peripheral speed of the wheel and the vehicle speed.
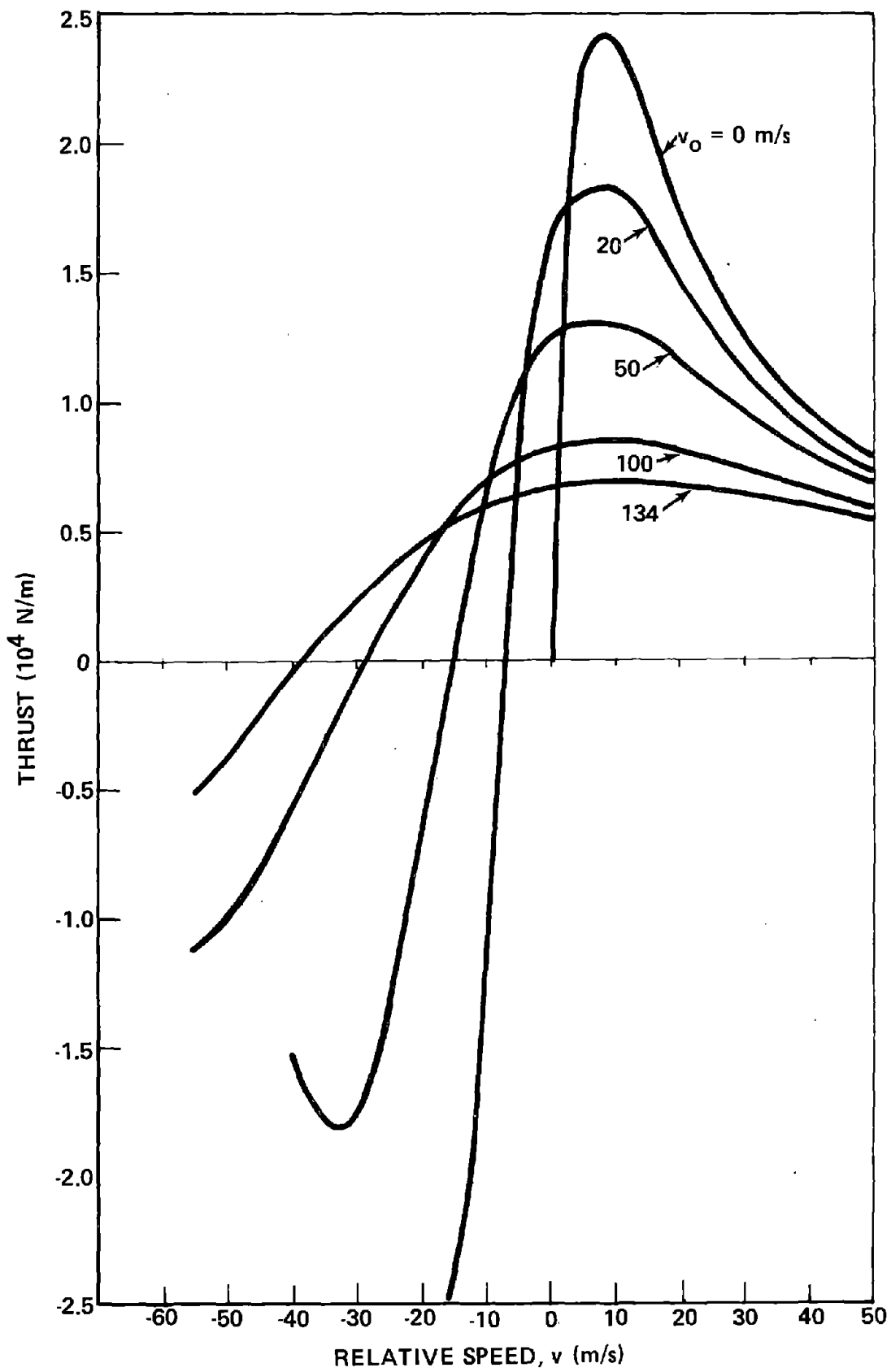
FIGURE 4-84. PADDLEWHEEL THRUST
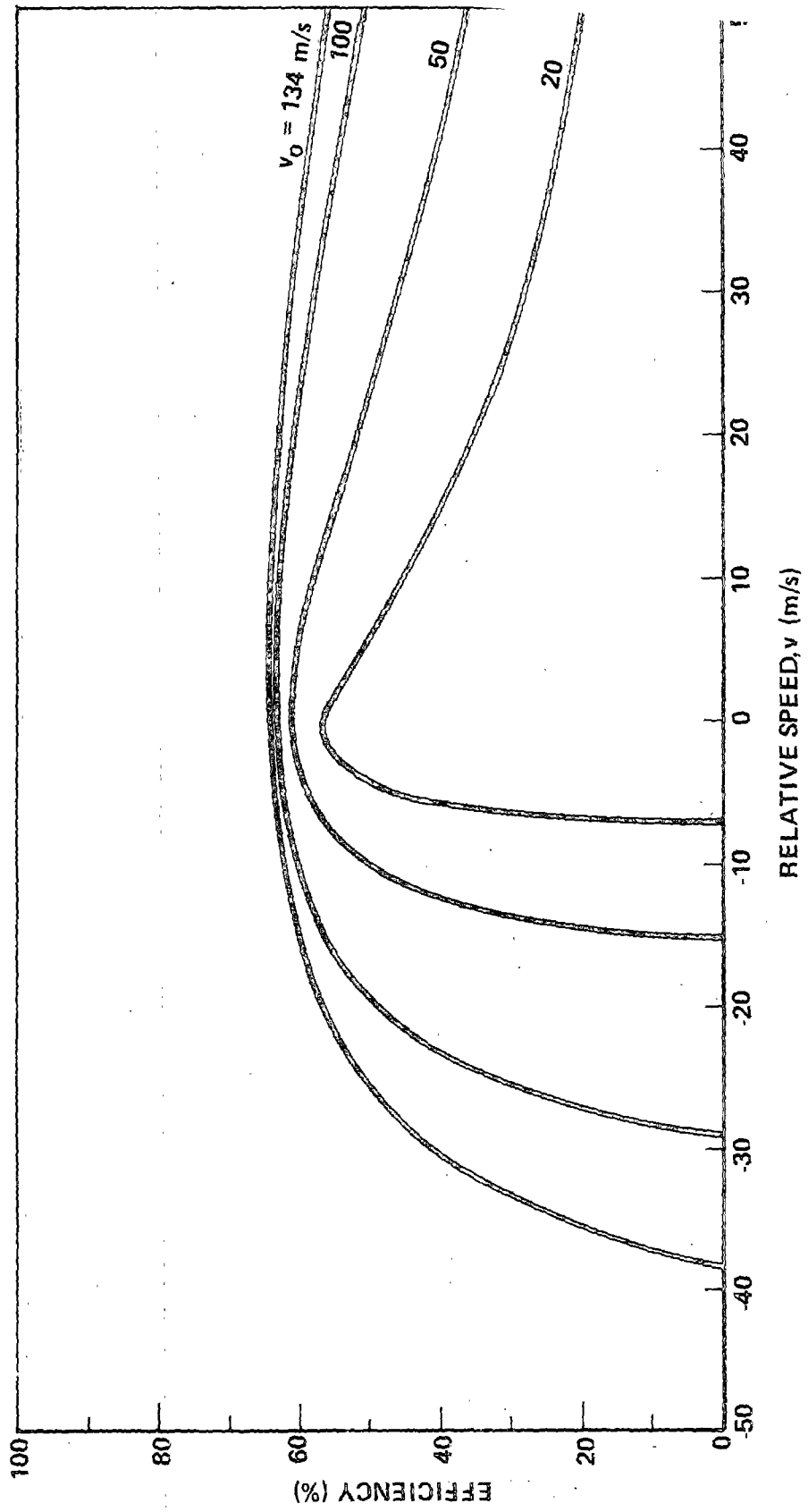
FIGURE 4-85. PADDLEWHEEL EFFICIENCY

vehicle speed and relative speed. Typical paddle wheel performance is shown in Figure 4-86, including the braking force available.
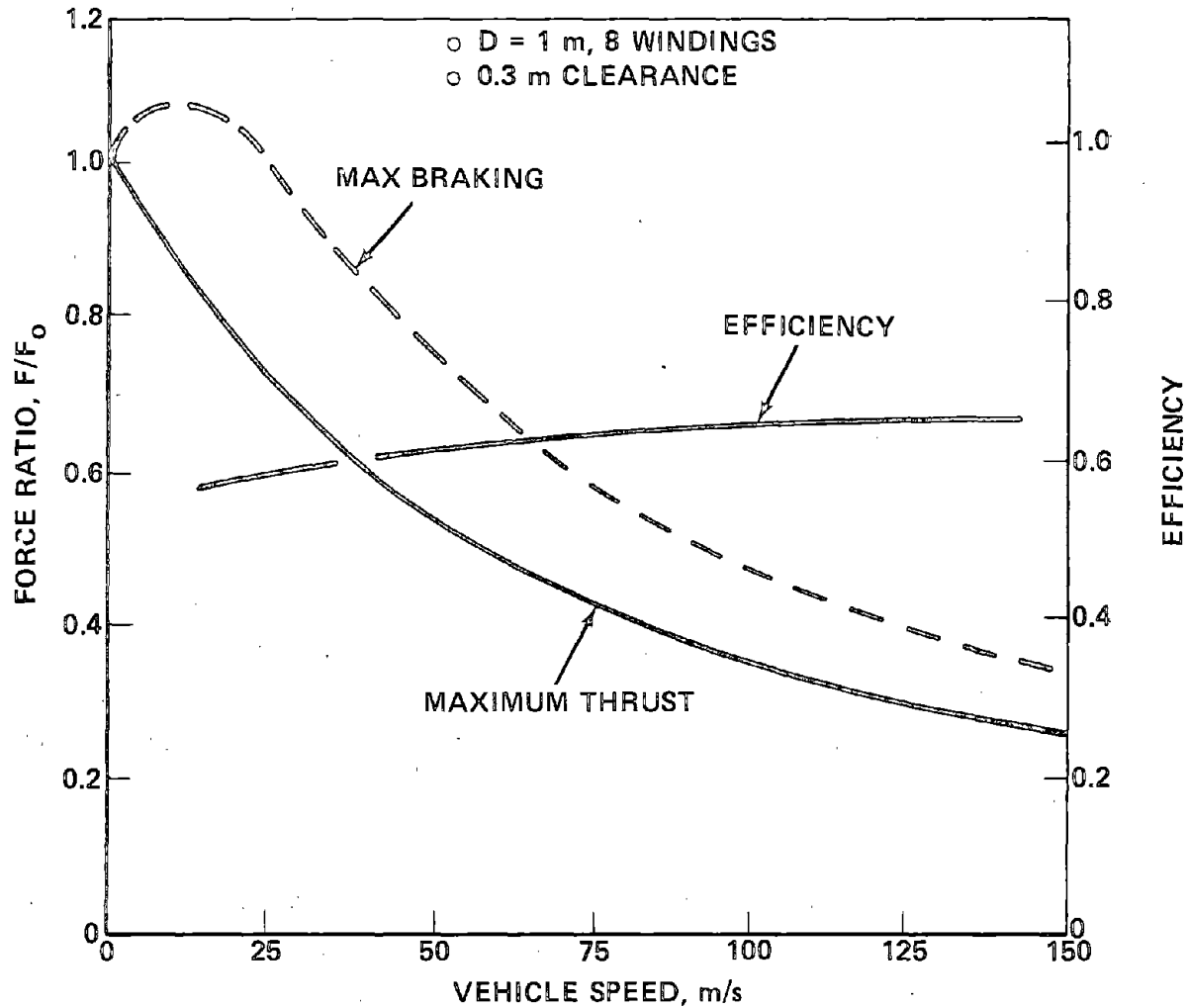
FIGURE 4-86. PADDLEWHEEL PERFORMANCE

In addition to the thrust force, there is an appreciable lift force generated that could augment and possibly eliminate at least one of the two support magnets in each of the levitation modules near the paddle wheel. It is even possible to provide four paddle wheels in the corners of the vehicle and completely eliminate the need for levitation magnets, relying solely on the lift force generated by the rotating paddle wheels. In this manner, magnetic drag — an undesirable by-product for the levitation magnets — is eliminated and becomes a useful thrust in the superconducting paddle wheel. Detailed

analyses are required to evaluate an integrated propulsion/suspension approach, particularly in the area of ride quality.

The proper matching of the thrust from the superconducting paddle wheel to that required for the vehicle requires more work to obtain the optimum guideway parameters and determine the desirability of using the lift force from the paddle wheel. For example, a 2 to 3 cm thick aluminum guideway may be too thick to provide adequate vehicle thrust with a 10^6 ampere-turn paddle wheel winding. Although a thinner aluminum section would decrease the lift-drag ratio of the levitation magnets, lift force from the paddle wheel can offset this decreased peformance. It should even be possible to provide an iron backing, similar to that of the single-sided linear induction motor (SLIM), to the high speed sections of the aluminum guideway to enhance the performance of the device. At high speed, the levitation magnets would not "see" the iron backing.

An 80-seat, 134 m/s vehicle has been synthesized for the superconducting paddle wheel propulsion scheme. Power is supplied to the paddle wheels by regenerative gas turbines arranged as shown in Figure 4-87. The installation is quite compact, with only a small increase in vehicle cross-section to allow for the engine air intakes. The gross weight of the vehicle is 365.4 kN (82,150 lb). Propulsion system weight is shown in Table 4-39.

The weight of each major component of the vehicle is given in Table 4-40. For the baseline 750 km, 5-stop route, the energy intensity, ψ, is approximately 1.71 MJ/seat-km (2,609 Btu/seat-mile). The variation of ψ with intercity distance is given in Table 4-41.

The estimated cost of the paddle wheels is $775,000, and the cost of the gas turbines is $725,000, for a total propulsion cost, per vehicle, of $1,500,000 exclusive of development. Total vehicle cost with the Paddle Wheel/GT propulsion system is estimated at $2,626,000. Note that at the current state of knowledge, the cost estimates for the paddle wheel must be considered very approximate.

A substantial amount of R&D effort must be devoted to this concept before its feasibility can be established. At this point in time, however, it has

TABLE 4-39. PADDLE WHEEL/GT VEHICLE WEIGHT BREAKOUT

COMPONENT	WEIGHT, KN (LB)	
● PADDLEWHEELS (2)	29.4	(6,610)
● GAS TURBINES (2)	14.2	(3,192)
● DUCTING	6.0	(1,349)
● GEARBOXES (2)	3.3	(742)
COMPONENT SUB-TOTAL	52.9	(11,893)
● FUEL (23.2 X 1.15)	26.7	(6,003)
TOTAL PROPULSION	79.6 KN	(17,896 LB)

TABLE 4-40. PADDLE WHEEL/GT VEHICLE WEIGHT BREAKOUT

COMPONENT	WEIGHT, KN (LB)	
● SUSPENSION	66.8	(15,019)
● STRUCTURE	53.3	(11,983)
● FURNISHINGS	24.5	(5,508)
● AUXILIARIES	21.0	(4,721)
● BRAKES	20.2	(4,541)
● CREW COMPARTMENT	15.6	(3,507)
● PAYLOAD	71.0	(15,962)
● PROPULSION	79.6	(17,896)
● CONTINGENCY	13.4	(3,012)
GROSS WEIGHT	365.4 KN	(82,149 LB)
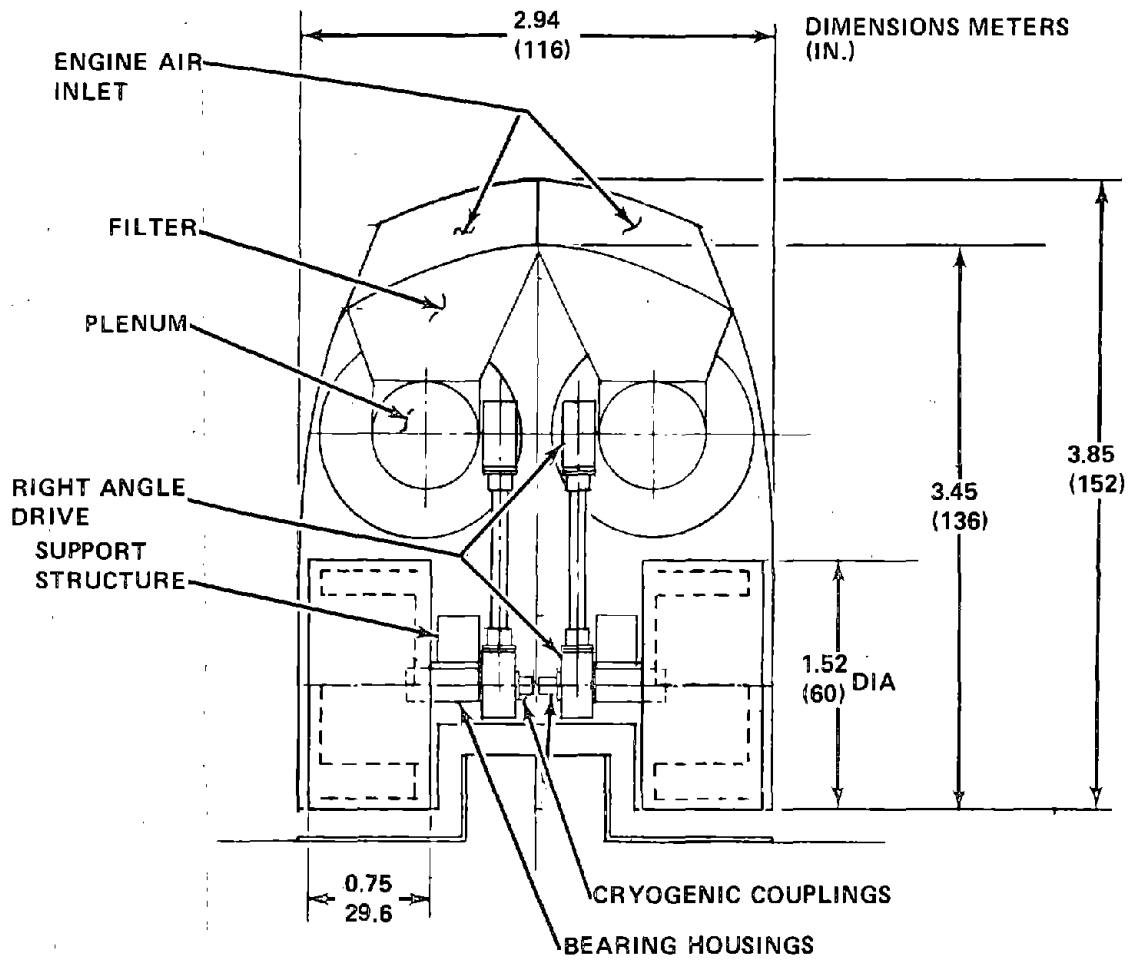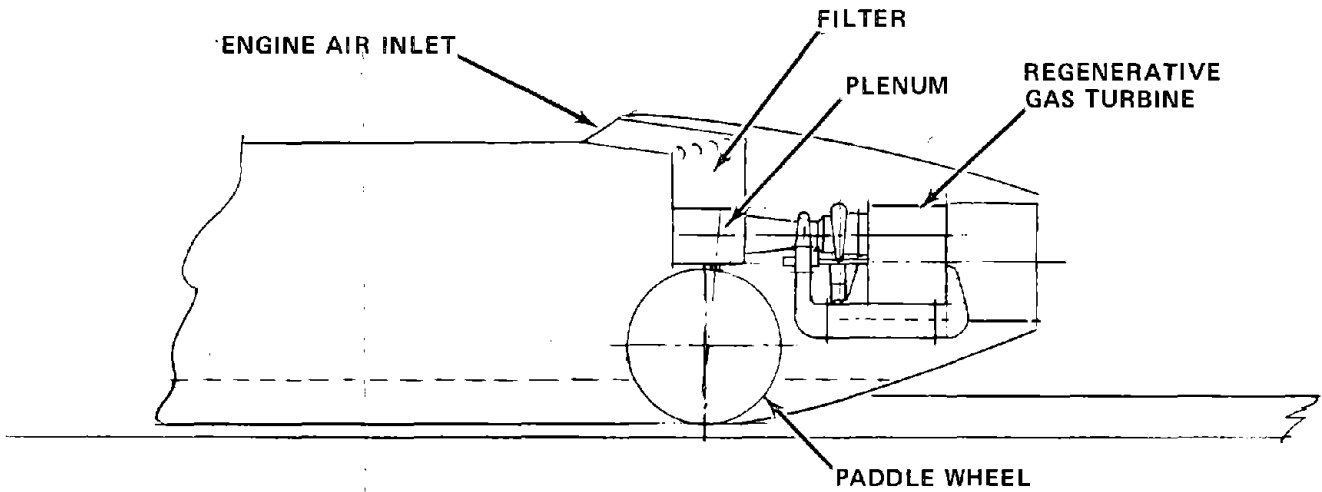
FIGURE 4-87. PADDLEWHEEL/ GT SYSTEM GENERAL ARRANGEMENT

TABLE 4-41. PADDLEWHEEL ENERGY INTENSITY

INTERCITY DISTANCE, KM	ψ, MJ/SEAT-KM (BTU/SEAT-MI)	
50	2.14	(3,265)
100	1.78	(2,715)
125	1.71	(2,609)
200	1.6	(2,441)
300	1.54	(2,349)
500	1.49	(2,273)
800	1.46	(2,227)

significant potential as a MAGLEV propulsion device. It is light and efficient and has relatively low energy consumption. It is a large gap device and is thereby quite compatible with the Repulsion MAGLEV concept. It can be driven by either gas turbines or superconducing electric motors (with wayside power pick-up) and is adaptable to the switching concept developed for the baseline guideway although the wheeled part of the suspension will probably have to be powered for off-ramp and station operations.

4.4.6 Evaluation of Propulsion Candidates

Table 4-42 summarizes the 80-seat, 134 m/s vehicle gross weight, vehicle cost, additional guideway-related cost (i.e., over the basic guideway), overall

TABLE 4-42. PROPULSION SYSTEM COMPARISON (80 SEAT VEHICLE)

	FAN/GT	FAN/REM	SLIM	LSM	PADDLE WHEEL/GT
○ VEHICLE GROSS WT (KN)	366.5	332.8	347.2	464	365.4
○ VEHICLE COST (10^3)	2316	2547	2013	2086	2626
○ ADD'L GUIDEWAY COST (10^3/KM)	0	494	901	734	0
○ OVERALL EFFICIENCY	0.209	0.149	0.188	0.196	0.243
○ ENERGY INTENSITY (MJ/SEAT-KM)	2.18	2.59	2.19	2.13	1.71

efficiency and baseline route energy intensity for each of the propulsion systems studied. Figure 4-88 shows the energy intensity for each propulsion scheme as a function of intercity distance. Although Section 5 presents a more complete cost analysis of the various systems, some general conclusions can be drawn relative to the propulsion systems studied herein.
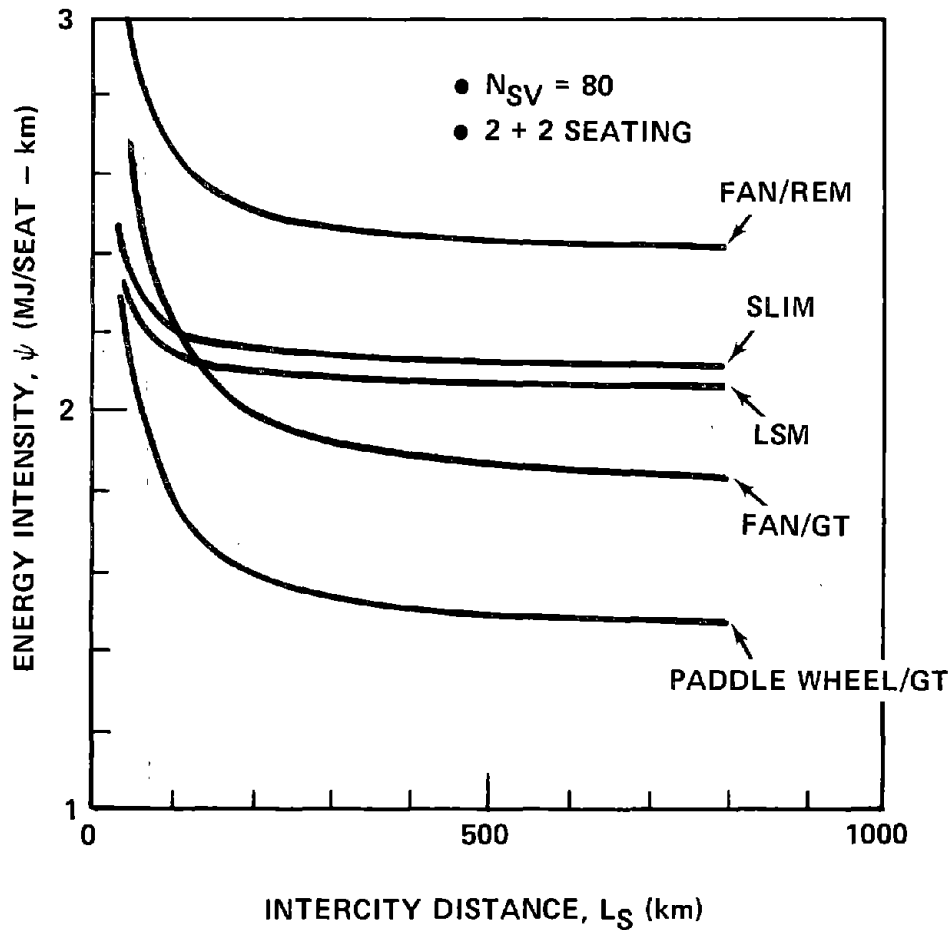
FIGURE 4-88. COMPARATIVE ENERGY CONSUMPTION

The most "realistic" system appropriate to the Repulsion MAGLEV concept is the gas turbine-driven ducted fan. Its development background is extensive and its reliability is firmly established. It is totally self-contained, and requires no power pick-up, thereby permitting great flexibility in guideway

4-198

design; it also serves as a single propulsion system for off-line as well as on-line operation. It is efficient and is definitely the "near-term" solution. The future chemical fuel situation is difficult to evaluate. However, there is reason to doubt that the U.S. will ever reach all-electric status, whatever the basic source of its energy, i.e., nuclear, solar, geothermal, etc. Synthetic fuels would thus appear necessary for energy applications which are not optimum for electricity. For this reason, a hydrogen-fueled MAGLEV system could be attractive. The emissions problem would essentially disappear with this approach, leaving the noise problem as the only negative feature. From the noise data presented, however, it seems clear that only the noise associated with the acceleration phase of vehicle operations ($\sim$ 90 dbA) remains of concern — and there is reason to believe that substantial improvement can be made in this area, as discussed in Appendix E.

Of the electric systems studied, the SLIM has the most extensive R&D background and can be considered a feasible system for Repulsion MAGLEV despite the requirement for operating it as a tug, i.e., with a separate suspension. With onboard power conditioning, the vehicle is heavy and energy consumption is adversely affected. Therefore wayside power conditioning is essential, and although not yet demonstrated, appears feasible. The appropriateness of the narrow-gap SLIM for a large-gap MAGLEV vehicle, however, is open to question. It is our judgement that neither the single- nor the double-sided linear induction motors will provide a good propulsion system for the Repulsion MAGLEV concept.

The LSM needs much more R&D to firmly establish its applicability; from an engineering viewpoint the LSM is not much more than a collection of mathematical equations at this point in time. Nevertheless, it has much potential for the future, particularly in view of its compatibility with the Repulsion MAGLEV concept. A vigorous research effort should be pursued on this scheme.

The (superconducting) electric motor-powered ducted fan is posed only as an alternate to the gas-turbine driven ducted fan in the event that circumstances force the U.S. to an all-electric society. The noise levels are lower (-3 db) but still of concern; this should be solvable however, well within the development cycle of the superconducting motor. The biggest disadvantage is

the high energy consumption, and this is because the poorest aspects of each concept are combined, i.e., the fan/duct with the electric generation chain. Its biggest advantage is compatibility with the Repulsion MAGLEV concept and its ability to handle both off-line and on-line operations.

The superconducting paddle wheel must be regarded as a far-out idea with long-term potential, paricularly for low energy consumption. It is compatible with Repulsion MAGLEV and also has the potential for integrated propulsion/levitation. Further research should be carried out on this concept.

4.5 GUIDEWAY SUBSYSTEM

The guideway subsystem consists of the aluminum levitation/guidance elements, the supporting guideway (both at-grade and elevated), switches, wayside power pick-up (if any), wayside communication and control, and right-of-way. Each of these items is discussed in the following sections.

4.5.1 Levitation/Guidance Element

A. Requirements. The aluminum elements in the guideway provide the source of the eddy currents which support the vehicle and provide the necessary guidance forces. The previous Ford work established the theoretical basis for the computation of the magnetic forces and moments and provided some preliminary system studies (Ref. 4-22). The tradeoff information presented in Section 5.3.2 shows typical results for the magnetic performance of the system. The tradeoff information and the Ford studies show:

o   The requirement for guidance forces (i.e., a 90° corner) introduces a significant increase in magnet drag compared to a flat plate, however, a corner configuration is considered to be the most practical aluminum shape.

o   The use of nearly pure aluminum alloy (1100-H14) offers a significant decrease in magnetic drag compared to a stronger alloy such as 6061-T6.

o   The magnetic lift-drag ratio increases with increasing aluminum thickness. The "optimum" thickness (minimum system cost) is a function of vehicle fuel costs as well as the aluminum costs. A thickness of 2.54 cm (1 in.) is "optimum" if the JP fuel cost rises to roughly ~20¢/liter (76 ¢/gallon) for the baseline Ducted Fan/Gas Turbine propulsion system, and has been selected as the baseline. (However, the optimum thickness of the aluminum is between 2 and 3 cm for a very side range of JP fuel cost, i.e., 5 to 30¢/liter.)

o   Studies at Ford have shown that the width of each aluminum ele-
    ment should be approximately twice the magnet coil width, and
    the height of the vertical guidance element should be approxi-
    mately one-half the width. Thus, the size of a 90° element is
    1 x 0.5 m. (These are the inside dimensions, the outside dimen-
    sions are 1.03 x 0.53 m.)

o   The vertical and horizontal parts of the element must be elec-
    trically connected if a combined lift/guidance magnet is used
    on the vehicle. However, separate (unconnected) aluminum guid-
    ance and lift elements may be used with separate guidance and
    lift magnets.

o   The presence of iron close to the levitation elements degrades
    the performance of the magnets, particularly at low speed. The
    approximate limits on the amount of steel reinforcing bars in
    the guideway are: have no bars closer than 5.1 cm (2 in.) to
    the bottom surface of the aluminum, and the bars at this dis-
    tance should not be larger than 1.9 cm (0.75 in.) or be closer
    together than 15.3 cm (6 in.) on the average. More steel can
    be used if located further away from the aluminum, for example
    at approximately 0.3 m (1 ft), a solid-steel structure could
    be used, at least for the high-speed portions of the guideway.

o   The effect of surface roughness on vehicle dynamics have been
    discussed in Section 4.3.2; a nominal roughness index, A, of
    1.5×10^{-6} m-rad (5×10^{-6} ft-rad) has been used as the base-
    line condition. The achievement of this roughness for prac-
    tical guideway construction is discussed in following sections.

o   Structual requirements such as maximum length of the sections,
    attachments, etc., are discussed in Paragraph E, below.

B.   Candidate Configurations and Evaluation. There are a number of pos-
sible shapes for the levitation/guidance elements; typical configurations are
shown in Figure 4-89. The aluminum portion of the guideway is indicated by
the solid dark lines. Note that all the candidates except one — the circular
shape — utilize a horizontal surface to provide lift and a vertical surface to
provide guidance forces. In addition to the five shapes shown in the figure,
others, such as an inverted Vee, were considered and eliminated. (The inver-
ted Vee guideway results in an unstable vehicle.)

In all cases the aluminum is not structural; it conforms to, and is sup-
ported by, the underlying guideway, therefore the construction tolerances of
the supporting structure becomes important from the standpoint of vehicle ride

4-201

HAT-SHAPE
(WIDE INVERTED TEE)

U-CHANNEL

CIRCULAR

CANTED
INVERTED TEE

INVERTED
U-CHANNEL
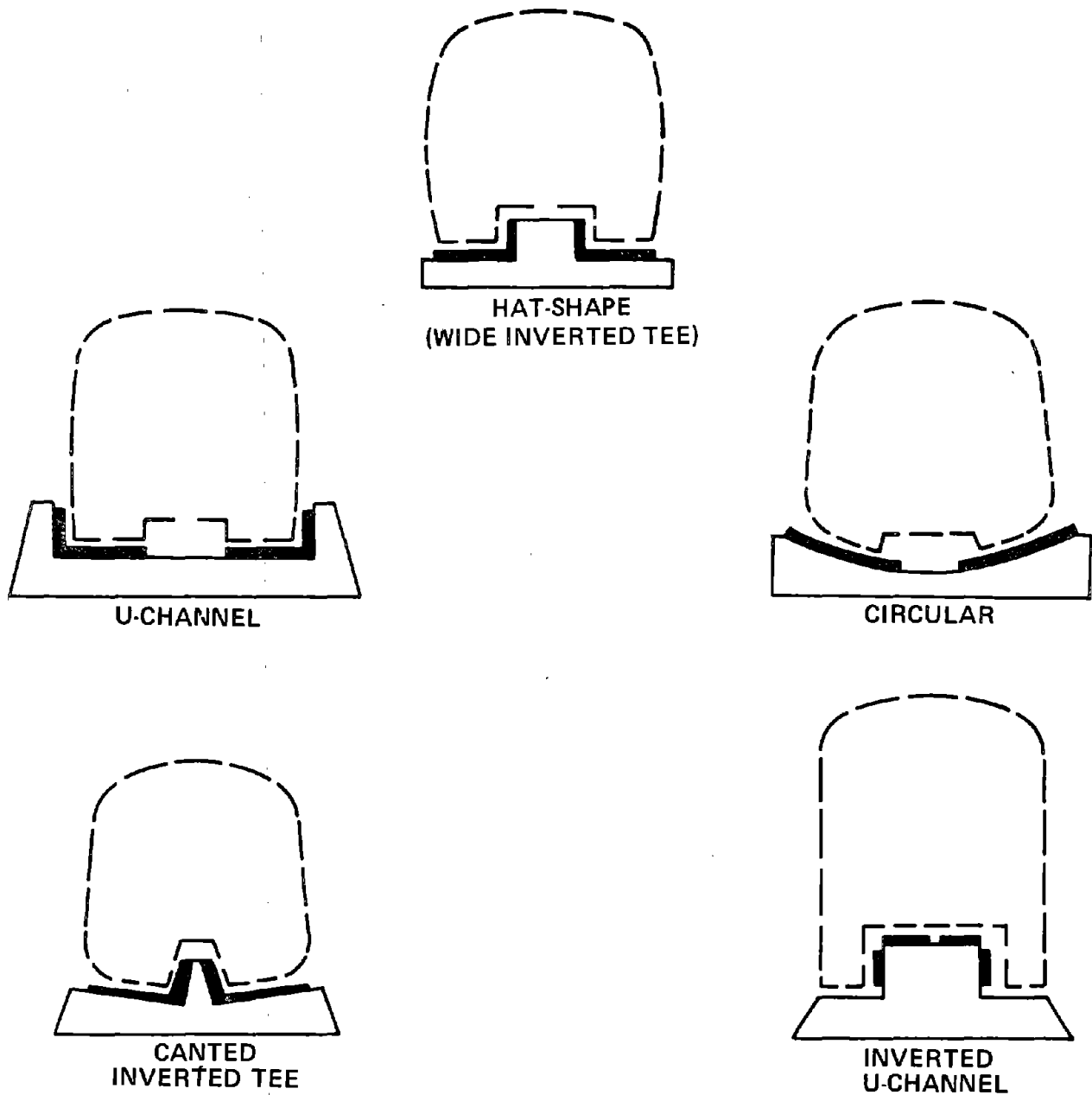
FIGURE 4-89.   CANDIDATE GUIDEWAY CONFIGURATIONS

4-202
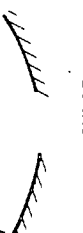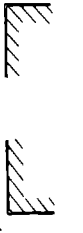
quality. Table 4-43 lists other important factors considered in the evalua-
tion of the various configurations. This table summarizes the advantages and
disadvantags of each. Based upon the current information, the overall rank-
ing is:

Rank	Guideway Configuration
1. (Baseline)	Hat Shape (Wide Inverted Tee)
2.	U Channel
3.	Inverted U Channel
4.	Canted Inverted Tee
5.	Circular

This ranking is based upon the assumption that the propulsion system has no
influence on the guideway design. This is obviously true only with an air
propulsion system, or a narrow superconducting paddle wheel which operates on
horizontal aluminum guideway elements. The U channel, inverted U channel, or
circular guideway are better geometrical shapes for SLIM or LSM propulsion
systems since they can more easily accommodate the propulsion elements down
the center of the track. However, they are not adaptable to the baseline fail-
safe switch concept without using auxiliary propulsion in the switch area.
Actually there is relatively little difference between the ranking of the first
three candidates even for the air propulsion system. Since guideway construc-
tion costs are very important for the overall system economics, an alternate
system such as the inverted U channel may ultimately become the leading con-
tender if the construction costs are the lowest. This proof, however, will
require a detailed site-specific analysis including the amount of elevated vs.
at-grade construction since this type of guideway may be quite economical for
elevated structures, but be at a disadvantage at-grade.

C. Stress Analysis. Problems with the Garrett LIMRV vertical reaction
rail at the test track in Pueblo, Colorado, have shown that care must be taken
in the installation of continuous aluminum elements. The aluminum portion of
the MAGLEV guideway has a considerably different configuration than a LIM
reaction rail; one of the primary differences is the presence of gaps rather
than a continuous guideway. There are some advantages to the vehicle ride and
forces on the magnet by having a continuously welded guideway, but there are

TABLE 4-43. GUIDEWAY EVALUATION

GUIDEWAY CONFIGURATION	COMPATIBILITY WITH VEHICLE AND GUIDEWAY STRUCTURE		SWITCHING TECHNIQUES	OTHER CONSIDERATIONS
	GENERAL EVALUATION	EFFECTS OF CURVES		
(1) HAT SHAPE (WIDE INVERTED TEE)	Baseline configuration, good ride quality characteristics. Design lends itself to efficient (economical) structural design.	Vehicle tends to lean in a favorable direction (inward) in a curve, but self banking effect is small.	Compatible with baseline "overhead" switch. Vehicle rolls on wheels while switching and low-speed travel. However, overhead switch not compatible with SLIM or LSM without auxiliary propulsion. At-grade switching possible as shown in alternate switch concept.	Vertical elements require only a single central support. Debris, snow, etc., will tend to collect in corners. Difficult to use with SLIM or LSM propulsion.
(2) CANTED INVERTED TEE	Ride quality good. Purpose of cant is to maximize lift of magnet, but effect is small. Structurally not as economical as (1).	Minor improvement in self-banking compared to (1).	Same as above except more difficult to have wheels extend below bottom of vehicle (optimum for slow-speed travel).	More difficult to fabricate than (1). Problem with debris/snow collection. Drain holes required in levitation elements. Same propulsion problems as (1).
(3) U CHANNEL	Good ride quality; similar to (1). Structural design not as efficient as (1) due to two outboard curbs.	Vehicle tends to roll in an unfavorable direction (outward) in a curve, but effect is small.	Same as (2). Best configuration for at-grade switch.	Sides on channel tend to reduce aerodynamic side forces and moments. Extended sides would reduce noise and aero effects. More compatible with center SLIM or LSM active track than (1) or (2). Problem with debris/snow collection and drainage.
(4) CIRCULAR	Detailed ride characteristics not evaluated. More difficult to fabricate circular shape.	Vehicle is "self-banking" in a curve, i.e., will automatically have a coordinated turn for any speed, however this causes some problems with SLIM or LSM due to excursions of vehicle.	Same as (2). Difficult with at-grade switch.	Predicted to be more expensive and difficult to fabricate than (1). Requires additional aluminum in curves if designed for off-nominal speeds. Problem with debris/snow collection and drainage. Compatible with center SLIM or LSM.
(5) INVERTED U CHANNEL (BOX BEAM)	Requires separate lateral guidance magnets on vehicle. Good ride quality. Least complicated design. More efficient structural design than (1), but requires extra material for at-grade locations.	Same as (1)	Same as (2). Difficult with at-grade switch.	Aluminum installation and cost optimum since only flat plates used. Simplest guideway fabrication and probably the lowest guideway cost except for at-grade guideways. Should be best for debris and snow problem. Requires more expensive vehicle due to lateral guidance magnets. Compatible with center SLIM or LSM.

also several disadvantages and a "gapped" or segmented aluminum guideway has been selected as the baseline, at least for the portions of the guideway where normal cruise speeds are reached. The effect of gaps becomes more pronounced at lower vehicle speeds, and continuous or nearly continuous aluminum may be required near switches, in urban regions, and in other low-speed areas. Both continuous and segmented guideways have been investigated as summarized below.

(1) Introduction. Sketches of possible guideway configurations are shown in Figure 4-89. The roadway beneath the levitation elements forms the primary structural support for the vehicle magnetic loads, and the levitation elements are not relied upon for this purpose. (The 2.5 cm aluminum plate could support the vehicle loads over spans on the order of about 0.5 meters if an economical roadway design could be devised to utilize this capability. This does not appear to be possible.)

The primary structural problem is produced by differential thermal expansion between the roadway and levitation elements. An unrestrained levitation element will expand on hot days and contract on cold days relative to the roadway. However, since the levitation element for MAGLEV must be secured to the roadway, compressive and tensile forces will develop in the aluminum on hot and cold days, respectively. The magnitude of the stresses produced by these forces has been estimated and compared with allowable stresses to establish the requirements for the levitation element.

(2) Analytical Model. Only axial stresses and deformation have been considered for this conceptual design study. Also the stresses and deformations were assumed to be constant over the cross section, bending was neglected, and the underlying roadway was conservatively assumed to be inextensible. The model assumed an axial member restrained by discrete attachments spaced along both free edges of the levitation element. The axial restraint of the attachments in an actual application will most likely be transmitted by frictional forces between the attachments and levitation surface. The effects of limited friction capability would be included in a more detailed analysis. For this analysis, however, the levitation element is considered to be elastically restrained from thermal expansion/contraction by evenly spaced, infinite friction attachments. The axial load distribution in the levitation element

can be determined for this idealized case from the solution of the following equation:

$$\frac{d^2P}{d\chi^2} - \frac{k}{AE} P = k\alpha (T - T_i)$$

where: P = axial load at position χ

χ = axial position measured from the midpoint of the element

k = axial spring rate of attachment divided by the attachment spacing

A = cross-sectional area

E = modulus of elasticity

α = coefficient of thermal expansion

T = temperature of element

T_i = temperature of levitation element at installation.

The other important parameters such as attachment loads, axial stresses, etc., can be derived from the solution for the axial load, P.

(3) General Results. Solutions of the above equation have been derived which demonstrate how the maximum stress at the midpoint of the levitation element increases with attachment axial stiffness, and how maximum axial displacement at the ends decreases with increasing axial stiffness of the attachments. The distribution of attachment restraining forces were also derived. The restraining forces for relatively stiff attachments are concentrated near the ends of the levitation element. Since high, unmanageable axial loads could theoretically develop in the attachments at the ends of the levitation element, a practical attachment scheme must allow relative motion at these attachment points. By allowing this relative motion, axial restraining forces will be limited by the frictional force that can be resisted at each attachment. In the case of a long, continuously welded or mechanically joined levitation element, sufficient frictional forces evenly distributed near the ends will completely restrain a large portion of the levitation element length, and the thermal stress will approach that in a completely restrained element (σ^* = $E\alpha$ ($T-T_i$)). For short, segmented levitation elements with expansion gaps the friction forces will not be enough to restrain the levitation element segments, and stresses will be significantly lower than σ^*; however, motion at

the ends will approach that of an unrestrained element. The continuous element versus segmented elements comparison is made schematically in Figure 4-90.

(4) <u>Conceptual Design Example</u>. To assess the impact of the analytical solutions, realistic values were selected for the important parameters, and calculations were made for a representative design. The values used for this example are summarized at the top of Table 4-44. The possible extreme metal temperatures were estimated to be -34.4°C (-30°F) and 60°C (140°F) for installations in the United States (Ref. 4-35). Axial frictional restraint will be provided by clamping the aluminum sheet to the concrete roadway at one meter intervals using bolts or a clip and bolt arrangement. The range of static coefficients of friction for various combinations of materials, i.e., aluminum on aluminum, aluminum on steel, and steel on concrete, is estimated to be 0.45 to 0.95 based on data in Ref. 4-36.

As an example, a realistic attachment design might use a 1.91 cm (0.75 in.) diameter bolt preloaded to 172 MN/m^2 (25,000 lb/in^2) clamping force. As outlined in Table 4-44, the levitation elements with lengths greater than 80 meters would probably develop thermal stresses equal to σ^* (the thermal stress in a completely restrained element) and thus could be considered equivalent to continuous elements. Levitation elements less than 40 meters long would develop lower stresses.

Table 4-44 gives the minimum material properties for two aluminum alloys (Ref. 4-37). The two alloys that were considered demonstrate the tradeoffs that exist between two widely different materials; a high-strength, weldable alloy (6061-T6), and one with a high electrical conductivity (1100-H14).

The results in Table 4-44 demonstrate that 1100-H14 alloy will be inadequate to support the thermally-induced stresses of the weld joints of continuous elements (>80 m long). Therefore, a higher strength material such as 6061-T6 will be required for long segments. For the baseline (segmented) guideway, the allowable stress levels of the parent material will be realized, and in addition, induced stresses will be lower. Therefore, the baseline system should be constructed from the (electrically) more desirable 1100-H14 aluminum with expansion joints approximately every 10 to 40 meters. In either

SHORT SEGMENTED ELEMENTS

LONG CONTINUOUS ELEMENT

ATTACHMENT POINTS

INFINITE FRICTION

LIMITED FRICTION

ATTACHMENT LOAD, $|q|$

STRESS, σ

σ (MAX)

THERMAL EXPANSION: $\Delta L \approx 2a (T - T_i)b$

THERMAL STRESS: σ (MAX) = $-E\alpha (T - T_i)$

$\Delta L \rightarrow a (T - T_i) L$

$|\sigma (MAX)| < -E\alpha (T - T_i)$
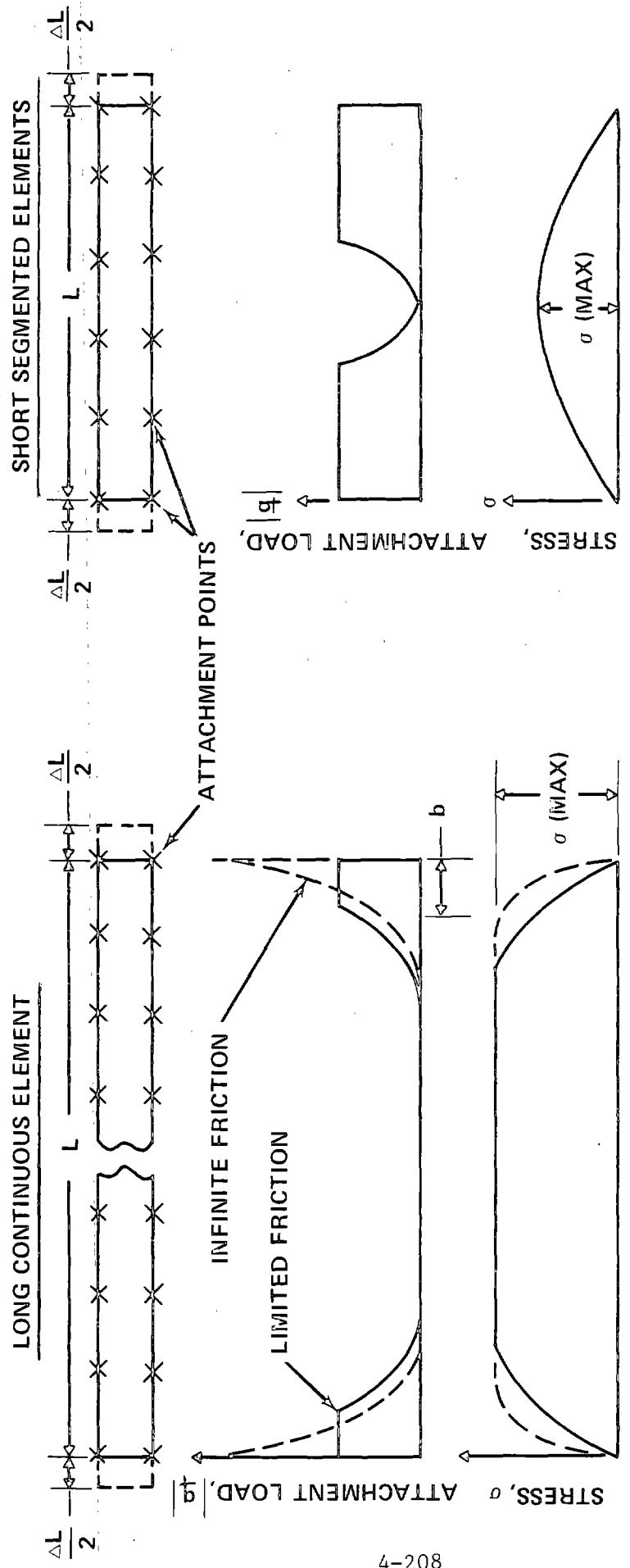
FIGURE 4-90. CONTINUOUS VERSUS SEGMENTED LEVITATION ELEMENT

4-208

TABLE 4-44. EXAMPLE OF CONCEPTUAL DESIGN OF GUIDEWAY ELEMENT

PROPERTIES AND CONDITIONS

$E = 68947.56 \text{ MN/m}^2$ (10×10^6 lb/in.^{2})

$\alpha = 23.59 \times 10^{-6} \, ^\circ\text{C}^{-1}$ ($13.1 \times 10^{-6} \, ^\circ\text{F}^{-1}$)

FRICTIONAL RESTRAINT BY ATTACHMENTS, $\mu = 0.45 - 0.90$

INSTALLATION TEMPERATURE, $T_i = 10^\circ\text{C} - 32^\circ\text{C}$ ($50^\circ\text{F} - 90^\circ\text{F}$)

ALUMINUM TEMP ON EXTREME HOT DAY, $T_h = 60^\circ\text{C}$ (140°F)

ALUMINUM TEMP ON EXTREME COLD DAY, $T_c = -34.4^\circ\text{C}$ (-30°F)

ATTACHMENTS AT 1m SPACING USING 1.91 cm (0.75 in.) DIA BOLTS PRELOADED TO 172.369 MN/m^2 (25,000 lb/in.^{2})

CROSS SECTION

0.53 M

2.54 CM

1.03 M

RESULTS

CONTINUOUS LEVITATION ELEMENT

L > 80m

MAX TENSILE STRESS = 101.316 MN/m^2 (16,000 lb/in.^{2})

MAX COMP STRESS = -81.358 MN/m^2 (-11,800 lb/in.^{2})

SEGMENTED LEVITATION ELEMENT

L < 40m

MAX TENSILE STRESS < 101.36 MN/m^2

MAX COMP STRESS > -81.358 MN/m^2

MATERIAL PROPERTIES

ALLOWABLE STRESSES FOR 2.5-cm-THICK ALUMINUM PLATE (MN/m^2)

ALLOY	PARENT MATERIAL		WELD ZONE		
	ULTIMATE STRENGTH	YIELD STRESS	ULTIMATE STRENGTH	YIELD STRESS	BUCKLING STRESS
1100 - H14	101.316 (16,000 lb/in.^{2})	96.527 (14,000)	75.842 (11,000)	31.026 (4500)	
6061 -T6	289.58 (42,000)	241.317 (35,000)	165.474 (24,000)	137.895 (20,000)	162.716* (23,600)

*Based upon the assumed attachment spacing.

case — continuous or segmented — an adequate margin against compressive buckling will be maintained by the use of a one-meter spacing between attachments. Since the maximum expected compressive stress (81.4 MN/m^2) is only 50 percent of the calculated elastic buckling stress (163 MN/m^2), amplification of any initial eccentricities in the flat aluminum surfaces during compressive loading will be limited. Considering the analysis of an initially imperfect column (e.g., Ref. 4-38 p. 554) and considering the analytical and experimental data presented in Ref. 4-39 for the LIM reaction rail (an aluminum plate structure), lateral deflection due to initial imperfections is expected to be limited to 50 percent of the initial imperfection for the worst case of thermal compression.

(5) Conclusions and Recommendations. The results demonstrate that a properly designed aluminum levitation element attached to the guideway at discrete points with axial motion restrained by limited frictional forces will survive the stresses thermally-induced by an extreme temperature variation. Frictional axial restraint is necessary since "hard" mounting can result in large unmanageable loads at attachment points near the ends of the element. It has been found that the levitation element should be installed at a temperature near the median of the expected temperature range. As stated above, the baseline segmented guideway can be constructed of nearly pure 1100-type aluminum alloy, whereas a continuous guideway will require a high-strength material such as 6061-T6. A segmented design with gaps every 10-40 meters is recommended from structural considerations since it requires no complicated load-carrying mechanical joining or welding of the aluminum levitation segments along the length of the guideway. This system should be more economical to install, and allows the use of high conductivity aluminum which maximizes the magnetic performance. Another advantage is the greater availability of 1100-type material in large production quantities due to the limited heat-treat facilities that are required for the stronger alloys.

D. Effects of Gaps and Joints. The discussion in Paragraph C demonstrated that gaps or joints are required between the sections if 1100-H14 aluminum alloy is used. These gaps give a discontinuity in the eddy currents as the magnets pass over them which results in a momentary loss of lift. A

change in the force in the longitudinal direction is also experienced in the vicinity of the gap. Measurements have been taken in the Ford Laboratory to estimate the magnitude of the effect, and the results evaluated in terms of the vehicle dynamics and the operation of a typical Revenue system. The discussion of vehicle dynamic response to gaps has been given in Section 4.3.2.

The initial estimates of the loss of lift gave roughly a 40% reduction (peak value) of lift for a butt joint. This was based on simple calculations and inductance measurements on a small-scale magnet coil and guideway. The second set of measurements was made using a laboratory magnet in various positions with respect to different types of joints; a simple butt joint, an "underlay" joint, and a lap joint. The second set of inductance measurements were performed using a larger coil (10 x 25 cm), and both the vertical (loss of lift) and horizontal force perturbations were measured. Typical results are shown in Figure 4-91 for a butt joint and a lap joint. The upper portion of the figure indicates a loss of lift starting as the magnet leading edge passes the gap, dropping to a maximum 23% for the butt joint when the magnet center is over the gap, and returning to full value when the trailing edge of the magnet leaves the gap. The corresponding maximum loss of lift for the lap joint is only 10%. The integrated loss in lift averaged over the magnet passage time is approximately 18% for the butt joint and 7% for the lap joint. A similar phenomenon is postulated to be experienced by the guidance force. The butt joint results shown in the figure were used to evaluate the effect of gaps on the vehicle dynamics.

The lower portion of the figure indicates a pulse effect in the fore and aft direction. First, a thrust-like pulse is produced as the forward portion of the magnet passes over the gap, followed by a drag-like pulse as the aft portion of the magnet passes over the gap. The gap between the aluminum sheets acts as a magnet "attractor" to produce this effect. The peak values of these pulses are approximately 9% of the nominal magnetic lift for the butt joint and 3% for the lap joint. For comparison, the nominal drag force is about 3% of the lift force at 134 m/s (300 mph).

The effects of these force variations impose very brief shock-type loads on the magnets which are transmitted through the various internal supports of

FIGURE 4-91.   EFFECT OF JOINTS ON LABORATORY
MAGNET LIFT AND AXIAL FORCE

the magnet module and attachment members to the vehicle. Although the overall vehicle dynamic response to a single gap is small (as shown in Figure 4-43), the dynamic response of the internal parts of the magnet to these loads is important and must be considered in the design. Table 4-45 summarizes the

TABLE 4-45. SUMMARY OF BUTT JOINT-INDUCED LOADINGS FOR BASELINE REVENUE SYSTEM (Based on Laboratory Measurements)

Nominal Magnetic Lift (N/magnet)	91,625	(20,600 lb)
Lift and Guidance Pulses Due to Gap		
● Pulse Time at 134 m/s (sec)	0.023	
● Maximum Change in Lift Force, (N/magnet)	-21,074	(-4,738 lb)
● Maximum Change in Guidance Force* (N/magnet)	-7,165	(-1,611 lb)
● Maximum Vehicle Vertical Accel (g's)	-0.23	
● Average Vehicle Vertical Accel (g's)	-0.18	
Thrust/Drag Pulse Due to Gap		
● Pulse Time, Each Direction at 134 m/s (sec)	0.012	
● Maximum Change in Thrust/Drag Force (N/magnet)	±8,063	(±1,813 lb)
● Maximum Vehicle Horizontal Accel (g's)	±0.088	
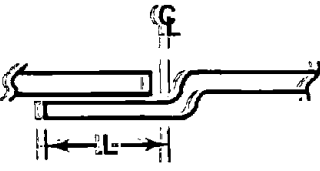
*Assuming variation in guidance force is the same as the variation in the lift force.

revenue vehicle loading situation based on the worst-case (butt joint) curves of Figure 4-91 for a typical revenue magnet and a velocity of 134 m/s. Although the values of the forces and accelerations produced by the butt gap appear to be large, it should be emphasized that the length of the pulse is very short ($\sim$ 0.02 sec), and the vehicle — with the exception of the magnet module itself — hardly responds to the individual shock loads. Also the results of the laboratory tests must be examined carefully; the initial results indicated a peak loss of lift nearly twice as large (40% vs. the current 23%). This difference is believed to be due to the small scale of the experiment used for the initial tests. For this reason, there was a question as to the scale effect of the experiment, and a third set of inductance measurements were made

for a larger coil of the same dimensions as the Task II Test System coil (25 x 75 cm). These final measurements confirmed the results presented in Figure 4-91.

If the shock loading on the magnets due to simple butt joints proves to be excessive, a different type of joint may be required. The maximum loss of lift for the three types of joints tested are shown in Table 4-46. A considerable improvement is seen for the underlay and lap joints, but these joints have the disadvantage of being more costly and difficult to construct. Details of the force profile for a lap joint are shown in Figure 4-91.

TABLE 4-46. MAXIMUM LOSS OF LIFT FOR VARIOUS JOINTS (Laboratory Tests)

TYPE OF JOINT	CONFIGURATION	CHARACTERISTIC DIMENSION, L	LOSS OF LIFT, $\frac{F_L}{F_{Lo}}$
Butt		---	0.77 (Fig. 4-91)
Underlay		30 cm (120%)*	0.94
		15.3 (61%)	0.93
		10 (40%)	0.92
		5 (20%)	0.87
Lap		4.5 cm (18%)	0.90 (Fig. 4-91)
		2.0 (8%)	0.89

*Percentage of test coil length

The inductance measurements were performed at one kHz which represents the high speed results. Two additional frequencies were used to indicate the velocity dependence of these perturbation forces, and the results shown in Table 4-47. This table shows that the loss of lift and the longitudinal force

TABLE 4-47. VELOCITY DEPENDENCE OF 4.5 CM LAP JOINT

MEASUREMENT FREQUENCY (KHZ)	EXPECTED SPEED RANGE	REFERENCE LIFT FORCE RATIO, $F_{L AT 3 kHZ}$	$\dfrac{F_L}{F_{L3 kHZ}}\Big\|_C$	$\dfrac{\Delta FX}{F_{L3 kHZ}}$
0.3	Low-Med	0.77	0.8	0.22
1.0	Med-High	0.99	0.89	0.06
3.0	Very High	1	0.96	0.04

ratios are greater at low speed, thus the low speed areas of the guideway may require special joints or perhaps a continuous guideway of higher strength aluminum.

As mentioned above, the effect of the loads must be included in the design and testing of the magnet module. Operation over 1100-type segmented aluminum guideways will subject the magnet to the shock-like loads on a continuous basis, therefore the fatigue resistance of the magnet structure must be very high. Each magnet will experience 9 pulses/second at 134 m/s for 15.2 m (50 ft) gaps. The large total number of pulses for a typical route is readily apparent.

4.5.2 Guideway Design

A. At-Grade

(1) Introduction. The results of guideway studies for air-cushion vehicles have shown that continuously-reinforced concrete pavements (such as used for highways and airport runways) can be constructed with a surface sufficiently smooth for the MAGLEV application. The guideway roughness for the Repulsion MAGLEV concept is established by the roughness of the underlying supporting roadbed assuming that the aluminum elements conform to the roadbed.

irregularities. Therefore, a smooth concrete roadbed is highly desirable (and desirable even if the aluminum does not exactly conform to the concrete). An alternate approach is to have a rougher roadbed and provide for post-installation adjustments of the aluminum relative to the roadbed to achieve the desired smoothness. Design provisions and procedures for adjusting an "L"-shaped element will be complicated and costly; whereas, standard construction methods for concrete pavements are well developed and relatively low cost. Therefore, a highway-type continuously-reinforced concrete pavement has been selected as the baseline roadbed.

(2) Baseline Design. Details of the baseline hat section guideway supported by a continuously-reinforced concrete pavement are shown in Figure 4-92. Typical roadbed cut and fill cross sections based on standard practices for slopes and drainage are illustrated in Figure 4-93. The thickness of the concrete pavement shown in Figure 4-92 is based upon the vehicle loads on the guideway. Vertical loads on the guideway due to levitation forces will be well distributed and not critical, and the possible dynamic interaction between the vehicle and at-grade guideways have been shown to be low by the analyses presented in Refs. 4-40 and 4-41. The controlling design loads are those produced by the landing wheels and the guidance forces. Transverse bending of the pavement slab was assumed to produce the critical stresses. Bending loads due to guidance forces are induced in the slab through the median curb that supports the vertical aluminum guidance surfaces.

The required slab thickness has been computed to be only 15.2 cm; however, 20.3 cm (8.0 in.) has been used since this is a standard thickness used in highway construction. More than adequate fatigue life is predicted for the 20.3-cm-thick slab subjected to the transverse bending stresses. The lateral guidance forces can be as high as 80,000 N (18,000 lb) at both the forward and aft magnets, and these forces are supported by a simple reinforced-concrete "curb." Detailed studies may show a less massive and costly support for the levitation element may be possible, but the conservative approach has been used for the baseline design.

4-216
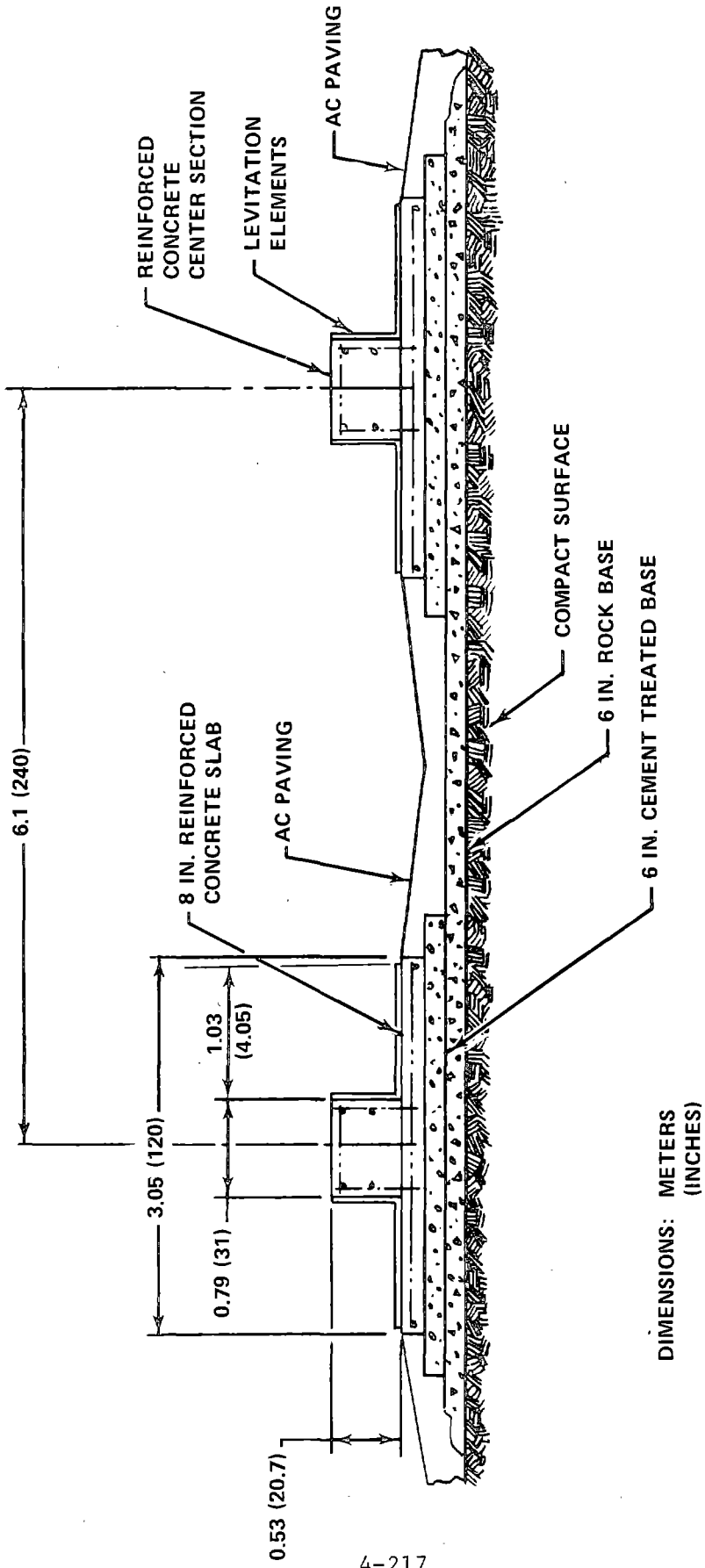
FIGURE 4-92. BASELINE AT-GRADE GUIDEWAY DESIGN

REINFORCED CONCRETE CENTER SECTION

LEVITATION ELEMENTS

AC PAVING

8 IN. REINFORCED CONCRETE SLAB

AC PAVING

COMPACT SURFACE

6 IN. ROCK BASE

6 IN. CEMENT TREATED BASE

6.1 (240)

3.05 (120)

1.03 (4.05)

0.79 (31)

0.53 (20.7)

DIMENSIONS: METERS (INCHES)

4-217

FILL

3.05 M   3.05 M   1.52 M

0.3 M

15 CM CEMENT TREATED BASE
15 CM ROCK SUBASE

2:1

COMPACT NATURAL SURFACE

C L

CUT

NATURAL SURFACE

ASPHALT PAVING

SLOPE 2:1

3.65 M

FIGURE 4-93. TYPICAL AT-GRADE GUIDEWAY CROSS SECTIONS

4-218

(3) Guideway Roughness Characterization. The achievement of an acceptable ride quality for a particular suspension system requires that construction techniques and specifications be identified which will produce a guideway that lies within an allowable surface irregularity tolerance. The vertical deviations for at-grade guideways can be assumed to be random and to be characterized by the power spectral density, $\Phi (\Omega)$, of the guideway elevation where Ω is the reduced frequency related to the wavelengths of the surface deviations by $\Omega = 2\pi/\lambda$, where λ is the wavelength. Insight into the roughness of concrete pavements was obtained by studying the measured roughness of highways and airport runways. Calculations of the power spectral density from measured data (see Ref. 4-42 for a summary) show that the roughness data can approximately be represented by:

$$\Phi (\Omega) = A/\Omega^n \qquad\qquad 4-12$$

where A and n are constants obtained by fitting measured data. For this study, a guideway roughness objective of $A = 1.5 \times 10^{-6}$ m-rad (5×10^{-6} ft-rad) and $n = 2$ have been selected. These values correspond to the specification for the DOT UTACV (now PTACV) guideway in Pueblo.

(4) Existing Roughness Data. The following airport runway roughness characterization suggested by Houbolt (Ref. 4-43) provides a comparison with the roughness objective:

$A = 2.0 \times 10^{-6}$ m-rad (6.7×10^{-6} ft-rad), $n = 2$ for "new construction"

$A = 0.61 \times 10^{-5}$ m-rad (2.0×10^{-5} ft-rad), $n = 2$ "needs repair"

Early runway roughness data (Refs. 4-44 and 4-45) indicate that the roughness for most of the runways that were measured approached the "needs repair" condition, and only one met the "new construction" condition. However, roughness measurements of a relatively new runway — measured in 1961 prior to being placed in service — showed that it was smoother than the "new construction" condition or the objective (see Ref. 4-46, Runway B). In fact, this newer runway was measured 7 years later and found to have experienced little change in roughness.

Another comparison of interest is the roughness measurement of the TACRV (now TLRV) guideway in Pueblo. Ref. 4-42 shows the TLRV guideway is considerably smoother than the UTACV specification, thus it is smoother than required for MAGLEV. Roughness measurements have only considered vertical irregularities with wavelengths up to about 90 m ($\sim$300 ft). For 134 m/s systems, wavelengths to about 300 m ($\sim$1000 ft) will be important from a ride quality standpoint; therefore, application of Equation 4-12 infers an extrapolation of existing data to longer wavelengths. Using this extrapolation and the measured roughness data for airport runways and the TLRV guideway, it has been determined that the MAGLEV roughness objective (A = 1.50 x 10^{-6} m-rad, n = 2) is achievable with a continuously-reinforced concrete pavement even though all such existing pavements may not meet this objective.

(5) Construction Tolerances. The required construction tolerances have been established by determining the allowable variations in the guideway profile. In general, the allowable mean square deviations for wavelengths less than a given λ_1, can be calculated from

$$\sigma^2 = \int_{\Omega_1 = 2\pi/\lambda_1}^{\infty} \Phi (\Omega)\, d\Omega \qquad\qquad 4\text{-}13$$

If the roughness is represented by Equation 4-12, Equation 4-13 gives

$$\sigma = \left(\frac{A}{n-1}\right)^{1/2} \left(\frac{\lambda_1}{2\pi}\right)^{\frac{n-1}{2}} \qquad\qquad 4\text{-}14$$

Houbolt (Ref. 4-43) suggests the maximum deviation, σ', is $\sqrt{2}\,\sigma$.

The allowable deviations in a distance L can be readily estimated for any given value of A and n by letting $\lambda_1 = 2L$ in the relationship for σ'. Estimates of tolerances for existing construction methods have been made using this equation.

A continuously-reinforced concrete guideway will normally be constructed with a standard wire-guided slip-form machine used for highway or runway construction. The expected surface irregularities for this type of construction can be derived from the following estimated tolerances.

4-220

- Established grade (survey accuracy): $\pm$1.27 cm per 1610 m ($\pm$0.5 in. per mile)

- Guidewire location relative to established grade: $\pm$0.4 cm ($\pm$0.157 in.) (including sag between supports)

- Paving machine accuracy: $\pm$0.318 cm ($\pm$0.125 in.)
  $\pm$0.159 cm ($\pm$0.063 in.), with heavy grinding

The total expected variation in the surface elevation can be assumed to be equal to the square root of the sum of the squares of the tolerances given above (see Ref. 4-47 for example).

The expected variations based on construction tolerances and the allowable variations derived from the power spectral density objective are compared in Figure 4-94. This figure shows that the roughness objection can be met for deviations within lengths of 18 m (60 ft) or greater with heavy grinding, and within lengths greater than 26 m (85 ft) without grinding. Deviations over lengths less than the 18 m should not be important for this system.

(6) Highway and Airport Runway Surface Finish Specifications. Since the study of the capability of standard slip-form construction methods indicates that the roughness objective can be met, it is of interest to explore possible explanations of the higher roughness levels measured for many existing highways and runways. First, the effects of roughness — especially that due to long wavelength deviations — are much less important at speeds considerably below 134 m/s. Therefore, little attempt is normally made to control the long wavelength deviations. The control of roughness of new California highway construction is based on the following specifications (see Ref. 4-48): (1) "When a straightedge 12-feet long (3.66 m) is laid on the finished pavement in a direction parallel to the centerline, the surface shall not vary more than 0.02 ft (0.61 cm) from the lower edge of the straightedge," and (2) "Equipment that produces a finished surface having a Profile Index of seven inches per mile or less for each profile as required hereinafter shall be used." The Profile Index is determined using a California-type Profilograph which measures the midchord offset for a 7.6 m (25 ft) chord length. A probabilistic analysis of the profilograph reported by TRW (Ref. 4-42) demonstrates that the specification of an index of 7.0 in./mile should lead to a
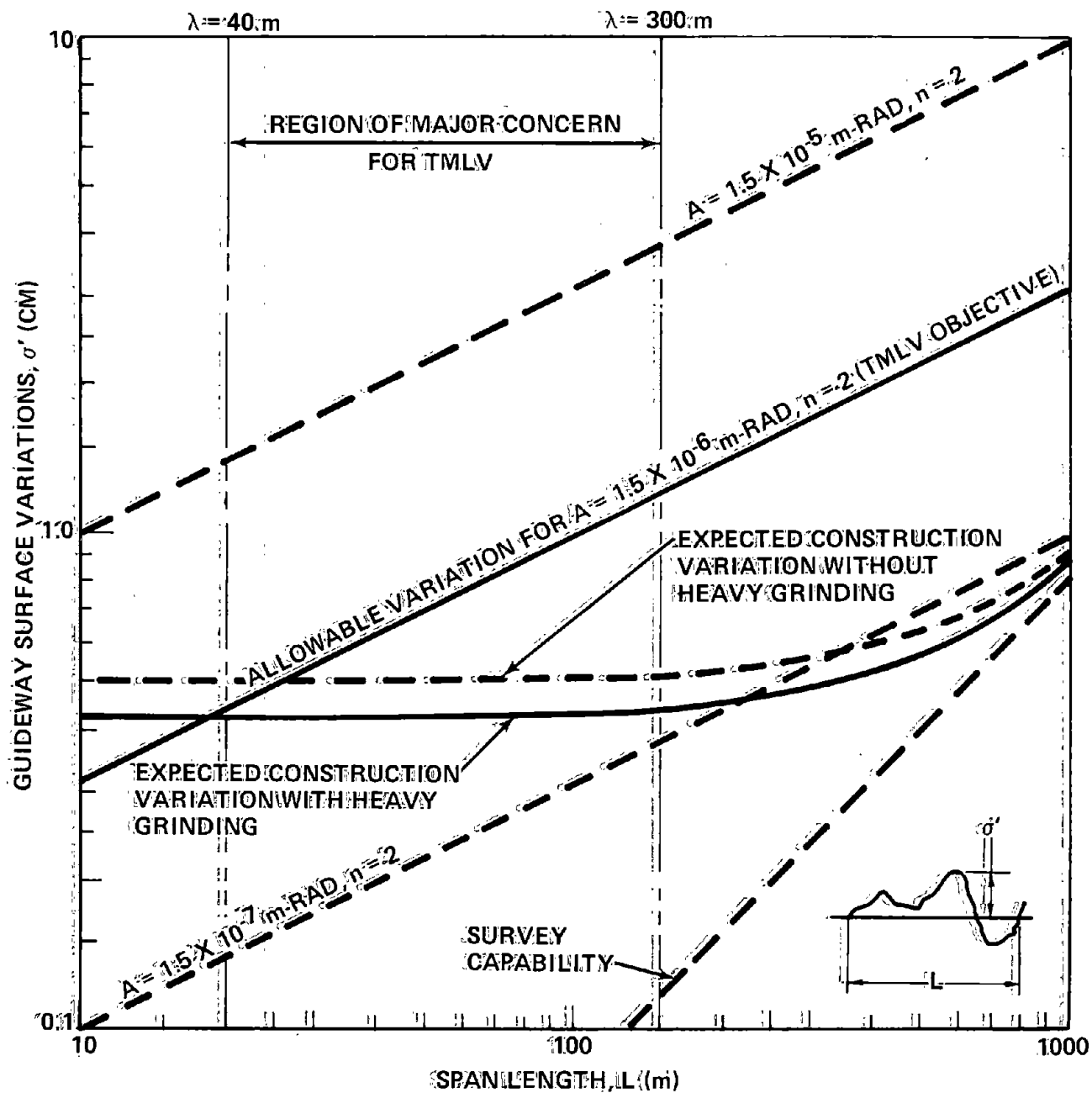
FIGURE 4-94. EXPECTED AND ALLOWABLE SURFACE VERTICAL VARIATIONS FOR AT-GRADE GUIDEWAYS

smoother guideway than the objective for short wavelength irregularities. However, a kinematic response analysis in the TRW report reveals that the profilograph response is considerably attenuated at wavelengths greater than 30 m (∿ 100 ft). For the 12-feet (3.66 m) straightedge test, a 0.02 ft (0.6 cm) variation from the lower edge corresponds to $\sigma' = 0.01$ ft (1.2 cm) in Figure 4-94. Figure 4-94 predicts a highway roughness somewhat greater than the $A = 1.5 \times 10^{-6}$ m-rad objective if the straightedge test is used as the control. Therefore, highway specifications will not necessarily give the required smoothness over either short distances (∿ 12 ft), or long distances where the profilograph is insensitive.

The FAA (Ref. 4-49) specifies the following for airport runway surfaces: (1) "Vertical deviation from established grade shall not exceed ±0.04 foot (12 mm) at any point," and (2) "Surface smoothness deviations shall not exceed 1/4 inch (6 mm) from a 16-foot (4.88 m) straightedge placed in any direction including placement along and spanning any pavement joint or edge." Comparison of the FAA specification with the allowable deviations given in Figure 4-94 indicates that even runways will not necessarily meet the roughness objective.

(7) Time Dependent Effects. A second reason that existing concrete pavement surfaces may not meet the TMLV objective is that over long periods of time the surface smoothness may degrade due to differential pavement motion caused by frost heave or earth settlement. Figure 4-49 shows that holding to the roughness objective allows little degradation of the surface with time. In fact, virtually no differential changes over distances on the order of 20 m (∿ 60 ft) can be accepted. Prediction of time-dependent effects on guideway roughness is strongly site-dependent and beyond the scope of this study. However, as noted above, the measurements of Runway B in Ref. 4-46 (which is smoother than the $A = 1.5 \times 10^{-6}$ m-rad objective) proved that time had little effect on the roughness for this particular case. Therefore, postconstruction differential earth movements can apparently be disregarded in some areas. An adjustable guideway design that allows periodic maintenance will likely be required to compensate for earth motions in areas of poor soil stability.

(8) <u>Conclusions</u>. A continuously-reinforced concrete pavement such as used for highways and airport runways is a desirable and cost-effective approach for the MAGLEV at-grade guideway. Since highway and runway construction specifications will not necessarily control the surface roughness to the degree required for the MAGLEV vehicle (especially over distances greater than 30 m), construction specifications must be derived which are consistent with the allowable surface deviations. The development of an adjustable guideway to meet a considerably lower roughness criterion (e.g., A $\approx$ 1.5 x 10^{-7} m-rad) or for use where unstable soil conditions exist, will require design and construction innovations. Much higher construction and maintenance costs are likely for an adjustable guideway approach. On the other hand, very little cost reduction will be realized by allowing a rougher guideway (for any conceivable improvement in vehicle suspension system) than that achievable with current highway and runway paving techniques. A higher allowable roughness would, however, be desirable to allow for time-dependent degradation from the as-constructed condition.

B. <u>Elevated Guideways</u>

(1) <u>Introduction</u>. A considerable portion of the TMLV guideway within cities and densely populated intercity areas will be elevated to maximize safety and to minimize conflict with existing transportation rights-of-way. Although a smaller percentage of the guideway in rural areas will be elevated, it is important even there to have innovative, low-cost elevated guideway designs. The results of conceptual design analyses for the baseline hat-shaped or wide inverted tee guideway are presented here.

A typical elevated guideway design is illustrated in Figure 4-95. Simply-supported prestressed concrete box beam girders are supported by periodic pier structures. Sliding joints at one end of each girder provide for differential thermal expansion, and pinned joints at the other end transmit longitudinal loads from the girders to the piers. Two L-shaped aluminum levitation elements are attached to the upper surface of each girder.

The elevated guideway must support the various vehicle and environmentally-induced loads and also provide a smooth surface to support and guide the vehicle without producing an unacceptable ride. The primary excitation of a vehicle

PIER

FOOTING

CONCRETE
BOX BEAM

DIMENSIONS: METERS
(FEET)

22.8
(75)

6.1
(20)
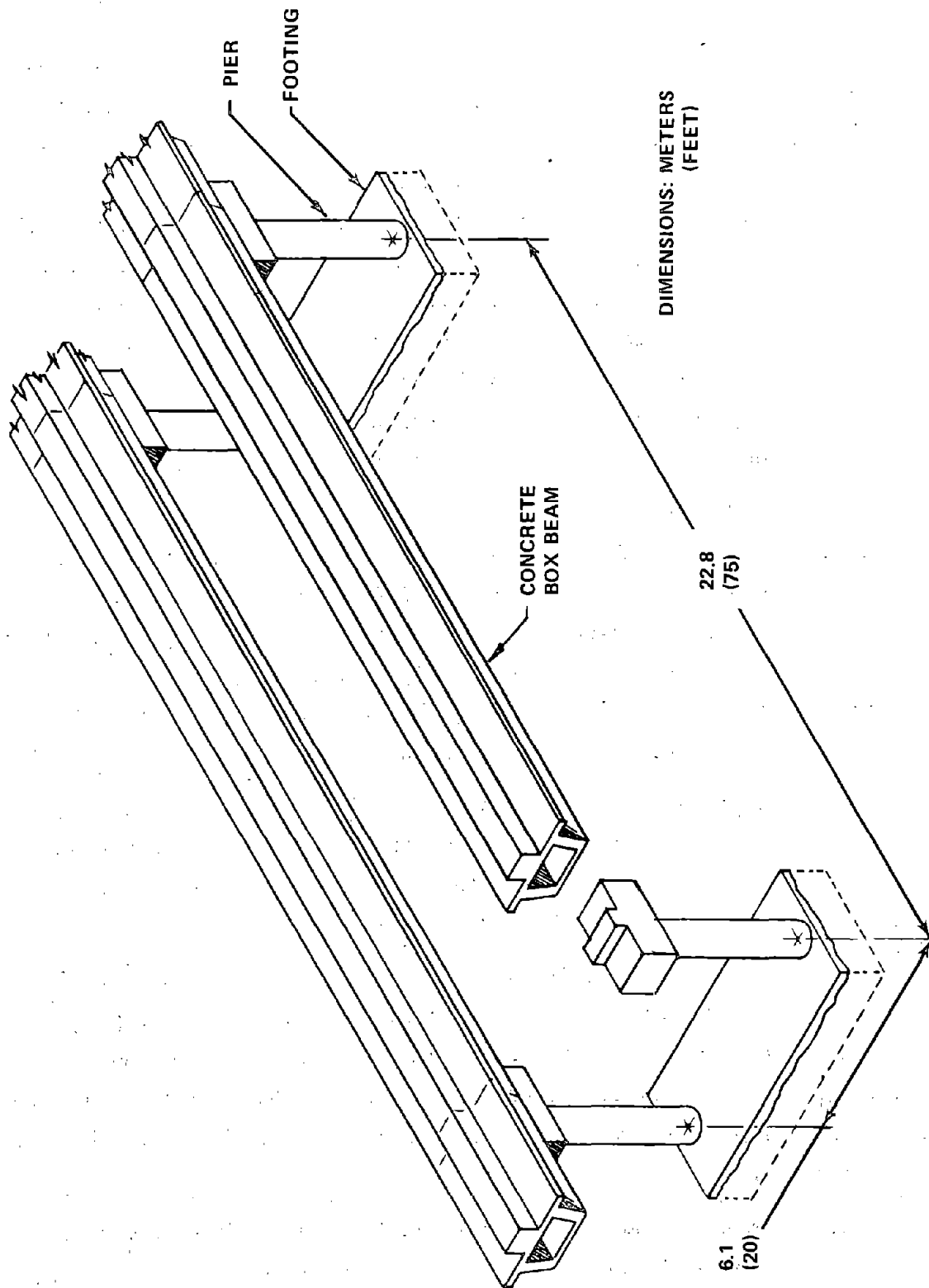
FIGURE 4-95. ELEVATED GUIDEWAY DESIGN

4-225

by an elevated guideway is periodic in nature and results from the deflection of the girders between the supporting piers. The effects of random guideway irregularities can be minimized by the adjustment of the girder positions on the supporting piers during installation. Excitation frequencies for a vehicle traveling at 134 m/s range from 4.4 Hz to 8.8 Hz for girder spans of 15.2 m (50 ft) to 30.4 m (100 ft), respectively. An allowable vehicle vertical acceleration of 0.05 g rms has been assumed for the 4.4 Hz to 8.8 Hz range, and the elevated guideway girders have been designed such that the predicted static and dynamic deflections will limit the vehicle vertical response to this value.

Span lengths of 15 to 30 meters have been considered. Similar designs could be used for somewhat longer spans, but the negotiation of rivers or other natural barriers usually requires very long spans (greater than 45 meters) of unique design. The study of long spans is beyond the scope of this effort.

Simply-supported guideway spans have been assumed for this analysis. Static stiffness and strength considerations suggest that continuous beams (beams allowing bending moment transfer from span-to-span) would be more efficient than simply-supported beams. However, the dynamic response characteristics of continuous beams can be much more severe than those of simply-supported beams, and, in fact, can be great enough to overshadow the gain in static stiffness and strength. Also, fabrication costs for a continuous-beam elevated guideway will likely be higher than for the simply-supported case. Therefore, no clear advantage can be discerned for continuous beams that outweigh the added analysis complexity that is required.

(2) <u>Previous Studies</u>. Many analytical and design studies of elevated guideways have been performed and reported in the literature, primarily for air-cushion vehicles (Refs. 4-50 through 4-62). Since the requirements for a repulsion MAGLEV elevated guideway design are quite similar to those for air-cushion vehicles — the vehicle parameters being the primary difference — a study of the cited references was made in order to utilize applicable existing analytical approaches and results. Many of the existing studies are purely analytical developments leading to computerized numerical solutions of the resulting equations of motion (Refs. 4-56 through 4-62). Several of the early studies (Refs. 4-53, 4-54, and 4-55) considered guideway designs based upon

static deflection and loading criteria. In some cases, viable designs were evolved based upon the requirements established by the analysis. A limited amount of data exist that analytically demonstrate predicted ride quality over actual guideway designs (Refs. 4-50, 4-51, and 4-52). Both Refs. 4-50 and 4-61 show that continuous spans give a degraded ride quality compared to a simply-supported span of the same cross section.

(3) <u>Vertical Stiffness Requirements and Vehicle Dynamic Loading</u>. Structural requirements have been derived to allow the guideway subcontractor (Cardan Co.) to develop guideway span designs. A prediction of worst-case dynamic response has been made to allow a preliminary bending stiffness requirement to be established, based upon the desired vehicle ride quality. The worst-case bending moment is also computed so that the structural capability can be predicted. A dynamic analysis of the resulting span designs has demonstrated the conservatism of these predictions.

Initially, the results of the vehicle/guideway dynamic interaction studies performed by Chiu, Smith, and Wormley at MIT (Refs. 4-59 and 4-60) were considered for application to the present system. This analytical model consists of a single-degree-of-freedom vehicle coupled to a simply-supported elevated guideway span by a parallel linear spring and viscous damper. For the vehicle excitation frequencies of interest ($> \sim 3$ Hz for spans less than 45 meters), the baseline MAGLEV control system minimizes the effects of relative damping but not the effects of absolute damping. Therefore, the MIT analysis —with only relative damping —will produce overly conservative results for the baseline system and higher guideway costs than necessary.

Since revision of the MIT analysis to reflect the baseline suspension characteristics was beyond the scope of the study, a simpler, but adequate approach has been devised. As noted in Ref. 4-63 and elsewhere, only a weak coupling exists between the vehicle and guideway in the case where allowable vehicle accelerations are small (< 0.05 g). Ride quality requirements limit allowable vehicle accelerations to about 0.05 g rms; therefore, the force of the vehicle on the guideway can be assumed to be a constant 445 kN (100,000 lb) traversing the span at a constant speed (note the final baseline vehicle weight is only 366.5 kN). The resulting dynamic span deflection can be used as an input to the vehicle motion analysis to determine ride quality.

The single-degree-of-freedom heave-motion model illustrated in Figure 4-96 has been used to estimate the allowable dynamic deflection of the span in terms of the allowable vehicle acceleration. The assumption of a deflected shape of the guideway allows the maximum guideway deflection to be calculated from the vehicle equation of motion. Typical results are also shown in Figure 4-96. An allowable peak vehicle acceleration of only 0.02 g has been used to compensate for unconservative features of the simple analytical model. The resulting allowable dynamic deflection has been used to determine the required span bending stiffness, assuming the front and rear magnets give two constant-pressure loads traversing the span at a constant speed. Wilson (Ref. 4-61) has developed a computer program to solve the moving pressure problem and has shown typical results of dynamic response calculations. One case is given in Figure 4-97, where the maximum dynamic-response-induced deflection and bending moment are given in terms of the non-dimensional vehicle speed, Ω_1/P_1. The required bending stiffness and maximum bending moment responses have been estimated from the results of Wilson and the allowable dynamic deflection given in Figure 4-96. Figure 4-97 also outlines the procedure for the above analysis and tabulates the results.

(4) <u>Guideway Loading</u>. The analysis of elevated guideways must include the bending moments induced by the vehicle as well as other types of vehicle loads. A list of the applicable load factors is given in Table 4-48. The loads are divided into three groups: (1) normal operating; (2) special conditions, and (3) emergency conditions. In the majority of cases, the "normal operating" loads will exist as the vehicle traverses the elevated guideway at 134 m/s. The "special conditions" loading shown in Table 4-48 will exist infrequently on the major portion of the guideway, but frequently near switches and terminals. Special designs may be necessary for these low-speed areas. Emergency landing loads should occur only at rare intervals. The guideway should be designed to a higher allowable stress for the less frequent loading conditions, consistent with good civil engineering practice. Realistic combined loading cases are also tabulated in Table 4-48.

Longitudinal loads on the guideway will be imparted by magnetic drag, braking forces, and some types of propulsive systems. (A fan-powered or air propulsion vehicle will not impart propulsive forces to the guideway.) The

VEHICLE CHARACTERISTICS

$$\left(\frac{\ddot{Y}_2}{g}\right)_{ALLOWABLE} = 0.02$$

$$r = 2\Omega_1/\Omega_n$$

$$\Omega_n = \sqrt{K/m} = 3.77 \text{ RAD/SEC } (0.6 \text{ HZ})$$

$$\zeta = \frac{c}{2m\Omega_n} = 1.0$$

ALLOWABLE DEFLECTION AT 134 M/S

s (m)	r	$Y_{1_{MAX}}$ (CM)	
		$\zeta = 0$	$\zeta = 1.0$
15.0	14.9	2.74	2.77
19.9	11.2	2.72	2.77
29.9	7.46	2.72	2.82
45.7	4.89	2.64	2.90

ANALYTICAL MODEL
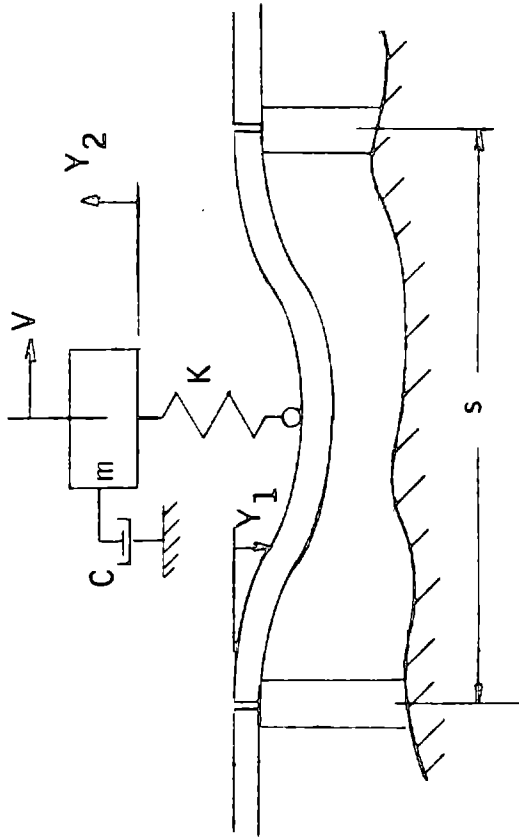
ASSUME: UNCOUPLED GUIDEWAY AND VEHICLE DYNAMICS

$$Y_1 = \frac{1}{2} Y_{1_{MAX}} (1 - \cos 2\Omega_1 t)$$

WHERE: $\Omega_1 = \pi V/S$

ALLOWABLE DYNAMIC DEFLECTION

$$Y_{1_{MAX}} = \frac{2\,(\ddot{Y}_2)_{ALLOWABLE}}{(2\Omega_1)^2} \sqrt{(1-r^2)^2 + 4\zeta^2 r^2}$$

FIGURE 4-96. ALLOWABLE DYNAMIC DEFLECTION
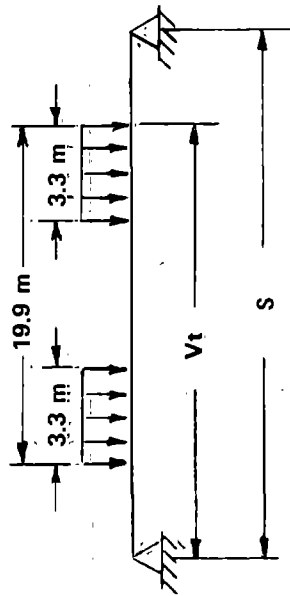
DESIGN PROCEDURE

1. GIVEN S AND Y_{1MAX}
2. DETERMINE Y_{1MAX}/Y_{MAX} STATIC FOR THE WORST CASE Ω_1/P_1^*
3. CALCULATE Y_{MAX} STATIC FROM (1) AND (2)
4. CALCULATE REQUIRED EI FROM (3)
5. DETERMINE M_{MAX}/M_{MAX} STATIC FOR THE WORST CASE Ω_1/P_1^*
6. CALCULATE M_{MAX} STATIC
7. CALCULATE M_{MAX} FROM (5) AND (6)

*FROM WILSON'S RESULTS

PRELIMINARY REQUIREMENTS

ELEVATED SPAN LENGTH ~ S	REQUIRED BENDING STIFFNESS (EI) $KN \cdot m^2$	ESTIMATED MAX. DYNAMIC BENDING MOMENT $MN \cdot m$
15.24 m (50 FT)	1.89×10^8 (0.658×10^{12} LB-IN.^{2})	2.20 (19.5×10^6 LB-IN.)
22.9 m (75 FT)	4.59×10^8 (1.6×10^{12} LB-IN.^{2})	2.37 (21×10^6 LB-IN.)
30.5 m (100 FT)	10.9×10^8 (3.8×10^{12} LB-IN.^{2})	3.44 (30.4×10^6 LB-IN.)

ANALYTICAL MODEL

TYPICAL RESULTS (Ref 4-61)

MOMENT — — —
DEFLECTION - - - -

P_1 = SPAN FUNDAMENTAL FREQUENCY

NONDIMENSIONAL SPEED Ω Ω_1/P_1

Y_{MAX}/Y_{MAX} STATIC & M_{MAX}/M_{MAX} STATIC
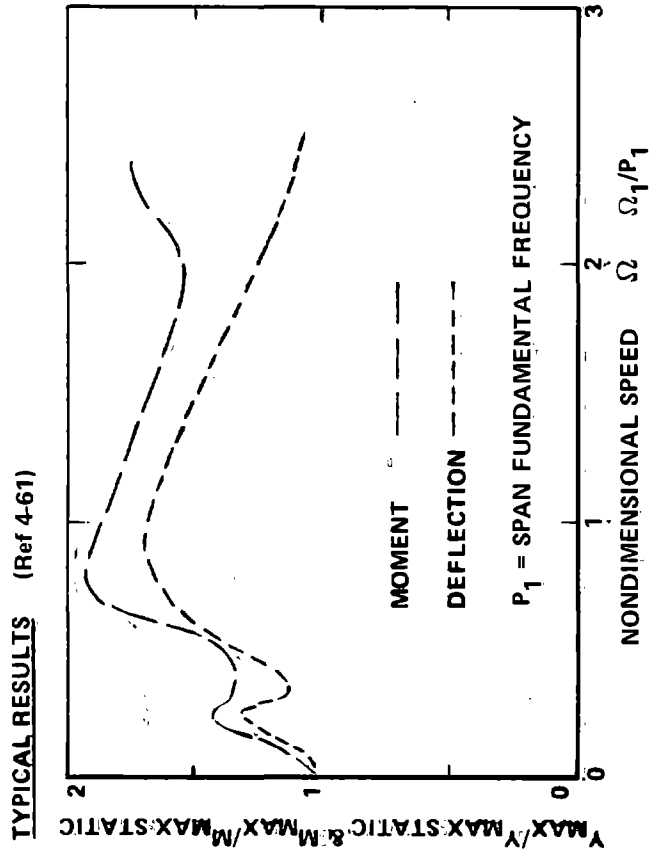
FIGURE 4-97. REQUIRED BENDING STIFFNESS

TABLE 4-48. GUIDEWAY LOAD FACTORS FOR A 445 KN (100,000 LB) VEHICLE

		LOADING CONDITION	DIRECTION		
			LONGITUDINAL (X)	LATERAL (Y)	VERTICAL (Z)
NORMAL OPERATING LOADING		① Net Propulsive/Drag Forces at 134 m/s (300 mph)	-0.022 (Fan Power)[1] +0.054 (LIM Power)[2]	0	0
		② Vehicle Dynamic Loads	0	+0.05 (Acting 16.22m Aft of Veh Nose)	1.1 to 2.75[3]
		③ High-Speed Banked Curve	0	+0.348 (Acting 16.22m Aft of Veh Nose)	0
SPECIAL CONDITIONS		④ Net Propulsive/Drag Forces at 30 m/s (67 mph)	+0.078 (Fan Power)[2] +0.0027 (LIM Power)[2]	0	0
		⑤ Operational Acceleration/ Deceleration Loads	±0.15 (LIM Power Only)	0	0
		⑥ Wheels Down Landing	0	0	Assume 1.5
		⑦ 26.8 m/s (60 mph) Crosswind[3] (Load on Vehicle)	0	±0.18[4] (Acting 8.2m Aft of Veh Nose)	0
DESIGN LOADS		Emergency Landing, Wheels Down	-0.4 Max (Wheel Brakes)	0	Assume 2.0
	COMBINED LOADS	Normal Operating Conditions On Straight Guideway ① + ②	+0.022 (Fan Power) +0.054 (LIM Power)	±0.05 (Acting 16.22m Aft of Veh Nose)	1.1 to 2.75[3]
		On Curved Guideway ① + ② + ③	+0.022 (Fan Power) +0.054 (LIM Power)	±0.398 (Acting 16.22m Aft of Veh Nose)	1.1 to 2.75[3]
		Special Conditions On Straight Guideway ② + ④ + ⑤ + ⑦ ① + ② + ⑤ + ⑦	-0.0790 (Fan Power) 0.204 (LIM Power)	±0.23 (Acting 9.94m Aft of Veh Nose)	1.1 to 2.75[3]
		On Curved Guideway ② + ④ + ⑤ + ⑦ + ③ ① + ② + ⑤ + ⑦ + ③	-0.0790 (Fan Power) 0.204 (LIM Power)	±0.578 (Acting 13.7m Aft of Veh Nose)	1.1 to 2.75[3]

NOTES:

[1] Net force transmitted to guideway to sustain vehicle at 134 m/s (300 mph). Includes 23.9 kN (5367 lb) of aerodynamic drag and 9.79 kN (2200 lb) of magnetic drag.

[2] Net force transmitted to guideway to sustain vehicle at 30 m/s (67 mph). Includes 1.2 kN (270 lb) of aerodynamic drag and 35.0 kN (7869 lb) of magnetic drag.

[3] Vertical guideway loads are affected by the dynamic interactions between the guideway and high-speed vehicle. A load factor of 1.1 is adequate for at-grade guideways. For elevated guideways, design bending moments have been conservatively predicted and are presented in previous figure.

[4] Load on vehicle due to 26.8 m/s (60 mph) crosswind. Additional wind load directly on the guideway must be considered for guideway structural analysis. The guideway must also be designed to withstand a 44.7 m/s (100 mph) crosswind without the vehicle.

4-231

higher longitudinal loads listed in the table for "special conditions" are due to increased magnetic drag at low speed and acceleration/deceleration forces. It has been assumed that a maximum longitudinal deceleration force of 0.4 g could be exerted on the guideway by wheel braking in an emergency landing. This is conservative since most, if not all, of the emergency braking is planned to be done with aerodynamic panels and an emergency parachute.

Vehicle guidance forces and crosswinds will produce the primary lateral loads on the guideway. In addition, loads due to the centrifugal acceleration of the vehicle must be accounted for on high-speed banked curves, and a maximum lateral acceleration of 0.05 g has been used. Crosswinds during vehicle operation were assumed not to exceed 26.8 m/s (60 mph). Support of the wind loads on the elevated guideway and support of the earthquake loads have been analyzed based on the standards of the American Association of State Highway Officials.

The vertical loads produced by wheels-down landings must also be considered. A landing gear design has been assumed that will limit vertical accelerations to 1.5 g during normal deceleration and landing, and 2.0 g during a high-speed emergency landing.

(5) Preliminary Span Designs. Prestressed concrete girder cross sections have been designed by the Cardan Co., for three span lengths based on the preliminary span requirements given in Figure 4-97. Two span designs — a twin-T configuration and a box beam — have been identified as the leading contenders. The twin-T beam is somewhat more economical, but has the disadvantages of being more susceptible to creep and having more camber due to the prestress and other manufacturing processes. Further discussion of these two designs is given below.

The first step in the analysis was to develop preliminary girder designs. The midspan dynamic response of the preliminary designs was evaluated using the computer code developed by Wilson (Ref. 4-61). According to Wilson, the midspan response is a good approximation of the maximum response along the span. The calculated midspan response for the complete speed range is plotted in Figures 4-98 and 4-99. In all cases, the results show that the calculated response is less than the predicted allowable response defined by Figures 4-96 and 4-97. Figures 4-98 and 4-99 also show that dynamic effects for the speed

$M_{MAX} = 2.0 \ X10^6$ N-m AT 134 m/s

$M_{MAX} = 2.01 \ X10^6$ N-m AT 112 m/s
($17.79X10^6$ LB-IN.)

$M_{MAX} = 2.95 \ X10^6$ N-m AT 134 m/s
($26.15X10^6$ LB-IN.)

15.2 m SPAN

$M_{MAX} = 3.13 \ X10^6$ N-m
($27.7X10^6$ LB-IN.)
AT 134 M/S

$M_{MAX} = 1.85 \ X10^6$ N-m
($16.36 \ X10^6$ LB-IN.)
AT 67 m/s

$M_{MAX} =$
$1.79 \ X10^6$ N-m
($15.82 \ X10^6$ LB-IN.)
AT 67 m/s

30.5 m SPAN

22.9 m SPAN

S (m)	M_{MAX} STATIC (10^6 N-m)
15.2	0.748
22.9	1.17
30.5	1.61

$$\Omega_1 = \frac{\pi V}{S}$$

222 KN (50,000 LB)   222 KN (50,000 LB)

→ V   → V

S=15.2 m (50 FT)

S=22.9 m (75 FT)

S=30.5 m (100 FT)

NONDIMENSIONAL SPEED, Ω_1/P_1

FIGURE 4-98. MIDSPAN BENDING MOMENT RESPONSE FOR ELEVATED GUIDEWAY BEAMS
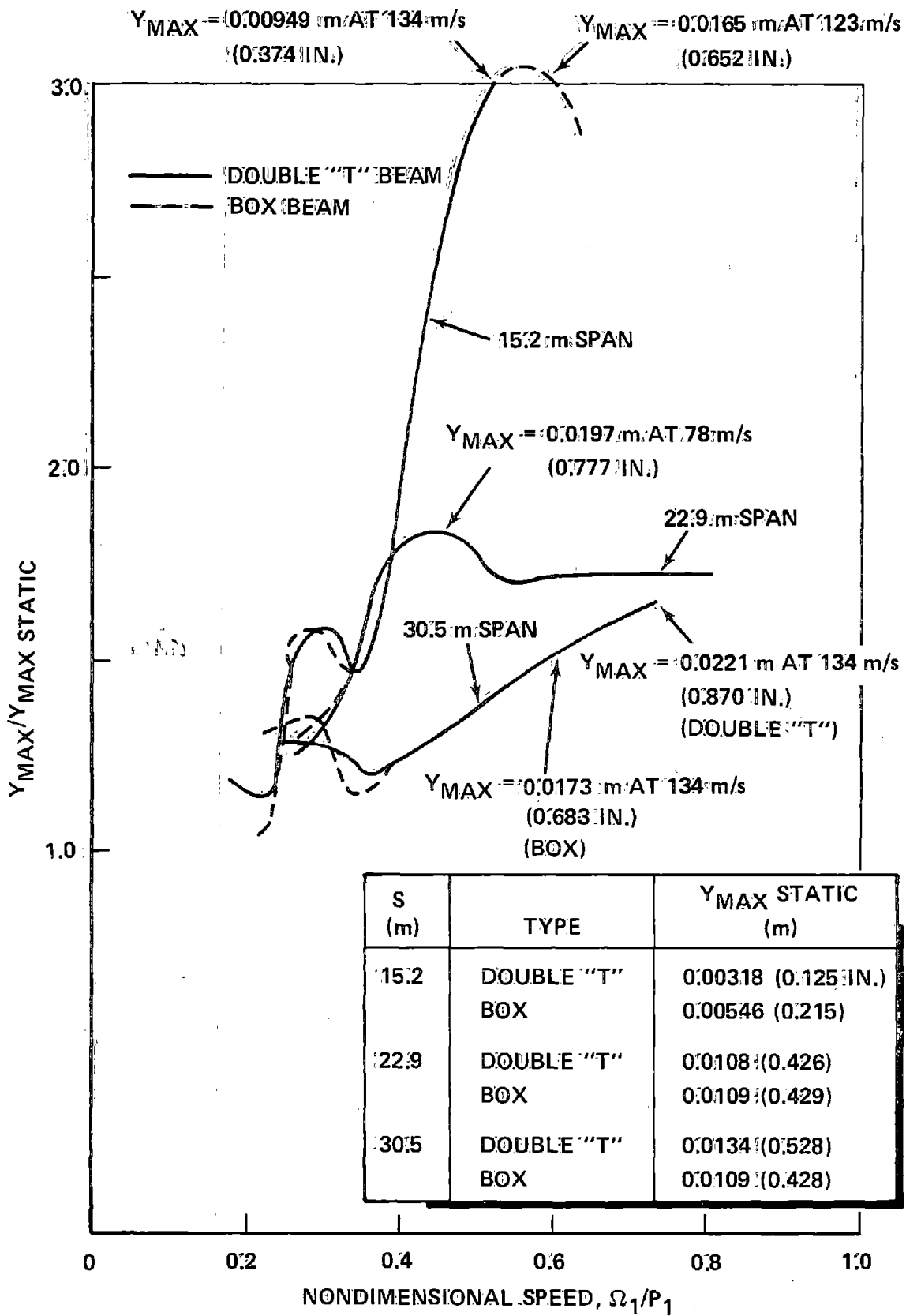
FIGURE 4-99. MIDSPAN DEFLECTION RESPONSE FOR ELEVATED GUIDEWAY BEAMS

4-234

range of interest will be greatest for the shorter spans. Such a result appears to be due to the fact that the superposition effects of the front and rear levitation forces are larger for short spans. The same effect can be seen in Figure 4-97 where Wilson's calculations give almost equal dynamic bending moments for 15.2 m and 22.9 m spans, even though static calculations would show a large difference.

Wilson's dynamic response computer program was modified to automate the calculation and plotting of girder deflections below the levitation coils as the vehicle traverses the span. Predicted deflections for the preliminary design of the 22.8 m (75 ft) twin-T girder are shown in Figure 4-100 and 4-101 for the front and rear levitation coils, respectively. The predicted deflections have somewhat different shapes than originally assumed (Figure 4-96), but the amplitudes are considerably lower than the initial predicted allowable. The results shown in Figures 4-100 and 4-101 were used in Section 4.3.2D to evaluate the vehicle response to periodic guideways.

(6) Final Elevated Span Designs. The final structural design of the girders included the analysis of the effects of the vehicle loads given by Table 4-48 and the consideration of other environmental effects. The resulting girder designs are presented in Table 4-49. These designs should be conservative based on the preliminary dynamic response calculations. Details of the 22.8 m (75 ft) prestressed concrete girders are illustrated in Figures 4-102 and 4-103 for the twin-T and box designs, respectively. A composite steel/concrete girder was also designed to have a cost comparison with the prestressed concrete girders. This girder is shown in Figure 4-104.

Appropriate pier and footing substructures were designed to support the elevated guideway. A typical design is given in Figure 4-105. Alternate piers have pinned girder attachments to support longitudinal guideway loads. The remaining piers (shown in Figure 4-105, by the dashed lines) have a smaller, rectangular cross section and a sliding girder attachment. This allows for thermal expansion but provides no support for longitudinal loads. Two footing designs, spread and pile, have been investigated to determine the effect of soil conditions on construction cost. The pile footing will, of course, be required in areas of poor soil conditions.

FIGURE 4-100. PRELIM. 22.8 M TWIN-T GIRDER, DYNAMIC DEFL; FRONT COIL GUIDEWAY DEFLECTION BELOW LEVITATION COIL
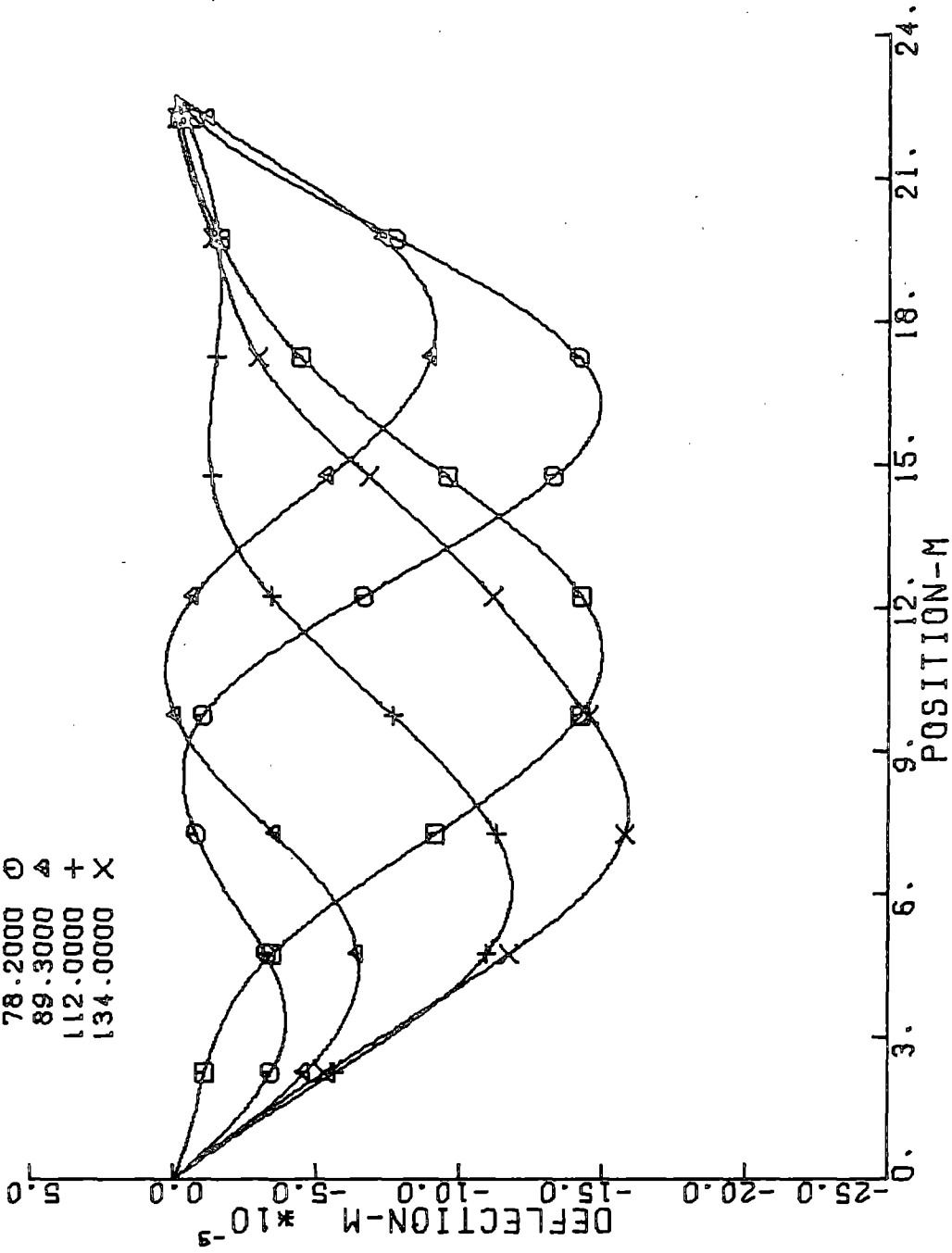
FIGURE 4-101. PRELIM, 22.8 M TWIN-T GIRDER, DYNAMIC DEFL; REAR COIL
GUIDEWAY DEFLECTION BELOW LEVITATION COIL

TABLE 4-49. FINAL GIRDER DESIGNS

PARAMETER	SPAN					
	15.24 m (50 ft)		22.9 m (75 ft)		30.5 m (100 ft)	
	TWIN "T"	BOX	TWIN "T"	BOX	TWIN "T"	BOX
DEPTH, d(cm)	127 (50 in.)	99 (39)	152 (60)	107 (42)	183 (72)	168 (66)
BENDING STIFFNESS, EI (kN-m^2)	5.05×10^6 (1.77×10^{12} lb-in.^{2})	3.70×10^6 (1.29×10^{12})	7.52×10^6 (2.62×10^{12})	5.02×10^6 (1.75×10^{12})	12.5×10^6 (4.37×10^{12})	15.5×10^6 (5.39×10^{12})
WEIGHT/LENGTH(N/M)	43,000 (2950 lb/ft)	39,000 (2700)	44,000 (3000)	43,000 (2950)	48,000 (3320)	50,000 (3450)

BOX DESIGN (BASELINE)

304 Cm (120 in.)

TWIN "T" DESIGN

304 Cm (120 in.)

0.79
(2.58)

0.15
(0.5)

0.53
(1.73)

0.4
1.3

REINFORCEMENT
LOCATIONS

1.52
(5)

DIMENSIONS: METERS (FEET)

0.2
(0.67)

1.93
6.33)

END SECTION ← | → MID-SPAN SECTION

3.04
(10)

₵ SPAN

5.8
(16.67)

11.43
(37.5)
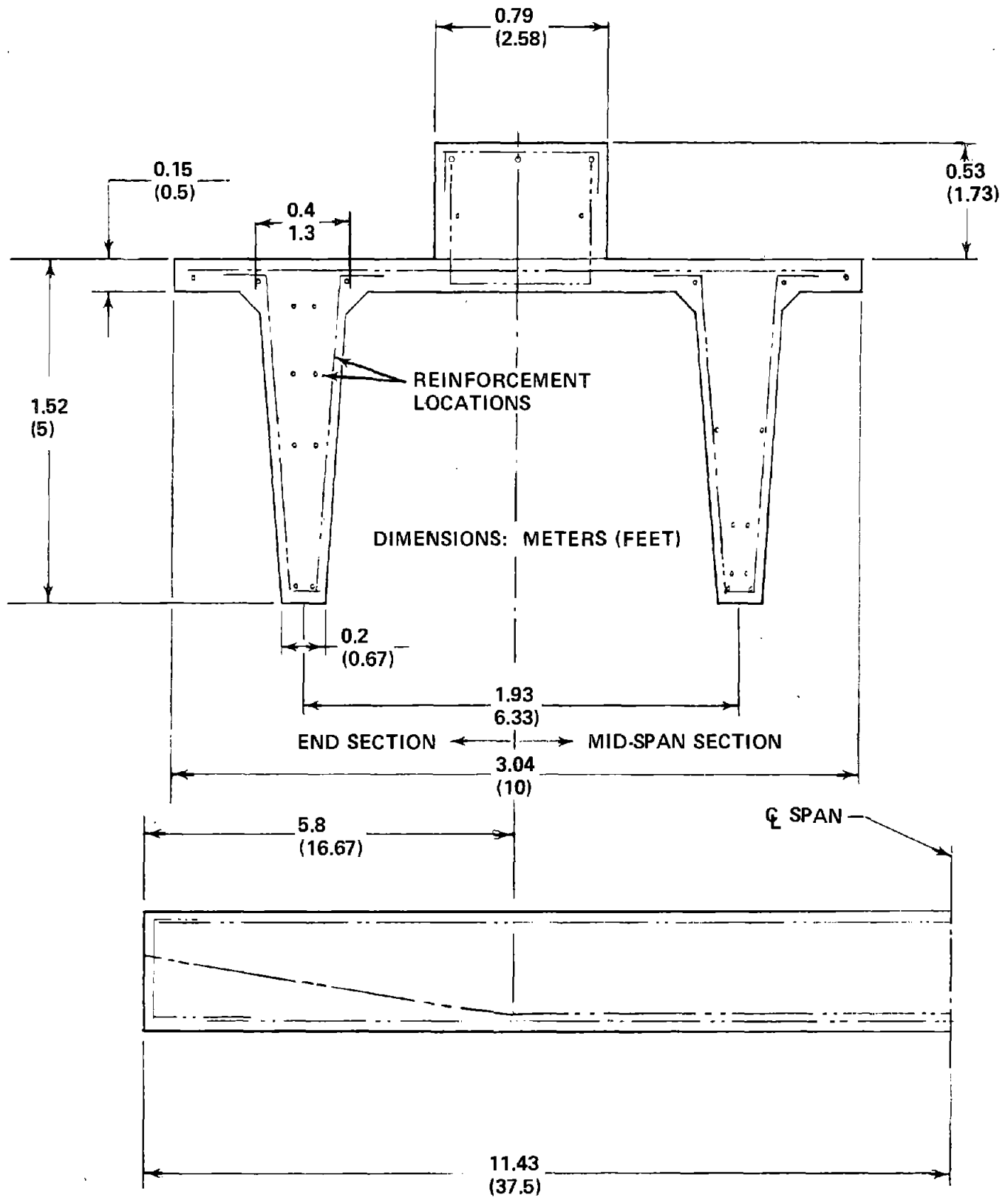
FIGURE 4-102. DETAILS OF 22.8 M (75 FT) SPAN - DOUBLE-TEE GIRDER

4-239

3.04
(10)

0.79
(2.58)

0.51
1.83

0.15
(0.5)

0.53
(1.73)

1.07
(3.5)

0.3
(1.0)

0.15
(0.50)

REINFORCEMENT
LOCATIONS

1.83
(6)

DIMENSIONS:
METERS (FT)

END SECTION ←→ MID-SPAN SECTION

5.8
(16.67)

C SPAN

11.43
(37.5)
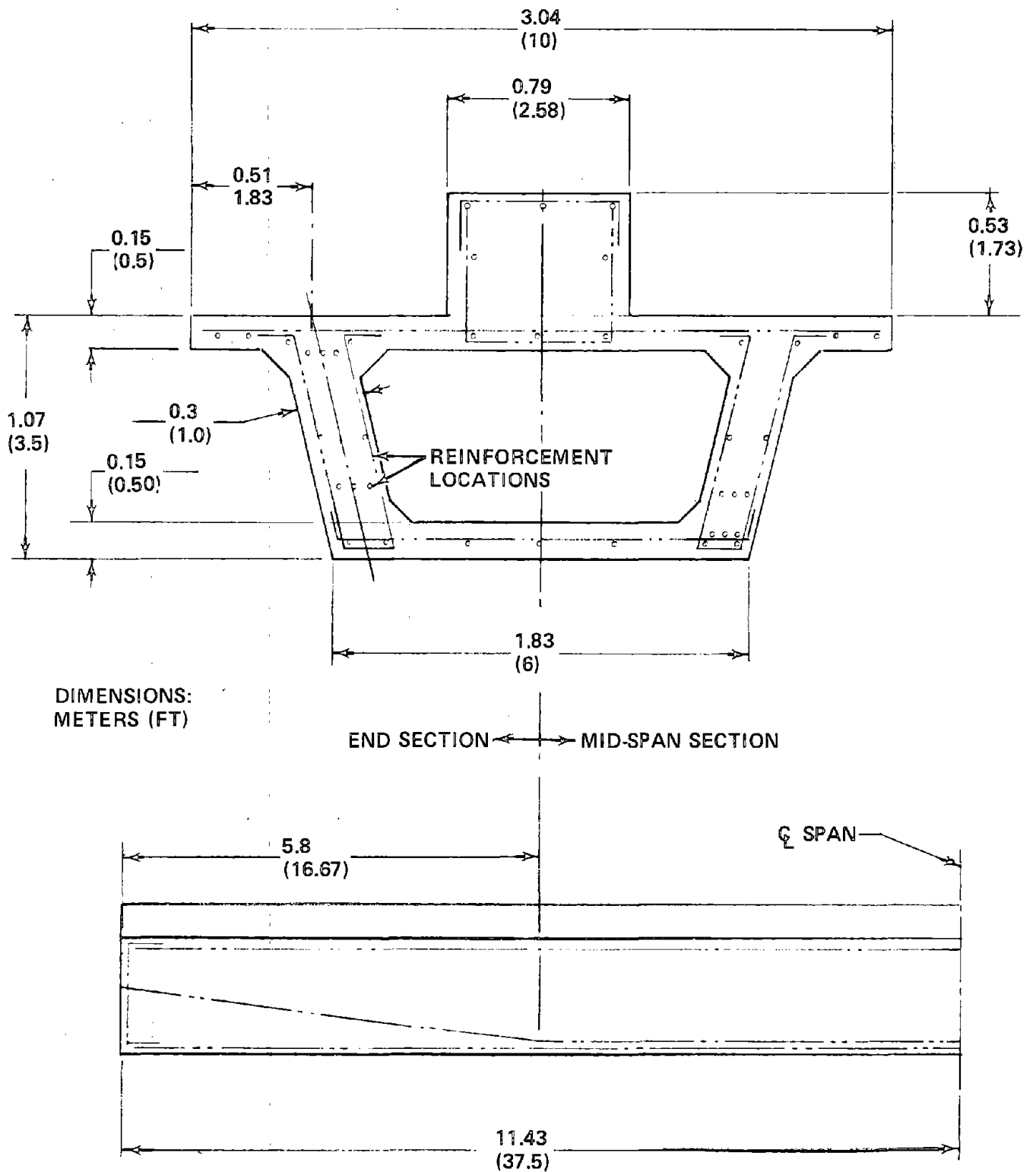
FIGURE 4-103. DETAILS OF 22.8 m (75 FT) SPAN - BOX GIRDER
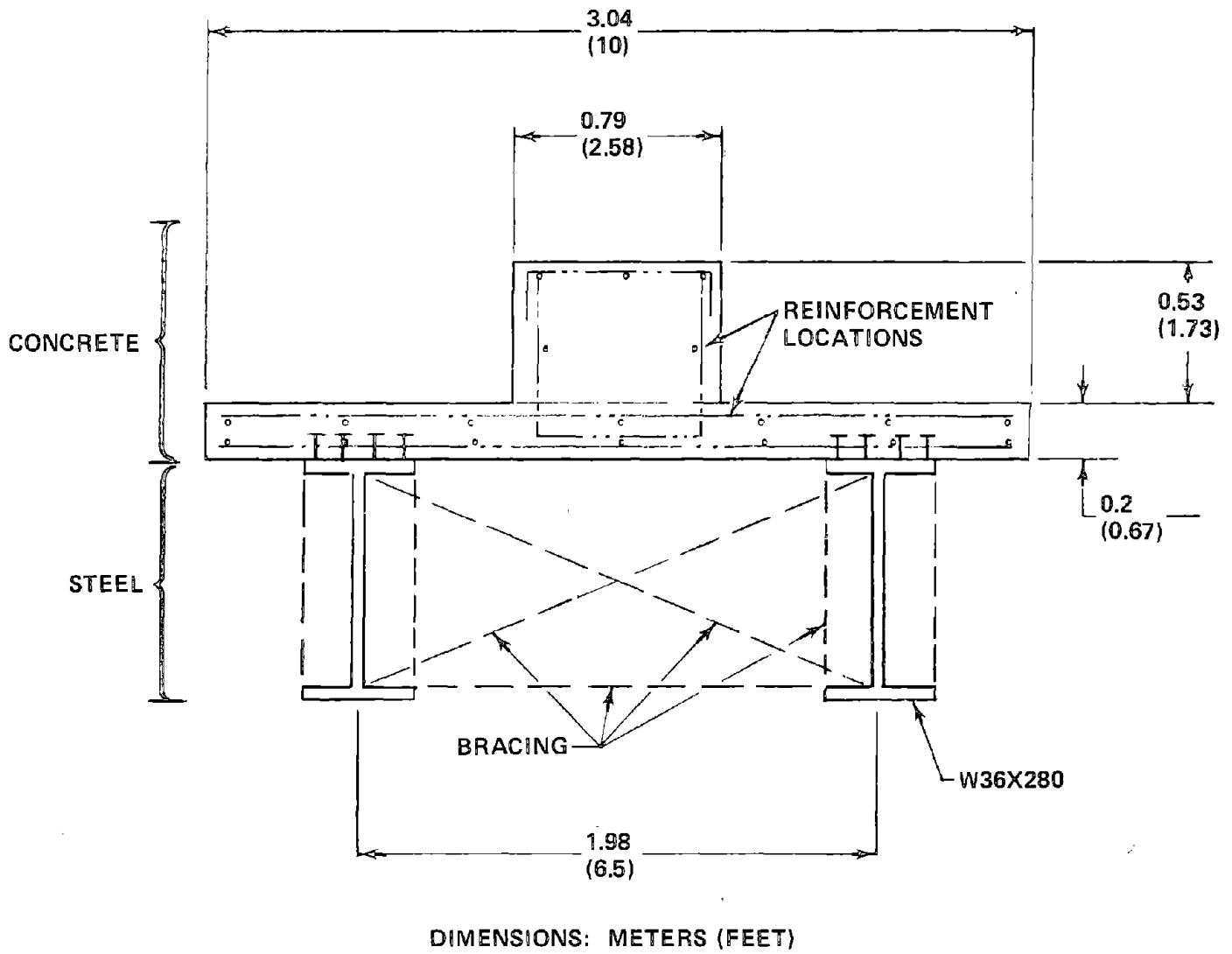
FIGURE 4-104. TYPICAL 22.8 M (75 FT) SPAN-COMPOSITE GIRDER

6.1 (20)

2.44 (8)

0.6 (2)

1.22 (4)

REINFORCEMENT LOCATIONS

0.91 (3)

PIER FOR SLIDING JOINT DESIGN

0.91 (3)

4.26 (14)

4.57 (15)

0.46 (1.5)

0.91 (3)

DIMENSIONS: METERS (FEET)

FINAL GRADE

1.22 (4)

3.88 12.75

PILE FOOTING

3.65 (12)

SPREAD FOOTING

3 EQUAL SPACED PILES FOR SLIDING JOINT DESIGN
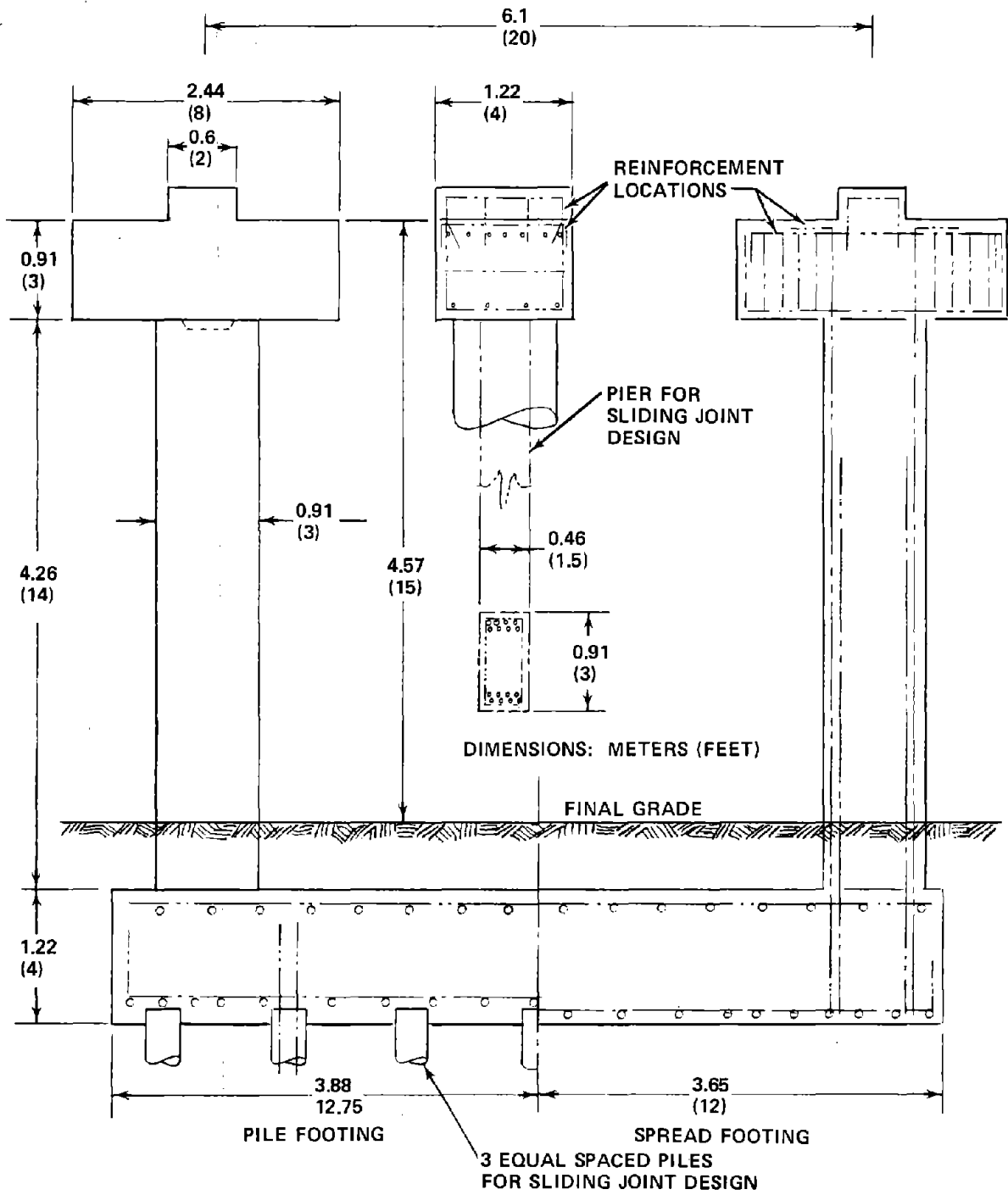
FIGURE 4-105. TYPICAL PIER AND FOOTING FOR 22.8 M (75 FT) SPAN

(7) <u>Girder Deflections and Ride Quality (Final Designs)</u>. The evaluation of the vehicle ride quality of different girder designs requires the consideration of static deflections and camber developed in the prestressed beams as well as the dynamic deflection. Table 4-50 lists the expected midspan deflections for the 22.8 m (75 ft) girders given in Table 4-49. Downward (negative) deflections result from the dead and dynamic loads; whereas, upward (positive) deflections are produced by the prestressing loads, creep deformations, and thermal distoration. The thermal distortion prediction of Table 4-50 is based on the assumption that the top surface of the girder is 15°C hotter than the lower surface. The dynamic deflections for the final 22.8 m girder design have been determined in the same manner as for the preliminary designs discussed in the previous paragraph. Figures 4-106 and 4-107 give the complete deflection histories for the final 22.8 m twin-T design.

Some compensation for girder deflection can be achieved by constructing the concrete girders with a built-in camber. However, due to analytical limitations in predicting precamber requirements, construction tolerances, and material property variations, the desired postconstruction camber can only be expected to be obtained within some tolerance. As a guideline, the Prestressed Concrete Manufacturers Association (PCMAC) has suggested the maximum deviation from the installed mean camber objective should be assumed to be ±0.318 cm per 3.05 m of span length (±0.125 in. per 10 ft). This tolerance is believed to be conservative because less uncertainty should exist after several girders of a particular design are designed, built and measured.

An example of the expected midspan deflection for the 22.8 m twin-T girder with a built-in precamber of -1.9 cm (downward) is given in Table 4-51. The range of possible girder deflections below the front levitation magnet of the vehicle is shown in Figure 4-108. The results of this figure include all the static and dynamic sources in Table 4-50 for the 22.8 m twin-T design. A preliminary vehicle ride quality calculation assuming only dynamic deflections resulted in the estimation of the maximum vertical acceleration of a vehicle of 0.055 g, very close to the objective of 0.05 g. This is based on the 22.8 m twin-T girder and the total predicted deflections in Figure 4-108.

TABLE 4-50. MIDSPAN DEFLECTIONS FOR 23m (75 FT) ELEVATED SPAN

MIDSPAN DEFLECTIONS (cm)	TWIN "T" DESIGN	BOX DESIGN
DEAD LOAD	-2.1	-3.0
PRE-STRESS CAMBER*	+2.5	+3.8
28 DAY CREEP*	+0.89	+1.2
LONG TERM CREEP*	+1.5	+1.1
THERMAL DISTORTION ($\Delta T = 15^{\circ}C$)	+0.66	+0.97
LIVE LOAD DEFLECTION	-0.57	-0.64

*CAN BE GREATLY REDUCED WITH UNIFORM PRE-STRESS REQUIRING 150% MORE PRE-STRESS FOR TWIN "T" OR 30% MORE PRE-STRESS FOR BOX
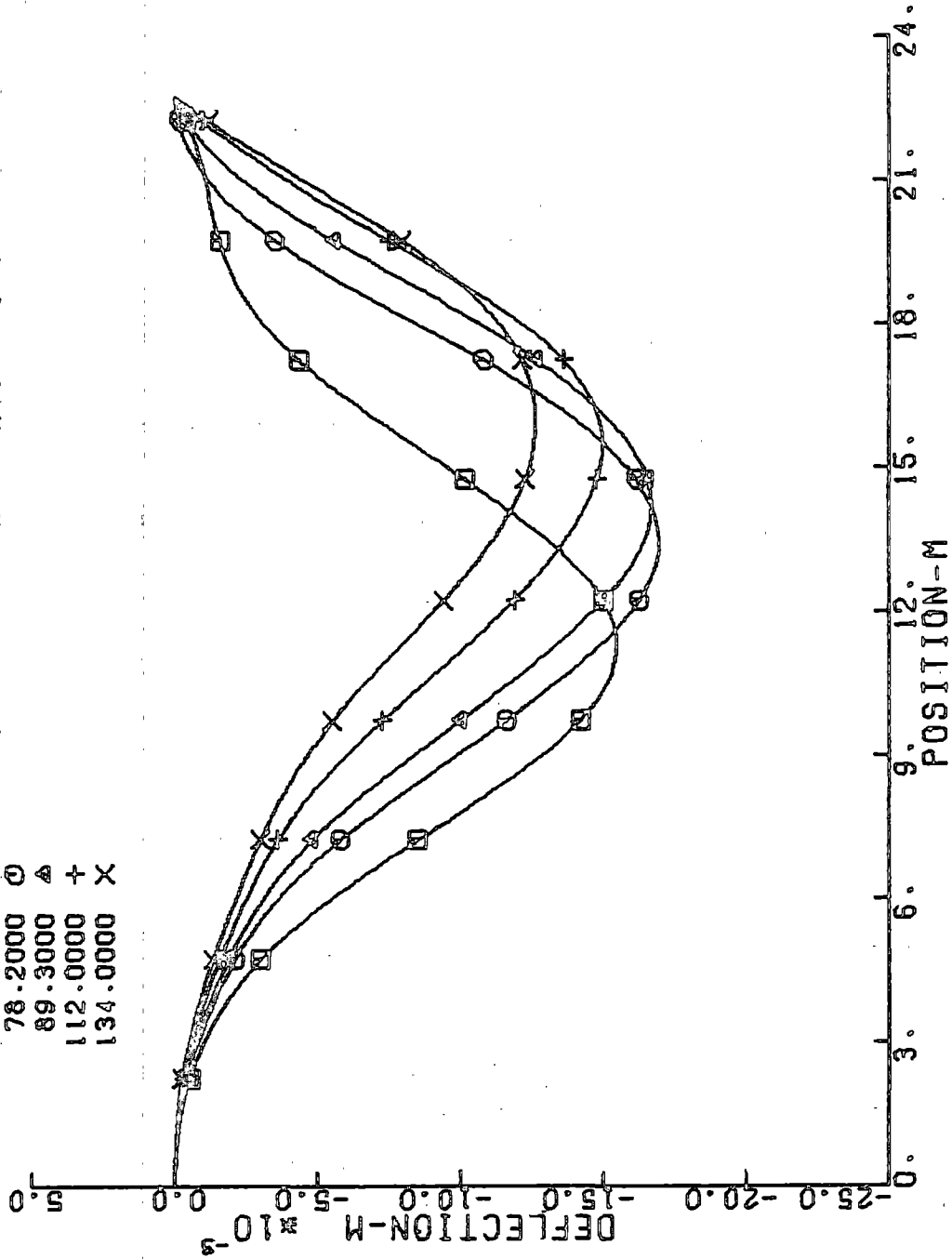

BOX BEAM

TWIN T

4-244

FIGURE 4-106. FINAL 22.8 M TWIN-T GIRDER, DYNAMIC DEFL; FRONT COIL
GUIDEWAY DEFLECTION BELOW LEVITATION COIL
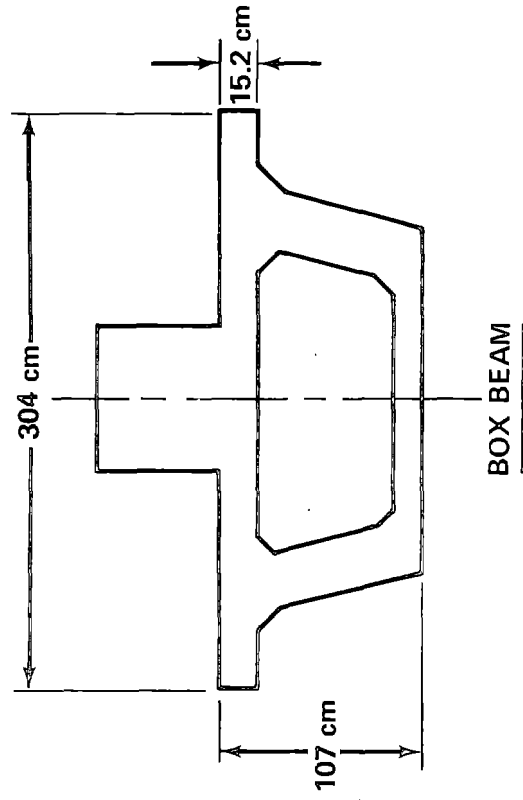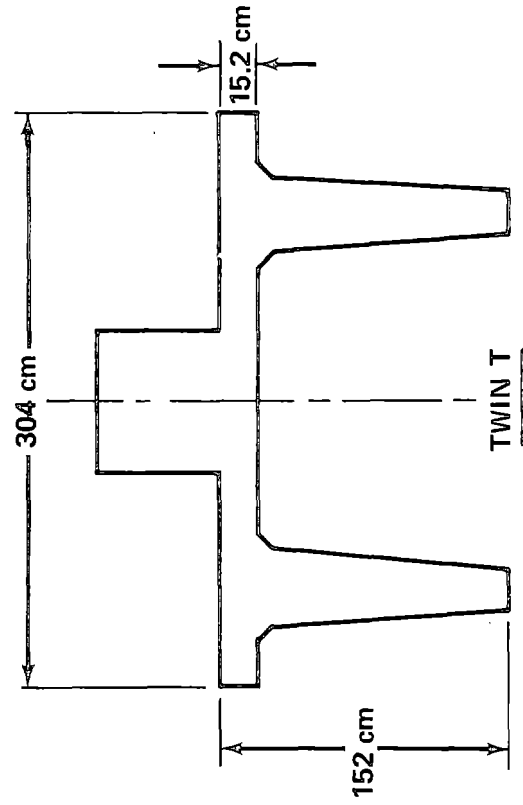
DATE 10 JAN 1975

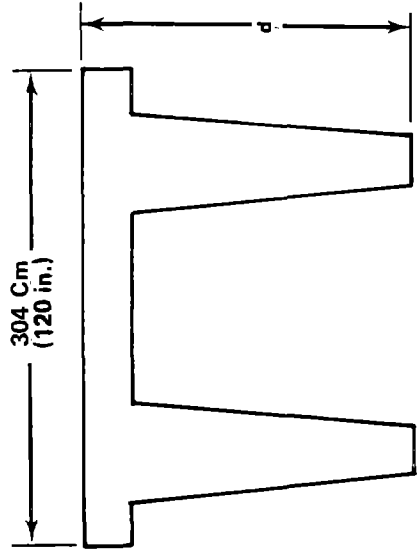SPEED (M/SEC)
55.8000
78.2000
89.3000
112.0000
134.0000

DATE 22 JAN 1975

SPEED (M/SEC)
55.8000
78.2000
89.3000
112.0000
134.0000
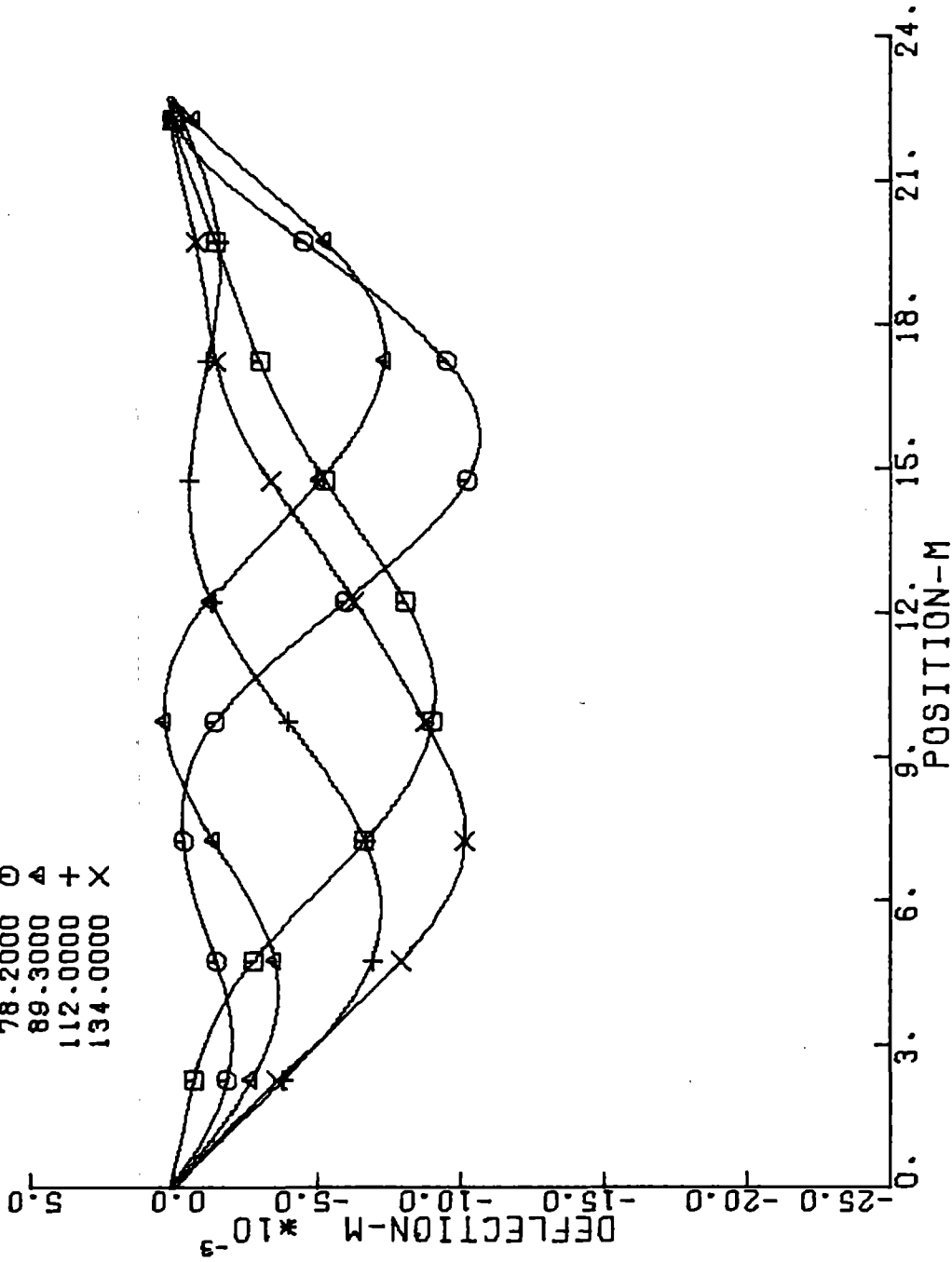
FIGURE 4-107. FINAL 22.8 M TWIN-T GIRDER, DYNAMIC DEFL.; REAR COIL
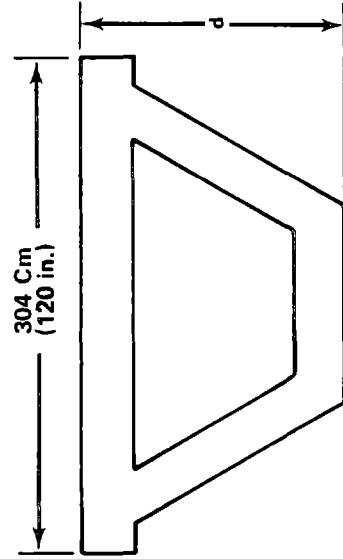GUIDEWAY DEFLECTION BELOW LEVITATION COIL

4-246

TABLE 4-51. TOTAL MIDSPAN DEFLECTIONS FOR 23 M (75 FT) TWIN-T GIRDER WITH ORDINARY PRESTRESS

(-1.9 CM BUILT-IN PRECAMBER)

AGE OF BEAM	LOADING CONDITION			RANGE OF MIDSPAN DEFLECTION (cm)
	STATIC ONLY	STATIC AND DYNAMIC[1]	STATIC, DYNAMIC AND THERMAL[2]	
Short Term (~28 Days after Fab)	X			-3.1 to 1.9[3]
		X		-3.7 to 1.3
			X	-3.0 to 2.0
Long Term	X			-1.5 to 3.5
		X		-2.1 to 2.9
			X	-1.4 to 3.6

[1]Dynamic loads for a vehicle speed of 134 m/s.

[2]Thermal loads based on a top surface 15°C hotter than lower surface.

[3]For this condition, the range of deflection is derived as follows: The nominal deflection of -0.6 cm is obtained by summing the dead load, the built-in camber, the prestress camber, and the short-term creep. The tolerance of ±2.5 cm is the recommended PCMAC maximum deviation.

It is desirable from a ride quality standpoint to reduce the girder roughness to a minimum, and the following alternatives exist for improving the guideway roughness:

- The girders can be prestressed more uniformly than normal to virtually eliminate the uncertain prestress camber and creep deformations (Ref. 4-53). Uniform prestress requires greater prestressing loads and could be implemented more efficiently for the box girder design rather than the more economical twin-T girder.

- Combine prestress with post-tension. Prestress to about 75% of the required load, and post-tension at installation so that the final camber adjustment can be made after some of the creep deformations have taken place.

- Add a concrete topping to the girders after installation and after much of the creep deformations have taken place.
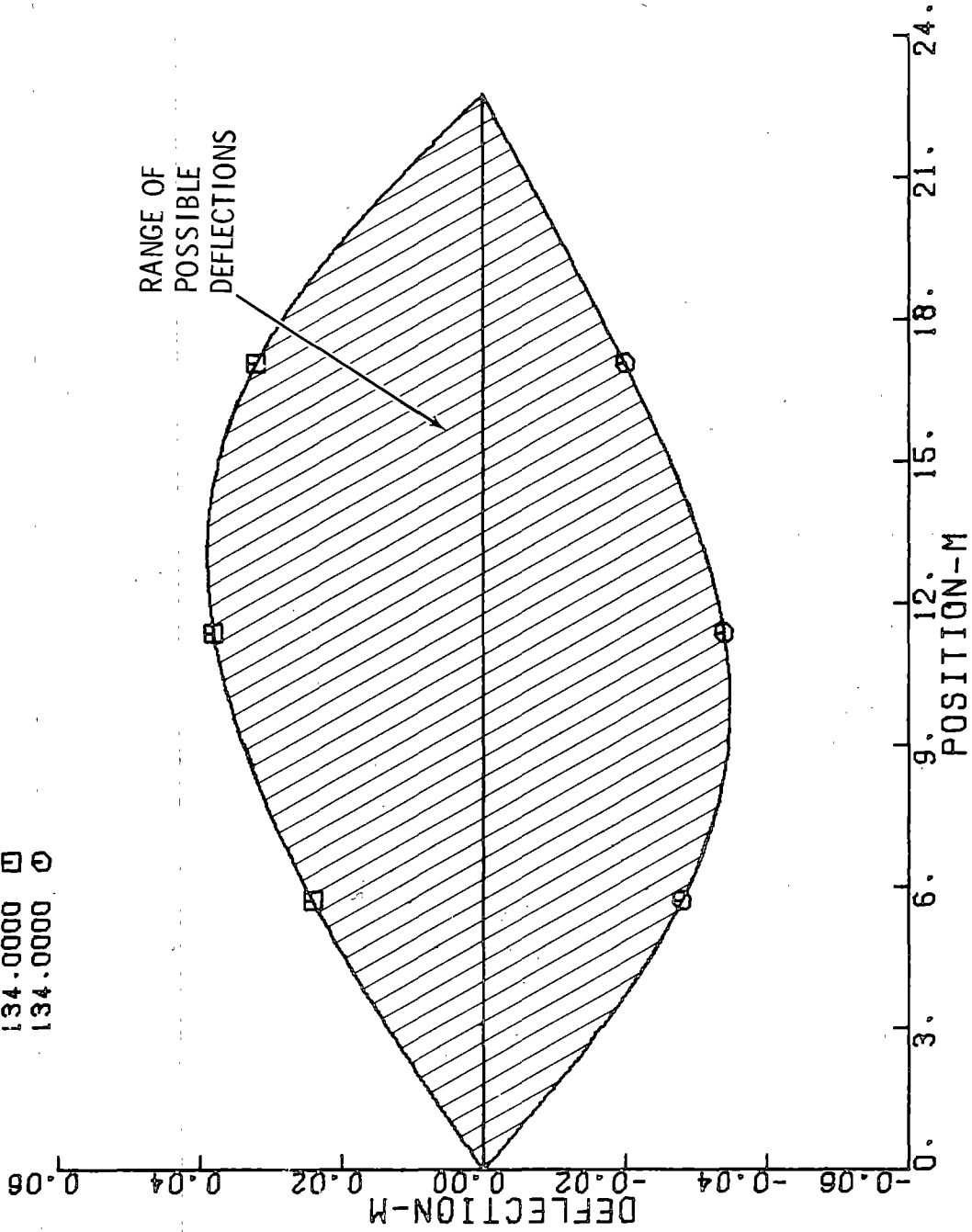
FIGURE 4-108. EST. TOTAL DEFL, FINAL 22.8 M TWIN-T GIRDER; FRONT COIL
APPROXIMATE DEFLECTION BELOW LEVITATION COIL

o   Provide for post-installation adjustments of the aluminum
    levitation/guidance elements relative to the concrete girders.

o   Install the aluminum levitation/guidance elements on aged girders;
    shim the aluminum relative to the girders to provide a smooth
    surface; and pressure grout any resulting voids between the
    aluminum and concrete.

The first option appears to be the most practical, and estimates have been made
to show the cost increases involved with uniform prestress. The baseline
design that was selected is the box beam with uniform prestress.

        (8) Comparison With Other Work. A comparison has been made between
the MAGLEV girder design and those derived for tracked air-cushion vehicles.
This comparison is summarized in Table 4-52. The early Aeroglide study listed
at the top of the table did not consider vehicle dynamics, and the spans were
designed to highway standards. This resulted in a relatively lightweight,
flexible span. Tracked Hovercraft Ltd., and Grumman derived heavier and less
flexible span designs when the dynamic interaction of the high-speed vehicle
and the guideway was considered. The MAGLEV vehicle has a low vehicle natural
frequency in heave (0.6 Hz) and a minimum relative damping which results in a
girder design which is relatively flexible compared to the Grumman TACRV
(now TLRV) design and the TRW/ABAM design for the TACV.

A further point of interest is shown in the last column of Table 4-52 for
the TRW/ABAM elevated span designs for the UTACV (now PTACV). Vehicle response
calculations were made for identical girder designs assuming simply-supported
spans in one case and continuous spans in another case. The ride quality for
a vehicle with a suspension heave frequency of 2.0 Hz was shown to be degraded
by using a continuous beam design. A small improvement in the ride quality
for a continuous beam design was predicted for a vehicle with a softened sus-
pension (1.0 Hz). The conclusion is that a continuous beam system is not
a priori a better solution to the elevated guideway problem even though TRW
showed a cost advantage (based upon the static deflection considerations in
Reference 4-55). Since continuous-beam elevated guideways have other potential
advantages such as the elimination of gaps at each support pier, a careful
study of continuous beam systems, including the evaluation of dynamic effects,
fabrication methods, and overall construction economics, is recommended for
future work.

4-249

TABLE 4-52. COMPARISON OF SIMPLY SUPPORTED ELEVATED GUIDEWAYS

STUDY	SPAN TYPE	SPAN LENGTH S m(ft)	SPAN WEIGHT kN/m (lb/ft)	SPAN BENDING STIFFNESS, EI kN-m² (lb/in.²)	SPAN FUND FREQ P_1 Hz	VEHICLE WEIGHT kN (lb)	VEHICLE SUSPENSION HEAVE FREQUENCY Hz	VEHICLE RESPONSE NONDIMENSIONAL VELOCITY* Ω_1/P_1	VEHICLE RESPONSE MAXIMUM ACCEL g
Aeroglide Sys Inc., (Ref. 4-53) (Dec. 1968)	Concrete twin-T with steel vertical guide	22.9 (75)	16.9 (1160)	2.34×10^6 (0.816×10^{12})	3.5	200 (45,000)	6.0	No Analysis	No Analysis
Tracked Hovercraft, Ltd. (July 1970) (Ref. 4-52)	Concrete channel	22.9 (75)	48.7 (3340)	6.60×10^6 (2.3×10^{12})	3.5	316 (71,000)	—	0.70 at 112 m/s	0.05
Grumman-TACRV (TLRV) (Ref. 4-51)	Concrete double box	22.9 (75)	50.2 (3440)	13.1×10^6 (4.57×10^{12})	4.8	173 (39,000)	0.8	0.46 at 134 m/s	0.03
						262 (59,000)			0.063
Present Study	Concrete twin T	22.9 (75)	44.0 (3000)	7.52×10^6 (2.62×10^{12})	3.9	445 (100,000)	0.6	0.75 at 134 m/s	0.055
		30.5 (100)	48.0 (3320)	12.5×10^6 (4.37×10^{12})	2.69			0.816 at 134 m/s	—
TRW-ABAM (Ref 4-50) UTACV (Now PTACV)	Concrete box	30.5 (100)	17.5 (1200)	4.50×10^6 (1.57×10^{12})	2.66	267 (60,000)	2.0 / 1.0	0.413 at 67 m/s	0.80 (0.89)** / 0.14 (0.11)**
TACRV (Now TLRV)	Concrete channel-box	30.5 (100)	33.0 (2260)	21.1×10^6 (7.36×10^{12})	4.24	409 (92,000)	0.8	No Analysis	No Analysis

*$\Omega_1 = \pi V/S$

**Continuous beam

4.5.3 Switching

The requirements and conditions that have been used in evaluating potential switching concepts are summarized below:

- The switch must be passive and failsafe, i.e., there should be no moving parts associated with the guideway.

- The through-traffic should be able to pass the switch at normal cruising velocity (134 m/s in lightly-populated areas).

- The switch should be simple.

- High-speed switching ($\geq$ 45 m/s or 100 mph) is impractical due to the turn radii required and other design considerations such as problems of moving the magnets relative to the vehicle.

The latter restraint has resulted in the selection of a nominal switching speed of 30 m/s (67 mph). Since this is approximately the lift-off speed, wheels can be employed; therefore the decision has been made to use the loading wheels as the onboard switching mechanism. A discussion of the design of the landing/ switching wheels is given in Section 4.2.7B.

The baseline switching system meets all of the requirements, and is simply two inclined ramps outboard of the normal guideway. The wheels onboard the vehicle are extended out and down until they contact these inclined ramps thus moving the vehicle up on the elevated switch. Figure 4-109 is an artist's conception of the switch in a greatly foreshortened view. The ramps have a gradual grade change so that the vehicles can make the transition to and from the main guideway without exceeding the ride quality requirements. Once back on the main guideway the vehicle will be at, or quickly reach, the lift-off speed, and the wheels will be retracted back into the vehicle.

The baseline switch has no moving parts, and should have maximum safety since there is no loss of guidance for through-traffic. Failure to extend the wheels simply means the vehicle safely passes the switch on the through-guideway with full guidance forces. Another possible failure mode is inadvertent extension of the wheels of a high-speed through-vehicle just before the switch is reached, but this is analogous to an airplane lowering its landing wheels prematurely; i.e., the chances should be very remote that this will occur. A dynamic pressure-actuated linkage will be provided to prevent this.

4-251

SWITCHING RAMP

HAT-SHAPED GUIDEWAY
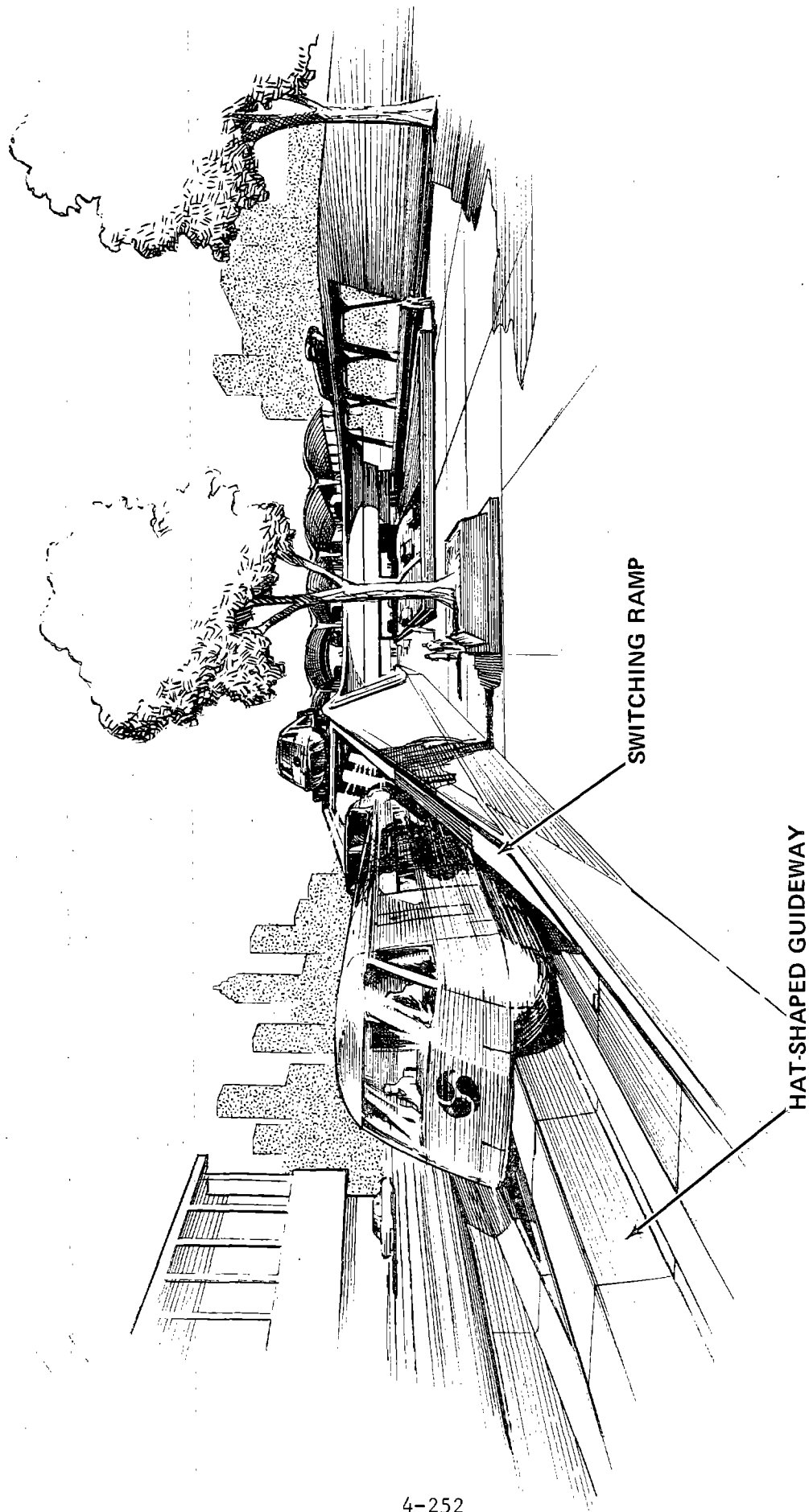
FIGURE 4-109. ARTISTS' DRAWING OF TERMINAL AREA AND BASELINE SWITCHING CONCEPT

The baseline switch is ideal for a vehicle propelled by a turbine-driven ducted fan since the switch will not affect its operation. The use of an electric motor-driven fan propulsion is complicated by the problem of switching the power pick-up. This will probably require two pick-ups, one on each side of the vehicle; one (say, the left) will be used for normal travel including through-traffic. The auxiliary or right-side pick-up will be extended and used upon entrance to the switch as the left one is disconnected. The reverse procedure will be used upon transition from the switching ramp to the main guideway.

The baseline overhead-type of switch may not be acceptable for SLIM, LSM, and paddle wheel driven vehicles because they will suffer a loss of power during switching as the vehicles move up and away from the guideway. This could be overcome by providing a secondary low-speed drive system through the wheels via rotary electric motors, but it may prove to be more desirable to use an at-grade switch for these types of propulsion systems. A conceptual design for an at-grade guideway is shown in Figure 4-110. This alternate approach uses a guide trail type of design similar to that used on several existing people-movers. All vehicles approaching the switch extend one of two onboard guide wheels, the left one for straight-through traffic, or the right guide wheel for switching to the right (see Figure 4-110). The disadvantages of this type of switch are obvious — first, through-traffic must extend a guide wheel in order to maintain guidance through the switch since the vertical aluminum surfaces normally used for lateral guidance are not present. Failure to do so would mean loss of control and the possibility of impacting the guideway or other objects. Second, through-traffic will be required to traverse the switch at reduced speed to assure a smooth transition with the guide rail, thereby penalizing the block speed. One advantage of the at-grade switch is that the landing wheels would only be required to extend down (not laterally), thereby simplifying the landing wheel design. However, the vehicle design would not be greatly simplified due to the addition of the guide wheels.

The at-grade switching concept in Figure 4-110 is shown with the baseline hat-shaped guideway. However, it will probably be more advantageous to use a U-channel guideway for SLIM and LSM, and have the SLIM rail or the LSM windings

GUIDE WHEEL
RETRACTED

GUIDE WHEEL
EXTENDED

GUIDE RAIL

GUIDE WHEEL EXTENDED
FOR STRAIGHT-THROUGH TRAVEL

GUIDE WHEEL EXTENDED
FOR SWITCHING VEHICLE

TOP VIEW

HAT-SHAPE
GUIDEWAY

GUIDE RAIL

AT-GRADE ALUMINUM
SURFACE

HAT-SHAPE OR
WIDE INVERTED
TEE GUIDEWAY
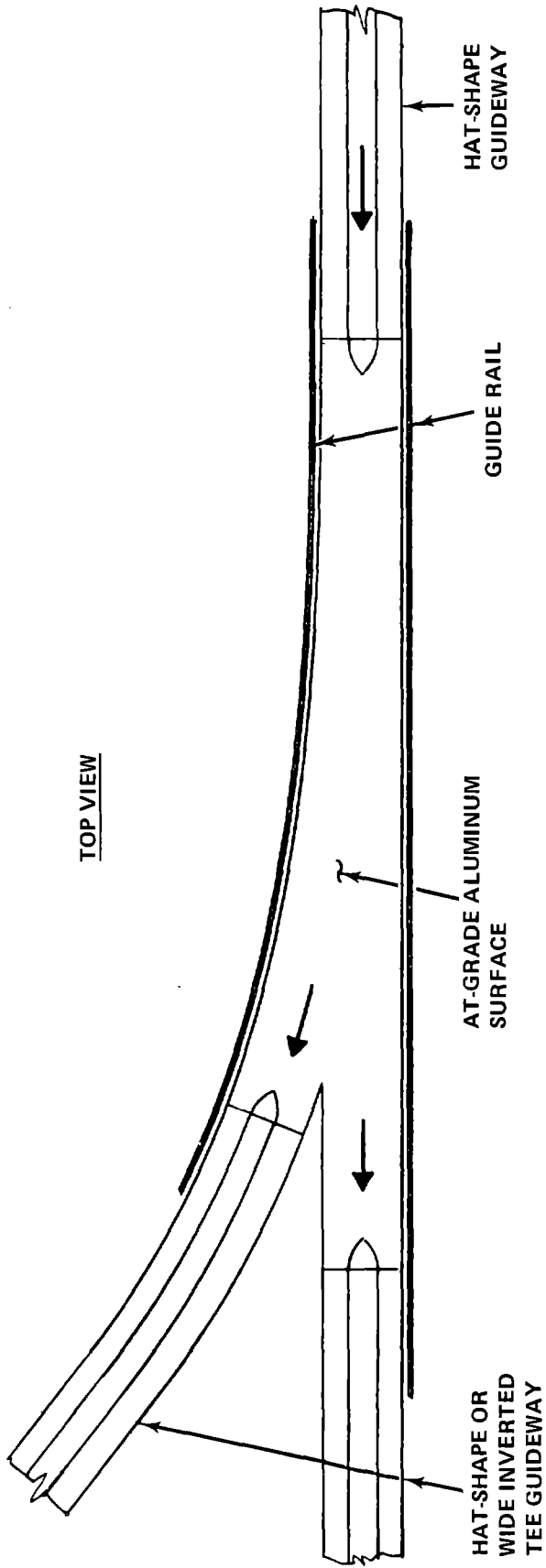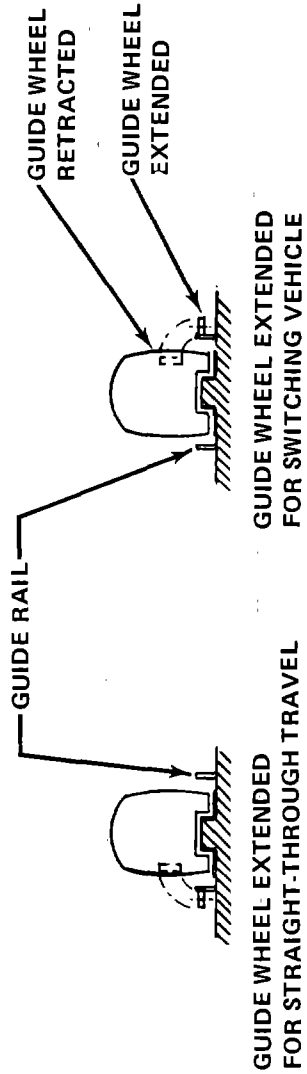
FIGURE 4-110. ALTERNATE AT-GRADE SWITCHING CONCEPT WITH HAT-SHAPED GUIDEWAY

down the center of the guideway. This will allow these systems to provide propulsion power through the at-grade switch, except, perhaps for a very short region where the roadbed propulsion rails or windings for the switching leg cross over the aluminum levitation surface.

4.5.4 Wayside Power Pick-up

Electrical power pick-up will be required for the superconducting rotary electric motor-driven fan or the SLIM propulsion systems. The pick-up can be of two basic approaches (Ref. 4-1): mechanical contact such as used on the TLRV or the more advanced contactless system. No studies have been made to determine which type will be the best for Repulsion MAGLEV, however it appears that both have a number of fundamental problems that require investigation, i.e.:

- The problem of switching the pick-up needs study. The approach discussed in the previous paragraph of having a separate pick-up for switching adds considerable complications to the system design. The system developed by Garrett for TLRV cannot be used in its present form without some means of releasing the captured pick-up at the same time the auxiliary pick-up is being engaged.

- The problem of arcing and proper power pick-up under all types of conditions and speeds must be solved and a design demonstrated.

- The problem of excessive wear of a mechanical contact pick-up must be solved before a practical solution is assured.

- Potential aerodynamic problems need to be investigated further. The overall force the pick-up exerts on the vehicle must be determined.

- The noise of the system must be studied to determine its contribution to the overall noise level.

- The potential problem of electromagnetic interference (EMI) of the arc on the onboard and nearby communications systems must be investigated.

The superconducting electric motor-driven fan propulsion requires DC, and it is likely that switching DC may be simpler than for AC, primarily due to one less conductor.

4.5.5 Communications and Control

A detailed study of the communications and control system for the guideway is beyond the scope of this study, however consideration has been given to the types of equipment needed to assure safety and schedule. Safety assurance comprises the functions of: (1) foreign object detection; (2) deleterious weather detection (e.g., excessive crosswinds); (3) detection of unsafe vehicle location spacing, closure rates and corrective action; and (4) detection of wayside equipment failures and corrective action.

Schedule control involves the routing, switching, and in-transit monitoring and control of the system traffic. These functions are implemented by a three-tier hierarchy of equipment. The first level consists of guideway-mounted equipment. It comprises safety and schedule control sensors and the requisite cabling and communication facilities to tie into the next level plus facilities to permit communication with vehicles enroute.

Wayside station equipment comprises the second tier. The elements needed are, first, communications repeaters with local access to the network. Second, safety equipment is needed to activate and monitor the guideway-mounted sensors plus facilities to detect unsafe conditions and initiate corrective action. Third, schedule control computer facilities are needed to analyze the route block status based upon inputs from guideway sensors and the vehicles in the block, and to initiate control instruction to these vehicles.

The central control facilities of the system comprise the third tier of wayside equipment. The central system computer, display and control consoles are located at this level. This equipment ties into wayside stations and the individual vehicles via digital data and voice links built into the guideways. It also interfaces with the commercial telephone net for access to the outside world and to provide alternate (back-up) digital and voice communications channels to the wayside stations. These facilities provide the means to monitor and control the total system traffic for both safety and scheduling purposes. Additional communications channels are provided to handle passenger service information to and from the individual vehicles and the outside world.

All of the technology to mechanize the wayside complex currently exists except for an adequate means of foreign object detection. A system capable of detecting objects with a vertical dimension of greater than 5 to 10 centimeters on the horizontal portions of the guideway is needed. Also, it is desirable to detect any foreign objects on the vertical members of the guideway. It is likely that this problem must be handled by a combination of instrumentation, security fencing, passivation of the wayside environment to prevent natural generation of foreign objects, and manual observation of the guideways.

4.5.6 Right-of-Way

A. Width Requirements. The minimum width requirements for the at-grade guideway is defined by the maximum of either:

o The distance required for noise requirements or safety, currently estimated at a minimum of 15.2 m (50 ft) from the centerline of the guideway, i.e., a total width of 36.6 m (120 ft) for a dual guideway.

● Or the distance required by the cuts and fills to make a level guideway through the terrain.

The latter requirement will be the controlling factor in many cases. Figure 4-111 is a plot of the distance from the centerline of the right-of-way versus the depth of the fill or cut for the typical 2:1 slopes used for the earth embankments or cuts (see Section 4.5.2A). The results show that a fill greater than 5.6 m (18.4 ft), or a cut greater than 3.2 m (10.5 ft), will exceed the current minimum sound and safety ROW of 36.6 m.

The edge of the ROW will be fenced for security purposes, and may have a single-lane road on each side for use by maintenance vehicles.

The right-of-way for elevated portions of the guideway will be determined primarily by the noise requirements. Safety should not be such an important factor due to the relative inaccessibility of the guideway. Preliminary estimates indicate the ROW for elevated sections in industrial areas may be as narrow as 22.9 m (75 ft) increasing to roughly 30.5 to 36.6 m (100 to 120 ft), or more, in residential areas. The final values will depend on the vehicle speed, the sound level generated by all sources, and the noise requirements.

4-257

FILL

0

SLOPE 2:1

10

FILL DEPTH ~ M

20

7.62 M

15.2 M (50 FT) DISTANCE (MIN)
FROM GUIDEWAY FOR SOUND
AND SAFETY REQ'S

25   20   15   10   5   0

DISTANCE FROM R.O.W. CENTERLINE ~ M

20

CUT

CUT DEPTH ~ M

SLOPE 2:1

10

11.27 M

7.62 M

0
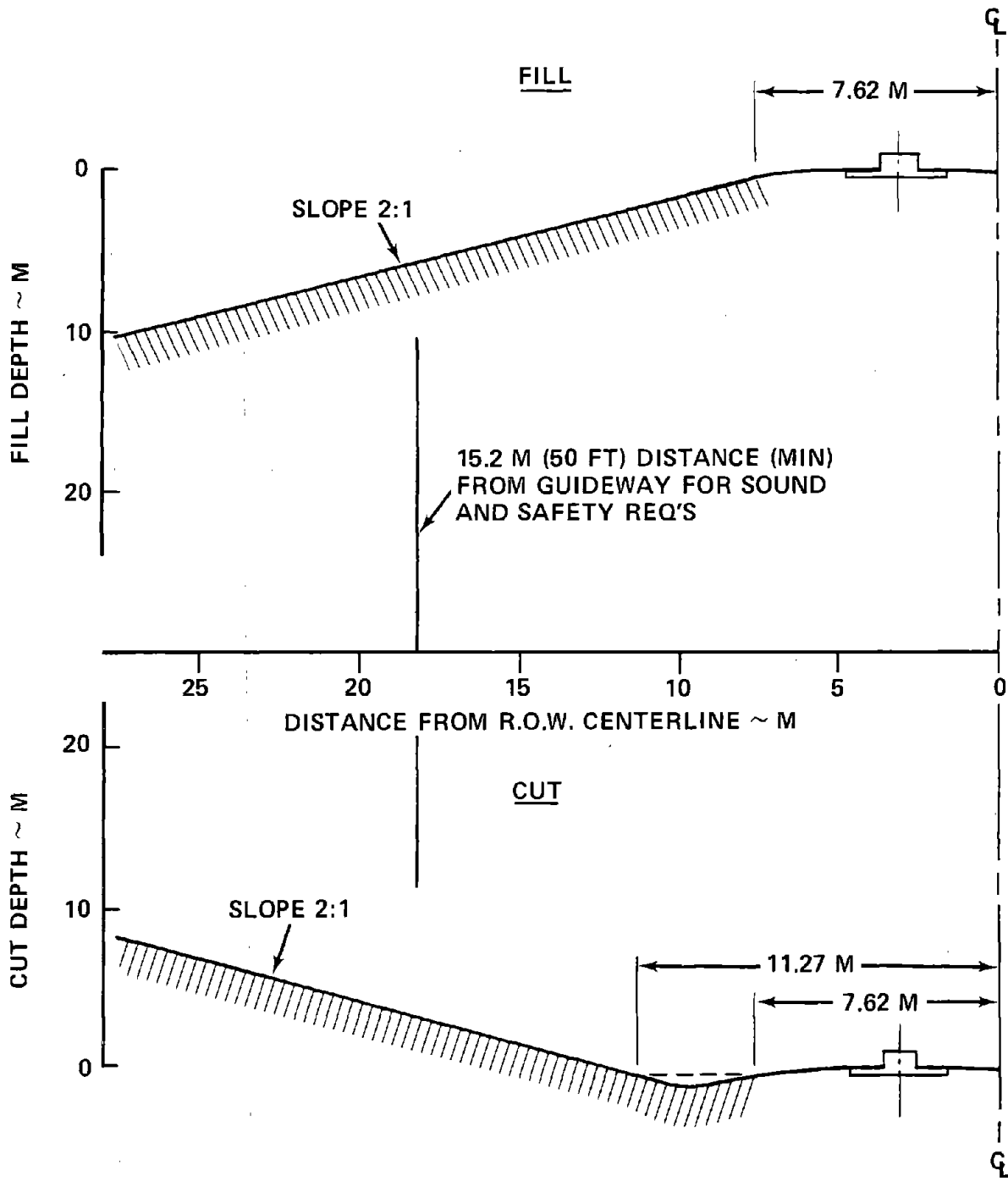
FIGURE 4-111. RIGHT-OF-WAY REQUIREMENTS BASED ON CUTS
AND FILLS

4-258

B. <u>Curve Radii and Transition Requirements</u>. The requirements for guide-way superelevation, vehicle bank limits, and speed are discussed in Section 3.2.2F. For any speed, a 24.6° bank angle and the specified 0.08 g lateral acceleration limit define the minimum radius turn. However, this maximum bank angle is impractical for a vehicle that does not have the capability of rolling the cabin with respect to the undercarriage, and a value of 10° guideway bank has been selected. The turn radius vs. vehicle speed for the two bank angles is shown in Figure 4-112. (This curve was originally given in Ref. 4-64.) The term "coordinated turn" is one with no lateral acceleration.

The minimum turn radius is one which subjects the passengers to 0.08 in the outward direction, however, some margin must be maintained in case the vehicle exceeds the design speed. Note from Figure 4-112 that the allowable variation in vehicle speed for a 10° bank angle is much greater than for 24.6°. Using 10° as the nominal guideway bank angle, the minimum turn radius for a speed of 134 m/s (300 mph) is approximately 7.6 km (25,000 ft). Even larger radii are required for a transition to a grade change (vertical curvature). These large horizontal and vertical radii will require careful selection of the roadbed site in order to minimize the right-of-way requirements and the amount of earthwork required.

Transition to a horizontal or vertical radius of curvature will consist of a cubic or spiral section so as not to exceed the jerk requirements. These transition sections will be approximately 670-800 m long (2200-2600 ft) or greater for cruise conditions (Ref. 4-64). Additional discussion of transition and grade requirements is given in Section 4.3.2.

4.6   REFERENCES

4-1   Meisenholder, S. G., McGinnis, N. F. and Graham, H. R., "Suspended Vehicle Systems (SVS); Volume I, System Engineering Studies," TRW, FRA-ORD&D-74-7, March 1974.

4-2   Bruhn, E. F., <u>Analysis and Design of Flight Vehicle Structures</u>, Tri-State Offset Co., Cincinnati, Ohio, 1965.

4-3   <u>Metallic Materials and Elements for Aerospace Structures</u>, MIL-HDBK-5B, Department of Defense, September 1, 1971.
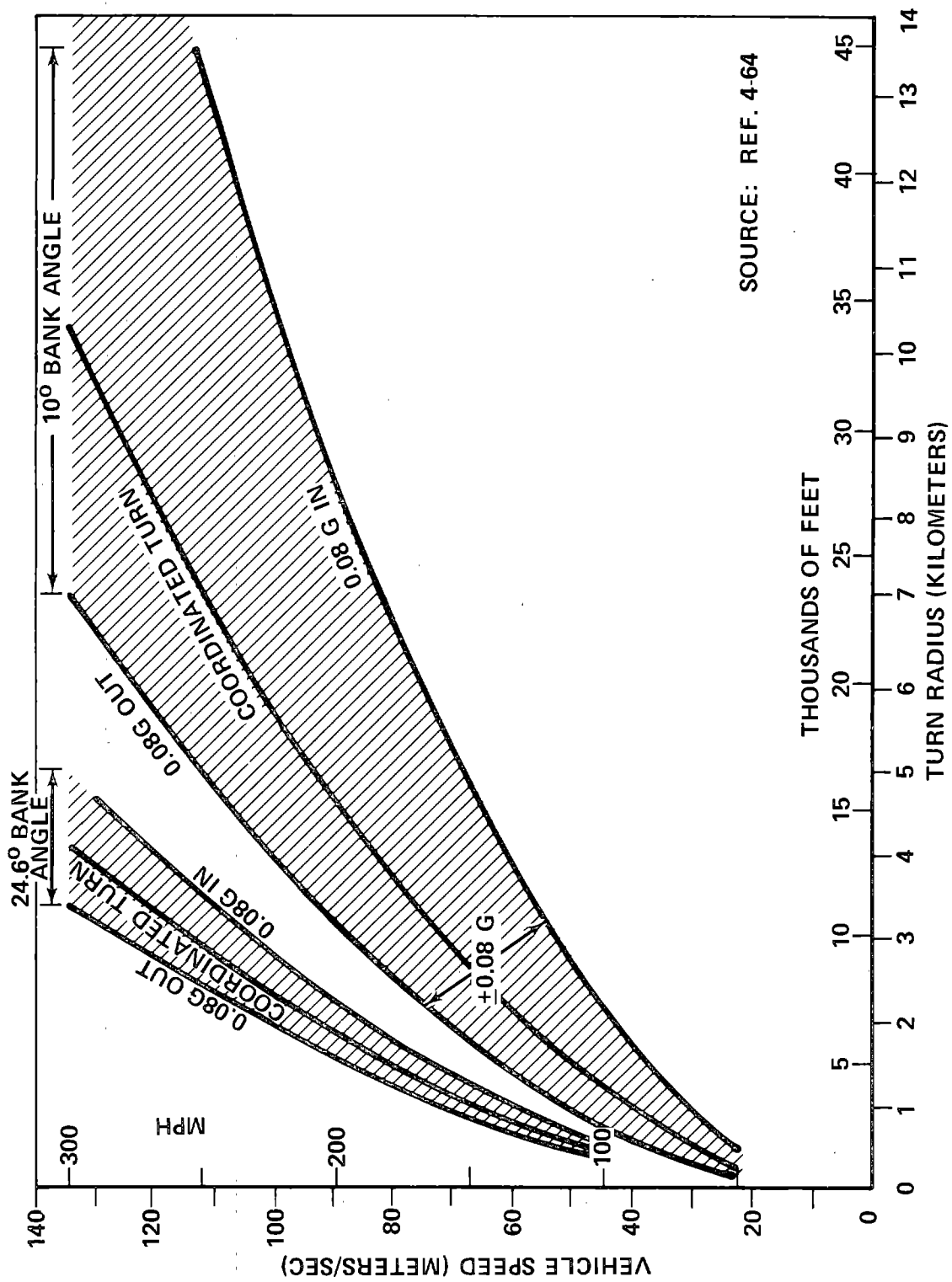
FIGURE 4-112. MINIMUM RADIUS OF CURVATURE TO SATISFY LATERAL
ACCELERATION CRITERION

SOURCE: REF. 4-64

4-4   Shanley, F. R., Weight-Strength Analysis of Aircraft Structures, Dover
      Publications, New York, 1960.

4-5   Burns, M. P., "Aerodynamic Analysis for the MAGLEV Revenue Vehicle,"
      Philco-Ford TMLV Technical Report 0026, 16 Oct. 1974.

4-6   Grunwald, K. J., "Aerodynamic Characteristics of Vehicle Bodies at Cross-
      wind Conditions in Ground Proximity," NASA TN D-5935, August 1970.

4-7   Bowman, W. D., "The Present Status of Automobile Aerodynamics in Automobile
      Engineering and Development," Proceedings of the AIAA Symposium on
      The Aerodynamics of Sports and Competition Autombiles, 20 April 1968.

4-8   Ruetenik, J.R. and Zartarian, G., "Development of Methods for Predicting
      Airloads on TACV Configurations Due to Strong Crosswind Gusts," Report
      No. DOT-TSC-171-1, March 1972.

4-9   Bowman, W. D., "Generalizations on the Aerodynamic Characteristics of Sedan
      Type Automobile Bodies", SAE Report 660389, 10 June 1966.

4-10 Tracked Hovercraft Ltd., "A Cost Comparison of Three Tracked Air Cushion
      Vehicle Configurations," Appendix B, NTIS Report No. PB 197501,
      July 1970.

4-11 Beauvais, F. N., Tignor, S. C., Turner, T. R., "Problems of Ground
      Simulation in Automotive Aerodynamics," SAE Report 680121,
      12 January 1968.

4-12 Hara, T., Kawaguti, M., Fukuchi, G., and Yamamoto, A., "Aerodynamics of
      High Speed Trains," IR. C.A.-UIC, High Speeds Symposium (Vienna), 1968.

4-13 "Aerodynamics of High-Speed Ground Transportation Vehicles," Appendix B
      of "Supporting Studies for HSGT System Reports," TRW, PB 193114, June 1970.

4-14 Hammitt, A. G., The Aerodynamics of High Speed Ground Transportation,
      Western Periodicals Co., 1973.

4-15 Kurtz, D. W., and Dayman, B., "The Importance of Aerodynamics in the
      Design of Intra-Urban Trains Traveling in Tunnels," High-Speed Ground
      Transportation Journal, Vol. 7, No. 3, 1973.

4-16 "Far Field Aerodynamic Noise Measurement Program," Lockheed-California
      Report LR 23640, June 1970.

4-17   Ward, E. J., "Noise in Ground Transportation," _Journal of High-Speed Ground Transportation_, Vol. 7, No. 3, pp. 297-306, Fall 1973.

4-18   "High-Speed Ground Transportation Alternatives Study," Office of the Assistant Secretary for Policy and International Affairs (DOT/TPI), U.S. Dept. of Transportation, TPI-13, (PB 220079), June 1973.

4-19   Internoise 1972 Proceedings, Washington, D.C., 4-6 October 1972.

4-20   Johnson, R. A., "Aerodynamic Drag and Stability Characteristics of a Magnetically Levitated Vehicle," AVSD-0391-72-CR, AVCO Systems Division, Wilmington, Mass., 1 November 1972.

4-21   "High Speed Ground Transportation Systems Engineering Study," TRW, Rept. FRA-RT-70-36, February 1970.

4-22   Reitz, J. R., Borcherts, R. H., Davis, L. C., Hunt, T. K., Wilkie, D. F., "Preliminary Design Studies of Magnetic Suspension for High Speed Ground Transportation," U.S. Dept. of Transportation Report FRA-RT-73-27, PB 223237, March 1973.

4-23   Stekly, Z, J. J., deWinter, T. A., Vitkevich, J. A., Tarrh, J. M., and Emanuel, A. E., "Design Study of Superconducting Magnetic Levitation Pads," Magnetic Corp. of America Report MCA-TP 124, 1972.

4-24   1974 Applied Superconductivity Conference, Oakbrook, Illinois, Sept. 30-Oct. 2, 1974. See papers by T. Fields, J. L. Smith, and A. Appleton.

4-25   "Cryogenic Materials Data Handbook" and Supplements; AD 609562, AD 679087, AD 618065, AD 611165, and AD 633388.

4-26   Ishizaki, Y., Kuroda, R., and Ohtsuka, T., "Sealed Cryostat System for Magnetically Levitated Vehicles," ICEC-5 Kyoto, Japan, May 1974; and Ohno, E., Iwamoto, M., Ogino, O., and Kawamara, T., "Development of Superconducting Magnets for Magnetically Levitated Trains," ICEC-5, Kyoto, May 1974.

4-27   Coffey, H. T., Colton, J. D., Solinsky, J.C., and Woodbury, J. R., "An Evaluation of the Dynamics of a Magnetically Levitated Vehicle," U.S. Department of Transportation Report FRA-ORD&D-74-41, March 1974.

4-28   Helms, H. E., "Quiet Clean STOL Experimental Engine Study Program," Detroit Diesel Allison Rept. EDR 7543, September 1972.

4-29 Doyle, T. J., "Superconductive Propulsion Motor Development at NSRDC," Naval Ship Research and Development Center, Annapolis, Md., August 1974.

4-30 "Linear Induction Motor Propulsion System for Philco-Ford's Repulsion MAGLEV Vehicle," Garrett AiResearch Mfg. Co., Rept. 74-10672, Rev. 1, 28 August 1974.

4-31 Elliott, D. G., "Single-Sided Induction Motor for a Repulsion MAGLEV Vehicle," JPL Letter Report No. 24, October 1974.

4-32 Tang, C. H. and Harrold, W. J., "Linear Synchronous Motor Studies, Final Report," (for Philco-Ford) Raytheon Co., ER 74-4420, December 1974 (see Appendix F of this report).

4-33 "Report on a Study of the Magneplane Power System and Guideway," United Engineers and Constructors, Inc., June 1973 (MIT P.O. ML-46235, Prime Contract NSF-C670).

4-34 Davis, L. C. and Borcherts, R.H., "Superconducting Paddlewheels, Screws, and Other Propulsion Units for High Speed Ground Transportation," J. Appl. Phys. Vol. 44, P. 3294, 1973.

4-35 "Research, Development, Test, and Evaluation of Material for Extreme Climatic Conditions," U.S. Army Regulation AR 70-38, effective 1 July 1969.

4-36 Baumeister, T., Standard Handbook for Mechanical Engineers, McGraw-Hill, 7th ed., 1967.

4-37 Alcoa Handbook of Design Stresses for Aluminum, Aluminum Co. of America, 1966.

4-38 Shanley, F. R., Strength of Materials, McGraw-Hill, 1957.

4-39 Williams, J. G., Haight, E. C., Hutchens, W. A., "Compressive Behavior of a Linear Induction Motor Reaction Rail," ASME Paper No. 73-ICT-159, September 1973.

4-40 Wilson, J. F., "Dynamics of Soil-Supported Guideways with Thermal and Air Cushion Vehicle Loading," ASME Paper 73-ICT-28, presented at the Intersociety Conference on Transportation, Denver, Colo., September 1973.

4-41 Katz, R. M., Nene, V. D., Ravera, R. J. and Shalski, C.A., "Performances of Magnetic Suspensions of High-Speed Vehicles Operating Over Flexible Guideways," Trans. ASME Journal of Dynamic Systems, Measurement and Control, Vol. 96, Series G, No. 2, pp. 204-212, June 1974.

4-42 Birkeland, P. W., Meisenholder, S. G., McCullough, B. F. and Oye, J., "Investigation of Reduced Cost Guideway Designs for the Tracked Air Cushion Research Vehicle," (advanced copy), TRW Systems, ABAM Engineers; TRW Report No. 96030-L003-0, Redondo Beach, Ca., December 1972.

4-43 Houbolt, J. C., "Runway Roughness Studies in the Aeronautical Field," Journal of the Air Transport Division--Proceedings of the ASCE, Vol. 127, pp. 427-448, 1962.

4-44 Walls, J. H., Houbolt, J. C. and Press, H., "Some Measurements and Power Spectra of Runway Roughness," NACA TN 3305, Langley Aeronautical Laboratory, November 1954.

4-45 Thompson, W. C., "Measurements and Power Spectra of Runway Roughness at Airports in Countries of the North Atlantic Treaty Organization," NACA TN 4303, Langley Aeronautical Laboratory, July 1958.

4-46 Hall, A. W., Hunter, P. A. and Morris, G. J., "Status of Research on Runway Roughness," NASA Aircraft Safety and Operating Problems, Volume 1, Langley Research Center, NASA SP-270, 1971.

4-47 Holman, J. P., Experimental Methods for Engineers, McGraw-Hill, 1966.

4-48 "Standard Specifications," State of California, Business and Transportation Agency, Department of Public Works, Division of Highways, January 1973.

4-49 "Slip-Form Paving; Portland Cement Concrete," Advisory Circular AC No. 150/5370-9; Department of Transportation, Federal Aviation Agency; 7 June 1973.

4-50 Birkeland, P. W., Magura, D. C., McCullough, B. F., Meisenholder, S. G. and Weidlinger, P., "Investigation of Low-Cost Guideway Concepts for Tracked Air Cushion Vehicles," TRW, TRW Systems, ABAM Engineers, TRW Report 96030-L009-0; Draft dated May 1973.

4-51 Pulgrano, L., "Tracked Air Cushion Research Vehicle -- Vehicle/Guideway Dynamics Analysis," Grumman Aerospace Corporation, Bethpage, New York, Technical Report No. PMT-B4-R71-07, 1971.

4-52 "A Cost Comparison of Three Air Cushion Revenue Configuration," Tracked Hovercraft Ltd., PB 197501, July 1970.

4-53 "A Preliminary Design Study of a Tracked Air Cushion Research Vehicle. Volume II, Guideway Study Report," Aeroglide Systems, Inc., New York, PB 183320, December 1968.

4-54 "Elevated Guideway Structures," TRW Systems Group, DOT Report No. FRA-RT-70-35, PB 191670, December 1969.

4-55 "Elevated Structures - Continuous Beams," TRW Systems Group, DOT Report No. FRA-RT-71-54, PB 194371, June 1970.

4-56 Kaplan, A., Lipner, N., Roberts, F. B., and Strom, R. O., "Train Elevated Guideway Interactions," TRW Systems Group, DOT Report No. FRA-RT-70-23, PB 190635, February 1970.

4-57 Lipner, N., Evensen, D. A., and Kaplan, A., "Dynamic Response of Continuous Beam Elevated Guideways. Volume I - Analysis," TRW Systems Group, DOT Report No. FRA-RT-71-42, PB 194137, July 1970.

4-58 Soux, A. L., "Train/Elevated Guideway Parametric Investigation," TRW Systems Group, TRW Report No. 06818-W018-R0-00, PB 194039, July 1970.

4-59 Chiu, W. S., Wormley, D. S., Smith, R. C., Richardson, H. H., "Coupled Dynamic Interactions Between High Speed Ground Transportation Vehicles and Discretely Supported Guideways," Massachusetts Institute of Technology, DOT Report No. FRA-RT-71-76, PB 199136, July 1970.

4-60 Chiu, W., Smith, R., and Wormley, D., "Influence of Vehicle and Distributed Guideway Parameters on High Speed Vehicle - Guideway Dynamic Interactions," Journal of Dynamic Systems, Measurement, and Control, Vol. 93, No. 1, pp 25 - 35, March 1971.

4-61 Wilson, J. F., "Dynamic Interactions Between Moving Loads and Their Supporting Structures, with Application to Air Cushion Vehicle - Guideway Design," Duke University, DOT Report No. FRA-RT-72-27, PB 205325, September 1971.

4-265

4-62   Biggers, S. B. and Wilson, J. F., "Dynamic Interactions of High Speed
        Tracked Air Cushion Vehicles with Their Guideways." Part I of a
        Parametric Study, Trans. ASME <u>Journal of Dynamic Systems, Measurement
        and Control</u>, Series G, Vol. 95, No. 1, pp 76 - 91, March 1973.

4-63   Richardson, H. H., and Wormley, D.N., "The Coupled Dynamics of Trans-
        portation Vehicles and Beam-Type Elevated Guideways," <u>Surveys of Research
        in Transportation Technology</u>, AMD Vol. 5, ASME, New York, 1973.

4-64   Walston, T. C., Graham, H. R., and Dietrich, W. H., "Operational
        Potential of Suspended Vehicle Systems (SVS)", Final Report, TRW,
        Report FRA-ORD&D-74-7B, July 1973.

SECTION 5

SYSTEM ANALYSIS

This section summarizes the results of a system analysis conducted as part
of the Task I TMLV effort. The primary objective of this analysis is to estab-
lish a simple economic model for preliminary evaluation of MAGLEV systems
employing the Repulsion principle. Major system parameters are identified and
traded off on the basis of cost and/or performance.

5.1 SYSTEM MODEL

A corridor-type system is selected to facilitate performance analysis.
The route characteristics are derived from those of the Northeast and California
corridors as given in Ref. 5-1. The vehicle and guideway characteristics are
derived from the data presented in preceding sections of this report.

Detailed cost data for the suspension subsystem and guideway construction
are given in Section 6.

Cost data for all vehicle subsystems, including propulsion, are derived on
this program and summarized in this section. United Aircraft Research Labora-
tories contributed cost data in support of this effort. Cost data for the
remaining elements of the system are derived from Refs. 5-1, 5-2, and 5-3.

5.2 ROUTE CHARACTERISTICS

A 750 km (466 mi.) linear, double track system is selected as described in
Section 3. For computation of vehicle performance during intra-city operation,
it is assumed that deceleration, switching, station dwell and acceleration take
place as described in Section 4.4 for the baseline Ducted Fan/Gas Turbine
vehicle. Between the cities, 10% of the route (75 km) is assumed to be at 2%
grade with a headwind of 13.4 m/s (30 mph), with the remainder of the inter-
city distance corresponding to level, no-wind operation at cruise speed.

5.2.1 Transit Performance

Figure 5-1 shows the influence of the number of equidistant, intermediate stops (N_i) on average speed and elapsed transit time (τ) for the baseline 80-seat vehicle at a cruise speed of 134 m/s (300 mph). Figure 5-2 shows the transit time as a function of cruise speed, for both $N_i = 0$ (the express case) as well as $N_i = 5$. For all analyses reported in subsequent paragraphs of this report, the baseline mission profile corresponds to the case where $N_i = 5$. For this profile, the transit time is 120 min. and the average speed is 104 m/s (233 mph).

5.2.2 System Capacity

The appropriate capacity equations for operation 16 hr/day, on a double-track at 60% load factor are as follows:

A. Number of Passenger-km Per Year, N_{PKY}

$$N_{PKY} = 3.154 \times 10^8 \, N_{ST}/\Delta t \qquad\qquad 5\text{-}1$$

where N_{ST} = Number of Seats/Train = $N_{SV} \times N_{VT}$

      N_{SV} = Number of Seats/Vehicle

      N_{VT} = Number of Vehicles/Train

      Δt = Headway, Min.

B. Number of Passengers Per hour, N_{PH}

$$N_{PH} = 72 \, N_{ST}/\Delta t \qquad\qquad 5\text{-}2$$

C. Number of Passengers Per Year, N_{PY}

$$N_{PY} = 4.205 \times 10^5 \, N_{ST}/\Delta t \qquad\qquad 5\text{-}3$$

D. Number of Vehicles Required, N_V

$$N_V = 2 \, \tau/\Delta t = 6.341 \times 10^{-9} \left(\frac{N_{PKY}}{N_{SV}}\right) \qquad\qquad 5\text{-}4$$

where τ = Time to Transit 750 km, min.

Figure 5-3 shows the influence of headway and train size on passenger capacity and offers a number of interesting observations. For example, the headway limit sets the maximum capacity of the system and is determined by safety considerations. Safety considerations are, in turn, influenced by
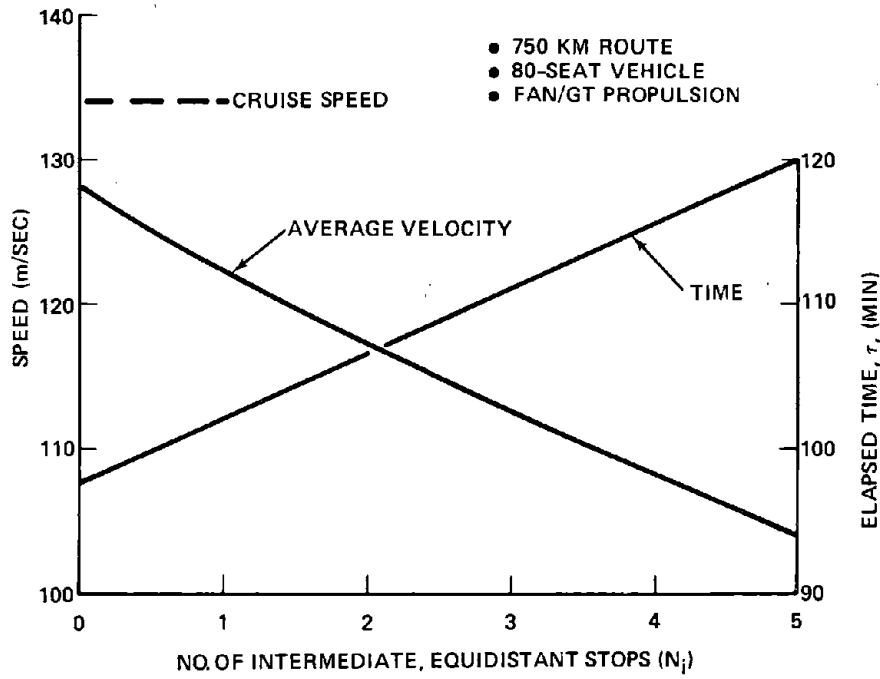
FIGURE 5-1. TRANSIT CHARACTERISTICS
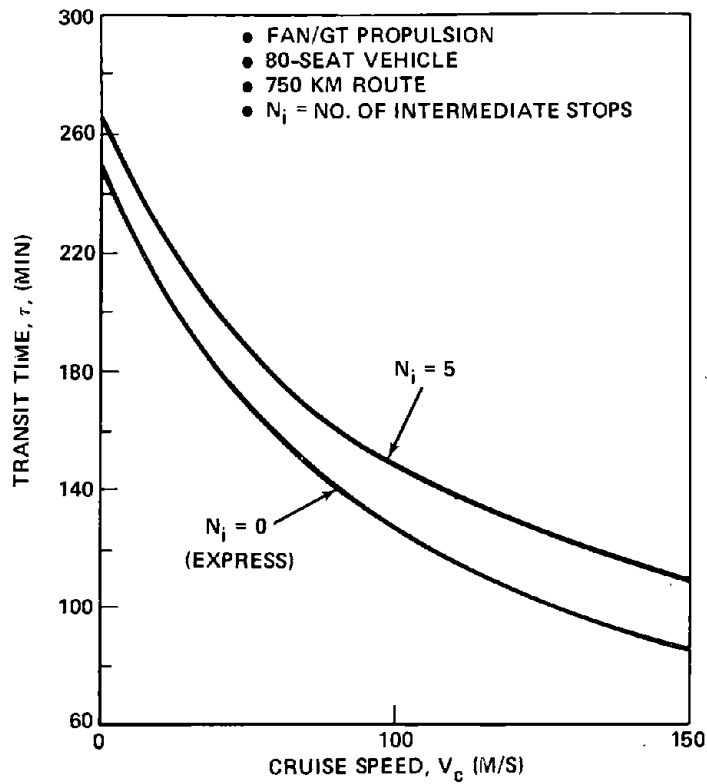
FIGURE 5-2. ONE-WAY TRANSIT TIME
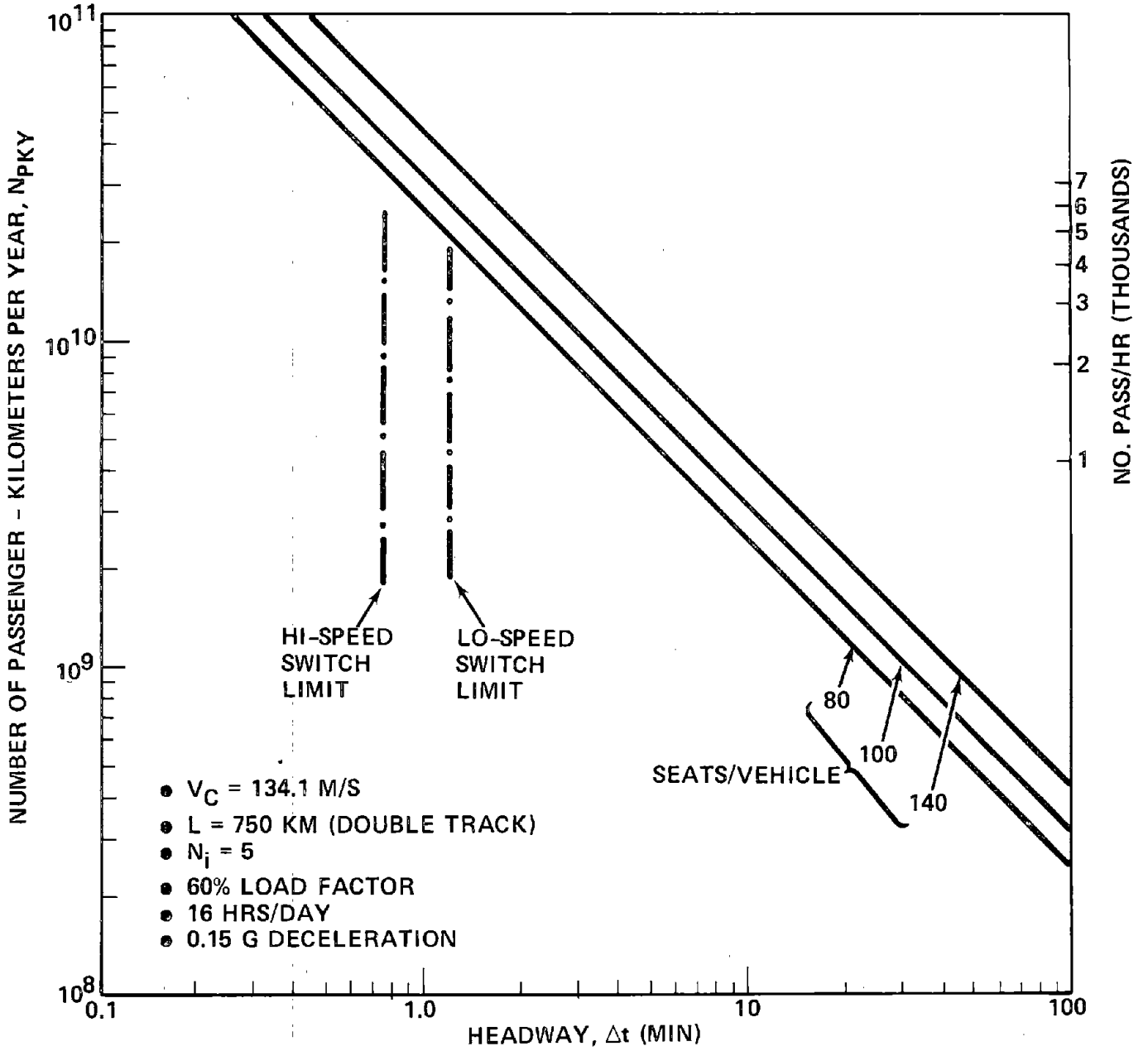
FIGURE 5-3. SYSTEM CAPACITY

switch operations, deceleration capability, station dwell time and overall
system reaction/communication time. If a high-speed switch is employed, i.e.,
where a vehicle does not slow down to transit off the main line, the minimum
headway limit is essentially determined by the distance required to come to a
stop in order to avoid collision with an obstacle (or another vehicle) on the
track. For 0.15 g deceleration from 134 m/s, this distance is 6.115 km
(3.8 mi), corresponding to 45.6 sec (0.76 min.) separation between vehicles at
134 m/s and neglecting system reaction time.

If a low-speed switch is employed, i.e., where a vehicle must decelerate
at 0.15 g to engage the switch, the required separation distance for the
trailing vehicle increases to 9.79 km (6.08 mi) corresponding to 73 sec
(1.22 min.) spacing at 134 m/s. The station dwell time, however, is estimated
to be 120 sec (2 min.) to allow for passenger loading/unloading. It is thus
unlikely that the headway will be less than two minutes, in which case there
appears to be no advantage of a high-speed switch from the standpoint of capac-
ity. Of course, actual operation will probably entail a mix of express and
local vehicles, requiring a more complex analysis than the simple example given
here. For system analysis purposes, however, it is assumed herein that minimum
headway for 134 m/s operation is two minutes.

At this headway and a load factor of 60%, the system with 80-seat vehicles
can handle 2880 passengers per hour (2-way operation) corresponding to 16.82×10^6
passengers per year and 1.262×10^{10} passenger-km per year. The system with
140-seat vehicles comes closest to meeting NEC projections, because it can handle
5040 passengers per hour at 60% load factor, corresponding to 29.43×10^6 pas-
sengers per year and 2.21×10^{10} passenger-km per year. As shown in subsequent
paragraphs, the larger vehicle offers significant reduction in cost per
passenger-km (as well as reduced energy intensity as shown in Section 4.2).

For headways larger than two minutes, or for peak capacities above 5040
passengers per hour, it will be necessary to couple at least two vehicles
together. As shown in Section 4.4, this results in a more favorable energy
intensity; however the consequences to the dynamic interaction between coaches
are unknown at this time.

Figure 5-4 shows the influence of passenger handling capacity, headway and vehicle size on the number of vehicles required in the system. Note that 120 vehicles are required for two minute headway. Figure 5-5 shows the influence of cruise speed on the number of 80-seat vehicles required. It is obvious that one significant advantage of a high-speed system is the substantial reduction in the number of vehicles required. Figure 5-6 shows the added capacity associated with coupling vehicles together.

5.3 VEHICLE/GUIDEWAY CHARACTERISTICS

Baseline vehicle physical characteristics are given in Section 4. In Section 4.2, a matrix of vehicles is synthesized to determine the influence of seating arrangement and capacity (from 80 to 140 seats) on energy intensity; all vehicles have the Ducted Fan/Gas Turbine propulsion system and operate at 134 m/s cruise speed over the baseline 750 km route. For systems analysis purposes, only the minimum energy design points from this matrix are considered. Vehicle physical parameters for these design points are given in Table 5-1. Table 5-1 also shows the amount of gas turbine (JP) fuel consumed and the associated energy intensity for the baseline route. Table 5-2 presents a weight breakout of the major vehicle components for the aforementioned vehicles.

5.3.1 Variable Cruise Speed Vehicles

To ascertain the influence of cruise speed on system performance and cost, additional syntheses were carried out for the 80- and 140-seat configurations. At each cruise speed, the propulsion system was sized to provide approximately the same rate of acceleration as achieved with the 134 m/s system. Fan diameter was held constant and the propulsive efficiency calculated and compared with 134 m/s figures. Propulsive efficiency, gross weight, fuel weight consumed, and energy intensity are given in Table 5-3 as a function of cruise speed. Note that more detailed analysis will be required to optimize the propulsion system at speeds substantially different from 134 m/s. This will undoubtedly entail varying fan diameter and performing tradeoffs relative to noise generation, studies beyond the scope of this effort. Nevertheless, the approximate technique used here is probably representative and certainly more realistic than analyses based only on steady-state conditions.
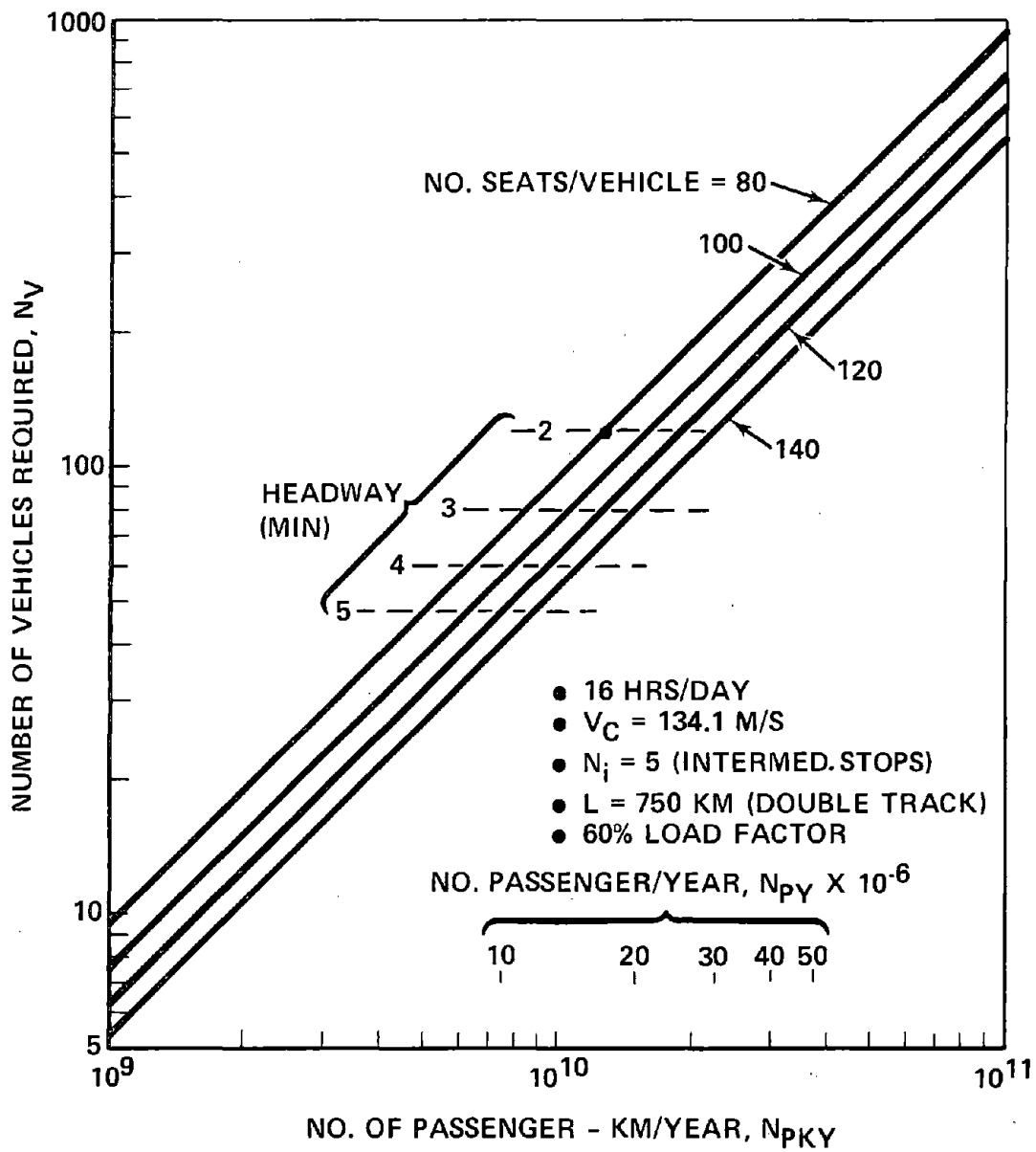
FIGURE 5-4. VEHICLE/SIZE REQUIREMENTS
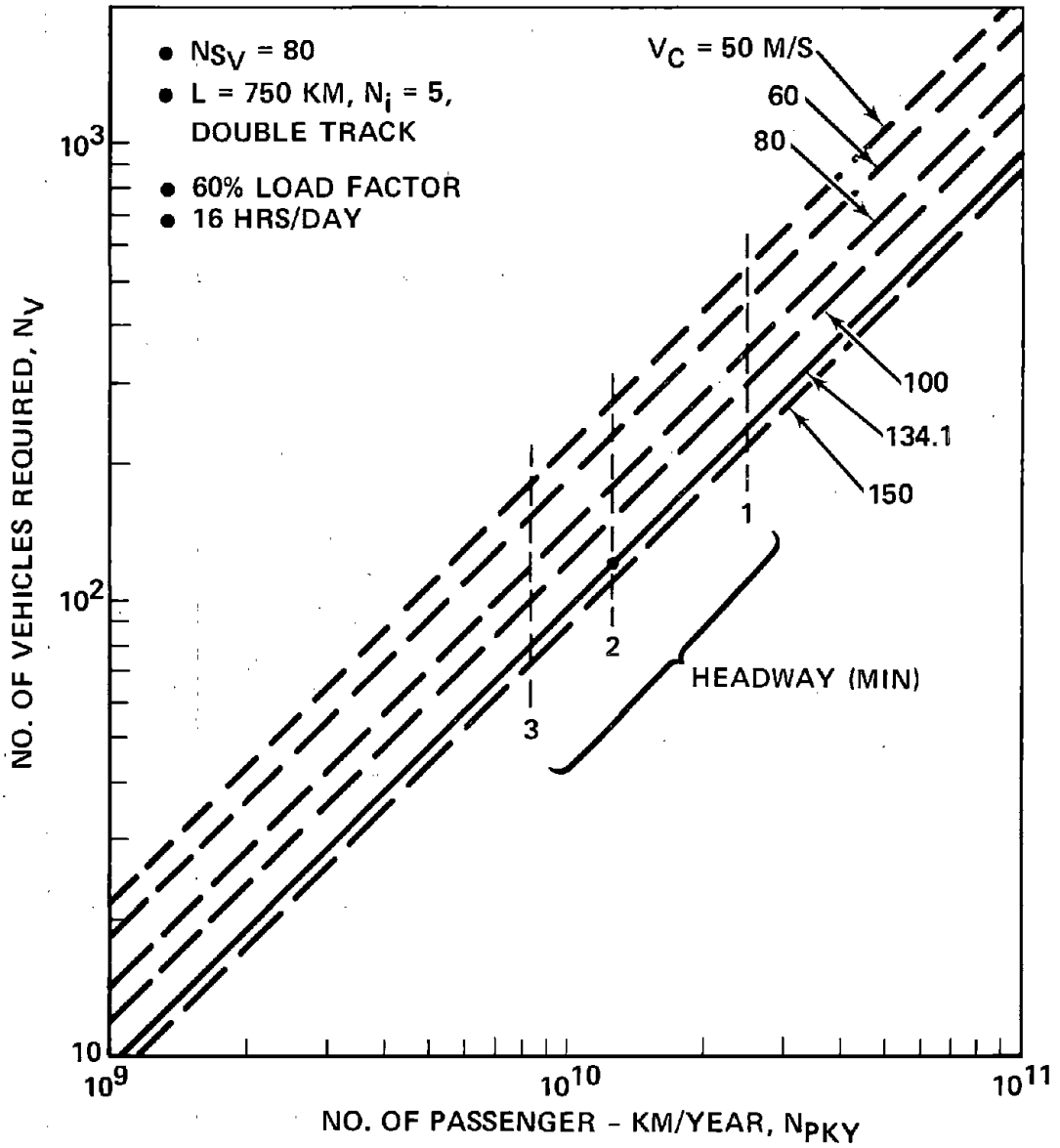
FIGURE 5-5. VEHICLE/SPEED REQUIREMENTS
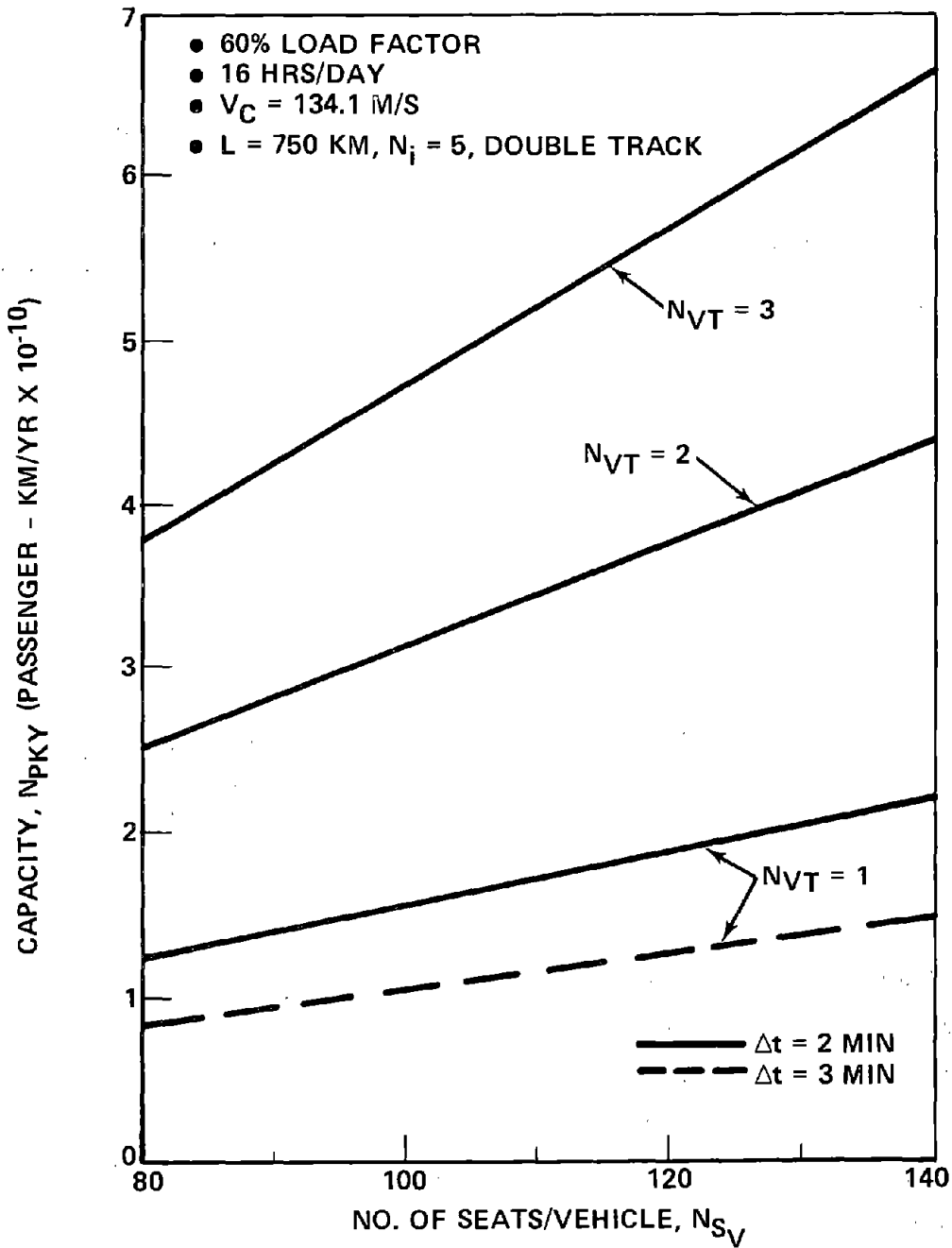
FIGURE 5-6. COUPLED VEHICLE CAPACITY

TABLE 5-1. VEHICLE PHYSICAL PARAMETERS[1]

PARAMETER	NO. SEATS/VEHICLE			
	80	100	120	140
SEATING ARRANGEMENT	2 + 2	2 + 3	2 + 3	2 + 3
HEIGHT (M)	3.454	3.454	3.454	3.454
WIDTH (M)	2.94	3.454	3.454	3.454
LENGTH (M)	33.67	33.6	39.1	42.9
FUEL WEIGHT[2] (kN)	29.7	33.4	37.6	39.3
ENERGY INTENSITY $\left(\frac{MJ}{SEAT\text{-}KM}\right)$	2.18	1.96	1.84	1.65

[1] FOR 134.1 M/S (300 MPH) CRUISE VELOCITY
[2] CONSUMED PER 750 KM, 5 INTERMEDIATE STOP TRANSIT

TABLE 5-2. VECHICLE WEIGHT BREAKOUT[1]

SYSTEM	NO. SEATS/VEHICLE			
	80	100	120	140
SUSPENSION	66.8 kN	68.2 kN	70.9 kN	73.4 kN
STRUCTURE[2]	53.4	41.8	51.9	59.9
FURNISHINGS	24.5	30.5	36.8	42.4
AUXILIARIES	21	26.2	31.5	36.7
PAYLOAD	71	89.9	109.9	129.7
BRAKES	20.2	21.3	23.9	25.9
PROPULSION[3]	80.6	87.1	94.1	100
OTHER[4]	29	29	29	29
GROSS WEIGHT	366.5 kN	394.0 kN	448.0 kN	497.0 kN

[1] FOR 134 M/S (300 MPH) CRUISE VELOCITY
[2] STRUCTURE WEIGHT IS LEAST FOR 100 SEAT VEHICLE DUE TO INCREASED STIFFNESS OF WIDER CROSS SECTION (SEE SECTION 4.2.6)
[3] INCLUDES FUELWEIGHT WITH 15 PERCENT RESERVE
[4] INCLUDES CREW COMPT AT 15.6 kN AND CONTINGENCY AT 13.4 kN

TABLE 5-3. VARIABLE CRUISE SPEED DESIGNS

CRUISE SPEED (M/S)	50	60	80	100	120	134	150
PROPULSIVE EFFICIENCY[1]	0.711	0.838	0.992	1.044	1.03	1.00	0.96
80 PASSENGER VEHICLE (NS$_V$ = 80)							
• GROSS WEIGHT (kN)	341.8	335.1	332.3	338.6	351.8	366.5	386
• FUEL WEIGHT[2] (kN)	24.6	19.9	17.2	19.1	23.9	29.7	36.5
• ENERGY INTENSITY $\left(\dfrac{MJ}{SEAT\text{-}KM}\right)$	1.81	1.46	1.26	1.40	1.76	2.18	2.68
140 PASSENGER VEHICLE (NS$_V$ = 140)							
• GROSS WEIGHT (kN)	464.7	454.8	451.6	457.9	475.3	497	521.9
• FUEL WEIGHT[2] (kN)	33.1	26.7	23.6	25.2	31.7	39.3	51.6
• ENERGY INTENSITY $\left(\dfrac{MJ}{SEAT\text{-}KM}\right)$	1.39	1.12	0.99	1.06	1.33	1.65	2.17

[1] RELATIVE TO SYSTEM AT 134 M/S
[2] CONSUMED PER 750 KM, 5 INTERMEDIATE STOP TRANSIT

5.3.2 Magnetic Performance

Levitation and guidance is achieved with at least four* superconducting magnets at fore and aft stations on the vehicle. At 134 m/s these magnets suspend the vehicle approximately 0.3 m above the aluminum guideway elements arranged in the baseline hat-shape, as a U-channel, or some other possible configuration.

The achievable magnetic lift-drag ratio is shown in Figure 5-7 as a function of speed and the type of aluminum used. The 90° corner results are compared with those of the infinite plate, showing that: (1) the requirement for guidance introduces significant increase in magnetic drag, and (2) the use of nearly pure (1100-H14) aluminum offers significant decrease in drag compared with an alloy (6061-T6). On this basis, it is concluded that the guideway should be carefully designed to permit the use of pure aluminum, particularly since it is no more expensive** than the alloy in quantity use. In view of the thermal stress problems with the pure material, it is necessary that transverse gaps be provided to permit expansion and contraction of the aluminum plates. (See Sections 4.3 and 4.5 for detailed discussion of gap effects).

Figures 5-8, 5-9, and 5-10 present additional performance data on the effect of magnet dimensions and aluminum plate thickness on lift-drag ratio. It is clear from these figures that the 0.5 x 3 m magnet configuration offers good performance, as does the 2.54 cm (1 inch) aluminum plate thickness. Cost tradeoffs on plate thickness are given in subsequent paragraphs. The resultant drag/speed curves are given in Section 4.4; the combination of aerodynamic drag and magnetic drag is unique to the Repulsion Concept and clearly shows that repulsion is not well suited for low-speed operations, e.g., below ~ 60 m/s (134 mph). The drag curves also show that for single vehicle operation, aerodynamic drag is much larger than magnetic drag despite the presumption of a

---

*As pointed out in Section 4-3, eight magnets are used, primarily for redundancy; each pair, however, is arranged so that performance is essentially equal to a single magnet of twice the length.

**According to Kaiser Aluminum, the mass of aluminum required (~ 3 x 10^8 kg) for a 750 km double track system is such that the cold-worked pure material would be cheaper and more readily available than the heat-treated alloy because of heat treatment facility limitations.
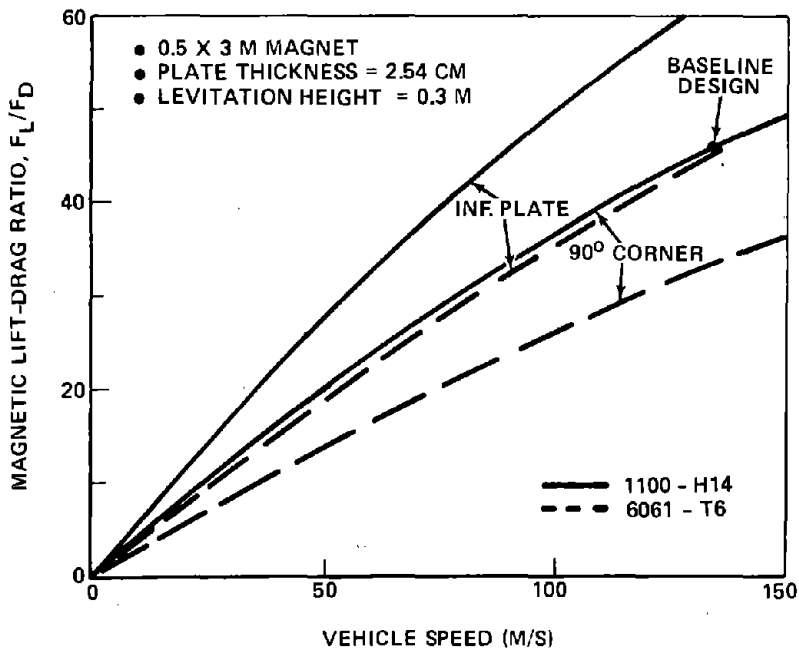
FIGURE 5-7. MAGNETIC PERFORMANCE
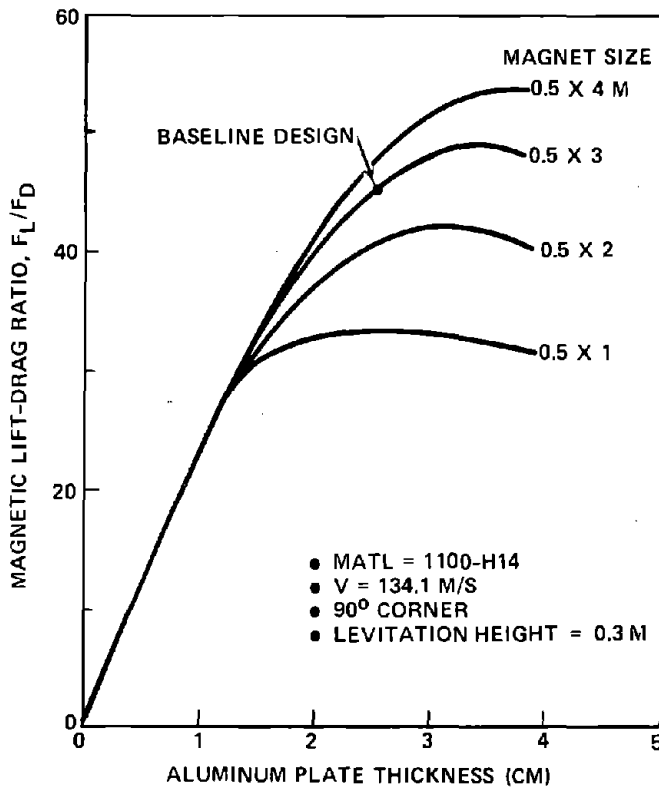
FIGURE 5-8. EFFECT OF PLATE THICKNESS

5-13
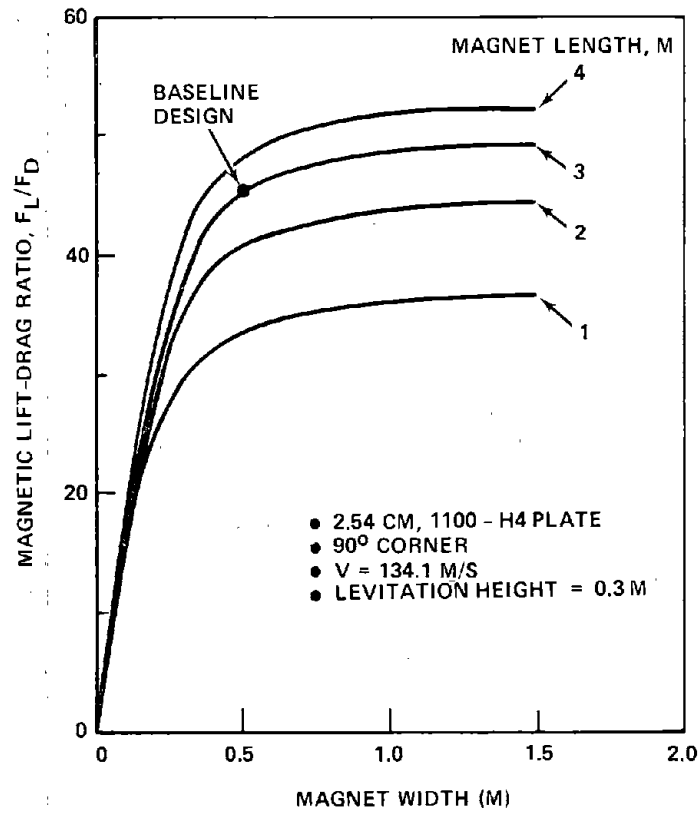
FIGURE 5-9. EFFECT OF MAGNET WIDTH
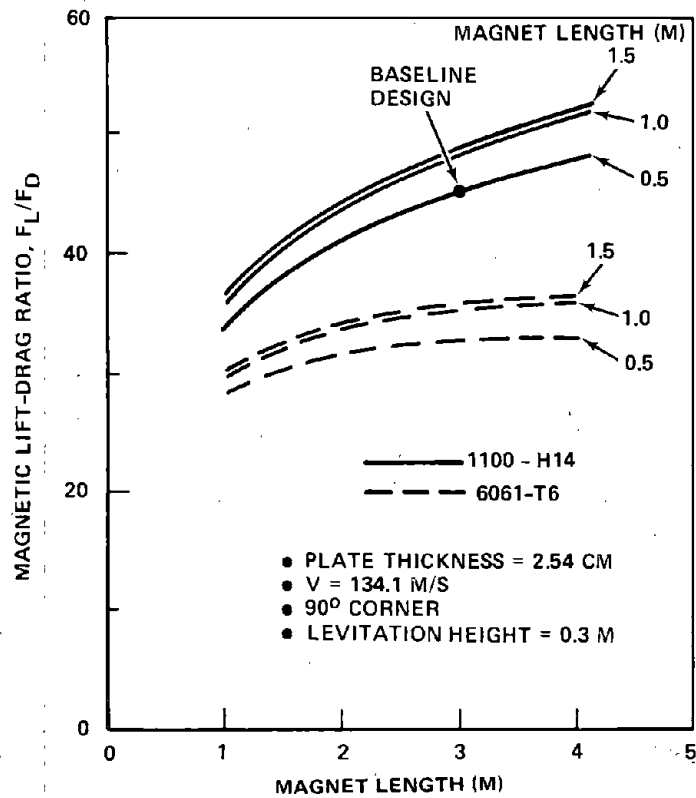
FIGURE 5-10. EFFECT OF MAGNET LENGTH

fairly "clean" vehicle configuration. Thus, in order to reduce the overall energy consumption of the system, major effort should be expended in reducing aerodynamic drag.

5.4 COST ANALYSIS

A simplified cost model is devised, based primarily on the approach and data given in Ref. 5-1 and 5-2. A semi-government type of corporation is envisioned to acquire and run the system; this conveniently permits the question of taxation to be ignored. As in Ref. 5-1, the useful life of the guideway and facilities is assumed to be 25 years, the vehicle's life to be 14 years, and capital is assumed acquired at a 10% interest rate. All cost elements are reduced to cents per passenger-km to facilitate comparative analysis.

5.4.1 Generalized Cost Data

Costs are identified in three broad categories: (1) Investment Costs (IC), (2) Direct Operating Costs (DOC) and (3) Indirect Operating Costs (IOC). The Investment Costs consist of the guideway (including land acquisition, guideway construction, route preparation, guideway equipment* and electrification, where appropriate), the vehicles, and facilities (including yards, shops, terminals, and communications equipment). The DOC consists of fuel, crew, and maintenance (both vehicle and guideway maintenance) costs as well as terminal operations costs. The IOC are those incurred in providing services but not directly related to vehicle operation. Refs. 5-1 and 5-3 differ significantly on the magnitude of these costs, particularly as to the influence of intercity distance; for this analysis, IOC are assumed constant at ~ 0.5¢/passenger-km. All other system costs are identified below.

    A.   Investment Costs (IC)

        (1) Guideway-Related

            a. Land Acquisition. Average land acquisition costs for both the Northeast and California corridors are given in Ref. 5-1. After adjusting these data for right-of-way width (from 61 m to 47 m) and 1974 dollars, the appropriate figures are as follows.

---

*Foreign object detection equipment, communications, trip identification loop, etc.

- Northeast corridor ~ $58,000/acre
- California corridor ~ $15,000/acre

An average cost of $30,000/acre is assumed for the baseline route used in this report.

b. <u>At-Grade Guideway</u>. The basic hat-shape configuration at-grade guideway cost is broken out in Table 5-4. Total cost with 2.54 cm thick aluminum levitation-guidance elements is estimated at $2,024,000/km ($3,257,000/mi), exclusive of the special equipment and/or electrification presented below in paragraph f. Detailed back-up of the basic at-grade guideway cost is given in Section 6.

c. <u>Elevated Guideway</u>. The basic hat-shape configuration elevated guideway cost is broken out in Table 5-5. Total cost with the 31.5 m right-of-way is $3,676,000/km ($5,916,000/mi) with spread footings and $3,964,000/km ($6,379,000/mi) with pile footings. The girders are fabricated of prestressed concrete in the twin-T shape* and the aluminum levitation-guidance elements are 2.54 cm thick. Detailed backup of the basic elevated guideway cost is given in Section 6.

d. <u>Bridges and Tunnels</u>. Ref. 5-1 is the basis for cost estimates on bridges and tunnels. With adjustment for 1974 dollars, the figures are:

- Bridges ~ $7,840,000/km (double track)
- Tunnels ~ $23,000,000/km (double tube)

Note that the bridge figure includes land acquisition costs.

e. <u>Overall Guideway Mix</u>. The guideway mix is assumed the same as that for the NEC, as given in Ref. 5-1, consisting of 1% bridges, 4% tunnels, 16% elevated and 79% at-grade. As shown in Table 5-6, the basic guideway total cost exclusive of special equipment and/or electrification is $2,409,330,000 for an average cost of $3.21 x 10^6/km ($5.17 x 10^6/mile).

f. <u>Other Costs</u>. It is assumed that a foreign object detection system, communication equipment, a trip identification loop system, and miscellaneous equipment such as anemometers are provided, at a cost of

---

*If uniform prestress is necessary for camber control, the box beam shape is preferred.

TABLE 5-4. ESTIMATED AT-GRADE GUIDEWAY COST

DOUBLE TRACK

		10^3/KM
LEVITATION–GUIDANCE COMPONENTS		962
• ALUMINUM	506.3	
• SHOP FAB	101.4	
• ATTACH HARDWARE	126.6	
• FIELD INSTALLATION	227.7	
ROADBED CONSTRUCTION		348
• CONCRETE PAVING	54.8	
• MEDIAN CONCRETE CURB	141.0	
• EXP. BOLTS	26.2	
• STEEL REINF.	64.2	
• BASE	8.0	
• SUB-BASE	18.0	
• ASPHALT	19.4	
• FILL	16.4	
SECURITY FENCING		37
DRAINAGE		87
SUB-TOTAL GUIDEWAY FAB	$	1,434
ROUTE PREPARATION		230
• MAXIMUM DEPTH OF CUT $\approx$ 6 M		
• EXCAVATION, ETC $\approx$ $3/YD		
LAND ACQUISITION		360
• 47 M RIGHT-OF-WAY		
• 12 ACRES/KM		
• $30,000/ACRE		
TOTAL COST		$2,024,000/KM

NOTE: GUIDEWAY-INSTALLED EQUIPMENT AND WAYSIDE COMMUNICATION
STATIONS ARE EXCLUDED.

TABLE 5-5. ESTIMATED ELEVATED GUIDEWAY COST

DOUBLE TRACK

			10^3/KM
LEVITATION-GUIDANCE COMPONENTS			962
● ALUMINUM	506.3		
● SHOP FAB	101.4		
● ATTACH HARDWARE	126.6		
● FIELD INSTALLATION	227.7		
GIRDER AND SUBSTRUCTURE CONSTRUCTION (TWIN "T")			2480-2770
● GIRDERS (22.8 M SPAN LENGTH)		2050	
● PIER (6.85 M COLUMN HEIGHT)		212	
● FOOTING (SPREAD FOOTING – PILE FOOTING)		217-505	
SUBTOTAL, GUIDEWAY FAB			3442-3730
LAND			111-234

	ALT NO. 1	ALT NO. 2	
● RIGHT-OF-WAY WIDTH	15 M	31.5 M	
● RIGHT-OF-WAY AREA	3.7 ACRE/KM	7.8 ACRE/KM	
● COST ASSUMPTION	$30K/ACRE	$30K/ACRE	

TOTAL COST (THOUSANDS OF $/KM)		
	ALT NO. 1	3553-3841
	ALT NO. 2	3676-3964

TABLE 5-6. COSTS OF BASIC GUIDEWAY

(750 KM CORRIDOR)

COMPONENT	PERCENT OF TOTAL LENGTH	LENGTH (KM)	UNIT COST, 10^3	TOTAL COST, 10^6
BRIDGES	1	8	7,840	62.72
TUNNELS	4	30	23,000	690.00
ELEVATED (SPREAD FOOTING)	8	60	3,676	220.56
ELEVATED (PILE FOOTING)	8	60	3,964	237.84
AT GRADE	79	592	2,024	1,198.21
			TOTAL	$2,409,330,000

$140,000/km ($225,300/mi). Total guideway cost, Cg, for the Ducted Fan/Gas Turbine system is thus $3.35 x 10^6/km ($5.39 x 10^6/mi). For electric propulsion systems (LIM and REM), the electrification costs from Ref. 5-4 are:

- Power Rail $497,000/km
- Power Station
    - With Wayside PCU   93,000
    - Without Wayside PCU   37,000
- Reaction Rail   311,000

From Ref. 5-5 the following cost estimates (including installation) are made for the LSM propulsion concept:

- Conductors and Attach Hardware $900,000/km
- Fixed Equipment   180,000/km
- Variable Equipment   234,000/km

The fixed equipment refers to 115 kV and 34.5 kV transmission systems. The variable equipment includes power distribution stations, PCUs, transformers, capacitors, circuit breakers, etc.; the quoted figures correspond to 2.5 km winding length, which Ref. 5-5 states to be the cheapest overall system cost arrangement.

(2) <u>Facilities</u>. Facilities costs are estimated from Ref. 5-1, adjusted for 1974 dollars and the 7-city baseline route assumed for this study. The figures are as follows:

- Yards and Shops $ 54.4 x 10^6
    - Storage, Service Shops, 4 @ $13 x 10^6
    - Major Overhaul Shop, 1 @ $2.4 x 10^6
- Terminals   142.4
    - Underground 2 @ $37 x 10^6
    - Downtown, 3 @ $15.6 x 10^6
    - Suburban, 2 @ $10.8 x 10^6
- Communications   18.9
    - Central Computer, 1 @ $14 x 10^6
    - Wayside Stations, 7 @ $700 x 10^3

TOTAL FACILITIES, C_{fa} $215.7 x 10^6

(3) <u>Vehicles</u>. Table 5-7 presents a cost break-out of a set of vehicles for 80- to 140-seat capacity, all synthesized* for a cruise speed of 134 m/s. Table 5-8 shows the cost break-out for the 80-seat vehicle synthesized* at cruise speeds from 50 m/s to 150 m/s. Table 5-9 shows similar data for the 140-seat vehicle. The costs (in 10^3) are determined by the following equations:

- Propulsion — $25.8 \, W_{PR} - 29.7 \, W_f$
- Suspension — $99 + 0.1061 \, W_g$
- Structure — $2.809 \, W_S$
- Furnishings — $5.714 \, W_{FURN}$
- Auxiliaries — $1.19 \, W_{AUX}$
- Brakes — $20.27 + 0.1935 \, W_g$

The weight parameters in kN, are as follows:

W_{PR} = Total propulsion system weight, including fuel

W_f = Fuel weight consumed

W_g = Vehicle gross weight

W_s = Structure weight

W_{FURN} = Furnishings weight

W_{AUX} = Auxiliaries weight

The propulsion costs are for the baseline Ducted Fan/Gas Turbine system. For the other propulsion systems considered, the onboard cost estimates (80-seat vehicle) are as follows:

- Fan/REM $1,450,000
  - Fan $500,000
  - REM   950,000
- SLIM   900,000
- LSM   868,000
- Paddle Wheel/GT   1,500,000
  - Turbines $700,000
  - Paddle Wheels   800,000

For the REM, LSM, and Paddle Wheel Systems, the added cryogenic subsystem cost is included with the cryogenic portion of the magnetic suspension system. The cryogenic part of the magnetic suspension for the SLIM tug is treated similarly.

---

*Weight and other physical parameters of these vehicles are given in Section 5-3.

TABLE 5-7. VEHICLE COST AT 134 M/S

(COST IN 10^3)

SUBSYSTEM	NO. SEATS/VEHICLE			
	80	100	120	140
SUSPENSION	138	141	146	152
STRUCTURE	150	117	146	168
FURNISHINGS	140	174	210	242
AUXILIARIES	25	31	37	44
BRAKES	91	96	107	117
PROPULSION[1]	1,200	1,256	1,310	1,357
OTHER[2]	572	572	572	572
TOTAL (THOUSANDS OF $)	2,316	2,387	2,528	2,652

[1]DUCTED FAN/GAS TURBINE, EXCLUDING FUEL COST

[2]INCLUDES RIDE CONTROL AT $272, COMMUNICATIONS AT $70, ASSEMBLY AND CHECK OUT AT $230

TABLE 5-8. 80 SEAT VECHICLE[1] COSTS AT VARIABLE CRUSE SPEED

(COST IN 10^3)

SUBSYSTEM	CRUISE SPEED, M/S						
	50	60	80	100	120	134	150
SUSPENSION	135	134	134	135	136	138	140
STRUCTURE	143	141	140	142	146	150	156
BRAKES	86	85	84	85	88	91	95
PROPULSION[2]	849	841	856	934	1,063	1,200	1,399
OTHER[3]	737	737	737	737	737	737	737
TOTAL (THOUSANDS OF $)	1,950	1,938	1,951	2,033	2,170	2,316	2,527

[1]2+2 SEATING ARRANGEMENT

[2]DUCTED FAN/GAS TURBINE, EXCLUDING FUEL COST

[3]INCLUDES FURNISHINGS AT $140, AUXILIARIES AT $25, RIDE CONTROL AT $272, COMMUNICATIONS AT $70, ASSEMBLY AND CHECK-OUT AT $230

TABLE 5-9. 140 SEAT VEHICLE[1] COST AT VARIABLE CRUISE SPEED
(COST IN 10^3)

SUBSYSTEM	CRUISE SPEED, M/S						
	50	60	80	100	120	134	150
SUSPENSION	148	147	147	148	149	152	154
STRUCTURE	160	157	156	158	163	168	175
BRAKES	110	108	108	109	112	117	121
PROPULSION[2]	921	903	926	1,011	1,184	1,357	1,575
OTHER[3]	858	858	858	858	858	858	858
TOTAL (THOUSANDS OF $)	2,197	2,173	2,195	2,284	2,466	2,652	2,883

[1] 2+3 SEATING ARRANGEMENT

[2] DUCTED FAN/GAS TURBINE, EXCLUDING FUEL COST

[3] INCLUDES FURNISHINGS AT $242, AUXILIARIES AT $44, RIDE CONTROL AT $272, COMMUNICATIONS AT $70, ASSEMBLY AND CHECKOUT AT $230

TABLE 5-10. MAGLEV SYSTEM INVESTMENT COSTS
(COST IN 10^6)

		NO. OF SEATS/VEHICLE	
		$N_{SV} = 80$	$N_{SV} = 140$
GUIDEWAY		2514.3	2514.3
● BASIC GUIDEWAY	2409.3		
● GUIDEWAY EQUIPMENT	105		
FACILITIES		215.7	215.7
● YARDS AND SHOPS	54.4		
● TERMINALS	142.4		
● COMMUNICATIONS	18.9		
VEHICLES (138, INCL SPARES)		319.6	366
● 80-SEAT VEHICLES AT 2.316			
● 140-SEAT VEHICLES AT 2.652			
TOTAL		$3050 X 10^6	$3096 X 10^6

(4) <u>Summary - Investment Costs</u>. Table 5-10 summarizes the investment costs for the 80- and 140-seat systems with the Ducted Fan/Gas Turbine propulsion option. The dominant aspects of the guideway are clearly evident. The annualized investment costs (principal plus interest payment) are as follows:

	$N_{SV} = 80$	$N_{SV} = 140$
● Guideway	277.1×10^6	277.1×10^6
● Facilities	23.8	23.8
● Vehicles	43.4	49.7
Total	344.3×10^6	350.6×10^6

B. <u>Direct Operating Costs (DOC)</u>. The following direct operating costs are estimated.

(1) <u>Fuel</u>. JP fuel cost is treated as a variable with minimum estimated to be 5.3¢/liter (20¢/gal.)

(2) <u>Crew</u>. Two crewmen and one cabin attendant are assumed, at a burdened rate of $20/hr.

(3) <u>Maintenance</u>. Annual vehicle maintenance is estimated as 10% of the initial cost of the vehicle. Maintenance of the basic guideway is estimated at $7000/km. For the electric propulsion options, annual guideway electrical maintenance is estimated at $20,000/km.

(4) <u>Terminal Operations</u>. Annual operating cost of each of the seven terminals is estimated at $500,000.

(5) <u>Summary - DOC</u>. Annual direct operating costs for the 80-seat and 140-seat configurations with fuel at 5.3¢/liter (20¢/gal) and two minute headway operation are:

	(Cost in 10^6)	
	$N_{SV} = 80$	$N_{SV} = 140$
● Fuel	69.74	96.74
● Crew	42.05	42.05
● Vehicle Maintenance	27.79	31.83
● Guideway Maintenance	5.25	5.25
● Terminal Operations	3.50	3.50
Total Annual DOC	148.33	179.37

It is clear from these figures that fuel costs are the dominant share ($\sim 50\%$) of the direct operating costs of the system. It is also apparent that the 140-seat configuration is significantly better than the 80-seat configuration (20% increase in DOC for 75% increase in capacity) provided, of course, the increased passenger capacity can be utilized.

   C. Summary - Total System Costs. Total annual system costs are as follows:

	(Cost in 10^6)	
	$N_{SV} = 80$	$N_{SV} = 140$
● Investment	344.3	350.6
● DOC	148.33	179.37
● IOC (0.5¢/passenger-km)	63.1	110.5
Total	555.73	640.47

These costs are also for fuel at 5.3¢/liter (20¢/gal) and with two minute headway operation. Note that the specific costs, i.e., ¢/passenger-km, for the two vehicle configurations are:

   ● 80-seats ($N_{PKY} = 1.262 \times 10^{10}$) $\sim$ 4.4¢/passenger-km

   ● 140-seats ($N_{PKY} = 2.21 \times 10^{10}$) $\sim$ 2.9¢/passenger-km

If the fuel cost is 10.6¢/liter (40¢/gal), the annual system cost for the 80-seat configuration would increase to 625.47×10^6 or 4.96¢/passenger-km, and the cost of the 140-seat configuration system would be 737.21×10^6 or 3.33¢/passenger-km.

   The following paragraphs present detailed tradeoffs of various system parameters, using specific cost as the tradeoff criteria.

5.4.2 Cost/Performance Tradeoffs

   The material presented in the following paragraphs constitutes a preliminary cost analysis of the various MAGLEV system elements. The objective is to permit general comparisons and to make preliminary judgments regarding certain system design parameters.

A. **Specific Cost Equations.** Specific costs, in ¢/passenger-km are:

(1) **Guideway**

$$\alpha_g = \frac{8265\ C_g}{N_{PKY}} = \frac{2.62 \times 10^{-5}\ C_g\ \Delta t}{N_{SV}\ N_{VT}}$$

5-5

where C_g = Guideway cost, $/km

(2) **Facilities**

$$\alpha_{fa} = \frac{11.02\ C_{fa}}{N_{PKY}} = \frac{3.494 \times 10^{-8}\ C_{fa}\ \Delta t}{N_{SV}\ N_{VT}}$$

5-6

where C_{fa} = Facilities cost, $

(3) **Vehicles**

$$\alpha_v = \frac{9.895 \times 10^{-8}\ C_v \tau}{N_{SV}}$$

5-7

where C_v = Vehicle cost, $

(4) **Fuel***

$$\alpha_f = 0.281\ \frac{C_f W_f}{N_{SV}}$$

5-8

where C_f = Fuel cost, ¢/ltr

W_f = Fuel weight consumed, kN

(5) **Crew**

$$\alpha_C = \frac{0.222\ \tau}{N_{SV}}$$

5-9

(6) **Vehicle Maintenance**

$$\alpha_{vm} = \frac{6.341 \times 10^{-8}\ C_v \tau}{N_{SV}}$$

5-10

(7) **Guideway Maintenance**

$$\alpha_{gm} = \frac{75000\ C_{gm}}{N_{PKY}} = \frac{2.378 \times 10^{-4}\ C_{gm}\ \Delta t}{N_{SV}\ N_{VT}}$$

5-11

where C_{gm} = Guideway maintenance cost, $/km

---

*For electric propulsion, $\alpha_E = 0.135\ \psi C_E$, where C_E = ¢/kW-hr and ψ = Energy Intensity, MJ/seat-km.

(8) Terminal Operations

$$\alpha_{TO} = \frac{3.5 \times 10^8}{N_{PKY}} = \frac{1.11 \, \Delta t}{N_{SV} \, N_{VT}}$$

5-12

For IOC = 0.5¢/passenger-km, C_{fa} = \$215.7 x 10^6 and N_{VT} = 1 (single vehicle operation), Equations 5-5 through 5-12 are summarized to give:

$$\alpha(\text{TOTAL}) = 0.5 + \frac{1}{N_{SV}} \left\{ \Delta t \left[2.62 \times 10^{-5} C_g + 2.378 \times 10^{-4} C_{gm} + 8.646 \right] \right.$$

$$\left. + \tau \left[1.623 \times 10^{-7} C_v + 0.222 \right] + 0.281 \, C_f W_f \right\}$$

5-13

where Δt = Headway, min.

τ = Time to transmit 750 km route

N_{SV} = Number of seats per vehicle

B. Baseline Ducted Fan/Gas Turbine Option. For the baseline system,

- C_g = \$3.35 x 10^6/km

- C_{gm} = \$7.0 x 10^3/km

and Equation 5-13 reduces to

$$\alpha(\text{TOTAL}) = 0.5 + \frac{1}{N_{SV}} \left\{ 98.08 \, \Delta t + \tau \left[1.6236 \times 10^{-7} C_v + 0.222 \right] + 0.281 \, C_f W_f \right\}$$

5-14

Equation 5-14 is the basis for the cost tradeoffs presented in the following paragraphs.

(1) System Cost Breakouts. Figure 5-11 shows total system specific cost for the 80- and 140-seat configurations as well as for a train set consisting of three 100-seat vehicles. The influence of vehicle size, train size, and headway limit is also shown in Figure 5-12.* These figures show clearly that high passenger capacity is the key to low specific cost. However, for a fixed level of passenger-km/year, the specific cost is nearly invariant with vehicle size as shown in Figure 5-12. If there is sufficient demand to run a MAGLEV HSGT system with headways on the order to two to three minutes, the

*Minimum energy seating is used in this figure.
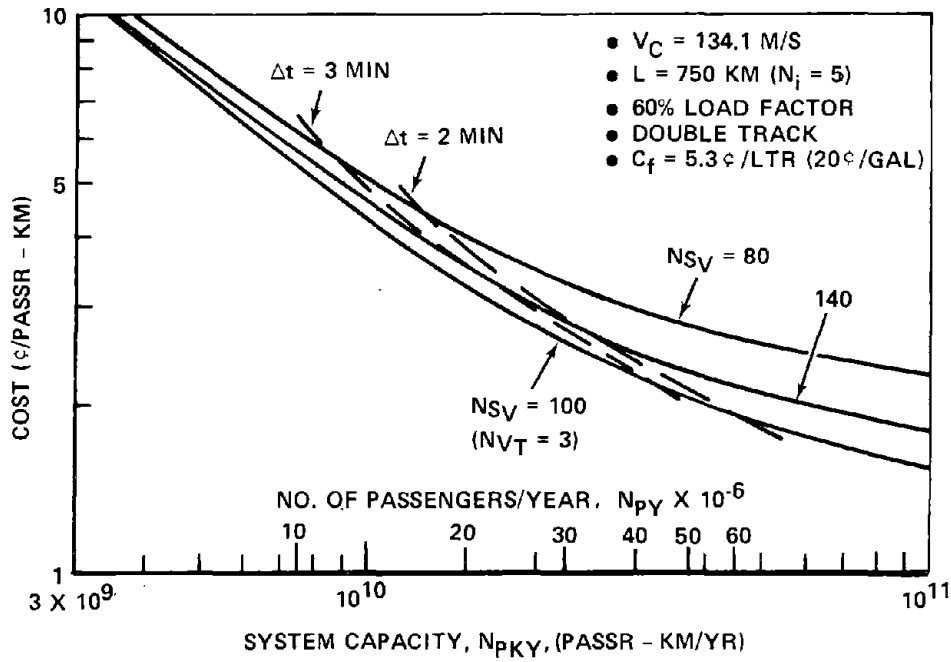
FIGURE 5-11. TOTAL SYSTEM COST

Figure 5-11 labels and annotations:

- COST ($\cent$/PASSR – KM) (vertical axis)
- $\Delta t = 3$ MIN
- $\Delta t = 2$ MIN
- $V_C = 134.1$ M/S
- $L = 750$ KM ($N_i = 5$)
- 60% LOAD FACTOR
- DOUBLE TRACK
- $C_f = 5.3\cent$/LTR ($20\cent$/GAL)
- $N_{SV} = 80$
- 140
- $N_{SV} = 100$ ($N_{VT} = 3$)
- NO. OF PASSENGERS/YEAR, $N_{PY} \times 10^{-6}$
- SYSTEM CAPACITY, N_{PKY}, (PASSR – KM/YR)

FIGURE 5-12. EFFECT OF VEHICLE SIZE

Figure 5-12 labels and annotations:

- TOTAL SYSTEM COST ($\cent$/PAX – KM) (vertical axis)
- 60% LOAD FACTOR
- $V_C = 134.1$ M/S
- $C_F = 5.3\cent$/LTR
- $L = 750$ KM, $N_i = 5$
- $\Delta t = 3$ MIN
- 1.26×10^{10} PASSENGER KM/YR
- $N_{VT} = 1$
- $N_{VT} = 2$
- $N_{VT} = 3$
- $\Delta t = 2$ MIN
- NO. OF SEATS PER VEHICLE, N_{SV}
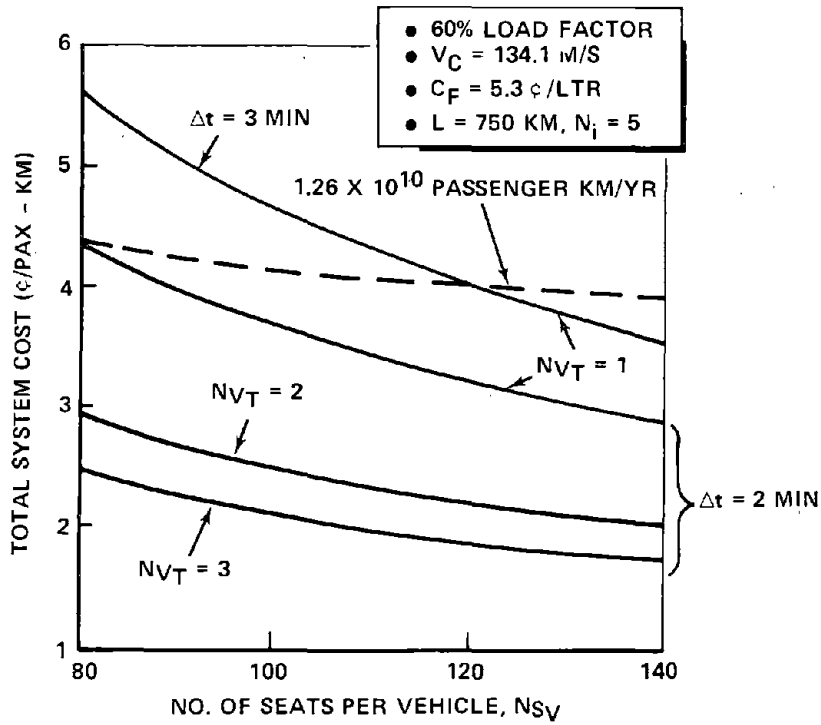
5-27

140-seat vehicles would be recommended, with provision for coupling at least two vehicles together to handle peak loads. Under such circumstances, system cost would be on the order of 3¢/passenger-km (4.8¢/passenger-mile) even with fuel on the order of 11¢/liter (41¢/gal).

Figures 5-13 and 5-14 show cost breakouts for the 80-seat configuration. Clearly, investment costs (primarily the guideway) dominate the cost picture, except at very high system capacity. Note further that the facilities and terminal operations costs - at the two minute headway limit - are quite small, i.e., less than 0.4¢/passenger-km (0.64¢/passenger-mile).

(2) <u>Parameter Tradeoffs</u>. A major parameter is the cost of fuel. Figure 5-15 shows the substantial effect of fuel cost on system cost for both the 80- and 140-seat configurations operating with two minute headway at 134 m/s cruise speed. However, even for fuel as costly as 30¢/liter ($1.13/gal), system cost for the 140-seat configuration is below 5¢/passenger-km (8¢/passenger-mile) with single vehicle operation, and below 4¢/passenger-km (6.4¢/passenger-mile) for dual vehicle operation.

Figure 5-16 shows the influence of aluminum plate thickness on system cost. To generate these data, a matrix of vehicles was synthesized and costed for operation over the aluminum guideway surfaces with plate thicknesses in the range of 1 to 3.5 cm.* System cost is nearly invariant with plate thickness except at very high fuel cost (above 16¢/liter). "Optimum" plate thickness is at or below 2.54 cm (1 inch) for a reasonable range of fuel cost.

Figure 5-17 shows the influence of cruise speed on system cost for both 80- and 140-seat configurations and for a range of fuel cost. "Optimum" or minimum cost cruise speed is approximately 110 m/s (246 mph) for fuel costing 5.3¢/liter (20¢/gal), dropping off slightly at higher fuel cost. However, the cost variation with speed is quite small - about 5% between the optimum speed and 134 m/s - for fuel costing about 12¢/liter (45¢/gal) or less. In view of uncertainty in the future cost of energy and its relationship to other system components, e.g. aluminum, as well as the difficulty of quantifying the benefit of speed, it is difficult at this time to specify a true

---

*Plate thickness influences drag and propulsion power and weight; the vehicle must then be redesigned to accommodate the changed propulsion system weight.
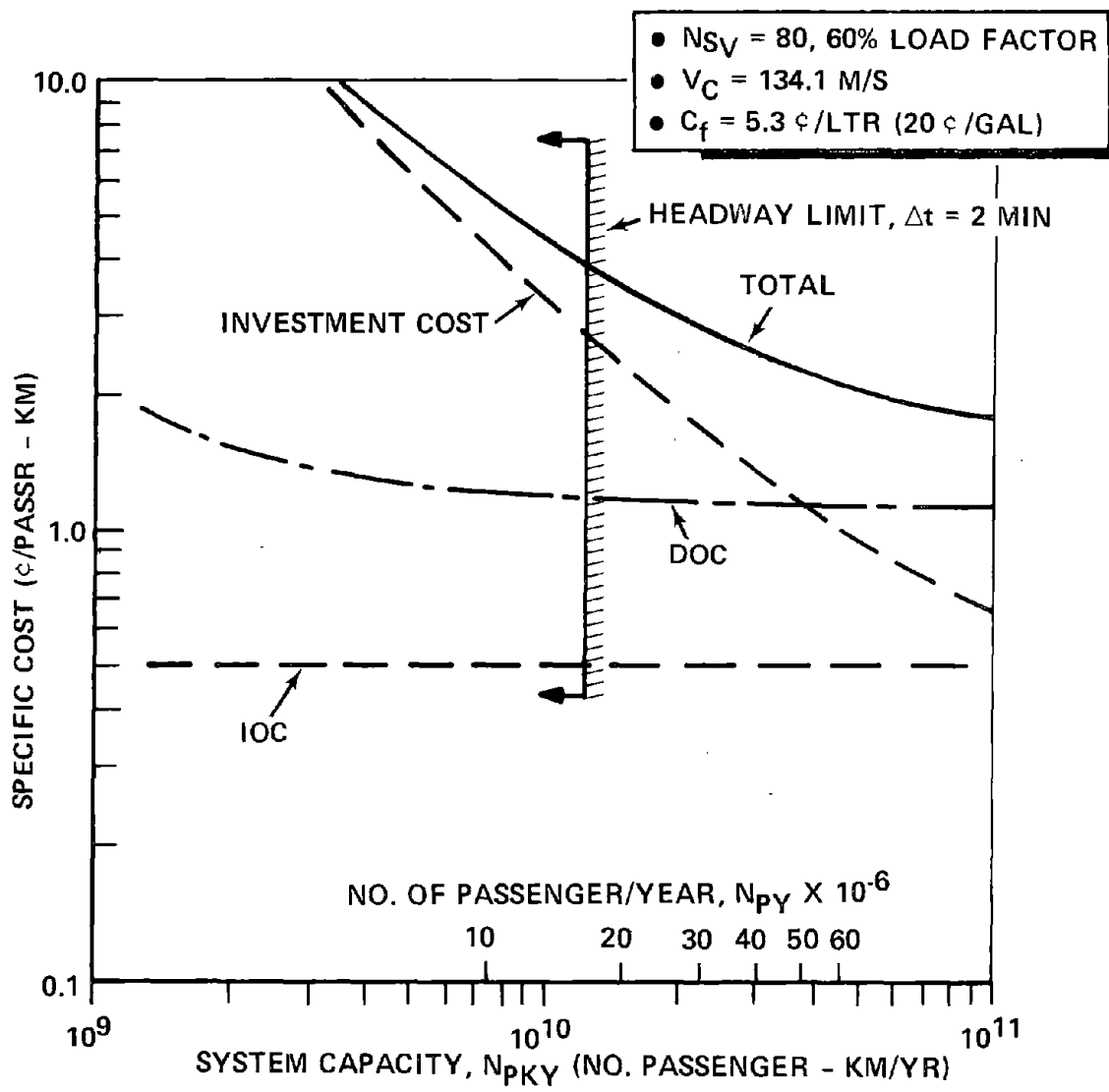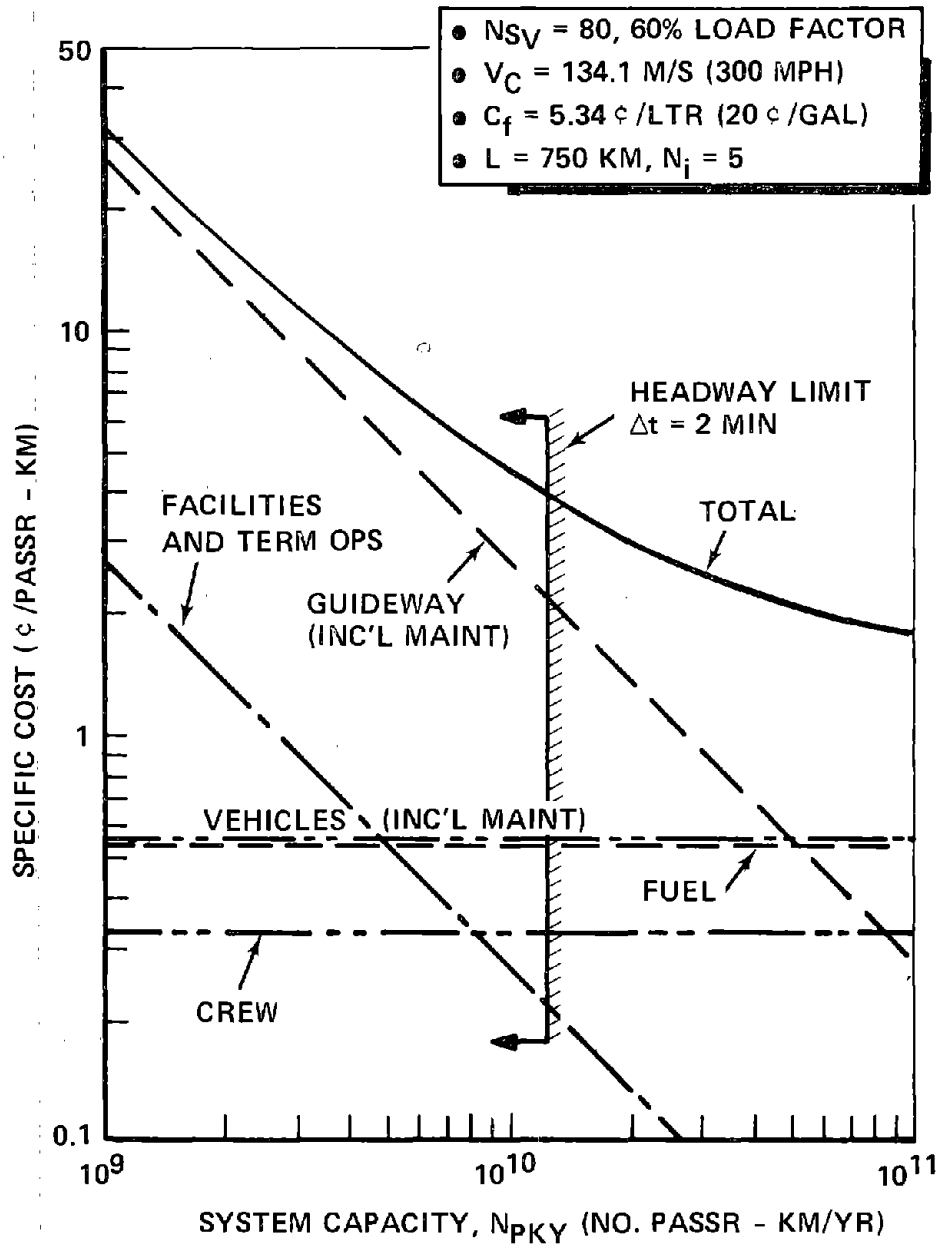
FIGURE 5-13. DISTRIBUTION OF MAJOR COSTS

FIGURE 5-14. SYSTEM COST BREAKOUT
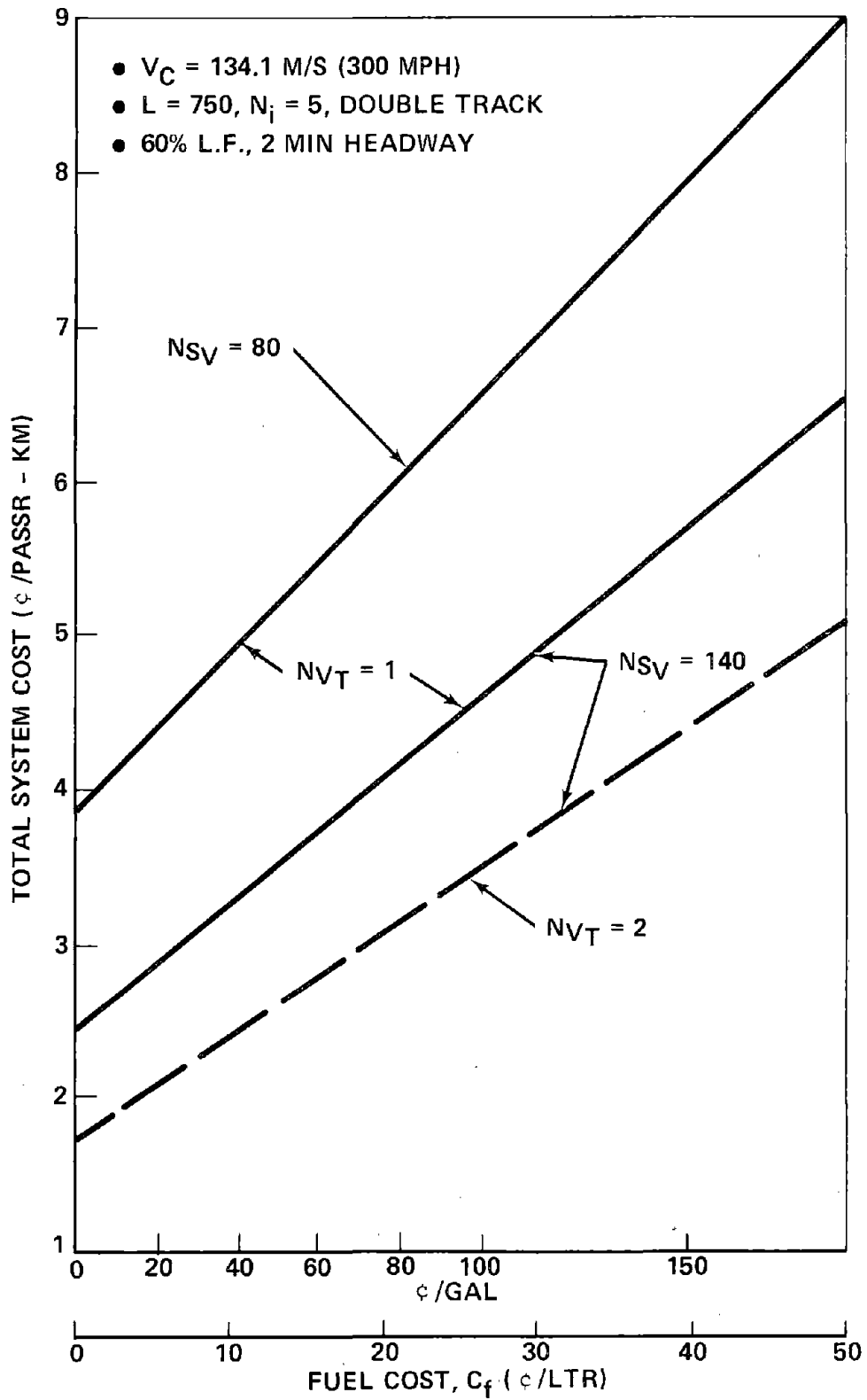
FIGURE 5-15. EFFECT OF FUEL COST
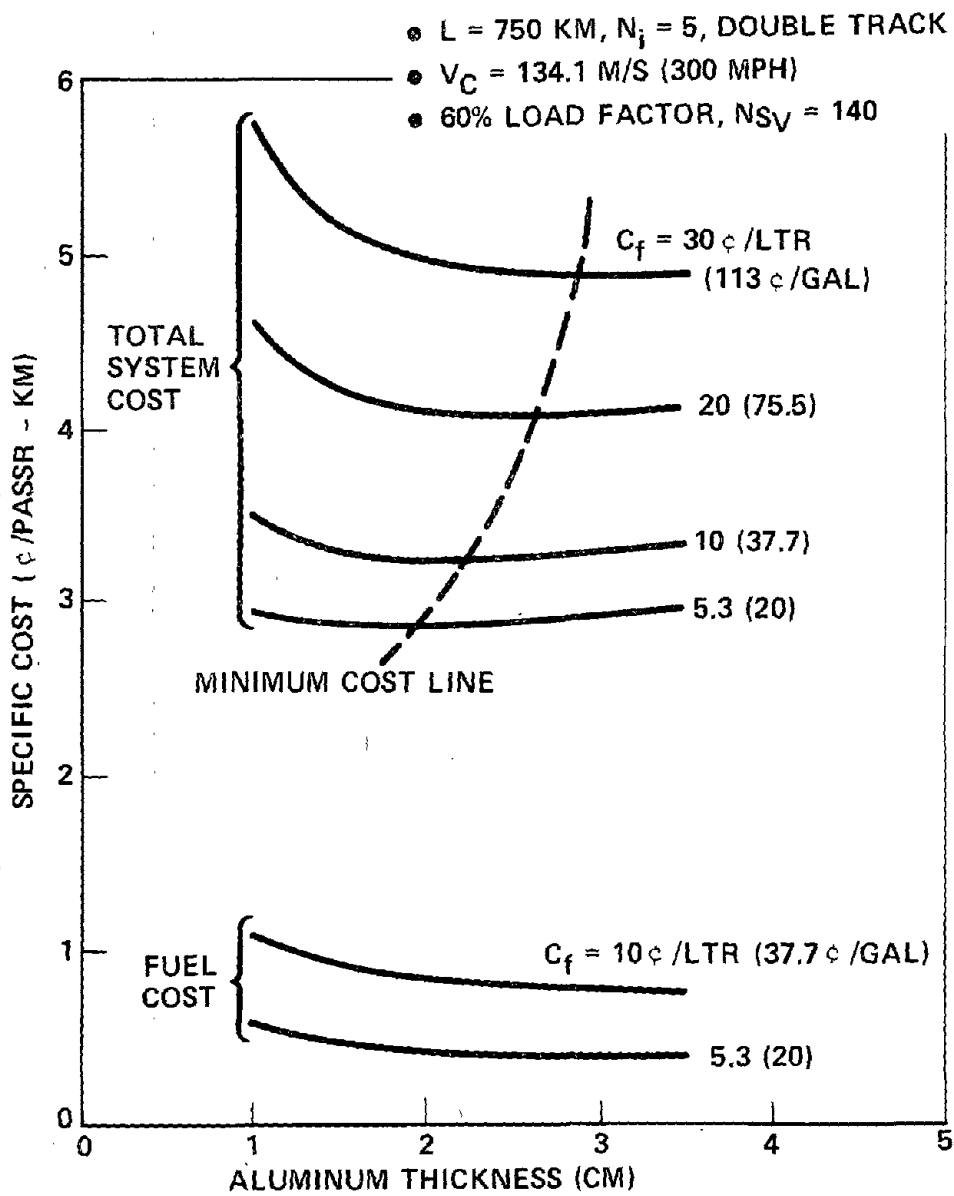
FIGURE 5-16. COST/THICKNESS TRADEOFF
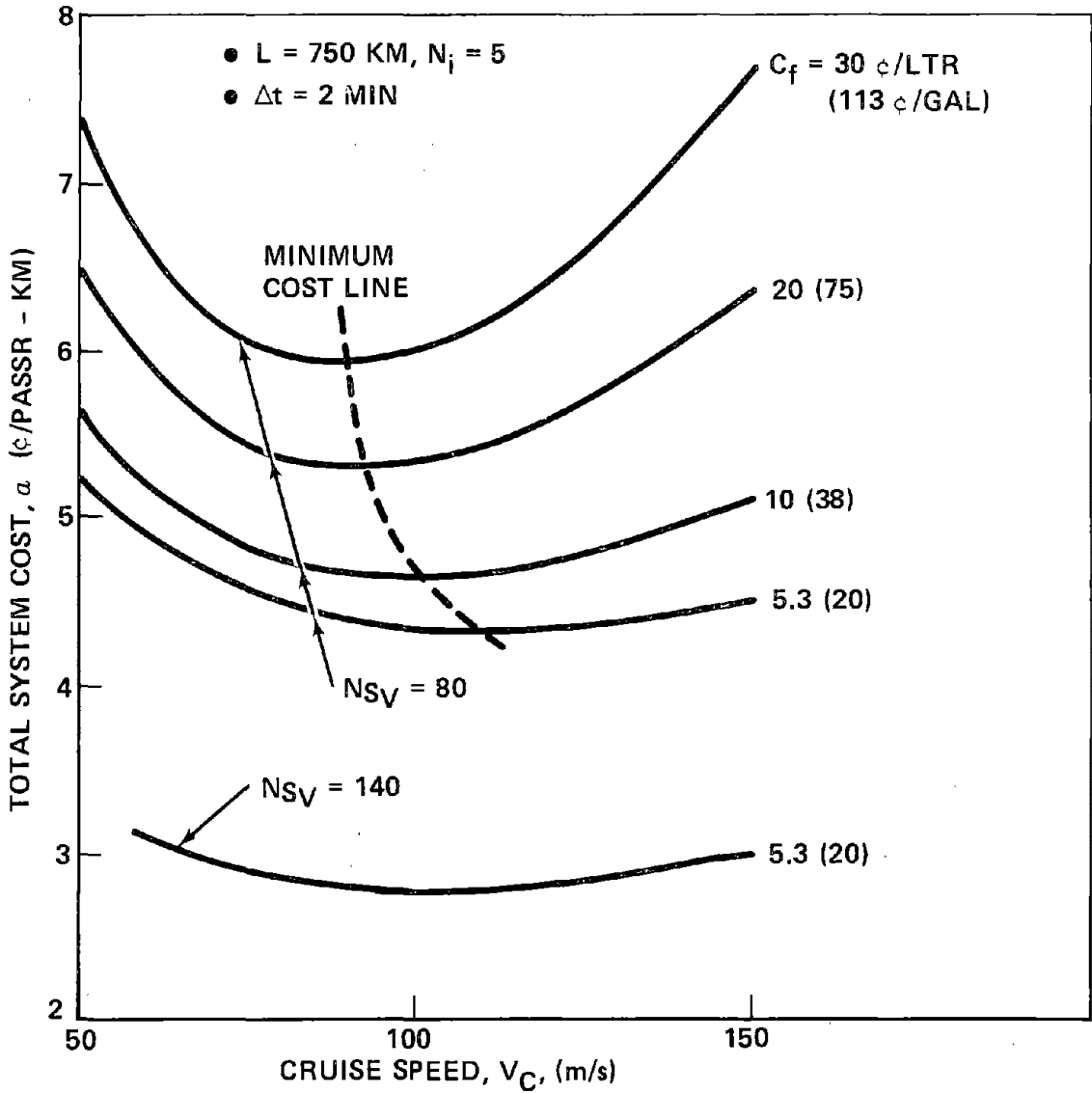
FIGURE 5-17. EFFECT OF CRUISE SPEED

"optimum" cruise speed. From the data at hand, it is our judgement that the optimum cruise speed would be in excess of 110 m/s (246 mph).

Figure 5-18 shows the influence of the route characteristics on total system cost. Between the extremes of no intermediate stops (the express case) and the 5 intermediate stop baseline route, the total cost variation is approximately 6%. The fuel expended for acceleration away from each city is a significant part of the total fuel consumption, particularly for large vehicles and/or numerous stops. However, with relatively cheap fuel the effect on total system cost is quite small, as shown in Figure 5-18.

C. Alternate System Comparison. Section 4.4 presents data on a number of propulsion systems applicable to MAGLEV, including the baseline Ducted Fan/Gas Turbine system. Eighty-seat vehicles are synthesized for each propulsion option to facilitate system comparison; comparative weight breakouts are shown in Table 5-11. The LSM vehicle is clearly the heaviest, due primarily to the large number of cryogenically-cooled superconducting magnets required for propulsion. Corresponding costs for these vehicles are shown in Table 5-12. Vehicle costs vary from approximately $2 x 10^6 to $2.6 x 10^6; however, some of the cost elements are very approximate at this time. For example, there is no valid base for estimating either the paddle wheel cost or the cost of the superconducting motor.

Table 5-13 summarizes the guideway cost for each propulsion concept. All concepts employ the basic hat-shaped guideway configuration. For the LSM concept, Ref. 5-5 data indicates a cost of $1,280,000/km for the conductors, after adjustment for 1974 dollars, whereas the $320,000 value listed in the table results from an increase in the number of vehicle LSM magnets and a corresponding reduction in the required guideway current. An optimization of LSM performance was not attempted.

Total system costs for the various 80-seat configuration are shown in Table 5-14; costs for the 140-seat configurations are shown for comparison. Operation is assumed at two minute headways for 16 hr/day over the baseline 750 km route with five intermediate stops. Conservative figures for energy cost are employed, i.e., 10.6¢/liter (40¢/gal) for JP fuel and 3¢/kw-hr for

electricity. For the 80-seat system, total cost varies about 1¢/passenger-km (~ 20%) for the range of propulsion systems studied; the variation is due primarily to variations in guideway cost. The total cost for the 140-seat system varies only about 0.4¢/passenger-km (~ 12%) since the increased capacity (from 1.262×10^{10} passenger-km/yr to 2.21×10^{10} passenger-km/yr) reduces the influence of guideway cost variations.

- o L = 750 KM
- o V_C = 134.1 M/S
- o C_f = 5.3¢/LTR (20¢/GAL)

N_{SV} = 80

N_{SV} = 140

TOTAL SYSTEM COST, a (¢/PASSR – KM)

NO. EQUIDISTANT, INTERMEDIATE STOPS, N_i
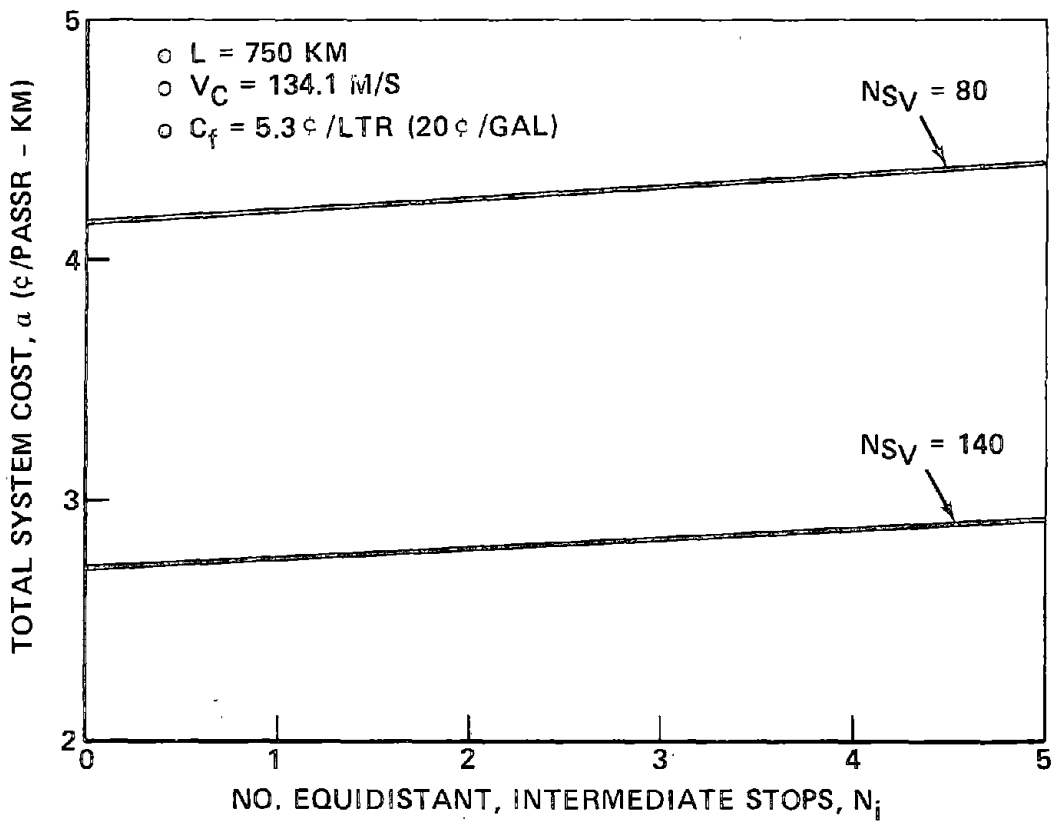
FIGURE 5-18. EFFECT OF MISSION PROFILE

TABLE 5-11. COMPARATIVE 80-SEAT VEHICLE WEIGHT

($V_C = 134.1$ M/S)

SUBSYSTEM	FAN/GT	FAN/REM	SLIM(1)	LSM	PADDLE WHEEL/GT
SUSPENSION(3)	66.8 kN	65.2 kN	62.5 kN	71.6 kN	66.8 kN
STRUCTURE	53.4	49.8	44.0	63.9	53.3
FURNISHINGS	24.5	24.5	24.5	24.5	24.5
AUXILIARIES	21	21	21	25	21
BRAKES	20.2	18.8	19.4	24.5	20.2
CREW COMPARTMENT	15.6	15.6	15.6	15.6	15.6
PAYLOAD	71	71	71	71	71
PROPULSION	80.6	53.5	75.8(2)	154.5(4)	79.6
CONTINGENCY	13.4	13.4	13.4	13.4	13.4
TOTAL, kN	366.5	332.8	347.2	464	365.4
(LB)	(82,300)	(74,800)	(78,100)	(104,300)	(82,150)

(1) WITH WAYSIDE PCU

(2) INCLUDES PROPULSION TUG AT 68 kN (MOTOR ~53, STRUCTURE ~9, LEV GUID MAGNETS AND CONTROL ~6) AND BODY-MOUNTED COOLING/CONTROL SYSTEM AT 7.8 kN

(3) INCLUDES LEV-GUIDE MAGNETS, CRYOGENICS, WHEELS AND RIDE CONTROL EQUIPMENT

(4) INCLUDES MAGNET SUBSYSTEM AT 111 kN, REFRIGERATION AT 43.5 kN

5-36

TABLE 5-12. COMPARATIVE 80-SEAT VEHICLE COST

(V$_c$ = 134.1 M/S)

SUBSYSTEM	FAN/GT	FAN/ REM	SLIM[1]	LSM	PADDLE WHEEL/GT
LEV-GUIDE MAGNETS + HARDWARE	$102 X 10^3	98	100[2]	112	101
CRYOGENICS	36	40[6]	40[6]	55[6]	50[6]
RIDE CONTROL	272	272	272	272	272
STRUCTURE	150	140	149[5]	179	148
FURNISHINGS[3]	140	140	140	140	140
AUXILIARIES[4]	25	25	25	50	25
WHEELS, BRAKES	91	85	87	110	90
PROPULSION	1,200	1,450	9000	868	1,500
COMMUNICATIONS	70	70	70	70	70
ASSEMBLY, CHECKOUT	230	230	230	230	230
TOTAL (THOUSANDS OF $)	2,316	2,550	2,013	2,086	2,626

[1]WITH WAYSIDE PCU

[2]INCLUDES LEVITATION-GUIDANCE MAGNETS FOR PROPULSION TUG

[3]INCLUDES CREW COMPARTMENT

[4]INCLUDES AIR CONDITIONING, APU, ETC.

[5]INCLUDES PROPULSION TUG STRUCTURE, THRUST BEARING, STRUTS, ETC.

[6]INCLUDES CRYOGENICS FOR PROPULSION OR SLIM TUG SUPPORT SYSTEM

TABLE 5-13. COMPARATIVE GUIDEWAY COST[1]

(DOUBLE TRACK)

	FAN/GT PADDLE WHEEL/GT	FAN/REM	SLIM (WAYSIDE PCU)	LSM
BASIC GUIDEWAY	$3,210 (X 10^3/KM)	3,210	3,210	3,210
GUIDEWAY EQUIPMENT[2]	140	140	140	140
		o POWER RAILS ___ 497	o POWER RAILS ___ 497	o CONDUCTORS ___ 320
		o POWER STATIONS ___ 37	o POWER STATIONS ___ 93	o FIXED[3] ___ 180
			o REACTION RAILS ___ 311	o VARIABLE[4] ___ 234
TOTAL COST (THOUSANDS OF $/KM)	3,350	3,844	4,251	4,084

[1]FOR NEC MIX, I.E., 1 PERCENT BRIDGES, 4 PERCENT TUNNELS, 16 PERCENT ELEVATED, 79 PERCENT AT GRADE

[2]INCLUDES FOREIGN OBJECT DETECTION, TRIP IDENTIFICATION LOOP

[3]INCLUDES 115 KV AND 34.5 KV TRANSMISSION SYSTEMS

[4]INCLUDES POWER DISTRIBUTION STATION, PCU'S, TRANSFORMERS, CAPACITORS, ETC.

TABLE 5-14. COMPARATIVE SYSTEM SPECIFIC COST[1]

(80-SEAT VEHICLES)

	FAN/GT	FAN/REM	SLIM	LSM	PADDLE WHEEL/GT
GUIDEWAY[2]	2.194 ¢/PASSR-KM	2.518	2.784	2.675	2.194
GUIDEWAY MAINTENANCE	0.042	0.161[3]	0.161[3]	0.161[3]	0.042
VEHICLES	0.344	0.378	0.299	0.309	0.390
VEHICLE MAINTENANCE	0.220	0.242	0.191	0.198	0.250
OTHER[4]	1.045	1.045	1.045	1.045	1.045
SUB-TOTAL	3.845	4.344	4.480	4.388	3.921
ENERGY[5]	1.106	1.048	0.886	0.842	0.860
TOTAL, 80-SEATS (¢/PASSR-KM)	4.951	5.392	5.366	5.230	4.781
TOTAL, 140-SEATS (¢/PASSR-KM)	3.30	3.55	3.495	3.406	3.169

[1] FOR 2 MINUTE HEADWAY, 16 HOUR/DAY OPERATION, 750 KM ROUTE

[2] INCLUDES BASIC GUIDEWAY, GUIDEWAY EQUIPMENT, ELECTRICAL SYSTEM AS APPROPRIATE

[3] INCLUDES ELECTRICAL MAINTENANCE AT 0.119¢/PASSR-KM

[4] INCLUDES CREW AT 0.333, FACILITIES AT 0.188, TERMINAL OPS AT 0.0277 AND IOC = 0.50 ¢/PASSR-KM

[5] JP FUEL AT 10.6 ¢/LTR (40¢/GAL), ELECTRICITY AT 3 ¢/KW-HR

5.5 REFERENCES

5-1 "High Speed Ground Transportation Alternatives Study", Office of the Assistant Secretary for Policy and International Affairs (DOT/TPI) U.S. Department of Transportation, TPI-13 (PB-220079), January 1973.

5-2 "Cost Analyses for NECTP", Vol. I, "High Speed Ground Modes", PB-190942, Resource Management Corp., December 1969.

5-3 Ward, J.D., "The Future Roles for Tracked Levitated Vehicle Systems", ASME Trans. Journal of Dynamic Systems, Measurement, and Control, Vol. 96, Series G, No. 2, pp 117-127, June 1974.

5-4 Communication from M. Guarino, DOT, via F. Gobetz, United Aircraft Research Laboratories, 18 November 1974.

5-5 "Report on a Study of the Magneplane Power System and Guideway", United Engineers and Constructors, Inc. (MIT P.O. ML-46235, Prime Contract NSF-C670), June 1973.

SECTION 6

SUSPENSION SUBSYSTEM AND GUIDEWAY CONSTRUCTION COSTS

This section presents detailed cost estimates for the suspension subsystem and the guideway construction. Details of the estimated costs of the onboard components of a typical linear synchronous motor (LSM) are also included. Other elements of the system are costed in Section 5.4.1.

6.1 SUSPENSION SUBSYSTEM

The suspension subsystem consists of the levitation components (levitation coil, control coil, shield coil (if any), dewar and associated cryogenic equipment), and the ride control subsystem (sensors, control and power electronics, power control unit, etc.).

6.1.1 Levitation Components

The cost breakdown for the levitation components was made by the Magnetic Corporation of America (MCA), and Ford Motor Company's Scientific Research Laboratory. The magnet configurations shown in Figures 4-16 and 4-18 were used in preparing the costs summarized in Table 6-1. As shown, the cost of four levitation modules and refrigeration system for a MAGLEV vehicle in volume production is approximately $121,000 without shielding coils and $137,000 with shielding coils. Engineering and development costs have not been included in these values; approximately a 25% increase in total cost is required if these are to be added.

Estimates have also been prepared for a low production volume case: for 12 vehicles, the cost of the levitation modules approximately doubles, but the refrigeration system remains unchanged. Therefore, the total cost of the levitation components per vehicle is $207,000 without a shielding coil and $240,000 with shielding. In addition, $500,000 of tooling is required. Again, no development or engineering costs are included in these values.

TABLE 6-1. LEVITATION MODULE AND REFRIGERATION COSTS [1]
(PER VEHICLE)

	WITHOUT SHIELDING COIL	WITH SHIELDING COIL
SUPERCONDUCTOR[2]	$ 41,400	$ 52,000
MAGNET CANS	770	1,570
PERSISTENT SWITCH	140	140
DEMOUNTABLE LEADS	370	370
OUTER CRYOSTAT	20,000	24,000
STRUTS	500	500
LEVEL DETECTORS	80	80
ELECTRICAL CONNECTIONS	80	80
SUPERINSULATION	300	400
LIQUID He RESERVOIR	1,200	1,200
LABOR	3,000	3,800
• SUB-TOTAL, LEV/GUIDE MAGNETS	$ 67,840	$ 84,140
UNIT ACCEPTANCE TESTING, SUBSYSTEM CHECKOUT AND TEST	2,720	2,720
RIDE CONTROL MAGNETS (CONTROL COILS)	14,820	14,820
• SUB-TOTAL, LEVITATION MODULES	$ 85,380	$101,680
REFRIGERATION SUBSYSTEM[3],[4]	35,600	35,600
• TOTAL LEVITATION SYSTEM	$120,980	$137,280

[1] 1974 PRICES ON 250 VEHICLES (1000 MODULES), NO DEVELOPMENT COSTS INCLUDED.

[2] SUPERCONDUCTOR COST IS APPROXIMATELY 1/2 CURRENT VALUES TO ALLOW FOR QUANTITY PRODUCTION.

[3] ADDITIONAL COMPRESSOR (@ $7,500) INCLUDED FOR REDUNDANCY

[4] REFRIGERATION COSTS BASED ON CURRENT PRICE FOR LOW VOLUME PRODUCTION. NOTE COST CAN BE REDUCED SUBSTANTIALLY BY HAVING A LARGE LIQUID HELIUM RESERVOIR ON-BOARD WHICH IS FILLED PERIODICALLY FROM WAYSIDE. THIS REQUIRES AN ON-BOARD HELIUM GAS CONTAINER AND COMPRESSOR SO THAT THE GAS CAN BE COLLECTED AND RELIQUEFIED BY A STATIONARY REFRIGERATOR.

6.1.2 Ride Control Subsystem

The cost figures developed for the ride control subsystem are based upon the following premises:

- 1974 prices for hardware fabrication, unit acceptance test, installation and subsystem checkout/acceptance test.

- 250 systems.

- High-reliability (screened) parts used throughout with separate costs for the basic subsystem elements and a failsafe configuration employing dual redundance where the basic configuration does not have inherent redundancy.

- Temperature and vibration testing included in the unit acceptance testing.

- No development costs included.

- All costs are engineering estimates based upon a brief analysis of requirements and available data on costs of current technology from catalogs and informal vendor contacts.

The elements in the ride control subsystem are identified in Figure 4-64. The following discussion is keyed to that figure.

A. Accelerometers. Costs are based upon use of a commercial unit which is currently in production for commercial instrumentation applications. Eight units are used in the basic system and 16 in the failsafe configuration. Base per unit cost of the commercial version of this device is $450. Assuming a factor of two increase for a high-reliability version and 0.7 or 0.55 quantity discount factors yields per system costs of:

Basic system cost = $450(8)(2)(0.7) = $5K

Failsafe configuration = $450(16)(2)(0.55) = $8K

B. Gap Sensors. A gap sensor applicable to the MAGLEV case remains to be developed. It is estimated that the per unit cost will be $5,000 in a high reliability configuration. Total costs using quantity discount factors of 0.8 and 0.55 are:

Basic system cost = $5,000(8)(0.8) = $32K

Failsafe configuration = $5,000(16)(0.55) = $44K

C. Longitudinal Velocity Sensors. A specific candidate for this requirement is not presently available, and adaptation of existing technology will be

required. The cost is estimated to be $3,000 per unit in a high reliability configuration. Total costs using a quantity discount factor of 0.8 are:

Basic system cost = $3,000(1)(0.8) = $2,400

Failsafe configuration = $3,000(2)(0.8) = $4,800

D. <u>Control Electronics</u>. As pointed out in Section 4.3.4B, the control electronics will benefit from the trend of development in LSI. However, care must be taken in making assumptions about the effect of LSI on cost since operating speed tends to suffer as large scale integration (LSI) circuit complexity increases. For example, the execution time of the MPLY instruction in the prototype PM 11 computer made by Toshiba is 40 microseconds. This computer employs standard American bi-polar small and medium scale chips. The LSI version of the PM 11 in P-MOS has an execution time of 120 microseconds for the MPLY instruction. A rough evaluation of the LSI speed problem indicates that they can be up to 1/5 as fast as current mini computers using bi-polar transistor-transistor logic (TTL).

It is possible to increase the effective speed of current micro processor chip sets by paralleling central processor units (CPU's) and/or complete computers. This approach tends to reduce the potential size and cost savings, however.

A second important point is the fact that mini computer and micro processor costs are frequently advertised for the basic memory and CPU without considering the cost of the options and I/O hardware necessary to make a useful system element. For this case, a multiplying factor of 3 to 5 over the basic CPU and memory hardware appears to be appropriate.

Using the above considerations, the control electronic costs are estimated as follows. The single-unit cost of present mini computers with I/O hardware applicable to the MAGLEV requirements ranges from approximately $13K for commercial versions (i.e., Computer Automation Alpha/LSI - 2/20G) to $40K for ruggedized military versions (i.e., ROLM Rugged Nova 1602). Taking the lower number, allowing a factor of 2 for high-reliability components and packaging, and taking a quantity discount factor of 0.8 and a net technology improvement factor of 0.5 yields a basic control electronics cost of $13,000(1)(2)(0.8)(0.5) = $10K. For the failsafe case, it is simply assumed

that the control electronics will increase by a factor of 2.5 to provide redundancy for the control electronics, and fault isolation and low-power switching control facilities for the total ride control subsystem.

E. _Power Control Unit_. The PCU hardware will be composed of relays and solid-state power conversion equipment. The cost, based upon past experience with this type of hardware, is $15,000 for the basic system and $24,000 for the failsafe configuration.

F. _Control Magnet Power Amplifiers_. The PA cost is estimated by taking a value of $125 per kilowatt of peak power as the base cost. This value is representative of costs for commercial SCR power amplifiers used for industrial motor control in the applicable power range. The peak power requirement of the system configuration with gap sensors is used for baseline costing purposes. Using a factor of two for a high-reliability unit and a quantity discount factor of 0.55 yields a total cost of

$$\$(125)(22)(8)(2)(0.55) = \$24.2K$$

It is assumed that adequate redundance is provided in the basic magnet PA configuration and no additional costs are incurred here for the failsafe configuration.

G. _Backup Power Supply_. A combination of batteries and a separate APU is used in the backup power supply. Batteries are used to power the low-level control and switching circuitry and to provide starting power for the APU. The APU provides the control magnet driver power which constitutes the main subsystem load. Two 24-volt aircraft type lead-acid batteries are needed. The cost of these items is $200.

The major cost element of the backup power supply is the APU and its associated generator. The base cost of a Garrett GPI-36 series APU adequate to handle the full load of the baseline system with gap sensor is $35K. The quantity discount factor is included in this figure. The unit is designed for commercial aircraft use, thus no further addition is made for reliability

improvement. The approximate cost of the generator is estimated at $25K. Total costs are then

Batteries	$0.02K
APU	35K
Generator	25K
TOTAL	$60.2K

These costs are quite large and are based on a first cut at the mechanization. This area is obviously worthy of additional cost comparison of alternatives.

H. Subsystem State Instrumentation. The subsystem state instrumentation includes a central signal conditioner and pick-off devices distributed throughout the subsystem elements. Costs are estimated on the basis of past experience with similar equipment. These costs are $10K for the basic system and $12K for the failsafe configuration.

I. Subsystem Cabling. The cabling costs are estimated at $5K for the basic system and $8K for the failsafe configuration, based upon past experience.

J. Acceptance Testing, Installation and Checkout. The breakdown of these costs is as follows:

Basic System

- Unit acceptance test of the subsystem elements, including temperature and vibration exposures, 24 hrs. @ $25/hr plus $250 facilities average each for 14 equivalent items of equipment in the basic subsystem (i.e., one set each of accelerometers, gap sensors, 1 control electronics, instrumentation, PCU, backup power supply; and 8 PA's) $12K

- Installation 80 hrs @ $25/hr   2K

- Installation materials, facilities, spares and rework at 10% of base equipment cost   16K

- Subsystem check out and acceptance testing 160 hrs @ $25/hr plus 2K facilities   6K

- Contingency @ 10% of total installation/test costs   4K

- Basic Subsystem Totals $40K

Failsafe Configuration

- Unit acceptance testing. Assume 5 additional items for a
  total of 19 @ $850 each $16K

o Installation 120 hrs @ $25/hr   3K

o Installation materials, facilities, spares, and rework   21K

- Subsystem check out and acceptance testing
  320 hrs @ $25/hr plus 4K facilities   12K

o Contingency @ 25% of total installation/test costs   _14K_

o Failsafe Subsystem Totals $66K

These estimates are based on past experience with similar equipment.

K. Summary Costs. Table 6-2 contains the cost data summary.

6.1.3 Linear Synchronous Motor (LSM)

Although the LSM is actually a propulsion system rather than a suspension
system, the costs have been included for completeness. The cost estimates
were provided by MCA for a typical LSM system consisting of five separate LSM
modules along the underside of the vehicle. The cost breakdown for the
modules is given in Table 6-3 for the case without shielding coils. If shield-
ing is required, the cost for the five modules increases by a factor of 1.8 --
to $868,500 per vehicle.

The refrigeration system for the combined LSM and levitation/guidance
magnets is estimated to cost $55,000. This includes an additional compressor
for redundancy, but only one large refrigerator.

6.2 GUIDEWAY CONSTRUCTION COSTS

The guideway construction cost estimates were made by the guideway sub-
contractor, The Cardan Company, Inc. of Beverly Hills, Ca. The at-grade and
elevated guideways were carried to the level of design sufficient to cost all
the major construction items, This included, for example, the amount, shape,
and location of the reinforcement bars in the concrete to withstand the various
loading criterion specified by Philco-Ford. The costs have been kept in the
standard English units used in the construction industry (cubic yards, pounds,
etc.). As stated in the introduction to Section 6, other elements of the
guideway costs, such as right-of-way, terminals, etc., have been given in
Section 5.4.1.

TABLE 6-2. RIDE CONTROL SUBSYSTEMS COSTS (PER VEHICLE)

	BASIC SYSTEM	FAILSAFE CONFIGURATION
ACCELEROMETERS (8)	$ 5,000	$ 8,000
GAP SENSORS (8)	32,000	44,000
LONGITUDINAL VELOCITY SENSOR (1)	2,400	4,800
CONTROL ELECTRONICS (1 SET)	10,000	25,000
POWER CONTROL UNIT (1)	15,000	24,000
CONTROL MAGNET POWER AMPLIFIERS (8)	24,200	24,200
BACKUP POWER SUPPLY	60,200	60,200
CONTROL SYSTEM STATE INSTRUMENTATION (1 SET)	10,000	12,000
SIGNAL AND POWER CABLING (1 SET)	5,000	8,000
● SUBTOTAL, EQUIPMENT	$163,800	$210,200
UNIT ACCEPTANCE TESTING, INSTALLATION AND SUBSYSTEM CHECKOUT AND ACCEPTANCE TEST	38,000	62,000
● TOTAL RIDE CONTROL SUBSYSTEM	$201,800	$272,200

6.2.1 At-Grade Costs

Construction cost data generated by the Cardan Co. for the baseline at-grade guideway configuration are itemized in Tables 6-4, 6-5, and 6-6. The costs of the roadbed shown in Table 6-4 — including concrete pavement, median curb, sub-base, and base — were calculated assuming the use of standard construction techniques used for highways and runways. The aluminum costs in Table 6-5 — including fabrication and installation expenses — were estimated from data contained in construction bids for the Task 2 test guideway and from DOT-supplied data for the cost of the PTACV LIM reaction rail.

TABLE 6-3. LSM COSTS (PER VEHICLE[1])

⊙ LSM MODULES

SUPERCONDUCTOR (NO SHIELDING COILS)	$307,500
MAGNET CANS	22,500
PERSISTENT SWITCHES	880
DEMOUNTABLE LEADS	230
OUTSIDE CONTAINER	104,000
SUPPORTS	715
LEVEL DETECTORS	200
ELECTRICAL CONNECTORS	200
SUPERINSULATION	3,000
ENVIRONMENTAL TESTING	20,000
LIQUID He RESERVOIRS	12,000
LABOR	19,000
TOTAL MODULE COST	$490,225[2]
● REFRIGERATION SUBSYSTEM[3]	$55,000
TOTAL SYSTEM COST	$545,225/VEHICLE[4]

[1] FIVE MODULES PER VEHICLE, 250 VEHICLES. NO DEVELOPMENT COSTS INCLUDED.

[2] $868,472/MODULE WITH SHIELDING COILS

[3] REFRIGERATION FOR BOTH THE LSM AND THE LEVITATION/GUIDANCE MODULES (ONE REFRIGERATOR AND TWO COMPRESSORS)

[4] $923,472/VEHICLE WITH SHIELDING COILS

TABLE 6-4. COST ESTIMATE - ROADBED CONSTRUCTION (AT-GRADE GUIDEWAYS)

ITEM	QUANTITY	UNIT PRICE	COST PER RUNNING FOOT $/FOOT
8 IN. CONCRETE PAVING	1.11 SQ YDS	$7.50/SQ YD	8.33
MEDIAN CONCRETE CURB	0.215 CU YDS	$100/CU YD	21.50
0.75 IN. DIA EXPANSION BOLTS	1 EA	$4.00/EA	4.00
REINFORCEMENT STEEL, PAVEMENT	21 LB	$0.35/LB	7.35
REINFORCEMENT STEEL, CURB	7 LB	$0.35/LB	2.45
CEMENT-TREATED BASE	0.222 CU YDS	$12.00/CU YD	1.22
SUBBASE	0.50 CU YDS	$5.50/CU YD	2.75
ASPHALT PAVING	0.19 TON	$15.50/TON	2.95
FILL UNDER ASPHALT PAVING	0.50 CU YDS	$0.50/CU YD	2.50
		TOTAL	$53.05/FT ($280,000/MILE)

TABLE 6-5. COST ESTIMATE – LEVITATION AND GUIDANCE ELEMENTS (PER ELEMENT)

ITEM	QUANTITY	UNIT PRICE	COST PER RUNNING FOOT . $/FOOT
ALUMINUM ELEMENTS	68.9 LB/FT	$0.56/LB	38.60
SHOP FABRICATION (FORM "L" SHAPE)	–	ASSUME 20% THE COST OF AL ELEMENTS	7.70
ATTACHMENT HARDWARE	–	ASSUME 25% THE COST OF AL ELEMENTS	9.66
FIELD INSTALLATION	–	ASSUME 45% THE COST OF AL ELEMENTS	17.40
		TOTAL	73.40/FT ($388,000/MILE)

TABLE 6-6. COST ESTIMATE – SITE PREPARATION (EARTHWORK) TWO-WAY TRACK

DEPTH OF CUT, H_1 FT	COST PER RUNNING FOOT $/FOOT	
5	14	ORIGINAL GRADE
10	30	FINAL GRADE
20	70	H_1 CUT
30	120	FILL H_2
40	180	$H_2 > H_1$

Site preparation costs (i.e., earthwork required to prepare for roadbed construction) are highly dependent on the route under consideration; therefore, only very preliminary cost estimations could be made relating to possible hypothetical terrain conditions and the attendant earthwork requirements. The amount of earth that would be moved for several required cut depths has been estimated to demonstrate the possible earthwork costs associated with providing a level surface through rough terrain. The typical cross sections shown in Figure 4-93 demonstrate that the cut must be smaller than the fill to balance the earth. The following assumptions were used to obtain the estimated earthwork costs given by Table 6-6: (1) the cut-fill earth balance is maintained; (2) an average cost for earth excavating, moving, filling and recompacting is $3.92/m^3 ($3.00/cu. yd.); and (3) elevation variation along the direction of travel can be approximated by a curve with a simple periodic waveform.

All guideway costs are summarized in Table 6-7, including an allowance for drainage. The estimated construction costs are shown to range from $1,450,000 per km ($2,330,000 per mile) for a two-way track in relatively smooth terrain (elevation deviations of about 3 m), to $1,990,000 per km ($3,200,000 per mile) for more severe terrain (elevation deviations of about 25 m). Cost estimates were not made for terrain having rock.

Cost Comparisons - Table 6-4 shows that a large part of the roadbed construction costs is associated with the median curb that supports the guidance surfaces. The high cost of this curb is due to the assumption that the curb is cast in place. A precast factory-made curb or the development of a slip-form type of machine to automate the curb construction should lead to a lower cost. Possible savings in curb construction has been estimated based on an assumption that an automatic process can be developed that will reduce the concrete cost per unit volume to that achieved with a slip-form paving machine. Based on this, a savings of $23,800 per km ($38,300 per mile) or about 14% of the roadbed construction cost should be possible.

A railroad tie roadbed such as suggested in Ref. 6-1 can be considered as an alternate guideway design. From the current cost of $9.97 each for ordinary railroad ties (Reference 6-2.), the 3.65 m-long (~12 ft.) ties

TABLE 6-7. ESTIMATED AT-GRADE GUIDEWAY CONSTRUCTION COST SUMMARY (TWO-WAY TRACK)

CONSTRUCTION COSTS - TWO WAY 1000 DOLLARS/KM (1000 DOLLARS/MILE)

COST ITEM	EARTHWORK REQUIREMENTS				
	H1* = 1.5 M (5 FT)	H1 = 3.0 M (10 FT)	H1 = 6.1 M (20 FT)	H1 = 9.1 M (30 FT)	H1 = 12.2 M (40 FT)
SITE PREPARATION	46 (74)	98 (158)	230 (370)	394 (634)	591 (950)
ROAD BED CONSTRUCTION			348 (560)		
DRAINAGE**			87 (140)		
LEVITATION AND GUIDANCE ELEMENTS			962 (1550) 4 ELEMENTS		
TOTAL, EXCLUDING LAND ACQUISITION	1450 (2330)	1500 (2410)	1630 (2620)	1790 (2890)	1990 (3200)

*H1 = DEPTH OF CUT REQUIRED
**COST OF DRAINAGE PROVISIONS IS ESTIMATE TO BE 25% OF ROADBED CONSTRUCTION COSTS

required for the MAGLEV guideway are estimated at least $13.30 each.* For ties spaced at 0.6 m (~2 ft), the cost of $13.30 ties would be $22,000 per km ($35,000 per mile), one way. From Table 6-4, the cost of finished concrete pavement including reinforcement steel is $51,500 per km ($83,000 per mile), one way. The railroad tie approach would then result in a potential savings if alignment of the awkward aluminum levitation/guidance elements relative to the ties can be accomplished for less than $29,000 per km ($48,000 per mile). It is doubtful if railroad ties will be less expensive when all the cost factors are considered, i.e., the cost of the installed ties, the cost of alignment and attachment of the aluminum to the ties, and the increased maintenance cost of ties. Also, ties will result in a rougher roadbed.

No clear advantage of any of the alternate guideway configurations over the baseline hat-shape is indicated from a guideway design or cost standpoint. The canted-inverted "T" involves the construction of a more complicated roadbed requiring the development of new machinery to automate construction. The "U" channel requires two separate curbs to support the guidance surfaces and would therefore be more expensive. A circular guideway may offer a cost advantage (due to the minimal amount of aluminum) if an innovative construction technique could be developed. The inverted "U" channel requires an increased amount of concrete for at-grade guideways unless a hollow beam is used. This design has the advantage of using separate aluminum plates for the horizontal and vertical (guidance) elements and would therefore eliminate the relatively expensive procedure of bending the aluminum. This necessitates having separate lift and guidance magnets on the vehicle, but having more expensive vehicles is generally cost effective if this results in a less expensive guideway.

6.2.2 Elevated Guideway Costs

Cost data were developed for the elevated guideway designs presented in Paragraph 4.5.2B. These data were generated by Cardan Co. as a function of the height of the pier, the span length, the type of footing (spread or pile), and whether ordinary prestress or uniform prestress is used in the beams. The unit price of the materials used to obtain the costs is tabulated in Table 6-8.

---

*Currently, the installed tie costs for some railroads (Penn-Central) are running at approximately $20 each, according to newspaper articles.

TABLE 6-8. UNIT MATERIAL COSTS FOR ELEVATED GUIDEWAYS

GUIDEWAY COMPONENT	MATERIAL/OPERATION	UNIT COST
Piers	Concrete, Forms, etc.	$105/cu yd
	Reinforcement Steel	$0.35/lb
Footings	Excavation	$6.00/cu yd
	Concrete, Forms, etc.	$85/cu yd
	Reinforcement Steel	$0.35/lb
	Backfill and Compaction	$9.00/cu yd
	Piles (if used)	$500/each
Girders	Fabricated Prestressed Girders (Concrete, Reinforcement, etc.)	Variable* From $400/cu yd to $800/cu yd
	Fabricated Center Curb (Concrete, Reinforcement, etc.)	$150/cu yd
	Erection Costs	Variable From $1200 (50 ft span) to $4100 (100 ft span)

*Cost depends on girder length, type of section and amount of prestress. The cost for a 75 foot uniform prestress box beam is $650/cu yd.

Figure 6-1 summarizes the substructure (piers and footings) and girder costs as a function of the length of the span. The girder costs predominate, especially for the long spans. The substructure costs decrease gradually with increasing span length since fewer, but larger, footings and piers are required. The twin-T girders with ordinary prestress have the lowest cost, but ordinary prestress beams have an undesirable amount of camber and creep (see Section 4.5.2B). A uniform prestress approach largely eliminates this problem. It is difficult and expensive to apply uniform prestress to a twin-T girder because of the shape of the section, but it is relatively easy to do
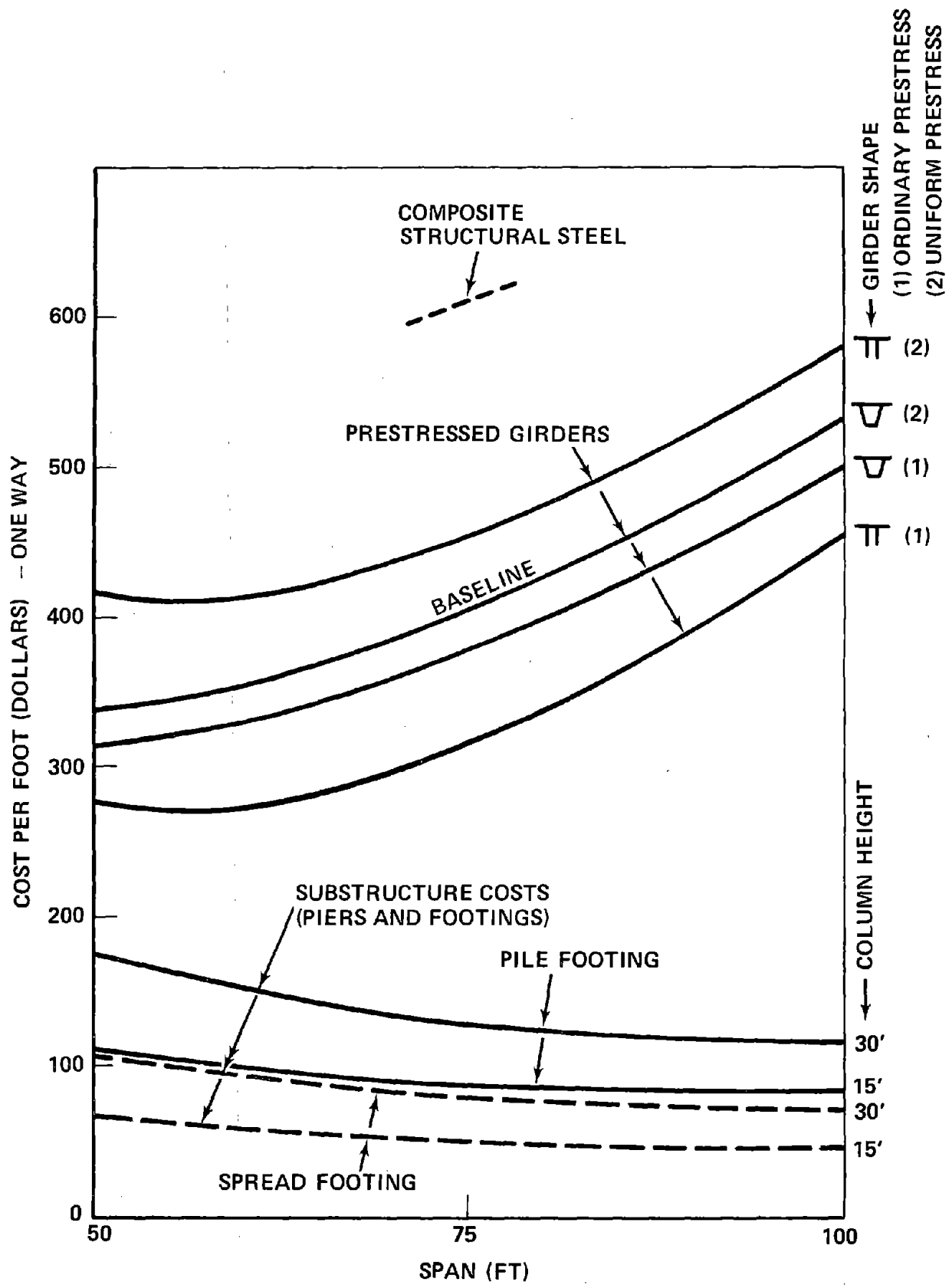
FIGURE 6-1.   GIRDER AND SUBSTRUCTURE COST

for a box beam. Therefore, the box beam with uniform prestress has been selected as the baseline elevated guideway. Note that a composite steel/concrete girder costs considerably more than all-prestressed concrete.

Figure 6-2 summarizes the cost of the complete structure for an elevated guideway except for the aluminum levitation elements on the top surface (aluminum costs are given in the previous section). The following conclusions can be drawn from the results:

- Span lengths on the order of 18 m (60 ft.) result in the lowest cost elevated guideway.

- Pile footings for poor soil conditions cost about 15% more than spread footings in terms of overall cost.

- Doubling the pier height from 4.5 m (15 ft.) to 9 m (30 ft.) increases the total cost by less than 15%.

- Total guideway costs using a uniformly prestressed box girder increase by less than 16% compared to the lowest-cost girder, i.e., a twin-T design with ordinary prestress.

Again, some cost savings can be obtained by prefabricating the center curb in a factory and simply bolting the sections to the guideway. The unit cost of $150/cu yd given in the table is for construction in the field. A cost savings of perhaps 5% in the girder cost (not guideway cost) may be possible with a prefabricated curb.

6.3 REFERENCES

6-1. Dyson, P., "Preliminary Estimates of Construction Costs for MAGLEV System Test Guideways," Mitre Corp., Report No. MTR-6622, March 1974.

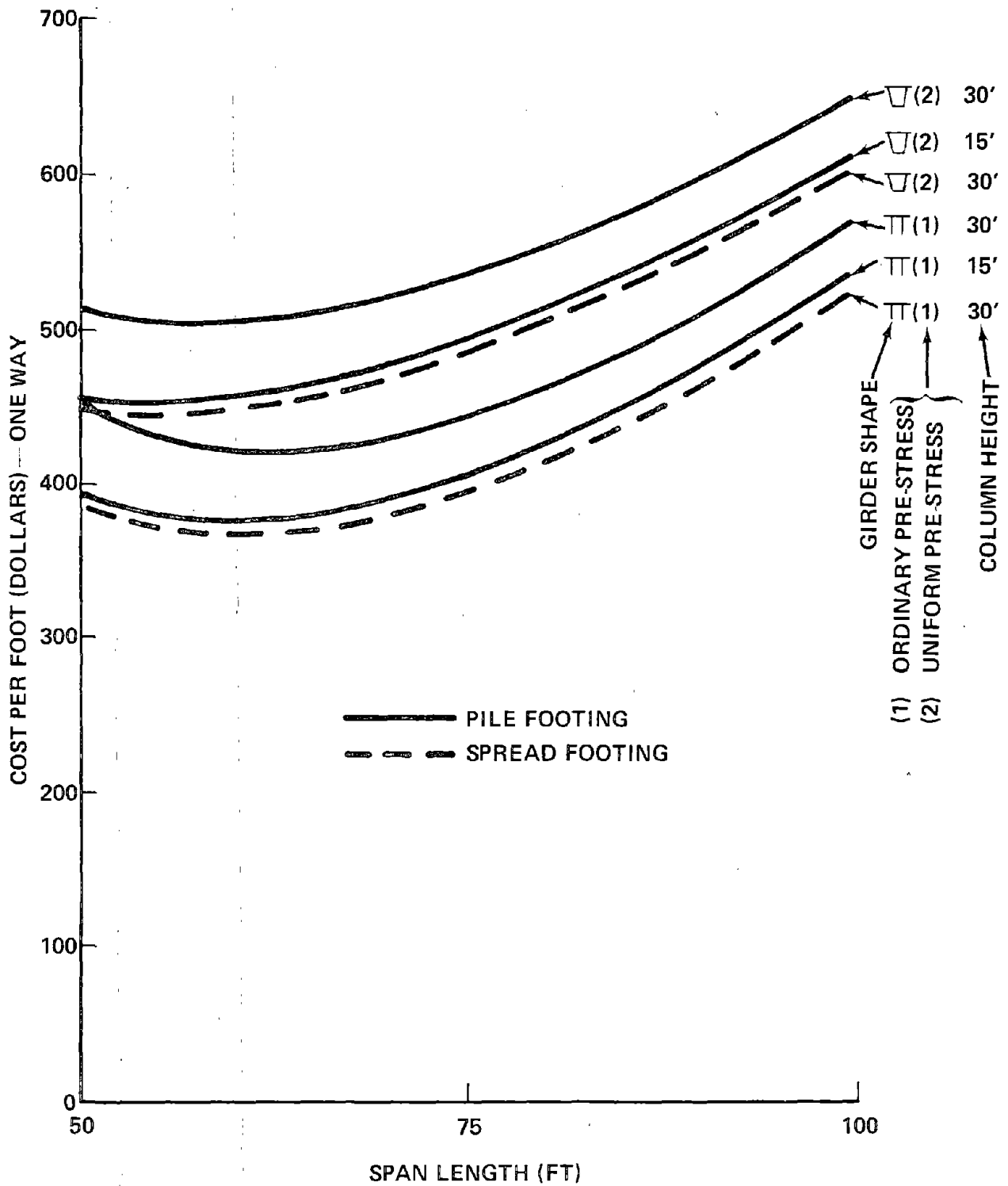6-2. "The World of Industry," Nation's Business, Vol. 62, No. 10, p. 442, October 1974.

FIGURE 6-2. TOTAL GIRDER AND SUBSTRUCTURE COST – ELEVATED GUIDEWAY

SECTION 7

CONCLUSIONS AND RECOMMENDATIONS

7.1 GENERAL STUDY RESULTS

The major study conclusions of this effort pertain to the technology aspects of a passenger-carrying TMLV, e.g., the vehicle suspension, the guideway, propulsion, and overall vehicle design/performance. Additional conclusions pertain to the general systems aspects, e.g., passenger capacity, total cost, and parameter optimization. The pertinent conclusions in each category are summarized below.

7.1.1 Vehicle Suspension

The passenger-carrying TMLV Revenue System conceptual design studies show that the repulsion-type of suspension for MAGLEV can be employed in a high-speed ground vehicle and meet all specified ride quality requirements at 134 m/s (300 mph) without the necessity for a super-smooth guideway or a secondary suspension. The ride quality requirements are achievable for a guideway with a statistical roughness coefficient, $A = 1.5 \times 10^{-6}$ m, without excessive vehicle excursion (maximum stroke $\leq$ 5 cm) or power consumption (30 to 50 kW) in all dynamic modes and in turns and transitions to a 2% grade as well as in straight and level transit. Several active ride control techniques were studied, i.e., those incorporating position feedback, acceleration feedback or heavy absolute damping, and all were found to have acceptable performance; quantitative comparison, however, is highly route-specific (primarily due to differing grade transition lengths) and no "optimum" control technique can be identified at this time. Total production cost of the baseline position feedback control system is estimated at $272,000 per vehicle.

The proposed design for the suspension system, i.e., the superconducting levitation/guidance magnets and associated refrigeration system, represents a very modest extension of state-of-the-art systems to produce a high-performance

design (lift-weight ratio ~16.8 with shielding; 20.8 W heat leak per vehicle).
All aspects of the proposed design (namely, high-current-density niobium-
titanium multi-filament wire, low-conductivity epoxy-fiberglass struts to
transmit mechanical forces, etc.) are currently available, but the combina-
tion embodied in the proposed design must go through a development test
program to ensure proper performance in the high-speed, vibratory field
environment. Eight suspension magnets are used in the design, combined in
pairs to make four suspension modules. Each module thus consists of two
redundant suspension magnets (each magnet encapsulated in a separate dewar),
thereby greatly increasing the reliability of the suspension system. Each
dewar contains a 16-liter liquid helium storage container to maintain its
cryogenic temperature in the event of failure of the refrigeration system.

Active shielding of the levitation/guidance magnets is accomplished with
bucking coils without introducing severe weight penalty. The average magnetic
field in the passenger compartment is quite low (5 to 10 gauss); the maximum
magnetic field at seat level (about 70 gauss) is directly over the magnets.*
The production cost of the suspension system is estimated at $138,000/vehicle.

7.1.2 Guideway

Although several guideway configurations are feasible, the hat-shaped
(or wide inverted Tee) configuration is preferred. It provides for stable
vehicle operation, is equally applicable to either elevated or at-grade use
and can be fabricated quite easily with conventional highway and airport
construction techniques and equipment. At the wavelengths of interest for a
vehicle at 134 m/s, the estimated guideway vertical roughness level achieved
with these conventional construction methods is actually less than that used
for the vehicle ride quality analyses. The lateral roughness level of the
central "spine" of the guideway is expected to be even lower. There is the
potential therefore, for further improvements in ride quality without resort
to expensive or exotic construction techniques. The hat-shaped guideway is
judged to be the most economical configuration; exclusive of land acquisition,

---

*In the baseline design, no passenger seats are actually located over the
magnets due to the placement of the magnets near the ends of the vehicle.

route preparation or electrical power, the double-track cost estimates are 1.4×10^6/km for at-grade-construction and 3.6×10^6/km elevated. These costs include the L-shaped levitation elements, which are fabricated from high-conductivity aluminum (1100-H14) to achieve high magnetic lift/drag ratio (~ 46).

7.1.3 Vehicle Design/Performance

The baseline, 80-seat vehicle with Ducted Fan/Gas Turbine propulsion exhibits minimum energy consumption per passenger with the 2 + 2 seating arrangement. The 140-seat vehicle, however, shows 24% less energy consumption per passenger and the optimum seating arrangement is 2 + 3. The aerodynamic drag of the baseline vehicle is approximately 2.5 times the magnetic drag at level cruise conditions, despite the assumption of a relatively "clean" configuration. Great care must be exercised in design, therefore, to assure conformity with aircraft practice regarding surface smoothness, the fit of joints, windows, doors, etc. Acceleration to cruise conditions and operation on an upgrade increases the importance of vehicle weight, and a lightweight design approach is highly desirable.

The vehicle sponsons (the lower vehicle sections required to straddle the hat-shaped guideway) are advantageous in that they provide a high section modulus with a relatively short vehicle (by encapsulating magnets, wheels, fuel, etc.), thus permitting a light-weight, low power vehicle design. The wheeled suspension system is easily packaged within the sponsons, and supports the vehicle during normal operation below lift-off speed ($\sim$ 30 m/s). The wheels also engage the switching ramps and provide the support for emergency landing. Vehicle-generated noise (exclusive of propulsion) is a major design factor since it bears on cruise speed selection, propulsion system performance, etc. The preliminary vehicle noise estimate is 92 dbA at 15 m for a vehicle traveling at 134 m/s; the DOT operating goal of 73 dbA is not reached until speed drops to 80 m/s (179 mph).

7.1.4 Propulsion

The propulsion system is a major factor in overall system design; it is the largest vehicle weight and cost element and directly influences the guideway and switch mode selection. The noise-suppressed Ducted Fan/Gas Turbine

system is clearly the leading candidate for a Repulsion MAGLEV vehicle for the near future. Its advantages relate to its development status, reliability, light weight, reasonable cost, performance, and its ability to provide propulsion for switching and off-line operation as well as on-line operations. An additional advantage is that it results in the cheapest guideway, e.g., when compared with electric propulsion systems. Noise and exhaust emission problems appear readily solvable within realistic requirement bounds.

In the event that chemical fuels (fossil or synthetic) are not available, recourse can be made to electric propulsion. All of the electric propulsion systems considered appear to be feasible, but there are a number of unresolved problems which prevent precise quantitative comparison. The linear induction motor (LIM) has the best development status of the electric systems, but it is excessively heavy unless wayside power conditioning is employed; although not yet demonstrated, wayside conditioning is probably feasible. The LIM requires power pickup and is difficult to switch safely, even in the single-sided version. The biggest difficulty, however, is the dynamic incompatibility between the narrow-gap motor and the large gap vehicle suspension; the motor cannot be suspended from the vehicle without adversely affecting ride quality and/or stroke. This problem is resolvable, in principle, by operating the motor as a tug, i.e., with its own separate suspension system. Nevertheless, it is our judgement that the linear induction motor will not be a good propulsion system for a Repulsion MAGLEV vehicle.

The linear synchronous motor has substantial potential for Repulsion MAGLEV applications. It is a large gap device, does not require a power pick-up and is efficient. Current indications are, however, that it is difficult to switch and is relatively heavy (with somewhat higher energy consumption). Nevertheless, with sufficient development the LSM could become the future MAGLEV propulsion system.

The noise-suppressed ducted fans can also be driven by rotary electric motors, preferably of the superconducting type for reduced size and weight. Despite the light weight of this propulsion arrangement, the overall energy consumption per passenger is the highest of all systems studied. Compared to

other electrically-powered systems, switching is easier because of the system's ability to provide propulsion for both on-line and off-line operations, and the additional guideway cost (above that for the gas-turbine driven fan) is only due to power rail and power distribution, not a reaction rail. The system will benefit from current military efforts to develop superconducting motors for ships.

The superconducting paddle wheel is a concept with long-term potential, including the possibility of integrating propulsion with levitation. It has high efficiency and, when driven by onboard gas turbines, has the lowest energy consumption of all systems studied. However, this concept has essentially zero development status and much more work is necessary to determine its characteristics.

7.1.5 Systems Analysis

The 140-seat vehicles can handle approximately 5000 passengers per hour, corresponding to $\sim 30 \times 10^6$ passengers per year or $\sim 2 \times 10^{10}$ passenger-km per year for the sample 750 km route. These results are based on 16 hour/day operation at 60% load factor and 2-minute headway between vehicles. For larger headways or for peak capacities of greater than 5000-passengers per hour, two or more vehicles must be coupled together. This results in a more favorable energy intensity (< 1 MJ/seat-km), but the vehicle dynamics aspects of coupled vehicles are unknown at this time.

Train sets composed of three 140-seat coaches operating at 134 m/s with Ducted Fan/Gas Turbine propulsion have a total operating cost of ~ 1.7¢/passenger-km for JP fuel at 5.3¢/liter (20¢/gal) and ~ 2.1¢/passenger-km for fuel at 10.6¢/liter (40¢/gal). Again, 60% load factor is used.

The optimum thickness of the aluminum guideway elements is between 2 and 3 cm for a very wide range of JP fuel cost. Cruise speed for minimum energy cost is between 80 m/s (179 mph) and 95 m/s (212 mph); cruise speed for minimum total system cost is between 90 m/s (201 mph) and 110 (246 mph), although total cost is not very sensitive to cruise speed in the range of current fuel costs.

Total double track guideway cost, assuming the Northeast Corridor compo-
nent mix* and with land at $30,000 per acre, ranges from ~ $3.3 x 10^6/km for
the Ducted Fan/Gas Turbine propelled system to ~ 4.1 x 10^6/km for the LSM-
propelled system.

For a single 80-seat vehicle operation with 2-minute headway, there is
approximately a 15% difference in cost/passenger-km between the Fan/GT system
and the highest cost electric system with JP fuel at 10.6¢/liter (40¢/gal)
and electricity at 3¢/kW hr, respectively. For a single 140-seat vehicle,
the difference is only 10%, reflecting the diminished importance of the guide-
way cost under high capacity operation.

7.2 RECOMMENDATIONS

The Philco-Ford-developed 5-DOF vehicle dynamics computer program should
be employed for in-depth parametric evaluation of various active control
schemes. Cruise speeds above and below 134 m/s should be considered and
emphasis should be placed on those control schemes which do not require a gap
sensor. This work should interface with route-specific analyses to derive
optimal turn and grade transition profiles and vehicle acceleration/speed
profiles.

Much more work based on either wind tunnel testing or free flight model
testing is necessary to obtain reliable aerodynamic data. This includes
cross-wind flow conditions with realistic guideway/vehicle simulation. A
similar recommendation is appropriate to the problem of vehicle-generated
noise. This is necessary to establish realistic noise requirements, partic-
ularly as they affect the propulsion system selection, operation near popu-
lated areas, etc.

More detailed analyses of various propulsion options should be carried
out, with possible subscale experimentation, and with careful attention to
overall systems aspects. Further consideration should be given to the problem
of vehicle switching. (Switching permits off-line loading and unloading, a
requirement for a high capacity, limited headway system.)

---

*1% bridges, 4% tunnels, 16% elevated, 79% at grade.

A field experimentation program, preferably with a subscale test vehicle, is necessary to ascertain performance of the superconducting magnets and associated equipment in a realistic environment. Measurement of vehicle ride quality, switch functioning, aerodynamic noise, and other system parameters is also desirable. Development should continue on the magnet to obtain a shielded, low weight, high lift, intrinsically stabilized design.

A gap sensor should be developed which will function in an all-weather environment and meet the requirements listed in Section 4.3.4A. Other instrumentation which should be developed is a device to detect objects on the track; ones large enough to interfere with passage of the vehicle.

1. Report No.	2. Government Accession No.	3. Recipient's Catalog No.
FRA-OR&D-75-21		PB247931

4. Title and Subtitle	5. Report Date
Conceptual Design and Analysis of the Tracked Magnetically Levitated Vehicle Technology Program (TMLV) - Repulsion Scheme; Volume I - Technical Studies	February 1975
	6. Performing Organization Code

7. Author(s)	8. Performing Organization Report No.
	Philco-Ford Report TMLV-37

9. Performing Organization Name and Address	10. Work Unit No. (TRAIS)
Ford Motor Co. Scientific Research Staff P.O. Box 2053, Dearborn, Michigan 48121 and Aeronutronic Div.; Philco-Ford Corp. Ford Road, Newport Beach, Ca 92663	
	11. Contract or Grant No.
	DOT-FR-40024

12. Sponsoring Agency Name and Address	13. Type of Report and Period Covered
U.S. Department of Transportation Federal Railroad Administration 400 7th Street, S.W., Room 5416A Washington, D. C. 20590	Final Report for Period of June 1974 to January 1975
	14. Sponsoring Agency Code

15. Supplementary Notes

16. Abstract

This report summarizes the studies of a program to establish the technology of magnetic suspension for ultimate use in a passenger-carrying high-speed ground transportation (HSGT) system - at speeds on the order of 134 m/s (300 mph). Magnetic Levitation (MAGLEV) is one of the advanced vehicle suspension concepts considered as alternatives to conventional transportation modes in the short-haul regime. These advanced systems have the potential of alleviating the heavy traffic congestion predicted for the highly populated regions of the U.S. in the 1985-1995 period. The national energy shortage has intensified the search for more energy-efficient and cost-effective transportation modes.

This volume summarizes the analyses and designs which demonstrate the performance of the system including the ability to meet the DOT ride quality standards on straight and level guideways as well as on curves and grade transitions. Conceptual designs and costs are shown for the vehicles, guideways, and the complete system. Various propulsion systems and guideway configurations are investigated, and a simple economic model is developed for the evaluation of MAGLEV systems on a cost per seat-mile or cost per passenger-mile basis.

17. Key Words	18. Distribution Statement
High Speed Ground Transportation, Magnetic Levitation, Vehicle Dynamics, Ride Quality, High Speed Vehicle Design, Superconducting Magnets, Guideway and Systems Analysis	Document is available to the public through the National Technical Information Service, Springfield, Virginia 22151

19. Security Classif. (of this report)	20. Security Classif. (of this page)	21. No. of Pages	22. Price
Unclassified	Unclassified	380	

Form DOT F 1700.7 (8-72)   Reproduction of completed page authorized   PRICES SUBJECT TO CHANGE